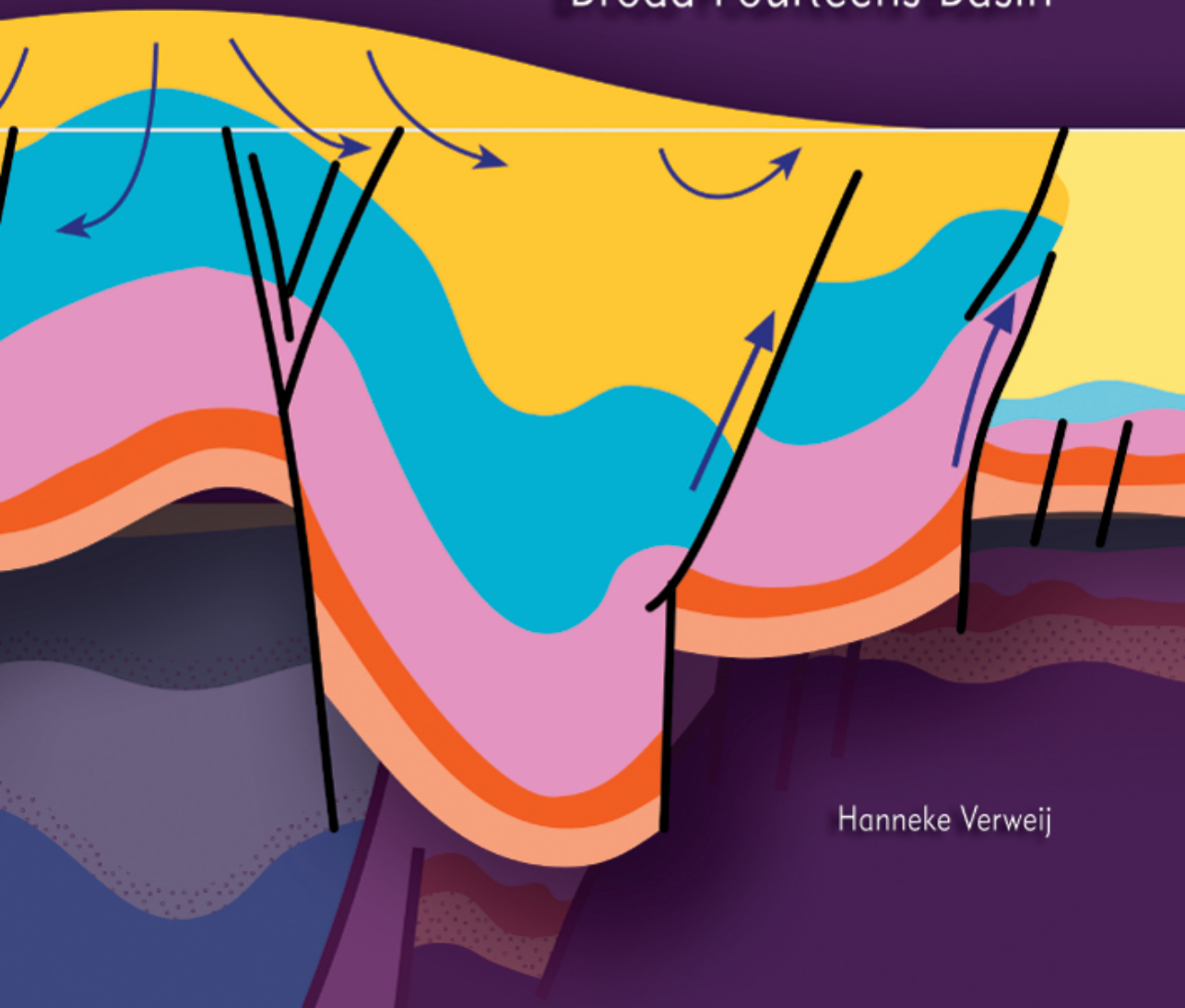


# Fluid flow systems analysis on geological timescales in onshore and offshore Netherlands

With special reference to the  
Broad Fourteens Basin



Hanneke Verweij

---

# Fluid flow systems analysis on geological timescales in onshore and offshore Netherlands

*With special reference to the  
Broad Fourteens Basin*

---

Hanneke Verweij

October 2003



Netherlands Institute of Applied Geoscience TNO  
– National Geological Survey

The research reported in this thesis was largely carried out at the Netherlands Institute of Applied Geoscience TNO – *National Geological Survey*

**Lay-out**

Jos Rietstap Vormgeving, Schiedam

**Printing**

Drukkaken, Rotterdam

Netherlands Research School of Sedimentary Geology (NSG) contribution No. 2003.09.05

**CIP-DATA**

Verweij, Johanna Maria

Fluid flow systems analysis on geological timescales in onshore and offshore Netherlands. With special reference to the Broad Fourteens Basin. – Doctoral Thesis Vrije Universiteit Amsterdam – with ref. – with summary in Dutch

Subject headings: fluid flow systems, groundwater systems, petroleum systems, paleo fluid flow, pore pressures, temperatures, basin analysis

ISBN 90-5986-035-7

©2003 J.M.Verweij, Delft

Published by the Netherlands Institute of Applied Geoscience TNO – *National Geological Survey*, Utrecht, the Netherlands

VRIJE UNIVERSITEIT

**Fluid flow systems analysis on geological timescales  
in onshore and offshore Netherlands**

With special reference to the Broad Fourteens Basin

ACADEMISCH PROEFSCHRIFT

ter verkrijging van de graad van doctor aan  
de Vrije Universiteit Amsterdam,  
op gezag van de rector magnificus  
prof.dr. T. Sminia,  
in het openbaar te verdedigen  
ten overstaan van de promotiecommissie  
van de faculteit der Aard- en Levenswetenschappen  
op woensdag 19 november 2003 om 15.45 uur  
in de aula van de universiteit,  
De Boelelaan 1105

door

Johanna Maria Verweij

geboren te 's-Gravenhage

promotoren: prof.dr. S.A.P.L. Cloetingh  
prof.dr. J.J. de Vries



---

*voor Hessel*



## Contents

|               |   |
|---------------|---|
| <b>1</b>      | <b>General introduction   1</b>   |
| 1.1           | Introduction   1  |
| 1.2           | Fluid flow systems in sedimentary basins: general concepts   2                                  |
| 1.3           | Analysis of fluid flow on geological timescales   13  |
| 1.4           | Objectives of this thesis   14  |
| 1.5           | Organisation   14   |
| <b>Part 1</b> | <b>Overview of the post-Carboniferous hydrogeohistory of onshore and offshore Netherlands</b>   |
| <b>2</b>      | <b>Introduction to Part 1   17</b>  |
| <b>3</b>      | <b>Geological history of onshore and offshore Netherlands   18</b>                              |
| 3.1           | Pre- and Early rift phase   19  |
| 3.2           | Main syn-rift phase   23  |
| 3.3           | Post-rift phase   23  |
| 3.4           | Syn-inversion phase   24  |
| 3.5           | Post-inversion phase   25   |
| <b>4</b>      | <b>Factors controlling the hydrogeohistory of onshore and offshore Netherlands   33</b>         |
| 4.1           | Tectonic control   34   |
| 4.2           | Sedimentary loading   35  |
| 4.3           | Erosional unloading   35  |
| 4.4           | Glacial loading/unloading   35  |
| 4.5           | Topography of the water table   36  |
| <b>5</b>      | <b>Present-day hydrogeological framework of onshore and offshore Netherlands   38</b>           |
| <b>6</b>      | <b>Present-day indicators of fluid flow conditions in onshore and offshore Netherlands   41</b> |
| 6.1           | Overview of indirect indicators derived from published studies   41                             |
| 6.2           | Identified periods of active fluid flow   44  |
| <b>7</b>      | <b>Present-day overpressures and fluid flow in onshore and offshore Netherlands   45</b>        |
| 7.1           | Distribution of overpressures   45  |
| 7.2           | Factors controlling present-day distributions of overpressure   48                              |
| 7.3           | Overpressures and fluid flow in Cenozoic sedimentary units   48                                 |
| 7.4           | Overpressures and fluid flow in pre-Tertiary sedimentary units: general observations   49       |
| 7.5           | Overpressures and fluid flow in Cretaceous units   50   |
| 7.6           | Overpressures and fluid flow in Upper Jurassic and Lower Triassic units   50                    |
| 7.7           | Overpressures and fluid flow in Upper Rotliegend units   51                                     |



|               |   |
|---------------|---|
| <b>8</b>      | <b>Hydrochemistry and temperatures in onshore and offshore Netherlands   53</b>   |
| 8.1           | Hydrochemistry   53   |
| 8.2           | Temperatures   66   |
| <b>9</b>      | <b>The present-day hydrodynamic setting of onshore and offshore Netherlands   79</b>  |
| 9.1           | Topography-induced fluid flow systems   79  |
| 9.2           | Artificial fluid flow systems   80  |
| 9.3           | Fluid flow systems induced by sedimentary loading and associated burial-related processes   80                                  |
| <b>10</b>     | <b>Discussion and conclusions Part 1   83</b>   |
| <b>Part 2</b> | <b>Fluid flow systems analysis of the Broad Fourteens Basin: Conceptual model of its geodynamic and fluid dynamic evolution</b> |
| <b>11</b>     | <b>Introduction to Part 2   85</b>  |
| <b>12</b>     | <b>Regional tectonic setting   86</b>   |
| 12.1          | Variscan phase   86   |
| 12.2          | Triassic and Early Jurassic extension and thermal subsidence   87   |
| 12.3          | Middle Jurassic domal uplift   87   |
| 12.4          | Late Jurassic to Early Cretaceous extensional tectonics   88  |
| 12.5          | Late Cretaceous to Earliest Tertiary closure of the Tethys Ocean and the creation of the Alpine fold chain   88                 |
| 12.6          | Tertiary creation of the Atlantic Ocean and seafloor spreading   89   |
| <b>13</b>     | <b>Geological history   91</b>  |
| 13.1          | Variscan sequence of Westphalian and Stephanian age   93  |
| 13.2          | Pre-rift and Early-rift sequence of Late Permian to Mid Jurassic age   93   |
| 13.3          | Main syn-rift sequence of Late Jurassic to Early Cretaceous age   95  |
| 13.4          | Post-rift sequence of Aptian-Albian to Late Cretaceous age   95   |
| 13.5          | Syn-inversion sequence of Late Cretaceous age   97  |
| 13.6          | Post-inversion sequence of Tertiary and Quaternary age   99   |
| <b>14</b>     | <b>Hydrogeohistory   101</b>  |
| 14.1          | Tectonic control   101  |
| 14.2          | Sedimentary loading   104   |
| 14.3          | Erosional unloading   104   |
| 14.4          | Glacial loading/glacial unloading   104   |
| 14.5          | Topography of the water table   104   |
| 14.6          | Overview of factors controlling the hydrogeohistory   106   |
| 14.7          | Present-day hydrogeological framework   107   |

|               |   |
|---------------|---|
| <b>15</b>     | <b>Indicators of present-day and paleo fluid flow conditions   110</b>                                    |
| 15.1          | Pressures   110   |
| 15.2          | Temperatures and steady-state heat flow   110   |
| 15.3          | Hydrochemistry   113  |
| 15.4          | Geochemistry   115  |
| 15.5          | Characteristics of petroleum fluid systems   118  |
| 15.6          | Identified periods of active fluid flow   120   |
| <b>16</b>     | <b>Conceptual model of geodynamic and fluid dynamic evolution   124</b>                                   |
| 16.1          | Conceptual model of geodynamic and hydrodynamic evolution   124   |
| 16.2          | Conceptual model of hydrodynamic evolution in relation to the evolution of petroleum systems   125        |
| <b>17</b>     | <b>Discussion and conclusions Part 2   129</b>  |
| <br>          |   |
| <b>Part 3</b> | <b>Fluid flow systems analysis of the Broad Fourteens Basin: results of integrated 2D basin modelling</b> |
| <b>18</b>     | <b>Introduction to Part 3   131</b>   |
| 18.1          | Principles of integrated 2D basin modelling   131   |
| 18.2          | Input data and boundary conditions   132  |
| 18.3          | Modelling procedure   132   |
| <b>19</b>     | <b>History of sedimentation, uplift and erosion   135</b>   |
| 19.1          | Reconstructed geological history   135  |
| 19.2          | Predicted history of sedimentation, uplift and erosion   135  |
| <b>20</b>     | <b>Thermal history   139</b>  |
| 20.1          | Selection of boundary conditions and input data   139   |
| 20.2          | Temperature and heat flow history   141   |
| 20.3          | Conclusions   145   |
| <b>21</b>     | <b>History of maturation and petroleum generation   149</b>   |
| 21.1          | Maturation and petroleum generation in the Limburg Group source rock   149                                |
| 21.2          | Maturation and petroleum generation in the Jurassic source rocks   153                                    |
| 21.3          | Conclusions   157   |
| <b>22</b>     | <b>Permeability history   158</b>   |
| 22.1          | Evaluation of the modelling scenarios   158   |
| 22.2          | Conclusions   160   |
| <b>23</b>     | <b>History of pore pressures and groundwater flow   161</b>   |
| 23.1          | History of pore pressures   161   |
| 23.2          | History of groundwater flow   166   |
| 23.3          | Discussion and conclusions   175  |

|                         |   |              |
|-------------------------|---|--------------|
| <b>24</b>               | <b>History of petroleum expulsion, migration and accumulation</b>   | <b>  181</b> |
| 24.1                    | Expulsion, migration and accumulation of gas  | 183          |
| 24.2                    | Expulsion, migration and accumulation of oil  | 188          |
| 24.3                    | Conclusions   | 194          |
| <b>25</b>               | <b>Relations between the groundwater flow system and the petroleum system</b>   | <b>  199</b> |
| 25.1                    | Influence of the groundwater flow system on the petroleum system  | 201          |
| 25.2                    | Influence of the petroleum system on the groundwater flow system  | 204          |
| 25.3                    | Influence of the groundwater and petroleum systems on permeability evolution  | 204          |
| <b>26</b>               | <b>Conclusions Part 3 and continued analysis of fluid flow systems on geological timescales</b>   | <b>  205</b> |
| 26.1                    | Conclusions   | 205          |
| 26.2                    | Continued analysis of fluid flow systems on geological timescales in sedimentary basins in onshore and offshore Netherlands                                 | 207          |
| <b>Summary</b>          |   | <b>  210</b> |
| <b>Samenvatting</b>     |   | <b>  219</b> |
| <b>Acknowledgements</b> |   | <b>  227</b> |
| <b>References</b>       |   | <b>  228</b> |
| <b>Appendices</b>       |   | <b>  239</b> |
| 1                       | Calculated bulk conductivities for offshore Netherlands   | 239          |
| 2                       | Temperature differences, temperature gradients and steady-state heat flows between successive temperature measurements in wells in the Broad Fourteens area | 248          |
| 3                       | Water analyses data from nine wells in the Broad Fourteens Basin  | 254          |
| 4                       | Conceptual model of basin history along the regional cross-section: input parameters and boundary conditions  | 256          |

# 1 General introduction

## 1.1 Introduction

Knowledge of the present-day fluid flow systems in the sedimentary fill of onshore and offshore Netherlands, and the related pore pressure distributions in its reservoirs and seals, is important for safe and economic drilling, oil and gas field exploration and exploitation, as well as for safe subsurface storage of energy and energy residues. Process-based understanding and prediction of present-day distributions of the characteristics of the rocks and geofluids, such as the distributions of the excess pore pressures, the diagenetic cements, and the oil and gas fields, require knowledge on the evolution of fluid flow systems on geological timescales.

To date there has only been very limited, non-proprietary information available on present-day physico-chemical characteristics of geofluids and fluid flow systems in the deeper subsurface of onshore and offshore Netherlands. In addition, the characteristics of this deeper subsurface have been described and explained in terms of their tectonic, structural and stratigraphic evolution (e.g. Rondeel et al. 1996; geological atlas of the deep subsurface of onshore Netherlands 1991-2002: RGD 1991-1996, TNO-NITG 1997-2002), not taking into account fluid flow evolution.

The general scope of this thesis is to provide an integrated description of the Netherlands earth system based on the premise that geodynamics and climate are the major external mechanisms influencing hydrogeological and hydrodynamic evolution, and with the concept of fluid flow system as the mechanism linking intrabasin processes. By so doing, the thesis aims to provide the fluid dynamics context to increase process-based understanding of the present-day characteristics of the sedimentary basin fill in the onshore and offshore parts of the Netherlands. The detailed study of the Broad Fourteens Basin aims to provide quantitative understanding of the hydrogeological and hydrodynamic response of the basin fill to its geodynamic and climatic evolution and to show the significance of this response for understanding and prediction of the present-day distributions of pore pressures and the distributions and characteristics of the oil and gas accumulations.

Tóth's hydraulic theory of petroleum migration (Tóth, 1980) triggered the author's interest in the interaction between large-scale groundwater flow systems and petroleum systems. In 1986, the author started the very first research – in the Netherlands – involving the analysis of fluid flow systems on geological timescales. This research aimed to assess the applicability of hydrogeological knowledge and methods for oil and gas exploration purposes in onshore and offshore Netherlands. First results included concepts and theories on qualitative and quantitative aspects of groundwater systems and petroleum systems and their interactions (Verweij 1989), an outline of the Cenozoic hydrogeohistory of onshore and offshore Netherlands (Verweij 1990a) and a preliminary assessment of the present-day patterns of petroleum migration in relation to this Cenozoic hydrogeohistory (Verweij 1990b). Continued research on groundwater flow systems in relation to petroleum systems for basin analysis purposes resulted in the publication of a book entitled 'Hydrocarbon migration systems analysis' (Verweij 1993). Continuation of the research of geofluid systems in sedimentary basins of the Netherlands was initially hampered

by the lack of publicly available data on the deep subsurface of onshore and offshore Netherlands. This situation improved during the late nineties. Research of geofluid systems in the Netherlands subsurface extended during the nineties (Bloch et al. 1993 (unpublished), Bouw 1999, Elderhorst and Zijl 1992, Kooi and De Vries 1998, Simmelink et al. 2003, Van Balen et al. 2000b, Verweij 2003, Wildenborg et al. 2000, Winthaegeen and Verweij 2003). The research on geofluid systems reported in this thesis, started in 1995 with the regional analysis of fluid flow systems in relation to geological processes that operated in onshore and offshore Netherlands from the Carboniferous to present-day (Verweij 1997, 1999). An updated and revised version of this research is presented in Part 1 of this thesis. Later, research was focussed on the geofluid systems of the offshore Broad Fourteens Basin (Verweij et al. 2000, 2001, Verweij and Simmelink 2002, Verweij et al. 2003). Part 2 and 3 of the thesis present the detailed results of this research.

The important role of fluid flow in the different geological processes is widely recognised; the worldwide interest in – and understanding of – fluid flow systems in relation to the various geological processes have advanced rapidly since the early 1990's (Bethke 1985, 1989, Doligez 1987, Garven 1985, Hubbert 1953, Tóth 1980, 1987; Al-Aasm et al. 2002, Bredehoeft and Norton 1990, Dahlberg 1994, Garven 1995, Ingebritsen and Sanford 1998, Jamtveit and Yardley 1997, Law et al. 1998, Lerche and Thomsen 1994, McCaffrey et al. 1999, Mitchell and Grauls 1998, Parnell 1994, 1998, Pueyo et al. 2000). These concepts on fluid flow systems in relation to various geological processes in different sedimentary basins have been valuable for the research in onshore and offshore Netherlands.

## 1.2 Fluid flow systems in sedimentary basins: general concepts

The two major components of a sedimentary basin fill are the rock framework and the geofluids it contains (Figure 1). It is the latter, the geofluids, that are the object of study of this thesis. The focus is on groundwater and to a minor extent on oil and gas.

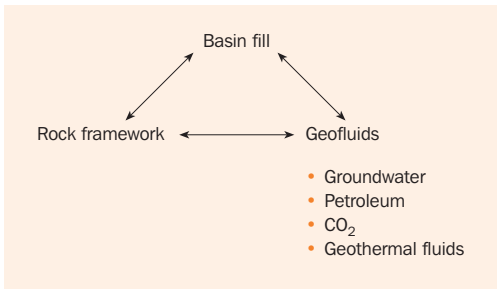


Figure 1 Two major components of a sedimentary fill

The physico-chemical characteristics of the rocks and geofluids evolve continuously during the development of a sedimentary basin. Through its physical, chemical and dynamic properties, groundwater continually interacts with its subsurface environment and other geofluids.

The important types of interaction between groundwater and the geological environment include (e.g. Tóth 1999): 1. Chemical interaction with processes of dissolution, hydration, oxidation–reduction, chemical precipitation, osmosis; 2. Physical interaction with processes of lubrication or pore pressure modification; 3. Kinetic interaction with transport processes of water, mass and heat. The process responsible for transporting the results of the different interactions is the transport of groundwater itself in flow systems. Indeed, groundwater's role as a general geologic agent is based on the interaction between groundwater and the geological environment and the transport of groundwater in flow systems are the basic causes (Tóth 1966, 1971, 1984, 1999).

The effects of groundwater's geological agency are created from the surface of the earth to depths of more than 15 km in the earth's crust, at widely varying scales of space and time (ranging from days to geological times) (Ingebritsen and Sanford 1998, Nur and Walder 1990). This thesis follows Ingebritsen and Sanford (1998) by using the term 'groundwater' in a broad sense as any subsurface, aqueous geofluid, including those of meteoric, connate and magmatic origin.

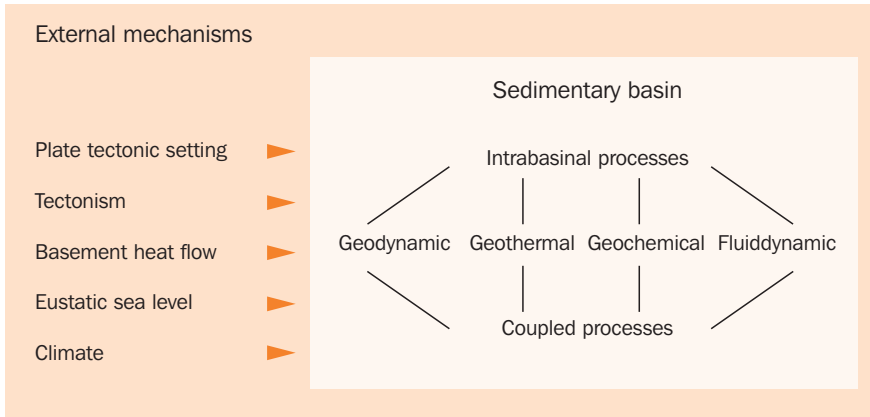


Figure 2 Different external and internal processes acting on the basin fill during basin evolution

The flow of geofluids in a basin, the mass transport of chemical compounds, the transport of heat and the deformation of the solid part of the basin are coupled processes (e.g. Ingebritsen and Sanford 1998, Person et al. 1996; Figure 2). Because no geological material can be considered impermeable to aqueous geofluids on a geological timescale (Neuzil 1995; Tóth 1995; Figure 3), these fluids are therefore the factor linking the different intrabasinal processes. The concept of fluid flow systems (Figure 4) offers a framework for the integrated study of these basin processes and for the interpretation of a wide range of physico-chemical characteristics observed in sedimentary basins.

Fluid flow systems are genetically related to external and internal processes acting on the basin, including processes such as tectonics, climatology, eustatic sea level changes, basement heat flow; sedimentation, erosion, sediment diagenesis, petroleum genesis (e.g. Garven 1995, Harrison and Tempel 1993, Person et al. 1996, Verweij 1993, 1994b, 1997, 1999; Figure 2). The fluid flow systems in sedimentary basins are differentiated genetically according to the dominant force or combination of forces/processes affecting fluid flow. The characteristics of such systems are furthermore strongly influenced by the hydrogeological framework of the basin. These forces/processes and the hydrogeology are strongly coupled to the formation

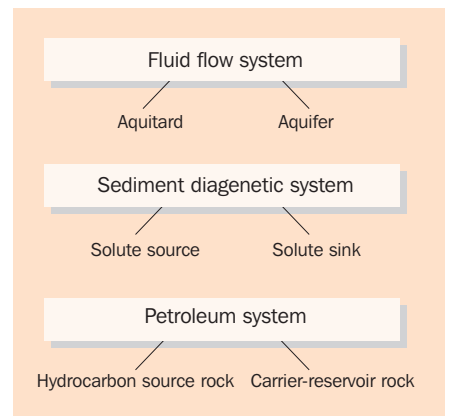


Figure 3 Different lithologies are interacting parts of a sedimentary basin (after Verweij 1999)

and evolution of the basin and its margins (Bethke and Marshak 1990, Garven 1995, Oliver 1986, 1992, Van Balen 1995, Van Balen and Cloetingh 1994, Verweij 1993, 1994a).

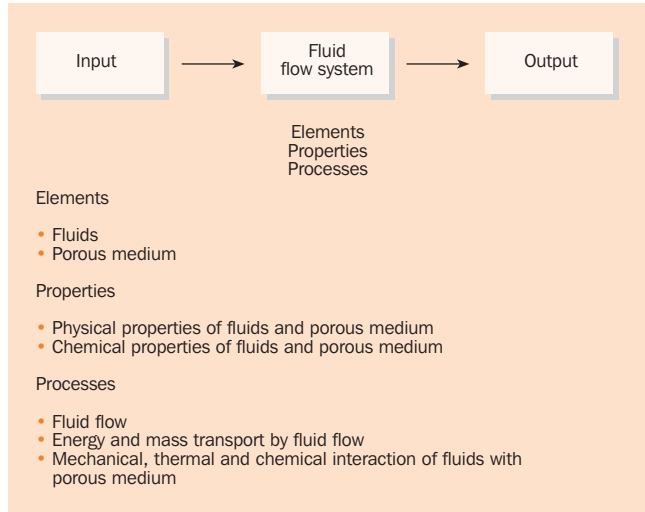


Figure 4  
Fluid flow system

### 1.2.1 Origin of overpressures

The dominating driving forces for one-phase fluid flow are fluid potential gradients, temperature gradients and hydrochemical gradients (Domenico and Schwartz 1998, Ingebritsen and Sanford 1998).

Fluid potential is the work necessary to transfer a unit volume of fluid from reference conditions (depth  $z = 0$ , gauge pressure  $P = 0$ ) to relevant subsurface conditions. At a certain depth  $z$ , the groundwater potential =

$$P - \rho_w g z = (P_{\text{hydrostatic}} + P_{\text{excess}}) - \rho_w g z = P_{\text{excess}}$$

(where,  $\rho_w$  = density of water;  $P_{\text{hydrostatic}} = \rho_w g z$  = hydrostatic pressure;  $P_{\text{excess}}$  = overpressure).

The overpressure or excess pressure of the groundwater at a certain depth is the difference between the pore pressure and the hydrostatic pressure at that depth (Figure 5). Flow is proportional to the gradient in groundwater potential – or gradient in overpressure – in the absence of other driving forces. The distributions of overpressures of groundwater in a basin and their changes in time largely control the evolution of hydrodynamic conditions in a basin.

The mechanisms controlling the development of the groundwater pressures during basin evolution are (Adams and Bachu 2002, Burrus 1998, McPherson and Garven 1999, Neuzil 1995, Osborne and Swarbrick 1997, Sibson 1995, 2000, Swarbrick and Osborne 1998):

— Stress-related processes (such as sedimentary loading, tectonic loading, glacial loading; erosional unloading; changing lateral tectonic stresses/changing

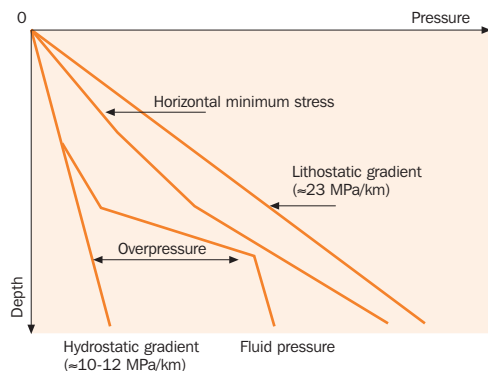


Figure 5 Relation between hydrostatic pressure, pore pressure and excess pressure

- of tectonic regimes; short-term stress fluctuations/seismicity);
- Flow of water (infiltration of meteoric water into the basin – creation of topographic relief of the water table; infiltration of seawater; flow into or out of a basin; flow in the basin itself);
- Sea level changes (these affect e.g. the topographic relief of water table);
- Heating and cooling (induced by climatic changes, changes in basal heat flow, tectonic subsidence or uplift and erosion);
- Changing groundwater volumes (induced by diagenetic reactions; dehydration of minerals; petroleum generation; heating/cooling);
- Changing groundwater salinities (these affect the groundwater densities and as a consequence the hydrostatic pressures of the groundwater).

Overpressures may be generated by: 1. increase in compressive stress, by e.g. sedimentary loading, vertical or lateral tectonic loading; 2. increase in fluid volume, induced by e.g. temperature increase, mineral diagenesis, gas generation and oil cracking; 3. fluid movement. An increase in density of the fluid, due to an increase in salinity, is associated with an increase in the hydrostatic pressure, but not with an increase in overpressure. Osborne and Swarbrick (1997) reevaluated the 3 mechanisms for generating overpressures in sedimentary basins and concluded – in accordance with previous evaluations (Bethke 1985, 1986b, England et al. 1987, Harrison and Summa 1991, Shi and Wang 1986) – that stress-related mechanisms are the most likely causes of overpressure in many sedimentary basins. Overpressure mechanisms related to changes in fluid volume require rocks with sufficiently low permeability. For example, aquathermal pressuring (temperature-induced increase in fluid pressure at constant fluid mass, Barker 1972) was found to be of negligible importance even in poorly permeable units (e.g. Daines 1982, Luo and Vasseur 1992). According to Osborne and Swarbrick (1997) the mechanism possibly could function effectively in units where near perfect sealing is more likely (in evaporite-rich units, or in very poorly permeable shales).

### *Sedimentary loading*

An important stress-related process is sedimentary loading. In a fluid-saturated rock pore, considering a certain time interval, sedimentary loading may induce: a. reduction in pore volume by increase in compressive stress (mechanical and chemical compaction); b. development of excess pore pressure; c. fluid flow from the pore. An overpressure distribution is thus controlled by the competition between the pressure-generating mechanism (sedimentary loading) and the pressure-dissipating mechanism (Darcy flow controlled by the overpressure gradients and hydraulic characteristics of the subsurface). Overpressures generated by past mechanisms will dissipate in time (controlled by hydraulic diffusivity of the subsurface).

The relation between these three effects of sedimentary loading can be illustrated by a modified Terzaghi's equation (Domenico and Schwartz 1998):

$$\sigma_z + \Delta\sigma_z = \sigma_e + (P_{\text{hydrostatic}} + P_{\text{excess}})$$

where  $\sigma_z$  is load stress,  $\Delta\sigma_z$  is the increment in load stress,  $\sigma_e$  is effective stress, and pore fluid pressure  $P$  consists of  $P_{\text{hydrostatic}}$  (hydrostatic pressure) and  $P_{\text{excess}}$  (overpressure). The load stress (= overburden stress = lithostatic stress) is due



to the force of gravity acting on a rock mass ( $\sigma_z = \rho gz$ ). The density ( $\rho$ ) is the bulk density of both rock and any fluids contained. This Terzaghi equation describes the effects of sedimentary loading assuming a number of limiting conditions, such as: vertical sedimentary loading is the only pressure generating mechanism; isothermal and isochemical conditions prevail; the rock matrix is compressible and behaves as a linear elastic solid; there is no horizontal compression or extension of the rock matrix; the solids are incompressible.

Under these assumed conditions an increase in the sedimentary load ( $\Delta\sigma_z$ ) will increase the pore fluid pressure and/or the effective stress. If the effective stress increases, pore volume will decrease and the rock will compact. Continued sedimentation and associated burial of the rock will induce continued reduction in porosity, provided that the pore water pressure increases according to the hydrostatic gradient. This will only occur if the sediments are able to dewater in response to the increasing sedimentary load. When fluid retention occurs at depths where permeability and sedimentation rate combine to prevent complete dewatering, the pore fluid will bear part of the incremental sedimentary load and become overpressured.

The pore pressure coefficient describes the percentage of the incremental load that is carried by the pore fluid for undrained conditions and compressible pore water (Domenico and Schwartz 1998, Flemings et al. 2002). The coefficient depends on the vertical compressibility of the rock matrix, the compressibility of the pore water and the porosity. The value of the pore pressure coefficient is  $\leq 1$ . Assuming that pore water is incompressible ( $\beta_w = 0$ ) the pore pressure coefficient is equal to 1 and the total incremental load will be carried by the pore water in the absence of flow. However, pore water is compressible ( $\beta_w = 4.8 \times 10^{-4} \text{ MPa}^{-1}$ ). The compressibility of sediments at depositional conditions varies widely; clays are most compressible, followed by silt, marl, sand and limestone. The compressibilities of the sediments at depositional conditions are  $>10^{-2} \text{ MPa}^{-1}$  (Mann et al. 1997), and the associated pore pressure coefficients are  $>0.95$ : the pore water will carry most of the change in sedimentary load. Compressibilities of sedimentary rocks decrease with decreasing porosities during burial. For porosities of 20% and 10% the compressibilities of the main clastic lithologies (clay, silt, marl, sand) decrease to  $10^{-3} \text{ MPa}^{-1}$  and  $2.7 \times 10^{-4} \text{ MPa}^{-1}$ , respectively (Mann et al. 1997), and the corresponding values of the pore pressure coefficient decrease to values below 0.90. When the compressibility of the rock matrix becomes much smaller than the pore water compressibility, the rock matrix will bear the load and the pore pressure will not change.

As another consequence of fluid retention, the increase in effective stress and the compaction slow down or even stop during continued sedimentary loading. The resultant trend of changing compaction or porosity with depth of burial will be out of equilibrium in an overpressured part of the sedimentary rock in comparison with a normally pressured part. This effect decreases in magnitude with increasing rock rigidity. Overpressuring in combination with undercompaction is most likely to occur in thick clay units subject to continuous sedimentary loading.

However, the pore pressures and porosities in a sedimentary basin subject to sedimentary loading are controlled by changes in mean stress, and not only by

changes in the vertical stress (e.g. Gouly 1998, Harrold et al. 2000, Palciauskas and Domenico 1989, Yassir and Bell 1996). The vertical stress and the mean horizontal stress change with depth. The change with depth of the ratio between mean horizontal stress and vertical stress (and as a consequence mean stress and vertical stress) seems to depend on the tectonic setting of a basin (e.g. Grauls 1997). For example, in the UK Central North Sea area, the sedimentary sequence is dominated by vertical stresses at shallow depths, and becomes more dominated by horizontal stresses at greater depths (Grauls 1997). The increasing horizontal stresses with depth will also affect the porosity and pore pressure development in the subsiding sediments. The magnitude of the changes of the horizontal stresses with depth is generally not known in present-day basins and during basin development. The significance of including the changes of horizontal stresses with depth in the evaluation of overpressure development due to sedimentary loading is not well established yet.

In reality, different pressure-influencing mechanisms may operate simultaneously during continuous burial of sedimentary units subject to sedimentary loading: not only the sedimentary loading itself, but also e.g. aquathermal pressuring, dehydration of minerals and generation of gas.

### *Tectonic control*

Tectonic forces include direct and indirect influences on fluid pressures. The indirect influence involves changes in the distribution of permeability and fluid pressure through opening and re-opening and closing of faults and fractures.

Tectonic forces exert influence on the hydrogeological and hydrodynamic conditions of a basin because of the interrelation between stress condition, fluid pressures and mechanical characteristics of the basin's rock framework (Jones et al. 1998, McCaffrey et al. 1999, Van Balen and Cloetingh 1994). Tectonic control includes both the static and dynamic influences on the permeability and storativity of the basin fill.

The static influence on permeability and storativity largely results from the influence of the state of stress, level of mean stress, and the orientation of principal stresses on existing stress-controlled features such as faults, fractures and stylolites (Sibson 1994, 1995). In general, permeability and storativity may tend to be higher in basins in an extensional stress regime compared with a compressional stress regime (e.g. Muir-Wood and King 1993, Sibson 1995, 2000). At a certain time during the basin's history, the orientation of existing fractures and faults relative to the orientation of the principal stresses will determine whether they are oriented such that they may become critically stressed for failure and are likely to be permeable, or to be impermeable (e.g. Muir-Wood and King 1993, Sibson 1995).

The dynamic influence of tectonics on storativity and permeability operates on different time scales related to gradual long-term changes in tectonic stress regime, pulse-like changes in compressive stress, as well as short-term stress fluctuations on time scales related to the earthquake cycle.

A change in tectonic regime from tensile to a compressive stress regime is

accompanied not only by changes in the direction of principal stresses but also by an increase in the mean stress and will lead to closure of the subvertical extension fractures, a decrease in storativity and permeability, fluid expulsion or, if fluid drainage is inhibited, an increase in fluid pressures (Sibson 1995, 2000). The magnitude of the pressure increase depends on permeability characteristics and the rate of stress change.

During periods of active deformation in the basin, short-term cycles of stress increase and subsequent stress-relaxation, i.e. short-term seismic events occur on time scales of 10 to 10,000 years (Sibson 1994). The type of stress-related hydrogeologic and hydrodynamic changes that may occur during active deformation depends on the type of stress regime and related style of fault displacements (Jones et al. 1998, Muir-Wood and King 1993). In an extensional regime, normal fault displacements may be accompanied by large changes in storativity and permeability (e.g. Muir Wood 1994) and pore pressure fluctuations. In a compressional regime, the changes in porosity, storativity and permeability will be small in comparison with those in an extensional regime, because of the high ambient horizontal stresses (Muir Wood 1994).

Tectonic processes influence pore pressures and fluid flow. Although Hubbert and Rubey (1959, Rubey and Hubbert 1959) recognised the influence of the increase in stresses of tectonic origin on the development of overpressures more than 40 years ago, the effect of horizontal loading on overpressure development is still poorly understood due to geological complexities of the basins in which lateral compression occurs (Osborne and Swarbrick 1997).

### 1.2.2 Fluid flow systems

Groundwater flow systems may be differentiated according to the dominant mechanism affecting flow: 1. Flow types controlled by groundwater potential gradients, including topography-induced flow, burial-induced flow, tectonically controlled flow, seismogenic flow, and 2. Flow types controlled by gradients in temperature and chemical components only, i.e. density-controlled flow, free thermal and thermo-haline convection. In this thesis the focus is on flow types controlled by groundwater potential gradients. The two most common flow types are the topography-induced groundwater flow system and the burial-induced flow system. The occurrence of tectonically-induced flow of groundwater has been proven (e.g. Ge and Garven 1989, Muir Wood 1994, Oliver 1986, 1992), but as yet no detailed tectonically controlled groundwater flow system has been defined.

#### *Topography-induced groundwater flow system*

Topography-induced groundwater flow systems (also known as gravity-induced groundwater flow systems) differing in their magnitude of extent and depth of penetration develop in subaerial basins or parts of basins and are genetically related to the topographic relief of the water table (e.g. Tóth 1963; Engelen and Kloosterman 1996; Figure 6). In a homogeneous and isotropic subaerial basin such hierarchically structured flow systems develop entirely in response to the relief of the groundwater table and are functions of the basin's geometry (that is water table relief and the basin's width and depth), assuming that chemically and/or thermally induced variations in fluid density do not influence flow. In each groundwater flow system,

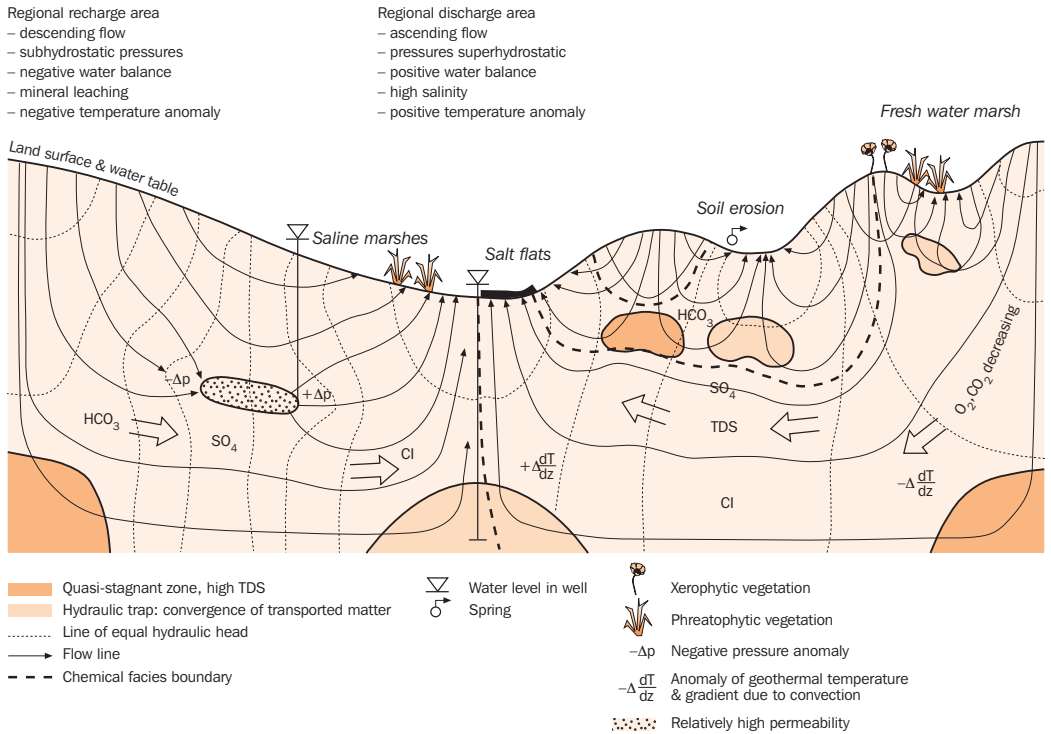


Figure 6 Topography-induced groundwater flow systems and associated physical, chemical and biological features (modified from Tóth 1999)

the flow is from a high-elevation recharge area, through a midline area towards a low-elevation discharge area. In the recharge area the groundwater flows vertically downwards. The corresponding groundwater potential decreases with depth and the associated groundwater pressures are subhydrostatic (the groundwater is underpressured, Figure 7). In the midline area the flow is lateral and the groundwater pressures change with depth according to the hydrostatic gradient. In discharge areas, the flow is vertically upward towards the ground surface. The groundwater potentials increase with depth and the groundwater pressures are superhydrostatic, i.e. the groundwater is overpressured (Figure 7). In most topography-induced flow systems the groundwater pressures remain relatively close to the hydrostatic gradient (perhaps within 10% of hydrostatic according to Ingebritsen and Sanford 1998).

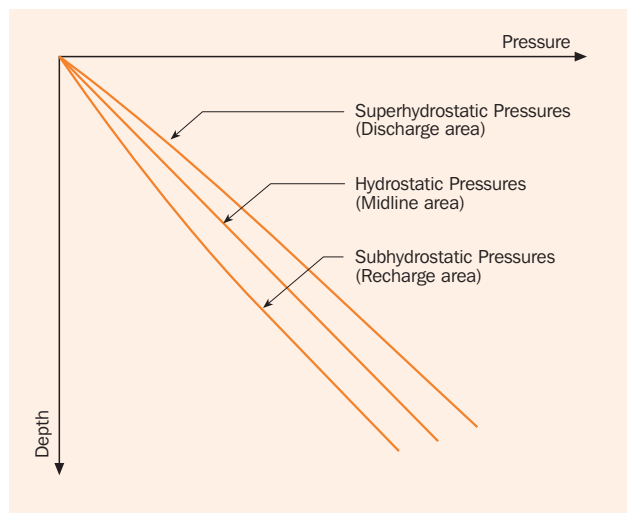


Figure 7 Change of groundwater pressure with depth in a simple topography-induced groundwater flow system

Two important influences of the hydrogeological framework on the pressure distribution and groundwater flow pattern are: the large losses of energy that are induced by poorly permeable hydrostratigraphic units and are reflected in the large differences in groundwater potential across such units; the regional flow that tends to be focussed into the relatively permeable hydrostratigraphic units (regionally extensive aquifers).

### *Burial-induced groundwater flow system*

The burial-induced groundwater flow systems are the combined result of the different pressure-influencing mechanisms operating on the sedimentary fill of a basin during its burial (Verweij 1993). Distinct patterns of overpressure and groundwater flow can be observed in such basins. As yet, we do not fully understand the processes behind the structure of the flow patterns and pressure distributions, especially in the deeper parts of the basins where temperature and pressure are high: researchers are trying to quantify the complex feedbacks between groundwater flow, rock deformation, heat transport and reactive mass transport that play a role on geological timescales; this is an area of active research (Person et al. 1996, Pueyo et al. 2000, Tuncay et al. 2000). As stated above stress-related mechanisms acting on the basin seem to be the most likely causes of overpressure.

Sedimentary loading of a basin's fill may induce compaction of the rock matrix, development of groundwater overpressures and groundwater flow. At shallow depth in young sedimentary basins, the still permeable sedimentary units dewater rapidly and the sediments compact mechanically in response to the increasing sedimentary load. The pressures of the groundwater remain approximately near-hydrostatic. This mechanical compaction is most effective in early shallow burial; at greater depths chemical processes (pressure solution and cementation) are the processes most reducing porosity (e.g. Bjørlykke and Hoeg 1997, Harrison 1990, Schneider et al. 1996). The transition zone for sandstones is around 1.5 km (Schneider et al. 1996). Mechanical compaction dominates porosity reduction in shales to much greater depths.

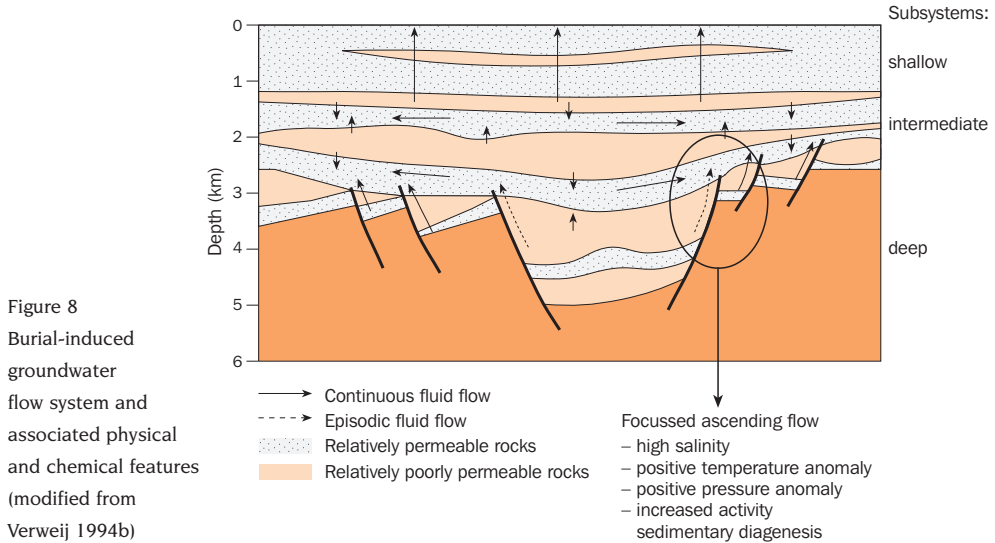
Poorly permeable compressible rocks (aquitards) are not able to dewater and compact rapidly in response to sedimentary loading and are susceptible to develop overpressures. In general, significant overpressured conditions are unlikely to develop in basins that subside less than 100m/My, with exceptions of parts of the basin with extensive layers of very poor permeability (e.g. Bethke 1986, Harrison and Summa 1991).

Burial-induced flow systems can be subdivided into shallow, transitional and deep subsystems, each with their characteristic flow pattern and overpressure distributions (Verweij 1993; Figure 8).

The flow of groundwater in an actively filling and subsiding basin is greatly influenced by both the space and time dependent porosity and permeability of the rock framework and the sedimentary loading characteristics.

**Shallow subsystem of burial-induced flow.** In general, in an actively filling and subsiding inhomogeneous sedimentary basin consisting of e.g. alternating continuous shales and sandstones, most groundwater flow tends to be crossformational and

vertically upwards during the earliest burial stages, i.e. in the relatively shallow part of the basin (<1000 - 1500 m) (Magara 1986, Bethke 1985, Harrison and Summa 1991; Figure 8). The groundwater potential increases only slightly with depth, i.e. the pressures of the groundwater are near-hydrostatic (Figure 9).



**Intermediate subsystem of burial-induced flow.** After continued burial, the groundwater flow at intermediate depths is focussed through the more permeable sandstones from the depocentre to the edges of the basin (Magara 1986, Bredehoeft et al. 1988); water is expelled vertically upward and downward from compacting shales towards the adjacent sandstones (Figure 8). At these intermediate depths there is no cross-formational flow through the shales: the groundwater potential in the shales is higher than the groundwater potential in the adjacent sandstone. The vertical change of groundwater pressure with depth over the sandstone unit is parallel to the hydrostatic pressure-depth relation, reflecting the lateral flow of groundwater (Figure 9). As long as the sandstones adjacent to overpressured shales in a subsiding basin provide a continuous escape way for the water, pressures can dissipate and no significant overpressured conditions will develop in the sandstones.

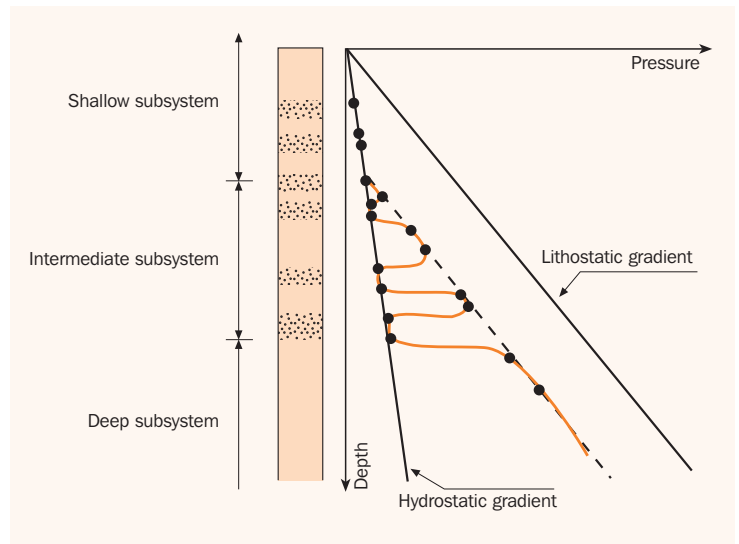


Figure 9 Change of groundwater pressure with depth in a burial-induced groundwater flow system

**Deep subsystem of burial-induced flow.** At continued burial of the sandstones, their porosity and permeability may decrease to such low values that flow becomes increasingly restricted. In addition, disruption of the lateral continuity of the sandstones by faults or salt structures in the deeper parts of the basin will restrict lateral flow and pressure dissipation. The deep subsystem is characterised by such restricted groundwater flow conditions: the groundwater in both shales and sandstones is significantly overpressured, and flow from the deep regime is either very slow and continuous, or rapid and discontinuous.

The maximum groundwater pressure that can be maintained in the subsurface is controlled by rock failure and by fracture opening and reopening conditions. The upper limit of groundwater pressure is controlled by the minimum principal stress and the tensile strengths of the rock (Du Rouchet 1981). Groundwater pressures close to maximum values occur frequently in deeper parts of e.g. the North Sea basins (Gaarenstroom et al. 1993). Episodic opening and reopening of fractures and faults allow groundwater to escape episodically from the deep subsystem (Nur and Walder 1990, Price 1980).

Each groundwater flow system, and each part of such a system, may influence the sediment diagenetic and petroleum system in a specific way. The largest impact of groundwater on the diagenesis and migration and accumulation of petroleum can be expected in zones of focussed active groundwater flow (continuous or episodic) and in zones where large groundwater potential gradients prevail (Verweij 1993, 1994a). Such zones are characterised by large net driving forces for groundwater flow; for instance related to pronounced topographic relief in the subaerial parts of a basin and high sedimentary and tectonic loading rates. These in turn are related to distinct periods of increased tectonic activity. This is in accordance with observations that distinct periods of increased groundwater flow seem to have a major influence on the sediment diagenetic system (e.g. Gaupp et al. 1993; Hendry 1993, Losh et al. 1999, Macaulay et al. 1997) and the petroleum system, through biodegradation and waterwashing of hydrocarbons (Connan 1984, Lafargue and Barker 1988, Tseng et al. 1998) and by influencing the migration and remigration of hydrocarbons (Davis, 1987, Dahlberg 1994, Giles et al. 2000, Hubbert 1953, Lerche and Thomsen 1994, Moretti 1998, Verweij 1993).

Each topography-induced and burial-induced flow system is characterised by its geometry and – as a result of groundwater's geological agency – by a specific distribution of physico-chemical characteristics of rocks and fluids in the basin (Figures 6 and 8). Tectonically-controlled upward flow of fluids through fault and fracture zones will be associated with positive pressure, temperature and salinity anomalies and associated diagenetic mineral assemblages at shallower depth in a basin.

During the development of a sedimentary basin, there is coexistence and interaction of different fluid flow systems (topography-induced flow, burial-induced flow, tectonically-controlled flow, density-controlled flow; Figure 10) (Garven 1995, Ge and Garven 1989, Gvirtzman and Stanislavski 2000a-b, Harrison and Summa 1991, Verweij 1990a-b, 1993, 1994a-b).

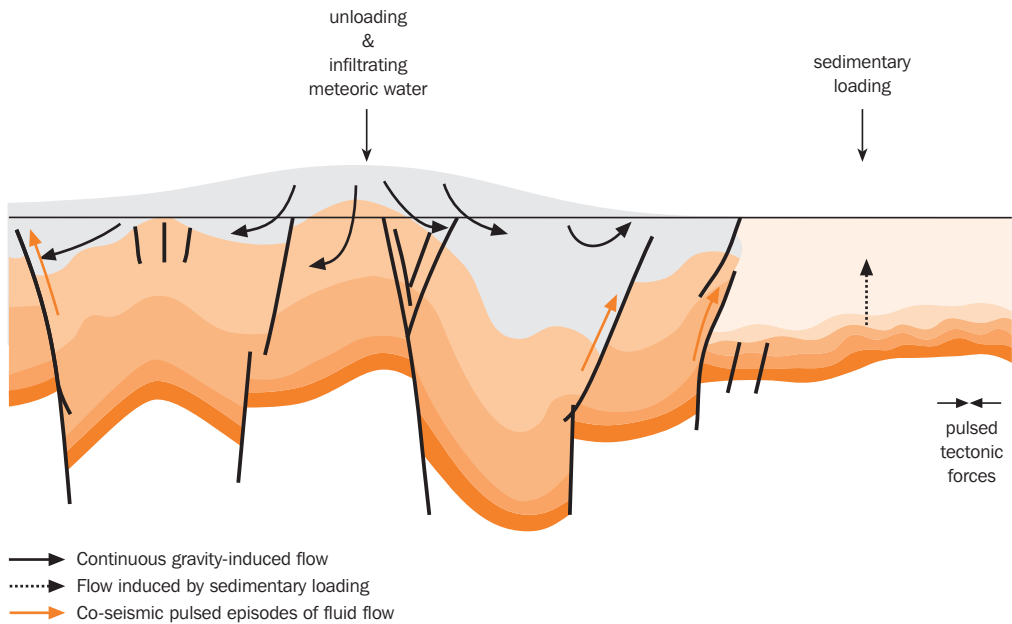


Figure 10 Different mechanisms control the development of groundwater pressures and groundwater flow systems at a certain time during basin development. Example illustrates situation during compression-induced inversion of basin.

### 1.3 Analysis of fluid flow on geological timescales

The procedure used in this thesis to study fluid flow systems on geological timescales is an extension of the concepts developed for topography-induced flow of groundwater (Engelen and Kloosterman 1996, Verweij 1993). As stated before, the procedure is based on the premise that geodynamics and climate are the major external mechanisms influencing the hydrogeological and hydrodynamic evolution and with the concept of fluid flow system as the mechanism linking intrabasinal processes. In the analysis, the evolution of fluid flow systems was reconstructed in relation to the major external and internal processes operating on the basin fill of onshore and offshore Netherlands. The various present-day manifestations of paleo and present-day fluid flow in the Netherlands subsurface were used to verify this evolution of fluid flow systems and to identify distinct periods of permeability alterations and distinct periods of fluid flow. The resulting conceptual model of the evolution of the geology, hydrogeology and fluid dynamics provided the basic understanding of the complexity of geofluid evolution in onshore and offshore Netherlands. The conceptual model and the database of present-day fluid and rock characteristics allowed the selection of a subbasin (the Broad Fourteens Basin) for subsequent more detailed analysis. In the second research phase the same analysing procedure was applied to the Broad Fourteens Basin and resulted in a powerful conceptual model that steered subsequent quantitative analysis of geofluid evolution by 2D basin modelling. This 2D basin modelling was used to acquire more quantitative understanding of the evolution of the coupled processes of sedimentation/uplift/erosion, heat transport, groundwater flow, maturation of source rocks, and generation, migration and accumulation of petroleum.



## 1.4 Objectives of this thesis

The strategic objective of the research was improvement of safety and economics of oil and gas field exploration and exploitation and of subsurface storage of energy and energy residues in onshore and offshore Netherlands. The thesis aims to contribute to this strategic objective by providing:

- A general description of the present-day hydrogeological framework of the sedimentary fill in onshore and offshore Netherlands and an overview of present-day characteristics of the fluids it contains (pressures, salinities, hydrochemical characteristics, temperatures);
- The fluid dynamics context for an improved process-based understanding of the present-day characteristics of the hydrogeological framework and the fluids in onshore and offshore Netherlands;
- A quantitative understanding of the hydrogeological and pore pressure and groundwater flow response of the basin fill of a selected basin – the Broad Fourteens Basin – to important aspects of its geological, geothermal and climatic evolution and an understanding of this response for the evolution of the oil and gas systems in the basin;
- A time framework for petroleum generation, migration, accumulation and preservation along a 2D cross-section in the Broad Fourteens Basin.

Specific research questions that are addressed in the thesis include:

- What are the main forces and processes that influenced, directly or indirectly, the hydrogeological, pore pressure and fluid flow conditions during the evolution of onshore and offshore Netherlands since the Late Carboniferous?
- What was the temporal and spatial distribution of these forces and processes?
- Could any of these processes have induced significant overpressuring of the subsurface in past or present?
- Are there any indications of distinct phases of increased fluid flow?
- What is the pattern of paleo fluid flow in the Broad Fourteens Basin (flow of groundwater and petroleum)?
- What causes the differences in observed geochemical compositions of oil accumulations in Broad Fourteens Basin?
- Where did all the gas go in the Broad Fourteens Basin?

## 1.5 Organisation

The unifying theme of this thesis is the analysis of the evolution of fluid flow systems on geological timescales.

The thesis is organised into three Parts that treat the analysis of fluid flow evolution in increasing detail. The analysis is applied to onshore and offshore Netherlands (Part 1) and the Broad Fourteens Basin (Parts 2 and 3). Each Part follows approximately the same systematic approach to assess the history of the fluid geology and the fluid dynamics. Because geology is the basis for the analysis, each Part starts with an outline of the geodynamic and geological history. Parts 1 and 2 present the approach for reconstructing the evolution of fluid flow systems based on the analysis and interpretation of a wide variety of data and information (geological, geophysical, thermal, geochemical, hydrochemical) both from published sources and public wells. The data analysis in Part 2 provided both the understanding as well as the input data,

boundary conditions and different scenarios required for the 2D basin modelling of the Broad Fourteens Basin treated in Part 3.

Another important organisational feature of the thesis is that the three Parts are self-contained.

The reader interested in obtaining a general understanding of the hydrogeohistory of onshore and offshore Netherlands should read Part 1. It provides an overview of the identified characteristic features of the external and internal processes acting on the sedimentary fill of onshore and offshore Netherlands and their role in shaping the hydrogeological and hydrodynamic setting of the Netherlands from Late Carboniferous to the present day. In addition it presents an overview of present-day characteristics of rocks and fluids of the study area.

Those readers especially interested in the Broad Fourteens Basin should read Part 2 and/or 3. Part 2 presents a conceptual model of the geological history of the Broad Fourteens Basin and its steering influence on the hydrogeological and hydrodynamic evolution of the basin. It provides additional results of the data analysis, such as present-day characteristics of the rocks and fluids in the basin and a time framework for important permeability alterations and distinct phases of fluid flow. Part 3 discusses the application and the results of the 2D integrated basin modelling along a SW-NE cross-section through the southern part of the Broad Fourteens Basin. Results of the 2D forward modelling include burial histories and histories of temperature and heat flow, maturation and petroleum generation from oil-prone Posidonia Shale Formation and Aalburg Formation and gas-prone Limburg Group source rocks, pore pressures and groundwater flow, and petroleum expulsion, migration and accumulation. Part 3 shows the significance of the combination of a powerful conceptual model with predictive abilities in geofluid evolution and the use of a wide variety of actual data with basin modelling for a process-based understanding of present-day characteristics of the hydrogeological framework and the fluids.

The reader interested in the integrated development of the analysis should read from cover to cover.



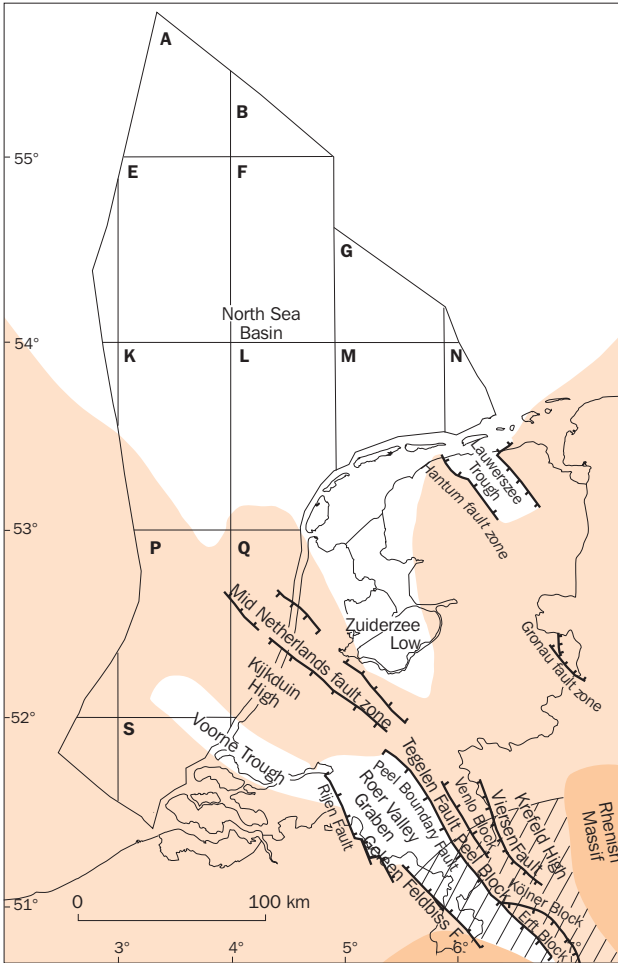
## 2 Introduction to Part 1

The overview of the fluid flow history on geological timescales presented below is a first step in providing the hydrodynamic context for a correct understanding of the present-day characteristics of the sedimentary basin fill in the onshore and offshore parts of the Netherlands. The geodynamic, sediment-geological, geothermal and climatic evolution of the Netherlands provided the basic information for a first reconstruction of its hydrogeohistory. The most significant aspects of this evolution for fluid flow analysis have been compiled from published sources, such as: the stratigraphic nomenclature of the Netherlands (Van Adrichem Boogaert and Kouwe 1993-1997), the Geological atlas of the deep subsurface of the Netherlands (RGD 1991-1996, TNO-NITG 1997-2002), and Glennie (1998), Rondeel et al. (1996), Van Wijhe (1987a-b), Vinken (1988), Zagwijn (1989) and Ziegler (1990a, 1992). In addition, the reconstruction of the hydrogeohistory was based on the analysis and interpretation of direct and indirect indicators of present-day and paleo fluid flow conditions (pressure, temperature, hydrochemistry, sediment-diagenetic characteristics). Hydrochemical data were available for public wells, while measured porosity, permeability, pressure and temperature data of offshore wells were derived in large part from ECL (1983), GAPS (1991), RRI (1984, 1985, 1988, 1990), webatlas of North Sea fields (1999) and onshore well data were derived from RGD 1991-1996. Published literature provided geochemical information.

The post-Carboniferous evolution of the external and internal processes acting on the sediments in onshore and offshore Netherlands provided the basis for the fluid flow systems analysis. Chapter 3 summarises the characteristic features of this evolution. Chapters 4 and 5 show the role of these processes in shaping the hydrogeohistory and hydrogeological framework of the onshore and offshore Netherlands. The indicators of present-day and paleo fluid flow conditions (Chapter 6, Section 7.1 and Chapter 8) refine the geology-based hydrogeohistory. Chapters 7 and 9 give an overview of the present-day hydrodynamic setting of the area as resulting from past and present influences.

### 3 Geological history of onshore and offshore Netherlands

The onshore and offshore Netherlands are located in the southeastern part of the Cenozoic Southern North Sea Basin (Figure 11). The sedimentary fill of the Southern North Sea Basin unconformably covers nine Mesozoic basins (Figure 12) that rest on the Southern Permian Basin, which in turn overlies the Variscan foreland basin.



▨▨▨ Lower Rhine Embayment

Figure 11 Dutch part of the Cenozoic North Sea Basin and Cenozoic structural elements (Van Adrichem Boogaert and Kouwe 1993-1997)

The dominant features of the present-day structural framework and the post-Carboniferous sedimentary fill of the Netherlands reflect a complex history of extension and compression related to changes in megatectonic setting (Glennie and Underhill 1988, Ziegler 1990). The post-Carboniferous sedimentary sequence rests on the northern foreland basin of the Variscan fold belt. The post-Variscan history has been influenced by the older Variscan geological and structural configuration of the area, that is by the NW striking wrench fault systems that dissected the Variscan fold belt and its northern foreland during the Late Carboniferous and the Early Permian. Many of the NW striking Variscan faults have been reactivated multiple times during the Mesozoic and Cenozoic (Dirkzwager et al. 2000, Dronkers and Mrozek 1991, Nalpas et al. 1995, Van Wijhe 1987a-b, Ziegler 1990a-b). Changes in the megatectonic setting of the basin are associated with changes in the regional tectonic stress regime. Since the Late Carboniferous, the onshore and offshore Netherlands have been in an intraplate setting. The development of the area took place in an active extensional stress regime from Triassic to Early Cretaceous and in a compressional stress regime from Late Cretaceous

onward. The present-day regime is characterised by NE-SW extension in the southeastern part of the onshore Netherlands and by NW-SE compression in the remaining area. Two major periods of tectonic activity are the Late Jurassic - Early Cretaceous extensional tectonic phase shaping the Mesozoic basinal structures, and the Late Cretaceous compressional phase inducing inversion of the Mesozoic basins.

In addition to changes in tectonic setting the sedimentary history of the area also clearly reflects the changes in sea level and changes in climatic setting relating to the continuous northward drift of the area from the equator in the Late Carboniferous to its present location.

On the basis of the relationship between changes in tectonic setting and sedimentary history, the sedimentary sequence above Carboniferous basement was subdivided for this study into 4 major tectono-stratigraphic sequences (Figure 13).

Figures 13 and 14 summarise the main characteristics of the post-Carboniferous geological history of the onshore and offshore Netherlands. Van Adrichem Boogaert and Kouwe (1993-1997) provide a detailed description of the sedimentary sequences.

### 3.1 Pre- and Early rift phase

In general, the Permian to Middle Jurassic sediments are a conformable megasequence, in most areas bounded at the base by Saalian and at the top by Mid Kimmerian regional unconformities. Thermal contraction of the lithosphere after the Saalian tectonic phase – associated with regional uplift, non-deposition and vulcanism – induced subsidence of the Southern Permian Basin (Van Wees et al. 2000, Ziegler 1990a). The Permian to Middle Jurassic sediments were deposited in the E-W trending Southern Permian Basin, a foreland basin located north of the London-Brabant Massif and the Rhenish Massif. These massifs, part of the northern rim of the Variscan orogenic belt (Geluk et al. 1996), were a sediment source for the Southern Permian Basin. The pre- and early rift sedimentary deposits thin towards these massifs. Time-dependent variations in sedimentation rate occurred in addition to lateral variations caused by the pronounced differences in synsedimentary subsidence of the Southern Permian Basin. Its depocentre was located in the northeastern part of offshore Netherlands.

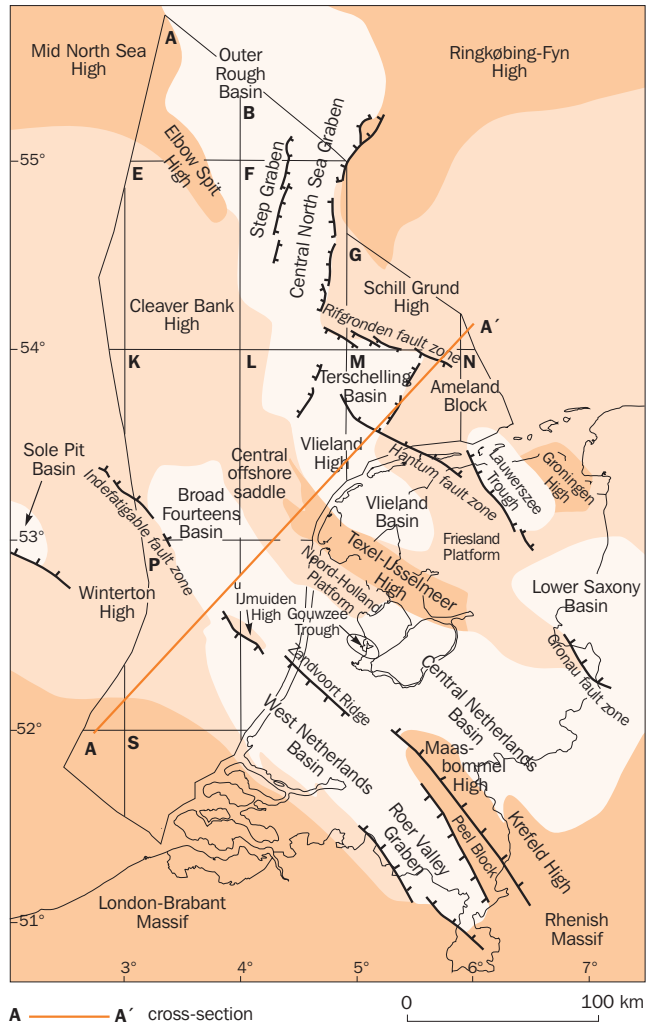


Figure 12 Late Jurassic–Early Cretaceous structural units in onshore and offshore Netherlands. Location of cross section presented in Figure 19

In the Late Permian, accumulation of terrestrial Rotliegend clastic (Slochteren Formation) and desert lake deposits (Silverpit Formation) was followed by deposition of marine Zechstein evaporites, carbonates and clays. The maximum long-time average sedimentation rate of the Upper Rotliegend Group is 80 metres per million years (80 m/My). Using sequence and cyclicity analysis, Yang and Nio (1993) calculated sedimentation rates for third-order stratigraphic sequences of the Upper Rotliegend Group of 60 - 110 m/My. The maximum long time average sedimentation rate of the Zechstein Group is estimated at 140 m/My for a present-day thickness of the Zechstein Group of 1000 m in basinal areas not affected by major halokinesis. In such areas, the Zechstein Group comprises up to five evaporite cycles. Potential deposition rates of halite can be extremely fast in comparison to other marine deposits (carbonates: 5 cm per thousand years (5 cm/ky), gypsum and anhydrite: 50 cm/ky, and halite: 5000 cm/ky; Einsele 1992). Non-evaporite deposition probably prevailed during most of the Zechstein period (Einsele 1992). Rotliegend and Zechstein deposits are still present in large part of the original sedimentation area. Subsequent structural development of the northern part of the area has been strongly influenced by the thick halite deposits present there. It has been suggested (e.g. Remmelts 1996) that active salt displacements are associated with periods of increased tectonic activity.

The Southern Permian Basin continued to subside during the Triassic. During the Early and Middle Triassic the Roer Valley Graben was the main feeder system of sediment (Ziegler 1990a); sediment also came from the London-Brabant Massif, which remained active during the Early Triassic (Geluk et al. 1996). The build-up of tensional stresses in the Triassic (Ziegler 1990a) induced the differential tectonic subsidence of subbasins within the Southern Permian basin (Off Holland Low, Ems Low, West Netherlands Basin and Roer Valley Graben) and the development of swells (Netherlands Swell, Cleaver Bank High) (e.g. Geluk and Röhling 1998). The Triassic axes of differential subsidence have a N-S and NNE-SSW orientation. The Hardeggen tectonic event induced uplift and caused deep erosion of the sediments of the Lower Germanic Trias Group on the swells. The first halokinetic movement of Zechstein salts started during Early Triassic and continued into the Neogene (Remmelts 1996). The Early Kimmerian tectonic phase – in the Late Triassic Carnian – caused rapid subsidence of a number of fault-bounded structures, such as the Central North Sea Graben, Broad Fourteens Basin and Ems Low, while regional subsidence and sedimentation resumed during subsequent Norian times (Geluk et al. 1996).

The Lower Germanic Trias Group is composed of lacustrine claystones and sandstones of aeolian and fluvial origin, and the Upper Germanic Trias Group consists mainly of lacustrine to shallow marine claystones, carbonates and evaporites (Figure 14). During the Triassic the long-time sedimentation rates calculated for the shifting depocentres decreased from 160 m/My (Lower Buntsandstein Formation) and 85 m/My (Main Buntsandstein and Röt Formations) to 40 m/My (Keuper and Muschelkalk Formations).

At the end of the Triassic the depositional environment changed from the previously continental to restricted marine towards open-marine. The Late Triassic transgression covered most of the highs in Northwestern Europe (Ziegler 1990a) and thick open-marine clays of the Altena Group (Sleen, Aalburg, Posidonia Shale, Werkendam and Brabant Formations) were deposited. Restricted conditions occurred during the

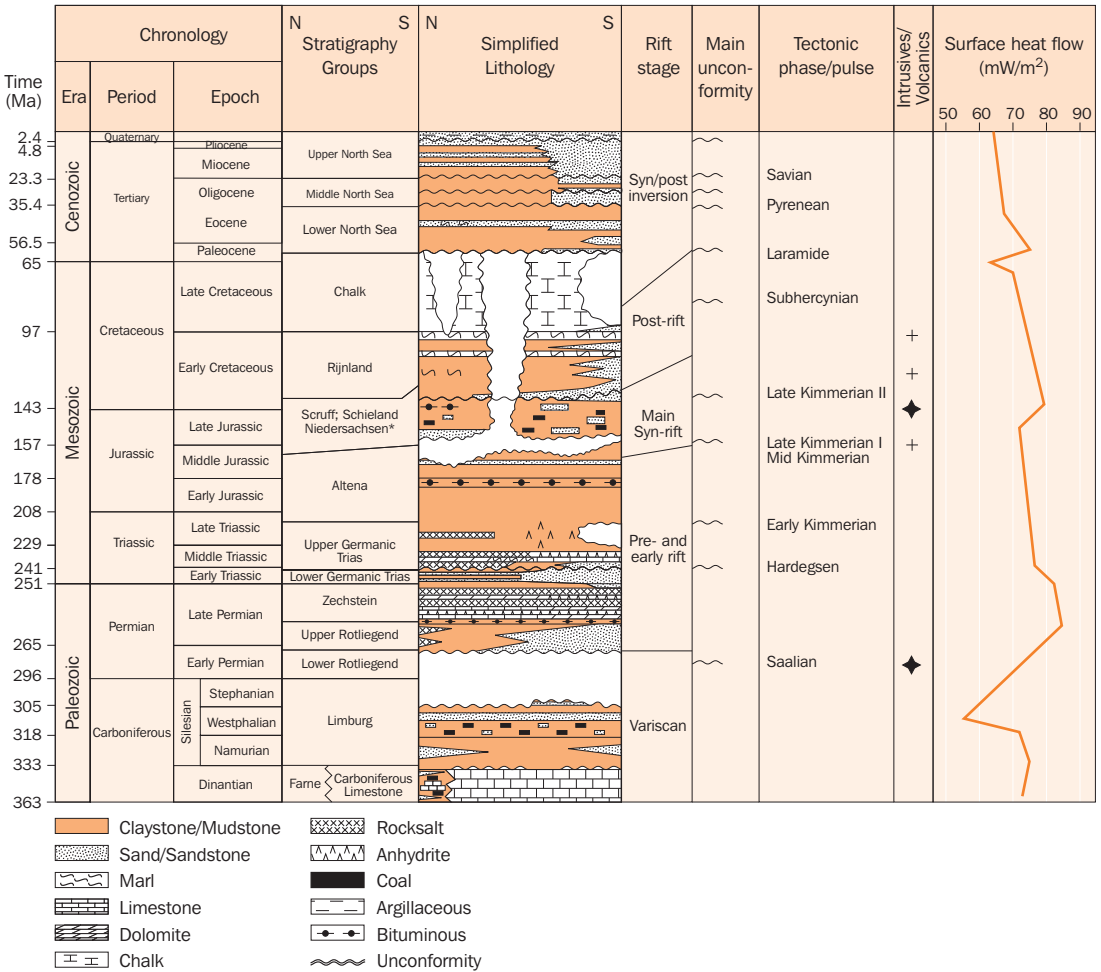


Figure 13 Lithostratigraphy, tectonic events and associated heat flow history in onshore and offshore Netherlands (From Verweij 1999).

Chronology after Harland et al. (1990) and for Permian and Triassic, Menning (1995); stratigraphy and lithology after Van Adrichem Boogaert and Kouwe (1993-1997); Tertiary stratigraphy also after Vinken (1988); intrusives and volcanism after Latin et al. (1990a-b); evolution of surface heat flow for southeastern flank of Roer Valley Graben after Veld et al. (1996)

Toarcian (Posidonia Shale Formation). The long-time average sedimentation rates of the Altena Group deposits vary between 3 and 34 m/My.

Thermal domal uplift of the central part of the North Sea area, which is associated with the Mid-Kimmerian tectonic phase (Glennie and Underhill 1998, Underhill and Partington 1993), decreased the area of deposition of the Altena Group. The present-day occurrence of the Altena Group is restricted to the Late Jurassic–Early Cretaceous basins (Figure 12) because of later erosion.



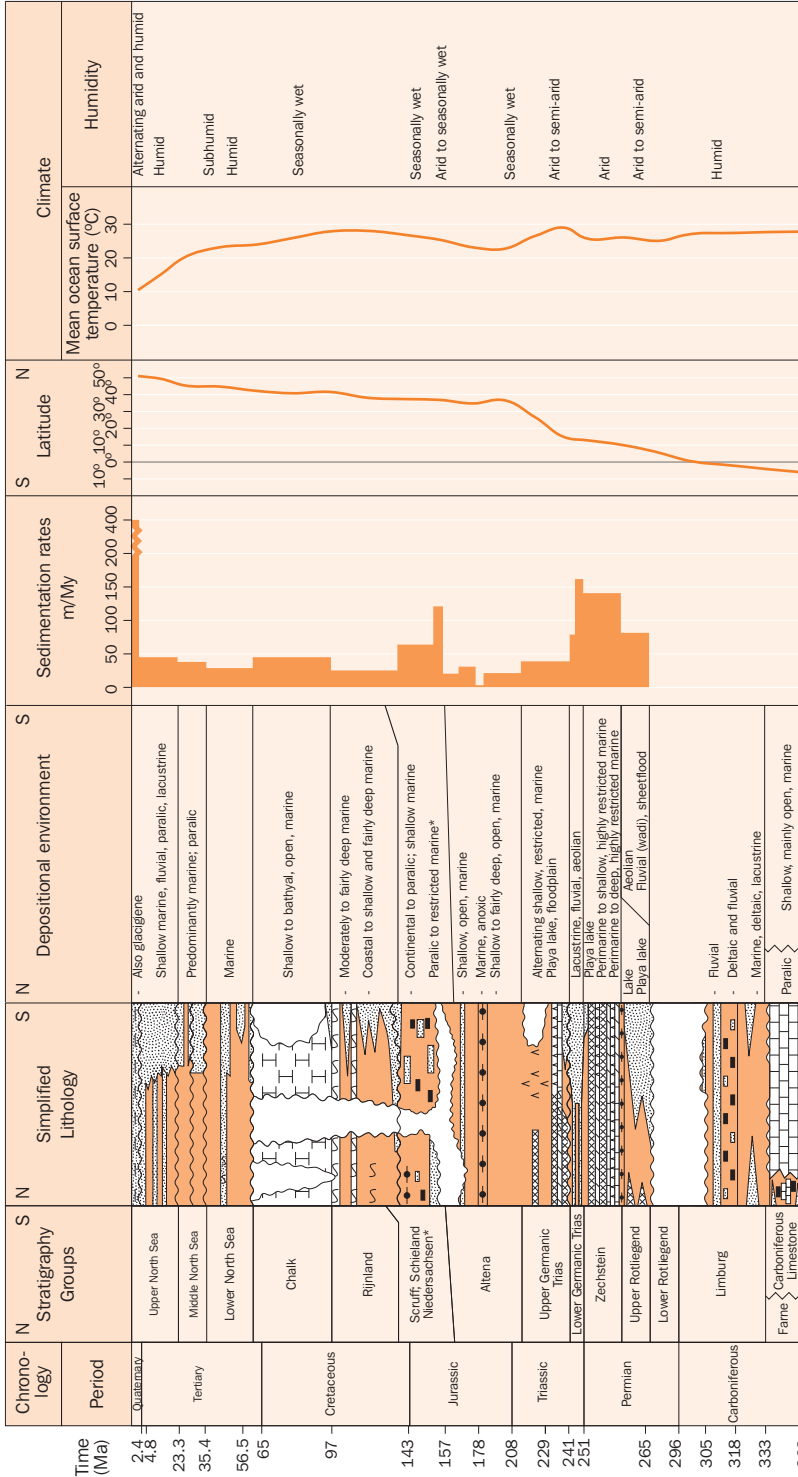


Figure 14 Lithostratigraphy and associated history of depositional environments, sedimentation rates and climatic conditions (From Verweij 1999).

Depositional environment based on Van Adrichem Boogaert and Kouwe (1993-1997) and Vinken (1988); Climate compiled from Frakes (1979), Hallam (1985), Yang and Nio (1993), Zagwijn (1975), Ziegler (1990a); mean ocean surface temperature compiled from Glennie (1990; Figure 2.7) and Welte et al. (1997; Figure 1.5); sedimentation rates compiled from different sources Caston (1977), Dronkert et al. (1989), Geluk et al. (1996), Sorensen et al. (1997), Van Adrichem Boogaert and Kouwe (1993-1997); Vinken (1988), Yang and Nio (1993)

### 3.2 Main syn-rift phase

Late Jurassic rifting followed the development of the Mid-Kimmerian thermal dome in the central North Sea and induced the Southern Permian Basin to break up into smaller subbasins. The orientation of the regional extensional stresses in the southern North Sea changed from ENE-WSW and E-W in Middle Jurassic times to NE-SW and NNE-SSW during the Late Jurassic (Nalpas et al. 1995). The Late Kimmerian I and II extensional tectonic phases resulted in the development of the following rapidly subsiding basins: N-S oriented Central North Sea Graben, the Terschelling Basin; NW-SE oriented Broad Fourteens Basin, West Netherlands Basin, Roer Valley Graben, Central Netherlands Basin; Lower Saxony Basin; and the Vlieland Basin and Lauwerszee Trough (Figure 12).

Sedimentation was concentrated in the rapidly subsiding basinal areas and was characterised by significant facies changes. Sedimentation rates were high: for example, the maximum long time average sedimentation rate of the Schieland Group sediments is 220 m/My.

Erosion proceeded on the adjacent uplifted highs (Figure 12). Uplift of the Elbow Spit High, Cleaverbank High and Schill Grund High had already started in the Middle Jurassic. Erosion on the Elbow Spit High reached the Lower Carboniferous and Devonian sedimentary sequences, while erosion on the Cleaverbank High affected Lower Triassic and locally Zechstein sequences. Deep erosion (down to Carboniferous) also occurred on the Texel IJsselmeer High (estimated amount of erosion 1000 m, Rijkers and Geluk 1996), Winterton High and Peel Block in the Early Cretaceous. Most erosion on these highs took place in the Early Cretaceous because of the Late Kimmerian II uplift in combination with a low sea level. Jurassic uplift of the London-Brabant Massif related to Kimmerian tectonism probably proceeded at an uplift rate of < 100 m/My, lasted several tens of millions of years and was accompanied by the erosion of a few thousand metres of sedimentary cover (Vercoutere and Van Haute 1993).

The present-day occurrence of main syn-rift sequences is mainly restricted to the basinal areas; on the highs these sequences are largely missing or thin.

The Late Jurassic – Early Cretaceous extensional tectonic phase was associated with magmatic activity in onshore and offshore Netherlands (Table 1) and an increase in heat flow (Figure 13). Magmatic activity seems to be concentrated in two periods, namely in the Jurassic (Callovian) – Early Cretaceous (Hauterivian), related to the Kimmerian tectonic phases, and in the Early Cretaceous Albian, probably associated with the Austrian tectonic phase (Van Wijhe 1987a, 1987b, Ziegler 1990a).

### 3.3 Post-rift phase

Extensional tectonic activity decreased during the later part of the Early Cretaceous and was followed by post-rift thermal subsidence. Marine sedimentation gradually overstepped the basin margins in the Aptian. By the Late Cretaceous, thermal, more regional subsidence coupled with a significant rise of sea level induced a transgression that inundated the previous highs (including the London-Brabant Massif in the Campanian-Maastrichtian). The influx of clastic material into the basin became

reduced and conditions became favourable for widespread deposition of chalk. The long-time average sedimentation rate of the Chalk Group is estimated at 50 m/My.

Table 1 Magmatism in onshore and offshore Netherlands during Mid-Late Jurassic and Early Cretaceous

| Area                   | Well           | Age (Ma)                 | Techniques             | Publication                      |
|------------------------|----------------|--------------------------|------------------------|----------------------------------|
| Cleaver Bank High      | E06-01         | 161 ± 1                  | K-Ar                   | Latin et al. 1990                |
| Vlieland Basin         | Zuidwal 1      | 145                      | K-Ar                   | Harrison et. al 1981*            |
|                        |                | 144 ± 1                  | 40Ar/30Ar              | Dixon et al. 1981*               |
|                        |                | 152 ± 3                  | 40Ar/36Ar-<br>40K/36Ar | Perrot and Van der<br>Poel 1987* |
| West Netherlands Basin | Heinenoord 1   | Late Jurassic            |                        | TNO-NITG 2001                    |
| West Netherlands Basin | Werkendam 1    | Hauterivien<br>(132-135) |                        | TNO-NITG 2001                    |
| West Netherlands Basin | Andel-4        | 133 ± 2                  | 40Ar/39Ar              | Dixon et al. 1981*               |
| Roer Valley Graben     |                |                          |                        |                                  |
| Roer Valley Graben     | Loon-op-Zand 1 | 132 ± 3                  | 40Ar/39Ar              | Dixon et al. 1981*               |
| Broad Fourteens Basin  | Q07-02         | 95 ± 2                   | 40Ar/39Ar              | Dixon et al. 1981*               |
|                        |                | 106 ± 2                  | 40Ar/39Ar              | Dixon et al. 1981*               |
| Broad Fourteens Basin  | L13-03         | 101 ± 1                  | 40Ar/39Ar              | Dixon et al. 1981*               |
| Step Graben            | PL1            | 99 ± 5                   | K-Ar                   | Latin et al. 1990                |

\* In: Latin et al. 1990

### 3.4 Syn-inversion phase

During the Late Cretaceous the regional stress regime changed from extensional to compressional (Ziegler 1990a). Regional subsidence was interrupted by initiation of compression-induced inversion movements related to the Late Cretaceous Subhercynian tectonic phase. The principal regional compressive stress direction for the Late Cretaceous was between N110° and N155° according to Huyghe and Mugnier 1994, and roughly N170° according to Nalpas et al. (1995). The compression-induced inversion of the Late Jurassic – Early Cretaceous basins (Broad Fourteens Basin, West Netherlands Basin, Central Netherlands Basin, Central North Sea Graben, Vlieland Basin, Lower Saxony Basin and Roer Valley Graben) reactivated their bounding normal faults as reverse faults (Burgers and Mulder 1991; Dirkzwager et al. 2000; Dronkers and Mrozek 1991; Nalpas et al. 1995; Van Wijhe 1987a). The intensity and timing of the inversion of the Late Jurassic – Early Cretaceous basins were different for each basin. The central parts of the Broad Fourteens Basin and West Netherlands Basin and the southeastern parts of the Central Netherlands Basin experienced the most severe inversion (Van Wijhe 1987a).

Structural inversion of the Broad Fourteens Basin began as early as the end of the Turonian (Hancock 1990; Huyghe and Mugnier 1994). This basin underwent its strongest uplift at the end of the Late Cretaceous. The Late Cretaceous inversion was probably induced by numerous short phases of uplift during 20 My (Huyghe and Mugnier 1994). The amount of basement (pre-Zechstein) uplift at the northeastern margin of the basin is estimated to be in the order of 2200 m (Hooper et al. 1995), increasing towards its centre. The associated minimum uplift rate for the basin margin

was estimated at 150 m/My. Nalpas et al. (1995) reconstructed a maximum erosion of the sedimentary cover of more than 3000 m in the central parts of the basin. The amount of erosion decreases towards the basin margin (Hooper et al. 1995, Huyghe and Mugnier 1995, Nalpas et al. 1995, Van Wijhe 1987a and 1987b).

Late Cretaceous, relatively mild, inversion of the Dutch Central North Sea Graben was strongest in the southern half of the graben (Van Wijhe 1987a) with associated erosion of 750 m (Dronkers and Mrozek 1991).

Herngreen et al. 1996 established that the deposition of chalk did not cease completely in the Vlieland Basin during its inversion (main inversion phases in Coniacian to Campanian): even on the inversion axis of the basin where maximum uplift occurred, a condensed sequence of sediments, representing almost all Upper Cretaceous stages occurs today. The Chalk sequence shows a profound thinning from the Texel IJsselmeer High towards the centre of the Vlieland Basin (Herngreen et al. 1996).

Tectonic inversion of the Roer Valley Graben, West Netherlands Basin and Central Netherlands Basin occurred in Santonian and Early Campanian (Bless et al. 1987, Gras and Geluk 1999, Van Wijhe 1987a). Erosion of the inverted Roer Valley Graben locally reached down to the Altena Group and the thickness of the eroded sediments is estimated at 1000 - 2000 m (Gras 1995). Inversion-related erosion in the Central Netherlands Basin reaches a maximum of 2000 m (TNO-NITG 1998).

From Late Maastrichtian to Danian deposition of chalk resumed in the Broad Fourteens Basin, Central Netherlands Basin, West Netherlands Basin and Roer Valley Graben (Bodenhausen and Ott 1981, Gras 1995, TNO-NITG 1998).

The rise of land masses surrounding the North Sea in Mid-Paleocene times in combination with the Mid-Paleocene low stand in sea level induced a regional phase of erosion and terminated Chalk deposition (e.g. Ziegler 1990a). Penetration of the inverted basins (Broad Fourteens, West Netherlands and Central Netherlands basins and the Roer Valley Graben), removing the post-inversion Chalk deposits, was followed by regional subsidence during Late Paleocene and Eocene.

While the sedimentary fill of the Late Jurassic – Early Cretaceous basins became folded, uplifted and subject to erosion, deposition of Chalk Group sediments continued in adjacent areas (e.g. north and northeast of the Broad Fourteens Basin, southwest of the Broad Fourteens Basin, east of the Central North Sea Graben (e.g. Oakman and Partington 1998), and also on the flanks of the West Netherlands Basin and the Roer Valley Graben).

### 3.5 Post-inversion phase

#### *Regional setting*

After the Early Eocene, the evolution of the North Sea area was governed by ongoing thermal relaxation of the lithosphere and sedimentary loading and in addition by fluctuations in compressional intraplate stresses (Ziegler, 1990, 1992). The stress regime in the North Sea area had an overall compressive character during the

Cenozoic (Kooi et al. 1989). The present-day compressive stress field in Northwest Europe, including the southern North Sea area, shows an overall NW-SE orientation for the compressive maximum horizontal stress (Müller et al. 1992, Zoback 1992). Changes in this intraplate stress regime are thought to have had a distinct influence on the Cenozoic subsidence and uplift history of the North Sea area (Cloetingh et al. 1990, Kooi et al. 1991, Van Wees and Cloetingh 1996). From Eocene to Recent the Cenozoic development of the North Sea area, including the Southern North Sea Basin, is dominated by regional subsidence. The Cenozoic depocentre of the North Sea Basin, where Tertiary and Quaternary deposits reach thicknesses of 3500 m, coincides with the UK and Norwegian part of the Central North Sea Graben (Ziegler 1990a). There are indications for Late Neogene acceleration of tectonic subsidence of the North Sea Basin, including the Netherlands North Sea area (Cloetingh et al. 1990, Kooi et al. 1991, 1998, Van Wees and Cloetingh 1996). The nature of the control on the Late Neogene subsidence of the North Sea is an area of active research (Kooi et al. 1991, Van Balen et al. 1998, Van Wees and Cloetingh 1996). Intraplate compression as an explanation for Neogene subsidence is one of the models investigated (Van Balen et al. 1998). The Cenozoic development of the southeastern part of the Southern North Sea Basin is dominated by reactivation of the Roer Valley Graben (e.g. Geluk et al. 1994, Van Balen et al. 2000a). The Roer Valley Graben strikes parallel to the present-day NW-SE orientation of maximum horizontal compressive stress. It is part of a mega-rift system crossing western and central Europe (Ziegler 1992, 1994). Renewed rifting of the Roer Valley Graben started during the Late Oligocene and continues today (Geluk et al. 1994, Houtgast and Van Balen 2000). Cenozoic faulting and recent seismicity is generally limited to areas surrounding the pre-existing boundary faults of the Roer Valley Graben (e.g. Dirkzwager et al. 2000, Houtgast and Van Balen 2000). The graben has subsided approximately 1000 - 1200 m since Late Oligocene (Geluk et al. 1994). The average subsidence rate in the Quaternary is 60 - 90 m/My (TNO-NITG 2001). Renewed uplift of the Rhenish Massif at the southeastern end of the graben occurred during Late Oligocene and accelerated during Mid-Late Miocene. Contemporaneous volcanic activity affected a broad area. Present uplift of the Rhenish Massif proceeds at 0.4 - 0.6 mm per year, with a maximum of 1 mm per year in the Eifel area (Ziegler 1994).

During the Late Pliocene and Quaternary the climate was characterised by repeated changes from very cold glacial conditions to warm-temperate interglacial conditions. These climatic changes exerted an important influence on the sedimentary evolution in the southern North Sea Basin.

### *Stratigraphy*

The total thickness of Cenozoic siliciclastic deposits of the Lower, Middle and Upper North Sea Group overlying the Laramide and Pyrenean unconformities in onshore and offshore Netherlands increases towards the north, reaching present-day values of approximately 2500 m (Figure 15). The Pyrenean and Savian unconformities mark the boundaries between the Lower and the Middle North Sea Group, and the Middle and Upper North Sea Group, respectively (Figures 13 and 14). Another important unconformity, found within the Upper North Sea Group between Pliocene and Pleistocene deposits, probably resulted from an eustatic drop in sea level, related to the first glacial stage. Early Tertiary deposits of the Lower and Middle North Sea

Group predominantly consist of marine clays and clayey sands. From the southeast, continental sedimentation progressively replaced marine sedimentation from the Miocene until, in the Early Quaternary, the sea withdrew completely from onshore Netherlands and predominantly fluvial sediments were deposited (e.g. Zagwijn 1989). The Miocene-Pliocene sediments of the Upper North Sea Group have been deposited in marine and – in the southeast – continental facies. A fan of fluvial deposits is present in the Roer Valley Graben area. Marine sedimentation remained absent from onshore Netherlands until far into the Middle Pleistocene. Clastic sediments were deposited in various environments in onshore and offshore Netherlands during the Quaternary (Pleistocene: glacial, continental and marine; Holocene: marine in offshore Netherlands and marine, coastal, fluvial deposits as well as peat accumulations in onshore Netherlands). Different centres of deposition developed successively in the North Sea Basin during the Cenozoic (Sørensen et al. 1997, Vinken 1988, Zagwijn 1989).

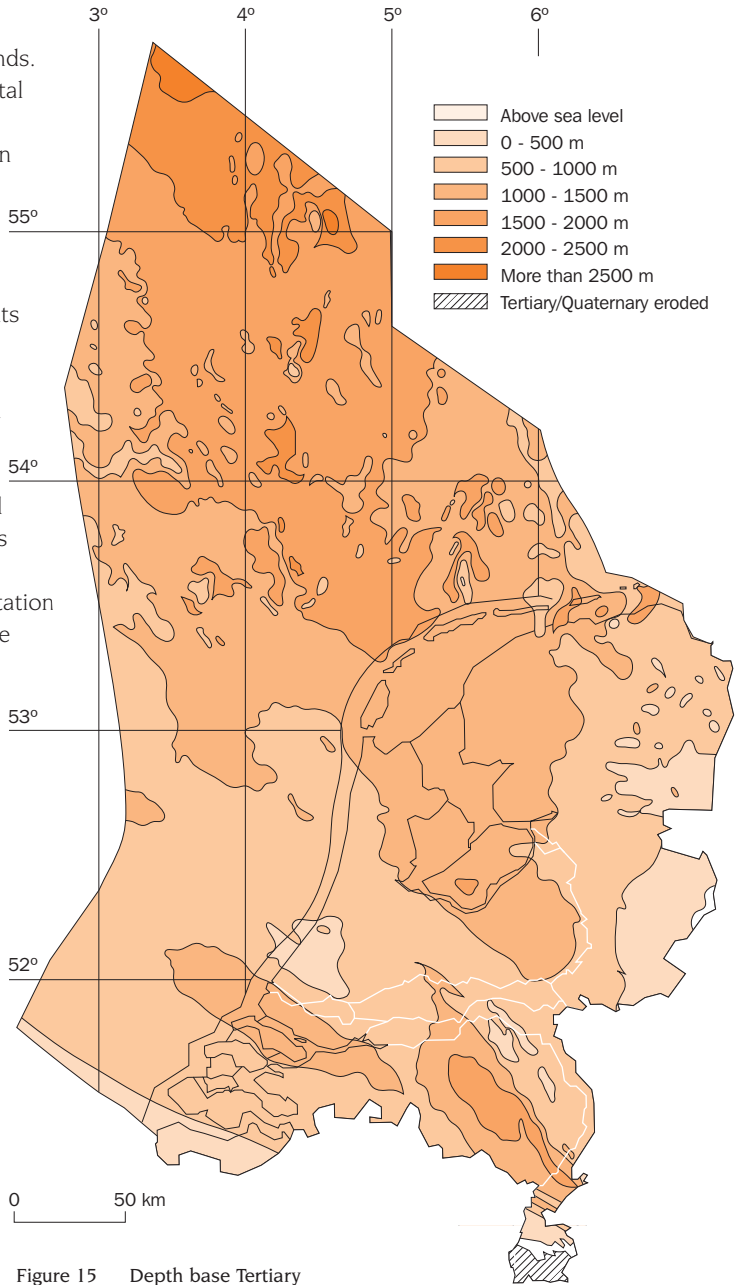


Figure 15 Depth base Tertiary (after Burgers and Mulder 1991)

**Sedimentation rates in shifting depocentres**

The largest residual thicknesses of Paleocene and Eocene sediments of the Lower North Sea Group occur in the Voorne Trough, the area to the northeast of the Broad Fourteens Basin and in the Lauwerszee Trough (Figure 12). The long-time average sedimentation rates calculated from the residual thicknesses in these areas are approximately 31 m/My. Polygonal fault patterns have been recognised in the Paleogene

Dongen Clay Formation (Netherlands offshore, block L8, Steeghs et al. 2000). Comparable fault patterns in Eocene–Lower Miocene mudstones in the UK Central North Sea developed during early burial by volume contraction of the muddy sediments (Cartwright and Lonergan 1996, Lonergan and Cartwright 1999).

Regional subsidence and deposition of the marine Lower North Sea Group sediments during Late Paleocene and Eocene was interrupted by the Late Eocene – Early Oligocene uplift related to the Pyrenean tectonic phase. Pyrenean compressive tectonics (orientation of the maximum principal compressive stress roughly N-S, Nalpas et al. 1996) involved reactivation of the Mid Netherlands Fault zone, resulting in uplift of the Southern Early Tertiary High, and the creation of the Kijkduin High (Van Adrichem Boogaert and Kouwe 1993 - 1997). Uplift-related erosion of Lower North Sea Group sediments has been recognised in the southeast and central parts of onshore Netherlands and in the West Netherlands and Broad Fourteens Basins (Bodenhausen and Ott 1981, Letsch and Sissing 1983, Nalpas et al. 1995).

The sea transgressed again over the erosion surfaces in the early Oligocene. Deposition of the Middle North Sea Group was concentrated in the southern part of the Netherlands (Voorne Trough and Roer Valley Graben). Long-time average sedimentation rates reached 42 m/My.

In the Neogene, deltas prograded from the south and southeast, and from the Fennoscandia border zone into the North Sea Basin (Ziegler 1990a). Sedimentation in the southern onshore parts of the Netherlands became in large part restricted to the Roer Valley Graben during the Miocene, Pliocene and Quaternary (Geluk et al. 1994). Long time average (residual) sedimentation rates of the Upper North Sea Group in the Roer Valley Graben is approximately 46 m/My in Miocene to Pliocene times and 80 m/My in Quaternary times. In the Middle Miocene the Zuiderzee Low was also a depocentre. After Miocene times the main depocentres developed in the northern offshore area (Figure 17). These depocentres gradually shifted from east to west and finally to the northwest after the Late Miocene (Sørensen et al. 1997, Overeem et al. 2001; Figure 17). Sedimentation rates in these offshore depocentres started to increase during the Pliocene and remained high during the Quaternary, reaching values of 400 m/My in Pliocene and Quaternary times. In Holocene times sedimentation rates reached values of 2 mm per year (calculated over Holocene time period, i.e. a period of only 10,000 years).

In conclusion, sedimentation rates varied during the Tertiary and Quaternary, but were generally highest during Pliocene – Quaternary times (Figure 14 and 18).

Note that the long-time average sedimentation rates presented here have been calculated from residual thicknesses in the depocentres not corrected for compaction and that sedimentation rates have been calculated over different time periods.

### *Present-day setting*

The burial history plots of Permian and Jurassic stratigraphic units located in different structural parts of the Netherlands outside the strongly inverted parts of the Broad Fourteens Basin, Central Netherlands Basin and West Netherlands Basin, show that these units are at their maximum depth of burial (Figure 18).



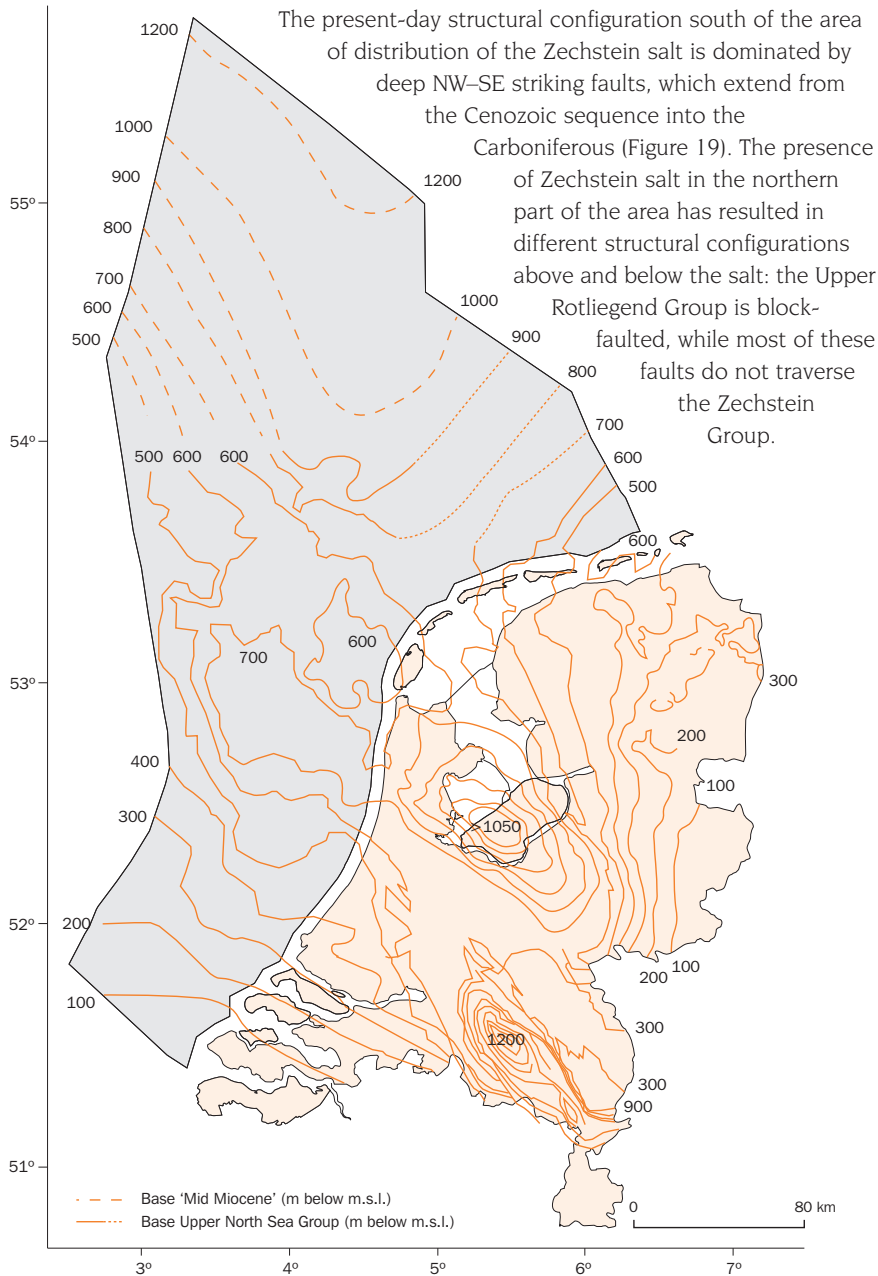
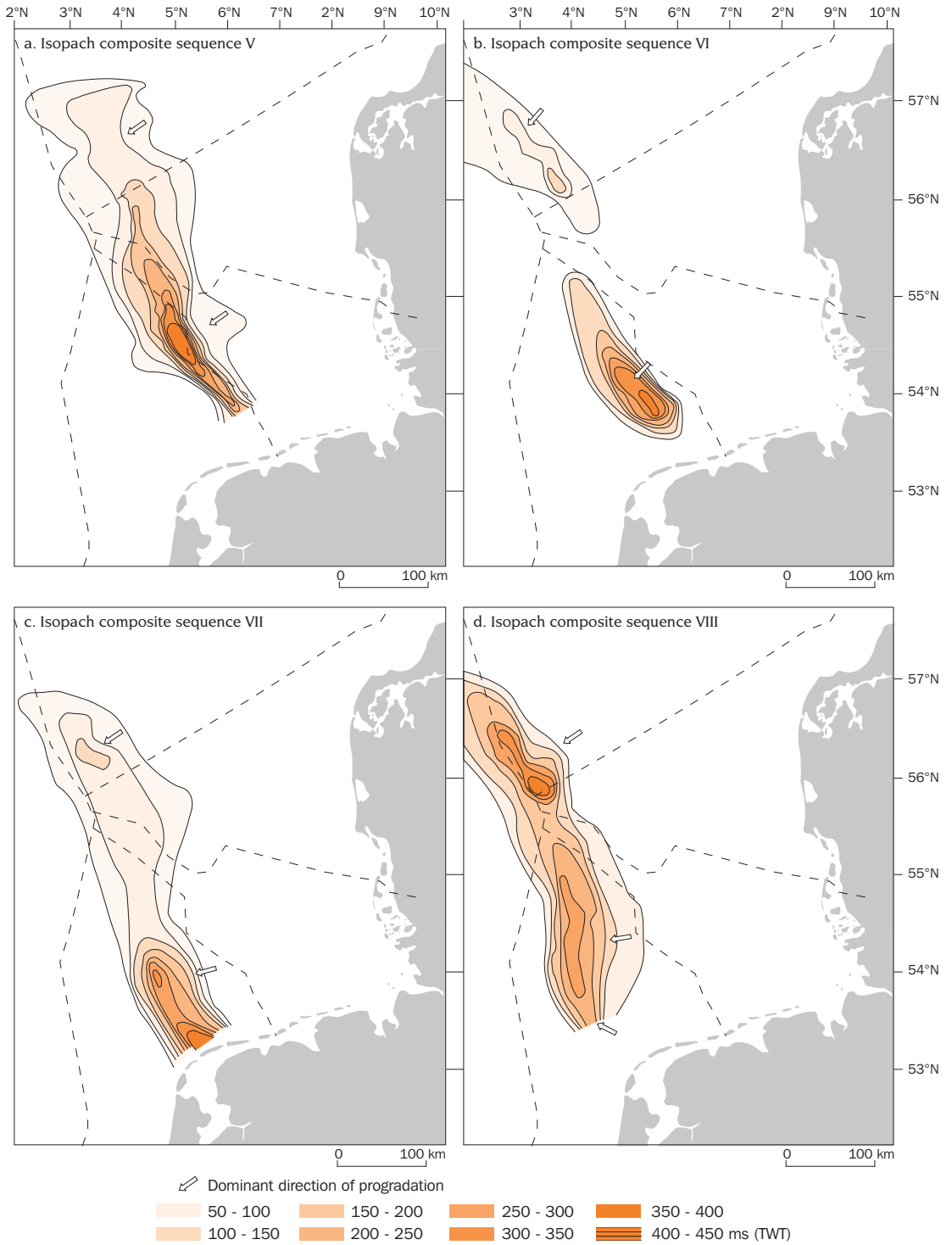


Figure 16 Base Upper North Sea Group (made available by De Lugt 2001) and base Mid Miocene (after Vinken 1988)

In the Central North Sea Graben, Step Graben and Terschelling Basin, strong salt movement, related to basement faults, occurred during Jurassic – Cretaceous rifting and during the inversion phases (Remmelts 1996). The resulting salt domes and salt walls disrupted the lateral continuity of Triassic to Tertiary sequences.





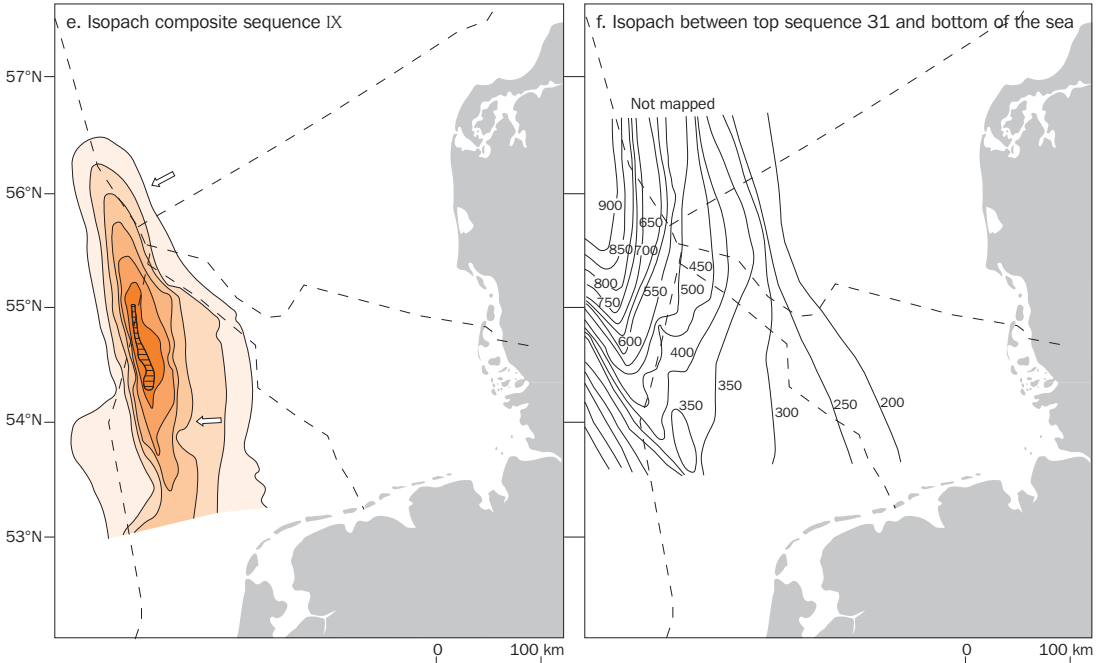


Figure 17 Shifting depocentres from 6 Ma to presentday (Modified from Sørensen et al. 1997).  
 a. Isopach composite sequence V (6 - 4.2 Ma); b. Isopach composite sequence VI (4.2 - 3.1 Ma);  
 c. Isopach composite sequence VII (3.1 - 2.4 Ma); d. Isopach composite sequence VIII (2.4 - 1.8 Ma);  
 e. Isopach composite sequence IX (1.8-1.1 Ma); Isopach of sediments between top sequence 31  
 and sea bottom (1.1 - 0 Ma)

The present-day compressive stress field in Northwest Europe documented by Zoback (1992) and Müller et al. (1992) shows a NW-SE orientation of the maximum principal compressive stress in onshore and offshore Netherlands. According to Grauls (1997) the change of the minimum principal stress with depth and the change of the minimum to vertical stress ratio with depth seem to be dependent on the tectonic regime. For the North Sea area, the ratio of minimum to vertical stress is 0.70 - 0.80 for the upper part of the basin dominated by vertical stress (depth between 0 m and about 3000 m) and increases to values ranging from 0.82 to 0.95 for the deeper more compressive part of the basin where the vertical stress becomes the intermediate stress (Grauls 1997).

The present-day low-lying flat onshore parts of the Netherlands are covered almost entirely by Quaternary deposits. The coastal area in the northern and western part of the country has been reclaimed from the sea (polders). About 30% of the total land area is below sea level. Only in the extreme southeast do altitudes above 200 m occur.

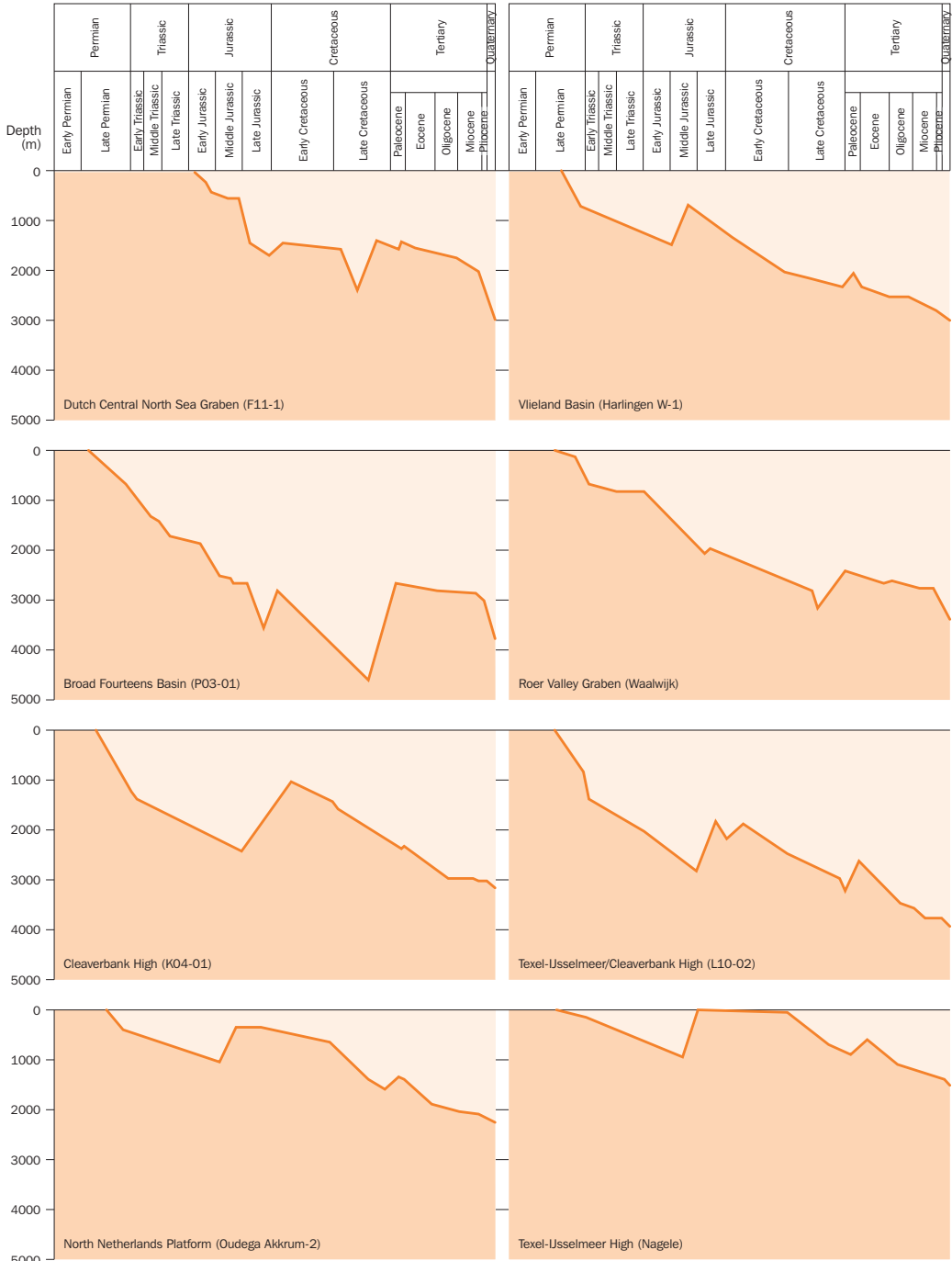


Figure 18 Burial history diagrams (From Verweij 1999).

Vlieland Basin, North Netherlands Platform and Texel IJsselmeer High after Geological Survey of the Netherlands (1993); Roer Valley Graben after Winstanley (1993); Texel IJsselmeer High/Cleaverbank High and Cleaverbank High after Intergeos (1991); Broad Fourteens Basin and Dutch Central Graben after RRI (1988)

## 4 Factors controlling the hydrogeohistory of onshore and offshore Netherlands

The climatic and geodynamic histories of onshore and offshore Netherlands, summarised in Figures 13 and 14, largely control the distribution in time and space of the major processes that directly or indirectly influence the hydrogeological (storativity and permeability of pores, faults and fractures) and hydrodynamic conditions (overpressure distributions; flow characteristics, such as no flow conditions, continuous or episodic flow conditions; invasion of water from different origins). Table 2 summarises the main mechanical and thermal forces and processes capable of exerting a controlling influence on fluid flow conditions in onshore and offshore Netherlands during its post-Carboniferous evolution.

Table 2 Main mechanical and thermal forces and processes that influenced fluid flow conditions during the evolution of onshore and offshore Netherlands

| Time period                | Area  | Primary driving force  | Secondary driving force                         |
|----------------------------|---|--|---|
| <b>Variscan</b>            |   |  |   |
| Early Permian              | The whole of the area<br>Area S and SE of Netherlands | Topography of water table  | Erosional unloading                             |
| <b>Pre- and Early rift</b> |   |  |   |
|                            | The whole of the area<br>Southern Permian Basin       | Sedimentary loading  |   |
|                            | – depocentre  | Sedimentary loading  |   |
|                            | – basin fringe  | Sedimentary loading  | Topography of water table                       |
|                            | Area S and SE of Netherlands                          | Topography of water table  |   |
| <b>Main Syn-rift</b>       |   |  |   |
|                            | Mesozoic basins                                       | Sedimentary loading<br>Tectonic forces   | (local) heating                                 |
|                            | Platform/highs<br>Area S and SE of Netherlands        | Topography of water table<br>Topography of water table                                     | Erosional unloading<br>Cooling                  |
| <b>Post-rift</b>           |   |  |   |
|                            | The entire area                                       | Sedimentary loading  |   |
| <b>Syn-inversion</b>       |   |  |   |
| Subhercynian-Laramide      | Inverted Mesozoic basins                              | Topography of water table<br>Tectonic forces<br>Erosional unloading                        | Cooling   |
| Pyrenean                   | Remaining area<br>Southern Early Tertiary High        | Sedimentary loading<br>Topography of water table<br>Tectonic forces<br>Erosional unloading |   |
| <b>Post-inversion</b>      |   |  |   |
|                            | Southern North Sea Basin                              | Sedimentary loading  | Topography water table<br>Ice loading/unloading |
| Oligocene-Recent           | Roer Valley Graben                                    | Topography of water table  | Sedimentary loading<br>Tectonic forces          |
|                            | Area southeast of Netherlands                         | Topography of water table  |   |

Additional processes influencing fluid flow, such as dehydration reactions, chemical diagenesis and gas generation, may have operated simultaneously. The deformation of Zechstein salt during different phases of basin development will have influenced

fluid flow and pressure distribution during times of active deformation (e.g. Tuncay and Ortoleva 2001). Fluid density gradients may have influenced fluid flow throughout the basin's evolution, including seawater intrusions in coastal areas and, in particular, density-driven flow near evaporites of the Zechstein Group and the Upper Germanic Trias Group.

#### 4.1 Tectonic control

Tectonic forces include direct and indirect influences on fluid pressures. The indirect influence involves changes in the permeability and pressure distribution through opening, re-opening and closing of faults and fractures (Chapter 1).

The orientation of the principal stresses has changed repeatedly over time: the orientation of the regional extensional stress was approximately E-W in the Mid Jurassic and NE-SW and NNE-SSW in the Late Jurassic (Nalpas et al. 1995); the direction of the maximum principal compressive stress was approximately N170° in the Late Cretaceous (according to Nalpas et al. 1996), roughly N-S in Late Eocene – Early Oligocene (Nalpas et al. 1996) and has an overall NW-SE orientation at present (Müller et al. 1992, Zoback 1992). During the Early and Late Oligocene the tectonic activity in the Roer Valley Graben suggests WNW-ESE extension. Since Miocene the orientation and the location of the main depocentre indicate a NE-SW extension (Michon et al. 2002). These changes in the direction of the principal stresses will have induced changes in the permeability of the fracture system.

Changes in tectonic stress during the evolution of onshore and offshore Netherlands include gradual long-term changes in tectonic stress regime from an active extensional stress regime (Triassic to Early Cretaceous) towards a compressional stress regime (Late Cretaceous to present-day), short-term stress fluctuations related to distinct rifting pulses (e.g. Late Jurassic rifting of the Mesozoic basins, Late Oligocene to recent rifting of the Roer Valley Graben) and pulse-like changes in compressive stress during the Late Cretaceous and Eocene – Oligocene. All these changes may have affected storativity and permeability and distributions of overpressure and fluid flow.

Major normal fault displacements in the Netherlands are related e.g. to the Late Kimmerian I rifting pulse. Active fault displacement in a compressional setting occurred in the basin during the Late Cretaceous and Eocene – Oligocene periods. During active deformation associated with Late Kimmerian I rifting, Late Cretaceous inversion and Eocene – Oligocene uplift and Late Oligocene to Recent rifting, faults and associated fractures may have acted as permeable pathways for fluids.

The maximum overpressure that can be sustained at a certain depth depends on the sum of the least principal stress plus the tensile strength of the medium at that depth (e.g. Du Rouchet 1981, Sibson 1994). Apart from being depth dependent, the minimum principal stress also depends on the tectonic regime (Grauls 1997), hence fluid expulsion through faults and fractures may have occurred at different depths and time intervals and maximum overpressures may have reached different magnitudes during the different tectonic regimes operating during geological evolution of the Netherlands.

## 4.2 Sedimentary loading

Sedimentary loading may induce porosity reduction by compaction of the rock matrix, development of groundwater overpressures and groundwater flow. The development of overpressures involves competition between increase in sedimentary load and dissipation of groundwater pressures by groundwater flow. Aquifers in hydraulic communication with the ground surface will allow groundwater flow induced by sedimentary loading, and as a consequence reduce or even prevent overpressures building up in the aquifer. Poorly permeable compressible rocks/aquitards are not able to dewater and compact rapidly in response to sedimentary loading and are susceptible to developing overpressured conditions of the groundwater. In general, significant overpressured conditions are unlikely to develop in basins that subside less than 100 m/My, with the exception of parts of the basin with extensive layers of very poor permeability (e.g. Bethke 1986, Harrison and Summa 1991). In contrast, rapid rates of sedimentation will cause groundwater overpressures in low permeable layers (e.g. Osborne and Swarbrick 1997).

The highest long-time average sedimentation rates (Figure 14) occurred in the depocentre of the Southern Permian Basin during the Zechstein (140 m/My) and Early Triassic (early rift sequence; 160 m/My), in the Mesozoic Basins during the Late Jurassic – Early Cretaceous (main syn-rift sequence; 220 m/My), and in the northern offshore of the Netherlands during Pliocene-Quaternary times (400 m/My). The Quaternary sedimentation rate of 400 m/My corresponds to an imposed vertical stress rate of approximately 8 MPa/My (assuming density Quaternary sedimentary rock = 2090 kg m<sup>-3</sup>).

## 4.3 Erosional unloading

Erosional unloading may give rise to pore volume increase, decrease of groundwater pressures (development of underpressures) and groundwater flow.

The most important phases of erosional unloading occurred during Late-Jurassic to Early Cretaceous uplift and erosion of the Mesozoic highs (such as Elbow Spit High, Cleaverbank High and Schill Grund High, Texel IJsselmeer High, Winterton High and Peel Block, Figure 12; estimated erosion on Texel IJsselmeer High 1000 m), Late Cretaceous – Early Tertiary inversion and erosion of Mesozoic basins (Broad Fourteens Basin, West Netherlands Basin, Roer Valley Graben, Dutch Central North Sea Graben: erosion between 750 and 3000 m), and Eocene – Oligocene uplift and erosion of the Southern Early Tertiary High (erosion Broad Fourteens Basin estimated at 500 m).

The maximum amount of inversion-related erosion during Late Cretaceous – Early Tertiary times was reported for the Broad Fourteens Basin: it was 3000 m in 20 million years or less, which corresponds to a minimum rate of erosional unloading in the order of 3.3 MPa/My. The erosional unloading during the Eocene – Oligocene inversion period is estimated at 3.7 MPa/My for the Broad Fourteens Basin (corresponding to a maximum erosion of 500 m in 3 My).

## 4.4 Glacial loading/unloading

Two Pleistocene periods of ice loading occurred in the Dutch part of the Southern North Sea Basin. At the maximum of the Elsterian glaciation the Scandinavian ice extended across the North Sea as far as the northwest coast of the Netherlands

and during the Middle Saalian ice extended farther south and reached the central parts of onshore Netherlands (e.g. Joon et al. 1990, Laban 1995). Three peaks in the southward extent of the Saalian ice sheet have been recognised at 155,000, 145,000 and at 135,000 years B.P. (Wildenborg et al. 2000). The minimum thickness of the Saalian ice sheet in the northern onshore parts of the Netherlands was estimated by Schokking (1990) at 195 m. Boulton et al. (1993) simulated the climate and the dynamics of ice sheet movement during the Saalian. The results of their study show that the advance and retreat of the ice sheets proceeded very rapidly at velocities of a few tens of metres to 200 - 300 metres per year. It is clear that glacial loading and unloading are very rapid processes of relatively short duration compared to sedimentary loading and unloading.

#### 4.5 Topography of the water table

During different time periods in the Permian to Recent history, a water table was able to establish in subaerial parts of the onshore and offshore Netherlands and in subaerial regions close to the Netherlands southern and southeastern borders. The post-rift period is the only time period without any subaerial exposure, and hence without any topography-induced flow. The main periods of topography-induced flow are indicated in Table 3. Supra-regional topography-induced flow systems with recharge areas in the highs south of the Netherlands border have probably been active repeatedly and for long periods of time: e.g. during the Permian, the Late Jurassic – Early Cretaceous main syn-rift period and from Miocene to the present-day (Table 3). Regional flow systems with recharge areas in onshore and offshore Netherlands probably developed in distinct intrabasinal highs, such as the main syn-rift highs, the Late Cretaceous inverted basins, and the Southern Early Tertiary High. In Quaternary times local and regional groundwater flow systems developed in onshore and offshore Netherlands in addition to the supra-regional Ardenno-Rhenish groundwater flow system (Verweij 1990a). The overall topography of the subaerial parts of the Netherlands North Sea Basin was dominated by the flat topography of the deltaic fan system that developed from the Late Tiglian. The local and regional topography-induced groundwater flow systems in such a flat lowland area will generally have limited depths of penetration. The Elsterian and Saalian glaciations modified the topography of the lowland area. During the Elsterian glaciation, deep valleys, locally reaching depths of more than 300 m were eroded in the northern parts of onshore Netherlands and the adjacent offshore areas (Zagwijn 1989, Laban 1995). Glacial lake sediments subsequently filled these valleys. The Saalian glaciation remodelled the ground surface topography: glacier tongue basins and ice-pushed ridges were formed (Joon et al. 1990). The basins were filled in during the Eemian interglacial. In the Weichselian the old Saalian relief was levelled further. However the present-day surface topography in the centre and east of onshore Netherlands is still dominated by the glacial features of Saalian origin. These positive glacial features act as recharge areas for local and regional topography-induced groundwater flow systems.

The repeated changes in sea level in Quaternary times exerted an important influence on the regional extent and depth of penetration and on the groundwater velocities of the topography-induced groundwater flow (e.g. Elderhorst and Zijl 1992, Oostrom et al. 1993).

Table 3 Main periods of topography-induced flow of groundwater in onshore and offshore Netherlands

| Subaerial exposure related to uplift and erosion/tectonic phase | Positive topographical features/highs  | Climate   | Flow system                           |
|---|--|---|---------------------------------------|
| Saalian   | London-Brabant Massif, Rhenish Massif  | Tropical, semi-arid                                 | 1. Supra-regional                     |
|   | London-Brabant Massif  | Arid to semi-arid                                   |                                       |
|   | London-Brabant-Massif  | Tropical, arid to semi-arid                         | 2. Supra-regional and regional        |
| Hardegsen   | Netherlands Swell, Cleaverbank High  |   |                                       |
| Late Kimmerian I  | Elbow Spit High, Cleaverbank High, Schill Grund High, Texel IJsselmeer High  | Subtropical, seasonally wet                         | 3. Supra-regional and regional        |
|   | Elbow Spit High, Cleaverbank High, Schill Grund High, Texel IJsselmeer High, Winterton High, Peel Block, London-Brabant Massif             |   |                                       |
| Late Kimmerian II   | Elbow Spit High, Cleaverbank High, Schill Grund High, Texel IJsselmeer High, Winterton High, Peel Block, London-Brabant Massif             |   |                                       |
| Subhercynian - Laramide Inversion                               | Broad Fourteens Basin, West Netherlands Basin, Central Netherlands Basin, Lower Saxony Basin, Central North Sea Graben, Roer Valley Graben | Subtropical, seasonally wet                         | 4. Regional                           |
| Pyrenean Inversion  | Broad Fourteens Basin/ Southern Early Tertiary High  | Warm, subhumid                                      | 5. Regional                           |
| Late Tertiary - Recent Uplift                                   | Ardennes - Rhenish Shield  | Cold, cool-warm temperate, alternating arid & humid | 6. Supra-regional, regional and local |
|   | Ardennes - Rhenish Shield  |   |                                       |

The type, magnitude and areal distribution of the identified driving forces and processes for fluid flow systems have changed continuously during the geological evolution of the Netherlands (Tables 2 and 3). During each tectonostratigraphic stage different forces have acted simultaneously on the fluids (Table 2), largely because of the differential subsidence and uplift history of the structural units. Different fluid flow systems have probably coexisted and interacted laterally and vertically in the onshore and offshore Netherlands. From the foregoing it is clear that the different geological histories for the different structural elements (Figure 18) will have induced different fluid flow histories for different locations: for instance different fluid flow histories can be expected for the Mesozoic basins in comparison with the platforms/highs, but also for the different basins (Roer Valley Graben and Central North Sea Graben, Tables 2 and 3).



## 5 Present-day hydrogeological framework of onshore and offshore Netherlands

The hydrogeological framework of the subsurface at a certain time describes the spatial distribution of the permeability of the subsurface. The framework is characterised by the distribution, thickness and dip of the hydrostratigraphic units and the location of the geological structures and tectonic elements of importance for subsurface fluid flow. Figure 20 shows the generalised present-day hydrostratigraphy of onshore and offshore Netherlands.

The most important poorly permeable units controlling past and present fluid flow conditions are the Salt Members of the Zechstein Group, because of their very poor permeability and their large areal continuity, and to a lesser extent the Salt Members of the Upper Germanic Trias Group. The remaining poorly permeable units mainly consist of claystones/mudstones/clays. The permeable units consist of sands, sandstones, limestones and chalk. The Chalk Group is considered here as an aquifer/reservoir rock in agreement with Megson (1992, 1998) and Barson et al. (1997). Its reservoir character is indicated by the numerous important oil and gas fields in the Chalk in the Norwegian and Danish parts of the Central Graben (Oakman and Partington 1998) and by the Harlingen gas field in the Netherlands (Van den Bosch 1983). Although there is ample evidence of hydrodynamic behaviour of the Chalk (Barson et al. 1997, Megson 1992), there is no consensus on whether the Chalk is a regional aquifer (see e.g. Caillet et al. 1997, Darby et al. 1996, Japsen 1998, Megson 1998).

Numerous deep faults and salt structures disrupt the lateral continuity of the sedimentary sequences (Figure 19). In general, the regional distributions in subsidence and inversion history have resulted in a restricted lateral continuity of permeable and poorly permeable units, especially of those of post-Zechstein to Tertiary age.

Heterogeneity in the porosity and permeability of each hydrostratigraphic unit is apparent both at basin and reservoir scale. Lateral variations of porosity in pre- and early rift sequences are clearly related to the differences in burial histories of the Late Jurassic – Early Cretaceous structural elements. The porosity-depth relation for

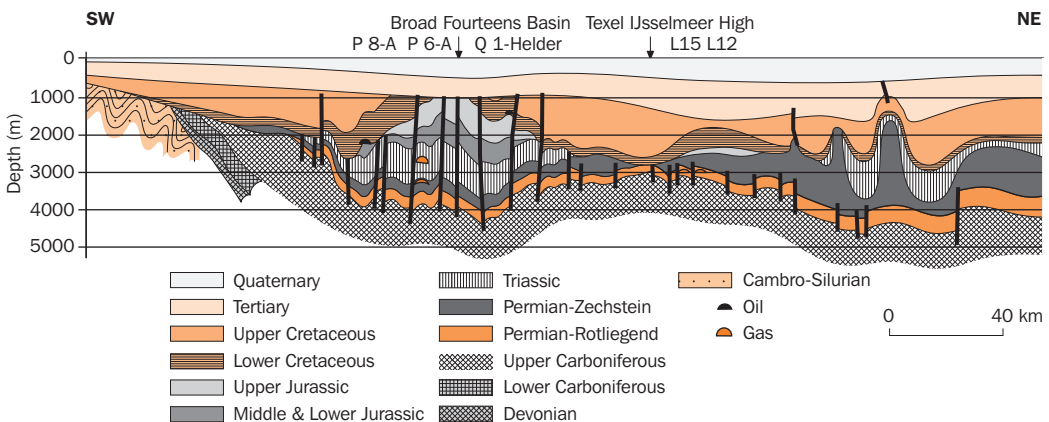


Figure 19 Regional stratigraphic cross-section (after Geological Survey of the Netherlands and IMNES 1984). Location of cross-section is indicated in Figure 12

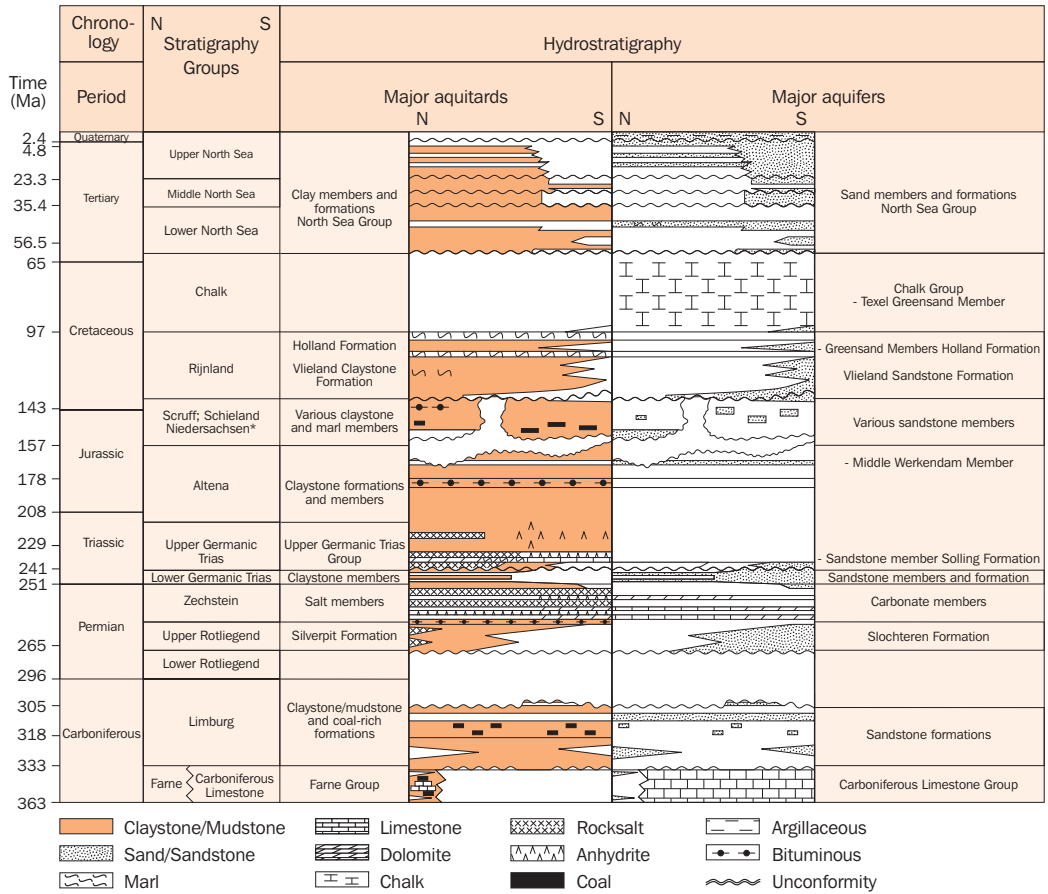


Figure 20 Generalised hydrostratigraphy of onshore and offshore Netherlands (From Verweij 1999)

the Slochteren hydrostratigraphic unit clearly illustrates this relationship (Figure 21). The Slochteren Formation is at its maximum depth of burial in structurally high areas (Figure 18) and the porosity-depth relation for these areas could be interpreted as an exponential trendline. The porosity-depth plot for the Slochteren Formation in the basal areas (Figure 21) does not follow a clear exponential trend. This is because the Slochteren Formation is not at its maximum depth of burial in the inverted Broad Fourteens Basin and part of the Central Netherlands Basin (Figure 18), and as a consequence the porosities are relatively low for present-day burial depths of the formation. The Slochteren Formation is at its maximum depth of burial in the Vlieland Basin. Here, the relatively low porosities result from the increased heat flow associated with the Zuidwal Vulcano of Late Jurassic – Early Cretaceous age (Figure 13). Giesen (1995) presented relatively high interval velocities for the Lower Germanic Trias Group in the central part of the Broad Fourteens Basin, which may also be an indication of relatively low porosities. The permeability-depth relation for the Slochteren Formation in structurally high areas is not as straightforward as the porosity-depth relation: different porosity-permeability relations have been identified for different scales of observation for the Slochteren Formation in structurally high areas. An important determinant of the porosity-permeability relation on core and reservoir

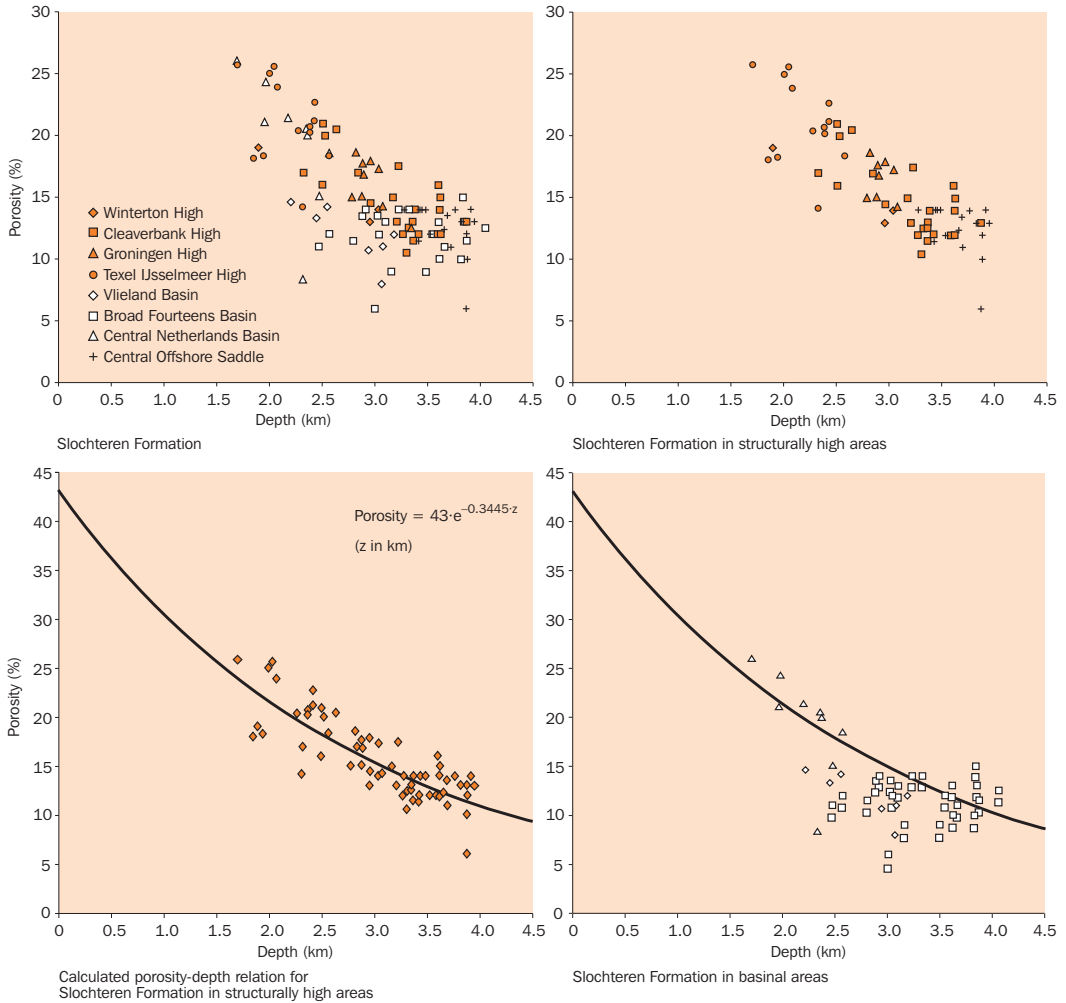


Figure 21 Porosity-depth relation for the Slochteren Formation (From Verweij 1999).

Porosity data from Geological Survey of the Netherlands 1991-1995 and RRI 1985, 1988

scale is type of cementation (e.g. Crouch et al. 1996, Ehrenberg 1990, Gaupp et al. 1993, Oele et al. 1981, Purvis and Okkerman 1996). More regional permeabilities are also affected by the presence of faults and fractures (sealing or otherwise) and differences in sedimentary facies (shale barriers).

The present-day porosity distribution in the syn-rift sedimentary sequences also reflect the influence of the Late Cretaceous–Early Tertiary inversion movements as indicated by, for example, the relatively high interval velocities for the Jurassic stratigraphic units – and the associated low porosities for present-day burial depth – in the Broad Fourteens area (Giesen 1995).

Relatively low porosities for present-day depth of burial are also well known for post-inversion units: the Pleistocene Potclay in the northern part of onshore Netherlands is currently overcompacted because of Pleistocene ice loading (Schokking 1990).

## 6 Present-day indicators of fluid flow conditions in onshore and offshore Netherlands

Being the effect of groundwaters' geologic agency, present-day physico-chemical characteristics of the sedimentary fill of onshore and offshore Netherlands are indicators of paleo and present-day fluid flow conditions (Chapter 1). Important indicators of periods of active paleo fluid flow in onshore and offshore Netherlands are present-day sediment diagenetic characteristics and characteristics of oil and gas accumulations.

### 6.1 Overview of indirect indicators derived from published studies

Tables 4 and 5 present an overview of the different types of indirect indicators and the related fluid flow events.

Table 4 Indirect indicators of northward topography-induced flow of groundwater originating at the southern and southeastern margins of the Netherlands during different times in geological history

| Indicator  | Fluid flow event  | Timing                 | Source                   |
|--|---|------------------------|--------------------------|
| 1. Composition of fluid inclusions and stable isotopes of ferroan calcites in fractures in Dinantian sediments (Belgium, SW of Maastricht) | – Meteoric origin mineralising fluids<br>– SE-NW topography-induced flow<br>– Discharge area Namur syncline<br>– Recharge area Ardennes Massif      | Kimmerian tect. phases | Muchez et al. 1994, 1995 |
| 2. Pb-Zn mineralisations of Bleiberg; Numerical modelling fluid flow and heat transport  | – Northward topography-induced flow<br>– Recharge area Ardennes Massif<br>– Discharge area Variscan front<br>– Focussed flow through fault zones    | Late Jurassic          | Lünenschloss et al. 1997 |
| 3. Present-day hydrothermal system Aachen hot springs (Germany); Numerical modelling of fluid flow and heat transport                      | – Northwestward topography-induced flow<br>– Recharge area Rhenish Massif<br>– Discharge area Variscan front<br>– Focussed flow through fault zones | Recent                 | Bayer et al. 1995        |

Studies on the genesis of Mississippi Valley-type Pb-Zn deposits (e.g. Muchez et al. 1994, 1995) and the results of modelling studies of elevated (paleo) temperatures (e.g. Bayer et al. 1995, 1996; Von Winterfeld et al. 1994) are consistent with the existence of large-scale north-flowing topography-induced fluid flow systems originating at the southern and southeastern margin of the Netherlands during different times in geological history (Late Carboniferous – Early Permian; Jurassic – Early Cretaceous; recent; Table 4). Studies on the diagenetic evolution of the continental sediments of the Slochteren Formation and the Lower Germanic Trias Group during the pre- and early rift stages (Table 5) confirm the existence of topography-induced (indicators 5, 7, 8) and density-induced fluid flow conditions (indicator 9) in the Southern Permian Basin. The data on sediment diagenetic evolution also reflects expulsion of water from poorly permeable units, e.g. by sedimentary loading in the basinal areas (indicator 10) and topography-induced flow from intrabasinal highs during the main syn-rift period (indicator 11), and are indicative of focussed fluid flow along faults during the periods of increased tectonic activity (indicator 10).

Table 5 Present-day indirect indicators of fluid flow events based on published sources

| Indicator  | Fluid flow event   | Timing                                      | Source  |
|--|--|---|---|
| 4. Anomalously high coalification Upper Carboniferous Coal Measures near Aachen thrust, Germany, and in SE Netherlands   | Northward forced fluid flow discharging along thrust fault zone near Aachen  | Late Carboniferous – Early Permian Variscan | Lünenschloss et al. 1997<br>TNO-NITG 1999   |
| 5. Dolomite, anhydrite and quartz cements in Slochteren Fm in CBH and NE of TYH; oxygen and strontium isotopic values of dolomite; sulfur isotopic values of anhydrite | Topography-driven flow of meteoric water from Permian basin margin to basin center   | Late Permian Pre-rift                       | Amthor and Okkerman 1998  |
| 6. Kaolin cement, leached K-feldspar in Slochteren Fm (e.g. in BFB)  | Expulsion acid CO <sub>2</sub> -rich water from Limburg Group into Slochteren Fm   | > 165 Ma<br>Early rift                      | Lanson et al. 1995, 1996<br>Rossel 1982<br>Platt 1993<br>Gaupp et al. 1993  |
| 7. Carbon, oxygen and strontium isotopic composition of dolomite cement in Main Buntsandstein Subgroup (offshore F17, 18; L2, 5, 6, 9)                                 | Flow of meteoric water through Main Buntsandstein Subgroup   | Early rift                                  | Purvis and Okkerman 1996  |
| 8. Dolomite and anhydrite cements in Volpriehausen Fm (offshore F15)   | Flow of meteoric water through Volpriehausen Fm  | Early rift                                  | Lepoutre et al. 1996  |
| 9. Halite cements in Detfurth Sandstone Fm (offshore L2, F15)  | Downward expulsion of brines from evaporites of Röt Fm into Detfurth Sandstone Fm  | Early rift                                  | Dronkert and Remmelts 1993<br>Lepoutre et al. 1996  |
| 10. Illite cements in Slochteren Fm and Lower Germanic Trias Group (BFB, WNB)  | – Hydrothermal flow along fault zones<br>– Expulsion K-rich water from Limburg Group and/or Zechstein Group into Slochteren Fm | 130 - 165 Ma<br>Main syn-rift               | Lanson et al. 1995, 1996<br>Lee et al. 1989<br>Leveille et al. 1997<br>Clauer et al. 1996<br>Gaupp et al. 1993<br>Platt 1993<br>Emery and Robinson 1993 |
| 11. Illite cements in Upper Rotliegend Group (NE onshore Netherlands; adjacent to WH); Reconstructed oxygen isotopic composition diagenetic fluid                      | Flow of meteoric water through Upper Rotliegend Group; Recharge area TYH<br>Recharge area WH                                   | 106 - 125 Ma<br>130 Ma<br>Main syn-rift     | Lee et al. 1989   |
| 12. Stable isotopes groundwater Vlieland Sandstone Fm (WNB)  | Flow of meteoric water through Vlieland Sandstone Formation  | <90 Ma                                      | Van der Weiden 1983   |

Table 5 (Continued)

|  |  |                              |   |
|--|--|------------------------------|---|
| 13. K-feldspar leaching in Vlieland Sandstone Fm (BFB)                                 | Flushing of Vlieland Sandstone Fm  | <90 Ma                       | De Jong and Laker 1992  |
| 14. Biodegraded oils in Upper Jurassic and Lower Cretaceous reservoirs (BFB, WNB)      | Flow of oxygen-rich meteoric water through Upper Jurassic and Lower Cretaceous reservoirs                          | <90 Ma (BFB)<br><60 Ma (WNB) | Roelofsens and De Boer 1991<br>De Jager et al. 1996<br>Van Balen et al. 2000<br>Verweij 1990a,b |
| 15. Illite cements in Upper Rotliegend Group near fault (NE onshore Netherlands)       | Fluid flow along fault zone  | 40 Ma                        | Lee et al. 1989<br>Platt 1993   |
| 16. Shallow gas accumulation; Shallow gas seepage                                      | Vertical fluid migration through Pliocene and Quaternary units   | Quaternary-Recent            | Schroot 2001<br>Schroot and Schüttenhelm 2003   |
| 17. Pockmarks at seabottom Netherlands offshore  | Fluids escaping at seabottom   | Recent                       | Laban 1999<br>Schroot and Schüttenhelm 2003   |
| 18. Current land subsidence (onshore Netherlands)                                      | Groundwater flow in Tertiary and Quaternary sediments induced by Late Pleistocene and Holocene sedimentary loading | Quaternary                   | Kooi et al. 1998<br>Kooi and De Vries 1998  |
| 19. Potclay (onshore Netherlands); overcompaction                                      | Expulsion of groundwater due to ice-loading  | Pleistocene                  | Schokking 1990  |
| 20. Fracture vents and sand boils (onshore Netherlands)                                | Liquefaction induced by Roermond (1992) earthquake   | Recent                       | Nieuwenhuis 1994  |
| 21. Hydraulic heads; chemical compositions groundwater; various groundsurface features | Topography-induced groundwater flow  | Quaternary-Recent            | e.g. Dufour 1998, 2000<br>TNO-GG 1991 - 1996  |

Hydrochemical, sediment-diagenetic as well as petroleum geochemical studies provide strong evidence for a period of active meteoric fluid flow through the Lower Cretaceous reservoirs in the West Netherlands Basin and the Broad Fourteens Basin, presumably during Late Cretaceous to Early Tertiary times (indicators 12, 13 and 14). A distinct period of illite cementation in the Upper Rotliegend Group in Northeastern Netherlands occurred during Eocene-Oligocene times (indicator 15). Lee et al. (1989) associate the cementation with a period of active fluid flow along a nearby fault zone.

Present-day fluid flow conditions in onshore Netherlands include fluid flow and related compaction as induced by recent sediment loading (Table 5, indicator 18: Kooi et al. 1998, Kooi and De Vries 1998). From the hydrochemical compositions of the groundwater in the west of onshore Netherlands it can be inferred that this water has been expelled from Quaternary sediments, by compaction (Stuyfzand 1993).

The location of oil and gas fields in on- and offshore Netherlands provides additional valuable information on fluid flow conditions and fluid pathways. For example, the widespread occurrence of Posidonia sourced oil fields in the Lower Cretaceous reservoirs in the West Netherlands Basin and the Broad Fourteens Basin (Rondeel et al. 1996) means that there must have been cross-formational flow or along-fault flow of oil through the Werkendam and Brabant Formations and the Upper Jurassic units. The gas fields in reservoirs of the Lower Germanic Trias Group in the Dutch Central North Sea Graben (e.g. F15, L2, Crépieux et al. 1998, Lepoutre et al. 1996) are sourced from Limburg Group coal measures. These gas fields must have been filled by paleo and/or present-day cross-formational migration through the poorly permeable Zechstein Group and part of the Lower Germanic Trias Group, via permeable fault and fracture zones or salt depletion zones in the Zechstein Group. Shallow gas accumulations in Pliocene–Pleistocene reservoirs in the offshore blocks A12 and A18 (Wride 1995) and shallow gas seepage along fault systems through Pliocene and Quaternary units in block F3 (Schroot 2001) reveal Quaternary to recent vertical fluid migration in northern offshore Netherlands (indicator 16). A number of pockmarks have been identified on the floor of the Netherlands North Sea (indicator 17: Laban 1999, Schroot and Schüttenhelm 2003). Pockmarks are indicators and recorders of focussed fluid flow (gas or liquid) (Hovland et al. 2002). The fluids escaping through pockmarks may be sourced or driven by changing overpressure conditions at any depth beneath the surface (Hovland et al. 2002).

## 6.2 Identified periods of active fluid flow

The present-day indicators of fluid flow allowed fluid flow/groundwater flow events in the different rifting stages to be recognised. The identified groundwater flow events are qualitatively related to the different types of driving mechanism as previously determined from geological history (Tables 2 and 3; Tables 4 and 5):

|                       |   |
|-----------------------|---|
| Pre-rift period       | — Topography of the water table (indicator 5)                         |
| Early-rift period     | — Expulsion (sedimentary loading) (indicators 6, 9)                   |
|                       | — Topography water table (indicators 1, 7, 8)                         |
| Main syn-rift period  | — Tectonic forces (Basins) (indicator 10)                             |
|                       | — Topography of the water table (Highs) (indicator 11)                |
|                       | — Topography of the water table (S, SE Netherlands) (indicators 1, 2) |
| Post-rift period      | — — — —   |
| Syn-inversion period  | — Topography of the water table (indicator 12, 13, 14)                |
|                       | — Tectonic forces (indicator 15)                                      |
| Post-inversion period | — Topography of the water table (SE Netherlands) (indicator 3)        |
|                       | — Topography of the water table (indicator 21)                        |
|                       | — Sedimentary loading (indicator 18, possibly also 16 and 17)         |
|                       | — Glacial loading (indicator 19)                                      |
|                       | — Tectonic forces (indicator 20)                                      |

Flow of groundwater during the post-rift period induced by sedimentary-loading could not be verified from the available indicators. Publications on petroleum systems infer a phase of oil and gas migration during the post-rift period (e.g. Bodenhausen and Ott 1981, De Jager et al. 1996).

## 7 Present-day overpressures and fluid flow in onshore and offshore Netherlands

### 7.1 Distribution of overpressures

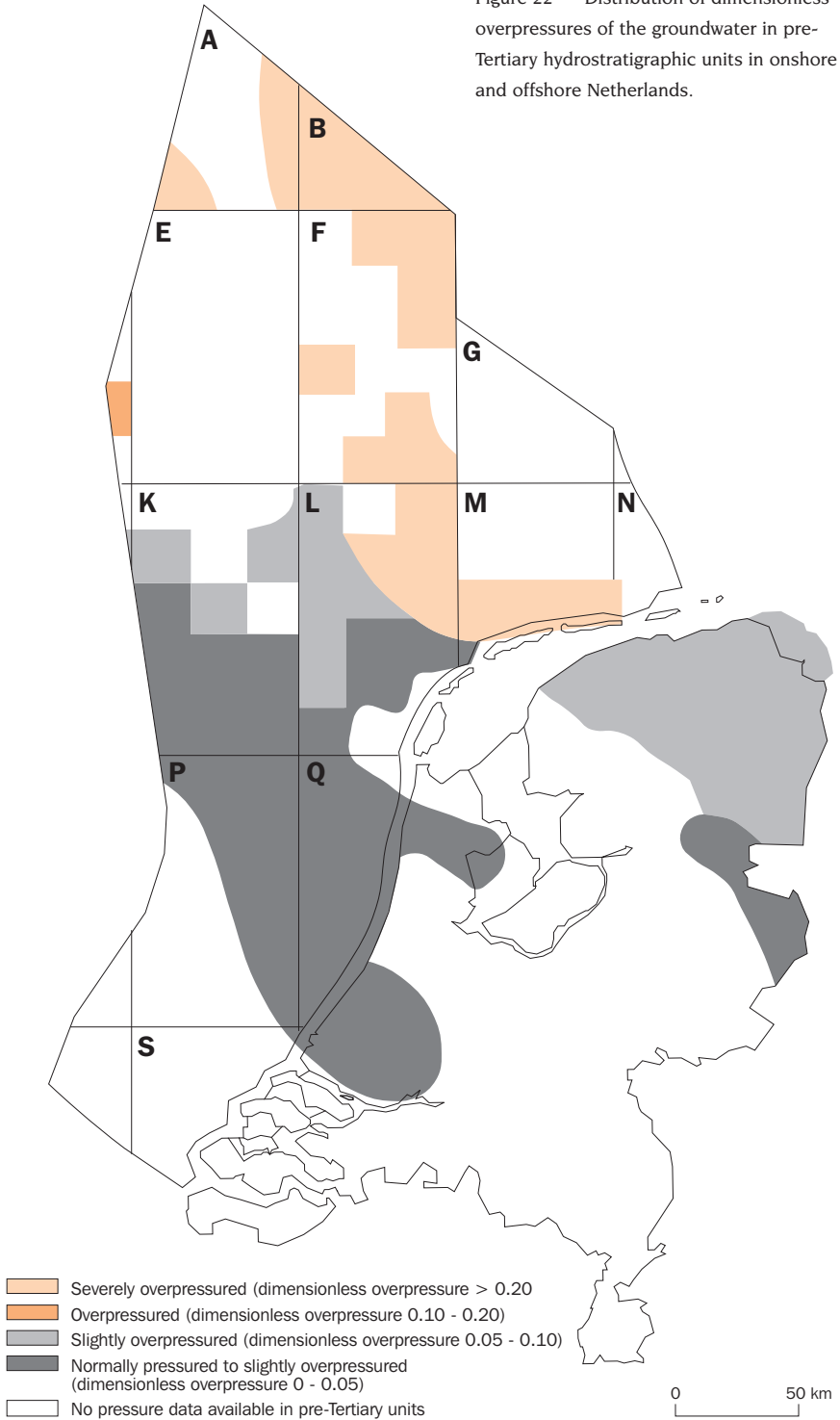
The direct indicators of fluid flow conditions in the subsurface are the distribution of groundwater potential, and the associated distribution of groundwater overpressures. The groundwater is overpressured if its pressure exceeds the hydrostatic pressure at a specific depth (Chapter 1). The dimensionless overpressure at a specific point is defined by  $(P_{\text{observed}} - P_{\text{hydrostatic}})$  divided by  $(P_{\text{lithostatic}} - P_{\text{hydrostatic}})$  (e.g. Domenico and Schwartz, 1998). In theory, the dimensionless overpressure varies between 0 and 1. The maximum groundwater pressure that can be maintained in the subsurface is controlled by rock failure and by fracture opening and reopening conditions. Hence, the upper limit of groundwater pressure is controlled by the minimum principal stress and the tensile strength of the porous medium (leak-off pressure corresponds to fracture initiation and can be considered as the upper bound of the minimum principal stress; Gaarenstroom et al. 1993, Grauls 1997). In the North Sea area the minimum principal stress corresponds to the minimum horizontal stress. Leak-off pressures and minimum horizontal stresses change with depth in this area (Crépieux et al. 1998, Gaarenstroom et al. 1993, Giles et al. 1999, Grauls 1997). As a consequence, the maximum value of the dimensionless overpressure will change with depth as well. Maximum values for dimensionless overpressures are 0.45 at 1000 m depth ( $\sigma_3/\sigma_z = 0.70$ ), 0.60 at 2500 m ( $\sigma_3/\sigma_z = 0.80$ ) and 0.80 at 4000 m ( $\sigma_3/\sigma_z = 0.90$ ). Wells have encountered highly overpressured brines and gases within Zechstein salt units, indicating that salt can hold overpressures close to lithostatic pressures (corresponding to maximum dimensionless overpressures of 1).

Figure 22 shows the distribution of the dimensionless overpressures of the groundwater in pre-Tertiary reservoir-type hydrostratigraphic units in onshore and offshore Netherlands. These values are based on pressure data from approximately 80 oil and gas wells (Cottençon et al. 1975, Fontaine et al. 1993, Lepoutre et al. 1996, RRI 1985, 1988, Stheeman 1963, Van den Bosch 1983, Van Wijhe et al. 1980, Verweij 1990a, b, Webatlas of North Sea fields) and additional information on overpressure distribution from Bloch et al. (1993), Crépieux et al. (1998), Japsen (1999) and Megson (1992).

Severely overpressured conditions occur in the Dutch Central North Sea Graben, Step Graben, Terschelling Basin and southwest of the Elbow Spit High. The dimensionless overpressures exceed 0.20. The pressures have been measured in different reservoir type hydrostratigraphic units and at different depths, and as a consequence vary widely. Dimensionless overpressure values of at least 0.20 in northern offshore Netherlands (A and B blocks) are representative of the pressure conditions in the Chalk Group (Megson 1992, 1998, Japsen 1998). Japsen (1998) analysed interval-velocity data for the Chalk Group in the UK, Norwegian, Danish and Dutch North Sea and identified an area of negative velocity anomalies in the central and northern parts of the North Sea Basin, including the eastern A blocks, B blocks, northern F blocks and northern G blocks in offshore Netherlands (Japsen identified negative velocity anomalies in wells A11-01, B13-02, F02-01, F03-06, G17-01 and L08-02). Giesen (1995) also mapped a clear northward trend of decreasing depth-corrected interval velocities for the Chalk Group in offshore Netherlands. Japsen (1998) related these negative velocity anomalies



Figure 22 Distribution of dimensionless overpressures of the groundwater in pre-Tertiary hydrostratigraphic units in onshore and offshore Netherlands.



with undercompaction and overpressuring of the Chalk Group. He identified the area north of the A and B blocks as the major zone of Chalk overpressuring.

In the Central North Sea Graben and the Terschelling Basin severely overpressured conditions also occur in the laterally and vertically restricted syn-rift hydrostratigraphic units and the pre-rift Triassic units. The dimensionless overpressures mapped in the F blocks (Figure 22) are mainly from the Central Graben Group, and vary between 0.20 and 0.30. An exception is the dimensionless overpressure in the Central Graben Group in the F3 block (at least 0.50 at 2500 m), that approaches its maximum value. In the southern part of the Central North Sea Graben and in the Terschelling Basin severely overpressured conditions have been encountered in the Lower Germanic Trias Group (e.g. in blocks F10, F15, L2, L3, L6, L9; e.g. Crépieux et al. 1998, Fontaine et al. 1993, Lepoutre et al. 1996). This is illustrated by the pressure conditions in the F15-A Triassic gas reservoir, which forms a structural compartment located between the Central North Sea Graben, the Terschelling Basin and the Schill Grund High (Fontaine et al. 1993; Lepoutre et al. 1996). This Main Buntsandstein reservoir, which is partly affected by salt cementation, is located between two major NNE-SSW trending salt ridges, a fault to the north and overlying formations plugged by salt. The pressure in this structurally and hydrodynamically restricted gas reservoir is approximately 67.5 MPa at 3520 m (Fontaine et al. 1993, Lepoutre et al. 1996, Matthis and Nieuwland 1999), which corresponds to a dimensionally overpressure value of approximately 0.7 which is close to its maximum value. Giles et al. (2000) also refer to fluid pressures that approach the minimum in situ stress in the nearby Terschelling Basin.

The pre-rift Upper Rotliegend Group is of reservoir quality in the area south of the Central North Sea Graben and the Terschelling Basin. Severe overpressures occur along the northern limit of the Upper Rotliegend Slochteren Formation below a thick Zechstein seal (e.g. in southern M blocks, and blocks L1, L8, K6). The overpressures dissipate rapidly in the direction of decreasing sealing capacity of the Zechstein Group, e.g. towards the Texel IJsselmeer High, and in the direction of increasing permeability of the Slochteren unit. The pressures in the Slochteren unit are near hydrostatic to slightly superhydrostatic in onshore and offshore Netherlands south of the High, where Zechstein salts are less thick and of limited areal extent.

The mapped dimensionless overpressures (Figure 22) are indicative of normal to slightly overpressured conditions in the main hydrostratigraphic units in the Broad Fourteens basin (Upper Rotliegend Group, Main Buntsandstein Subgroup, Delfland Subgroup, Vlieland Sandstone Formation) and in the Vlieland Sandstone Formation of the West Netherlands Basin.

It should be kept in mind that no pressure data were available for poorly permeable units (shales, evaporites) of pre-Tertiary age. It cannot be excluded that overpressured conditions do exist in shales and evaporites adjacent to normally pressured reservoir units.

## 7.2 Factors controlling present-day distributions of overpressure

In general, an overpressure distribution is controlled by the competition between the pressure-generating mechanisms and the pressure-dissipating mechanisms (such as fluid flow, unloading, cooling; Chapter 1). The possible main mechanisms responsible for the observed overpressure distribution as derived from geological history are summarised in Tables 2 and 3. Sedimentary loading was the main pressure influencing mechanism in the offshore Netherlands, outside the inverted basins from Cretaceous times onward (Table 2). During post-inversion times sedimentary loading was the main mechanism in the entire offshore area. For the entire onshore and offshore Netherlands, mechanical forces and processes influencing fluid pressure conditions since the Oligocene included sedimentary loading, topography of the water table, tectonic forces and ice loading and unloading (Table 2). Fluid density differences, gas generation, and most recently also human activities are additional factors of influence. Present-day pressure distributions will reflect these relatively recent forces and processes to a greater or lesser extent.

A large number of studies in the Central North Sea/UK Central Graben, indicate that the dominant factors controlling present-day pore pressure distribution in the Central North Sea are sedimentary loading, fluid flow and the permeability framework (e.g. Mann and Mackenzie 1990, Yardley and Swarbrick 2000). Additional controlling factors identified are late gas generation and the cracking of oil to gas (e.g. Cayley 1987, Holm 1996). Sedimentary loading is probably also a major factor of influence on the present-day distribution of overpressure in the Southern North Sea Basin (Table 2, Figure 22).

Overpressure distribution is the direct indicator of present-day fluid flow. The relation between observed overpressures and fluid flow are described below.

## 7.3 Overpressures and fluid flow in Cenozoic sedimentary units

In argillaceous sediments the dominant process responsible for reducing porosity is mechanical compaction (e.g. Rieke and Chilingarian 1974). The Tertiary units in offshore Netherlands are predominantly argillaceous (Figure 13). Japsen's (1999) study of interval velocities of the Cenozoic revealed an area of relatively low velocities for the depth of burial of the Paleogene in the northern offshore of the Netherlands (A and B blocks and northern F blocks) and adjacent Central North Sea area. No anomaly was found for the Neogene part of the Cenozoic. Japsen suggested that the identified velocities of the Paleogene are low relative to depth because of overpressured and undercompacted conditions related to rapid late Cenozoic sedimentary loading. The Neogene is normally compacted and not overpressured. Japsen's findings are qualitatively supported by the fact that the Pliocene to recent depocentres in the northern offshore of the Netherlands have shifted from east to west and finally to the northwest (Figure 17) and the thickest package of Upper North Sea Group sediments is found in the northern offshore (Figure 16). There are no pressure data available for the Tertiary to confirm Japsen's interpretation or to assess whether overpressured conditions are more widespread in the thick claystone units of the Lower and Middle North Sea Group (e.g. corresponding to one of the other Neogene depocentres). The first results of an analysis of sonic and 3D seismic data in the southeast of the Central North Sea Graben indicated regional undercompaction and overpressuring

of the shales of the Lower North Sea Group (Winthagen and Verweij 2003). These results suggest that the region of undercompaction and overpressuring may extend further southward than the main region identified before by Japsen (1999).

Fault zones cutting through the Tertiary units provide vertical escape routes for fluids as indicated by occurrences of shallow gas in the northern offshore (Chapter 6). Relatively permeable fault zones will only dewater claystones/shales in a limited area surrounding the fault – in contrast to the dewatering of permeable reservoir rocks – and as a consequence will not reduce the overpressures in the claystones away from the fault zone.

Undercompaction of the Lower and Middle North Sea Groups seems to occur in an area where the present-day thickness of the Upper North Sea Group exceeds 1000 m (Figure 16). The sand content in the Lower and Middle North Sea Group increases towards the southeast of the study area, reducing the likelihood of undercompaction and overpressured conditions in the southeast. This is confirmed by studies done by Kooi and De Vries (1998) and Kooi et al. (1998) for onshore Netherlands. Their numerical modelling of the influence of Quaternary sedimentary loading and normal compaction of the Cenozoic sedimentary sequence in the western part of the Netherlands (Kooi and De Vries 1998, Kooi et al. 1998) predicted present-day rates of land subsidence in the order of 0.1 mm per year. They contended that this present-day subsidence is mainly caused by rapid sedimentation that occurred during the early Holocene. Expulsion of water derived from compaction of Quaternary deposits is confirmed by hydrochemical compositions of the groundwater (Stuyfzand 1993).

#### 7.4 Overpressures and fluid flow in pre-Tertiary sedimentary units: general observations

The mapped distribution of dimensionless overpressures in pre-Tertiary reservoir units (Figure 22) reveals a clear distinction between the northern overpressured area and a southern normal to slightly overpressured area. This difference in overpressure of the groundwater can be explained by differences in magnitude and/or duration of the pressure-generating mechanisms and/or differences in hydraulic characteristics of the basin fill in both areas. Assuming sedimentary loading is the major pressure generating mechanism, it is important to realise that the most recent and most rapid sedimentation took place in the northernmost offshore area, although Neogene-Quaternary depocentres exist in the onshore Roer Valley Graben and Central Netherlands Basin as well as in the Broad Fourteens Basin. The total amount of sediments deposited during the Tertiary and Quaternary increases towards the north (Figure 15). In addition, sedimentation during the Cenozoic is more continuous in the northern offshore area than the southern area; for example, in the Broad Fourteens Basin and the onshore Early Tertiary High significant uplift and erosion occurred during the Eocene-Oligocene phase. The most notable difference in hydraulic characteristics of the basin fill in the northern and southern parts of the Southern North Sea Basin result from the distribution and sealing characteristics of the Zechstein Salt Members. Zechstein salts are the most important sealing cap rocks for the Upper Rotliegend Group and Carboniferous reservoirs. Numerous salt diapirs and walls in the northern offshore and in the northern part of the Broad Fourteens Basin disrupt the lateral continuity of reservoirs in the basins.

The normal to slightly overpressured conditions in the southern part of the study area suggest that fluid flow from the pores in the reservoir units can keep pace with the Late Tertiary and Quaternary sedimentation rates.

### 7.5 Overpressures and fluid flow in Cretaceous units

Dimensionless overpressures of at least 0.20 have been identified in the northern offshore (Section 7.1). The published overpressures in the Chalk Group occur in an area where the present-day thickness of the Upper North Sea Group exceeds 1000 m (Figure 16). Japsen (1998) calculated that the main part of the measured overpressures in the Chalk in the Central North Sea could be related to Neogene and Quaternary sedimentary loading. Major overpressuring of the Chalk occurs to the north of offshore Netherlands. Hence, present-day overpressure gradients in the Chalk – being the potential driving forces for lateral fluid migration – slope southwards towards offshore Netherlands.

The only data on dimensionless overpressure of the groundwater in the Lower Cretaceous reservoir units are from the southern part of the study area. They indicate that the Vlieland Sandstone Formation is normally pressured in the southern offshore.

### 7.6 Overpressures and fluid flow in Upper Jurassic and Lower Triassic units

Severely overpressured conditions were encountered in the laterally and vertically restricted syn-rift reservoir units and pre- and early rift Triassic units in the Central North Sea Graben and the Terschelling Basin. In order to evaluate the (Cenozoic) sedimentary loading as a possible cause of the identified magnitudes of overpressure, an example calculation is given for the F15-A Triassic reservoir ( $P = 67.5$  MPa at 3520 m). The simplified calculation is based on the assumption that Neogene to Recent sedimentary loading is the only pressure-generating mechanism, the loading is 1D, the basin is laterally constrained and undrained conditions prevail, i.e. no groundwater flow takes place. The pore pressure coefficient (Chapter 1) that describes the percentage of the incremental load that is carried by the pore water in the Triassic sandstones is taken as 0.85.

The vertical change in stress that gives rise to the development of overpressure is 8.6 - 11 MPa (for: thickness Neogene + Quaternary = 1000 m; density Neogene + Quaternary sequence = 1900 - 2150 kg m<sup>-3</sup>;  $g = 9.8$  ms<sup>-2</sup>; density of the groundwater = 1020 kg m<sup>-3</sup>). For a pore pressure coefficient of 0.85, the maximum overpressure that can be generated in the Triassic reservoir by the Neogene and Quaternary increase in load is 7.3 - 9.3 MPa.

The hydrostatic pressure at depth of 3520 m (assuming a hydrostatic gradient of 10 - 11 MPa/km) is 35.2 - 38.7 MPa. The maximum pressure in the Triassic reservoir at 3520 m resulting from 1D Neogene and Quaternary sedimentary loading is  $38.7 + 9.3 = 48$  MPa. Clearly, this sedimentary loading is not adequate to explain the measured pressure of 67.5 MPa. It is possible that sedimentary loading over a longer time is still reflected in the observed pressure; for example, sedimentary loading since the beginning of the Tertiary. For a sedimentary load of 1500 m and the same assumptions, the maximum generated pressure at 3520 m is 53 MPa. Yet this prolonged sedimentary loading still only explains part of the measured overpressure.

In addition, the assumed undrained condition (i.e. no flow during 60 My) is obviously very restrictive, and loading has not been continuous during the entire Cenozoic: the generated pressures due to Cenozoic sedimentary loading will most probably be less than the calculated values. The observed dimensionless overpressure in the Triassic reservoir (0.7) is close to its maximum value, indicating that present-day conditions are probably favourable for hydraulic fracturing of brittle rocks allowing groundwater flow and pressure reduction.

Tertiary and Quaternary sedimentary loading is an important pressure generating mechanism, but cannot explain completely the observed present-day overpressures. Possible additional pressure-generating mechanisms acting on Triassic units during the Cenozoic include: a. mechanisms related to ongoing deeper burial of the reservoir (pore volume reduction by chemical compaction and salt cementation; pressure redistribution by groundwater flow; aquathermal pressuring of the pore water); b. increasing lateral compressive stresses; c. pressure redistribution by density-controlled flow of groundwater; d. salt deformation during the Cenozoic. The decrease of pore volume in sandstones related to sedimentary loading includes mechanical compaction (predominant in the first 1500-2000 m of burial) as well as chemical compaction, which is of increasing importance at greater burial depth (e.g. Bjørlykke 1989). The Jurassic and Triassic units in the northern offshore are at burial depths of  $\geq 2000$  m. Therefore, volume reduction by chemical compaction has the potential to help generate some of the overpressure observed in these reservoir units. In addition, it is known that Triassic units have been affected by salt cementation (e.g. Purvis and Okkerman 1996). Whether the process of salt cementation was also active during the Cenozoic is not known to the author. The characteristics of changes in intraplate compressive stresses during the Cenozoic are an area of active research (Chapter 3) and so is their possible influence on overpressure distribution (Chapter 1). The occurrence of Carboniferous sourced gas accumulations in Triassic reservoirs indicates the present-day or past existence of permeable pathways through the Zechstein seal (zones of salt depletion, fault zones). Such permeable pathways will also allow flow of groundwater and associated transfer of pressures from pre-Zechstein units to Triassic units.

The severely overpressured conditions show that flow in the syn-rift reservoir units and the pre-and early-rift Triassic units in the Central North Sea Graben and the Terschelling Basin is restricted to flow within compartments bounded by salts and faults. Flow from such compartments probably only occurs episodically as indicated by the dimensionless pressures being close to maximum values in both Triassic and Jurassic units.

## 7.7 Overpressures and fluid flow in Upper Rotliegend units

Much of the dimensionless overpressure distribution in the offshore blocks L and M, and the onshore provinces of Friesland and Groningen (Figure 22) is based on pressure observations in the Upper Rotliegend Group. Figure 22 shows that sharp changes of dimensionless overpressure occur in the area between the Central North Sea Graben and the Central Offshore Saddle/Texel IJsselmeer High, between the Terschelling Basin and the Vlieland High, and in the area of the Waddenzee between the southern M blocks and onshore Netherlands (see Figure 12 for location of the structural units).

The overpressure distribution in the Upper Rotliegend Group (Slochteren Formation) seems to demonstrate the influence of the sealing capacity of cap rocks (Zechstein salt Members) and, to a minor extent, the influence of fault zones on the lateral distribution of permeability and on fluid flow. Severe overpressures occur along the northern limit of the Slochteren Formation below a thick Zechstein seal. The magnitude of overpressures decreases in the direction of decreasing sealing capacity of the Zechstein Group, e.g. towards the Texel IJsselmeer High, and in the direction of increasing thickness and permeability of the Slochteren Formation (Verweij 1990a). The groundwater in the Slochteren unit is near hydrostatic to slightly overpressured in onshore and offshore Netherlands south of the High, where Zechstein salts are less thickly developed and of limited areal extent. Here, pressure-generating mechanisms and fluid flow seem to be in equilibrium. The Slochteren Formation is dissected by numerous faults. It seems that the fault zones reduce the lateral permeability of the Slochteren Formation (adjacent fault compartments can have very different pore pressures) but do not prevent the lateral flow of groundwater and associated pressure redistribution on a regional scale. The distributions of the overpressures in the Slochteren hydrostratigraphic unit south of the Central North Sea Graben suggest a south and southwestward lateral dissipation of overpressures, which may be associated with a general pattern of flow directed from the Cenozoic depocentres in the northern offshore towards the Central Offshore Saddle and the Texel IJsselmeer High. Because of increasing disruption of the lateral continuity of the Zechstein Salt Members towards the south in both offshore and onshore Netherlands, vertical flow between pre-Zechstein and younger permeable units becomes possible, allowing the overpressures to dissipate (Verweij 1990a).

Also interesting is the difference in overpressure observed in the Triassic unit and the Slochteren Formation in an L-block: the highest overpressures values are reported for the Triassic units. A possible explanation is that while overpressures are able to dissipate laterally from the Slochteren Formation, the overpressures are maintained in the Triassic unit (possibly due to lateral and vertical sealing of the unit by Zechstein salt structures and overlying Triassic evaporites).

## 8 Hydrochemistry and temperatures in onshore and offshore Netherlands

Present-day data of water resistivity, water analyses and temperature data provide additional characterisation of the subsurface fluid conditions. In addition, the data were analysed with the objective to reconstruct present-day and paleo fluid flow conditions.

### 8.1 Hydrochemistry

#### 8.1.1 Factors influencing present-day chemical compositions of groundwater

Groundwater chemistry and the chemical composition of rocks are dynamically coupled by mineral-water equilibria and by the rate and mechanisms of groundwater transport (Ingebritsen and Sandford 1998). The present-day chemical composition of the groundwater in a basin is the combined result of the original composition of the syn-sedimentary water, initial geochemistry of the sedimentary rocks, the throughflow of groundwater, the source(s) of the flowing groundwater and water-rock interaction during basin evolution. Basin evolution influences the type of fluids and solutes that can be generated and the distribution and characteristics of fluid flow pathways (Burley 1993). From this it can be inferred that, the post-Carboniferous evolution of subsidence, sedimentation, uplift and erosion of onshore and offshore Netherlands influenced not only the fluid sources, fluid flow and fluid flow pathways but also the lateral and vertical distribution of the potential solute sources and their relationships to permeable hydrostratigraphic units (acting as solute sinks). The main solute sources and solute sinks (Figure 23) in the Netherlands subsurface coincide largely with the major aquitards and aquifers, respectively, as given in Figure 20 (see also Chapter 1, Figure 3). The main solute sources include: shales and coals of the Limburg Group; carbonates and evaporites (anhydrite/gypsum, halite, K-Mg salts) of the Zechstein Group; evaporites, carbonates and shales of the Upper Germanic Trias Group; shale and bituminous shales of the Altena Group; claystone members of the Schieland, Scruff and Rijnland Groups; marine clay members of the North Sea Supergroup.

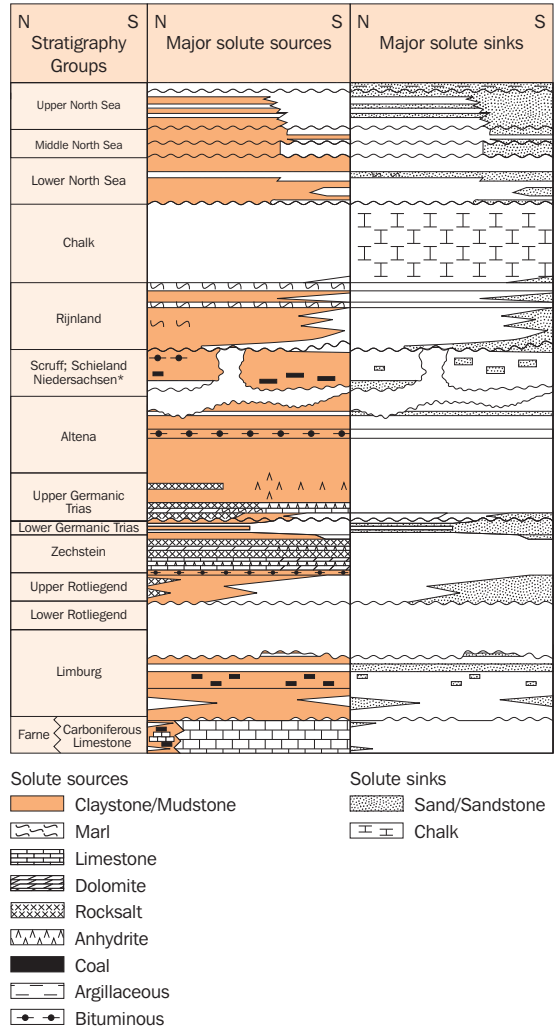


Figure 23 Main solute sources and solute sinks in the subsurface of onshore and offshore Netherlands



In this study the Chalk Group is considered to be a permeable hydrostratigraphic unit and, following Burley (1993), also a solute sink.

Most groundwater flow during basin evolution is expected to be concentrated through the major aquifers and distinct permeable fault and fracture zones. Most solutes are transported predominantly by advection through these permeable zones, and they may be transported into adjacent poorly permeable zones by diffusion.

Meteoric water has an extremely small content of total dissolved solids, is slightly to moderately acidic and has a high oxygen content. After infiltration in a recharge area of a topography-induced groundwater system, the chemical characteristics of groundwater evolve systematically in the direction of flow (Bredehoeft et al. 1982, Collins 1975, Herczeg et al. 1991, Ingebritsen and Sanford 1998, Tóth 1980, 1999). The salinity increases with depth and along the flow path, mainly because the solubility of most minerals increases with increasing temperature, and the water reacts with the more readily soluble minerals along its flow paths. The waters tend to evolve from a dilute calcium bicarbonate type in recharge areas toward a more concentrated sodium chloride or calcium chloride type. Systematic changes in the present-day shallow topography-induced groundwater flow systems in onshore Netherlands are well known, including the widespread influence of mixing of waters of marine and meteoric origin (e.g. Stuyfzand 1993, Nolte 1996).

In an actively filling and subsiding basin (Chapter 1) the initial modifications to the original chemical composition of the groundwater of marine or continental origin take place in the shallow subsystem of groundwater flow induced by sedimentary loading, characterised by cross-formational vertical upward groundwater flow. Water and dissolved ions move from the compacting aquitards / solute sources into the overlying aquifers, increasing their salinity. In addition, shaly aquitards may act as semi-permeable membranes that retard the passage of dissolved ions while allowing relatively unrestricted passage of neutral water molecules across the aquitard (Bredehoeft et al. 1963, 1982, De Sitter 1947, Graf 1982). As cross-formational flow and the selective filtration of cations and anions continue, the groundwater on the influent side of a shale membrane – that is in the underlying aquifer – will become progressively more saline (Hanor 1994).

In the intermediate subsystem, there is no cross-formational flow through the aquitards: hence no membrane filtration and only vertical expulsion of water and dissolved ions from the aquitards towards the adjacent aquifers. In addition, flow is focussed laterally through the aquifers. The groundwater flow conditions allow groundwater of different origins and chemical compositions to be introduced into the aquifer and the chemical composition of the groundwater in the aquifers of the intermediate system may become extremely variable. In general, the different transport processes act to increase the salinity of the aquifers.

In the deep (severely overpressured) subsystem, the flow of groundwater through both the aquifer and aquitard units is restricted. As a consequence, transport of solutes by groundwater flow is restricted and diffusion (transport of mass in response to concentration gradients) becomes the main process of mass distribution (e.g.

Bjørlykke 1989, Ranganathan and Hanor 1987). In the absence of active groundwater flow, the groundwater in the aquifers at greater depths and associated higher temperatures will tend to be in equilibrium with most minerals present (Bjørlykke 1989). Hanor (1994) suggests that thermodynamic buffering by silicate-carbonate  $\pm$  (halide) mineral assemblages exerts a first order control on groundwater compositions, even at temperatures of less than 100 °C.

In addition to the generally observed increase in salinity of the groundwater in the aquifers/reservoir units in an actively filling and subsiding basin, such as the present North Sea Basin, the difference between the salinity of groundwater in fine-grained aquitards and the adjacent coarser-grained aquifers seems to increase with depth (Dickey 1988, Hunt 1979). The total dissolved solids of the groundwater in the aquifers often exceed those in the aquitards (e.g. Fertl 1976). Two processes may explain these observations. In the shallow and intermediate subsystems, both water and dissolved ions may move from the compacting aquitards into the adjacent aquifers. However, the movement of some water molecules is inhibited by their adsorption on mineral surfaces of the fine-grained rocks (structured water), while the dissolved ions are relatively free to move into the coarse-grained rock, increasing the salinity of its groundwater. As compaction proceeds, all the larger pores in the aquitard lose their salts to the aquifers, until finally only small pores with fresh (structured) water remain (Hinch 1980). The dehydration of clay minerals at greater depths and associated higher temperatures and pressures works to reduce the salinity in the aquitards (e.g. Bjørlykke 1989).

Many sedimentary basins contain brines, i.e. groundwater with salinities well in excess of the average sea water salinity of 35 000 mg/l. Subaerial evaporation of marine and continental waters and the subsurface dissolution of evaporites have the potential for producing brines having both the salinities and dissolved chloride concentrations of most subsurface brines (Hanor 1994). The subsurface dissolution of mineral salts in particular may produce very saline water whose composition depends on the particular minerals present, such as halite, anhydrite and sylvite (e.g. Domenico and Schwartz 1998, Hanor 1994). Dissolution of halite can lead to large increases in sodium and chloride. This will initially result in enhanced groundwater salinity near salt layers and diapirs (e.g. Morton and Land 1987). The subsequent movement of the resulting brine through aquifers or permeable fault and fracture zones may spread brines over large distances, as shown for example by Hanor and Sassen (1990), and Gvirtzman and Stanislavski (2000a, b). A halite-saturated groundwater can reach maximum salinities of 250 000 - 300 000 mg/l NaCl equivalent. In the Dutch part of the southern North Sea Basin abundant amounts of salts (Zechstein Group, Upper Germanic Trias Group) are available for dissolution and for increasing the salinity.

### 8.1.2 Salinity of groundwater

The depth-contour map of the interface between fresh and brackish groundwater (at 150 mg Cl<sup>-</sup>/l) for onshore Netherlands shows that the maximum depth of occurrence of fresh groundwater is 500 m in the southeasternmost onshore part of the Netherlands (Figure 24d). In the Holocene western and northern part of the Netherlands the fresh-brackish and brackish-salt (> 1000 mg Cl<sup>-</sup>/l) groundwater interfaces are metres to tens of metres apart. In the Roer Valley Graben, the interfaces are hundreds of metres apart (Zuurdeeg et al. 1989). The maximum depth of occurrence

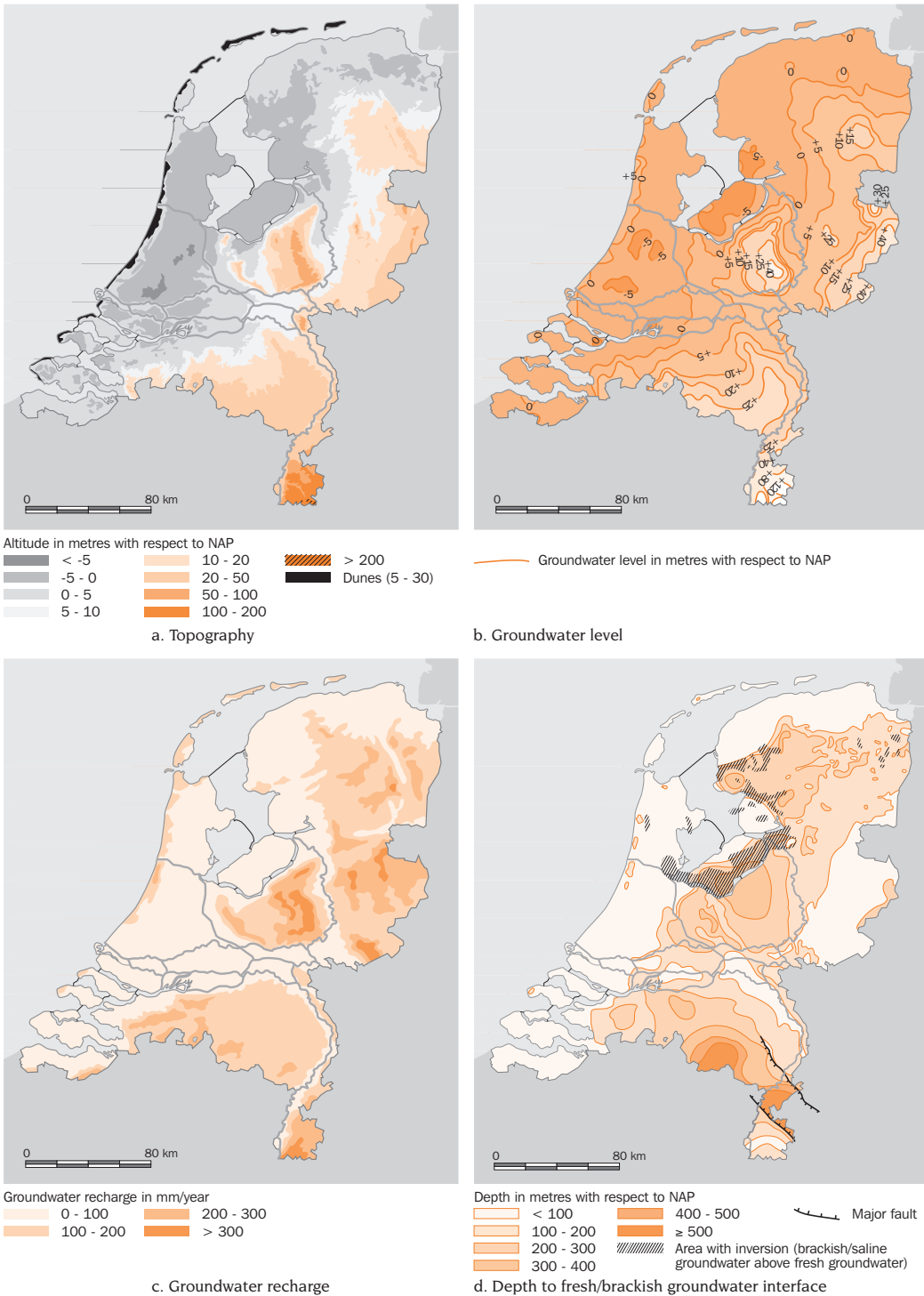


Figure 24 Surface topography of the Netherlands in relation to the elevation of the water table and depth of the fresh-brackish groundwater interface (From Dufour 2000)

of fresh groundwater is an indication of the minimum depth of penetration of recently active flow of groundwater of meteoric origin. Much of the groundwater of meteoric origin below the present fresh-salt water contact is of pre-Holocene origin (see Table 4.2 in Verweij 1990a). The dating of groundwater in discharge areas of supra-regional topography-induced groundwater flow systems in the southern onshore parts of the Netherlands has also revealed Pleistocene ages for the groundwater in this currently active groundwater flow system (>30 000 year; Stuurman et al. 2000).

Additional information on the salinity distribution of the groundwater in onshore and offshore Netherlands has been derived from measured resistivity values of the groundwater; the resistivity of subsurface waters is a proxy measure of the total quantity of ions in solution (TDS = total dissolved solids): the higher the TDS, the lower the groundwater resistivity. TDS can be expressed by the equivalent NaCl concentration (= salinity). For this purpose a database of approximately 230 measured resistivity values for Lower Cretaceous and older units was compiled from different published sources (mostly from ECL 1983, RRI 1985, 1988, 1990, Warren and Smalley 1994). Reported resistivity values were converted to values expressed in Ohmm at 25 °C (Schlumberger Log Interpretation Charts 1989). As the accuracy of the reported values varies considerably, only general conclusions can be drawn about the salinity distribution. More than 90% of the resistivity values vary between 0.12 and 0.04 Ohmm at 25 °C (Figure 25), corresponding to water salinities of approximately 55 000 to >200 000 mg/l NaCl. The groundwaters in the Lower Cretaceous and older units are predominantly brines. Highly saline waters with resistivities of less than 0.05 Ohmm at 25 °C are present in each of the units. The salinity of the groundwater shows large variations in all units. The waters in the Central Graben Subgroup and the Upper Rotliegend Group show the least variation in salinity. There is no obvious depth trend in salinity nor is there a trend of increasing salinities with increasing age of the stratigraphic units. Grouping the resistivity data per structural unit (basin, structural high) did not reveal such trends either. It is interesting to note that the least saline conditions are found in the oldest stratigraphic units (Figure 26), that is in the Carboniferous units in wells S02-01, E02-01 and in onshore well Apeldoorn (in well S02-01 and E02-01 the Carboniferous subgroups the Chalk Group).

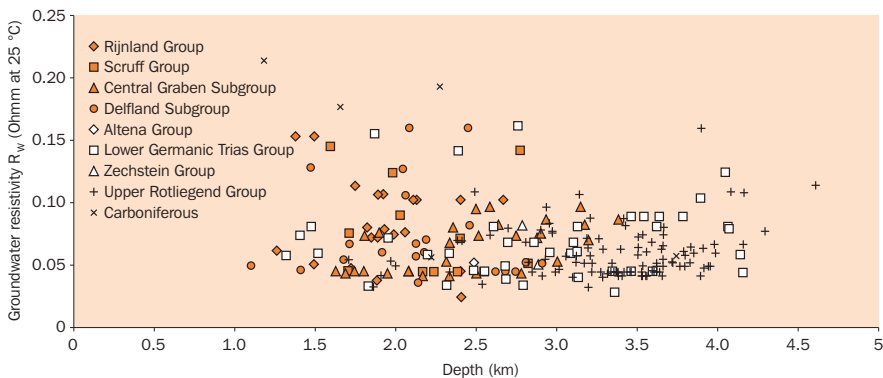


Figure 25 Groundwater resistivities in 9 stratigraphic units in offshore and onshore Netherlands (15 wells) (based on information from ECL 1983, RRI 1985, 1988, 1990 and the North Sea Formation Waters Atlas of Warren and Smalley 1994)

The resistivities of groundwater in the syn-rift Central Graben Subgroup are less than 0.10 Ohmm at 25 °C (>70 000 mg/l NaCl). The occurrence of the Central Graben Group is restricted to the Central North Sea Graben. Its lateral continuity is disrupted by Zechstein Salt structures. Lateral contact between the permeable units of the Central Graben Subgroup and Zechstein salt may explain the overall high salinity in the Central Graben Subgroup. In contrast the resistivities of the groundwater in the Delfland Subgroup, also of main syn-rift age, are more variable: from 0.035 to more than 0.15 Ohmm at 25 °C. The Delfland Subgroup is present in the southernmost part of the Central North Sea Graben and in the southern basins, i.e. partly outside the area of occurrence of Zechstein salt. Figure 26 shows that the least saline conditions are encountered in blocks Q10, Q11 and Q16, which are outside the area of occurrence of Zechstein salt.

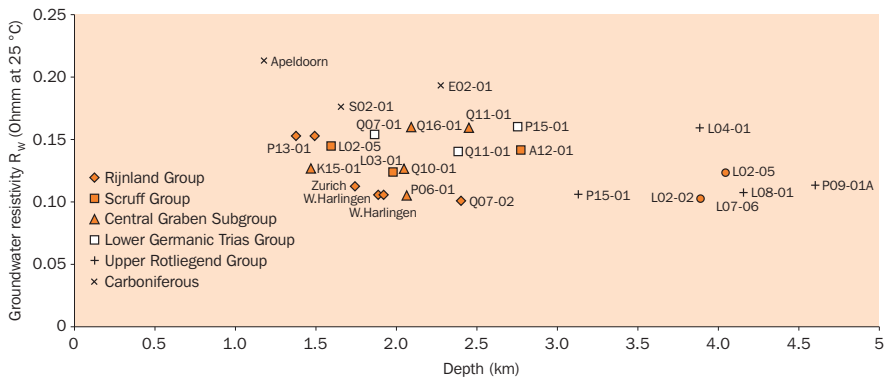


Figure 26 Groundwater resistivity values of more than 0.10 Ohmm at 25 °C in relation to stratigraphic unit, depth of measurement and well location

The least saline conditions in the Lower Germanic Trias Group also occur in the same area outside the distribution area of Zechstein salt (P15-01, Q07-01, Q11-01; however other  $R_w$  measurements in blocks P15 and Q7 indicate highly saline conditions).

The Rijinland Group shows large variations in resistivity of its groundwaters. The highest resistivity values occur in the southernmost part of the North Sea Basin (P13 block at 1400 m). Relatively saline conditions are observed in F18-04, L15-01, L16-01, P06-04a and Q01-04 ( $R_w < 0.05$  Ohmm at 25 °C).

The least saline conditions in the Rijinland Group, the Delfland Formation and possibly also the Lower Germanic Trias Group occur in the southernmost part of the North Sea Basin.

### 8.1.3 Chemical composition of groundwater

Water analyses data from groundwater and oil and gas wells provide information on the hydrochemical characteristics of the permeable hydrostratigraphic units of the North Sea Supergroup, Chalk Group, Rijinland Group, Lower Germanic Trias Group, Zechstein Group, and the Upper Rotliegend Group (Table 6). The data quality of available water analyses varies and is often uncertain (see e.g. Warren and Smalley 1994). A total of 118 individual water analyses from 28 offshore oil and gas

wells were available for this study. A large number of the water analyses of these Dutch offshore wells indicate minor to heavy contamination of the subsurface water by mud filtrate as reported by the analysing laboratories. The samples of 9 wells are not considered to be representative of actual subsurface waters, because analyses showed them to be either mud filtrate or subsurface water heavily contaminated with mud filtrate (findings based on laboratory reports). Table 6 includes water analyses data from wells with minor or no drilling fluid contamination. Qualitative reliability codes were assigned to the water analyses of the offshore wells: a. water analysis representative of subsurface water; b. water analysis probably representative of subsurface water: reliability cannot be deduced from the available analysis data only; c. water samples reported to have been contaminated to some extent with mud filtrate. Table 6 also includes previously published water analyses data.

The compositions of the water samples indicate that groundwaters of Upper Permian to Lower Cretaceous hydrostratigraphic units are chloride-dominated brines. Total dissolved solids were calculated by summing the concentration of all major and minor ions and are in the range of 60 000 mg/l to more than 300 000 mg/l. In all water samples sodium comprises 65 - 99% of the total cations and chloride comprises 93 - 99% of the total anions (in mg/l). Most brines can be classified as sodium-calcium cation facies waters. The composition of the brine at M07-01x classifies as calcium-sodium cation facies and the brines in P12-04, P06-06 and Nieuweschans are of sodium-potassium cation facies.

Cross plots of ionic concentrations as a function of total dissolved solids (Figures 27 and 28) show that salinity correlates strongly with chloride, sodium and calcium. Chloride and sodium data show an approximate 1 : 1 slope and calcium an approximate 2 : 1 slope with respect to total dissolved solids on the log-log cross plot (Figure 28). All chloride data are on the linear trend line in the cross plots. Not all the sodium data are on the linear trend line: relatively low sodium concentrations occur in the Upper Rotliegend Group at well M07-01x ( $\text{Na}^+ = 27\,500 - 30\,400$  mg/l for a TDS = 265 000 - 267 000 mg/l at a depth of 3245 - 3460 m) and to a lesser extent in the Houthem Formation at well Asten 2 (Table 6).

The increase in calcium concentration with increasing total dissolved solids is clearest for the waters in the Upper Rotliegend Group and in the Vlieland Sandstone Formation. A high content of total dissolved solids (>250 000 mg/l) in the Upper Rotliegend Group at well M07-01x coincides with relatively high concentrations of calcium ( $\text{Ca}^{++} = 59\,800 - 60\,900$  mg/l). In contrast the calcium concentrations are relatively low at high concentrations of total dissolved solids in the Detfurth Formation (P06-05:  $\text{Ca}^{++} = 15\,200 - 15\,800$  mg/l; P06-06:  $\text{Ca}^{++} = 310$  mg/l) and in the Zechstein Group (P02-05:  $\text{Ca}^{++} = 10\,650 - 11\,700$  mg/l).

The cross plots in Figures 27 and 28 do not show a regular increase of potassium with increasing total dissolved solids. Concentrations of potassium exceed 1000 mg/l in the Upper Rotliegend Group and the Detfurth Formation, and maximum values are observed in the Zechstein Group at P02-05 (at TDS > 300 000 mg/l,  $\text{K}^+ = 6150 - 7000$  mg/l). The magnesium concentration increases irregularly as a function of total dissolved solids. The highest concentrations of magnesium are observed in the Upper Rotliegend Group at M07-01x ( $\text{Mg}^{++} = 4590 - 6770$  mg/l). Concentrations exceeding 2000 mg/l occur in the Detfurth Formation (P06-05) and the Vlieland Sandstone Formation (P08-03).

Table 6 Water analyses data

| Well no.  | Structure   | Depth<br>(m) | TDS<br>mg/l | Na<br>mg/l   | K<br>mg/l | Mg<br>mg/l | Ca<br>mg/l | Sr<br>mg/l |
|---|-------------|--------------|-------------|--------------|-----------|------------|------------|------------|
| <b>North Sea Groups: Rupel Formation</b>              |             |              |             |              |           |            |            |            |
| Asten-2   | RVG         | 1500-1520    | 51475       | 16769        | 175       | 599        | 1400       | 123        |
| Broekhuizenvorst                                      | Venlo Block | 531-539      | 22130       | 7200         | 185       | 290        | 610        |            |
| <b>North Sea Groups: Dongen Formation</b>             |             |              |             |              |           |            |            |            |
| Nieuweschans  | Gron. High  | 537-582      | 122443      | 43000        | 290       | 870        | 2200       | 147        |
| <b>Chalk Group: Houthem Formation</b>                 |             |              |             |              |           |            |            |            |
| Asten-2   | RVG         | 1641-1651    | 47100       | 15950        | 191       | 616        | 1665       | 140        |
| (m –surface)  |             |              |             |              |           |            |            |            |
| <b>Rijnland Group: Vlieland Sandstone Formation</b>   |             |              |             |              |           |            |            |            |
| Wassenaar 27  | WNB         | 1310-1316    | 92730       | 30312        | 131       | 859        | 3977       | 289        |
| Wassenaar 12  | WNB         | 1200-1300    | 91040       | 29639        | 129       | 867        | 3958       | 288        |
| Meyendel 1  | WNB         | 1275-1283    | 91670       | 29862        | 129       | 851        | 4021       | 291        |
| Zoetermeer 14   | WNB         | 900-1000     | 75020       | 24280        | 126       | 878        | 3135       | 222        |
| Zoetermeer 37   | WNB         | 1130-1136    | 76440       | 24954        | 105       | 828        | 3118       | 225        |
| Pynacker 3  | WNB         | 1741-1790    | 110200      | 35857        | 165       | 854        | 5073       | 364        |
| Ysselmonde 22   | WNB         | 960-996      | 91210       | 29819        | 217       | 851        | 3588       | 540        |
| Ridderkerk 13   | WNB         | 1175-1449    | 80600       | 26402        | 239       | 856        | 2966       | 470        |
| De Lier 43  | WNB         | 1729-1770    | 87260       | 29295        | 128       | 681        | 2963       | 510        |
| De Lier 23A   | WNB         | 1733-1789    | 95250       | 31879        | 135       | 727        | 3419       | 496        |
| Q01-03  | BFB         | 1300         | 95360       | 27940        | 380       | 770        | 7360       |            |
|   | BFB         | 1300         | 97600       | 29620        | 480       | 760        | 6600       |            |
| Q04-04  | BFB         | 1023-1087    | 74200       | 24830        | 215       | 920        | 2400       | 155        |
| P08-03  | BFB         | 2830-2839    | 142930      | 40710        | 270       | 4300       | 7400       | 655        |
| <b>Scruff Group: Scruff Greensand Formation</b>       |             |              |             |              |           |            |            |            |
| F03-07  | CNSG        | 2485         |             |              |           | 1000       | 7400       |            |
| <b>Lower Germanic Trias Group: Detfurth Formation</b> |             |              |             |              |           |            |            |            |
| P06-05  | BFB         | 1335         | 312340      | 99660        | 2040      | 2550       | 15800      | 470        |
|   | BFB         | 1335         | 320640      | 100470       | 3200      | 4070       | 15200      | 440        |
| P06-06  | BFB         |              | 331920      | 128260       | 1010      | 4.8        | 310        | 6.9        |
| <b>Zechstein Group</b>                                |             |              |             |              |           |            |            |            |
| P02-05  | BFB         | 3011         | 311080      | 101080       | 7100      | 1760       | 11750      | 300        |
|   | BFB         | 3011         | 306910      | 100110       | 6100      | 1840       | 11700      | 370        |
|   | BFB         | 3011         | 303730      | 100700       | 7000      | 1530       | 9850       | 300        |
|   | BFB         | 3011         | 309920      | 102450       | 6500      | 1650       | 10650      | 325        |
|   | BFB         | 3011         | 312000      | 102260       | 6150      | 1720       | 11700      | 395        |
| <b>Upper Rotliegend Group: Slochteren Formation</b>   |             |              |             |              |           |            |            |            |
| Q07-01  | BFB         | 2375-2408    | 256084      | 83841 (Na&K) |           | 1290       | 13555      |            |
| L07-06  | COS         | 3929-3952    | 228121      | 63000        | 2100      | 3405       | 17335      |            |
| L10-19ST  | COS         | 3988-4019    | 78170       | 18020        | 3730      | 2040       | 4420       | 115        |
|   | COS         | 3988-4019    | 79380       | 18720        | 3840      | 1990       | 4450       | 115        |
|   | COS         | 3988-4019    | 60880       | 15290        | 2010      | 1400       | 3680       | 110        |
| K12-03  | BFB         | 3600         | 257445      | 76906        |           | 3246       | 17495      |            |
| L07-07  | COS         | 3655-3677    | 260901      | 76333        | 2066      | 4499       | 14830      |            |
| L11-01  | COS         | 3620         | 217506      | 63351        |           | 2176       | 16874      |            |
|   | COS         |              | 191888      | 56160        |           | 1513       | 15190      |            |
| P05-01  | BFB         | 3053-3088    | 103152      | 35600        | 1160      | 61         | 3210       |            |
|   |             |              | 50513       | 16500        | 700       | 61         | 2000       |            |
|   | BFB         | 3053-3088    | 152311      | 49700        | 1580      | 300        | 7310       |            |
|   | BFB         | 3053-3088    | 149978      | 49000        | 1590      | 426        | 7010       |            |
| M07-01x   | VH          | 3245-3460    | 265000      | 27500        | 1620      | 6770       | 59800      |            |
|   | VH          | 3245-3460    | 267000      | 30400        | 1620      | 4590       | 60900      |            |
| P12-04x   | WNB/YMH     | ± 3000       | 142670      | 50220        | 1150      | 1475       | 2250       | 30         |
|   |             |              | 143040      | 50990        | 1030      | 1280       | 2050       | 30         |
| K05-02  | CBH         | 3548-3555    |             | 71700        | 2390      | 1640       | 2530       |            |
|   | CBH         | 3548-3555    |             | 21500        | 1240      | 730        | 1040       |            |

1 Van der Weiden 1983 (concentrations given in ppm)    2 Zuurdeeg et al. 1989    3 Glasbergen 1984    4 Released well data

| Ba mg/l | Cl mg/l | HCO <sub>3</sub> mg/l | SO <sub>4</sub> mg/l | PO <sub>4</sub> mg/l | Fe total mg/l | Fe mg/l | Sample | Date | Data source | Reliability |
|---------|---------|-----------------------|----------------------|----------------------|---------------|---------|--------|------|-------------|-------------|
| 7.9     | 31500   | 44                    | <0.23                | 43.4                 |               | 149     |        | 1988 | 2           |             |
|         | 12939   | 514                   | 230                  | 0                    |               | 3.28    |        | 1983 | 3           |             |
|         | 73867   | 163                   | 1740                 |                      |               | 9.9     |        | 1983 | 3           |             |
| 60      | 27600   | 273                   | 8.4                  | 29.4                 |               | 7       |        | 1987 | 2           |             |
| 48.8    | 56600   | 90                    | 89.6                 | 11.5                 |               | 18.4    | Prod   | 1983 | 1           |             |
| 45.6    | 55610   | 90                    | 90.9                 | 6.61                 |               | 23.9    | Prod   | 1983 | 1           |             |
| 37      | 56010   | 90                    | 88.3                 | 9.75                 |               | 19.2    | Prod   | 1983 | 1           |             |
| 48.2    | 45830   | 150                   | 66.1                 | 4.53                 |               | 21.1    | Prod   | 1983 | 1           |             |
| 21.1    | 46690   | 150                   | 65.6                 | 4.53                 |               | 35.1    | Prod   | 1983 | 1           |             |
| 31.7    | 67190   | 100                   | 157.4                | 10.8                 |               | 31.7    | Prod   | 1983 | 1           |             |
| 40.1    | 55370   | 270                   | 78.8                 | 6.27                 |               | 27.5    | Prod   | 1983 | 1           |             |
| 40.3    | 49000   | 210                   | 64.8                 | 5.22                 |               | 16.1    | Prod   | 1983 | 1           |             |
| 27.5    | 52880   | 230                   | 61.3                 | 16.4                 |               | 35.1    | Prod   | 1983 | 1           |             |
| 31      | 57830   | 230                   | 74.9                 | 14.3                 |               | 55.9    | Prod   | 1983 | 1           |             |
| 27      | 58380   | 270                   | 230                  |                      | 13            | 0.1     | DST    | 1979 | 4           | a           |
| 25      | 59880   | 230                   | 10                   |                      | 33            | 0.2     | DST    | 1979 | 4           | a           |
| 20      | 45360   | 260                   | 43                   |                      | 15            | 0.5     |        | 1983 | 4           | a           |
| 7.4     | 89050   | 68                    | 345                  |                      | 250           | 125     | DST    | 1983 | 4           | a           |
|         | 114000  |                       |                      |                      |               |         | Prod   | 1981 | 4           | b           |
| 0.1     | 191090  | 50                    | 510                  |                      | 810           | 170     | DST    | 1979 | 4           | c           |
| 0.1     | 196410  | 130                   | 670                  |                      | 220           | 45      | DST    | 1979 | 4           | c           |
| <0.1    | 190740  | 235                   | 11350                |                      | 4.0           | <0.1    | RFT    | 1980 | 4           | c           |
| 39      | 187140  | 355                   | 1520                 |                      | 185           | 3.3     | DST    | 1983 | 4           | c           |
| 48      | 185310  | 255                   | 1130                 |                      | 825           | 14      | DST    | 1983 | 4           | c           |
| 30      | 182550  | 315                   | 1390                 |                      | 2000          | 14      | DST    | 1983 | 4           | c           |
| 38      | 186680  | 255                   | 1310                 |                      | 3160          | 13      | DST    | 1983 | 4           | c           |
| 40      | 188320  | 250                   | 1130                 |                      | 1850          | 5       | DST    | 1983 | 4           | c           |
|         | 156555  | 232                   | 450                  |                      | 161           |         |        | 1973 | 4           | a           |
|         | 140764  | 586                   | 438                  |                      |               | 491     | DST    | 1974 | 4           | a           |
| 1.8     | 46230   | 800                   | 950                  |                      | 1860          |         |        | 1979 | 4           | a           |
| 2.3     | 47220   | 485                   | 930                  |                      | 1630          |         |        | 1979 | 4           | a           |
| 2       | 37010   |                       | 410                  |                      | 970           |         |        | 1979 | 4           | a           |
| 0       | 159007  | 12                    | 483                  |                      |               | 297     | DST    | 1976 | 4           | b           |
|         | 162216  | 366                   | 373                  |                      |               | 218     | DST    | 1975 | 4           | b           |
|         | 134012  | 238                   | 411                  |                      |               | 444     | DST    | 1971 | 4           | b           |
|         | 117349  | 470                   | 888                  |                      |               | 318     | DST    | 1971 | 4           | b           |
|         | 58800   | 854                   | 3340                 |                      |               | 111     | DST    | 1968 | 4           | b           |
|         | 27200   | 480                   | 3210                 |                      |               | tr      | DST    | 1968 | 4           | b           |
|         | 90400   | 732                   | 2150                 |                      |               | 111     | DST    | 1968 | 4           | b           |
|         | 88460   | 732                   | 2620                 |                      |               | 111     | DST    | 1968 | 4           | b           |
|         | 169000  | 110                   | 270                  |                      |               |         | DST    | 1969 | 4           | c           |
|         | 169000  | 250                   | 280                  |                      |               |         | DST    | 1969 | 4           | c           |
| 3.4     | 85020   | 580                   | 1940                 |                      | 1.5           | <0.1    | DST    | 1983 | 4           | b           |
| 3.5     | 85260   | 610                   | 1790                 |                      | 1.2           | <0.1    | DST    | 1983 | 4           | b           |
|         | 120000  |                       |                      |                      |               |         | Prod   | 1985 | 4           | c           |
|         | 38200   |                       |                      |                      |               |         | Prod   | 1985 | 4           | c           |



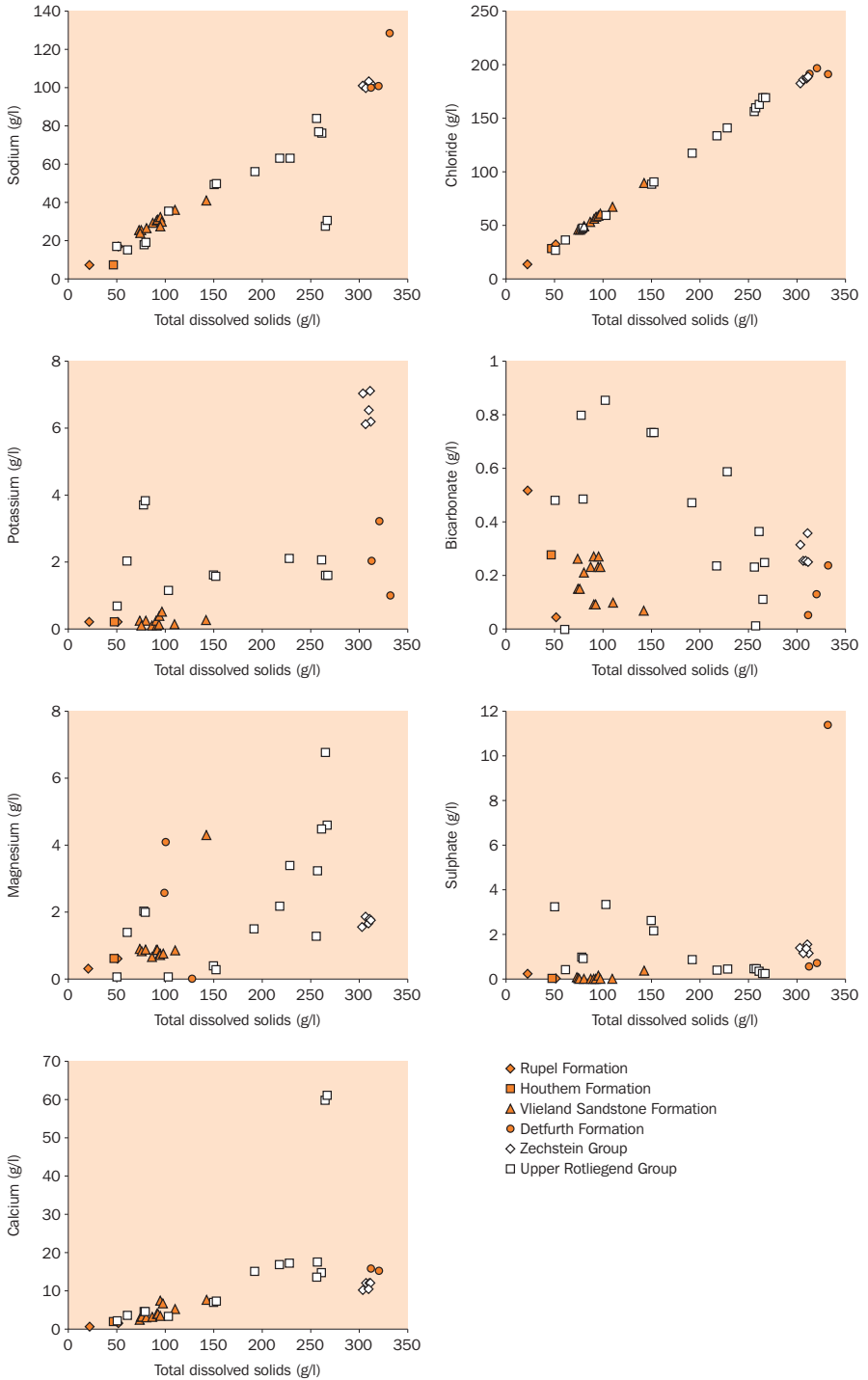


Figure 27 Cross plots of ionic concentrations as a function of total dissolved solids for the onshore and offshore Netherlands

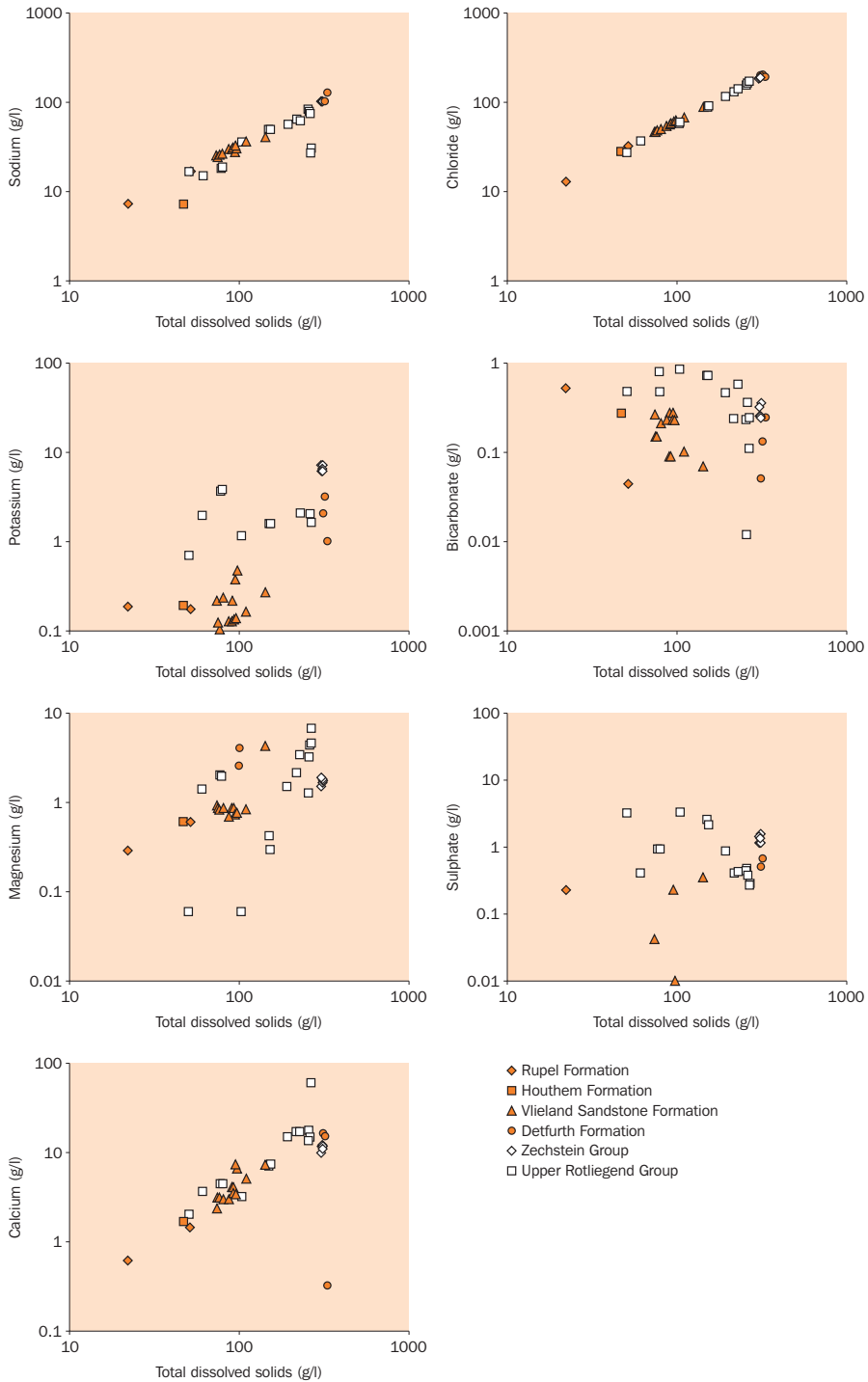


Figure 28 Log-log plots of ionic concentrations as a function of total dissolved solids for onshore and offshore Netherlands

The bicarbonate concentration shows a general decrease with increasing total dissolved solids in the Upper Rotliegend Group for TDS > 100 000 mg/l. A weak trend of decreasing bicarbonate concentrations can be recognised in Figure 27 for the Vlieland Sandstone Formation ( $\text{HCO}_3^-$  content decreases from 260 mg/l at TDS = 74 200 mg/l in Q04-04 to 68 mg/l at TDS 142 930 mg/l in well P08-03). The two water analyses available for the Rupel Formation in onshore Netherlands (Asten2 and Broekhuizenvorst) also show a sharp decrease of bicarbonate content with increasing total dissolved solids (Table 6).

Figures 27 and 28 do not show a clear trend in the cross plots of sulphate as a function of total dissolved solids. Low sulphate concentrations occur in the Vlieland Sandstone Formation (Q01-03, Q04-04, Q01-03) and in the Rupel Formation (Broekhuizenvorst). The highest concentration of sulphate is reported for the water in the Detfurth Formation at P06-06 (Table 6).

Previous studies provide additional information on the sources and evolution of groundwater in the North Sea Groups and the Vlieland Sandstone Formation in onshore Netherlands. Glasbergen (1984) and Zuurdeeg and Coenegracht (1986) reconstructed the evolution of the chloride-dominated brine with a sodium-potassium cation facies encountered in the Eocene Dongen Formation at Nieuweschans in the northeastern part of onshore Netherlands (Table 6). The waters are in large part of meteoric origin and contain a large amount of dissolved evaporites (Glasbergen 1984). Glasbergen reports a  $^{14}\text{C}$  age of only  $\geq 19\,000$  years for the brine in the Dongen Formation at Nieuweschans. Zuurdeeg and Coenegracht (1986) reconstructed the chemical characteristics of groundwater from claystone and sandstone samples of the Dongen Formation and found that the claystones contain the least saline waters today. They suggest that the originally marine pore water of the Dongen Formation started to be replaced by water of meteoric origin in the Tertiary during periods of nondeposition and erosion, e.g. during the Eocene-Oligocene, and continued in Pliocene-Pleistocene times when continental conditions prevailed. This flushing by waters of meteoric origin probably reached a minimum depth of 600 m and lowered the salinity to at least 4300 mg/l Cl (Zuurdeeg and Coenegracht 1986). At the end of the Pleistocene the Dongen Formation at Nieuweschans was part of a topography-induced groundwater flow system that also included salt structures: the infiltrating groundwater could interact with a salt diapir before reaching Nieuweschans (Glasbergen 1984, Zuurdeeg and Coenegracht 1986). Dissolution of rock salt and gypsum or anhydrite turned the fresh meteoric waters into brines. The subsequent flow of brines towards Nieuweschans was focussed through the aquifers of the Dongen Formation and increased the groundwater salinity in the aquifer at Nieuweschans, while the salinity in the adjacent claystones remained relatively low. Zuurdeeg et al. (1989, Heederik and Hurdeman 1988) found a relatively low content of chlorides (well below the chloride content of seawater) in the groundwater of clay members of the Rupel Formation at depths of 1400-1500 m at Asten in the Roer Valley Graben. The chloride content of the adjacent sand members of the Rupel Formation is higher than the chloride content of seawater. Zuurdeeg et al. (1989) suggested that the relatively low content of chlorides indicate a former deeper extension of the topography-induced groundwater flow system in comparison with the present-day systems.

In the West Netherlands Basin, brines in the Vlieland Sandstone Formation at depths of approximately 1000 to 1800 m are of meteoric or partly meteoric origin. Originally the formation contained syndepositional marine waters. The meteoric origin of the present-day groundwaters was inferred by Van der Weiden (1983) from the isotopic composition ( $\delta D$  and  $\delta^{18}O$ ) of four water samples from wells Wassenaar27, Pijnacker3, IJsselmonde22, De Lier23A.

In conclusion, the groundwaters of Upper Permian to Lower Cretaceous hydrostratigraphic units are chloride-dominated brines. The total dissolved solids correlate strongly with chloride, sodium and calcium. There is a weak trend of increasing magnesium concentration and of decreasing bicarbonate concentration with increasing total dissolved solids. These general characteristics of the deeper subsurface waters in onshore and offshore Netherlands are consistent with the chemical characteristics of groundwater in other sedimentary basins influenced by salt domes, such as the UK southern and central North Sea basin (Bjørlykke 1989, Warren and Smalley 1994) and Gulf of Mexico Basin (e.g. Hanor 1994). Hanor (1994) suggested, for the Gulf of Mexico area, that the first order controls on chemical composition of the groundwater are dissolution of halite and subsequent buffering of pore water composition by multi-phase silicate-carbonate mineral assemblages. He states that dissolution of salt alone should produce a progressively NaCl dominated fluid without significant increase in calcium, magnesium, potassium and strontium. The groundwaters in the deeper subsurface of onshore and offshore Netherlands show a clear increase in calcium and magnesium indicative of (prolonged) water-rock interaction. When groundwater reaches saturation with respect to halite, the sodium concentration progressively declines with increasing salinity, while chloride continues to increase. The buffering of the groundwater will shift from a strictly silicate-carbonate assemblage to one involving halite as well; and as a consequence with increasing total dissolved solids calcium and potassium become increasingly important solutes (Hanor 1994). The characteristics of the water analysis of M07-01x clearly illustrate Hanor's observations: TDS at M07-01x exceeds 265 000 mg/l, the sodium content is relatively low and the calcium and magnesium concentrations are relatively high. Relatively high concentrations of potassium in relation to highly saline brines occur in the Zechstein Group at well P02-05.

Very saline brines of high salinity in the Netherlands subsurface are not necessarily very old, stagnant waters, as shown by the age and chemical composition of the water sample of Nieuweschans (age approximately 19 000 years, TDS = 122 443 mg/l; Table 6).

The groundwater resistivities and the water analyses data show that the least saline groundwaters in Tertiary and older hydrostratigraphic units occur in the southern onshore and offshore parts of the Netherlands. Two conditions in these southern areas may be responsible for the less saline groundwaters in the subsurface: 1. absence of major evaporite (halite) deposits and 2. meteoric flushing during Tertiary and especially Quaternary times. Zechstein evaporites are absent in the southern parts of the Netherlands, and therefore no major solute source is available for producing very saline waters. During Tertiary and Quaternary times continental conditions prevailed more often in the southern part of the study area and associated topographic relief of the ground surface was larger in comparison with the northern parts. For example, uplift of the Southern Early Tertiary High at the Eocene-Oligocene boundary, uplift

of the Ardenno–Rhenish Massif since Oligocene times and subaerial conditions in the southern part of onshore and offshore Netherlands from Waalian to the beginning of the Eemian in Pleistocene times (Chapter 2) all favoured the development of topography-induced groundwater flow and associated flushing of the subsurface by infiltrating meteoric waters.

The flow of groundwater as described by the generalized Darcy equation (e.g. De Marsily 1986) depends on the density and viscosity of groundwater. The density and viscosity of groundwater are controlled by the concentration of dissolved solids, and by the temperature and pressure of the groundwater. The viscosity is most strongly influenced by temperature (e.g. Garven and Freeze 1984a). The density increases with increasing concentration of dissolved solids and increasing pressures, whereas a temperature increase cause a decrease in density (e.g. Adams and Bachu 2002, Garven and Freeze 1984b). Over the range of conditions encountered in a basin, the salinity (TDS) may have the greatest impact on density followed by temperature (Adams and Bachu 2002). Differences in the density of the groundwater are a driving force for groundwater flow (Chapter 1) and as a consequence may also enhance or retard flow induced by other mechanisms (e.g. Bachu 1995). In onshore and offshore Netherlands the concentration of total dissolved solids varies from freshwater concentrations at very shallow depths in onshore Netherlands (Figure 24) and approximately 22 000 mg/l in Tertiary units at 500 m depth in onshore Netherlands to 330 000 mg/l in Triassic and Zechstein hydrostratigraphic units in offshore Netherlands (Table 6). The water resistivity and the water analyses data pointed to large variations in concentration of total dissolved solids in all units. The associated variations in density of the groundwater result in variations in hydrostatic pressures of the groundwater (Chapter 1) in all hydrostratigraphic units in addition to density related variations in hydrostatic pressure between units. Such variations in density also influence present-day fluid flow and over-pressure conditions.

## 8.2 Temperatures

### 8.2.1 Factors influencing present-day temperature and heat flow distribution

The geothermal system in the crust is governed mainly by input of heat from the mantle, heat generated internally by the decay of radioactive isotopes in crustal rocks, the temperature at the earth's surface and the transport of heat through the crust towards the surface. The main mechanisms of heat transport are conduction and convection by flowing fluids.

#### *Thermal diffusivity*

Heat conduction is largely responsible for the general increase of temperature as a function of depth. The heat transferred by conduction depends solely upon the thermal diffusivity and the temperature gradient, where thermal diffusivity is the ratio of the thermal conductivity to the volumetric heat capacity of the medium (rock matrix and pore fluids). The volumetric heat capacity  $c$  of a medium is the amount of heat per unit volume required to raise the temperature 1K and is the product of the specific heat capacity ( $c_r$  or  $c_w$ ) at constant pressure and of density ( $\rho_r$  or  $\rho_w$ ) of the rock or fluid. The specific heat capacity of water is four times as high as that of rocks. For the

great majority of rock matrix the magnitude lies within 20% of  $2.3 \times 10^6 \text{ Jm}^{-3}\text{K}^{-1}$  (Beck 1988). For porous rocks, the volumetric heat capacity is the geometric mean of the rock matrix and the pore fluid heat capacities. ( $c_r \rho_r \sim 1000 \text{ Jkg}^{-1}\text{K}^{-1} \times 2300 \text{ kgm}^{-3} = 2.3 \times 10^6 \text{ Jm}^{-3}\text{K}^{-1}$ ;  $c_w \rho_w \sim 4200 \text{ Jkg}^{-1}\text{K}^{-1} \times 1000 \text{ kgm}^{-3} = 4.2 \times 10^6 \text{ Jm}^{-3}\text{K}^{-1}$ ; assuming 10% porosity the heat capacity of the porous medium is  $c = 0.1 c_w \rho_w + 0.9 c_r \rho_r = 2.5 \times 10^6 \text{ Jm}^{-3}\text{K}^{-1}$ ). Hence, the thermal diffusivity of a basin fill is approximately  $10^{-6} \text{ m}^2\text{s}^{-1} = 32 \text{ km}^2 \text{ My}^{-1}$ , assuming a bulk thermal conductivity of  $2.5 \text{ Wm}^{-1}\text{K}^{-1}$  and a volumetric heat capacity of  $2.5 \times 10^6 \text{ Jm}^{-3}\text{K}^{-1}$ .

### Fluid flow

Groundwater flow has the potential to be an effective agent for redistribution of heat in the subsurface (Chapman and Rybach 1985, Deming 1994a-b, Jessop and Majorowicz 1994, Lampe and Person 2000, Person and Garven 1992, Willet and Chapman 1987): in addition to the flow aspects, this is because the specific heat capacity of water is more than four times as high as that of rocks. Vertically directed fluid flow, i.e. flow perpendicular to the isotherms, can, in particular, induce temperature and heat flow anomalies. The magnitude of the thermal anomaly caused by groundwater flow increases exponentially as depth of flow system and flow velocity increase linearly (Deming 1994b). Deming calculated the reduction of surface heat flow (and geothermal gradient) as a function of groundwater velocity and depth of a groundwater system for steady state conditions: for example, downward flow through 1000 m at a Darcy velocity of 10 mm per year resulted in a 40% reduction of the surface heat flow, while downward flow through 5000 m at a velocity of 1 mm per year resulted in a 23% reduction. Focussed flow of groundwater through aquifers or permeable fault and fracture zones in topography and sedimentary loading induced groundwater flow systems may result in localised heat advection through less permeable adjacent rocks where heat conduction remains the dominating mechanism (Vasseur and Demongodin 1995).

The Peclet number (Pe) may be used for a quick assessment of the possible influence of a regional groundwater flow on heat transport (assuming steady state 2D flow and homogeneous hydrogeological conditions) (Deming 1994b, Domenico and Palciauskas 1973):

$$Pe = (q \Delta z c_w \rho_w) / 2\lambda$$

where,  $q$  = Darcy velocity;  $\Delta z$  = depth of system,  $\lambda$  = thermal conductivity of porous medium).

The threshold Peclet number for significant advective influence is in the order of 1 (Domenico and Palciauskas 1973), although according to Deming (1994b) for  $Pe \sim 0.1$  the magnitude of advective heat transport will still be significant.

Two example calculations for a local and a supraregional groundwater system (Section 9.1: Figure 32) provide indications of the potential influence of groundwater flow on the present-day distribution of temperature and heat flow in the Netherlands. For a local topography-driven groundwater flow system in the coastal dunes of the Netherlands:  $Pe \gg 1$

( $K = 50 \text{ m/day} = 6 \cdot 10^{-4} \text{ m/s}$ ;  $\Delta z = 100 \text{ m}$ ; hydraulic gradient  $\Delta h/L = 3 \cdot 10^{-4}$ ;  
 $q = K (\Delta h/L) = 2 \cdot 10^{-8} \text{ m/s}$ ;  $\rho_w = 1000 \text{ kg/m}^3$ ;  $c_w = 4200 \text{ J/kgK}$ ;  $\lambda = 2 \text{ W/mK} \Rightarrow Pe \approx 20$ ).  
 For a supraregional topography-driven groundwater flow system in southern parts of

the Netherlands (e.g. Figure 32, Kempen system - Roer Valley Graben):  $Pe \approx 0.3$ .  
 $(K = 10^{-6} \text{ m/s}; \Delta z = 500 \text{ m}; \text{hydraulic gradient } \Delta h/L = 6 \cdot 10^{-4}; q = K (\Delta h/L) = 6 \cdot 10^{-10} \text{ m/s}; \rho_w = 1000 \text{ kg/m}^3; c_w = 4200 \text{ J/kgK}; \lambda = 2.3 \text{ W/mK} \Rightarrow Pe \approx 0.3)$ .

The magnitude of the Peclet number is linearly related to the groundwater velocity and, through the Darcy equation, to the magnitude of the permeability. In the above calculations, conservative values for the permeability are used. Groundwater flow in local and regional systems in the shallow onshore parts of the Netherlands can be expected to influence the distribution of temperature and heat flow.

### Sedimentation

In addition to groundwater flow, uplift and erosion as well as subsidence and sedimentation can affect the temperature and heat flow distribution in a basin (Deming 1994a,b, Ingebritsen and Sanford 1998). Subsidence and sedimentation tend to decrease the near-surface temperature and heat flow, while uplift and erosion have the opposite effect. Among the factors controlling the magnitude of these effects are the rate and duration of sedimentation, somewhat similar to the effects of vertical groundwater flow (Ingebritsen and Sanford 1998). According to Ingebritsen and Sanford uplift or subsidence rates in the order of 1000 m/My can detectably influence the geothermal system. Deming (1994a) presented results of 1D numerical modelling studies that indicate that heat flow is significantly depressed by sedimentation rates  $\gg 100 \text{ m/My}$ .

Sedimentation rates in the study area started to exceed 100 m/My in the Pliocene. The sedimentation took place in shifting depocentres, and at each of these the total duration of the period with high sedimentation rates was geologically short. The highest sedimentation rates, reaching values  $>400 \text{ m/My}$ , occurred in the northern offshore area. It seems that, both the short duration of the sedimentation plus the rate of sedimentation over a large part of the area did not allow the present-day surface heat flow to be lowered significantly. The high sedimentation rates in the northern offshore area in the Early Quaternary may have depressed its surface heat flow.

### Top and bottom temperature boundary conditions

Boundary conditions for the heat flow system in a sedimentary basin include the ground surface temperature and the temperature distribution along the basin's lower boundary or the distribution of the input of basal heat flow into the basin. The time (t) it takes for changes in boundary conditions to propagate a certain distance ( $\Delta z$ ) through a basin fill with thermal diffusivity ( $D_t$ ) is (Lachenbruch and Sass 1977)  
 $t = (\Delta z)^2/4D_t$ .

### Ground surface temperature

The evolution of ground surface temperatures in onshore and offshore Netherlands during the last 75 000 years is (Van Gijssel 1995):

|                          |          |                          |          |
|--------------------------|----------|--------------------------|----------|
| 0 - 5000 years BP        | : 8 °C   | 25 000 - 60 000 years BP | : -2 °C  |
| 5000 - 10 000 years BP   | : 4 °C   | 60 000 - 70 000 years BP | : -10 °C |
| 10 000 - 13 000 years BP | : -2 °C  | 70 000 - 75 000 years BP | : -5 °C  |
| 13 000 - 25 000 years BP | : -10 °C |                          |          |

In the period 75 000 - 10 000 years BP, the groundsurface temperature was  $\leq -2$  °C. During these 65 000 years the low groundsurface temperature could propagate its influence on subsurface temperatures to a depth of  $\Delta z = \sqrt{t \cdot 4D_t}$ .

The volumetric heat capacity of the Cenozoic sequence:  $c = 0.4 c_w \rho_w + 0.6 c_r \rho_r = 3.06 \cdot 10^6 \text{ Jm}^{-3}\text{K}^{-1}$  (assuming porosity is 40%) and  $c = 2.87 \cdot 10^6 \text{ Jm}^{-3}\text{K}^{-1}$  (assuming porosity is 30%). Taking the thermal conductivity of the Cenozoic  $\lambda = 1.5 \text{ W/mK}$ , its thermal diffusivity is 15-16  $\text{km}^2/\text{My}$  and  $\Delta z = \sqrt{t \cdot 4D_t} \geq 2000 \text{ m}$ . By 10 000 years BP the influence of these glacial surface temperatures had reached depths of at least 2000 m. It is interesting to evaluate whether this influence of glacial temperatures has since dissipated. In a period of 10 000 years, these glacial temperature anomalies will dissipate over a depth range of 800 m. Thus in the depth range of 800 to at least 1200 m, negative temperature anomalies can be expected to prevail at today. The present-day temperatures in the shallow subsurface (to depths of approximately 565 m) will have adjusted to the ground surface temperature of approximately 8 °C that has prevailed during the last 5000 years.

The thickness of Cenozoic deposits thin out southwards (Figure 15) and so the propagation time of thermal disturbances will be increasingly influenced by the larger magnitude of thermal diffusivities of the pre-Cenozoic deposits. For example, in the southern offshore parts of the Netherlands, the influence of glacial temperatures may have penetrated deeper by the end of the Pleistocene. On the other hand, these glacial influences will also have dissipated more rapidly through the pre-Cenozoic deposits.

#### *Basal heat flow*

Goes et al. (2000a) have analysed models of the P and S seismic wave speeds for the European upper mantle to obtain a picture of mantle temperature variation beneath Europe. Relatively low temperatures of the upper mantle were found under the Netherlands, where geotherms at 200 km depth are slightly below or just reach adiabatic mantle temperatures (Goes et al. 2000b). In contrast, maximum shallow mantle temperatures inferred from P and S wave velocities are located under the Rhenish Massif, to the southeast of the Netherlands and correlate with recent volcanism and accelerated uplift of the area (Goes et al. 2000b). The range of modelled surface heat flow values for onshore and offshore Netherlands based on mantle P wave velocities is 55-70  $\text{mW/m}^2$  (Goes et al. 2000b).

The increased heat flow associated with rifting during the main syn-rift period has equilibrated and is not reflected in the present-day distribution of temperature and heat flow. The thermal effects of rifting also include the more local transient increases in temperature surrounding the syn-rift igneous intrusions. The thermal conductivities and radiogenic heat productivity of intrusive and extrusive rocks under the Netherlands continue to play a role in determining the present-day temperature distribution.

Assuming that heat flow from the mantle is fairly constant, differences in the thermal structure and thickness of the overlying crust may result in spatial variation in heat flow into – and temperatures at – the base of a certain stratigraphic unit, for example the Carboniferous Limburg Group. No information is available on the pre-Carboniferous



and its thermal characteristics. Rijkers and Duin (1994) reconstructed a southward thickening thickness of the crust in the southern part of offshore Netherlands (the Moho depth, reconstructed from the seismic reflection line, increases from 28 to 36 km).

The above evaluation indicates that the following factors will have influenced to a greater or lesser extent the present-day temperature distribution in onshore and offshore Netherlands:

- the basal heat flow input into the Dutch sedimentary basins;
- distribution of the bulk thermal conductivity of the subsurface ( rocks and fluids)
- recent groundwater flow
- paleo ground surface temperatures.

And possibly also:

- Late Tertiary and Quaternary subsidence and sedimentation, especially in the northern offshore part of the Netherlands.

It is clear that groundwater flow is only one of several possible influences that may be reflected in the present-day temperature distributions. In order to be able to use temperatures as an indicator of groundwater flow, the other factors of influence were evaluated first.

If rates of groundwater flow and basin uplift or subsidence and sedimentation are sufficiently slow, heat transport is conduction-dominated. Under steady-state conditions the conduction of heat is controlled by the thermal conductivity of the rock matrix and the pore fluids.

### 8.2.2 Thermal conductivities

Bulk thermal conductivities were calculated for the following chronostratigraphic units: Quaternary, Tertiary, Upper Cretaceous (Chalk Group), Lower Cretaceous, Jurassic, Upper Triassic, Lower Triassic, Upper Permian (Zechstein Group), Upper Permian (Upper Rotliegend Group) and Carboniferous at 52 offshore well locations (Appendix 1, Table 7). These bulk thermal conductivities are based on the matrix thermal conductivities given by Andrews-Speed et al. (1984) and on the groundwater temperature-dependent thermal conductivities given in Somerton (1992), and they take into account the influence of porosity. The temperature dependence of the thermal conductivity of halite and carbonates was also included in the calculations. In addition to the above stratigraphic units in the subsurface, mantle-derived intrusive rocks of Early Cretaceous age have been encountered in wells in the West Netherlands Basin, Broad Fourteens Basin (Andel-2,-4, Loon-op-Zand 1, Berkel, K14-FA103, L13/3, Q7/2) and Central North Sea Graben and extrusive rocks have been encountered in well Zuidwal 1 in the Vlieland Basin (Dixon et al. 1981, Latin et al. 1990a-b). No data are available on thermal conductivities or radiogenic heat productivity of these rocks. The calculated thermal conductivities vary by less than a factor 4.

Because the thermal conductivity of salt decreases as a function of increasing temperature, and therefore depth, the deeper salt units tend to act thermally similarly to other sediments. However, within the shallower part of a basin, salt diapiric structures can significantly disturb heat flow.

The variations in the thermal conductivity of the Netherlands subsurface are only minor in comparison with the variations in the hydraulic conductivity: these exceed 10 orders of magnitude. As a consequence, conductive heat transport is dominantly vertically upwards. Deviations from vertical conductive heat transport only occur where lateral contrasts in thermal conductivity are large. Conductivity contrasts will refract the flow of heat from the medium that is less conductive to the medium that is more conductive and heat flow will be focussed through the more conductive zones. Such lateral contrasts in thermal conductivity in onshore and offshore Netherlands can be expected near salt structures, igneous intrusions and along basin boundary fault zones.

### 8.2.3 Temperature data base

Published information on temperature distribution in the study area includes temperature maps (reconstructed isotherms at 500, 1000, 2000 and 3000 m depth) and a map of the surface heat flow of onshore and offshore Netherlands (Ramaekers 1992; Rijkers and Van Doorn 1997); an accurate and reliable temperature study of Van Dalfsen (1983) including isotherm maps of the shallow onshore part of the Netherlands (upper 250 m), and temperature-depth relations of deep subsurface temperatures in the Roer Valley Graben and the adjacent Peelhorst (Van Balen et al. 2002). The publications of Ramaekers (1992) and Rijkers and Van Doorn (1997) do not provide the original temperature data used for compiling the temperature and heat flow maps. The maps are constructed assuming steady-state conductive heat flow conditions and uniform thermal conductivities for each chronostratigraphic unit. That is, the lithology, porosity and temperature influences that may induce variations of present-day thermal conductivities within a certain chronostratigraphic unit have not been taken into account. Table 7 shows that such variations do occur in the Netherlands subsurface. As a consequence the published maps cannot be used

Table 7 Bulk thermal conductivities of chronostratigraphic units in offshore Netherlands (Appendix 1 provides information on the calculation of these thermal conductivities)

| Chronostratigraphic unit                  | Bulk thermal conductivity<br>$Wm^{-1}K^{-1}$ |
|---|--|
| Quaternary                                | 1.5  |
| Tertiary                                  | 1.3 - 1.6                                    |
| Upper Cretaceous<br>(Chalk Group)         | 1.8 - 2.5                                    |
| Lower Cretaceous                          | 1.8 - 2.2                                    |
| Jurassic                                  | 1.9 - 2.5                                    |
| Upper Triassic                            | 2.2 - 3.2                                    |
| Lower Triassic                            | 2.4 - 2.8                                    |
| Upper Permian<br>(Zechstein Group)        | 2.8 - 5.0                                    |
| Upper Permian<br>(Upper Rotliegend Group) | 2.5 - 3.7                                    |
| Carboniferous                             | 1.8 - 2.2                                    |

for deriving the possible influence of groundwater flow from temperature anomalies in the temperature distribution. The studies of Van Dalfsen (1983) and Van Balen et al. (2002) are included in the interpretation of present-day temperatures outlined in the next section.

Regrettably, the original temperature data of 130 released offshore wells and 334 onshore wells (underlying Ramaekers 1992 maps) were not available for the present study, and so the published temperature data from 65 offshore wells (RRI 1984, 1988, 1990) were used.

The temperatures at the sediment–water interface in the offshore vary between 7 and 9.5 °C. These sediment–water interface temperatures were calculated for a mean sea-surface temperature of the North Sea of 9.9°C (Wassing 1968) and a change of temperature with water depth given by Evans and Coleman (1974).

## 8.2.4 Interpretation present-day temperature distribution

### *Netherlands offshore*

Figure 29 shows the change of temperature with depth in the offshore Netherlands, based on published temperature data from 65 wells. Most of these published temperature data are derived from bottom hole temperature measurements. No information is available on the quality and reliability of the published temperatures, but it is recognised that measured bottomhole temperatures and corrected bottom hole temperatures are generally unreliable (e.g. Deming 1989, Hermanrud et al. 1990). In general, temperatures derived from bottom hole temperature data are cooler than true formation temperatures, while the magnitude of the deviation increases with depth (Deming 1989). The present-day temperature gradient is approximately 31 °C/km (based on a linear trendline passing through the published temperature data and the interception point at depth = 0 m and a sediment-water interface temperature = 8 °C, Figure 29). The calculated temperature gradient for a trendline calculated for the subsurface data points only is approximately 29.5 °C/km. This difference may be the result of too low BHTs at greater depth. Figure 30 shows the temperature–depth relation in the onshore Roer Valley Graben. The offshore gradient seems relatively low in comparison with the increase of temperatures with depth in the onshore Roer Valley Graben based on corrected temperature data (Van Balen et al. 2002).

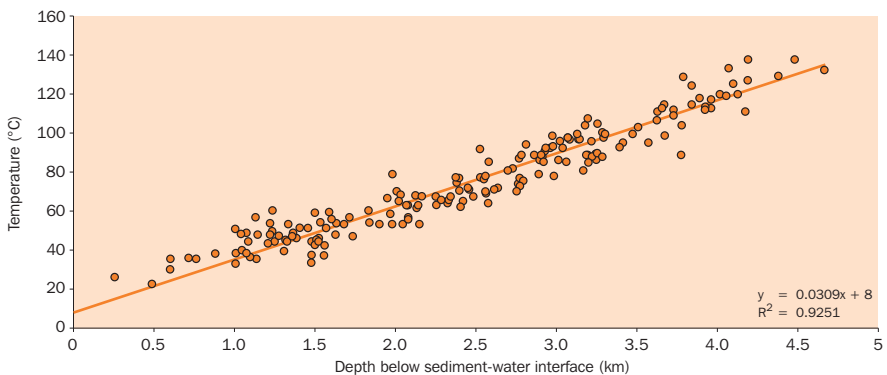


Figure 29 Temperature versus depth for offshore Netherlands based on published temperature data from 65 wells

Taking into account all temperature data observed at depths of approximately 600 - 1600 m, the temperature gradient for shallow depths in the offshore Netherlands is 34 °C/km. Temperature gradients of less than 30°C/km are frequently encountered at shallow depths in the northern part of offshore Netherlands (blocks A12, E17, F3, F18, L2, L8, L11, L12), while temperature gradients exceeding 35°C/km occur in the southern offshore area (observed at wells P03-01, P05-01, P12A-01, Q01-05, Q04-01, Q10-01, Q11-01S). Shallow temperature gradients exceeding 35°C/km also occur locally in the northern offshore, associated with salt diapirs (e.g. at wells F09-01, G17-01).

Conductive heat flows were estimated for each well location based on the published temperature data, the thermal conductivities (Appendix 1) and the sediment-water interface temperatures. The 1D conductive heat flow through the basin fill, calculated for temperature data at the deepest point of measurement (measurement depths between 1334 and 4660 m below sea floor) is 59 mW/m<sup>2</sup>. This heat flow is within the range of the modelled heat flow values (55 - 70 mW/m<sup>2</sup>) based on mantle P wave velocities (Goes et al. 2000a). The calculated heat flow for the depth interval of 0 - 1000 m is approximately 50 mW/m<sup>2</sup> and for depths exceeding 1000 m it is 67 mW/m<sup>2</sup>. Table 8 shows the clearly decreasing heat flow towards the surface in the areas of the Central North Sea Graben and the Step Graben (blocks A12, F3, F18). The mean trend of increasing rates of heat flow with depth is less pronounced or even absent in the southern offshore parts of the Netherlands (Table 8). In addition to the observed variations in heat flow and temperatures with depth, the data indicate that shallow heat flow in the northern part of the basin is less than the average heat flow of 50 mW/m<sup>2</sup> (namely 46 mW/m<sup>2</sup>; at 24 wells in blocks A, B, E, F, G, K, L). In contrast, the shallow heat flow is greater in the southern offshore (57 mW/m<sup>2</sup>; at 21 wells in P and Q blocks). The relatively high values of the shallow heat flow, presented in Table 8, are observed at wells located at or near the Cenozoic highs/Cenozoic active zones (offshore extension Mid Netherlands Fault zone: Q04-01; IJmuiden High: P12A-01, P12-1x; Winterton High: P05-01; Kijkduin High: P15-02, Q13-02, Q16-01).

The observed difference in shallow temperatures and heat flows between the southern and the northern offshore parts of the Netherlands probably result from a combination of factors:

- Difference in thickness of Tertiary and Quaternary units in combination with the poor thermal conductivity of these units. The maximum thickness of the Cenozoic sequence in the West Netherlands Basin (Kijkduin High) is only about 450 m. The Cenozoic sequence is more than 1500 m in the Central North Sea Graben and Step Graben, and exceeds 2000 m in the northernmost offshore.
- The thermal conductivity of Tertiary and Quaternary deposits in the northernmost offshore will be relatively small because of undercompaction of part of the Tertiary and the occurrence of gas in the shallow subsurface.
- The West Netherlands Basin is not a Pliocene-Quaternary centre of deposition. In contrast, in the northern offshore there was significant subsidence and sedimentation: here the Quaternary sedimentation rates exceed 400 m/My and may act to decrease the shallow subsurface temperatures to some extent.
- Although changes in paleo groundsurface temperature are approximately the same for the whole area, in the southern offshore the relatively low subsurface temperatures at the end of the Pleistocene could probably dissipate more rapidly, and as a consequence over greater depths, because of the greater thermal diffusivity of its subsurface.
- Possible influence related to tectonic activity of Mid Netherlands Fault zone and its offshore extension.

The more local influence of conductivity contrasts with the present-day temperature distribution is recognisable at several locations. For example, the influence of salt structures on temperature and heat flow can be clearly illustrated for a number of wells penetrating the Zechstein Group. High values for the heat flow were calculated

Table 8 Contrast in change of heat flow with depth in northern and southern parts of offshore Netherlands

| Location                       | Heat flow ( $\text{mWm}^{-2}$ )<br>depth < 1000 m | Heat flow ( $\text{mWm}^{-2}$ )<br>depth > 1000 m | Heat flow ( $\text{mWm}^{-2}$ )<br>depth > 2000 m |
|--------------------------------|---|---|---|
| <b>Northern offshore</b>       |   |   |   |
| A12 and F3 blocks<br>(4 wells) | 47  | 67  | 92  |
| F18 block<br>(4 wells)         | 45  | 61  | 70  |
| <b>Southern offshore</b>       |   |   |   |
| P05-01                         | 60  | 59  | 69  |
| P12A-01                        | 79  | 40  | 42  |
| P12-1X                         | 60  | 54  | 59  |
| P15-02                         | 57  | 54  | 66  |
| Q04-01                         | 72  | 62  | 54  |
| Q13-02                         | 57  | 44  | 61  |
| Q16-01                         | 57  | 38  | n.a.  |

for the Zechstein at well A12-01 (206  $\text{mW/m}^2$ ), E17-01 (109  $\text{mW/m}^2$ ), K15-03-S1 (114  $\text{mW/m}^2$ ), K15-07 (191  $\text{mW/m}^2$ ), K17-02 (126  $\text{mW/m}^2$ ) and N04-01 (87  $\text{mW/m}^2$ ). The heat flow within the Zechstein Group at these well locations is generally higher than that in the pre- and post-Zechstein units. Already in 1975 Van Engen observed an increase in the vertical rate of heat flow within the onshore Annerveen-Veendam salt dome, and found that relatively low temperatures in pre-Zechstein units

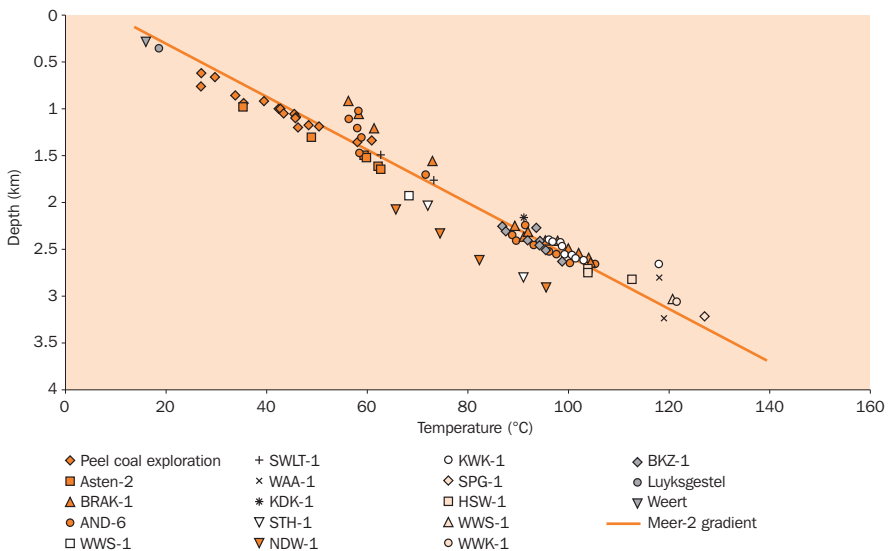


Figure 30 Temperature versus depth in the Roer Valley Graben, onshore Netherlands: DST, RFT, geothermal and Horner corrected temperature data (Modified from Van Balen et al. 2002) and additional temperature data from groundwater wells at Luyksgestel and Weert (data from Van Dalfsen 1983).

correspond to the presence of overlying salt structures. The rapid transfer of heat produces positive temperature anomalies in sedimentary units overlying the salt structures (e.g. at K15-03, N04-01, and F09-01, G17-01). The location of Zechstein salt structures is associated with basement boundary faults (Remmelts 1996) and as a consequence the lateral and vertical changes of heat flow induced by the relatively great thermal conductivity of the Zechstein salt units, will concentrate and coincide with the basin boundaries. In theory, positive temperature anomalies at basin boundary fault zones may also result from focussed vertical upward flow of groundwater. Such cross-formational flow of hot brines has been reported from near salt domes outside the Dutch part of the North Sea (e.g. Jensenius and Munkgaard 1989, Liewig et al. 1987). It was not possible to distinguish the thermal conductivity and the flow effects from the available temperature data.

Similarly, conductivity contrasts are responsible for the focussing effect of the extrusive Zuidwal volcano units that produce the positive temperature anomaly above the extrusive units recognised by Rijkers and Van Doorn 1997. The igneous intrusions in onshore and offshore may have a similar effect on the subsurface temperature distribution. The presence of the igneous intrusions observed in the Andel 2 and 3 wells (Roer Valley Graben) provide an alternative explanation for the positive temperature anomalies measured in the nearby Andel 6 and Brakel 1 wells (see below).

The evaluation of the published offshore data allow the assessment of the local and regional influence of thermal conductivity contrasts on vertical and lateral temperature and heat flow distributions in the offshore Netherlands. The data did not allow the selection of temperature and heat flow anomalies indicative of focussed groundwater flow selected: these are probably small scale and subtle.

**Onshore Netherlands**

Isotherm maps for depths of ≤250 m in onshore Netherlands clearly show the relation between relatively low temperatures and regional recharge areas of Veluwe and Utrechtse Heuvelrug and to a minor extent of the glacial plateau of Drente (Van Dalfsen 1983; Verweij 1990a).

Figure 30 shows the temperature-depth relation for the Roer Valley Graben. The temperatures at Luyksgestel, Weert, Giesen at depths of <350 m, and at Asten at depths of ≤1250 m in the Roer Valley Graben are well below the gradient of 34-35 °C/1000 m observed at well Meer-2 located on the stable high bounding the Roer Valley Graben. The measured temperature gradient at very

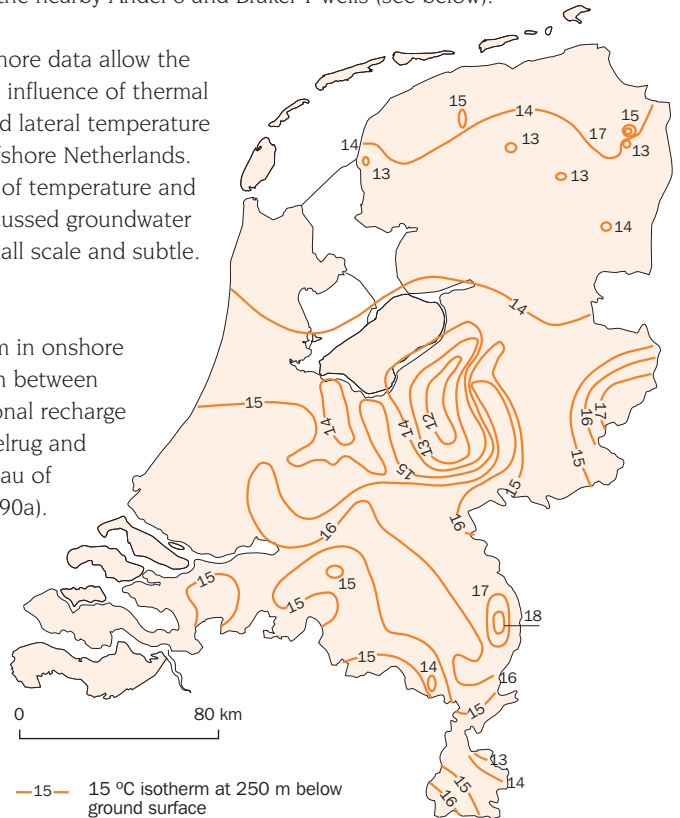


Figure 31 Temperature distribution at a depth of 250 m below ground surface (after Van Dalfsen 1983)

shallow depths in the Graben is 23 °C/1000 m (0 - 200 m at Giesen), 24 °C/1000 m (0 - 275 m at Weert) and 27 °C/1000m (0 - 350 m at Luyksgestel). The temperature gradient calculated from the ground surface temperature and an observed temperature of 35.5 °C at depth of 964 m at Asten-2 (Heederik and Huurdeman 1988) is 26 °C/1000 m). Based on temperatures measured at depths of  $\geq 2000$  given in Figure 30 (not taking into account NDW-1 and STH-1) the temperature gradient at greater depths is 34 - 35 °C/1000 m, and is in accordance with the Meer-2 gradient. Such relatively low values for the shallow subsurface temperature gradient also occur in the northern offshore area where, as well as in the Roer Valley Graben, Cenozoic deposits – with their relatively low thermal conductivities – reach thicknesses of more than 1500 m.

Calculated changes in heat flow with depth for the Asten-2 well shows that heat flow increases from 25 mW/m<sup>2</sup> (0-250 m), and 45 mW/m<sup>2</sup> (250 - 1000 m) to 65 mW/m<sup>2</sup> (1000 - 1500 m). Values of 45 mW/m<sup>2</sup> for depths of less than 1000 m were calculated for the northern offshore. Because no temperature measurements were available in the shallowest depth range in the offshore area, it is not known if the very low heat flow rates of 25 mW/m<sup>2</sup> occur in the offshore region as well.

As shown by the calculated Peclet number reported in Section 8.2.1, the temperature and heat flow distribution in southeastern Netherlands may have been influenced by Quaternary topography-induced groundwater flow. Most flow in the Roer Valley Graben takes place through the upper 250 m (e.g. Wiers 2001). The low heat flow value of 25 mW/m<sup>2</sup> may partly result from the cooling effect of this groundwater flow.

Inspecting Figure 30, a clear positive temperature anomaly can be recognised at depths of approximately 900 to 1200/1300 m corresponding to temperatures measured during repeat formation tests in the wells Brakel-1 and Andel-6. One possible explanation for this anomaly, given by Van Balen et al. (2002), is that these temperatures were probably collected shortly after completion of the well and circulating drilling mud may have caused the wall of the shallow part of the well to heat up. A more geologically-based approach offers an alternative explanation for the anomaly. Igneous intrusions have been recognised in Middle Jurassic sedimentary units in the nearby Andel-2 and Andel-4 wells (Dixon et al. 1981). The top of the Middle Jurassic sediments, corresponding to base Schieland Group, is at 1167 m below msl (Andel-2) and at 1369 m below msl (Andel-4). The Andel wells are located near N-S and E-W trending faults cutting through the Jurassic sedimentary units (TNO-NITG 2001, map XIII Breda-Valkenswaard). The measured positive temperature anomaly occurs right above the igneous intrusions, and may be related to the occurrence of these intrusions (similar to the relation between the Zuidwal volcanic rocks and the associated positive temperature anomalies recognised by Rijkers and Van Doorn (1997) and/or the fault systems and possible fault-related fluid flow. The temperatures measured at well NDW-1 are systematically about 15 °C lower than average temperatures in the Roer Valley Graben in the same depth range (2000 - 3000 m). After evaluating different possible causes of this anomaly, including deep-reaching groundwater flow, Van Balen et al. (2002) conclude that the data are probably affected by a measurement error.

### *Conclusion*

On the basis of theory, one would expect that focussed vertical upward flow of fluids along, for example, permeable fault and fracture zones and salt diapirs in the northern offshore, and along currently active fault zones (such as the Mid Netherlands Fault zone and its offshore extension) and topography-induced groundwater flow at different scales would have an observable effect on the present-day geothermal field. The accurate and reliable temperature data for the shallow onshore (Van Dalssen 1983) do indeed illustrate the influence of regional topography-induced flow on temperature distribution. The calculated low heat flows suggest that concentrated groundwater flow of the supra-regional groundwater flow system in the upper 250 m of Roer Valley Graben may have a cooling effect on the temperatures. The temperature data available for the offshore were neither sufficiently accurate nor sufficiently reliable for these expectations to be verified.



| Type of flow system | Age (years)                               | Scale            | Maximum present-day depth of flow system (m) | Maximum depth fresh groundwater (m) |
|---------------------|---|------------------|--|-------------------------------------|
| 1                   | 30 - 55                                   | Local - regional | n.a.   | -                                   |
| 2                   | <800                                      | Local - regional | 200  | -                                   |
| 3                   | <7000                                     | Local            | 100  | -                                   |
| 4                   | <5000                                     | Local - regional | 150  | 150                                 |
| 5                   | Young dunes: <1000<br>Coversands: <11 000 | Local - regional | 400  | 400                                 |
| 6                   | Ice-pushed hills: <130 000<br><3 000 000  | Supra-regional   | >1000  | ≥500                                |
| 7                   | From recent to >>5 000 000                | Basinal          | >>1000                                       | -                                   |

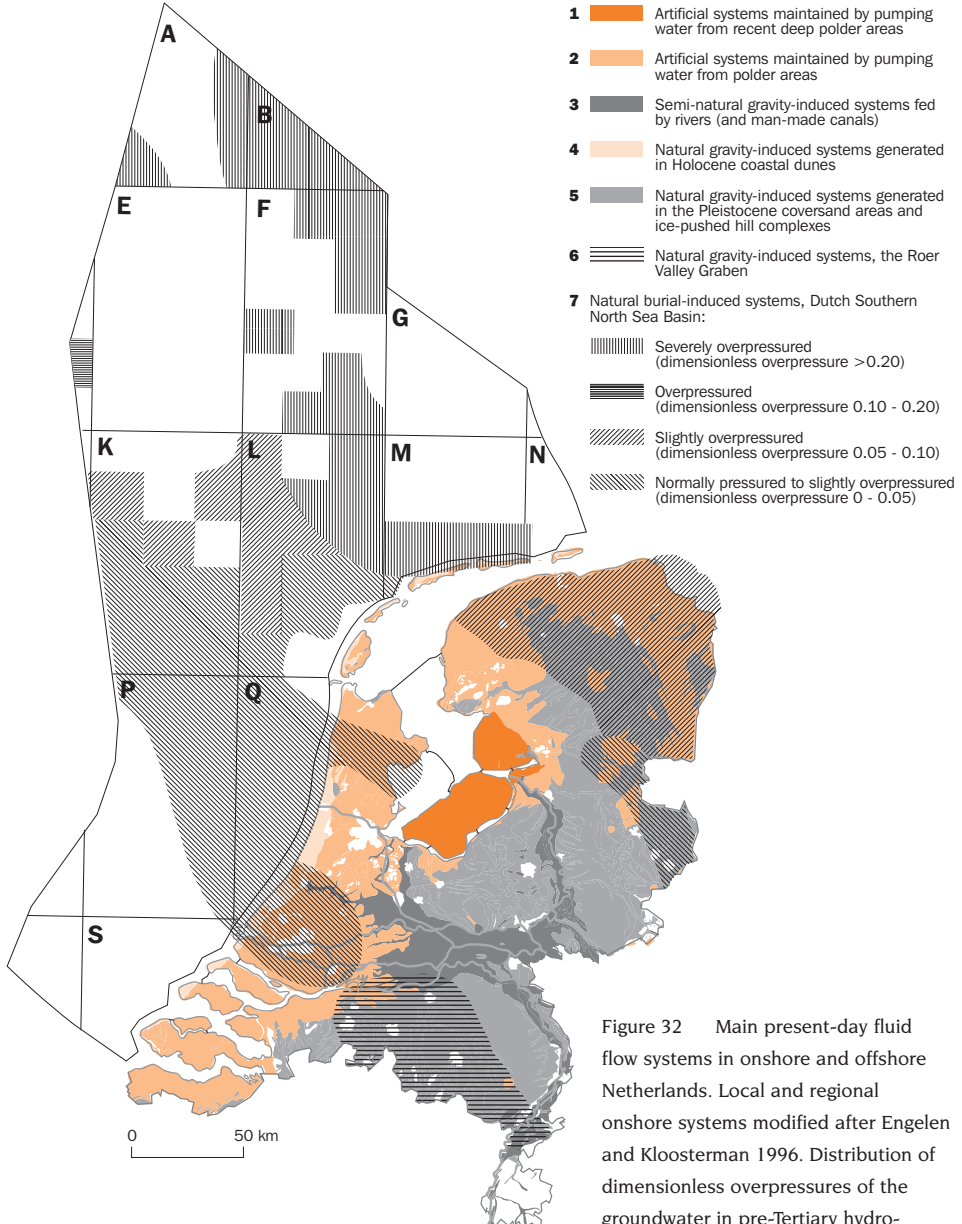


Figure 32 Main present-day fluid flow systems in onshore and offshore Netherlands. Local and regional onshore systems modified after Engelen and Kloosterman 1996. Distribution of dimensionless overpressures of the groundwater in pre-Tertiary hydrostratigraphic units is according to Figure 22 (Modified from Verweij 1999)

## 9 The present-day hydrodynamic setting of onshore and offshore Netherlands

The natural topography-induced, the artificial fluid flow systems and the density-induced fluid flow in shallow parts of onshore Netherlands today and their related physico-chemical characteristics have been described and modelled in great detail (see e.g. the 'National analysis of regional groundwater flow systems' of TNO-GG 1991-1996, and the overview publication of groundwater in the Netherlands of Dufour 1998, 2000).

From the Miocene onward, an increasing part of the southeastern part of the Southern North Sea Basin emerged above sea level (Chapter 3). Since that time three types of topography-induced groundwater flow system developed in the Netherlands (Table 3; Chapters 6 and 8): two of these – the local and regional systems – originating in the Dutch lowland area itself; the third is a supraregional system that originated at the southern and southeastern margins of the Netherlands. Local and regional topography-induced groundwater flow had relatively limited depths of penetration. Evidence for a prolonged existence of a supra-regional system with northward flow is provided by dating of the groundwater, hydrochemical indicators of flow and results of modelling studies concerning elevated temperatures (Chapters 6 and 8). The results of hydrochemical studies suggest that a pre-Holocene supra-regional groundwater flow system extended more deeply than the present-day system (Chapter 8).

Chapter 7 discussed the relation between Tertiary and Quaternary sedimentary loading and present-day distributions of fluid flow and observed overpressures.

These main characteristics of the present-day hydrodynamic setting of onshore and offshore Netherlands are summarised below. Figure 32 shows the hydrodynamic setting.

### 9.1 Topography-induced fluid flow systems

Figure 24 shows the close relation between the present-day surface topography of onshore Netherlands in relation to the elevation of the water table and depth of the fresh-brackish groundwater interface. As observed before, the isotherm map at 250 m depth shows the cooling effect of meteoric waters infiltrating in regional recharge areas of Veluwe and Utrechtse Heuvelrug.

The present-day depths of penetration of local and regional topography-induced fluid flow systems originating in the Netherlands lowland area are in the order of tens to hundreds of metres (Figure 32). The present-day main recharge areas of supra-regional fluid flow systems are the Belgian Kempenland and Ardennes, and the German Eifel, Sauerland and Teutoburgerwald, and their offshoots. An important part of this supra-regional flow is concentrated in the Roer Valley Graben, where meteoric water has been able to infiltrate since the Miocene. Although topography-induced fluid flow probably penetrates to a depth of  $\geq 1000$  m in the Graben, most flow is concentrated in the upper 250-500 m (e.g. Wiers 2001). Most of the groundwater below the fresh-brackish groundwater interface under the Netherlands participating in the supra-regional flow systems is pre-Holocene (Chapter 8).

The fresh-brackish and brackish-salt groundwater interfaces in the Roer Valley Graben are hundreds of metres apart. This is probably because the supra-regional flow system used to extend much deeper than today as indicated by the relatively low content of chlorides in groundwater in clays at depths of 1400 - 1500 m in the Roer Valley Graben (Chapter 8).

## 9.2 Artificial fluid flow systems

Figure 32 shows the distribution of the major artificial fluid flow systems in the onshore Netherlands.

People have been lowering the groundwater levels in the peat and clay areas in the western and northern parts of the Netherlands since the Middle ages. Apart from influencing the natural groundwater flow systems, the lowering of the groundwater levels also resulted in extensive irreversible mechanical compaction of Holocene peat and clay layers and associated surface subsidence (e.g. Huisman et al. 1998). There has been additional artificial compaction of shallow and deeper parts of the subsurface as a result of human-induced loading of the subsurface (e.g. houses) and gas production (Doornhof 1992), respectively.

Extensive abstraction of fresh groundwater for public water supply and groundwater use and abstraction for industry and agriculture have affected local, regional and supraregional groundwater flow systems in onshore Netherlands (e.g. Dufour 2000, Stuurman and Vermeulen 2000, Stuurman et al. 2000, Wiers 2001).

## 9.3 Fluid flow systems induced by sedimentary loading and associated burial-related processes

Evaluation of observed groundwater pressure distributions (Chapter 7) identified a qualitative relation between the pressure distributions, fluid flow and Tertiary and Quaternary sedimentary loading.

Late sedimentary loading showed relations with groundwater flow, compaction, and normal pressures in sediments of the Upper North Sea Group today (Japsen 1999, Kooi and De Vries 1998, Kooi et al. 1998, Stuyfzand 1993). Neogene and Quaternary sedimentary loading was found to be related to undercompaction and overpressures in the Lower and Middle North Sea Groups and Chalk Group in the northernmost offshore part of the Netherlands (Japsen 1999, Winthaegeen and Verweij 2003). Ongoing active expulsion of compaction-derived water from poorly permeable Tertiary and Quaternary hydrostratigraphic units probably occurs in onshore and offshore Netherlands (corresponding to the shallow subsystem of burial-induced flow, Chapter 1) except in the northernmost offshore area, where compaction disequilibrium conditions probably prevail in the Lower Tertiary.

Major overpressuring of the Chalk occurs in the northern offshore. These overpressure gradients are indicative of southward flow through the Chalk. Such flow conditions are characteristic for the transitional subsystem of the burial-induced flow system (Chapter 1). The normally pressured Lower Cretaceous reservoirs in the West Netherlands Basin and the Broad Fourteens Basin contain chloride-dominated brines with TDS of approximately 74 000 - 140 000 mg/l. In the West Netherlands Basin,

water with the highest content of dissolved solids (TDS = 140 000 mg/l) occurs in the most deeply buried formation. In addition, the calcium content increases with increasing TDS, probably resulting from increasing water-rock interaction. These chemical characteristics point to only little groundwater flow through these Lower Cretaceous reservoirs in the southern part of the study area. This is in accordance with only minor late sedimentary loading of the area (Chapter 3).

It was found that Neogene and Quaternary sedimentary loading and even sedimentary loading since the start of the Tertiary can only explain part of the observed overpressures in pre-Cretaceous sedimentary units in the northern offshore. More prolonged sedimentation or other processes and forces must also have been involved in shaping the present-day overpressure distribution. A wide variety of additional mechanisms may be jointly responsible for the overpressure distribution: a. mechanisms related to ongoing deeper burial of the reservoir not directly related to mechanical loading (pore volume reduction by chemical compaction and salt cementation; pressure redistribution by groundwater flow; aquathermal pressuring of the pore water); b. gas generation in e.g. Jurassic source rocks; c. changes in lateral compressive stresses; d. pressure redistribution by density-controlled flow; e. salt deformation during the Cenozoic. Overpressures in these pre-Cretaceous units in part of the Central North Sea Graben and in the Terschelling Basin are close to the regional maximum values indicating that present-day conditions are probably favourable for hydraulic fracturing of brittle rocks allowing groundwater flow. The Jurassic and Early Cretaceous claystones form a thick seal for the underlying severely overpressured syn-rift reservoir-type hydrostratigraphic units. The early-rift reservoir type units of the Lower Germanic Trias Group are sealed by evaporites and shales of the Upper Germanic Trias Group. Fluid flow from these severely overpressured units is probably episodic and concentrated through hydrofractures or reactivated pre-existing fractures and faults resulting from the constant interaction between the fluid pressure and the stress regime (such restricted flow conditions correspond to the deep subsystem of characteristics of the burial-induced flow system; Chapter 1). In the North Sea, severe overpressures occur along the northern limit of the Slochteren Formation below a thick Zechstein seal. Zechstein salts may hold overpressures close to lithostatic. The magnitude of overpressures decreases in the direction of decreasing sealing capacity of the Zechstein Group, e.g. towards the Texel IJsselmeer High, and in the direction of increasing thickness and permeability of the Slochteren Formation.

The available data on overpressures in pre-Tertiary reservoir units indicate a clear distinction between the northern overpressured area and a southern normal to slightly overpressured area. A possible explanation for this is the combined effect of differences in magnitude and duration of Cenozoic or Late Cenozoic sedimentary loading and in distribution and sealing capacity of the Zechstein Group.

Figure 32 includes the geographical distribution of the pressure that is thought to be related to burial-induced groundwater flow systems.

The identified forces and processes operating during Tertiary and Quaternary times may all have contributed to present-day pressure and fluid flow conditions: sedimentary loading, the topography of the water table, tectonic forces and ice loading (Table 2).

Fluid density differences, gas generation and, most recently, human activities, are additional factors of influence. Present-day fluid flow systems and the associated groundwater potential and pressure distributions will reflect these relatively recent driving forces and processes to a greater or lesser extent. The available data and information alone were not sufficient to evaluate the importance of each of these forces and processes on present-day fluid flow conditions.

The foregoing showed that from the Miocene onward, an increasing part of the southeastern Southern North Sea Basin emerged above sea level. It was considered plausible that since that time the Dutch part of the basin has contained at least two major types of groundwater flow system: a topography-induced groundwater flow system in which water of meteoric origin is driven by the relief of the water table and the flow system activated by sedimentary loading and associated processes related to ongoing burial of the sediments. Sedimentary loading influenced groundwater flow and pressure conditions throughout onshore and offshore Netherlands to a greater or lesser extent. These natural groundwater flow systems are presented in Figure 32 together with the artificial flow systems. The figure shows the widely different temporal and spatial scales associated with this present-day hydrodynamic setting of onshore and offshore Netherlands.

## 10 Discussion and conclusions Part 1

Analysis of the geodynamics, sedimentary geology, geothermics and climatology of onshore and offshore Netherlands from Late Carboniferous onwards resulted in the identification and timing of the main mechanical and thermal forces and processes that exerted a controlling influence on the evolution of fluid pressures, fluid dynamics and permeability. The type, magnitude and areal distribution of these driving forces and processes influencing fluid flow systems have changed continuously during the geological evolution of the Netherlands. This study demonstrated that during each tectonostratigraphic stage different forces have acted simultaneously on the fluids, largely because of the differential subsidence and uplift history of the various structural units. Hence, different fluid flow systems have probably coexisted and interacted laterally and vertically in onshore and offshore Netherlands.

Direct and indirect indicators of fluid flow (pressure, sediment-diagenetic minerals, salinity, hydrochemistry, and to a minor extent temperature) were a valuable tool in delineating and characterising present-day and paleo hydrodynamic conditions.

The present study on overpressure distribution in pre-Tertiary reservoir units found a clear difference between the northern overpressured area and the southern normal to slightly overpressured area. The combined effect of differences in magnitude and duration of (Late) Cenozoic sedimentary loading and in distribution and sealing capacity of the Zechstein Group probably are the main factors explaining this difference.

The absence of Zechstein evaporite deposits in the southern onshore and offshore is also considered one of the factors explaining the observation that the least saline groundwaters occur in these southern areas. A combination of factors is probably responsible for the identified difference in present-day shallow temperature gradients and heat flows between the southern and northern offshore parts of the Netherlands; in the northern offshore the temperature gradients and heat flows at shallow depths are less than average for the entire area. The most important factor is probably the difference in thickness of Tertiary and Quaternary units in combination with the poor thermal conductivity of these units.

The analysis of fluid flow systems on geological timescales presented in Part 1 provide a general fluid dynamics context and a data set for an improved process-based understanding of the present-day characteristics of the hydrogeological framework and the fluids in onshore and offshore Netherlands. It is the basis for more detailed geoscientific studies, including more detailed applications of the concept of fluid flow systems analysis on geological timescales. In general such more detailed fluid-related studies should focus on

1. Characterisation of present-day fluid flow systems (overpressure distributions, flow characteristics, hydrochemical and thermal characteristics).

Information on physico-chemical characteristics of geological media in the deeper subsurface of onshore and offshore Netherlands and the fluids it contain, is generally only available for reservoirs that have been explored and developed for petroleum exploitation. Pressures and temperatures have been recorded

in exploration and production wells for over 40 years. However, these pressure and temperature measurements were not available for this research. Published studies include a selection of the pressure and temperature information. This thesis used the published information to describe the present-day overpressure and fluid flow characteristics. Currently, the author is involved in a joint industry project in which the unique data set of the petroleum wells in offshore Netherlands is used to set up a quality-controlled database of pressures, temperatures and salinities (Simmelink et al. 2003). This will allow a more detailed characterisation of present-day fluid flow conditions in the deeper subsurface of offshore Netherlands. The identified lack of pressure data for poorly permeable units, such as clays and shales, triggered the development of methodologies to estimate pressure conditions in such units in the Netherlands (Winthagen and Verweij 2003).

2. Characterisation of the hydrogeohistory (dating, timing and characterisation of paleo fluid flow; quantification of paleo fluid flow conditions).

A wide diversity of techniques is available to date, time and characterise paleo-fluid flow (e.g. Parnell 1998, Pueyo et al. 2000). Characteristics of fluids from which diagenetic minerals precipitated are retained in fluid inclusions and in the isotopic composition of the mineral. The application of detailed petrographic, fluid inclusion and isotope geochemical studies, often in combination with burial history or basin modelling studies, have become common place for characterising hydrogeohistories. Such petrographic, fluid inclusion and isotope geochemical studies of the main reservoir horizons in the different Dutch basins and their flanking regions would greatly help to constrain the timing and duration of the multiple fluid flow events identified in this thesis and to trace the origin of the fluids.

The Broad Fourteens Basin was selected for this study as the most appropriate basin for executing a more detailed and quantified study of the evolution of fluid flow systems on geological timescales (see Parts 2 and 3). The selection of this inverted offshore basin was based on the findings of the present research: the nature of its geological history, the identified factors controlling its hydrogeohistory, the presence of oil and gas accumulations, and the wide variety of information publicly available for the basin.

## 11 Introduction to Part 2

The Broad Fourteens Basin (Figure 33) was selected for a detailed analysis of fluid flow systems on geological timescales. This selection was based on the nature of its geological history, the identified factors controlling its hydrogeohistory, the presence of oil and gas accumulations, and the wide variety of information publicly available for the basin (Part 1).

The study of the Broad Fourteens Basin aims to provide quantitative understanding of the hydrogeological and hydrodynamic response of the basin fill to its geodynamic and climatic evolution and to show the significance of this response for understanding and prediction of the present-day distributions of pore pressures and the distributions and characteristics of the oil and gas accumulations.

The basin has been extensively studied in the past and there is a wide range of information – geological, geophysical, thermal and geochemical – available on it (e.g. Gauthier et al. 2000, Goh 1996, Hastings et al. 1991, Lee et al. 1989, Oele et al. 1980, Nalpas et al. 1995, Roelofsen and De Boer 1991, Van der Poel 1989, Van Wijhe 1987a, Wong et al. 2001). In addition water analyses data were available for public wells, and porosity, permeability, pressure and temperature data were derived in large part from ECL (1983), GAPS (1991), RRI (1984, 1985, 1988, 1990), and the webatlas North Sea fields (1999). Part 2 presents the first phase of the basin study that involved the analysis of the data following the approach outlined in Chapter 1.



## 12 Regional tectonic setting

The Broad Fourteens Basin is a northwest–southeast trending Mesozoic basin, approximately 120 km long and 45 km wide (Figure 33). The basin is now inverted and unconformably overlain by the sedimentary fill of the Cenozoic Southern North Sea Basin.

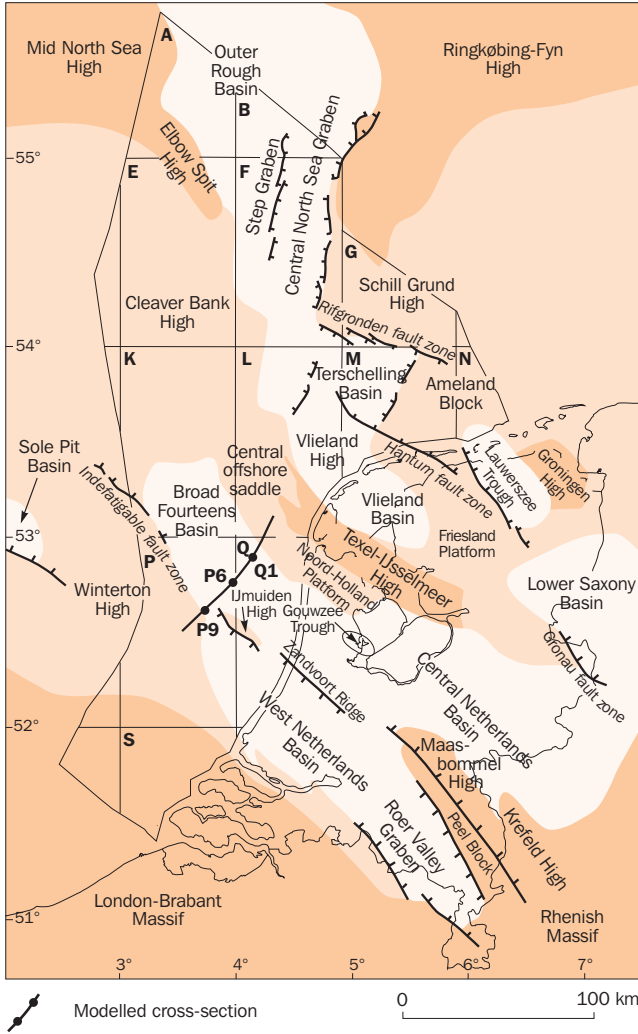


Figure 33 Location of the Broad Fourteens Basin in offshore Netherlands

Changes in regional tectonic setting of a basin control its structural geological, sediment geological and geothermal history and as a consequence the fluid flow history of the basin (Chapter 1, Part 1). In order to identify, characterise and understand the main factors that control the fluid geological and fluid dynamic history of the Broad Fourteens Basin, the analysis starts with an outline of the regional tectonic setting of the basin.

### 12.1 Variscan phase

The Late Carboniferous Variscan orogeny, associated with a compressional tectonic setting, marks the closure of the southern Proto-Tethys ocean and the creation of the supercontinent Pangea (Glennie and Underhill 1998). The area of the southern North Sea was part of the subsiding northern foreland basin of the Variscan fold belt. During the Westphalian to Stephanian the southern North Sea area was only marginally affected by compressional deformations associated with the Variscan orogeny (Glennie and Underhill 1998).

The Variscan fold belt and its northern foreland basin became subjected to post-orogenic wrench deformation and associated intrusive and extrusive magmatism during the Stephanian and Early Permian Autunian (Van Wijhe 1987b, Ziegler 1990a). Vulcanism started around 293 Ma and lasted to about 288 Ma (Glennie and Underhill 1998). It was most intense in Germany, Poland and the eastern North Sea area, while the Broad Fourteens area remained essentially volcanic-free. In the southern North Sea area NW trending wrench fault systems developed in response to the prevailing regional stress pattern. A long

(10 - 20 My) period of thermal uplift and erosion followed the period of vulcanism (Glennie and Underhill 1998). The erosion pattern of top Carboniferous in the southern North Sea area indicates the existence of NW–SE trending horst and graben systems during the uplift phase (Van Wijhe 1987b).

The relaxation of lithospheric thermal anomalies that were introduced during the Autunian phase of wrench faulting plus the vulcanism, induced the Southern Permian Basin to subside (Van Wees et al. 2000, Ziegler 1990).

Since the Late Carboniferous, the North Sea area has effectively been in an intraplate setting. The Late Permian subsidence of the Southern Permian Basin was largely governed by thermal contraction of the lithosphere, and its loading by water and sediments. Glennie and Underhill (1998) suggest an early Late Permian (267 - 265 Ma) initiation of rift formation in the North Sea (initiation of Viking and Central Grabens), and as a consequence an extensional influence on the subsidence of the Southern Permian Basin (tectonic subsidence has been recognised in the Broad Fourteens area in Late Permian, Kooi et al. 1989). Geluk (1999), however, suggests that Late Permian tectonic activity represents the aftermath of the Variscan orogeny and not the initiation of – Kimmerian – rifting. The later Broad Fourteens Basin mainly evolved in response to the build-up of regional extensional stress fields governing the Triassic – mid Jurassic break-up of Pangea and the Late Jurassic – Paleogene disintegration of Laurasia (Ziegler 1992). With the Early Eocene onset of seafloor spreading in the northern North Atlantic and the Norwegian-Greenland Sea, the North Sea Basin, including the Broad Fourteens Basin, became tectonically quiescent and its subsequent evolution was governed by thermal relaxation of the lithosphere, sedimentary loading and fluctuations in compressional intraplate stresses (Ziegler 1992).

The following five regional tectonic events and associated stress fields have exerted a major influence on the post-Variscan – Triassic to recent – history of the Broad Fourteens area. For detailed information on the evolution of the megatectonic setting of the North Sea area, see Glennie and Underhill (1998) and Ziegler (1990a-b, 1992).

## 12.2 Triassic and Early Jurassic extension and thermal subsidence

The general pattern of subsidence in the southern North Sea as started in the Late Permian, indicated by the location of the Southern Permian Basin, continued during the Triassic and Early Jurassic. The main driving mechanism for subsidence was the relaxation of Permo-Carboniferous thermal anomalies (Ziegler 1990a-b, 1992). In the Early Triassic, the North Sea area became subjected to regional tensional stresses related to increasing rifting activity in the Norwegian Greenland Sea and in the Tethys domain (Ziegler 1990a-b). This build-up of tensional stresses in the Triassic induced the differential tectonic subsidence of sub-basins within the Southern Permo-Triassic Basin, for example, the NNE-oriented Off Holland Low (Fisher and Mudge 1998, Geluk and Röhling 1997).

## 12.3 Middle Jurassic domal uplift

Domal uplift of the central part of the North Sea area occurred in response to the development of a transient mantle plume head (Glennie and Underhill 1998, Underhill

and Partington 1993). This Mid-Kimmerian uplift was associated with vulcanism and widespread erosion in the central North Sea area. In the central North Sea area, crustal extension persisted during the uplift phase (Ziegler 1992). During Mid Jurassic Aalenian and Oxfordian times, regressive sequences were deposited in the Broad Fourteens area in response to the regional domal uplift (e.g. Van Adrichem Boogaert and Kouwe 1993-1997). Erosion in the Broad Fourteens area occurred in the late Mid Jurassic, at the transition from Oxfordian to Kimmeridgian (Van Wijhe 1987).

#### 12.4 Late Jurassic to Early Cretaceous extensional tectonics

Extensional tectonic activity in the North Sea increased as a result of processes governing the break-up of Laurasia (Ziegler 1990), i.e. the creation of the Atlantic Ocean and the separation of Laurasia into North America and Eurasia (Glennie and Underhill 1998, Ziegler 1992). This peak in tectonic activity, corresponding to the Late Kimmerian rifting pulse, also affected the Broad Fourteens area. By reactivating NW-SE trending Carboniferous-Permian faults it induced rapid subsidence of the Broad Fourteens Basin and uplift of its flanking highs: Winterton High, IJmuiden High, Cleaver Bank High, Texel-IJsselmeer High (Van Wijhe 1987a, 1987b). The renewed uplifted London Brabant Massif remained subaerial.

The orientation of the regional extensional stresses in the southern North Sea changes from ENE-WSW and E-W during Middle Jurassic times to NE-SW and NNE-SSW during the Late Jurassic (Nalpas et al. 1995).

An Early Cretaceous period of increased tectonic activity preceded and accompanied the mid-Aptian crustal separation between Iberia and the Armorican shelf, thus opening the Bay of Biscay (Ziegler 1990a). This Austrian tectonic rejuvenation of the North Sea area also affected the Broad Fourteens area as indicated by the emplacement of dykes and sills in the basin around 100 Ma (Dixon et al. 1981, Latin et al. 1990a-b, Van Wijhe 1987a,b, Ziegler 1990a).

During the later parts of the Early Cretaceous tectonic activity decreased and subsidence of the North Sea area became increasingly dominated by the relaxation of thermal anomalies that had been introduced during the preceding Triassic to Early Cretaceous extension stage (Ziegler 1990a). As a consequence, the Broad Fourteens Basin ceased to subside differentially around Albian (or possibly Aptian) times. Late Cretaceous regional subsidence coincides with a major eustatic rise in sea level.

#### 12.5 Late Cretaceous to Earliest Tertiary closure of the Tethys Ocean and the creation of the Alpine fold chain

The intraplate stress regime in the North Sea area during the Late Cretaceous - Paleocene is related to reorganisation of plate boundaries in the Arctic North Atlantic and the Tethys region: it is the combined result of the northward compressional stress field related to the onset of convergence of Africa with the Eurasian plate and the weakening extensional components related to the late rifting stage of the North Sea area (e.g. Oakman and Partington 1998, Ziegler 1990a-b). The pulsed, buildup of a regional northward oriented compressional stress-field during the Late Cretaceous to Paleocene induced the inversion of the Broad Fourteens Basin, which probably involved a pulsed uplift of the basin (Huyghe and Mugnier 1994, 1995). This inversion

started in the Turonian (Huyghe and Mugnier 1995, Nalpas et al. 1996). Oakman and Partington (1998) distinguish the following main compressive events in Turonian to Maastrichtian times: Early to Mid Turonian; Early Campanian; Campanian-Maastrichtian boundary; middle Late Maastrichtian. The Coniacian – Early Campanian event corresponds to the Sub-Hercynian phase. Major thrust structures developed in the northern Broad Fourteens Basin during the Coniacian to Early Santonian (Huyghe and Mugnier 1995). The middle Late Maastrichtian compressive pulse heralded the continent to continent collision in the Alpine domain (Ziegler 1990b). Huyghe and Mugnier (1995) suggest that the basin underwent its strongest uplift at the end of the Late Cretaceous. The regional direction of the maximum principal compressive stress in the Late Cretaceous is roughly N170° (Nalpas et al. 1995). This compression from the south was oblique to the major pre-Cretaceous fault systems (fault direction N140°, Nalpas et al. 1995). The compressional movements reactivated these pre-existing normal basin boundary faults (Brun and Nalpas 1996, Nalpas et al. 1995). Reversed movements along reactivated normal faults also involved oblique slip and strike slip movements (Brun and Nalpas 1996, Nalpas et al. 1995, 1996).

## 12.6 Tertiary creation of the Atlantic Ocean and seafloor spreading

The latest Cretaceous to Paleocene development of the Thulean (Icelandic) hot spot preceded crustal separation in the northern Atlantic and the Norwegian-Greenland Sea. Thermal uplift of the British Isles at the transition from Early to Late Paleocene, which is related to the development of the Iceland hot spot, terminated chalk deposition in the North Sea area (Ziegler 1990a).

Crustal separation between Laurentia, Greenland and Eurasia was achieved at the transition from the Paleocene to the Eocene (Ziegler 1990a). The crustal separation of Greenland and Europe ended the rifting stage of the North Sea area. Following the Late Eocene – Early Oligocene reorganisation of seafloor spreading patterns and plate boundaries in the Arctic North Atlantic, spreading axes stabilised in their current position (Ziegler 1990a).

After the early Eocene onset of seafloor spreading in the northern Atlantic and the Norwegian Greenland Sea, the evolution of the North Sea area was governed by ongoing thermal relaxation of the lithosphere and sedimentary loading and in addition by fluctuations in compressional intraplate stresses associated with changes in the rate of seafloor spreading and the Alpine collision of African and Eurasian plates and their suturing along Alpine fold belts (Ziegler 1990a, 1992). The overall character of the stress regime in the North Sea area was compressive during the Cenozoic (Kooi et al. 1989). Changes in this intraplate stress regime are thought to have had a distinct influence on the Cenozoic subsidence and uplift history of the North Sea area, including the Broad Fourteens Basin (Cloetingh et al. 1990, Kooi et al. 1991, Van Wees and Cloetingh 1996).

Neogene exhumation of margins of the North Sea Basin and accelerated sedimentation rates in the basin centre during Cenozoic (Japsen 1997, 1998, 1999, Kooi et al. 1991) may be explained by changes in intraplate stress fields (Cloetingh et al. 1990, Kooi et al. 1991, Van Wees and Cloetingh 1996). In addition, Late Eocene – Early Oligocene

uplift of the Broad Fourteens Basin, which is contemporaneous with the last phase of plate boundary reorganisation in the Arctic–North Atlantic region and the main phase of Alpine orogeny, probably results from the overriding influence of the build-up of intraplate compressional stresses induced by Alpine collision (Ziegler 1990a). The Late Eocene – Early Oligocene direction of compression was approximately N-S (Nalpas et al. 1996).

The present-day compressive stress field in Northwest Europe, including the southern North Sea area, shows an overall NW-SE orientation for the maximum compressive horizontal stress (Müller et al. 1992, Zoback 1992). This regional pattern of tectonic stress has been related to a combination of the ridge push force associated with the Mid-Atlantic ridge and collisional boundary forces along European-African plate boundaries (Gölke and Coblenz 1996, Müller et al. 1992). Frikken (1999) reports a present-day maximum principal stress direction of NNW-SSE in the Broad Fourteens Basin.

At present, the area of the Broad Fourteens Basin is not seismically active (Houtgast, pers com. 1999).

The bulk of crustal extension across the Broad Fourteens Basin occurred during Late Permian/Triassic to Early Cretaceous times; shortening was concentrated in the Late Cretaceous. Van Wees and Beekman (2000) estimated the amount of crustal stretching and shortening of the Broad Fourteens Basin by forward modelling the tectonic history of the basin for a well in the northern part of the basin, incorporating two phases of uniform extension (one in Triassic to Early Jurassic times and a second phase from Late Jurassic to start Late Cretaceous) and the inversion phase. The forward modelling resulted in a cumulative stretching factor of  $\delta = \beta = 1.29$  for the extensional phases. For the inversion phase Van Wees and Beekman (2000) adopted a stretching factor of  $\delta = \beta = 0.847$ , in accordance with 15% shortening of the basin. Rijkers and Duin (1994) estimated the amount of crustal stretching across the Broad Fourteens Basin for the Jurassic – Early Cretaceous phase of extension by comparing the length of base Upper Cretaceous and base Jurassic sediments along a 2D section:  $\delta = 1.07$ . The amount of shortening perpendicular to the orientation of the basin during Late Cretaceous inversion is estimated at 10 to 12% (Hooper et al. 1995, Huyghe and Mugnier 1994, Nalpas et al. 1995). The amount of relative dextral strike slip displacement of lateral platforms of the Broad Fourteens Basin in accordance with 10% shortening is estimated at 4.5 km (Nalpas et al. 1995). De Jong and Laker (1992) reported a lateral displacement of 3 km along faults in northeastern part of the basin.

The tectonic evolution of the North Sea area has resulted in the crust in the area of the Broad Fourteens Basin being only 29 - 30 km thick (Rijkers and Duin 1994). The thickness of the crust increases southwestward to about 38 km beneath the London Brabant Massif (Rijkers and Duin 1994).

Rheological modelling of the evolution of the Broad Fourteens Basin has indicated that a permanent weakening of the lithosphere exists and that deformation in the basin is concentrated on the basin boundary faults (Dirkzwager et al. 2000).

### 13 Geological history

This chapter outlines the geological history of the Broad Fourteens Basin. It focusses on those aspects of its history, that are considered important for reconstructing the fluid geological and fluid flow history of the basin.

The Westphalian to recent sediments present in the the Broad Fourteens area reach a thickness of more than 6 km. On the basis of the relationship between changes in tectonic setting and sedimentary history, in this thesis the Westphalian to recent stratigraphy has been subdivided into six major tectonostratigraphic sequences. A more detailed description of sedimentary sequences in offshore and onshore Netherlands is given in the stratigraphic nomenclature of the Netherlands (Van Adrichem Boogaert and Kouwe 1993–1997).

Figures 34 and 35 summarise some of the important characteristics of the geological setting of the Broad Fourteens Basin.

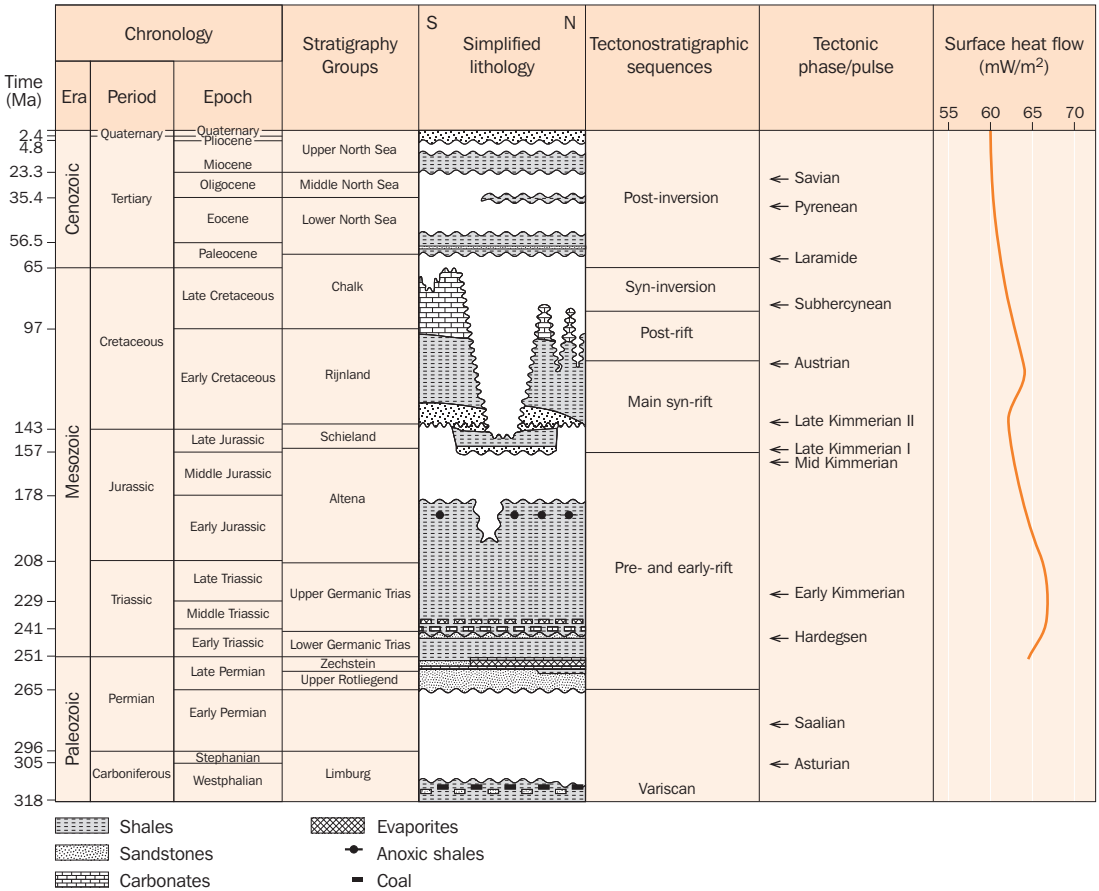


Figure 34 Stratigraphy, lithology and history of tectonic events and surface heat flow of the Broad Fourteens Basin. The evolution of the surface heat flow is derived from in-house tectonic forward modelling of the tectonic subsidence curve of well P09-01A

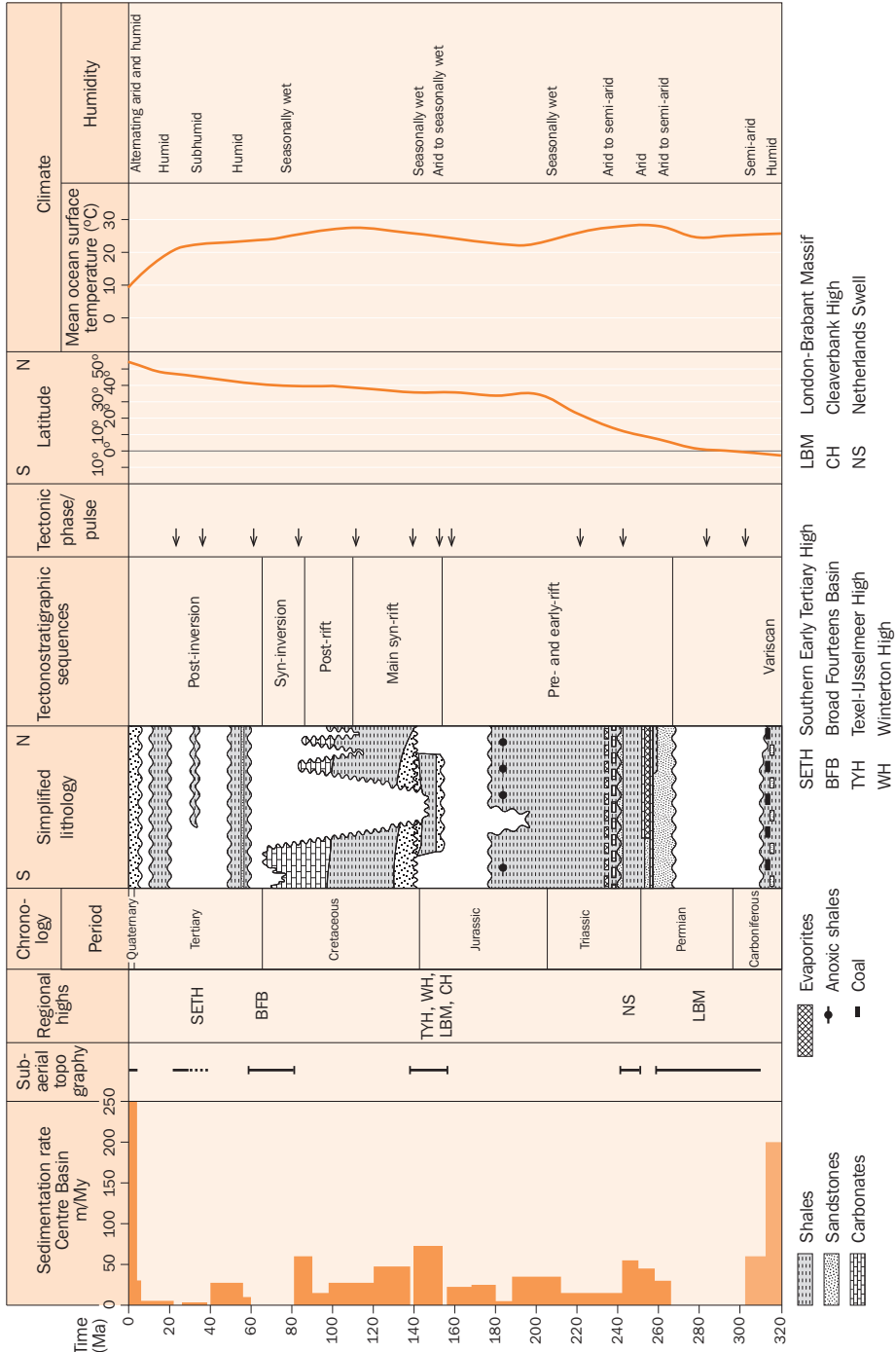


Figure 35 Tectonostratigraphy and lithostratigraphy and associated history of the subaerial topography, sedimentation rates and climatic conditions in the Broad Fourteens area (latitude from Glennie 1990; Figure 2.7; ocean surface temperatures for paleolatitudes estimated from Welte et al. 1997; Figure 1.5)

### 13.1 Variscan sequence of Westphalian and Stephanian age

During the Westphalian – Stephanian, regional deposition in the Broad Fourteens area took place in a regressive foreland basin setting, initially under a humid tropical climate and, during Westphalian D and Stephanian, under dry conditions. The result was a thick succession of predominantly lacustrine, deltaic and fluvial fine-grained siliciclastic deposits with intercalated coal seams belonging to the Caumer Subgroup (Baarlo, Ruurlo and Maurits Formations) and the Dinkel and Hunze Subgroups. The estimated total restored thickness of the succession is 2000 m (Quirk and Aitken 1997). The coal content varies laterally and vertically within the succession. The most frequent intercalations of coal seams occur in the Ruurlo and Maurits Formations. The Dinkel Subgroup comprises coarse-grained sandstone deposits derived from the uplifted hinterland in Westphalian C times (Leeder and Hardman 1990).

Regional thermal uplift of the Southern North Sea area in Stephanian – Early Permian times induced widespread differential erosion of the sedimentary succession. The estimated thickness eroded from the Broad Fourteens area varies between 800 and 1200 m (estimated from Figure 4C in Van Adrichem Boogaert and Kouwe 1993 - 1997 and the pre-Permian subcrop of chronostratigraphic units given in Gas Atlas 1998). The Dinkel and Hunze Subgroups are only preserved locally below the Saalian unconformity. As the Caumer Subgroup, including its coal measures, was only partly eroded, coal measures are preserved in the Broad Fourteens area. These coal measures are considered to be the main source rock for gas in the Broad Fourteens Basin (e.g. Van Wijhe 1987a, Van Wijhe et al. 1980).

The Base Permian Saalian unconformity is the erosive upper boundary of the Westphalian and Stephanian succession. The succession rests on the mudstones of the Namurian Epen Formation. These mudstones are coal free, but do contain dispersed carbonaceous matter. Along the northern flanks of the London Brabant Massif, the basal deposits of the Namurian consist of marine bituminous shales (Geverik Member). These shales were taken into account as a possible oil-prone source rock in studies of the West Netherlands Basin (Van Balen et al. 2000, Van Bergen 1998). It is not known if the Geverik Member is present in the Broad Fourteens Basin and, as a consequence was not taken into account in the present study.

### 13.2 Pre-rift and Early-rift sequence of Late Permian to Mid-Jurassic age

Also in the Broad Fourteens Basin, the Late Permian to Middle Jurassic sediments form a conformable megasequence, bounded at the base by Saalian and at the top by Mid Kimmerian regional unconformities (Chapter 3). The Late Permian to Middle Jurassic sediments in the Broad Fourteens area were deposited in the southern parts of the E-W trending Southern Permian Basin. The important sediment sources of the basin were the Variscan Mountains and the London-Brabant Massif, located south of the Permian Basin. The regionally deposited sedimentary sequence generally thins towards the massif.

In the Broad Fourteens Basin, sedimentation started in 267 Ma with accumulation of the terrestrial coarser-grained clastic (Slochteren Formation) and finer-grained desert lake deposits (Silverpit Formation) of the Upper Rotliegend Group. This group



has not been affected by later erosion in the Broad Fourteens Basin. The present-day thickness of the Upper Rotliegend Group varies between approximately 200 and 300 m and consists predominantly of eolian and fluvial sandstones of the Slochteren Formation. Intercalations of the Silverpit Formation in the group increase towards the north.

Lateral and time-dependent variations in syn-sedimentary subsidence in the area of the Broad Fourteens basin occur from Late Permian Zechstein onwards.

The marine to continental Zechstein deposits, composed of claystone, carbonate, anhydrite and rock-salt, in the southern part of the Southern Permian Basin thin out rapidly towards the London Brabant Massif (Van Adrichem Boogaert and Burgers 1983, Geluk et al. 1996). The Zechstein Group in the southern parts of the Broad Fourteens area is 200 - 300 m thick and is rich in siliciclastics. Zechstein salt is absent in the southeasternmost part of the future location of the basin. The clastic content of the Zechstein deposits decreases rapidly northwards and is replaced by carbonates and evaporites. In the central part of the future Broad Fourteens Basin, the present-day thickness of Zechstein salt deposits varies between 0 - 400 m and in the northwestern part the thickness of Zechstein salt varies between 400 and 600 m and there are numerous salt diapirs are present (Brun and Nalpas 1996). The Zechstein salt in the northern half of the basin has strongly influenced its subsequent tectonic and sedimentary development (e.g. Brun and Nalpas 1996, Nalpas et al. 1995). The first halokinetic movement of Zechstein salt in the Netherlands started during the Early Triassic and continued into the Neogene (e.g. Remmelts 1996).

During the Triassic, the Southern Permian Basin continued to subside differentially and the London Brabant Massif was a residual positive structural feature. The depositional thickness of the Lower and Upper Germanic Trias Groups in the future Broad Fourteens basin varied between approximately 900 and 1200 m (Geluk et al. 1996, Ziegler 1990a). The Lower Germanic Trias Group is composed of lacustrine claystones and sandstones of aeolian and fluvial origin. The Upper Germanic Trias Group consists mainly of lacustrine and shallow marine claystones, carbonates and evaporites. In the Early Triassic, initially widespread subsidence of the Southern Permo-Triassic Basin resulted in regional deposition of the Lower Buntsandstein Formation of the Lower Germanic Trias Group. Subsequently, sedimentation in the basin became progressively influenced by the development of swells (Netherlands Swell and Cleaverbank High) and lows, such as the Off Holland Low and West Netherlands Basin. The Hardegsen tectonic event induced uplift of these swells and caused deep erosion of sediments of the Lower Germanic Trias Group on the swells and minor erosion in the lows (Geluk and Röhling 1997). The Hardegsen tectonic event is associated with an unconformity at the base of the Upper Germanic Trias Group in the Broad Fourteens area.

At the end of the Triassic the depositional environment changed from continental towards restricted marine and open-marine. The Late Triassic transgression covered most of the previous swells, and thick open marine clays of the Altena Group (Sleen, Aalborg, Posidonia Shale, Werkendam and Brabant Formations) were deposited regionally in the Early to Middle Jurassic. The restricted marine conditions during

the Toarcian are associated with the deposition of bituminous clays of the Posidonia Shale Formation. This Formation is considered to be the most important oil source rock in the Broad Fourteens area (e.g. Oele et al. 1981, Roelofsen and De Boer 1991). Thermal uplift of the Central North Sea Dome decreased the area of deposition of the Altena Group and changed the depositional environment from open marine to shallow marine. Deposition of shallow marine sandy carbonates of the Brabant Formation ended in the Late Oxfordian when the Broad Fourteens area became subaerial and was subjected to erosion (Van Wijhe 1987a).

### 13.3 Main syn-rift sequence of Late Jurassic to Early Cretaceous age

Following erosion, the Late Kimmerian I rifting pulse induced rapid subsidence of the Broad Fourteens Basin and uplift of its flanking platforms and highs. Late Jurassic – Early Cretaceous deposition of the Delfland Subgroup was concentrated in the rapidly subsiding basin (Figure 36). The deposits thicken towards the basin centre across each of the major faults (Hooper et al. 1995) and attained a thickness of more than 800 m in the basin. The lacustrine, coastal plain and fluvial deposits of the Delfland Subgroup are characterised by significant facies changes and consist of carbonaceous silty claystones and fine- to coarse-grained sandstones with dispersed lignitic matter. During deposition in the basin, erosion proceeded on the adjacent platforms and highs. This erosion was intensified during the Late Kimmerian II tectonic pulse (Early Cretaceous Ryazanian) by the combined influence of uplift of the Mid-Late Kimmerian Highs, in combination with low sea levels. Rijkers and Geluk (1996) estimated an erosion of 1000 m on the Texel-IJsselmeer High (Chapter 3). Contemporaneous erosion in the basin centre was limited.

Sedimentation in the Broad Fourteens area resumed in Valanginian times with deposition of the Vlieland Sandstone Formation (Rijnland Group). During deposition of the coastal to shallow marine sands of the Vlieland Sandstone Formation and the open marine clays of the Vlieland Claystone Formation the basin continued to subside differentially. Sedimentation rates were significantly lower in comparison with the previous syn-rift sedimentation rates. During deposition of the Vlieland Claystone Formation marine sedimentation gradually overstepped the basin margin.

Albian tectonic activity resulted in emplacement of magmatic intrusions in the area of the Broad Fourteens Basin (Chapter 12). Undersaturated basaltic igneous rocks have been encountered in sandstones of the Upper Rotliegend Group (K14-FA-103), in Triassic sediments (Q07-02) and in salts of the Zechstein Group (L13-03) (Dixon et al. 1981). Figure 37 shows the reconstructed thickness of the Early and Main syn-rift sequences of the Triassic to Early Cretaceous as given by Nalpas et al. 1995.

### 13.4 Post-rift sequence of Aptian-Albian to Late Cretaceous age

Differential subsidence decreased further during the subsequent regional deposition of the marls and clays of the marine Holland Formation in Aptian/Albian times. By Albian times, the Texel-IJsselmeer High had also been incorporated in the regionally subsiding North Sea Basin (Rijkers and Geluk 1996). Continued regional subsidence in combination with a major eustatic rise in sea level inundated the remaining highs, such as the London–Brabant Massif. As a consequence of inundation of the highs,

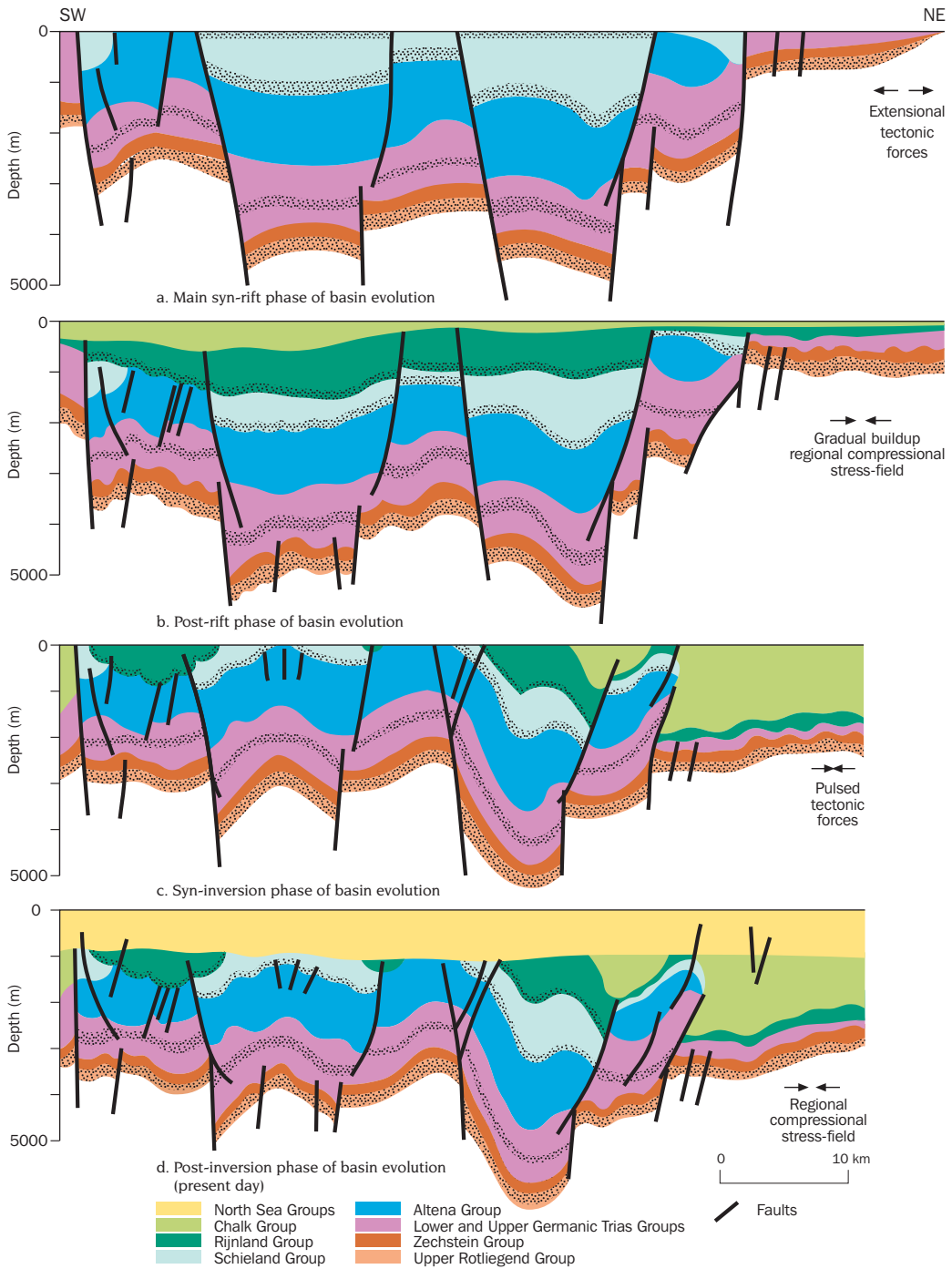


Figure 36 Balanced cross-sections through the Broad Fourteens Basin (Modified from Huyghe and Mugnier 1995) showing: a. Main syn-rift phase of basin evolution; b. Post-rift phase of basin evolution; c. End of syn-inversion phase of basin evolution: Paleocene geometry of the basin showing result of peneplanation of the basin and its flanks following Late Cretaceous inversion; d. Post-inversion phase of basin evolution

the influx of clastic material into the North Sea Basin diminished and conditions became favourable for the widespread deposition of limestones and marly chalk of the Texel Formation and the chalks of the Ommelanden Formation.

This post-rift regional subsidence became interrupted in the Broad Fourteens Basin in Turonian times by initiation of the inversion movements induced by the pulsed build-up of the regional compressional stress field (Section 12.5; e.g. Huyghe and Mugnier 1994, 1995, Nalpas et al. 1996).

### 13.5 Syn-inversion sequence of Late Cretaceous age

Pulsed inversion of the Broad Fourteens Basin took place from Turonian to Maastrichtian times (Brun and Nalpas 1996, Huyghe and Mugnier 1994). Hooper et al. (1995) interpreted the inversion of the basin to be diachronous: uplift started first in the central parts of the basin and later spread to the margins. The inversion was most intense at the end of the Late Cretaceous (Huyghe and Mugnier 1994). Along-strike variations in inversion style have been related to variations in the thickness of the Zechstein salt (Brun and Nalpas 1996, Dronkers and Mrozek 1991, Nalpas et al. 1995, 1996, Figure 38). In the northern and middle parts of the basin the Zechstein salt served as a décollement surface for the overlying sedimentary sequence during inversion. Here inversion was accompanied by folding and the development of thrust faults in the post-Zechstein basin fill along the basin margins, allowing the syn-extension sediments to be expelled over the basin flanks (e.g. Hooper et al. 1995, Nalpas et al. 1995). Salt diapirs were preferential sites for thrust fault development (Brun and Nalpas 1996). A major early phase

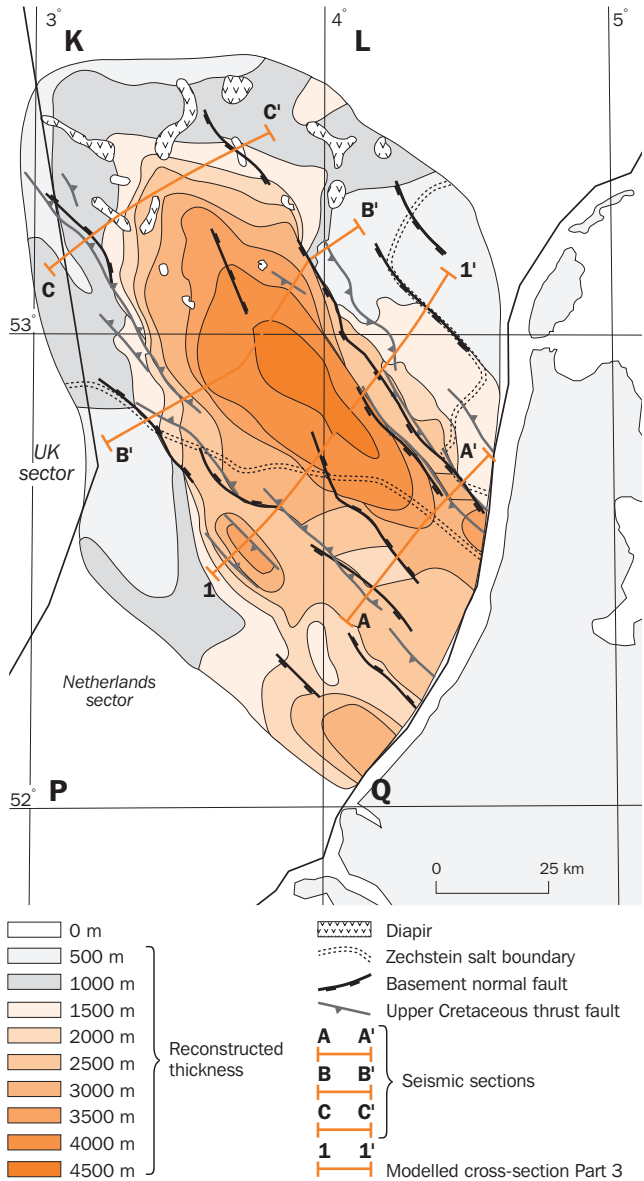


Figure 37 Reconstructed thickness of the Early and Main Syn-rift sequences of Triassic to Early Cretaceous age (Modified from Nalpas et al. 1995; some of the data are from maturation modelling by Trichon and Lescoeur 1993). Locations of seismic sections A-A', B-B', C-C' shown in Figure 38. Section 1-1' is modelled cross-section discussed in Part 3

of inversion-related thrusting in Coniacian to Early Santonian times is recognised in the northern part of the basin (Huyghe and Mugnier 1995). In the southernmost parts of the basin, where Zechstein salt is absent, inversion involved folding and basin fill uplift along steep, reverse, faults that pass downward into steep basement normal faults (Brun and Nalpas 1996). A hiatus between Danian and Campanian sedimentary units in the southern part of the basin (blocks Q8/Q10, pers. com. Geluk 2000) is indicative of an important early, pre-Campanian, phase of uplift and erosion. A similar major pre-Campanian phase of inversion-related erosion has also been observed in the nearby Vlieland Basin (Herngreen et al. 1996).

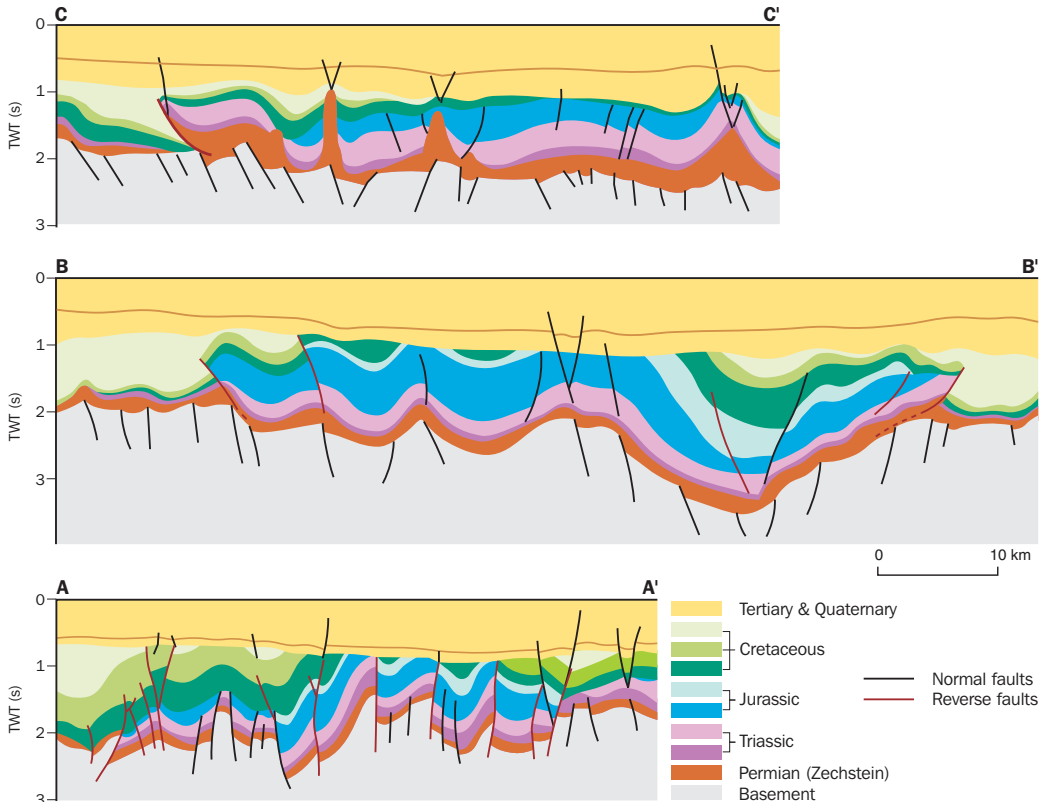


Figure 38 Seismic sections of the southern, middle and northern parts of the Broad Fourteens Basin showing differences in structural style (modified after Nalpas et al. 1995). Location of seismic sections is indicated on Figure 37

During Turonian to Maastrichtian times the deposition of Chalk Group sediments continued outside the inverted basin area reaching a maximum total thickness of approximately 2000 m (Nalpas et al. 1996). Various internal hiatuses as well as marly and sandy intercalations have been observed in the chalk deposits surrounding the basin. They are interpreted to be contemporaneous with periods of uplift of the basin (Bouw 1999, Huyghe and Mugnier 1994, Nalpas et al. 1995, Roelofsen and De Boer 1991). The uplifted sedimentary basin fill was strongly eroded during the inversion. Erosion was greatest in the centre of the basin and decreased towards the basin margins (Hooper et al. 1995, Huyghe and Mugnier 1995, Nalpas et al. 1995, Van Wijhe

1987a, 1987b; Figure 39). In parts of the basin where Zechstein salt deposits are present, the strongest erosion gradients are located along reverse faults (Brun and Nalpas 1996). Figure 39 indicates a reconstructed maximum erosional thickness of more than 3000 m. In addition to the pre-Campanian erosion, significant erosion probably also occurred in the Maastrichtian, because of the combination of inversion of the basin and a major fall in sea level in the Late Maastrichtian.

Chalk deposition persisted outside the inverted basin during the Early Paleocene (Danian). Late Maastrichtian to Danian Chalk overstepped the inverted basin. The rise of land masses surrounding the North Sea Basin (including the thermally uplifted British Isles) in Mid Paleocene times, in combination with the Mid-Paleocene low sea level, induced a regional phase of erosion and, as a consequence, terminated deposition of chalk (Section 12.6). Peneplanation of the Broad Fourteens Basin and its flanks (Figure 36) was followed by regional subsidence during Late Paleocene and Eocene.

### 13.6 Post-inversion sequence of Tertiary and Quaternary age

Regional subsidence and sedimentation in the Early Tertiary resulted in a sequence of marine fine-grained clastics (predominantly clays)

belonging to the Landen and Dongen Formations of the Lower North Sea Group. The Pyrenean compressive event at the Eocene–Oligocene boundary induced regional uplift of the Southern Early Tertiary High in the southeastern part of the Dutch part of the North Sea Basin (Van Adrichem Boogaert and Kouwe 1993-1997, Wong et al. 2001). The northwestern offshore extension of this High includes the Broad Fourteens area. Compression-induced uplift of the basin was responsible for 400 to 500 m of erosion of Lower Tertiary deposits in the southern part of the Broad Fourteens Basin (Nalpas et al. 1995, Wong et al. 2001). The original thickness of the Lower North Sea

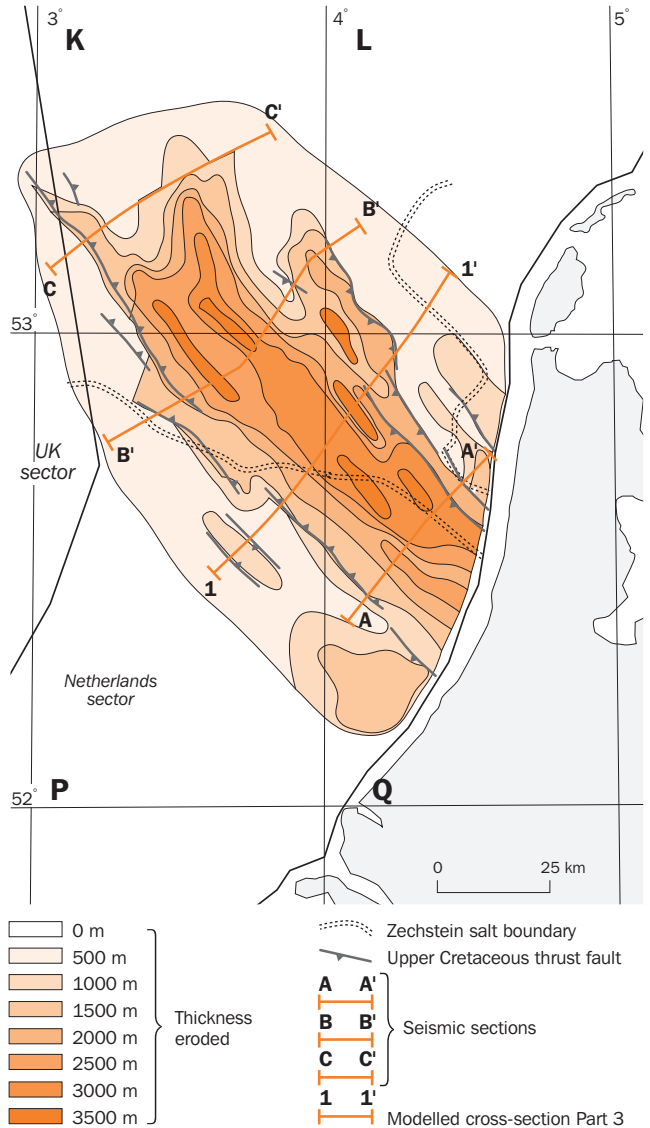


Figure 39 Pre-Tertiary erosion related to Late Cretaceous inversion (modified after Nalpas et al. 1995; some of the data are from maturation modelling by Trichon and Lescoeur 1992)

Group in the basin was approximately 600 m. This thickness has been derived from present-day residual thicknesses of 500 to 700 m of Lower Tertiary clastics surrounding the basin (Vinken 1987). During the Early Oligocene the sea again transgressed across the eroded basin. Oligocene sedimentation was concentrated in depocentres outside the area of the Broad Fourteens Basin (Chapter 3). This marine sedimentation of deposits belonging to the Middle North Sea Group was interrupted at the end of the Oligocene. The interruption is related to the Savian phase of regional uplift. From the south-eastern part of the Netherlands, continental sedimentation progressively replaced marine sedimentation since the Early Neogene (Zagwijn 1989). The depocentres in the onshore parts of the Netherlands have shifted to the NNW since the Middle Miocene (Zagwijn 1989), whereas in the northern offshore the depocentres gradually have shifted from east to west in the period between Late Miocene and Pliocene/Early Quaternary times (Sørensen et al. 1997) (Part 1, Figure 17). During Late Tertiary times sedimentation in the Broad Fourteens Basin occurred outside the main depocentres. Sedimentation rates started to increase during the Pliocene and remained relatively high during the Quaternary. In the Quaternary a local depocentre developed again in the Broad Fourteens Basin (Wong et al. 2001). Marine sedimentation persisted in the Broad Fourteens area during Miocene to Early Pleistocene times (siltstones and clays of the Breda, Oosterhout, Maassluis/Westkapelle Ground Formations of the Upper North Sea Group). Predominantly fine to medium grained sands and to a minor extent clays were deposited in various depositional environments during the remaining part of the Quaternary (Pleistocene: glacial – continental – marine; Holocene: marine). In the Pleistocene the Elsterian and Saalian ice sheets only just covered the Broad Fourteens Basin during their maximum advance (e.g. Joon et al. 1990, Laban 1995).



## 14 Hydrogeohistory

The main mechanisms capable of exerting a controlling influence on the fluid flow conditions in the Broad Fourteens Basin during its evolution were selected from its climatic, tectonic and geological history (Chapters 12 and 13; Figures 34 and 35). The mechanisms are discussed below.

### 14.1 Tectonic control

The general influence of tectonic forces and processes on the hydrogeologic and hydrodynamic conditions of a basin were outlined in Chapter 1. Here, these tectonic controlling mechanisms are discussed in close relation with the geological history of the Broad Fourteens Basin.

Chapter 1 outlined that tectonic control includes both static and dynamic influences on the permeability and storativity of the basin fill, and as a consequence on pore pressures and fluid flow. It should be realised that various processes operating during and after deformation may reduce the porosity and permeability of faulted rock. They include deformation-induced porosity reduction by disaggregation and mixing; pressure solution; cataclasis; cementation; clay smearing (e.g. Fisher and Knipe 1998).

The static influence on permeability and storativity results largely from the influence of the state of stress, level of mean stress, and the orientation of principal stresses on existing stress-controlled features such as faults, fractures and stylolites (Sibson 1994, 1995). In general, permeability and storativity tend to be higher in basins in an extensional stress regime than in a compressional stress regime (e.g. Muir-Wood and King 1993, Sibson 1995, 2000). Fractures close normal to the maximum compressive stress direction, whereas fractures oriented normal to the minimum stress direction will tend to dilate. In both normal and strike-slip tectonic regimes, enhanced permeability will tend to be along vertical fractures and steep normal faults, while in a compressional regime, enhanced fracture permeabilities are expected to be bedding-parallel (Du Rouchet 1981, Muir-Wood and King 1993). At a certain time during the basin's history the orientation of existing fractures and faults relative to the orientation of the principal stresses would have determined whether they were likely to become critically stressed for failure and were likely to be permeable, or to be impermeable. This means that changes in the direction of the principal stresses will have induced changes in the permeability of existing fractures. The orientation of the principal stresses changed repeatedly during the evolution of the Broad Fourteens Basin (for example: the regional extensional stress was oriented E-W in the Mid Jurassic and NE-SW and NNE-SSW in the Late Jurassic; the direction of the maximum principal compressive stress was approximately N170° in the Late Cretaceous, roughly N-S in Late Eocene – Early Oligocene and is NNW-SSE at present, Chapter 12). Frikken (1999) and Gauthier et al. (2000) studied the fracture orientations, present-day and paleo stress directions and permeability characteristics of fractures in the Upper Rotliegend Group in the northern part of the Broad Fourteens area. Gauthier et al. (2000) recognised three phases of fracturing in the basin: 1. A Triassic phase in which deformation during shallow burial resulted in particulate shear fractures, filled with dolomite cement, with NW-SE to NNW-SSE and NE-SW to ESE-WNW trends; 2. A Late



Jurassic phase of fault-related fracturing associated with fracture sets with NW-SE, NE-SW and N-S orientations; 3. A Late Cretaceous phase of dilational shear and joint propagation along existing NW-SE and NE-SW trends. At present, the fractures of Triassic origin and the Jurassic NE-SW and N-S fault-related shear fractures are cemented and may act as lateral barriers to fluid flow (Gauthier et al. 2000). In contrast, the NW-SE trending fault-related vertical dilational shear fractures and joints of Late Cretaceous age are often partly open (Gauthier et al. 2000). Frikken (1999) also observed that present-day NNW-SSE trending subvertical fractures associated with a reverse fault are parallel to present-day principal compressive stress directions and as a consequence have become minor dilational shear fractures. The present-day NNW-SSE orientation of maximum principal compressive stress is also roughly parallel to the inversion-related folding axes of the basin. As a consequence, tensile fractures related to the folding process may still be open, assuming cementation has not filled in the fracture pore space. In addition to the open fractures in the Upper Rotliegend Group, presently permeable fractures of inversion-related origin have been reported from Zechstein 3 Carbonates in block P6 (Van der Poel 1989) and in a small oil structure (Dronkers and Mrozek 1991).

The dynamic influence of tectonics on storativity and permeability in the Broad Fourteens Basin operates on different time scales related to various changes: gradual long-term changes in the tectonic stress regime from an active extensional stress regime (Triassic to Early Cretaceous) towards a compressional stress regime (Late Cretaceous to present day); pulse-like changes in compressive stress during the Late Cretaceous and beyond; and short-term stress fluctuations on time scales related to the earthquake cycle.

A change in tectonic regime from tensile to a compressive stress regime is accompanied by an increase in the mean stress level as well as by changes in the direction of principal stresses and will lead to closure of the subvertical extension fractures, a decrease in storativity and permeability, fluid expulsion or, if fluid drainage is inhibited, an increase in fluid pressures (Sibson 1995, 2000). The magnitude of the pressure increase depends on permeability characteristics and the rate of stress change.

Tectonic compression during Late Cretaceous times imposed a horizontal stress rate on the basin, resulting in the basin becoming 10 - 15 % shorter (Chapter 12). Assuming the main phase of shortening was from Coniacian to Maastrichtian, the estimated long-term horizontal shortening rate is 5000 m/ 23 My (0.22 mm/yr). The calculated shortening rate can be considered to be a minimum rate, because shortening of the Broad Fourteens Basin during Late Cretaceous probably took place in response to pulse-like changes in compression. In between the distinct shortening phases, compressional stresses will have built up to a level at which the (shear) strength of the rocks was exceeded and deformation (fault displacement, folding) could take place, relaxing the stresses.

During periods of active deformation in the basin, short-term cycles of stress increase and subsequent stress-relaxation, i.e. short-term seismic events occur on time scales of 10 to 10 000 years (Sibson 1994). The type of stress-related hydrogeological and hydrodynamic changes that may occur during active deformation depends on the

type of stress regime and related style of fault displacements (Jones et al. 1998, Muir-Wood and King 1993). In an extensional regime, normal fault displacement and stress relaxation is accompanied by the partial closing of extension fractures and groundwater expulsion from the fault and fracture zone, while during the interseismic period the fractures will dilate again (Muir Wood 1994, Muir-Wood and King 1993, Sibson 1994). Because these fractures are located in a stress regime of reduced ambient horizontal stress, they are likely to be highly strain sensitive and hence undergo large changes in aperture (Muir Wood 1994), i.e. large changes in storativity and permeability. Major normal fault displacements in the Broad Fourteens Basin are related to the Late Kimmerian I rifting pulse.

According to Muir-Wood and King (1993) reverse fault displacement and stress relaxation in a compressional regime will involve the dilation of high angle fractures and flow of groundwater towards the deformation zone. In the interseismic period, when compressive stresses build up again, groundwater will again be expelled from the fractures. In a compressional regime, the changes in porosity, storativity and permeability will be small in comparison with those in an extensional regime, because of the large ambient horizontal stresses (Muir Wood 1994). In contrast to Muir Wood, Sibson (1994, 1995) is in favour of expulsion of groundwater from the active reverse fault zone by way of seismic fault valving. Fault valve behaviour leading to post-failure discharge may occur in any tectonic setting where overpressuring has developed. Sibson considers it especially active in compressional and transpressional fault systems, and particularly associated with steep reverse faults. In Sibson's model, the – steep reverse – fault is impermeable and fluid pressures increase due to tectonic compression during the interseismic period, the increase in fluid pressure plays a role in initiating fault failure, and finally the fault functions as a permeable pathway for groundwater flow immediately post-failure. The groundwater flow through the fault zone is from a deep overpressured zone towards shallower zones. In neotectonic areas Muir Wood (1994) did not find field evidence of water coming out of reverse faults at the surface. He postulated that seismic valving is a process that only exists deep in the crust. Active fault displacement in a compressional setting occurred in the basin during the Late Cretaceous and Eocene–Oligocene periods. It was concentrated along the pre-existing normal basin boundary faults (Brun and Nalpas 1996, Dirkzwager et al. 2000, Nalpas et al. 1995). These fault displacements also included strike-slip components. In strike-slip faulting, local compressional and extensional structures are produced. It seems that less groundwater is released from active strike-slip fault zones compared with active normal faults (Muir-Wood and King 1993).

In conclusion, during active deformation of the Broad Fourteens Basin associated with Late Kimmerian I rifting, Late Cretaceous inversion and Eocene–Oligocene uplift, faults (especially the basin boundary faults) and associated fractures may have acted as permeable pathways for fluids.

At present, the Broad Fourteens Basin is in a compressive regime and the area is not seismically active today. Anyhow, the present-day compressive stress field will exert a static control on hydrogeological and hydrodynamic conditions. As described above, favourably oriented fracture systems in the basin tend to be partly open. Presently misoriented and/or cemented fracture systems have relatively poor

permeability and will have an adverse effect on fluid flow (e.g. Frikken 1996, 1999, Gauthier et al. 2000, Hastings et al. 1991).

## 14.2 Sedimentary loading

From Permian to Late Tertiary the average long-term sedimentation rates in the southern part of the Basin did not exceed 100 m/My (Figure 35), corresponding to an imposed vertical stress rate of approximately 2 MPa/My. The highest sedimentation rates occurred during the Early Triassic (Early rift sequence), the Late Jurassic – Early Cretaceous (syn-rift sequence), during deposition of the post-rift chalks, and in the Quaternary. In Quaternary times sedimentation rates reached values exceeding 250 m/My. This sedimentation rate corresponds to an imposed vertical stress rate of approximately 5 MPa/My (density Quaternary sedimentary rock = 2090 kg m<sup>-3</sup>). In the northern part of the basin, average long-time sedimentation rates also exceeded 100 m/My during deposition of evaporites of the Zechstein Group (Bouw 1999).

Significant overpressured conditions are unlikely to develop in basins that subside less than 100 m/My, except in the parts of the basin with extensive layers of very poor permeability (e.g. Bethke 1986, Harrison and Summa 1991). In contrast, rapid rates of burial (high sedimentation rates) will cause overpressure in poorly permeable layers (e.g. Osborne and Swarbrick 1997).

## 14.3 Erosional unloading

The maximum amount of inversion-related erosion during Late Cretaceous – Early Tertiary times was 3000 m. The inversion-related erosion rate in the inverted centre of the basin was 3000 m in 20 million years or less, which corresponds to a minimum rate of erosional unloading in the order of 3.3 MPa/My. During the Eocene – Oligocene inversion period the erosional unloading is estimated at 3.7 MPa/My (corresponding to a maximum erosion of 500 m in 3 My).

## 14.4 Glacial loading/glacial unloading

The southernmost extension of the Elsterian and Saalian ice sheets did just reach the Broad Fourteens Basin. Glacial loading and unloading will have affected the basin fill during and, probably shortly, after these glaciations.

## 14.5 Topography of the water table

During different time periods in the basin's history, a water table was able to establish in the subaerial parts of the Broad Fourteens area (Figure 35). The only time period without any subaerial exposure, and hence without any topography-induced flow is the post-rift period. The main periods of topography-induced flow are indicated in Table 9. During three time periods the Broad Fourteens area was part of major supraregional flow systems with recharge areas outside the basin (flow periods 1, 2 and 3). During syn-rift times the subsiding Broad Fourteens Basin was probably the discharge area of different supraregional flow systems originating in the highs surrounding the basin, such as the Texel IJsselmeer High, Winterton High and Cleaverbank High. Deep syn-rift erosion of these uplifted highs (Chapters 3 and 13) exposed e.g. Triassic and Rotliegend reservoir units to infiltrating meteoric water. The dip direction of these units favoured subsequent flow towards the Broad Fourteens Basin. During the Late Cretaceous and Pyrenean inversion phases regional flow

Table 9 Main periods of topography-induced flow in the Broad Fourteens Basin

| Time period                           | Flow period | Subaerial exposure related to continental depositional setting | Subaerial exposure related to uplift and erosion/tectonic | Positive topographic features/highs phase                                      | Climate                                       | Flow system                        | Duration |
|---------------------------------------|-------------|--|---|--|---|------------------------------------|----------|
| Variscan                              | 1a          | Dinkel Subgroup; fluvial fan, floodplain                       |   | London-Brabant Massif  | Tropical, semi-arid                           | 1: Supra-regional (lateral inflow) | >47 My   |
|                                       | 1b          |  | Saalian   | London-Brabant Massif  | Tropical, semi-arid                           |                                    |          |
| Pre- and Early rift                   | 1c          | Upper Rotliegend Group; eolian, fluvial                        |   | London-Brabant Massif  | Arid to semi-arid                             | 2: Supra-regional (lateral inflow) | 9 My     |
|                                       | 2a          | Lower Germanic Trias Group; fluvial, basin fringe, lacustrine  |   | Netherlands Swell  | Tropical, arid to semi-arid                   |                                    |          |
|                                       | 2b          |  | Hardegsen   | Netherlands Swell  |   |                                    |          |
| Main Syn-rift                         | 3a          |  | Late Kimmerian I  | Texel IJsselmeer High  | Subtropical, seasonally wet                   | 3: Supra-regional (lateral inflow) | 17 My    |
|                                       | 3b          | Schieland Group; continental                                   |   | Texel IJsselmeer High, Winterton High, Cleaverbank High, London-Brabant Massif |   |                                    |          |
|                                       | 3c          |  | Late Kimmerian II   | Texel IJsselmeer High, Winterton High, Cleaverbank High, London-Brabant Massif |   |                                    |          |
| Syn-inversion                         | 4           |  | Late Cretaceous Inversion                                 | Broad Fourteens Basin  | Subtropical, seasonally wet                   | 4: Regional                        | >14 My   |
|                                       | 5           |  | Pyrenean Inversion  | Broad Fourteens Basin / Southern Early Tertiary High                           | Warm, subhumid                                | 5: Regional                        | 3 My     |
| Post-inversion (Mid-Late Pleistocene) | 6           | Upper North Sea Group; glaciogene, fluvial, marine             |   |  | Cold-cool temperate, alternating arid & humid | 6: Local                           | <<1 My   |

systems were probably able to develop in the Broad Fourteens area. For example, during the Late Cretaceous inversion period, the Broad Fourteens Basin was a regional high surrounded by the Late Cretaceous sea. The island-like character of the inverted basin and the topographic relief of the ground surface induced by inversion-related uplift, in combination with abundant precipitation, were favourable conditions for the development of a water table with sufficient relief to induce a deep circulation of groundwater of meteoric origin. The process of intrusion of meteoric water into the subsurface of the basin can be compared with the well-known process of the development of freshwater lenses below dunes: the uplifted central parts of the Broad Fourteens Basin may have been major recharge areas (Verweij 1990a). The

hydrogeological framework of the inverted basin also favoured deep infiltration of meteoric waters. The inversion-related permeable fault and fracture zones may have enhanced the deep infiltration. The tilting of the hydrostratigraphical units due to inversion movements exposed different permeable units to meteoric flushing.

#### 14.6 Overview of factors controlling the hydrogeohistory

Table 10 gives an overview of the main forces and processes that exerted a controlling influence on the fluid flow conditions in the basin during its evolution. In addition to the – mechanical and thermal – forces given in Table 10, other processes influencing fluid flow conditions and related pressure conditions, such as dehydration reactions, chemical diagenesis and gas generation, may have operated simultaneously. Fluid density gradients may have influenced fluid flow locally throughout the basin's evolution (for example near evaporites in the central and northern part of the Broad Fourteens Basin, and in coastal depositional environments, by way of seawater intrusion; Chapter 1). Table 10 clearly indicates that different processes have been active and have influenced the fluid flow conditions simultaneously at a certain time during the history of the Broad Fourteens Basin.

Table 10 Main mechanical and thermal forces and processes that influence fluid flow conditions during the evolution of the Broad Fourteens Basin

| Time period                        | Area                           | Primary driving force     | Secondary driving force   |
|------------------------------------|--------------------------------|---------------------------|---|
| Variscan                           |                                |                           |   |
| Carboniferous                      | Broad Fourteens Basin & flanks | Topography of water table | Sedimentary loading   |
| Permian                            | Broad Fourteens Basin & flanks | Topography of water table | Erosional unloading   |
| Pre- and Early rift                | Broad Fourteens Basin & flanks | Sedimentary loading       | Topography of water table   |
| Main Syn-rift                      | Broad Fourteens Basin          | Sedimentary loading       | Tectonic forces (local) heating                                     |
|                                    | Flanks/highs                   | Topography of water table | Erosional unloading<br>Cooling*                                     |
| Post-rift (Albian-Late Cretaceous) | Broad Fourteens Basin & flanks | Sedimentary loading       |   |
| Syn-inversion (Late Cretaceous)    | Broad Fourteens Basin          | Topography of water table | Cooling*  |
|                                    |                                | Tectonic forces           |   |
|                                    |                                | Erosional unloading       |   |
|                                    | Flanks                         | Sedimentary loading       |   |
| Post-inversion (Oligocene-present) | Broad Fourteens Basin & flanks | Sedimentary loading       | Topography of water table<br>Cooling**<br>Glacial loading/unloading |

\* Cooling: temperature decrease in sedimentary units because of erosion

\*\* Cooling: temperature decrease in sedimentary units because of climate change/decrease surface temperature

Table 11 summarises the large number of mechanisms and related processes that operated during basin evolution and that are expected to have controlled the pressure development in the basin to a greater or lesser degree.

Table 11 Mechanisms controlling the development of overpressures of the groundwater in the Broad Fourteens Basin during its evolution

|   |
|---|
| Stress related processes  |
| – Sedimentary loading*  |
| – Erosional unloading*  |
| – Changing lateral tectonic stresses/changing tectonic regime (extension → compression) |
| – Tectonic stress fluctuations (short term)/seismicity                                  |
| – Glacial loading/unloading   |
| Fluid flow  |
| – Infiltration of seawater  |
| – Infiltration of meteoric water (creating topographic relief of groundwater table*)    |
| – Flow of fluids in the basin*  |
| – Lateral flow of fluids into basin   |
| – Lateral flow of fluids out of basin*  |
| Heating and cooling   |
| Changing groundwater volumes/fluid volumes by   |
| – (Heating/cooling)   |
| – Diagenetic reactions  |
| – Dehydration of minerals   |
| – Petroleum generation*   |

\* Mechanisms included in 2D basin modelling Broad Fourteens Basin

## 14.7 Present-day hydrogeological framework

Shaly deposits of poor matrix permeability dominate the sedimentary fill of the basin. In addition, very poorly permeable Zechstein Salt Members are present in the central and northern parts of the basin. The main reservoir type units are the Upper Rotliegend Slochteren Formation, Carbonate Members of the Zechstein Group, Sandstone Members of the Lower Germanic Trias Group, Solling Formation of the Upper Germanic Trias Group, Middle Werkendam Member of the Altena Group, Sandstone Members of the Schieland Group, Vlieland Sandstone Formation of the Rijnland Group and Quaternary sands (Figure 40). The lateral continuity of pre-Tertiary hydrostratigraphic units is restricted by numerous faults in the basin (Figure 38) and in the northern part of the basin is also affected by the presence of salt diapirs.

The very poor permeabilities of Upper Permian and Lower Triassic sandstone units in the inverted central part of the basin have been related to the syn-rift illite cementation of these units (e.g. Lee et al. 1989, Oele et al. 1981; for more detailed information see section 15.4). Present-day porosity distributions in the pre-, early- and syn-rift sequences reflect the influence of the Late Cretaceous – Early Tertiary inversion movements. In a large part of the Broad Fourteens Basin, these sequences are not at their maximum depth of burial. The sequences show signs of overcompaction, that is their porosities, and as a consequence their permeabilities, are relatively low for the present-day burial depths of the sequences. Figure 41 shows

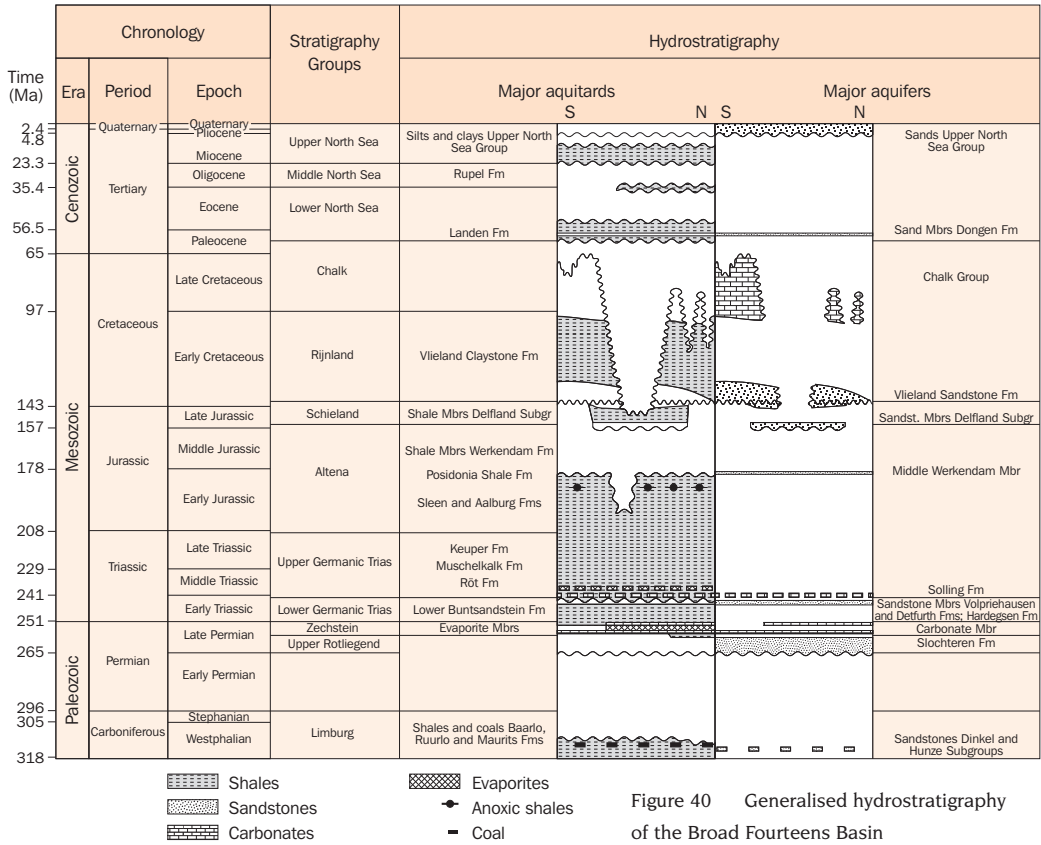


Figure 40 Generalised hydrostratigraphy of the Broad Fourteens Basin

examples of relatively poor porosities of the Slochteren Sandstone Formation in the strongly inverted parts of the basin. The overcompacted nature of the Lower Germanic Trias Group is also indicated by the relatively high sonic velocities, determined by Giesen (1995), for this Group in blocks K17, P2, P3, P6 and to a minor extent in blocks P9 and Q4 (see also Nalpas et al. 1995).

The overall permeability of the hydrostratigraphic units in the basin is the combined result of the matrix permeability and the fracture permeability. The fracture permeability of the hydrostratigraphic units in the Broad Fourteens Basin is influenced by the orientation of the fractures vis-à-vis the present-day orientation of maximum compressive stress. Studies of fractures of Triassic, Late Jurassic and Late Cretaceous origin have demonstrated this influence on present-day permeability in the Upper Rotliegend hydrostratigraphic unit (section 14.1). At present, the NW-SE oriented Late Cretaceous and Late Jurassic fractures and joints are partly open, while Triassic and Jurassic NE-SW and N-S oriented fractures are cemented and act as lateral barriers to flow (e.g. Gauthier et al. 2000).

Open, favourably oriented inversion-related tension fractures increase the overall porosity and permeability of the sequences in distinct parts of the basin.

Table 12 summarises the present-day indicators of changing permeability conditions during basin evolution.

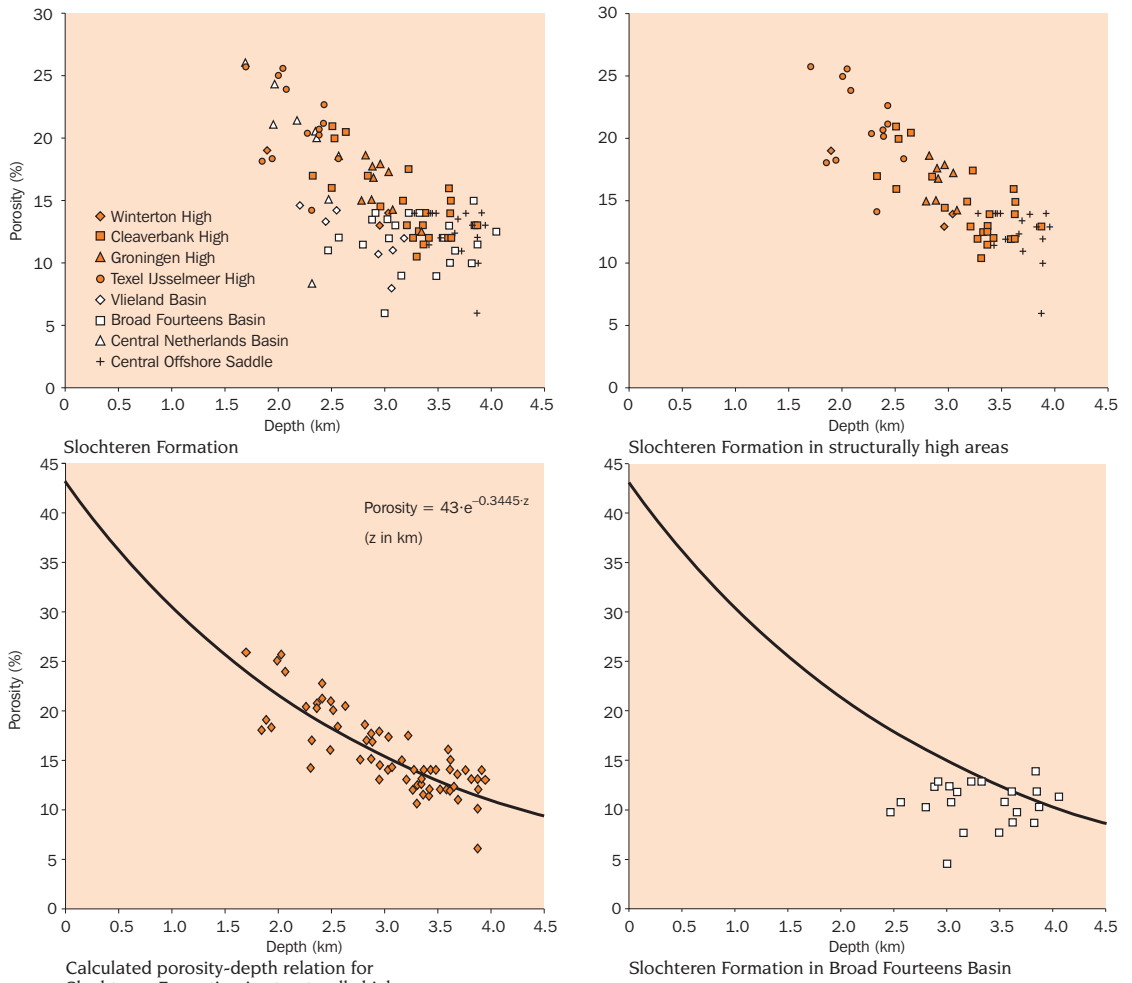


Figure 41 Porosity-depth relations for the Slochteren Formation in sedimentary basins and structural highs. Porosity data from Geological Survey of the Netherlands 1991 - 1995; RRI 1985, 1988

Table 12 Present-day indicators of changing permeability conditions

| Indicator  | Event  | Timing        | Source   |
|--|--|---------------|--|
| Relatively low matrix porosity in pre-inversion units in central part of basin | Uplift                                       | Syn-inversion | Giesen 1995<br>Nalpas et al 1995<br>Verweij 1999 |
| Disrupted permeability in Slochteren Fm and Triassic sandstones                | Illitization                                 | Main syn-rift | Oele et al 1981<br>Lee et al 1989                |
| Fractures of different orientation in Slochteren Fm                            | ± E-W extension                              | Early-rift    | Frikken 1999                                     |
|  | ± NE-SW extension                            | Main syn-rift | Gauthier et al 2000                              |
|  | ± N170° compression                          | Syn-inversion |  |
| Fractures in Z3 Carbonates   |  | Syn-inversion | Van der Poel 1989                                |
| Partly open NW-SE fractures in Slochteren Fm                                   | NNW-SSE direction maximum compressive stress | Present-day   | Gauthier et al 2000                              |



## 15 Indicators of present-day and paleo fluid flow conditions

Part 1 showed that during most of the post-Carboniferous history of onshore and offshore Netherlands, different forces have acted simultaneously on the fluids, and different fluid flow systems will have coexisted laterally and vertically. The same observation applies to the Broad Fourteens Basin and its flanking regions (Tables 9 and 10). The characteristics of these inferred fluid flow systems can be verified with the help of direct and indirect indicators of present-day and paleo-hydrodynamic and hydrogeological conditions. These indicators include the present-day physico-chemical characteristics of rocks and fluids, such as pressures, temperatures, heat flow, hydrochemical characteristics, sediment-diagenetic characteristics, and characteristics of oil and gas accumulations.

### 15.1 Pressures

Published pressure data are available for a restricted number of reservoir-type units of the Upper Rotliegend Group, Main Buntsandstein Subgroup, Delfland Subgroup and Rijnland Subgroup (Table 13). These groundwater pressures, measured between depths of 1200 and 3900 m, are near-hydrostatic to slightly superhydrostatic. Slightly overpressured conditions of the groundwater (1 - 2.6 MPa) are observed in the Upper Rotliegend Group in the northern part of the basin (blocks K11-K15) and in its flanking highs (blocks L14, P5). These overpressures are calculated, assuming a hydrostatic gradient of 10.3 MPa/km. Because the hydrostatic gradient changes with water salinity, temperature and pressure (Chapter 1), the actual overpressure may deviate from the values in Table 13; for waters with a very high concentration of dissolved solids located at shallow depths, the actual overpressure will be smaller than indicated in the table. No measured pressure data were available for the poorly permeable units.

### 15.2 Temperatures and steady-state heat flow

Figure 42 shows the change of temperature with depth in the Broad Fourteens area based on published temperature data from 18 wells (Appendix 2). Most of these data were derived from bottom hole temperature measurements. No information is available on their quality and reliability. It is recognised that the reliability of the measured bottomhole temperatures and corrected bottom hole temperatures is poor (e.g. Deming 1989, Hermanrud et al. 1990). In general, temperatures derived from bottom hole data are cooler than true formation temperatures; the magnitude of the deviation increases with depth (Deming 1989). The present-day temperature gradient of the Broad Fourteens Basin is approximately 32 °C/km (based on a linear trend line passing through the published temperature data and the interception point at depth = 0 m and temperature = 8 °C). The calculated temperature gradient for a trend line calculated for the subsurface data points only is approximately 28 °C/km. This gradient seems relatively low in comparison with recently calculated temperature gradient for the onshore Roer Valley Graben based on corrected temperature data (Van Balen et al. 2002). The temperature data suggest that there is a difference between the temperature gradient in the basin and the gradient in its flanking highs. In the flanking highs the temperatures in the shallow part of the subsurface are relatively high and in the deeper parts relatively low in comparison with the temperatures in the basin itself.

Table 13 Measured reservoir pressures Broad Fourteens area

| Location              | Stratigraphic unit          | Depth        | Reservoir P       | Hydrocarbon-water contact | Pw    | Hydrostatic Pw     | Overpressure | Data source     | Hydrostatic gradient |
|-----------------------|-----------------------------|--------------|-------------------|---------------------------|-------|--------------------|--------------|-----------------|----------------------|
|                       |                             | m –sea-level | (measured)<br>MPa | m –sealevel               | MPa   | (estimated)<br>MPa | MPa          |                 | Pa/m                 |
| Broad Fourteens Basin |                             |              |                   |                           |       |                    |              |                 |                      |
| K11-02                | Upper Rotliegend Group      | 3085.5       | 34.59             | 3185.5                    | 34.79 | 32.81              | 1.98         | DST; RRI 1985   | 10300                |
| K11 gas field         | Upper Rotliegend Group      | 3135         | 34.79             | 3188                      | 34.79 | 32.83              | 1.96         | Webatlas 1999   | 10300                |
| K12-02                | Upper Rotliegend Group      | 3500         | 37.68             | 3555                      | 37.78 | 36.62              | 1.16         | Webatlas 1999   | 10300                |
| K12-03                | Upper Rotliegend Group      | 3495.6       | 39.23             | 3568.6                    | 39.34 | 36.75              | 2.59         | DST; RRI 1988   | 10300                |
| K13-04                | Upper Rotliegend Group      | 2466         | 27.47             | 2521                      | 27.58 | 25.97              | 1.61         | DST; RRI 1988   | 10300                |
| K13 DE structure      | Upper Rotliegend Group      | 2450         | 27.44             | 2517                      | 27.58 | 25.93              | 1.65         | Webatlas 1999   | 10300                |
| K14-01                | Upper Rotliegend Group      | 2875.4       | 33.88             | 3115.4                    | 34.35 | 32.09              | 2.26         | ProdT; RRI 1985 | 10300                |
| K14 gas field         | Upper Rotliegend Group      | 3000         | 34.05             | 3114                      | 34.33 | 32.07              | 2.26         | Webatlas 1999   | 10300                |
| K15 FB gas field      | Upper Rotliegend Group      | 3875         | 43.19             | 3979                      | 43.57 | 40.98              | 2.59         | Webatlas 1999   | 10300                |
| K 17 gas field        | Upper Rotliegend Group      | 2865         | 29.99             | 2882                      | 30.08 | 29.68              | 0.4          | Webatlas 1999   | 10300                |
| P6 gas field          | Main Buntsandstein Subgroup | 2650         | 30.23             | GDT: 2750                 | 30.58 | 29.40              | 1.18         | Webatlas 1999   | 10300                |
|                       |                             |              |                   | GWC estimated: 2854       |       |                    |              |                 |                      |
| Q01-02                | Upper Rotliegend Group      | 2972         | 31.07             | 2982                      | 31.09 | 30.71              | 0.38         | DST; RRI 1985   | 10300                |
|                       | Upper Rotliegend Group      | 2956         | 31.32             | 2982                      | 31.37 | 30.71              | 0.66         | DST; RRI 1985   | 10300                |
|                       | Upper Rotliegend Group      | 2971         | 30.59             | 2982                      | 30.61 | 30.71              | 0.10         | DST; RRI 1985   | 10300                |
| Q01-03                | Vlieland Sandstone Form.    | 1191.6       | 12.79             | 1288.6                    | 13.69 | 13.14              | 0.55         | DST; RRI 1988   | 10204                |
|                       | Vlieland Sandstone Form.    | 1215.6       | 12.86             | 1288.6                    | 13.76 | 13.14              | 0.62         | DST; RRI 1988   | 10204                |
| Q01-03                | Vlieland Sandstone Form.    | 1275         | 13.44             | 1289                      | 13.57 | 13.15              | 0.42         | Webatlas 1999   | 10204                |
| Basin flanks          |                             |              |                   |                           |       |                    |              |                 |                      |
| K13 B structure       | Main Buntsandstein Subgroup | 1300         | 14.29             | 1347                      | 14.47 | 13.87              | 0.60         | Webatlas 1999   | 10300                |
| L14-02                | Upper Rotliegend Group      | 3165.7       | 34.95             |                           | 34.95 | 32.61              | 2.34         | DST; RRI 1988   | 10300                |
|                       | Upper Rotliegend Group      | 3182.7       | 34.13             |                           | 34.13 | 32.78              | 1.35         | DST; RRI 1988   | 10300                |
|                       | Upper Rotliegend Group      | 3101.7       | 34.07             |                           | 34.07 | 31.95              | 2.12         | DST; RRI 1988   | 10300                |
| L14-03                | Upper Rotliegend Group      | 3154         | 31.79             |                           | 31.79 | 32.47              | <0           | DST; RRI 1988   | 10300                |
|                       | Upper Rotliegend Group      | 3198         | 35.02             |                           | 35.02 | 32.94              | 2.08         | DST; RRI 1988   | 10300                |
| L16-01                | Upper Rotliegend Group      | 3271.4       | 37.23             | GDT: 3336.4               |       |                    |              | DST; RRI 1985   | 10300                |
|                       | Upper Rotliegend Group      | 3526.4       | 38.14             |                           | 38.14 | 36.32              | 1.82         | DST; RRI 1985   | 10300                |
| P05-01                | Upper Rotliegend Group      | 2890.2       | 30.91             |                           | 30.91 | 29.77              | 1.14         | DST; RRI 1985   | 10300                |
|                       | Upper Rotliegend Group      | 3055.2       | 32.70             |                           | 32.70 | 31.47              | 1.23         | DST; RRI 1985   | 10300                |
| P12-01                | Upper Rotliegend Group      | 3490.4       | 37.01             |                           | 37.01 | 35.95              | 1.06         | DST; RRI 1985   | 10300                |
| Q08-01                | Upper Rotliegend Group      | 2213         | 22.60             |                           | 22.60 | 22.58              | 0.02         | DST; RRI 1988   | 10204                |
| Q08-02                | Main Buntsandstein Subgroup | 1920         | 21.47             | 1962                      | 21.53 | 20.02              | 1.51         | DST; RRI 1988   | 10204                |
| Q10-01                | Delfland Subgroup           | 2107         | 21.49             |                           | 21.49 | 21.49              | 0            | FIT; RRI 1988   | 10204                |

Steady-state heat flows were calculated from the temperature data using porosity-dependent bulk thermal conductivities for the chronostratigraphic units (Appendix 2). These porosity-dependent bulk thermal conductivities are based on matrix thermal conductivities given by Andrews-Speed et al. (1984) and temperature-dependent thermal conductivities of groundwater given in Somerton (1992; see also Chapter 8).

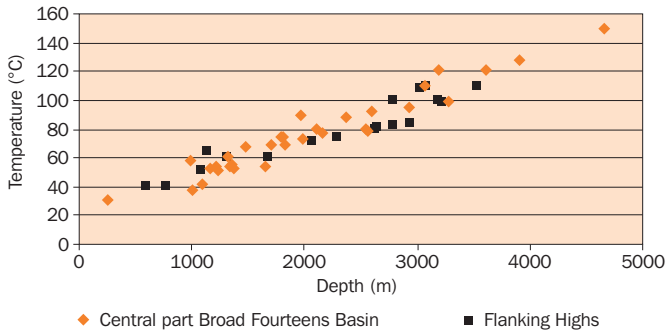


Figure 42 Measured temperatures versus depth for the Broad Fourteens Basin and adjacent highs (temperature data and well locations are given in Appendix 2)

The temperature dependence of the thermal conductivity of halite and carbonates was also included in the calculations. The steady-state heat flow in the basin, calculated for temperature measurements at depth between 0 m and at least 3000 m, is approximately 62 mW/m<sup>2</sup> (Appendix 2 and Table 14). The calculated steady-state heat flow for this range of depth is 58 mW/m<sup>2</sup> at the Winterton High, is 55 mW/m<sup>2</sup> at the IJmuiden High and is 65 mW/m<sup>2</sup> at the Zandvoort Ridge. These heat flow values are within the range of the modelled heat flow values for the Netherlands based on mantle P wave velocities (Goes et al. 2000a-b). The calculated steady-state heat flow in the study area changes with depth (Table 14). Heat flow in the basin and its flanking highs at depths of less than 2000 m was calculated to decrease to 53 mW/m<sup>2</sup>. In the flanking highs the heat flow seems to increase again in the shallowest part of subsurface (Table 14).

Table 14 Calculated steady-state heat flow in the Broad Fourteens Basin and flanking highs

|  | Basin<br>(15 wells) | Flanking Highs             |  |                              |
|--|---------------------|----------------------------|--|------------------------------|
|  |                     | Winterton High<br>(P05-01) | IJmuiden High<br>(P12-A-01,<br>P12-1X, Q10-01) | Zandvoort Ridge<br>(Q11-01S) |
| Heat flow (mW/m <sup>2</sup> )<br>0 m to >3000 m | 62                  | 58                         | 55   | 65                           |
| Heat flow (mW/m <sup>2</sup> )<br>>2000 m        | 84                  | 69                         | 51   | 105                          |
| Heat flow (mW/m <sup>2</sup> )<br>0 m to 2000 m  | 53                  | 54                         | 54   | 52                           |
| Heat flow (mW/m <sup>2</sup> )<br>0 m to 1000 m  | 53                  | 60                         | 60*  | 62                           |

\* Heat flow (mW/m<sup>2</sup>) 0 m to 1000 m for P12-A-01: 79 mW/m<sup>2</sup>

In addition to these regional variations in steady-state heat flow, more local variations can be observed due to the occurrence of Zechstein salt deposits in the northern part of the basin. Heat flow through Zechstein salt deposits was calculated to increase to values of 190 mW/m<sup>2</sup> in well K15-07 (thickness Zechstein Group = 904 m) and 124 mW/m<sup>2</sup> in well K17-02 (thickness Zechstein Group = 1010 m). The presence of igneous intrusions in the basin may exert a local influence on the heat flow and temperature distribution (Chapter 8). This could not be confirmed by the temperature data available.

### 15.3 Hydrochemistry

The waters in the Lower Cretaceous and older units in the Broad Fourteens Basin are brines, i.e. they are more concentrated than seawater. The measured resistivity values of waters in these units vary between approximately 0.12 and 0.04 Ohmm at 25 °C, corresponding to water salinities of approximately 55 000 to >200 000 mg/l NaCl (Figure 43).

The water salinity shows large variations in all units. The largest variations seem to occur in the younger units. Highly saline waters, with resistivities of less than 0.05 Ohmm at 25 °C, have been observed in each of the units. All water resistivities in Permian and Triassic units at depths of more than 3000 m indicate highly saline conditions in these older units. Brines of relatively low salinity occur in the southern part of the basin (wells Q07-01, Q07-02 and Q08-02), coinciding with the offshore extension of the Early Tertiary High. There is no obvious depth-trend in salinity, but the variability in salinity seems to decrease with depth.

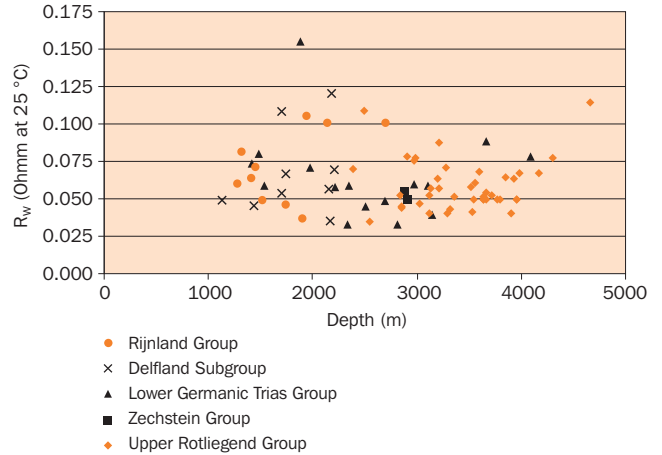


Figure 43 Measured groundwater resistivities in five stratigraphic units of the Broad Fourteens Basin

Water analyses data from 9 wells provided information on the hydrochemical characteristics of the Vlieland Sandstone Formation, the Detfurth Formation, the Z2 Formation and the Slochteren Formation in the Broad Fourteens Basin (Appendix 3). The quality of the data analysed varies, largely because sample contamination by mud filtrate or completion brine modified the groundwater samples, making the data potentially unreliable. Appendix 3 shows the results of chemical analyses of the 16 most representative samples, selected from a total of 55 individual water analyses available for released wells. The reliability of the data from well P02-05 is uncertain; the sample may have been contaminated to some extent with mud filtrate, as stated in the laboratory report. The data from well P06-06 are also of questionable reliability: the sample of water was taken during a repeat formation test (RFT), and therefore more prone to contamination by drilling fluids than samples taken during drillstem tests (DSTs) (Warren and Smalley 1994).

The compositions of the water samples indicate that groundwaters of Upper Permian to Lower Cretaceous stratigraphic units are Na-Cl type brines. Total dissolved solids, calculated by summing the concentration of all major and minor ions, are in the range of 74 000 mg/l to more than 300 000 mg/l. The less saline waters occur in the Vlieland Sandstone Formation at depths of 1300 m or less. In all water samples sodium comprises 76 - 99% of the total cations and chloride comprises 93 - 99% of the total anions. As a consequence of these large variations in total dissolved solids, water densities and hydrostatic pressures will also vary in the basin.

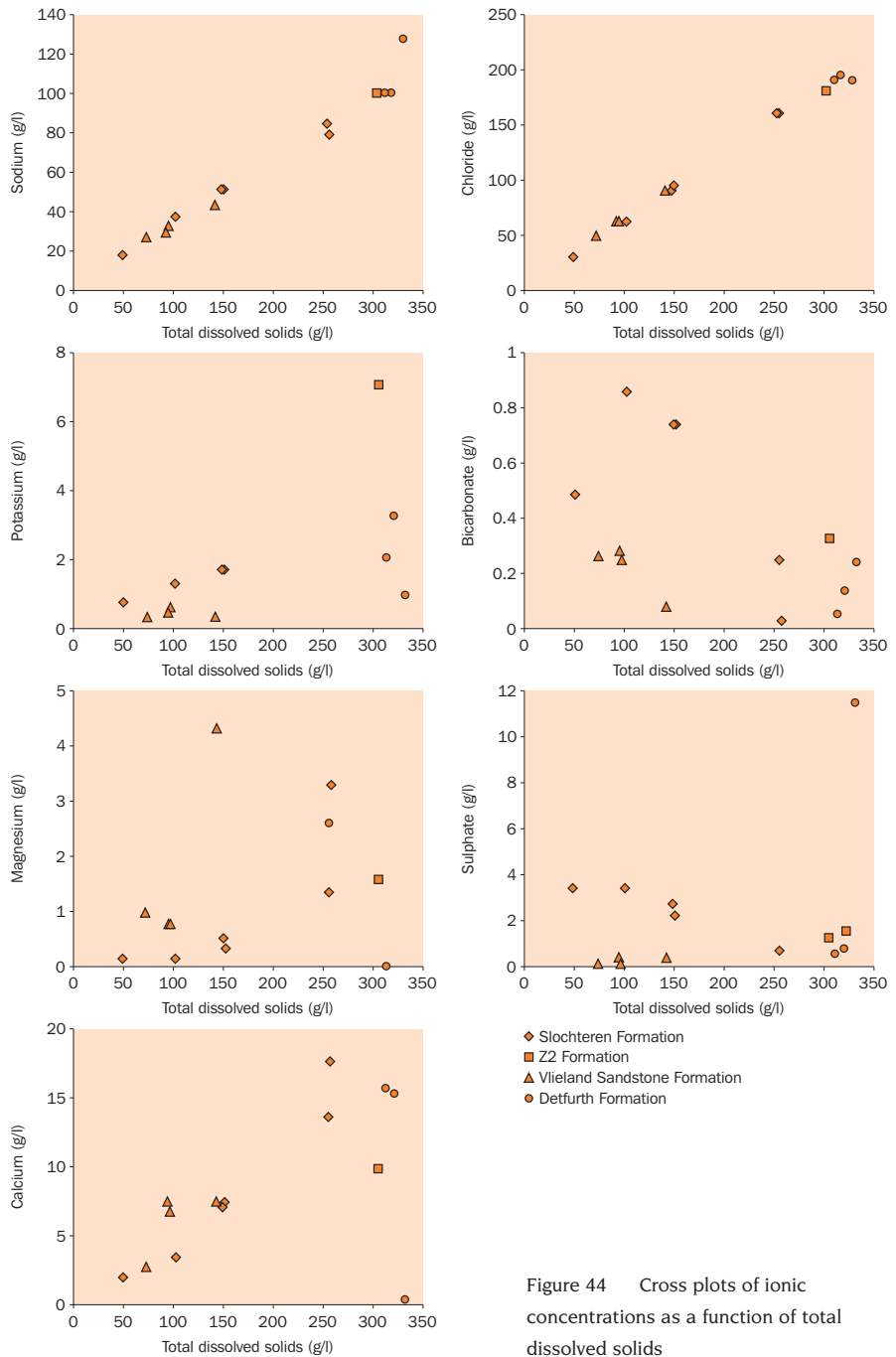


Figure 44 Cross plots of ionic concentrations as a function of total dissolved solids

Cross plots of ionic concentrations as a function of total dissolved solids (Figure 44) show that salinity correlates strongly with sodium and chloride, and also with calcium (anomalous calcium composition from well P06-06). The increase in calcium may be indicative of prolonged water-rock interaction (Chapter 8). No clear correlation was found between total dissolved solids and magnesium, bicarbonate and sulphates.

The sulphate content was less than 3500 mg/l in all samples but one (sample P06-06, which had a high magnesium content).

## 15.4 Geochemistry

Diagenesis is the sum of all those physical, chemical and biological post-depositional processes prior to the onset of metamorphism by which originally sedimentary assemblages and their interstitial pore-waters react, and attempt to reach equilibrium with their evolving geochemical environment. Each time the mineral pore-water assemblage is exposed to changes in temperature, pressure or pore-water chemistry, the sedimentary assemblage reacts via the interstitial pore waters in an attempt to equilibrate with the newly established conditions. Diagenesis is strongly related to the availability and interrelations between solute sources and solute sinks in the basin fill and to the development and evolution of a sedimentary basin. Figure 23 (Part 1) showed the main solute sources and solute sinks in the Netherlands subsurface and their relation with the major aquifers and aquitards, respectively. Such relations are also valid for the Broad Fourteens Basin. Three conceptual regimes of diagenesis can be recognised: depositional environment related diagenesis; burial diagenesis and meteoric water diagenesis (Keary 1993).

The porosity-reducing effects of burial diagenesis in particular strongly influence the hydrogeological characteristics of sediments during continuous burial. Initially the sediments become less porous as the sediments are mechanically compacted in accordance with the increasing mechanical load and associated increasing mean effective stresses. This mechanical compaction is most effective in early, shallow, burial, while chemical processes are the most significant porosity-reducing mechanisms at greater depths (e.g. Bjørlykke and Hoeg 1997, Harrison 1990, Schneider et al. 1996). According to Schneider et al. (1996), the transition zone is probably at a depth of a few hundred metres for carbonates and around 1.5 km for sandstones. The main chemical processes are pressure solution and cementation (diagenetic process by which authigenic minerals are precipitated in the pore space). The source of most cement and the mechanism for removing dissolved constituents is probably water moving through the subsurface. During burial, moving pore-water undersaturated with respect to one or more of the major mineral phases present in the sediments may also create secondary porosity by dissolution.

Meteoric water diagenesis takes place where the existing pore water is flushed from the sediments by the ingress of meteoric waters. Meteoric waters, i.e. groundwaters that originated from atmospheric precipitation and reach the phreatic zone by infiltration, are characteristically very dilute, oxidising, saturated in CO<sub>2</sub> and may be acidic in nature. They are highly reactive towards sediments deposited in a marine environment or those that have experienced burial diagenesis prior to uplift and inversion (Keary 1993).

Below a selection is presented of those diagenetic features of the Broad Fourteens Basin that could be related to important permeability alterations in the basin and to distinct phases of fluid flow. The relevant published studies on the diagenetic evolution of sediments in the Broad Fourteens Basin focus principally on the Upper Rotliegend Group (Gaps 1991, Lanson et al. 1995, 1996, Lee et al. 1985, 1989, Rossel

1982, Seemann 1979). Information is also available on the diagenetic characteristics of the Z3 Carbonate Member (Van der Poel 1989), the Lower Germanic Trias Group (Dronkert et al. 1989) and the Vlieland Sandstone Formation (De Jong and Laker 1992).

The general diagenetic sequence observed by Lanson et al. (1995, 1996) in the Upper Rotliegend Group is: 1. Early crystallisation of carbonates and possibly sulphates; 2. Progressive infilling of primary pores by carbonates (ferroan dolomite to ankerite), quartz overgrowths, and kaolin aggregates. Dissolution of plagioclase and K-feldspar is concomitant with the crystallisation of carbonates, kaolin and quartz. There is a clear increase in dissolution of detrital K-feldspar and /plagioclase with burial depth; 3. Illitisation at the expense of kaolin; 4. Late crystallisation of sulphates (anhydrite and barite). These sulphate cements post-date illitisation and locally seal both primary and secondary porosity.

Dissolution of K-feldspar and crystallisation of kaolin is favoured by the active flow of acid – CO<sub>2</sub>-rich – water. During burial such waters may have been introduced into the Upper Rotliegend Group from the underlying Carboniferous Coal Measures, as suggested by different authors (Gaupp et al. 1993, Lanson et al. 1995, 1996, Platt 1993, Rossel 1982). The present-day concentrations of kaolinite decrease towards the Broad Fourteens Basin and kaolinite becomes rare or even absent in the central part of the basin, while the highest concentrations of illite are found in the basin (Gaps 1991, Lee et al. 1989, Oele et al. 1981).

Abundant illite cementation in the Upper Rotliegend Group has been identified close to fault zones, e.g. in Groningen (Lee et al. 1989) and in Germany (Clauer et al. 1996, Gaupp et al. 1993, Platt 1993). Knowledge on the time of formation and the distribution of illite is very important for petroleum related studies as illite is well known for greatly reducing the permeability (e.g. Lee et al. 1989, Leveille et al. 1997, Seemann 1979). K/Ar ages of illite cements in the Upper Rotliegend Group of the Broad Fourteens Basin obtained by Lanson et al. (1995, 1996) and Lee et al. (1989) from different burial depths vary between 145 - 165 Ma and 130 - 160 Ma, respectively. The dating of the illite indicates that the illite precipitated within a geologically short period of time, coinciding with the main syn-rift period of basin evolution. The formation temperatures of potassium-bearing clay-minerals, including illites, reconstructed for several locations in Europe are reported to be higher than 150 °C (Clauer et al. 1996). These temperatures appear to be higher than the temperatures at maximum burial of the sediments estimated from burial history and normal geothermal gradients in the different locations (Clauer et al. 1996). The rapid illitisation in the Broad Fourteens Basin during the main syn-rift period requires a – sudden – increase in temperature in the Upper Rotliegend Group (Lanson et al. 1995, 1996). During the main syn-rift period of extensional tectonic activity, heat may have been released from the continental crust through the hydrothermal flow of fluids along deep-reaching fault zones, a process described by e.g. Deming (1992). Waters flowing upward along active normal fault zones may not reach the surface if very poorly permeable sedimentary deposits prevent any connection between basement and surface. In that case, permeable units below such very poorly permeable sedimentary deposits may provide outlet zones for the upward flowing fluids: the fluids will enter the permeable sedimentary unit and subsequently flow laterally away from the fault

zones (Fleming et al. 1998, Muir-Wood and King 1993). Such a process may have been responsible for the required increase in temperature in the Upper Rotliegend Group in the Broad Fourteens Basin during tectonically active times, especially near the deeply penetrating active normal fault zones and in parts of the basin where the Upper Rotliegend sandstones are covered by very poorly permeable Zechstein evaporites. Lanson et al. (1996) reports a period of increased heat flow in the Broad Fourteens basin around 155 Ma. In addition to an increase in heat, the illitisation of the kaolin-group of minerals requires a flow of potassium-rich fluids through the sediments, and according to Lanson et al. (1995, 1996, Leveille et al. 1997) this should be an external fluid source of potassium. They favour the overlying and laterally adjacent Zechstein evaporites as a source of potassium, in line with studies of Rossel (1982) and in accordance with 'evidence' for the influx of pore fluids from the Zechstein derived from studies on fluid sources for anhydrite cementation in the Rotliegend sandstones in the UK part of the North Sea (e.g. Leveille et al. 1997, Ziegler et al. 1994). In contrast, Clauer et al. (1996), Gaupp et al. (1993) and Platt (1994) show clear indications that the Carboniferous Coal Measures were the source for fluids influencing the illitisation process in the German Rotliegend sandstones. Illite cements have also been identified in Triassic sandstones in the P and Q blocks of the Broad Fourteens Basin (Dronkert et al. 1989).

Late crystallisation of sulphates (anhydrite and barite) occurred after the period of illitisation. Several authors describing the diagenesis of Upper Rotliegend sandstones in the Sole Pit Basin indicate that the sulphate in the anhydrite cements present in the sandstones originated from Zechstein-derived waters (McNeil et al. 1998, Sullivan et al. 1994). Lanson et al. (1995, 1996) observed that the sulphate cements in the Upper Rotliegend sandstones in the Broad Fourteens Basin are especially abundant close to the overlying Zechstein evaporites. Based on strontium isotopic ratios, however, Sullivan et al. (1994) argue that the fluids involved in the crystallisation of anhydrite were of mixed origin and suggest that the Zechstein evaporites as well as the Carboniferous shales provided the strontium found in the anhydrite cements. In addition, McNeil et al. (1998) suggest that the barium in the barite cements is probably sourced from the Carboniferous as well. The timing of sulphate precipitation in the Sole Pit Basin and associated expulsion of pore waters from adjacent Zechstein and Carboniferous units has been related to the period of basin inversion (McNeil et al. 1998, Sullivan et al. 1994). In the Broad Fourteens Basin, crystallisation of sulphates postdates the phase of illitisation and Gauthier et al. (2000) identified anhydrite cements in inversion-related joints and dilational shears, suggesting that the late crystallisation of sulphates in the Dutch basin is also inversion-related.

The diagenesis of the Z3 Carbonate Member in block P6 is described by Van der Poel (1989). Following depositional environment related diagenesis, burial diagenesis started with dolomitisation and anhydritisation, followed by calcitisation and some leaching. Van der Poel suggests that calcitisation and leaching may have been enhanced by – CO<sub>2</sub>-rich – gases generated and expelled from Carboniferous source rocks. Continued burial induced compaction and stylolitisation.

The diagenesis of the Lower Cretaceous Vlieland Sandstone Formation, as described by De Jong and Laker (1992) for the Kotter Field Vlieland sandstone, is characterised



by minor cementation and grain dissolution. Secondary porosity enhancement resulted from a late phase of intense dissolution of alumina-silicate framework grains, which caused strong leaching of feldspar and clay casts. The lack of cementation and the secondarily enlarged pores have resulted in a good to excellent present-day permeability of the sandstones.

The Helm, Helder, Hoorn and Haven fields reservoired in the Vlieland Sandstone Formation in block Q1 contain waterwashed and biodegraded oils (Roelofsen and De Boer 1991). The waterwashed and biodegraded nature of the oils result from meteoric water diagenesis: the bacteria, oxygen and trace nutrients needed for the biodegradation of the oil (e.g. Connan 1984, Palmer 1993) may have been introduced into the subsurface by infiltrating meteoric waters. In the direction of flow, i.e. away from the recharge area of a topography-induced groundwater system, the oxygen and nutrients will be used by the bacteria and their concentration in the groundwater will decrease. In the process of waterwashing, the more soluble (i.e. light) hydrocarbons from the oil are taken into solution by the groundwater. In relatively permeable units and close to the main recharge area, the flux of groundwater will be the largest, and so will be the groundwater's capacity to transport hydrocarbons in solution. Hence, the intensity of biodegradation and waterwashing of oils is controlled by the permeability of the reservoir unit and its openness to meteoric water invasion (Ahsan et al. 1997) and will decrease from recharge to discharge areas. The biodegradation and waterwashing phenomena in the Broad Fourteens Basin increase towards the axis of the basin (Roelofsen and De Boer 1991). Verweij (1990a) pointed out that this is consistent with a regional topography-induced groundwater flow system that developed in the inverted part of Broad Fourteens Basin during the Late Cretaceous syn-inversion period.

### 15.5 Characteristics of petroleum fluid systems

The first successful exploration well drilled by Mobil in the Broad Fourteens Basin encountered gas in Zechstein carbonates and Triassic sandstones in the P6 block in 1968. The first oil fields (Helm and Helder fields) were discovered by Union Oil in block Q1 in 1979 (Knaap and Coenen 1987).

Figure 45 shows the location of oil and gas fields in the Broad Fourteens Basin. Most of the fields are located along the margins of the basin. Figure 46 illustrates the stratigraphic position of the source rocks and reservoir rocks.

#### *Reservoirs and seals*

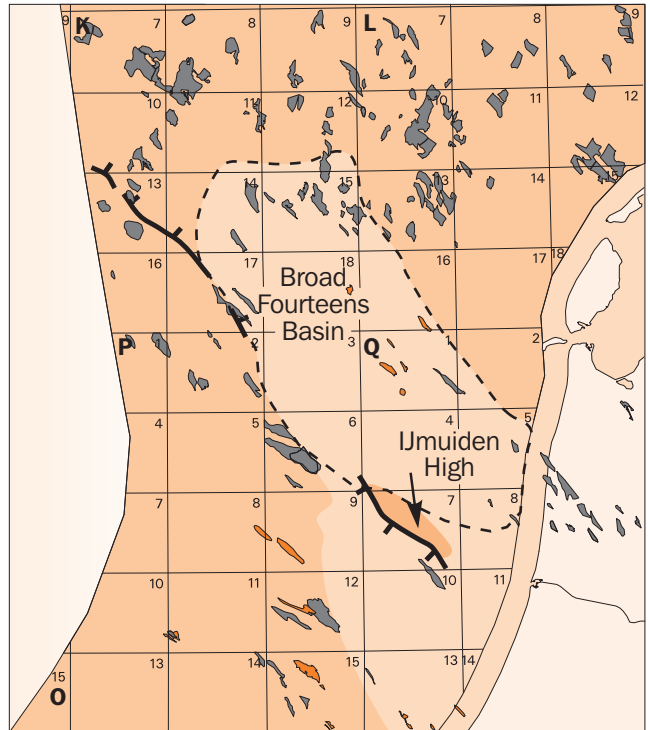
Important commercial gas accumulations are present in the Upper Permian Slochteren Formation and, in addition, in Zechstein Carbonate Members and in the Triassic Main Buntsandstein Subgroup (Table 15). The principal top seal of the Slochteren reservoir consists of Zechstein evaporites (e.g. Frikken 1996, Oele et al. 1981, Roos and Smits 1983). Triassic traps in block K13 were formed during the Late Cretaceous – Early Tertiary inversion.

The commercial oil accumulations are principally reservoired in the Lower Cretaceous Vlieland Sandstone Formation, and, to a minor extent, in the Late Jurassic – Early Cretaceous Delfland Subgroup. The Vlieland Claystone Formation is the top seal for oil accumulations in blocks Q1 and K18 (De Jong and Laker 1992, Roelofsen and De Boer 1991). The majority of the current faulted anticlinal traps in the Vlieland

Sandstone Formation formed during the Late Cretaceous – Early Tertiary inversion (Dronkers and Mrozek 1991, Hastings et al. 1991, Roelofsen and De Boer 1991).

### Source rocks

The dominantly gas-prone Westphalian coal measures of the Caumer Subgroup are considered to be the main source rock for gas in the basin (e.g. Glennie 1998, Oele et al. 1981, Van Wijhe et al. 1980, Van Wijhe 1987a). The source rock is of kerogen type III. Reconstructed burial histories of the Westphalian source rocks and maturation calculations indicate that source rock horizons reached maturity in large part of the basin prior to inversion (Oele et al 1981, Van der Poel 1989, Van Wijhe 1987a). Van Wijhe (1987a) showed that present-day vitrinite reflectance values reach up to  $2.4\%R_o$ , at the top of the coal measures along the pre-inversion axes of the basin, indicating present-day overmature conditions. During the Cenozoic post-inversion period gas generation took place outside the inverted part of the basin (Oele et al. 1981, Van Wijhe 1987).






-  Broad Fourteens Basin
-  Gas accumulations
-  Oil accumulations

Figure 45 Location of the oil and gas fields in the Broad Fourteens Basin

The Posidonia Shale Formation, a kerogen type II source rock (Cornford 1998), is considered to be the most important source rock for oil in the Broad Fourteens Basin (De Jong and Laker 1992, Goh 1996, Roelofsen and De Boer 1991). Roelofsen and De Boer (1991) consider the bituminous shale of the Delfland Subgroup to be a secondary source rock for oil. In addition, Cornford (1998) suggests that Lower Jurassic shales may have developed oil and gas potential in the basin. Maturation studies for the Posidonia Shale Formation indicate that oil generation from this source rock started in the Early Cretaceous in the centre of the basin (De Jong and Laker 1992, Roelofsen and De Boer 1991).

### Oil and gas composition

Table 15 shows the gravities of the reservoir oils. The Helm, Helder, Hoorn and Haven fields in block Q1 contain waterwashed and biodegraded oils (Roelofsen and De Boer 1991).

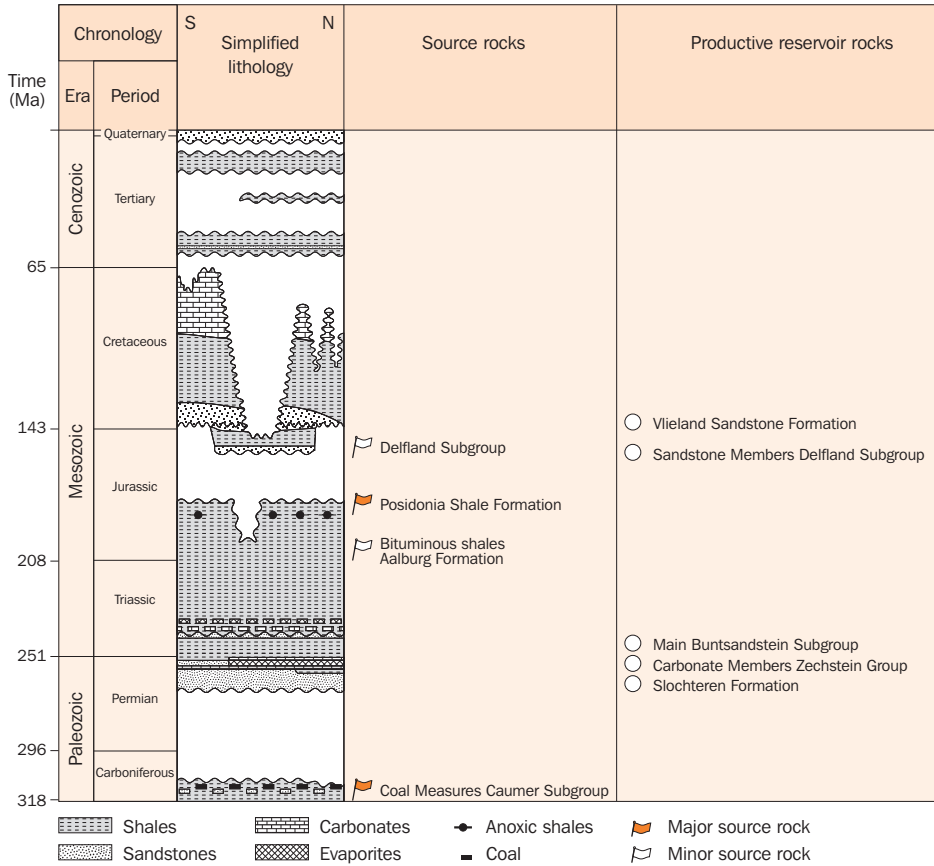


Figure 46 Source rocks and productive reservoir rocks in the Broad Fourteens Basin

The methane content of gas reservoir in the Upper Permian Slochteren Formation in the northern part of the Broad Fourteens Basin varies on average between 85% and 95% (Gas Atlas 1998). Locally, the gas contains a high % of CO<sub>2</sub> (in K15-FB: 24% CO<sub>2</sub>, Oele et al. 1981). In the Zechstein reservoirs the gas compositions are characterised by 90 - 95% of CH<sub>4</sub> in the southern part of the basin and by a variable CH<sub>4</sub> content, between 60 - 65% and 80 - 85% (Gas Atlas 1998), and locally high values of nitrogen (20 - 30% N<sub>2</sub>) in the northern part of the basin. Gas fields in Triassic reservoirs contain variable percentages of methane: the CH<sub>4</sub> content in the reservoir gas varies between 90-95% in the southeastern part of the basin and 60 - 65% in the northern part. In these northern parts locally high values of nitrogen (20 - 30% N<sub>2</sub>) are also encountered in Triassic reservoirs.

## 15.6 Identified periods of active fluid flow

The physico-chemical characteristics of the rocks and fluids in the basin described above, provide information on the evolution of fluid flow conditions in the Broad Fourteens Basin. The pressures in the basin are direct indicators of present-day fluid flow conditions. The published present-day groundwater pressures in reservoir horizons between depths of 1200 and 3900 m represent near-hydrostatic to slightly overpressured conditions. Published overpressures of the groundwater reach values

Table 15 Characteristics of oil and gas fields in the Broad Fourteens Basin

| Field             | Well no | Reservoir unit   | Depth unit<br>m –sea-<br>level | OWC<br>m –sea-<br>level | Gravity<br>API ° | Data<br>source |
|-------------------|---------|--|--------------------------------|-------------------------|------------------|----------------|
| <b>Oil fields</b> |         |  |                                |                         |                  |                |
| Kotter            | K18-02  | Vlieland Sandstone Formation<br>Breeveertien Formation |                                | 1782                    | 32               | 1              |
| Logger            | L16-6   | Vlieland Sandstone Formation                           | 1836                           |                         | 34               | 2              |
| P9                | P09-02  | Vlieland Sandstone Formation                           | 1973-2129                      |                         | 30               | 1              |
| Haven             | Q01-08  | Vlieland Sandstone Formation                           | 1550                           |                         | 28               | 3              |
| Helder            | Q01-07  | Vlieland Sandstone Formation                           |                                | 1425                    | 22               | 3              |
| Helm              | Q01-03  | Vlieland Sandstone Formation                           |                                | 1289                    | 18               | 3              |
| Hoorn             | Q01-16  | Vlieland Sandstone Formation                           | 1450                           |                         | 26               | 3              |
| <b>Gas fields</b> |         |  |                                |                         |                  |                |
|                   |         |  |                                | GWC<br>m –sea-<br>level |                  |                |
| K8                | K08-03  | Upper Rotliegend Group                                 |                                | 3334                    |                  | 4              |
| K11               |         | Upper Rotliegend Group                                 |                                | 3188                    |                  | 4              |
| K12               | K12-03  | Upper Rotliegend Group                                 |                                | 3569                    |                  | 4              |
| K13A              | K13-01  | Main Buntsandstein Subgroup                            |                                | 1543                    |                  | 5              |
| K13B              | K13-02  | Main Buntsandstein Subgroup                            |                                | 1347                    |                  | 4              |
| K13E              | K13-04  | Upper Rotliegend Group                                 |                                | 2503                    |                  | 5              |
| K13F              | K13-05  | Upper Rotliegend Group                                 |                                | 2608                    |                  | 5              |
| K14               |         | Upper Rotliegend Group                                 |                                | 3114                    |                  | 4              |
| K15FA             |         | Upper Rotliegend Group                                 |                                | 3410                    |                  | 6              |
| K15FB             |         | Upper Rotliegend Group                                 |                                | 3980                    |                  | 6              |
| K17               |         | Upper Rotliegend Group                                 |                                | 2882                    |                  | 4              |
| P6                |         | Main Buntsandstein Subgroup<br>Zechstein Group (ZEZ3C) |                                | 2750 (GDT)              |                  | 4<br>4         |

- ECL 1983
- Goh 1996
- Roelofsen and De Boer 1991
- Webatlas 1999
- Roos and Smits 1983
- Oele et al. 1981

in the order of 1 - 2.6 MPa in the Upper Rotliegend Group in the northern part of the basin. The restricted number of published pressure measurements available for the permeable hydrostratigraphic units only, do not permit the detailed characterisation of a present-day groundwater flow system. Overpressure is a transient condition during basin evolution and the pressure distribution at a certain time is a reflection of the pressure-generating mechanism as well as of the dissipating mechanism (e.g. groundwater flow). The observed near-hydrostatic pressures in the Broad Fourteens Basin indicate that the sedimentary loading of the basin after its Late Cretaceous uplift and erosion did not lead to widespread overpressuring of the reservoir units at present-day. This suggests that Tertiary and Quaternary sedimentary loading and other pressure generating mechanisms were not powerful enough to induce overpressuring and/or that the permeability and continuity of the reservoir units in question allowed groundwater flow to dissipate the overpressures.

The groundwaters in Lower Cretaceous and older units are chloride dominated brines (total dissolved solids in the range of 74 000 mg/l to 300 000 mg/l). Hydrochemistry indicates that, at present, there is no fresh water of meteoric origin, nor unevolved sea water present in reservoir horizons at depths of more than 1200 m. The large variations in concentration of total dissolved solids in the groundwaters and the associated variations in density of the groundwater in the basin constitute a controlling factor on present-day pressures and fluid flow conditions.

The published temperature data do not allow a hydrodynamic interpretation.

Important indicators of periods of active paleo-fluid flow in the basin are its present-day sediment diagenetic characteristics and the characteristics of its oil and gas accumulations. A number of diagenetic features of the Broad Fourteens Basin can be related to important permeability alterations in the basin and to distinct phases of fluid flow.

The indicators and the associated/inferred paleo fluid flow conditions are listed below.

*Kaolin cements, and leached K-feldspar, in the Upper Permian Slochteren Formation.*

- Expulsion of acid CO<sub>2</sub>-rich waters from the Carboniferous Limburg Group into the Slochteren Formation during burial (Gaupp et al. 1993, Lanson et al. 1995, 1996, Platt 1993, Rossel 1982);
- Flow period contemporaneous with the Early-rift period of basin evolution (period of burial before 165 Ma; Lanson et al. 1995, 1996).

*Illite cements in the Upper Permian Slochteren Formation.*

- Hydrothermal flow along fault zones (increased heat flow in basin around 155 Ma reported by Lanson et al. 1996);
- Expulsion of potassium-rich waters from Zechstein Group (Lanson et al. 1995, 1996, Leveille et al. 1997) and/or Limburg Group (Clauer et al. 1996, Gaupp et al. 1993, Platt 1993) into the adjacent Slochteren Formation;
- Both fluid flow events (hydrothermal flow and expulsion of potassium-rich waters) occurred during the main syn-rift period of basin evolution (130 - 165 Ma; from illite age dating by Lanson et al. 1995, 1996, Lee et al. 1989).

*Anhydrite and barite cements in the Upper Permian Slochteren Formation.*

- Flow of sulphate-rich waters from both the Zechstein Group (evaporites) (Lanson et al. 1995, 1996, McNeil et al. 1998, Sullivan et al. 1994) and the Limburg Group (McNeil et al. 1998) into the adjacent Slochteren Formation;
- Flow is contemporaneous with syn-inversion period of basin evolution (indicated by anhydrite cements in inversion-related joints: Gauthier et al. 2000; crystallisation of sulphates postdates illitisation: Lanson et al. 1995, 1996).

*Calcite cements in the Z3 Carbonate Member.*

- Flow of CO<sub>2</sub>-rich fluids (gases) from the Limburg Group into the Z3 Carbonate Member (Van der Poel 1989);
- Flow is contemporaneous with early rift to syn-rift period of basin evolution.

*Biodegraded and waterwashed nature of oils in Lower Cretaceous Vlieland Sandstone Formation (block Q1; Roelofsen and De Boer 1991).*

- Flow of oxygen-rich meteoric groundwater through the Vlieland Sandstone Formation;

— Flow occurred during subaerial exposure of the basin due to uplift and/or changes in sea level (after 90 Ma).

*Secondary porosity and leached K-feldspars in the Lower Cretaceous Vlieland Sandstone Formation (De Jong and Laker 1992).*

- Flushing of Vlieland Sandstone Formation with waters capable of grain dissolution, K-feldspar leaching;
- Flushing occurred after 90 Ma.

And in addition:

*Gas fields in the Upper Permian Slochteren Formation, Zechstein Carbonate Members and Triassic Main Buntsandstein Subgroup (e.g. Oele et al. 1981, Van Wijhe et al. 1980, Van Wijhe 1987a).*

- Petroleum fluid flow from Carboniferous source rocks into Upper Rotliegend, Zechstein and Triassic reservoirs presently located at the edges of the basin. Flow from the source rock into the reservoirs was both vertical and lateral.

*Oil fields in the Lower Cretaceous Vlieland Sandstone Formation and Late Jurassic – Early Cretaceous Delfland Subgroup (e.g. De Jong and Laker 1992, Goh 1996, Roelofsen and De Boer 1991).*

- Petroleum fluid flow from Jurassic source rocks into overlying reservoirs included both vertical and lateral components.

Table 16 shows the timing of inferred paleo-fluid flow events during basin evolution.

Table 16 Present-day indicators of fluid flow events

| Indicator  | Fluid flow event  | Timing                      | Source  |
|--|---|-----------------------------|---|
| Kaolin cement, leached K-feldspar in Slochteren Formation        | I.<br>Expulsion acid CO <sub>2</sub> -rich water from Limburg Group into Slochteren Formation   | < 165 Ma<br>Early rift      | Lanson et al. 1995, 1996<br>Rossel 1982<br>Platt 1993<br>Gaupp et al 1993   |
| Calcite cements in Z3 Carbonate Member                           | I.<br>Expulsion CO <sub>2</sub> -rich fluids from Limburg Group into Z3 Carbonate Member  | Early to syn-rift           | Van der Poel 1989   |
| Illite cements in Slochteren Formation                           | II.<br>- Hydrothermal flow along faultzones<br>- Expulsion K-rich water from Limburg Group and/or Zechstein Group into Slochteren Formation | 130-165 Ma<br>Main syn-rift | Lanson et al 1995, 1996<br>Lee et al 1989<br>Leveille et al 1997<br>Clauer et al 1996<br>Gaupp et al 1993<br>Platt 1993 |
| Anhydrite and barite cements in Slochteren Formation             | III.<br>Expulsion sulphate rich water from Limburg Group and Zechstein Group into Slochteren Formation                                      | Syn-inversion               | Lanson et al 1995, 1996<br>McNeil et al 1998<br>Sullivan et al 1994<br>Gauthier et al 2000                              |
| K-feldspar leaching in Vlieland Sandstone Formation              | IV.<br>Flushing of Vlieland Sandstone Formation   | >90 Ma                      | De Jong and Laker 1992  |
| Biodegraded and waterwashed oils in Vlieland Sandstone Formation | IV.<br>Flow of oxygen-rich meteoric water through Vlieland Sandstone Formation  | >90 Ma                      | Roelofsen and De Boer 1991  |

## 16 Conceptual model of geodynamic and fluid dynamic evolution

### 16.1 Conceptual model of geodynamic and hydrodynamic evolution

The indicators of fluid dynamic and permeability conditions of the Broad Fourteens Basin (Chapter 15 and 14) in combination with the identified processes influencing these conditions – as reconstructed from the data on the geodynamic, climatic and sedimentary geologic evolution of the basin (Chapter 14, Tables 9 and 10) – are the basis of the conceptual geofluid model. Figure 47 schematically illustrates the conceptual model for four important phases of basin evolution.

- **Main syn-rift period.** Syn-rift deposition of the Schieland Group – concentrated in the rapidly subsiding basin – induces cross-formational vertical upward flow of fluids in the shallow and relatively permeable part of the basin (shallow subsystem of burial-induced flow; Chapter 1), while in the deeper parts fluid flow directions are stratigraphically controlled (intermediate subsystem of burial-induced flow; Chapter 1; Figure 47a). Hydrothermal flow along deeply penetrating active normal faults enters permeable units (e.g. the Slochteren Formation) in the basin during periods of extensional tectonic activity in the early part of the main syn-rift phase (section 13.3). In addition, fluid flow through the temporarily active and permeable fault and fracture zones in the basin drains the relatively permeable units in particular. During syn-rift times, water tables and topography-induced flow systems develop in the uplifted basin flanks and adjacent highs.
- **Post-rift period.** Continuous subsidence and sedimentation during the post-rift phase of basin evolution (Figure 47b) maintain cross-formational vertical upward flow of fluids in the shallow part of the basin and stratigraphically controlled flow in its deeper parts. At the end of the post-rift phase the continuous burial and associated compaction of the hydrostratigraphic units favour the development of overpressured conditions in the deepest parts of the basin, especially in the poorly permeable units such as Carboniferous shales and Zechstein evaporites. In addition, the gradual build-up of regional compressional stresses may influence the distribution of overpressure and fluid flow in the basin. This effect was not studied in detail in the present study. It was studied in a separate project involving geomechanical modelling of compressive stress and overpressure in the Broad Fourteens Basin (Simmelink et al. 2001).
- **Syn-inversion period.** During the subsequent syn-inversion phase of basin evolution (Figure 47c) different mechanisms operate to dissipate the inferred post-rift overpressured conditions in the central part of the basin: sedimentary loading as a pressure-producing mechanism is absent, there is erosional unloading, the geometrical framework is changing, and there is increased permeability of fault zones during tectonic activity. The elongated island-like character of the inverted central part of the basin and the topographic relief of the ground surface favour topography-induced fluid flow and the development of a freshwater lens (Verweij 1990). The geometrical framework of the inverted basin favours deep infiltration of meteoric water, e.g. the inversion-related tilting of geological units exposes different permeable units to the inflow of meteoric water. Extension fractures in the uplifted infiltration area enhance deep infiltration. Bouw (1999) studied

the syn-inversion development of a freshwater lens in the northern (salt-dominated) part of the basin by applying a density-dependent groundwater flow model. The results of her different modelling scenarios show that the main factor influencing the development of a freshwater lens is the distribution of permeability; predicted near steady-state flow conditions are established within 4 My; the maximum depth of the fresh-salt water interface is 1200 m (for a high permeability scenario). In the conceptual model the dynamic permeability of repeatedly reactivated faults, and the associated fracture zones allows fluid flow during inversion tectonic activity (co-seismic pulsed episodes of fluid flow; Figure 47c). Meanwhile, subsidence and sedimentation continue to influence the pressure distribution and fluid flow in the platform area adjacent to the basin.

- **Post-inversion period.** Figure 47d shows that at present the main mechanism influencing the pressure distribution and fluid flow in the basin is assumed to be the sedimentary loading during the Late Tertiary and Quaternary. The regional compressive stress field is assumed here to exert a static influence only (Chapter 14).

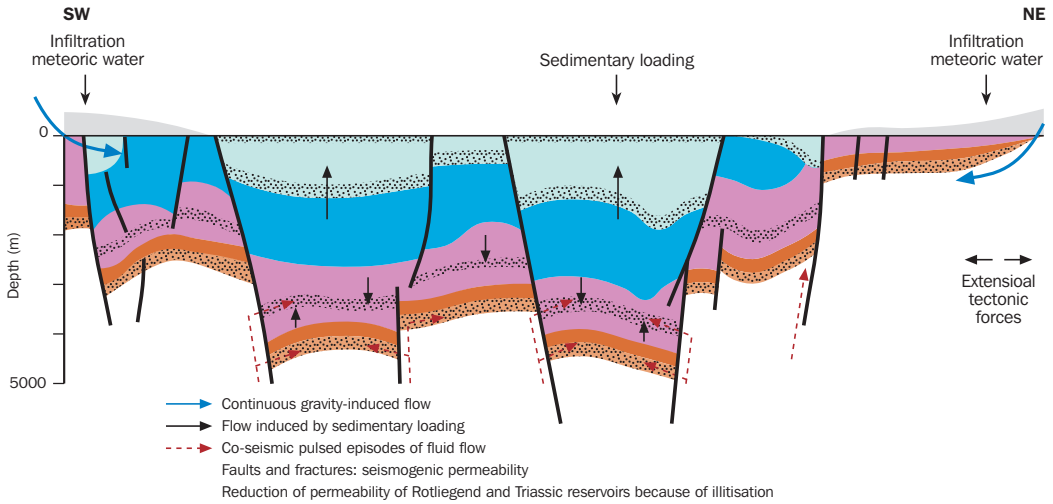
## 16.2 Conceptual model of hydrodynamic evolution in relation to the evolution of petroleum systems

The hydrogeological and hydrodynamic response of a basin fill to its geodynamic evolution may exert a direct and indirect influence on all subsystems of the petroleum systems in the basin (Verweij 1993, 1997; Table 17). In the Broad Fourteens Basin,

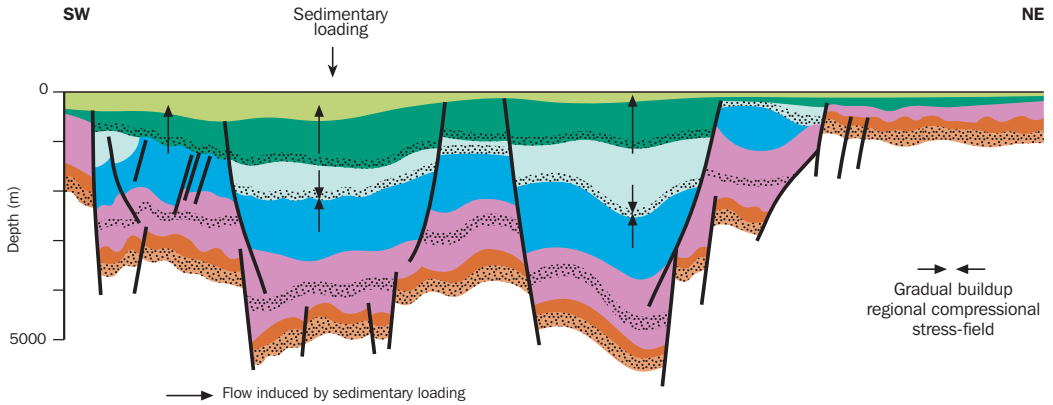
Table 17 Possible direct and indirect influences of the groundwater system on the petroleum system

| Groundwater system  | Petroleum system   |
|---|--|
| Distribution groundwater potential gradient<br>(≈ distribution overpressure gradient) | <ul style="list-style-type: none"> <li>— Expulsion</li> <li>— Migration pattern</li> <li>— Migration losses</li> <li>— Entrapment</li> <li>— Hydrocarbon-water contacts</li> <li>— Preservation, remigration</li> <li>— Sealing capacity rocks and faults<br/>(pressure sealing, water drive leakage)</li> </ul>   |
| Overpressures   | <ul style="list-style-type: none"> <li>— Sealing capacity rocks and faults<br/>(hydraulic fracturing, fault failure)</li> <li>— Porosity and permeability rocks<br/>(undercompaction)</li> </ul>   |
| Active groundwater flow   | <ul style="list-style-type: none"> <li>— Porosity and permeability rocks and faults<br/>(through rock-water interaction)</li> <li>— Petroleum composition (geochemical water-petroleum interaction: e.g. compositional fractionation, waterwashing; biochemical water-petroleum interaction: biodegradation)</li> <li>— Petroleum generation (by influencing temperature distribution through forced convection of heat)</li> <li>— Petroleum migration (gas in solution)</li> </ul> |

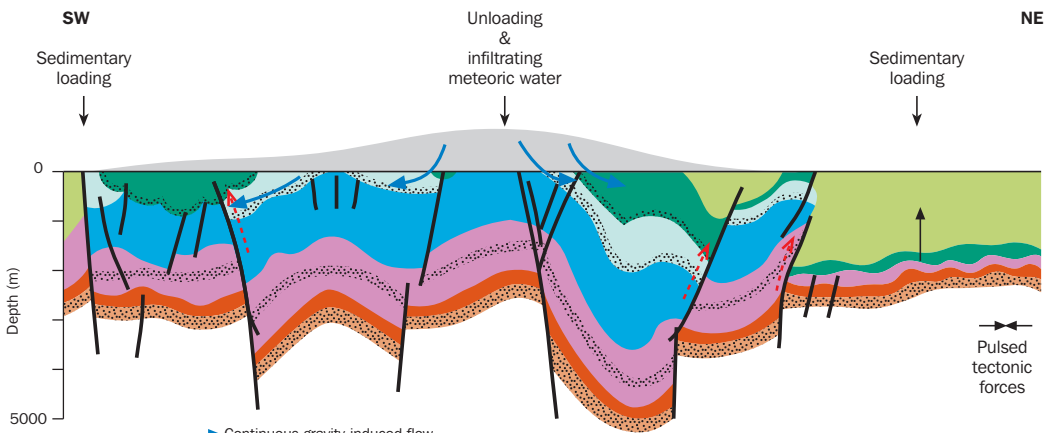




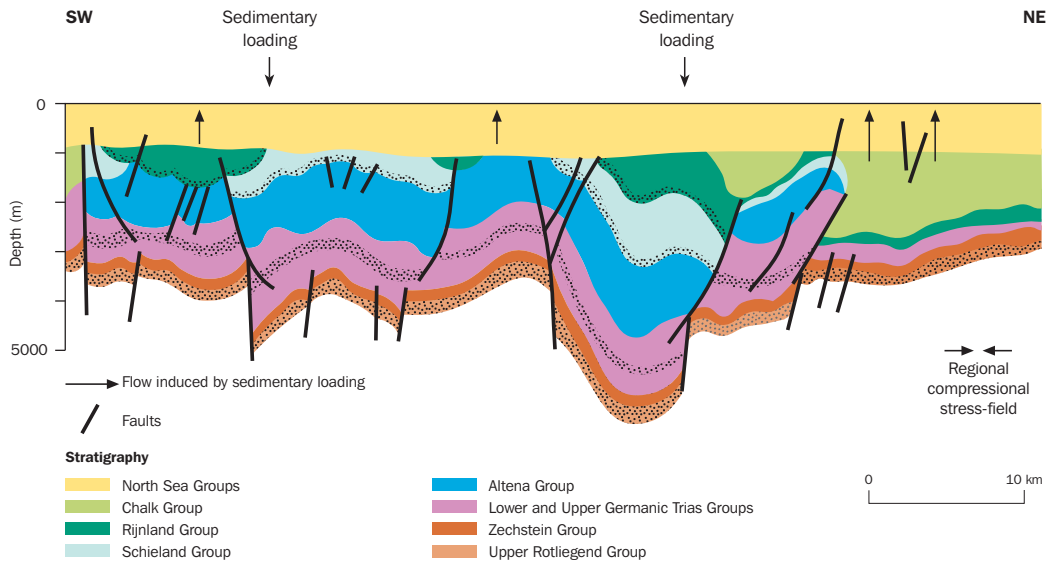
a. Main syn-rift phase of basin evolution



b. Post-rift phase of basin evolution



c. Syn-inversion phase of basin evolution



d. Post-inversion phase of basin evolution (present day)

Figure 47 Overview of the processes influencing fluid flow conditions during the different phases of basin evolution of the Broad Fourteens Basin: a. Main syn-rift phase; b. Post-rift phase; c. Syn-inversion phase; d. Post-inversion phase (present-day). The geological cross-sections of the post-Paleozoic sequences are modified from the balanced cross-sections presented by Huyghe and Mugnier (1995)

the identified rapidly changing permeability of fault and fracture zones and changing of dips of the hydrostratigraphic units during the main syn-rift period and the syn-inversion period affect both the groundwater and the petroleum systems. The largest impact of groundwater conditions on rock permeability and petroleum migration, accumulation and preservation can be expected in zones of active groundwater flow, in zones where large groundwater potential gradients exist and in severely overpressured zones (Chapter 1). Such zones are generated by large net driving forces for groundwater flow that in turn are related to, for example, a large topographic relief of the water table, high sedimentary loading rates or high tectonic loading rates.

The analysis indicated that the major groundwater flow events active during the development of the Posidonia Shale oil system were the topography-induced flow and the co-seismic flow events during the syn-inversion period and, to a minor extent, the flow induced by sedimentary-loading in Pliocene-Quaternary times. Both topography-induced flow and co-seismic flow are able to influence the migration, accumulation and remigration of oil. Assuming that the active topography-induced groundwater flow actually reached the realm of the oil system, the groundwater flow may also have affected the oil composition by waterwashing and biodegradation. During post-rift times the oil system was probably not affected by overpressures that – according to the conceptual model – developed in the deeper parts of the basin, and were induced by sedimentary loading.

The development of the gas system started with the deposition of the Coal Measures of the Limburg Group during Late Carboniferous times and, as a consequence, all

inferred major groundwater flow events since that time may have influenced the gas system. Gas generation started prior to inversion, but there is no information on its exact timing in the published literature. Assuming that the gas generation process was already active during main syn-rift times, the changing permeability framework and the co-seismic flow event will have influenced gas expulsion and migration in the basin. In contrast to the oil system, the deeper gas system was probably in the realm of the inferred overpressured zone that was induced by continuous sedimentary loading during post-rift times. The gradients of overpressure might have influenced the expulsion of gas from the source rock as well as the sealing capacities of the cap rocks. The combined influence of a rapidly changing permeability framework and co-seismic flow during syn-inversion might have favoured the remigration and accumulation of gas in the basin and possibly also the escape of gas from the basin.

## 17 Discussion and conclusions Part 2

The first phase of the Broad Fourteens Basin study involved the analysis and interpretation of a wide variety of publicly available data on rocks and fluids in the basin. The results of the data analysis included: a. the present-day geological and hydrogeological framework of the basin and an overview of the present-day characteristics of the fluids it contains; b. a conceptual model of the geological history of the Broad Fourteens Basin and its steering influence on the hydrogeological and hydrodynamic evolution of the basin.

In addition to its geological and hydrogeological framework, it was possible to characterise the Broad Fourteens Basin by its temperature and heat flow distribution, distribution of groundwater pressures, distribution of hydrochemical properties, and distribution and characteristics of petroleum accumulations:

- **Hydrogeological framework.** Identified important characteristics of the sedimentary fill controlling fluid flow conditions are the dominance of shaly deposits of poor matrix permeability in the basin and the occurrence of Zechstein Salt Members of very poor permeability in the central and northern parts of the basin. The lateral continuity of pre-Tertiary hydrostratigraphic units is restricted by the numerous faults in the basin. Lateral continuity in the northern part of the basin is also affected by the presence of salt diapirs. In much of the basin the pre-rift, early-rift and syn-rift sequences are not at their maximum depth of burial due to the previous inversion of the basin and show signs of overcompaction. Fracture permeability affects the overall permeability of the hydrostratigraphic units in the basin. Based on the distribution of Zechstein Salt Members, the basin can be subdivided hydrogeologically in a northern area where the Zechstein Group is laterally and vertically sealing reservoir units, and a southern area where the Zechstein Group is increasingly clastic and as a consequence less sealing.
- **Temperatures.** The present-day temperature gradient of the Broad Fourteens Basin, based on the published data, was calculated at approximately 28 °C/km. Heat flow calculations indicated a relatively low heat flow in the shallow parts of the basin and heat flows increasing with depth.
- **Groundwater pressures and chemical compositions.** The published pressure data indicated near-hydrostatic to slightly overpressured conditions in reservoir units at depths exceeding 1200 m. No pressure data were available for poorly permeable units. The composition of water samples revealed that groundwaters of Upper Permian to Lower Cretaceous hydrostratigraphic units are chloride-dominated type brines. The salinity of the water showed large variations in all units.
- **Oil and gas.** It was observed that most oil and gas accumulations are located along the margins of the basin. Four oil fields in block Q1 contain waterwashed and biodegraded oils.

The nature and distribution of the presented characteristics of the basin clearly revealed the need for additional information on rock and fluid properties and in addition gave rise to a lot of questions concerning the origins of the identified characteristics. Specific questions emanating from the data analysis include:

- Why are the observed pressures in the reservoir units near-hydrostatic to only slightly superhydrostatic?

- What are the processes and conditions responsible for these present-day pressure conditions?
- Is it likely that poorly permeable units (shales, evaporites) are overpressured today?
- Is there any fluid flow in the basin today?
- What are the processes and conditions responsible for the observed increase of heat flow with depth in the basin?
- What are the processes and conditions responsible for the large salinity variations in the basin today; what is the influence of these salinity variations on fluid flow, today and in the past?
- Why are the oil and gas fields concentrated along the margin of the basin, while the oil- and gas-prone source rocks are present in the entire basin?
- Is it likely that oil and gas are generated in the basin today?
- What are the fluid flow processes and conditions responsible for the waterwashed and biodegraded nature of the oil accumulations in the Q1 block; is it likely that these processes and conditions also influenced the characteristics of oils in other parts of the basin?

A general aim of this thesis was to provide the fluid dynamics context to increase process-based understanding of present-day characteristics of the hydrogeological framework and the fluids in Netherlands sedimentary basins (Chapter 1). The data analysis in Part 2 led to the identification of the major mechanical processes involved in overpressure and fluid flow evolution in the basin (sedimentary loading and unloading, tectonic compression and extension, topography of the water table) and the establishment of a time framework for the important permeability alterations in the basin and the distinct phases of fluid flow. In general the data analysis provided the basis for such a fluid dynamics context, i.e. the conceptual model of geodynamic and fluid dynamic evolution of the Broad Fourteens Basin.

Ideally, a detailed explanation of the identified present-day characteristics of the basin fill and the prediction of the missing fluid properties and fluid flow conditions requires more quantitative knowledge on the integrated evolution of all the identified forces and processes that exerted influence – to a greater or lesser extent – on the fluid geological framework and fluid flow in the basin (Tables 10 and 11). The second phase of the Broad Fourteens study is a first step to provide such quantitative knowledge; it involves the 2D numerical modelling of integrated basin evolution (Part 3). The results of the data analysis presented here in Part 2 provided both the essential data and the a priori understanding of the basinal processes required for this modelling study.

## 18 Introduction to Part 3

This final part of the thesis discusses the quantitative analysis of fluid flow systems on geological timescales. It aims to provide 1. a quantitative understanding of the hydrogeological and pore pressure and groundwater flow response of the basin fill of the Broad Fourteens Basin to important aspects of its geological, geothermal and climatic evolution and an understanding of this response for the evolution of the oil and gas systems in the basin; 2. a time framework for petroleum generation, migration, accumulation and preservation in the basin (Chapter 1). In addition it addresses specific research questions that resulted from the extensive data analysis of the Broad Fourteens Basin (see Part 2, Chapter 17).

The Temispack 2D basin modelling package (versions 2.5 and 2.6, Breicip-Franlab 1997) was used to analyse the geofluid evolution along a SW-NE cross-section through the southern part of the Broad Fourteens Basin (Figure 33, Part 2). The modelling work was carried out at the Netherlands Institute of Applied Geoscience TNO – *National Geological Survey*.

The data analysis presented in Part 2 provided both the input data and boundary conditions required for the numerical modelling, and the necessary a priori understanding of the basinal processes and their interactions.

### 18.1 Principles of integrated 2D basin modelling

Temispack is a finite-volume model that uses a two-D mesh to simulate the following conditions during basin evolution (Burrus et al. 1991, Ungerer et al. 1990):

- Sedimentation, erosion and compaction. The model simulates changes in geometrical framework of the model layers based on normal porosity-depth curves defined for each lithology, and taking into account the paleogeography and the vertical displacements of the layers.
- Heat flow and temperature. The calculation of temperature history is based on a transient heat flow equation that uses lithology and porosity dependent thermal conductivities, heat capacities and radiogenic heat production based on lithology, and takes into account the evolution of the sediment-water interface temperatures and the evolution of basal heat flow.
- Source rock kerogen maturity and petroleum generation. The input for the maturity module includes kerogen type, total organic carbon (TOC) values and temperature history from the previous module. In this study, Temispack default kerogen types and the associated kinetic model were used. The maturity module computes the transformation ratios for each source rock type and the amount of petroleum generated. Vitrinite reflectances are computed for Type IV reference kerogen.
- Fluid flow. The history of pore pressures and groundwater flow is calculated to be the combined result of sedimentary loading and unloading, the relief of the water table and, in addition, the generation of hydrocarbons. The module requires the input of the relationships between porosity and effective stress for each lithology, as well as the permeabilities derived from the lithology-related porosities by applying the Kozeny-Carman equation, and finally, the anisotropies.
- Petroleum expulsion, migration and accumulation. The petroleum migration module links the previous modules and calculates the expulsion and migration history by using a two-phase Darcy equation. It requires additional input of relative permeability functions, petroleum density and viscosity, and capillary pressures.

The following assumptions underlying the basin modelling of the Broad Fourteens Basin have important implications for the evaluation of the previously identified processes and forces that might have influenced the overpressure and fluid flow evolution in the basin (Tables 10 and 11):

1. The cross-section is laterally constrained: no horizontal compression or extension of the basin fill;
2. The changes in porosity and pore pressure are related to changes in vertical effective stress by coupling of a water flow equation (Darcy's Law) and a deformation equation (Terzaghi's Law; this law is treated in Chapter 1);
3. The densities of the fluids (water, oil, gas) are assumed to be constant; e.g. the density of water is not influenced by changes in temperature or changes in concentration of total dissolved solids.

As a consequence of assumption 1 it will not be possible to assess the influence of the identified long-term changes in lateral tectonic stresses and short-term stress fluctuations (Tables 10 and 11) on the evolution of the fluid systems. Chapter 1 outlined that changes in porosity and pore pressure are related to changes in mean stress and not to changes in vertical stress only; in the modelling the changes in porosity and pore pressure are related to changes in vertical stress (assumption 2). Chemical diagenesis and their influence on porosity and permeability evolution are not included in the modelling. However, the effects of these geochemical processes (pressure solution, cementation) are incorporated in the calibrated porosity-depth relations. Because of assumption 3 the basin modelling study cannot provide information on the influence of heating and cooling and the influence of density differences on the development of pore pressures and water flow.

It is clear that the basin modelling does not incorporate all the previously identified processes and forces influencing the pore pressure, fluid geology and fluid dynamics in the Broad Fourteens Basin (Part 2). Application of the 2D basin modelling to the cross-section in the southern Broad Fourteens Basin does allow to study quantitatively the integrated history of sedimentation, erosion, porosity, permeability, water table elevation, pore pressure and water flow in the basin. In addition, the basin modelling permits to examine the interaction of sedimentation/uplift/erosion, heat transport, maturation of source rocks, and the generation, migration and accumulation of oil and gas, the latter also in relation to the evolution of pore pressure and water flow.

## 18.2 Input data and boundary conditions

The present study included the assessment of a detailed conceptual model of basin history along the regional cross-section. This conceptual model provided the input data and the boundary conditions required for the modelling. Appendix 4 presents the reconstructed quantified history of sedimentation, uplift and erosion along the cross-section and gives an extensive overview of the input data and boundary conditions.

## 18.3 Modelling Procedure

The first step was to prepare the data using the information given in Appendix 4. The geological cross-section (Figure 48) was divided into 42 geochronological events and 31 lithotypes, and was divided laterally into 83 vertical columns. This resulted in a mesh of 42 × 83 grid blocks at present-day. Secondly, the present-day section was

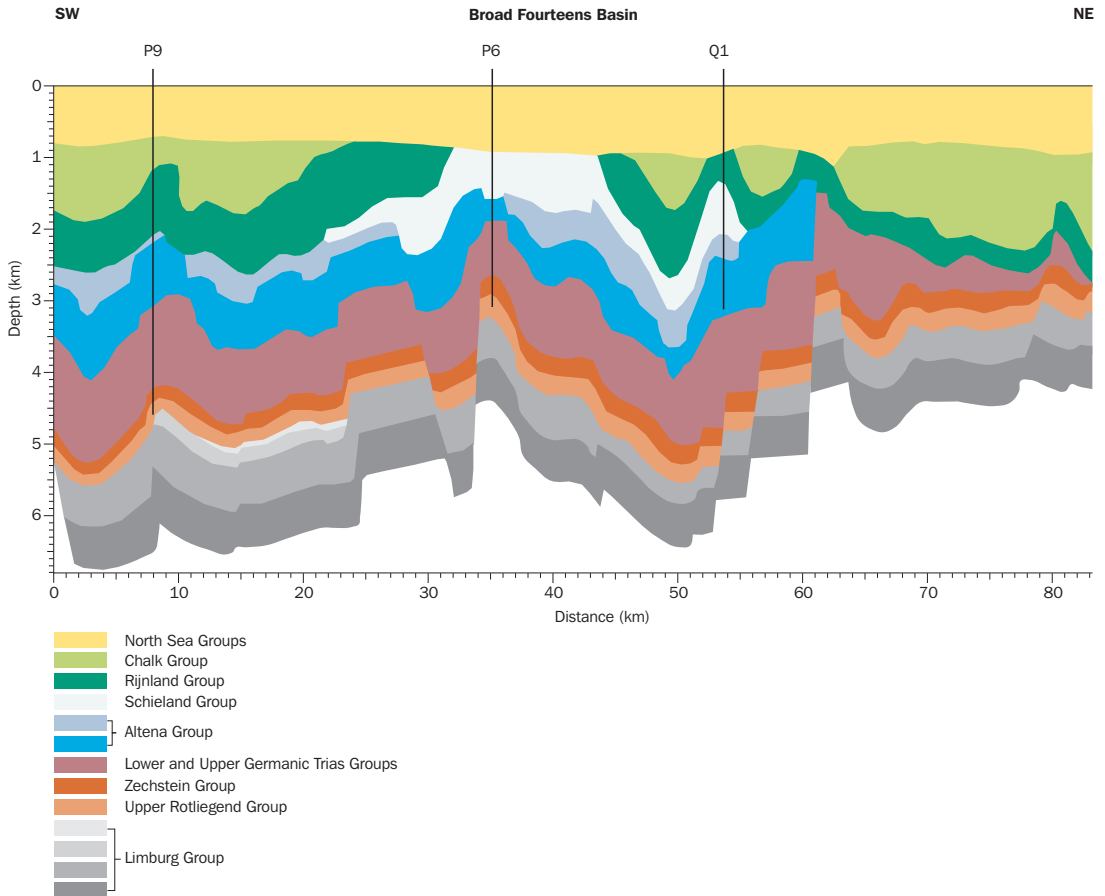


Figure 48 Geological framework along cross-section through southern part of the Broad Fourteens Basin. The geological framework is based on in-house interpreted seismic sections SNS-83-02 and NNS-6, published geological cross-sections (Burgers and Mulder 1991), declassified well-data and regional information (Quirk 1993, Quirk and Aitken 1997, RRI 1988, Van Adrichem Boogaert and Kouwe 1993-1997, and Van Wijhe et al. 1980). Figure 33 shows the location of the cross-section

backstripped and the sedimentary history was calculated. Subsequently, this history of sedimentation, uplift and erosion in combination with the geothermal history along the cross-section from the Late Carboniferous to present-day was verified against present-day temperature, vitrinite reflectance and porosity data. This resulted, amongst other things, in the selection of the most appropriate thermal boundary conditions and parameters that were used during subsequent modelling phases. The third important step was to calibrate the permeability structure. Initially, the history of pore pressures and groundwater flow was calculated with a simple fluid flow model, including sedimentary loading and unloading and the relief of the water table as pressure-influencing mechanisms, assuming no-flow bottom and lateral boundary conditions. The results of the fluid flow modelling were verified against present-day measured pore pressures and measured or published petrophysical parameters.



On the basis of this, the permeabilities were adjusted by adapting the initial anisotropies. In order to evaluate the adapted permeability structure, the pressure history was simulated again, now taking into account hydrocarbon generation as an additional pressure-influencing mechanism. For this purpose the petroleum migration and accumulation history was also simulated. The known distribution of oil and gas accumulations along the section was compared with the reconstructed migration and accumulation history. This step also included the analysis of the influence of time-dependent permeability of faults on the pressure history and the evolution of the petroleum systems. The final modelling step was to incorporate the results of the previous steps and to represent the favoured modelling scenario for the quantitative reconstruction of the evolution of temperature, source rock maturation, petroleum generation, pore pressure and water flow, petroleum expulsion, migration and accumulation. Below, the results of the integrated forward modelling are discussed in relation to the conceptual model of the evolution of the Broad Fourteens Basin described in Part 2 (see also Verweij et al. 2000, 2001, 2003, Verweij and Simmelink 2002).

## 19 History of sedimentation, uplift and erosion

### 19.1 Reconstructed geological history

The geological history of the entire Broad Fourteens Basin was outlined in detail in Part 2.

Appendix 4 discusses the quantitative reconstruction of the history of sedimentation, uplift and erosion along the cross-section. It includes the quantified uninterrupted time-stratigraphic sequence of events during the evolution of the basin for three key wells along the cross-section (P09-01A, P06-02, Q01-03) and for two wells along the northern extension of the cross-section (L17-02, L14-02) (Appendix 4, Tables 19 - 23).

### 19.2 Predicted history of sedimentation, uplift and erosion

Figure 49 illustrates the predicted history of sedimentation, uplift and erosion along the cross-section. The forward modelling of the changes in geometry along the cross-section includes the simplest conditions for the Late Cretaceous and Danian history (Appendix 4). This is geohistory scenario 1. Figure 49 clearly shows the occurrence of major changes in the geometry during basin history, i.e. changes of the magnitude and directions of dip. The predicted burial histories for geohistory scenario 1 conditions are given in Figure 50. The burial histories of pre-inversion tectono-stratigraphic units show large differences along the cross-section. The Variscan to Early-rift tectonostratigraphic units in the central parts of the basin reached their maximum depth of burial at pre-inversion times and are presently not at their maximum depth of burial, with the possible exception of a small area at 50 km. In the southern part of the section, the units are presently approximately at pre-inversion depth at the structural high corresponding to well location P9, and at maximum burial depth southward (0 - 7 km) and northward of the high (10 - 20 km). To the north of the actual basin (62 - 78 km; northern platform Figure 48) the Carboniferous and Triassic units are presently at their maximum depth of burial.

As outlined in Chapter 18 lateral displacements of layers and lateral changes in the dimension of the basin could not be incorporated in the modelling, because the Temispack modelling package does not allow such lateral changes. However, these types of displacement did occur during the evolution of the Broad Fourteens Basin, especially during the syn-inversion phase: e.g. shortening of the Broad Fourteens Basin of approximately 10 - 15%, and northward thrusting of the basin fill in the Q1 area (see Part 2; Roelofsen and De Boer, 1991).

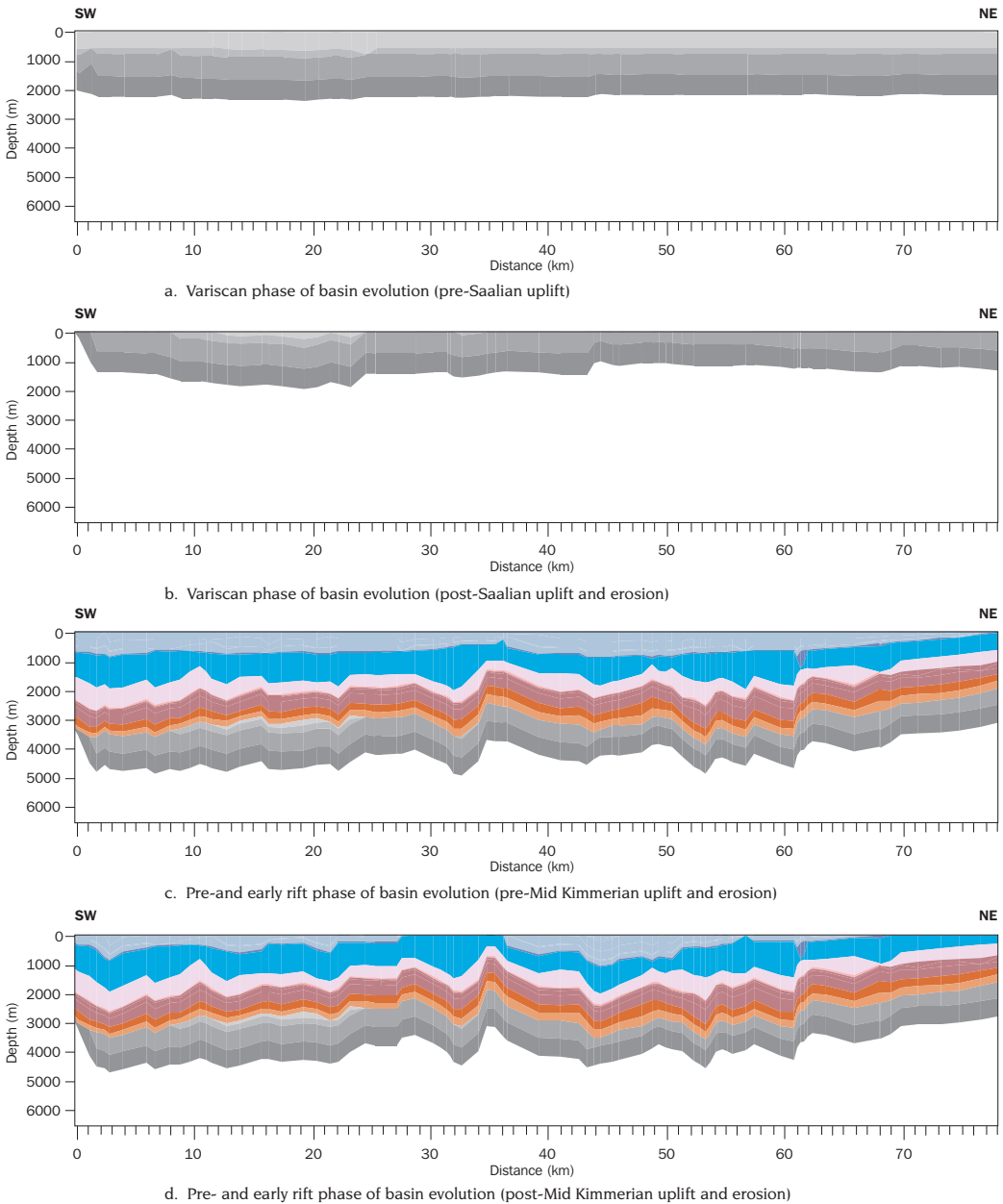
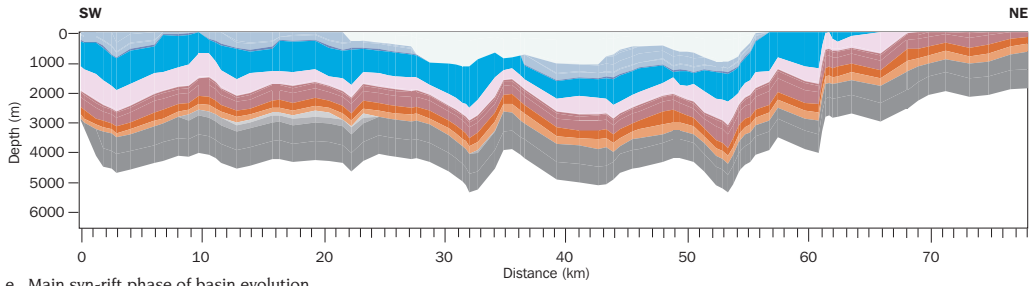
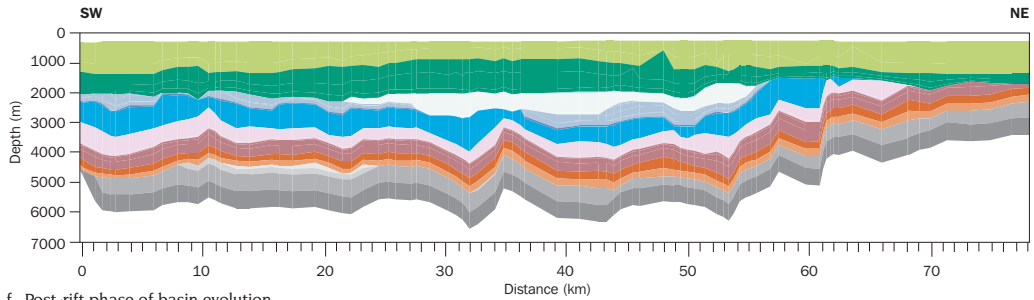


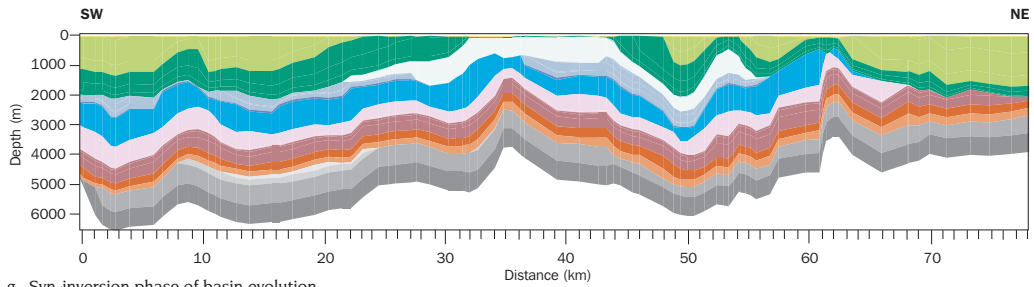
Figure 49 Predicted geometries of the basin fill along the cross-section through the southern part of the Broad Fourteens Basin related to the different phases of basin evolution (forward modelling assuming scenario 1 conditions of Cretaceous and Danian geological evolution): a. Variscan phase of basin evolution (pre-Saalian uplift); b. Variscan phase of basin evolution (post-Saalian uplift and erosion); c. Pre- and early rift phase of basin evolution (pre-Mid Kimmerian uplift and erosion); d. Pre- and early rift phase of basin evolution (post-Mid Kimmerian uplift and erosion); e. Main syn-rift phase of basin evolution; f. Post-rift phase of basin evolution (pre-inversion); g. Syn-inversion phase of basin evolution; h. Post-inversion phase of basin evolution (present-day)



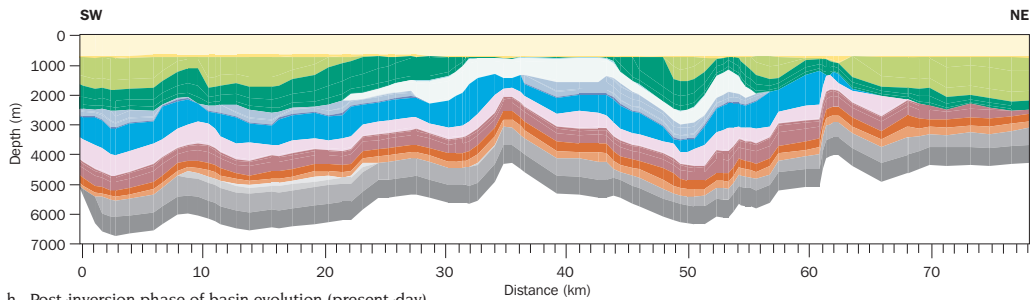
e. Main syn-rift phase of basin evolution



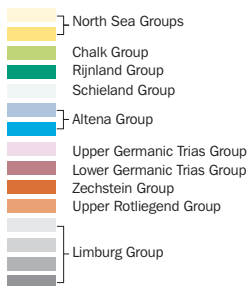
f. Post-rift phase of basin evolution



g. Syn-inversion phase of basin evolution



h. Post-inversion phase of basin evolution (present-day)



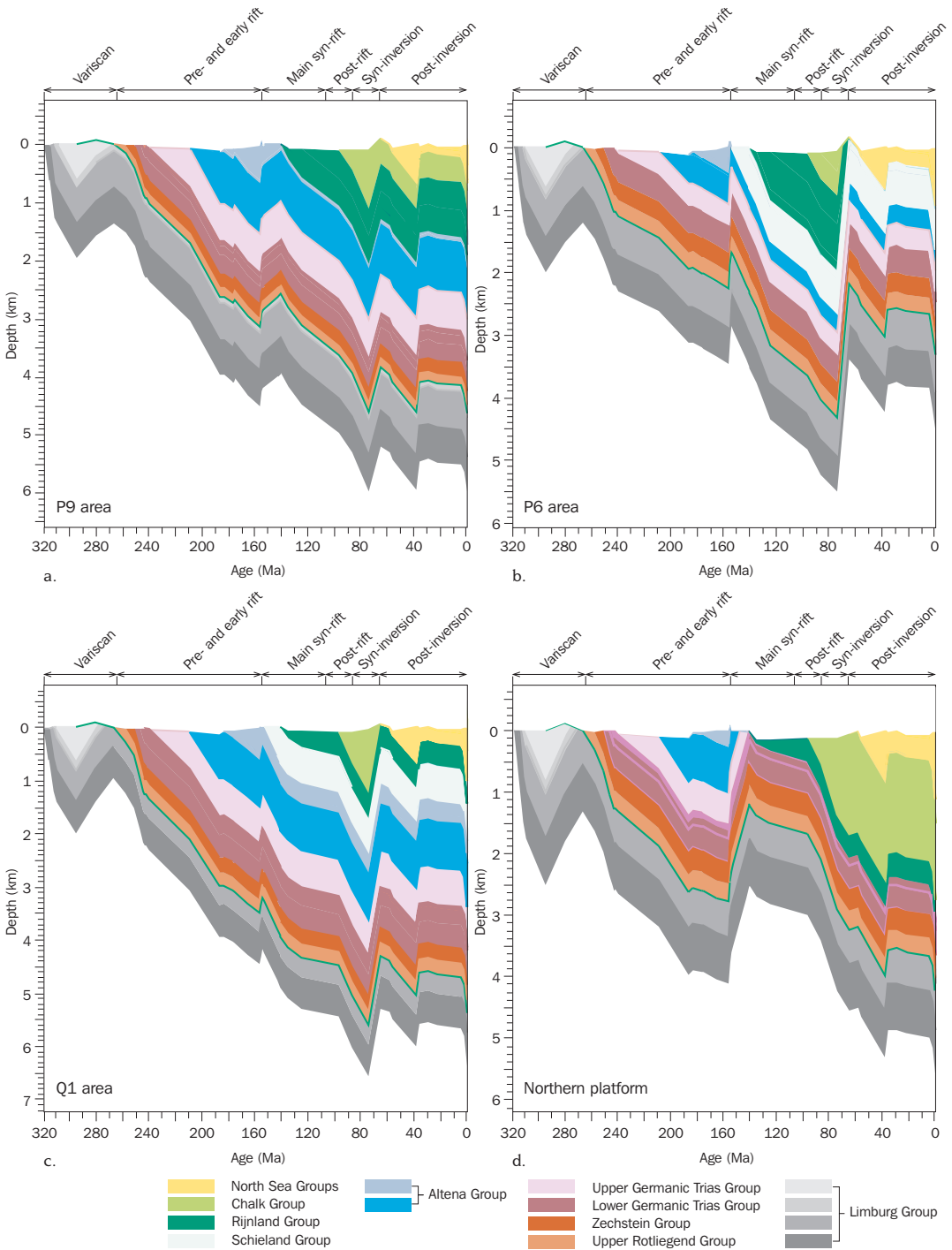


Figure 50 Predicted burial histories at four locations along the cross-section through the southern part of the Broad Fourteens Basin: a. Predicted burial history for P9 area; b. Predicted burial history for P6 area; c. Predicted burial history for Q1 area; d. Predicted burial history for the northern platform area

## 20 Thermal history

### 20.1 Selection of boundary conditions and input data

The simulations of the temperature and heat flow history started with a simplified thermal model of the basin using the scenario 1 of the geological history, applying default thermal conductivities and heat capacities, while neglecting radiogenic heat production, and assuming a generalised temperature history as top boundary condition, a constant basal heat flow as bottom boundary condition, zero heat flow across lateral boundaries, and a steady state heat flow in the basin. Gradually more realistic conditions were added and the influence of these changes on the thermal history was evaluated (see Simmelink and Verweij 2000). The most important effects are summarised below.

The validity of the temperature predictions in the different simulations was evaluated with the help of present-day temperatures based on bottom hole temperatures at wells P09-01A, P06-02 and O01-03 given in Robertson Research International (1985, 1988), and the vitrinite reflectance measurements at well P09-01A.

Running and validating the simplified thermal model with a constant basal heat flow at the bottom upper crust of 35 to 40 mW/m<sup>2</sup> led to adaptations of the matrix thermal conductivities and the selection of 40 mW/m<sup>2</sup> as the most appropriate constant basal heat flow boundary condition. In subsequent runs the adjusted, generally higher matrix thermal conductivities were applied, based on the results of heat flow studies in the southern North Sea area (Andrews-Speed 1984, Part 1), given in Appendix 4 (Table 25).

The temperatures and heat flow in a basin are influenced by geological processes such as subsidence and sedimentation, and uplift and erosion. The actual magnitude of the change in heat flow and temperature depends on the thermal conductivities of the sediments and the rate and duration of sedimentation or erosion. In the present study, the magnitude of the transient influences of these processes was examined by comparing the results of a simulation based on a steady state heat flow equation with the results based on a transient heat flow equation. In the Broad Fourteens Basin the predicted transient effects were found to be significant during different phases of basin evolution. For example, application of the transient heat flow model resulted in significantly lower present day heat flows and temperatures because of the transient influence of the Late Tertiary and Quaternary phase of sedimentation and a significantly higher heat flow and temperatures following the Eocene-Oligocene phase of uplift and erosion (e.g. temperature differences of more than 7 °C were predicted for the deeper part of basin, Simmelink and Verweij 2000). The disparity in the results for temperature produced by steady state and transient modelling generally increased with depth. From this it is clear that to model the geodynamic evolution of the Broad Fourteens Basin, which is characterised by significant differential vertical displacements, the best approach is transient thermal modelling.

The history of basal and surface heat flow along the cross-section was estimated by in-house tectonic forward modelling, using the reconstructed history of sedimentation, uplift and erosion of three wells (Appendix 4). The predicted present-day surface heat

flow was approximately  $60 \text{ mW/m}^2$ , which is the lowest predicted heat flow since Carboniferous. The tectonic modelling of heat flow evolution revealed two periods in which heat flow increased: after the Triassic and Late Jurassic rifting phases (but with a time lag). Such increases in heat flow following rifting phases were also deduced from tectonic forward modelling of the inverted West Netherlands Basin (Van Balen et al. 2000). The incorporation of the time-dependent changes in basal heat flow into the boundary conditions for the thermal basin modelling resulted in higher calculated temperatures, especially in the deeper parts of the basin during the two periods of rifting-related increased heat flow.

The evolution of the sediment-water interface temperatures is an important boundary condition in reconstructing temperatures and heat flow. Initial runs of the thermal module assumed a sediment-water interface temperature of  $8 \text{ }^\circ\text{C}$  for the period between 10 Ma and present-day. Simulations taking into account a detailed temperature evolution from Pliocene to recent times (with temperatures fluctuating between  $-10$  and  $+8 \text{ }^\circ\text{C}$ ; Appendix 4) reveal that these fluctuating surface temperatures have a major cooling effect on present-day temperatures in the basin. A calculated maximum present-day cooling effect of approximately  $10 \text{ }^\circ\text{C}$  occurs along the section at 900 - 1000 m depth.

The incorporation of radiogenic heat production resulted in generally higher temperatures in the basin.

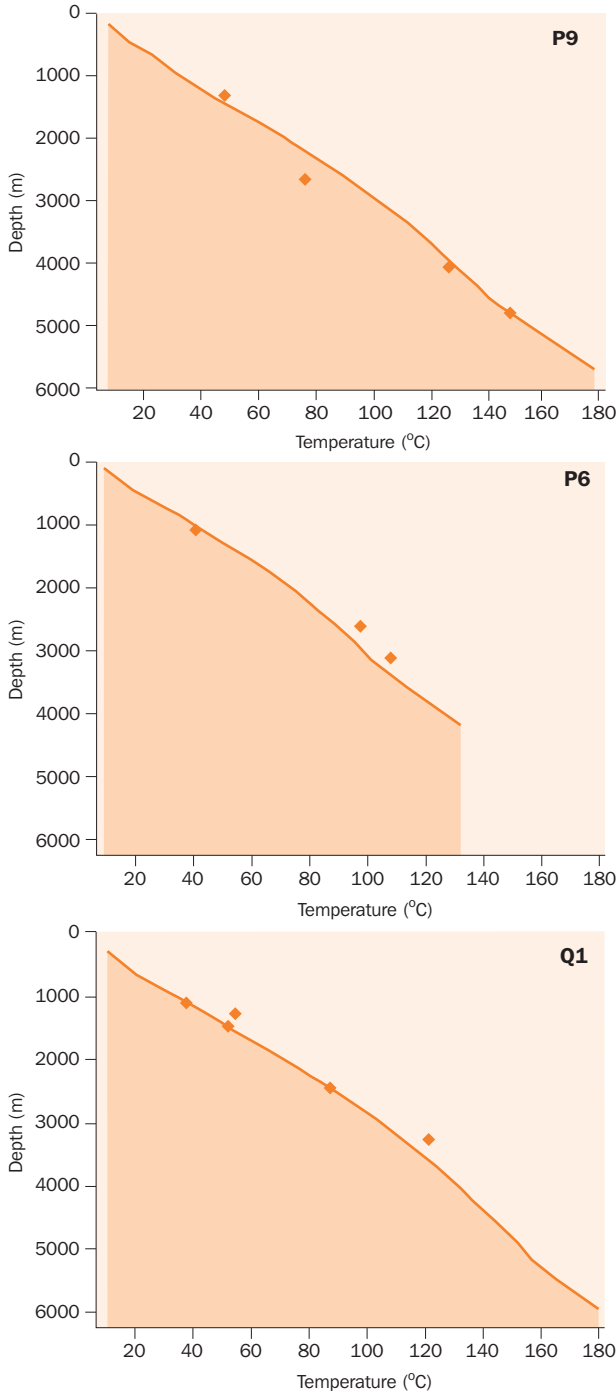
In the course of the study of the Broad Fourteens basin a more detailed reconstruction of the Late Cretaceous and Danian geological history was completed. This scenario 2 of the geological history was used in subsequent modelling studies.

The favoured scenario for reconstructing the temperature and heat flow history along the section incorporates the following conditions and parameters (values are given in the Appendix 4):

- The more detailed Scenario 2 of the geological history (geohistory scenario 2);
- Matrix thermal conductivities based on results of heat flow studies in the southern North Sea area (Andrews-Speed 1984; Part 1);
- Default heat capacities;
- Radiogenic heat production in the sediments.
- Evolution of sediment-water interface temperatures as top boundary condition, including detailed Pliocene to recent temperature fluctuations;
- Evolution of the basal heat flow as the bottom boundary condition;
- Zero heat flow across lateral boundaries;
- Transient heat flow.

The reconstruction of temperature and heat flow history resulted in calculated present-day temperatures and vitrinite reflectances that could be compared with measured data (Figures 51 and 52). Figure 51 shows that the predicted present-day temperatures for wells P09-01A, P06-02 and Q01-03 generally match the observed temperatures. The reliability of these – bottom-hole – temperatures in the Broad Fourteens Basin were discussed in Chapter 15 and it was recognised that the reliability of these temperature data is generally poor. Despite these restrictions of the available temperature data base, the above scenario was considered the most

appropriate one for the modelling, because of the careful reconstruction of the geological history along the cross-section, and the independent estimations of the basal heat flow, the sediment-water interface temperatures and the radiogenic heat production in the sediments. The predicted vitrinite reflectances, calculated by the



model for type IV reference kerogen, and measured vitrinite reflectances at two locations are given in Figure 52. For well P09-01A the measured and predicted values match. As explained in Appendix 4, the measured vitrinite reflectance of the Posidonia Shale Formation at well Q01-03 has limited value as calibration data for the basin modelling, because in the Q1 region there has been lateral displacement of pre-inversion units (certainly of the Altena and younger units) from the deeper central parts of the basin towards the north. These lateral displacements, that cannot be handled by Temispack, caused a doubling of the thickness of the Altena Formation at well Q01-03.

## 20.2 Temperature and heat flow history

The transient effects of tectonic vertical displacements of the basin and the accompanying sedimentation or erosion on the magnitude of the heat flow through the basin were clearly visible in the predicted heat flow distributions, especially after rifting, after inversion and at present day. The results of the thermal modelling revealed lateral variations in heat flow along the section.

Figure 51 Predicted temperature-depth relations at present-day and observed temperatures for wells P09-01A, P06-02 and Q01-03



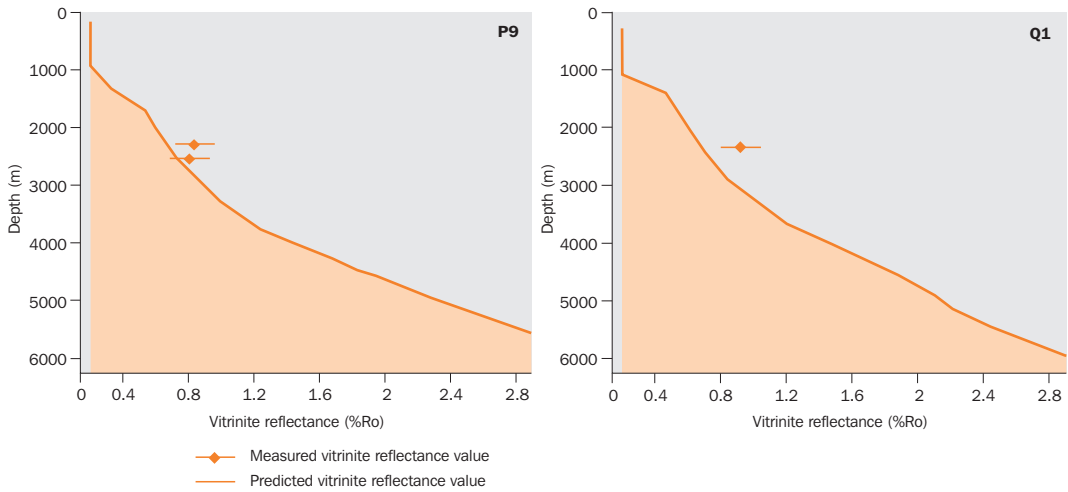
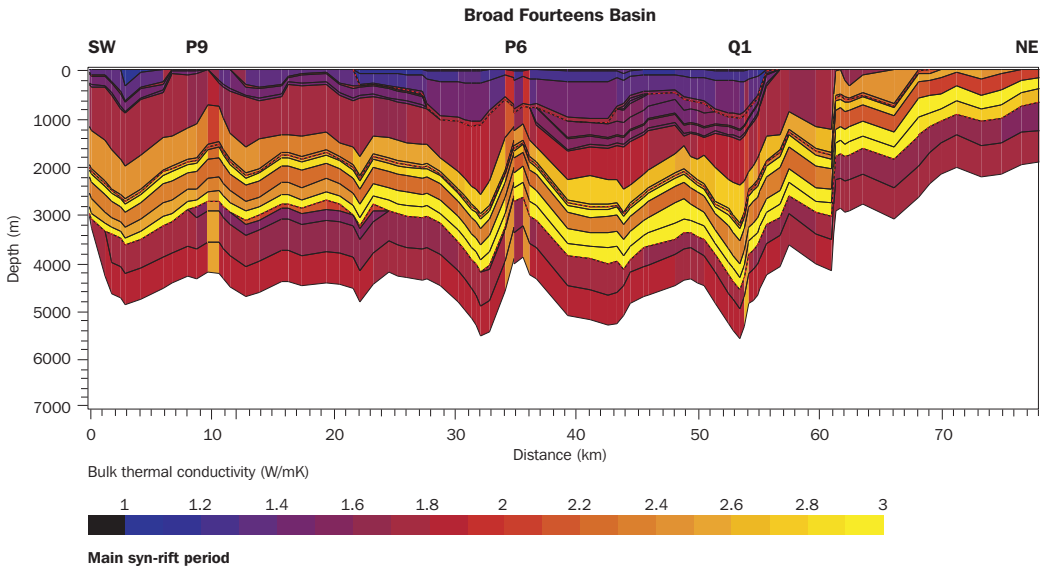


Figure 52 Predicted values of vitrinite reflectance and measured values of vitrinite reflectance for wells P09-01A and Q01-03

During the main syn-rift and syn-inversion phases of basin development, the central part of the basin and the northern platform underwent contrasting uplift and subsidence histories (Figure 49), resulting in differences in lithostratigraphy as well as in porosities between both areas. The recently deposited sediments have high porosities. The higher the water-filled porosities of a certain lithotype, the lower its bulk thermal conductivity. The resulting differences in bulk thermal conductivities between the basin and the northern platform (Figures 53 and 54) induce lateral variations in heat flow along the cross-section. This effect is augmented by the transient effect of tectonic vertical displacements on heat flow described before. Modelling results at depths between 400 and 2000 for the syn-rift period of basin evolution show a relatively decreased heat flow in the central part of the basin ( $64 \text{ mW/m}^2$ ) in comparison with the heat flow ( $72 \text{ mW/m}^2$ ) at the simultaneously uplifted and eroded northern platform. The results for the syn-inversion period, in contrast, predict a relatively high heat flow ( $74 \text{ mW/m}^2$ ) in the uplifted centre of the basin in comparison with the subsiding platform ( $66 \text{ mW/m}^2$ ) at these depths (Figure 55).

The predicted present-day heat flow distribution clearly reflects the effects of Pleistocene temperature fluctuations and recent sedimentation. At the start of the Pliocene (5.2 Ma) the predicted mean heat flow throughout the basin was approximately  $65 \text{ mW/m}^2$ . At 2.4 Ma the predicted shallow mean heat flow was approximately  $65 \text{ mW/m}^2$  in the recently deposited Pliocene Oosterhout Formation. The combined influence of the relatively low ground surface temperatures during Pleistocene times and – to a minor extent – the increased Quaternary sedimentation rates in combination with the relatively high porosities of the newly deposited sediments is reflected in the predicted relatively low mean heat flow values of less than  $55 \text{ mW/m}^2$  in the Pliocene Oosterhout Formation and Quaternary Formations at present-day (Figure 56). The predicted present-day magnitude of the heat flow increases with depth (Figure 57). This general trend of a relatively low heat flow at shallow depths is in accordance with the steady state heat flows calculated from measured bottom hole temperatures

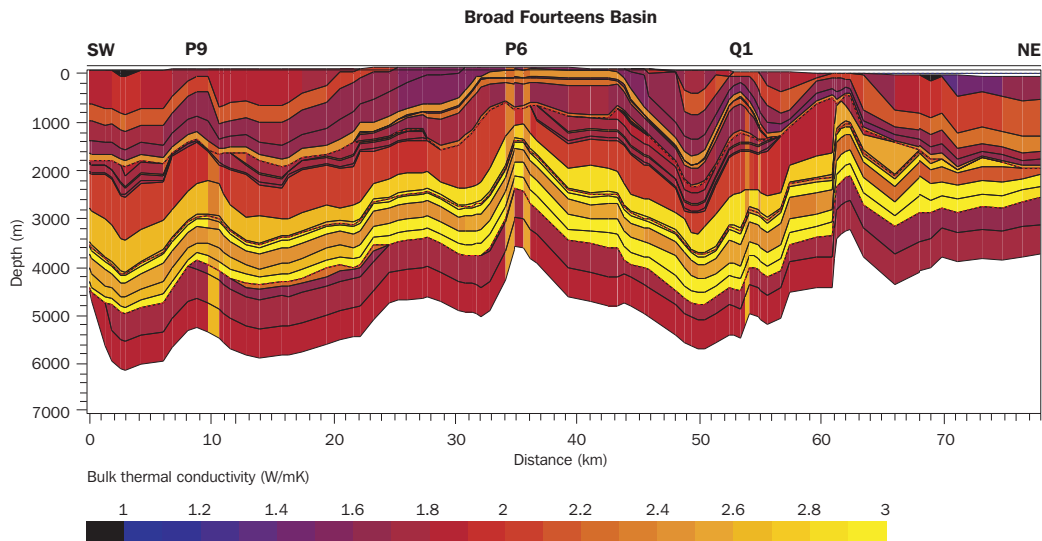


**Main syn-rift period**

Figure 53 Calculated distribution of bulk thermal conductivities in the Broad Fourteens Basin during the main syn-rift period

in the Broad Fourteens Basin (calculated heat flow = 53 mW/m<sup>2</sup> for shallow depths between 0 and 1000 m; see Part 2).

The simulated temperature history for the Carboniferous source rocks and the oil-prone Posidonia Shale Formation are given in Figures 58 and 59, respectively. It can be seen that the temperature history largely follows the burial histories of



**Syn-inversion period**

Figure 54 Calculated distribution of bulk thermal conductivities in the Broad Fourteens Basin during the syn-inversion period

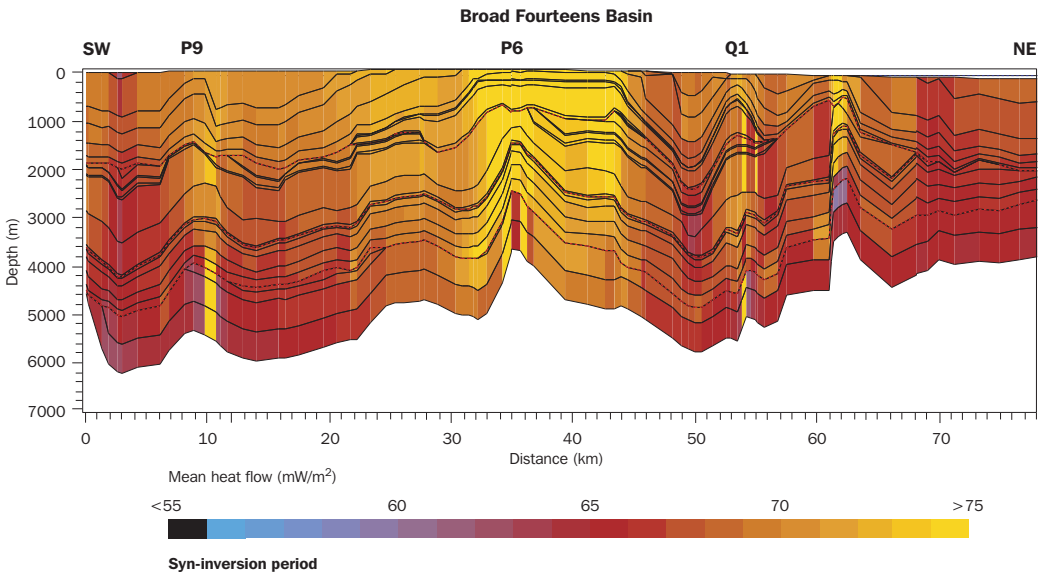


Figure 55 Predicted heat flow distribution in the Broad Fourteens Basin during the syn-inversion period

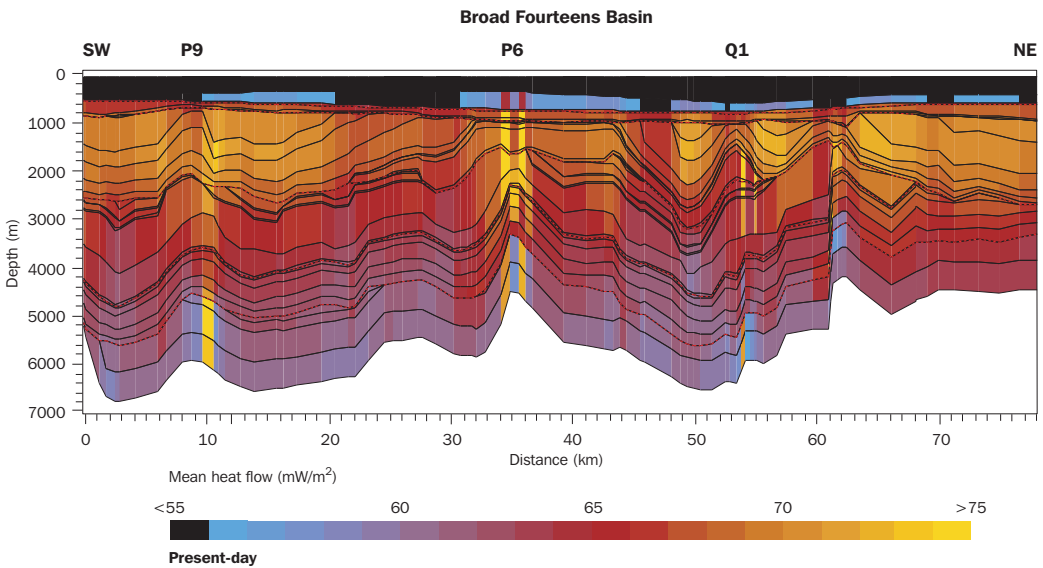


Figure 56 Predicted present-day heat flow distribution in the Broad Fourteens Basin

Carboniferous and Jurassic source rocks (Figure 58d, see also Figure 50). The temperatures increase in the source rocks with increasing depth of burial, and decrease during uplift and erosion. However during the Mid to Late Tertiary times, the temperatures in the source rocks decrease during burial. This temperature decrease during burial seems to be the result of the changing thermal boundary conditions. Between the Pyrenean phase of erosion and the start of the Pliocene the surface temperatures dropped dramatically from approximately 22 °C to 8 °C.

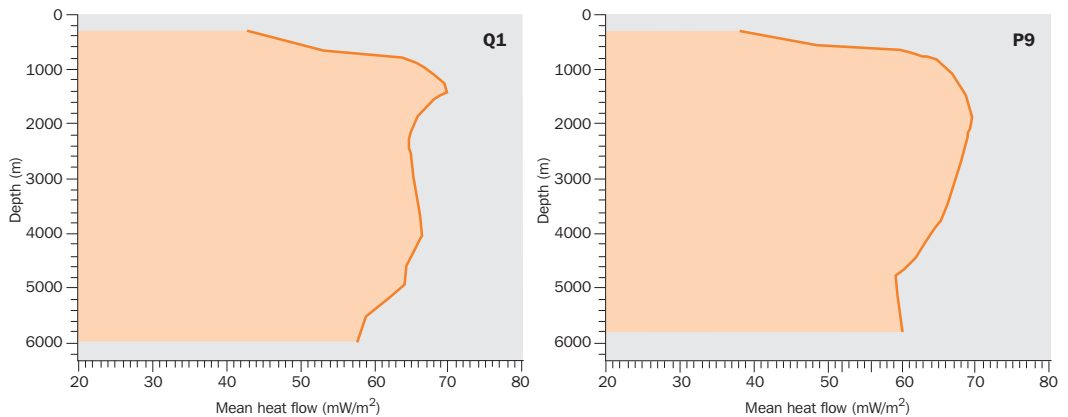


Figure 57 Predicted mean heat flow versus depth relation for P9 and Q1 area at present-day

What caused the continuous drop of temperatures in these source rocks was the influence of these decreasing surface temperatures together with the relatively low input of basal heat flow and the relatively minor sedimentation and corresponding burial of the Carboniferous and Jurassic source rocks in that period (Figure 60, Figure 50). Figures 58 and 59 show that temperatures started to increase again under the influence of increasing burial during the Pliocene and, especially, the Quaternary. Notwithstanding these recent temperature increases, the present-day temperatures in the Carboniferous and Jurassic source rocks along the entire cross-section are lower than maximum temperatures experienced during previous burial (Figures 58 and 59). Even in the platform area north of the basin where the Carboniferous rocks are at their maximum depth of burial, the present-day temperatures in the Carboniferous section were calculated to be below the maximum temperatures reached during basin evolution. In the southern part of the basin (e.g. at 13 km) the Carboniferous and Jurassic source rocks reached their maximum temperatures in the Early Tertiary, just before Eocene-Oligocene uplift (Figures 58 and 59). In the central most inverted part of the basin, the source rocks experienced maximum temperatures just before the Late Cretaceous inversion phase. The modelling results predict that in a small area around 50 km, the source rocks reached and even slightly exceeded pre-inversion temperatures during the Early Tertiary. In the northern platform area the Carboniferous units reached maximum temperatures in the Early Tertiary.

Figure 61 gives the predicted present-day temperature distribution along the section.

### 20.3 Conclusions

The thermal modelling revealed lateral and vertical variations in heat flow along the cross-section at different times during basin history. These variations could be related to vertical displacements of the basin and the evolution of the thermal boundary conditions, for example:

- The contrasting uplift and subsidence histories of the central part of the basin and the northern platform during the main syn-rift and the syn-inversion phase of basin evolution, resulted in lateral variations in heat flow along the cross-section of approximately  $8 \text{ mW/m}^2$ .

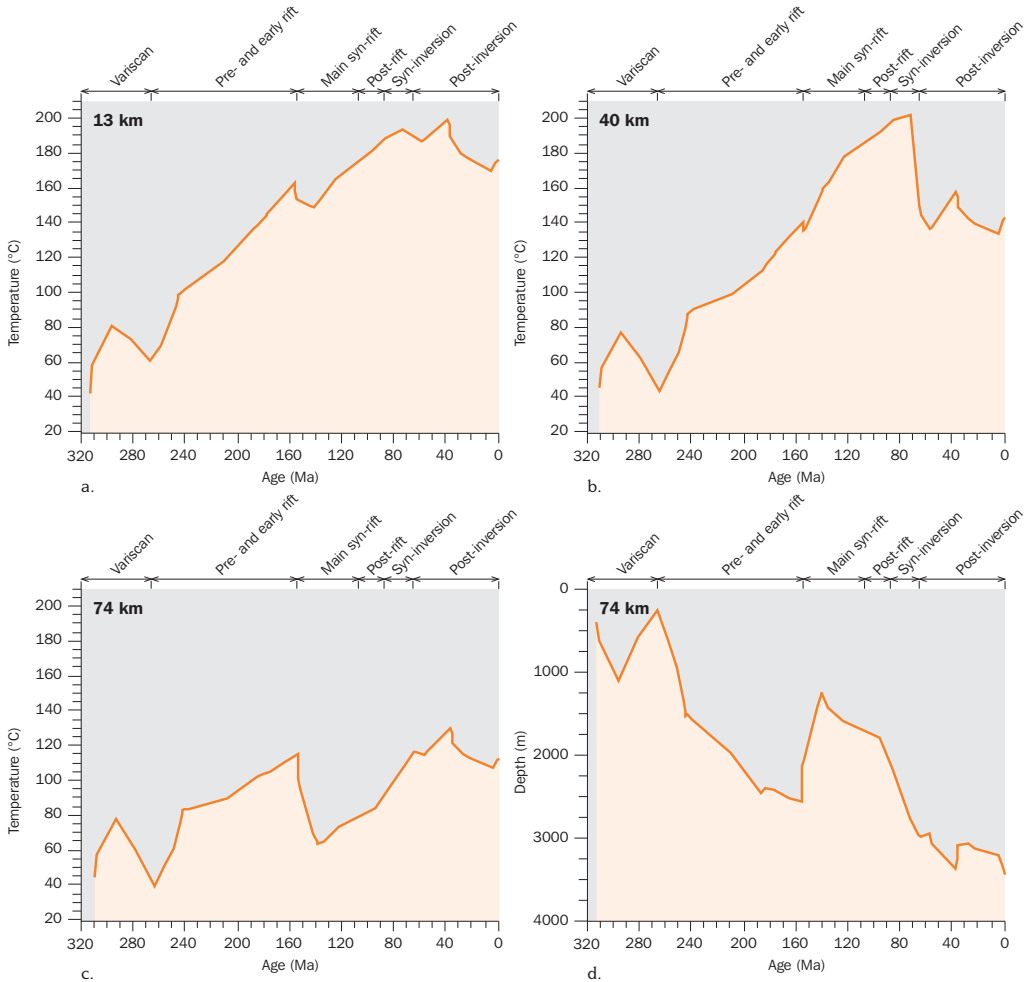


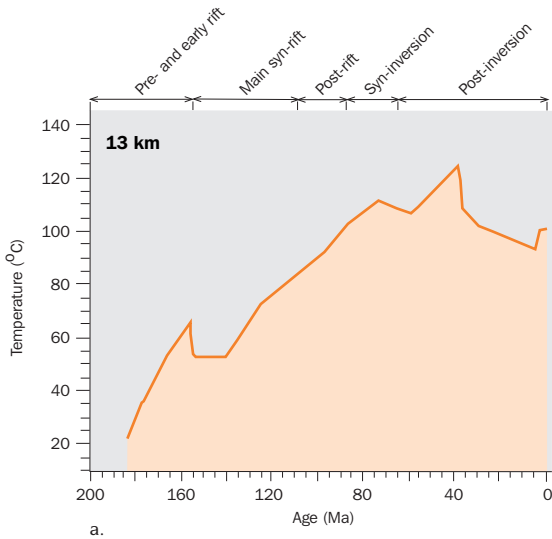
Figure 58 Predicted temperature evolution in the Limburg Group source rock in: a. the southern, b. the central and c. the northern parts of the cross-section; burial history Limburg Group source rock in northern part of the cross-section (d.)

— The predicted present-day heat flow distribution in the basin clearly reflects the effect of Pleistocene surface temperature fluctuations in combination with the relatively high porosities of the newly deposited sediments and – to a minor extent – the recently increased sedimentation rates: the predicted mean heat flow in the basin at the start of the Pliocene drops from approximately  $65 \text{ mW/m}^2$  to less than  $55 \text{ mW/m}^2$  at present day in the shallow part of the basin.

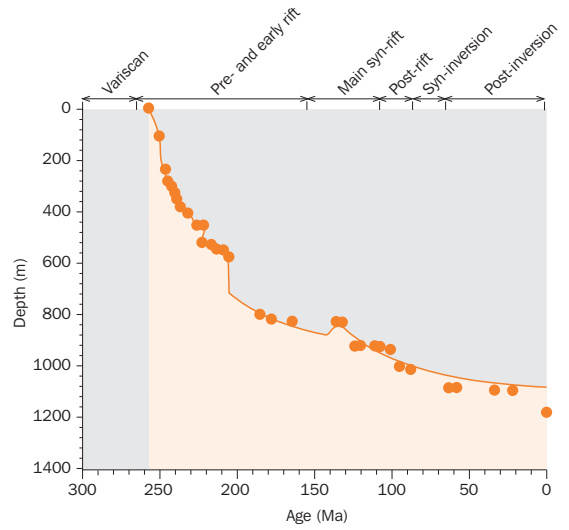
The simulated temperature history of the source rocks largely follows the burial histories of these rocks, except during Mid to Late Tertiary times.

The noteworthy modelling results of the temperature history of the source rocks are:

— The present-day temperatures in the Carboniferous and Jurassic source rocks along the entire cross-section are lower than the maximum temperatures experienced during previous burial.



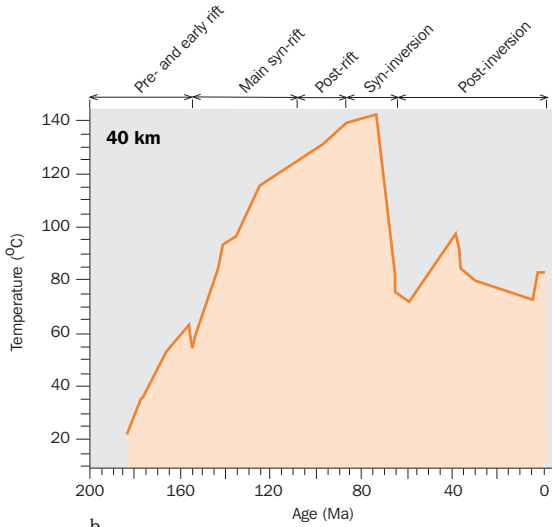
a.



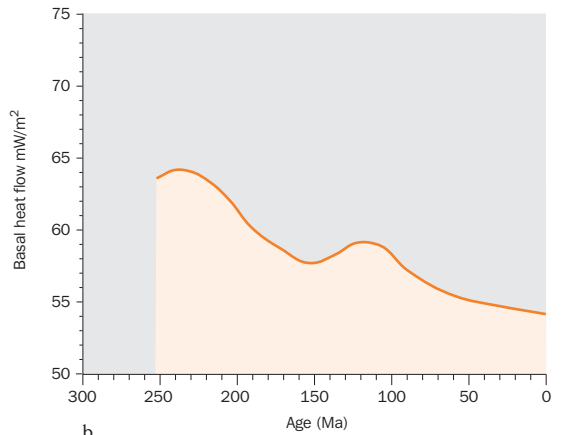
● Tectonic subsidence reconstructed by backstripping analysis

— Tectonic subsidence curve obtained by tectonic forward modelling

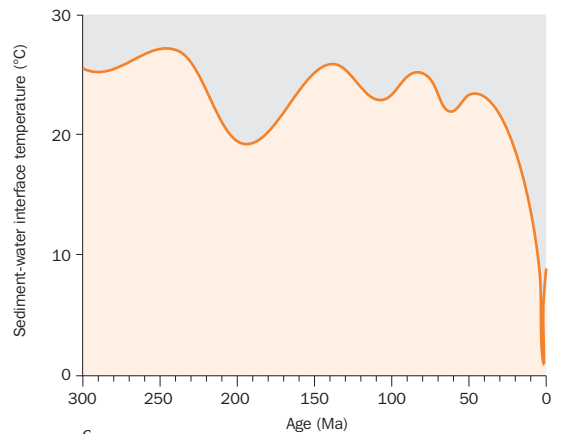
a.



b.



b.



c.

Figure 59 Predicted temperature evolution in the Posidonia Shale Formation in the southern and central parts of the cross section

Figure 60

- a. Tectonic subsidence curve for well P09-01A;
- b. Evolution basal heat flow derived from in-house tectonic forward modelling of the tectonic subsidence curve of well P09-01A;
- c. Evolution of sediment-water interface temperatures.

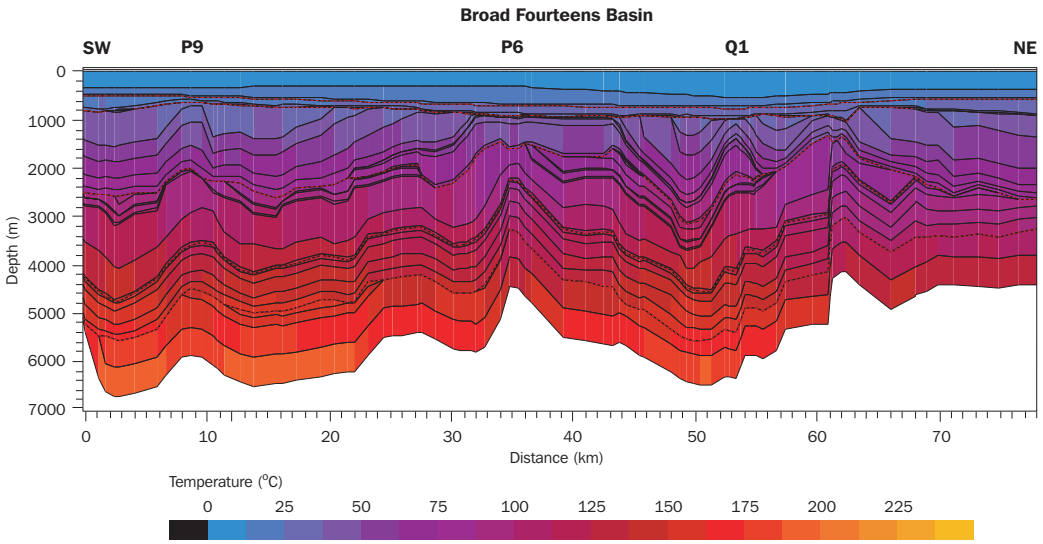


Figure 61 Predicted present-day distribution of temperatures along the cross-section

- In the southern part of the cross-section and in the northern platform area the source rocks reached their maximum temperature just prior to the Eocene-Oligocene uplift.
- In the central, most inverted part of the basin, the source rocks reached maximum temperatures just prior to the Late Cretaceous syn-inversion phase.

The simulated temperature and heat flow history offers a process-based understanding of the observed present-day temperature and heat flow variations in the Broad Fourteens Basin today, such as the observed relatively low heat flow in the shallow part of the basin and the increasing heat flows with depth (Chapter 15). It is recognised that a reliable database of present-day temperatures and more vitrinite reflectance data will increase the confidence of the applied thermal modelling.

## 21 History of maturation and petroleum generation

The model includes three source rock intervals: the Carboniferous coal measures of the Limburg Group, the Jurassic Posidonia Shale Formation, and the Aalburg Formation (Appendix 4). The gas-prone coal measures of the Limburg Group are of kerogen type III and include the Baarlo Formation, Ruurlo Formation, Maurits Formation and the Dinkel and Hunze Subgroups, with TOC contents of 0.7%, 2.8%, 4.2% and 0.7%, respectively. Van Balen et al. (2000) proposed a second gas system based on a Namurian source rock. Such a system may also be present in the Broad Fourteens Basin, but the occurrence of Namurian source rock in the basin has not been proven. Therefore it has not been included in the modelling. The oil-prone Posidonia Shale Formation is of kerogen type II with a TOC content of 5%. The Aalburg Formation was taken into account as an additional kerogen type II source rock for oil with a TOC content of 1%. The maturation of a source rock summarises the kerogen conversion processes including petroleum generation. The conversion of kerogen to petroleum is controlled by kinetic reaction processes, which are temperature and time dependent. The maturity model of the Temispack modelling program calculates indicators of maturity, such as the transformation ratio and vitrinite reflectance values. The transformation ratio is the ratio of generation of petroleum to potential petroleum in a source rock. The model computes the values of vitrinite reflectance from the transformation ratio.

### 21.1 Maturation and petroleum generation in the Limburg Group source rock

As expected, the predicted maturity history of the gas-prone Limburg Group source rock (Figure 62) is closely related to the temperature history. Figure 63 illustrates this relationship for the Ruurlo Formation. Increasing temperatures of the source rock correspond to increasing vitrinite reflectance values, i.e. increasing maturities.

Figure 63 shows that after periods of uplift and erosion and corresponding decreasing temperatures of the source rock, the maturity does not start to increase again until the source rock has been reburied beyond its previous maximum depth (i.e. maximum temperature). Such time lags are predicted to be significant in the periods following the Saalian and Mid-Kimmerian tectonic phases. For example, notwithstanding the subsidence and temperature increase related to deposition of Upper Rotliegend and Zechstein Group sediments in the period between 266 and 251 Ma there

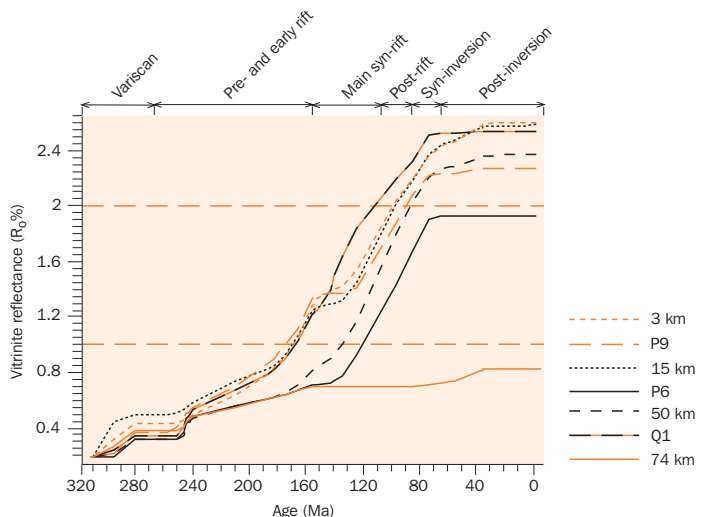


Figure 62 Predicted maturity history of the Limburg Group source rock (Ruurlo Formation) at seven locations along the cross-section through the Broad Fourteens Basin



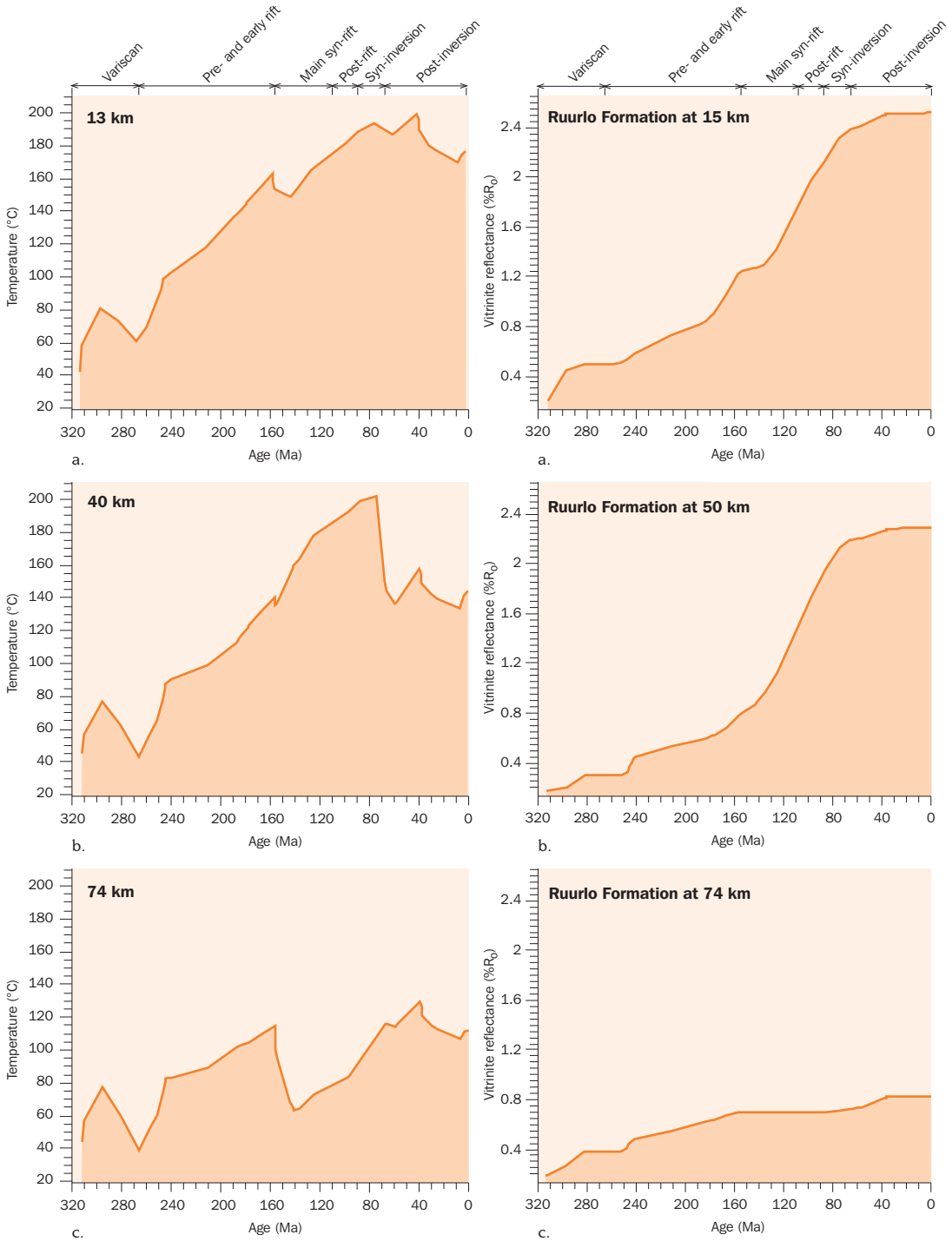


Figure 63 Predicted temperature history and associated maturity history of the Limburg Group source rock in the southern (at 13 - 15 km), central (at 40 - 50 km) and northern (at 74 km) part of the cross-section through the Broad Fourteens Basin

is no increase in vitrinite reflectance value of the Ruurlo Formation between 280 and 250 Ma at all seven locations along the cross-section, (Figures 62, 63 and 64).

The burial histories of the Limburg Group source rock show large differences along the cross-section (Figure 50) resulting in very different temperature (Chapter 20) and associated maturity histories for the source rock that depend on its structural position. Rapid subsidence in the Early Triassic induced a sharp increase in temperature and maturity along the entire cross-section (Figures 62, 63 and 64). During the remaining early-rift phase the maturities continued to increase but at diminished rates. In the northern platform area and in the P6 area, the Altena Formation deposited in the early-rift phase, was thinner than in the remaining part of the section; as a result, the increase in temperature and maturity was less in the northern platform and the P6 area. This is reflected in the calculated vitrinite reflectance values of the Ruurlo Formation at the end of the early-rift period just prior to the Mid-Kimmerian phase: the vitrinite reflectance value of the Ruurlo Formation in the northern platform and the P6 area is approximately  $0.7\%R_o$ , while a value of  $1.25\%R_o$  is predicted at 15 km along the cross-section (Figure 62).

In the central and southern parts of the cross-section the calculated vitrinite reflectance values and transformation ratios increased rapidly during syn-rift and post-rift burial and associated heating of the gas-prone source rock. In the most inverted parts of the basin (P6 and Q1 areas) Carboniferous source rock intervals attained their maximum temperatures prior to the Late Cretaceous period of inversion. The predicted vitrinite reflectance values in the P6 and Q1 areas increased until inversion started but then remained stable ever since (Figure 64). In the less inverted parts of the basin, reburial of the source rocks due to sedimentation in the Early Tertiary resulted in a slow and only minor increase in vitrinite reflectance values (Figure 62). The Eocene-Oligocene phase

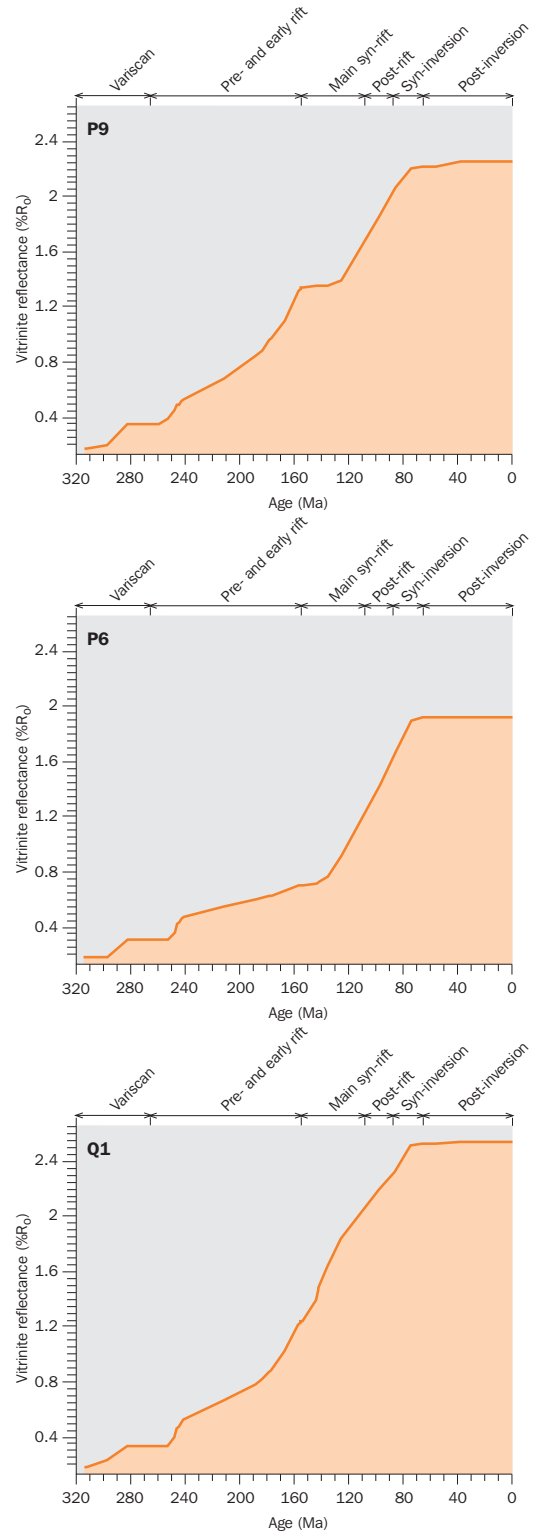


Figure 64 Predicted maturity history of the Limburg Group source rock (Ruurlo Formation) in the P9, P6 and Q1 areas of the Broad Fourteens Basin

of uplift stopped this maturation process. The temperature evolution after the Eocene–Oligocene phase (Chapter 20) did not allow the resumption of the maturation process of the Limburg Group source rock (Figure 62, 63 and 64).

The uplift and erosion of the northern platform area during the main syn-rift period halted the maturation process in the Limburg Group source rock (Figure 63c). The model predicted that maturity in the platform area started to increase again during syn-inversion sedimentation. In this area, the Limburg Group source rock reached maximum maturities prior to the Eocene–Oligocene phase of uplift. This maximum maturity for the Ruurlo Formation in the northern platform area corresponds to a calculated vitrinite reflectance value of  $R_o = 0.83\%$ .

At present-day, the predicted vitrinite reflectance values of the Limburg Group source rocks exceed  $R_o = 2\%$  in the basinal part of the Broad Fourteens area (Figure 62). This is in accordance with e.g. Van Wijhe (1987a), who reported that present-day  $R_o$  values reach up to 2.4% at the top of the Carboniferous coal measures in the central part of the Broad Fourteens Basin.

The predicted history of vitrinite reflectance values and transformation ratios (Figure 65) indicates that the Limburg Group source rock first entered the gas window at the end of early-rift times, except for the northern platform area and the area between P6 and 50 km (assuming gas generation starts at approximately  $R_o = 1.0\%$  for Westphalian source rocks as indicated by Crépieux et al. 1998). In the basinal area between P6 and 50 km the gas window was reached later during syn-rift times (Figure 62). According to the model the Limburg Group source rock in the central and southern part of the cross-section reached transformation ratios exceeding 90% prior to the syn-inversion period (Figure 65). Inversion of the Broad Fourteens Basin stopped the generation of gas in the central and southern part of the cross-section. Outside the most inverted parts of the basin (that is outside the P6 and Q1 areas) the model predicted minor increases in vitrinite reflectance values during the early post-inversion period (Figures 63a, 63b). Because the vitrinite reflectance values of the source rock in a large part of the pre-inversion basin had already exceeded 2%, that is the source rock had already reached very mature conditions, only minor additional gas is expected to have been generated in this early post-inversion period. The model results show that in the most deeply buried source rocks in the northern platform area the Limburg Group source rock only just reached maturity for gas generation.

The total amount of gas generated during the evolution of the Broad Fourteens Basin is largest in the southern part of the cross-section (Figures 66 and 67). This is because in the southern part of the basin, the Maurits Formation has been preserved after Saalian erosion (Chapter 19, Figure 49) and the Maurits Formation source rock interval has the highest assigned TOC content of the Limburg Group source rocks.

The production of  $\text{CO}_2$  from the Carboniferous source rocks peaked just before the beginning of catagenesis (corresponding to the 0.8–0.95%  $R_o$  interval; Crépieux et al. 1998). Hence, the maximum production of  $\text{CO}_2$  in the Broad Fourteens basin probably occurred in its basinal area in early-rift times and during syn-rift times will have

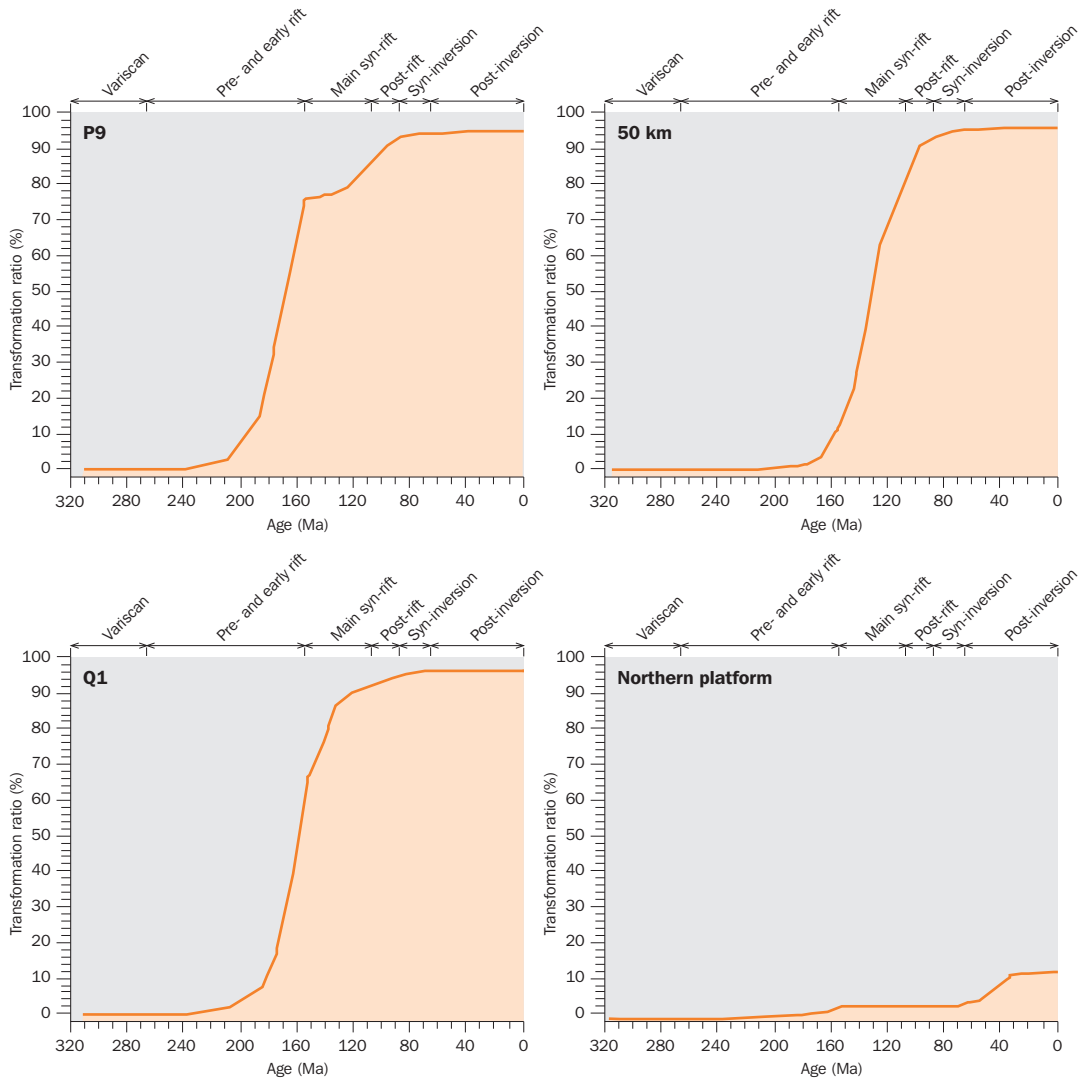


Figure 65 Predicted history of the transformation ratio of the Limburg Group source rock (Ruurl Formation) at P9, 50 km and Q1 in the Broad Fourteens Basin and in the northern platform area

continued in the area between P6 and 50 km. The Limburg Group source rock in the northern platform area is in the window for CO<sub>2</sub> production since syn-inversion times.

## 21.2 Maturation and petroleum generation in the Jurassic source rocks

The original distribution of the oil-prone Posidonia Shale Formation along the cross-section is restricted to the central and southern part of the Broad Fourteens Basin (Appendix 4). After the Mid and Late Kimmerian I tectonic phase the Posidonia Shale Formation was preserved in two separate areas along the cross-section: one in the southern part between 0 and 28 km and one in the central part of the basin between 37 and 56 km. The burial and temperature histories of the Posidonia Shale Formation

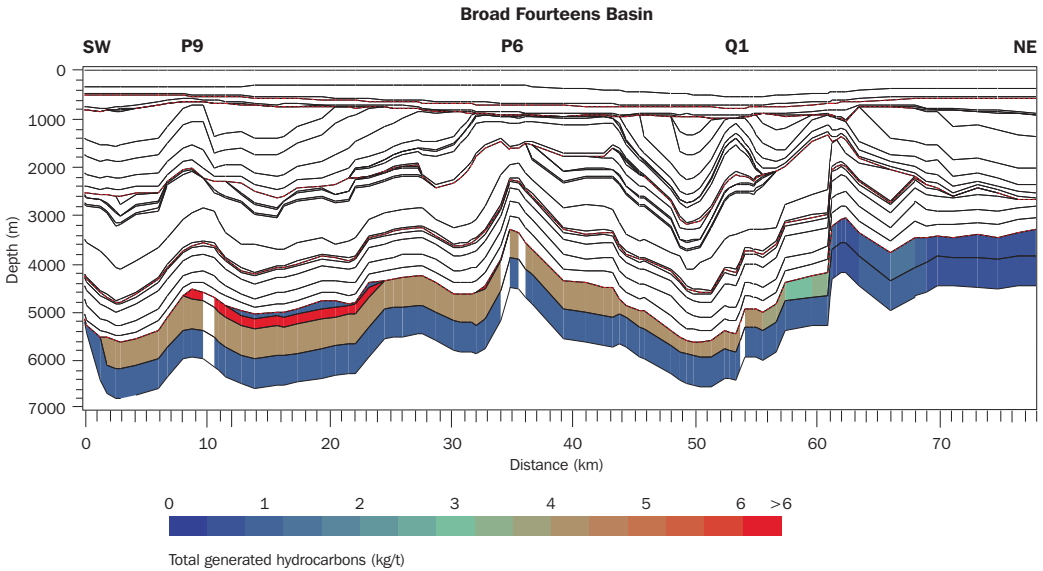


Figure 66 Predicted total amount of hydrocarbons generated in the Limburg Group source rocks along the cross-section through the Broad Fourteens Basin

in these two parts of the basin are different. The associated distinct maturity histories of the source rock are given in Figure 68.

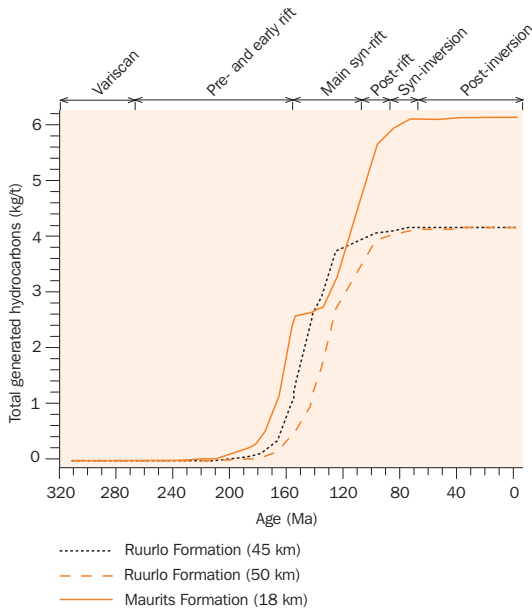


Figure 67 Predicted history of hydrocarbon generation in the Ruurlo Formation in the central part of the Broad Fourteens Basin and in the Maurits Formation in the southern part of the basin

During the main syn-rift phase, rapid subsidence of the Posidonia Shale Formation in the central part of the basin, which is related to deposition of Schieland Group sediments, started the maturation process in the source rock. This is reflected in the increasing values of vitrinite reflectance (Figure 68, location 50 km and Q1). The southern part of the basin south of 22 km was outside the area of deposition of the Schieland Group. Subsidence of the basin resumed here with the deposition of the Lower Cretaceous Rijnland Group sediments. Figure 68 shows that the predicted vitrinite reflectance values of the Posidonia Shale Formation in the southern part of the basin started to increase approximately 20 - 25 My later than the values predicted for the central part.

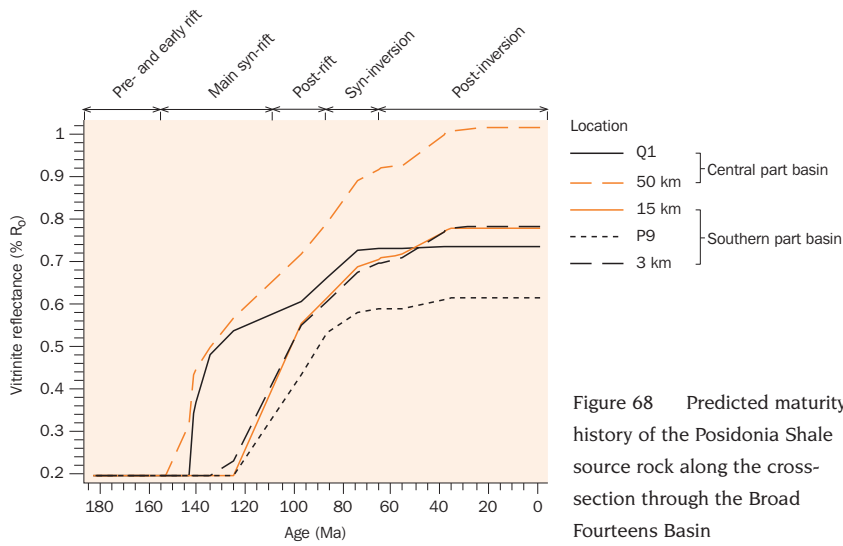


Figure 68 Predicted maturity history of the Posidonia Shale source rock along the cross-section through the Broad Fourteens Basin

Ongoing regional sedimentation in the later stage of the main syn-rift period and in the post-rift period resulted in continued maturation of the Posidonia Shale Formation in both the southern and the central part of the basin. Late Cretaceous inversion stopped the maturation process at the strongly inverted Q1 location and slowed down the maturation process at the other locations in the basin. The predicted vitrinite reflectance values and transformation ratios just prior to inversion are highest for the deepest part of the pre-inversion central part of the basin (at 50 km: 0.9% $R_0$ , transformation ratio 80%; Figure 68 and 69). The pre-inversion vitrinite reflectances in the southern part of the cross-section reached maximum values of 0.68% $R_0$  (at 15 km).

Post-inversion reburial of the Posidonia Shale Formation in Early Tertiary times continued the maturation process of the source rock, especially in the southern part of the basin. The calculated vitrinite reflectance values and transformation ratios just prior to the Eocene-Oligocene tectonic phase are: % $R_0 = 0.78$ , transformation ratio = 60% (at 3 km and 15 km, Figures 68 and 69). The model results indicate that after the Eocene-Oligocene tectonic phase the maturation process levelled out at all locations along the cross-section in accordance with the temperature evolution in the basin (Chapter 20).

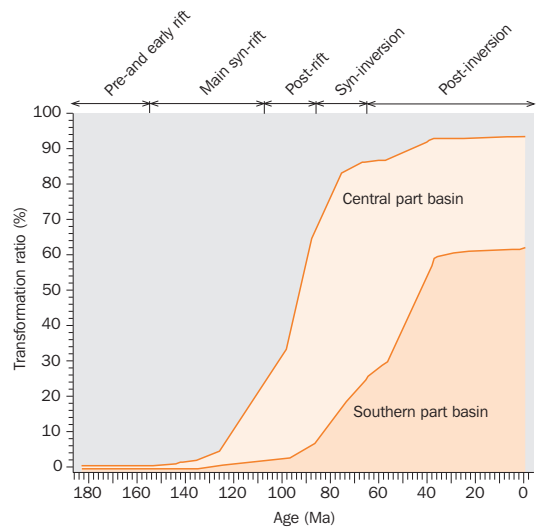


Figure 69 Predicted history of the transformation ratio for the Posidonia Shale source rock in the southern and central parts of the Broad Fourteens Basin

In the central part of the basin, most oil was generated prior to the syn-inversion period (Figure 70). In the southern part of the basin the Early Tertiary post-inversion period was an important phase of oil generation (Figure 71).

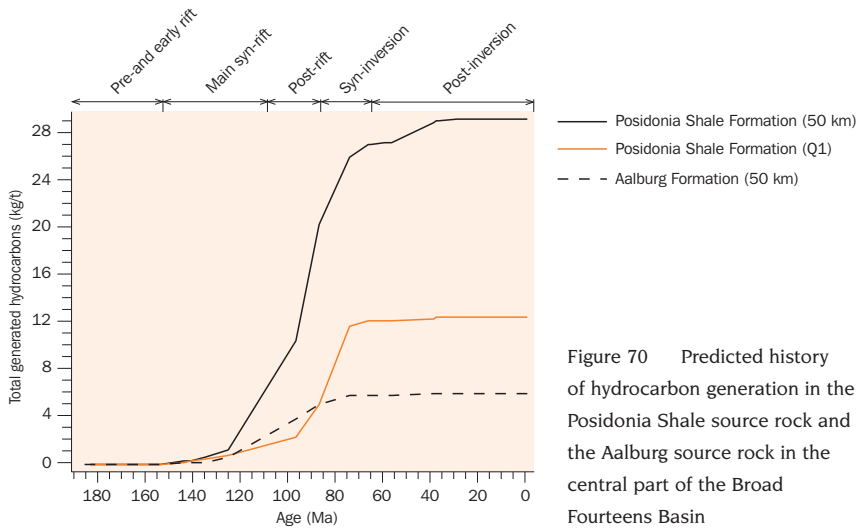


Figure 70 Predicted history of hydrocarbon generation in the Posidonia Shale source rock and the Aalburg source rock in the central part of the Broad Fourteens Basin

The modelling results indicate that in the period between Eocene-Oligocene tectonic phase and present-day little or no oil was generated from the Posidonia Shale Formation.

Originally, the oil-prone Aalburg Formation was present along the entire cross-section. After the Mid and Late Kimmerian I and II uplift and erosional phases, the shales are absent in the northern platform area. The pattern of the history of oil generation from these Aalburg shales is the same pattern as that of the Posidonia Shale Formation (Figure 70 and 71). However, at the same location, the total amount of oil generated (in kg/t) from the Aalburg Formation is less than the amount generated from the Posidonia Shale Formation.

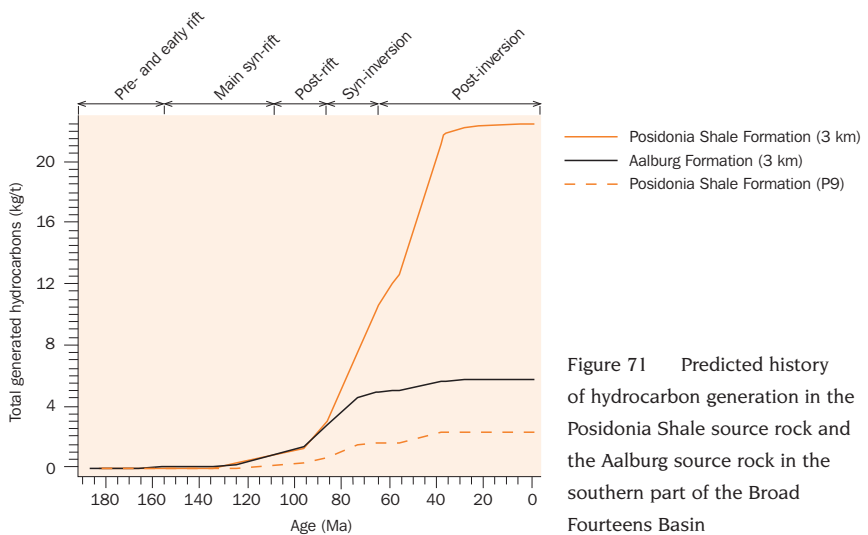


Figure 71 Predicted history of hydrocarbon generation in the Posidonia Shale source rock and the Aalburg source rock in the southern part of the Broad Fourteens Basin

### 21.3 Conclusions

The modelling demonstrates that large differences in the burial histories of the gas-prone Carboniferous source rocks along the cross-section result in very different temperature and maturation histories for the source rocks depending on their structural position. The Limburg Group source rock in the central and southern part of the basin first entered the gas window at the end of early-rift times, except for the basinal area between P6 and 50 km along the cross-section. Here, the gas window was reached during the main syn-rift period. Most gas was generated prior to the syn-inversion period. In the northern platform area, maximum maturity was reached in the Early Tertiary post-inversion period, initiating a first phase of gas generation in the most deeply buried rocks. The predicted total amount of gas generated during the evolution of the Broad Fourteens Basin is largest in the southern part of the cross-section. Based on the modelling results it was deduced that in the basinal area CO<sub>2</sub> generation peaked during early syn-rift times, while in the northern platform area CO<sub>2</sub> was not generated until syn-inversion times.

The modelling revealed that there was major generation of oil from the Posidonia Shale Formation in the central part of the basin during post-rift times prior to inversion. The Early Tertiary post-inversion period was an important phase of oil generation in the southern part of the cross-section. Little or no oil generation was predicted along the entire cross-section after the Eocene-Oligocene tectonic phase. The pattern of the simulated history of oil generation from the Aalburg Formation was the same pattern as the one for the Posidonia Shale Formation, but the total amount of oil generated (in kg/t) from the Aalburg Formation was smaller.

Based on the modelling results, it seems likely that today there is no to only minor generation of gas from the Limburg Group source rocks and no to only minor generation of oil from the Posidonia Shale Formation along the cross-section. This answers one of the research questions listed in Chapter 17, namely 'Is it likely that oil and gas is generated in the basin today'.



## 22 Permeability history

To validate the relations between porosity and effective stress and between porosity and permeability used in the modelling these relations were compared with reservoir porosity and permeability data (Appendix 4; Simmelink and Verweij 2000). Subsequently, various modelling scenarios were evaluated.

### 22.1 Evaluation of the modelling scenarios

First the history of pore pressures and groundwater flow was simulated with the adapted porosity-permeability model and a simplified one-phase fluid flow model, including sedimentary loading and unloading and the relief of the water table as pressure-influencing mechanisms, and assuming no-flow bottom and lateral boundary conditions (pressure modelling scenario P1).

#### Modelling scenario P1

Forward modelling showed that syn-rift and post-rift sedimentation induced overpressured conditions in restricted parts of the basin: that is mainly in the deeper poorly permeable Carboniferous shales and Zechstein evaporites. Pre-inversion overpressured conditions disappeared during inversion. The predicted present-day pressures were near-hydrostatic to slightly overpressured in reservoir horizons, but increased in the poorly permeable Carboniferous units. The calculated overpressure history in the reservoir unit (Upper Rotliegend Group) overlying the Carboniferous shales shows that overpressures never exceeded 2 MPa during basin evolution. The present-day pressures mainly resulted from sedimentation during Quaternary times (Figure 72, overpressure scenario P1). The predicted present-day overpressures are in accordance with known pressure conditions in reservoir units in the basin. This modelling scenario however, is too simple in comparison with the conceptual model (Part 2); the modelling scenario should also take into account the evolution of gas systems as a potential influence modifying the development of overpressure.

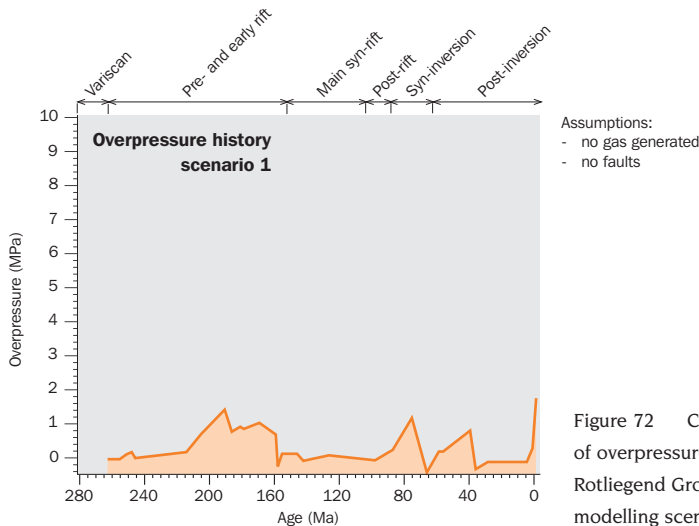


Figure 72 Calculated history of overpressures in the Upper Rotliegend Group for overpressure modelling scenario P1

### Modelling scenario P2

The second scenario, P2, also incorporated the evolution of the gas system. The modelling based on scenario P2 conditions predicted present-day gas saturations in the Permian Slochteren Formation in the P6 area that are higher than those observed. The simulated overpressure history of the basin for scenario P2 conditions shows pre-inversion and present-day overpressured conditions not only in the deeper poorly permeable sections of the basin, but also in the permeable Slochteren Formation. The predicted present-day overpressure of the Slochteren reservoir unit was  $P_{ex} = 8 - 8.5$  MPa in the area between the structural crest at P6 and the northern boundary of the cross-section. These calculated present-day overpressures of approximately 8 MPa in the central and northern parts of the cross-section through the southern Broad Fourteens Basin (Figure 73) are not consistent with published near-hydrostatic to slightly overpressured conditions in reservoir horizons (Table 13 in Part 2).

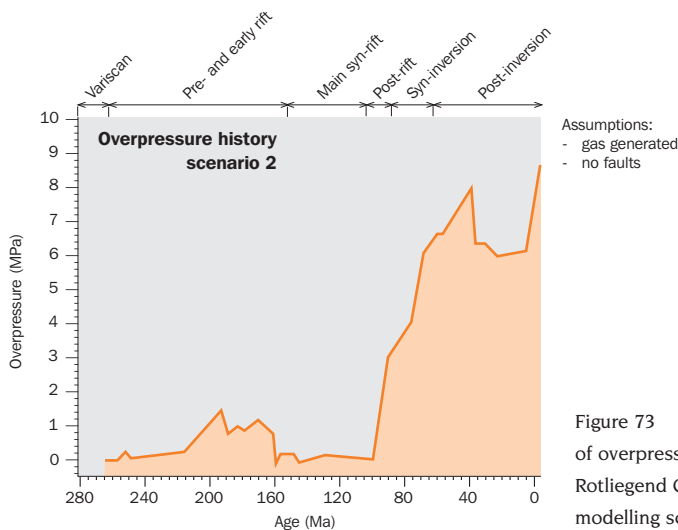


Figure 73 Calculated history of overpressures in the Upper Rotliegend Group for overpressure modelling scenario P2

In order to evaluate the permeability structure of the cross-section the Posidonia Shale - Vlieland Sandstone oil system was also studied. The forward modelling of the oil system assuming overpressure scenario P1 conditions did not reproduce the known oil accumulation in the Q1 area.

### Modelling scenario P3

The mismatch between results of forward modelling of the development of gas and oil systems assuming scenario P2 and the present-day characteristics of the basin, that is with published pressure conditions and known distributions of oil and gas accumulations is not surprising. Modelling scenarios P1 and P2 did not include all the mechanisms influencing groundwater and petroleum fluid flow and permeability, that were identified in the conceptual model of the evolution of the Broad Fourteens Basin (e.g. Tables 10 and 11). Given that tectonic processes play an important role during different phases of basin development (Part 2), the dynamic permeability of fault and fracture zones in the basin may have allowed fluids to flow through these zones during periods of tectonic activity. This is confirmed by present-day diagenetic features and fracture characteristics in the basin that indicate permeability alterations

and paleo fluid flow during distinct periods of tectonic activity in the basin, e.g. during Late Jurassic rifting and Late Cretaceous inversion of the basin (Part 2). From the three initial groundwater and petroleum modelling results discussed above, I concluded that the forward modelling required a new scenario that included a mechanism to increase vertical fluid migration. This scenario, P3, incorporated dynamic fault zone permeability. For this purpose four vertical fault columns were introduced into the cross-section at locations corresponding to major fault zones identified from the seismic sections (Figures 48 and 74). These fault columns were defined to be of poor permeability ( $k_h = k_v = 3 \times 10^{-5}$  mD at 10% porosity; capillary pressure  $C_p = 0.1$  MPa) except during periods of tectonic activity (Late Jurassic rifting and Late Cretaceous inversion and – for faults in the P9 and Q1 area – also during Eocene–Oligocene uplift), when the permeabilities in the fault zone are allowed to increase to  $k_h = 3 \times 10^{-2}$  mD and  $k_v = 3 \times 10^{-1}$  mD (for 10% porosity;  $C_p = 0.1$  MPa). The modelling with scenario P3 including dynamic permeable fault zones in the P9, P6 and Q1 areas reproduced the known oil accumulation and gas saturations along the modelled cross-section and gave a pressure prediction in reservoir units that agreed reasonably with published present-day conditions (see below). This third scenario P3 was therefore used in subsequent groundwater and petroleum fluid simulations. The scenario included sedimentary loading, erosional unloading, topography of water table and generation of gas as the pressure-influencing mechanisms, and took into account the dynamic permeable fault zones.

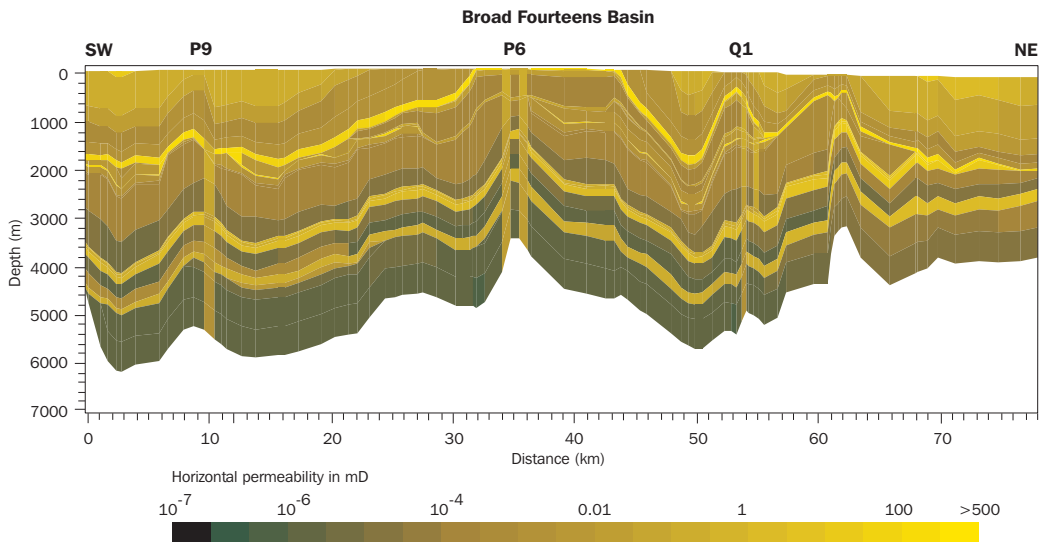


Figure 74 Predicted distribution of horizontal permeability during the syn-inversion phase of basin evolution, including location of fault zones with dynamic permeability

## 22.2 Conclusions

Model scenario P3 was selected to simulate the permeability history as part of the groundwater and petroleum fluid simulations. This scenario is based on geohistory scenario 2 (Appendix 4) and includes sedimentary loading, erosional unloading, topography of the water table and generation of gas as the pressure-influencing mechanisms, and takes the dynamic permeable fault zones into account.

## 23 History of pore pressures and groundwater flow

The hydrogeology of the Broad Fourteens Basin along the cross-section as presented here, includes the permeability history and the history of groundwater pressures and groundwater flow. Groundwater flow systems are characterised by the distribution of overpressures/hydraulic head, the groundwater flow pattern and the flow rates. The dominant force driving groundwater flow is the groundwater potential gradient, which is given by the overpressure gradient, assuming groundwater of constant density. The overpressure or excess pressure of the groundwater ( $= P_{ex}$ ) at a certain depth is the difference between the pore pressure and the hydrostatic pressure at that depth (Chapter 1, Figure 5). The modelled overpressures are calculated in relation to hydrostatic pressures for the assumed constant water density  $\rho_w = 1030 \text{ kg/m}^3$ .

One of the additional objectives of modelling the pore pressure and groundwater flow was to establish whether there had ever been overpressured conditions in the basin (Chapter 1, Chapter 17).

Unless otherwise stated, the history of pore pressures and groundwater flow was calculated for scenario P3 conditions and the following boundary conditions: no-flow conditions at the lateral boundaries and at the lower sediment-basement interface, while the upper boundary condition is given by the hydraulic head related to the topography of the ground surface.

### 23.1 History of pore pressures

Figures 75 to 79 illustrate the development of overpressures in subsequent phases of basin evolution. Figure 80 shows the history of overpressures in the Carboniferous Limburg Group, the Permian Slochteren Formation and Zechstein Group in the central part of the basin.

#### *Early-rift phase*

At the end of the early-rift phase, that is at the end of a prolonged period of regional sedimentation and before the start of gas generation in Carboniferous source rocks, minor overpressured conditions of 1 - 3 MPa occurred in the shaly Carboniferous formations and the Zechstein evaporites (Figure 75). Because of uplift and erosional unloading during mid-Kimmerian tectonic phase, pressures returned to near-hydrostatic values in all hydrostratigraphic units, with the exception of the pressures in a small part of the Carboniferous Baarlo Formation at 42 km along the cross-section. This formation maintained overpressures of 2 MPa.

#### *Main syn-rift phase*

Following erosion, syn-rift deposition of the Delfland Subgroup was concentrated in the rapidly subsiding basin and induced minor overpressures in the deeper poorly permeable units in the central part of the basin (at 40 - 44 km: in Baarlo Formation  $P_{ex} = 3 - 3.8 \text{ MPa}$ , in Ruurlo Formation and Zechstein evaporites  $P_{ex} \leq 2.5 \text{ MPa}$ ). Pressures remained near-hydrostatic in the Slochteren Formation. During the early part of the main syn-rift phase (156 - 140.7 Ma) the fault zones of increased permeabilities were able to dissipate the overpressures in the relatively permeable units (Figure 76).

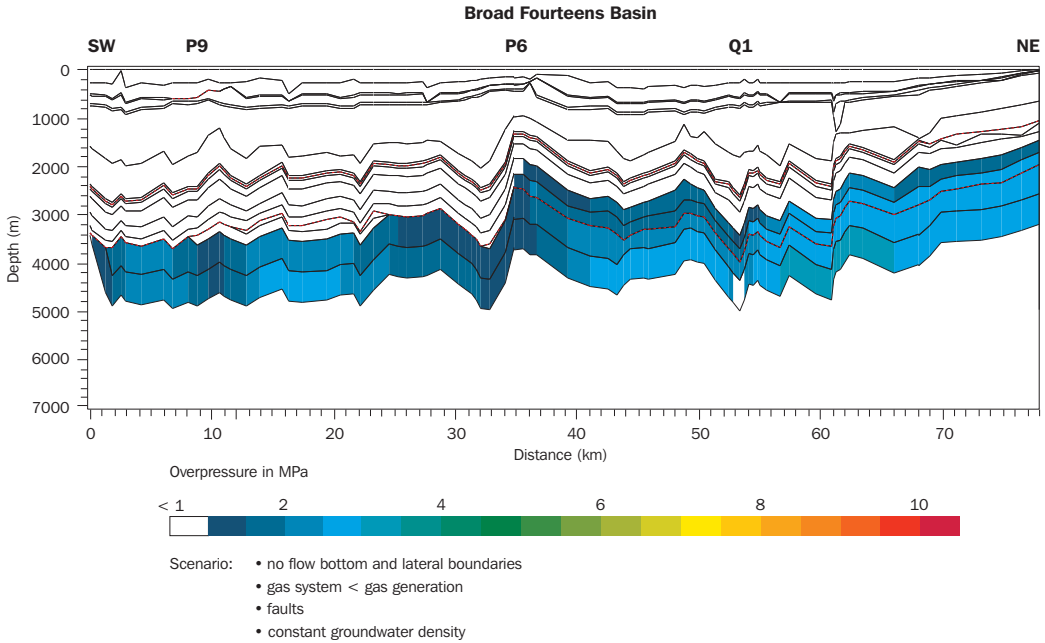


Figure 75 Predicted distribution of overpressures at the end of the early-rift phase of basin evolution (at 156 Ma; modelling scenario P3)

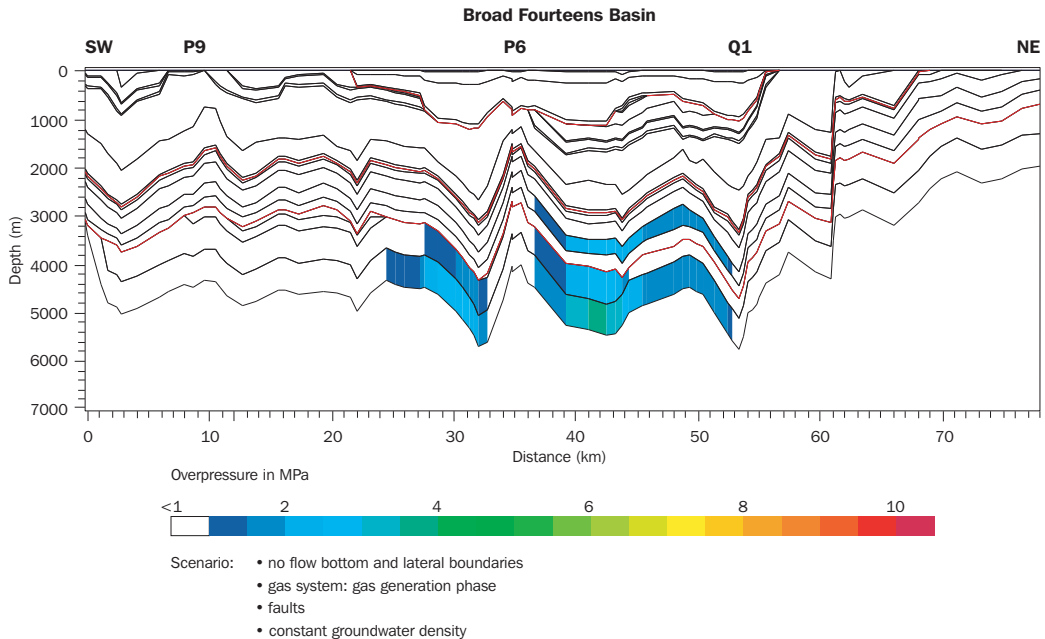


Figure 76 Predicted distribution of overpressures during the main syn-rift phase of basin evolution (at 140.7 Ma; modelling scenario P3)

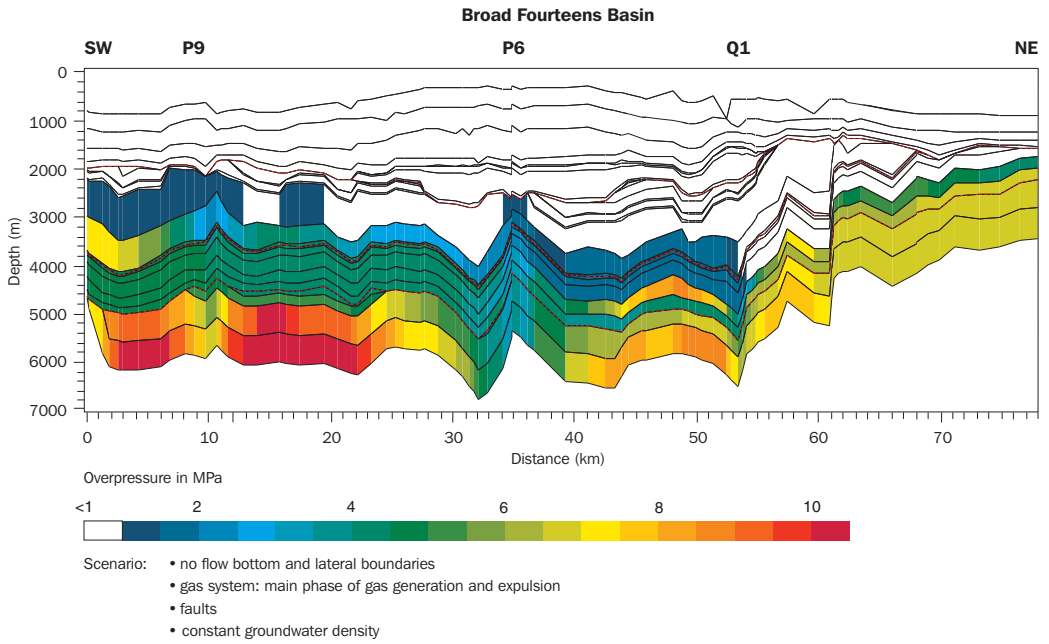


Figure 77 Predicted distribution of overpressures at the end of the post-rift phase of basin evolution (at 74 Ma; modelling scenario P3)

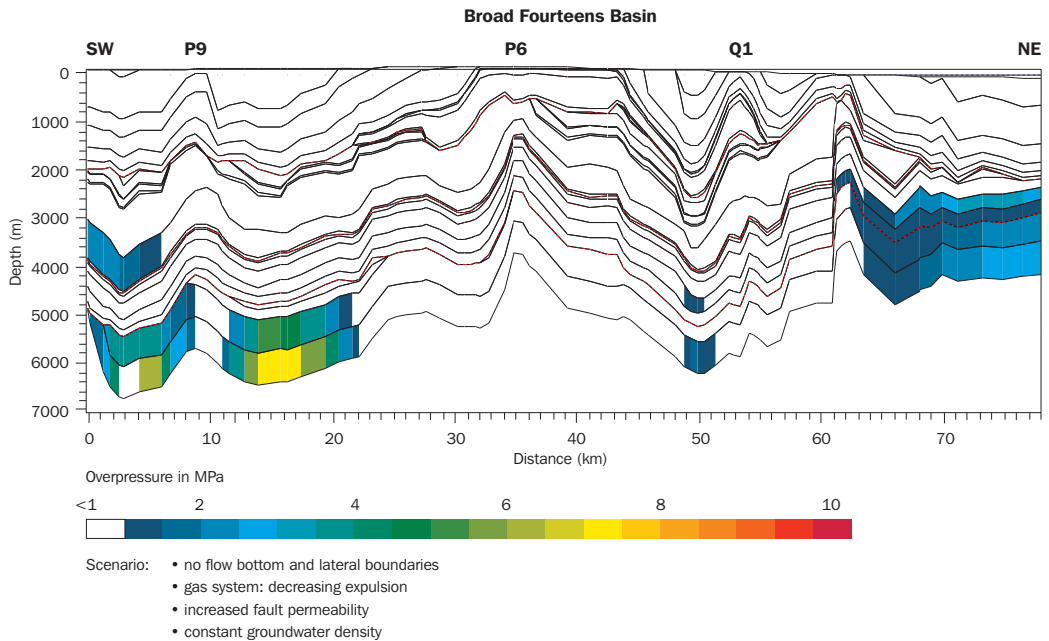


Figure 78 Predicted distribution of overpressures during the syn-inversion phase of basin evolution (at 65.9 Ma; modelling scenario P3)

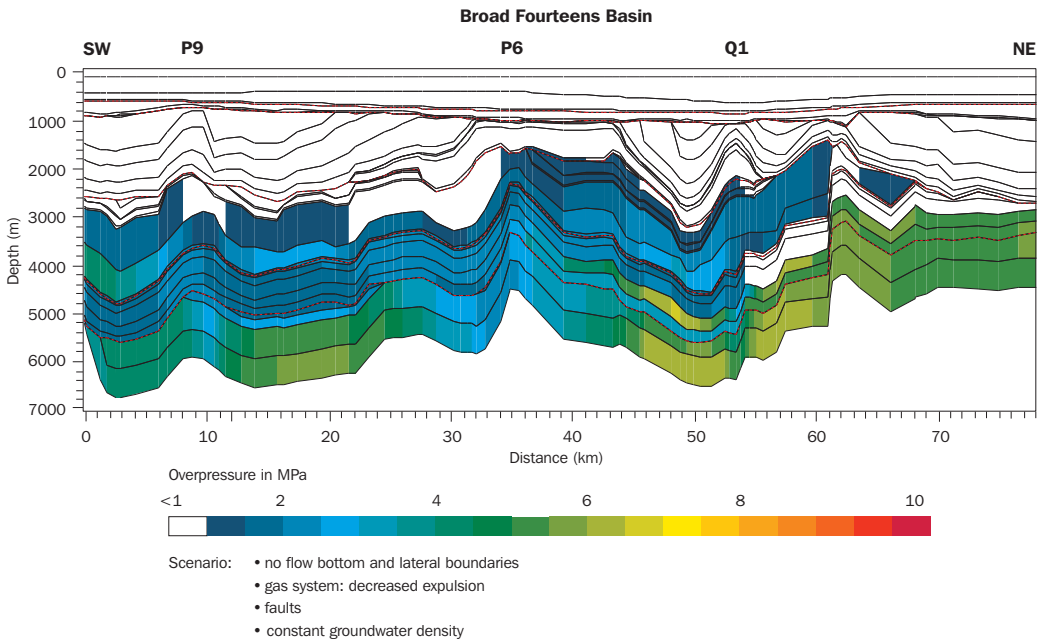


Figure 79 Predicted distribution of overpressures at present-day (modelling scenario P3)

Overpressured conditions built up in the Carboniferous formations along the entire cross-section during the Early Cretaceous syn-rift period because of continued differential subsidence and sedimentation and gas generation in the Carboniferous source rocks. At 125 Ma, maximum overpressures of 7 MPa occurred in the Ruurlo and Baarlo Formations in the central part of the basin (at 40 - 44 km). During this period the fault zones were poorly permeable again and, as a consequence, the overpressures in the Slochteren Formation could not dissipate from the central part of the basin (between areas P6 and Q1):  $P_{ex} \leq 3$  MPa. In addition, the modelling predicted minor overpressures in Triassic units south of the P6 area.

### Post-rift phase

The results of the modelling indicated that post-rift regional subsidence and sedimentation in combination with the continuous generation of gas extended the overpressured area in the basin. Figure 77 shows the predicted distribution of overpressures in the basin at pre-inversion time. The most significantly overpressured part of the section was the area south of P6: here minor overpressures were predicted in the Jurassic shales (1 MPa); in the Triassic (RB and RN), Zechstein and Slochteren Formations ( $P_{ex} \leq 4$  MPa); maximum overpressure values were predicted in the Baarlo Formation ( $P_{ex} = 11$  MPa), Ruurlo Formation ( $P_{ex} = 10$  MPa) and Maurits Formation ( $P_{ex} = 5$  MPa). In the central part of the basin the Triassic to Carboniferous formations were overpressured (Triassic  $P_{ex} \leq 1.7$  MPa, Zechstein  $P_{ex} = 4 - 8$  MPa, Slochteren Formations  $P_{ex} = 4$  MPa; Ruurlo Formation  $P_{ex} \leq 6$  MPa) and Baarlo Formation  $P_{ex} \leq 8.7$  MPa). The model results predicted overpressuring in the northern platform area as well: Zechstein Group  $P_{ex} = 4 - 5$  MPa in the Zechstein Group and  $P_{ex} = 6.5$  MPa in the Slochteren Formation. These maximum overpressures in poorly permeable units at the end of the post-rift period are well below minimum in-situ stresses (for

example: the maximum overpressure in the Baarlo Formation at  $\geq 5000$  m is  $P_{ex} = 11$  MPa, corresponding to a pressure of 61.5 MPa; the lithostatic pressure at 5000 m is approximately 115 MPa, which for a minimum to vertical stress ratio at these depths of  $\geq 0.8$  (Grauls 1997) corresponds to a minimum horizontal stress of 92 MPa).

The overpressure distribution during this pre-inversion time clearly shows the difference in hydraulic behaviour between the poorly permeable and permeable units. The overpressures showed large lateral variations in the poorly permeable Carboniferous and Zechstein units. For example, the overpressures varied between 6 and 11 MPa in the Baarlo Formation south of P6, and between 4 and 8 MPa in the Zechstein Group between P6 and Q1. These lateral variations in overpressures in the Carboniferous and Zechstein units show that in these poorly permeable units the groundwater flow did not equilibrate the overpressures. In contrast, the relatively permeable Slochteren Formation permitted lateral flow of groundwater and the associated redistribution of overpressures: the overpressure values in the permeable Slochteren Formation showed little variation laterally:  $P_{ex} \approx 4$  MPa.

The modelling accounts for the influence of regional subsidence and sedimentation in combination with the continuous gas generation on the distribution of overpressures in the basin. The gradual build-up of regional compressional stresses at the end of the post-rift phase (Part 2) may also have influenced the distribution of overpressures and groundwater flow in the basin. The Temispack programme does not allow incorporation of this effect in the modelling. It was studied in a separate project involving the geomechanical modelling of compressive stress and overpressure in the Broad Fourteens Basin (Simmelinck and Orlie 2001, Simmelink et al. 2001).

### Inversion phase

The combined effects of the absence of sedimentation as a pressure-generating mechanism, decreased rates of gas generation, erosional unloading, a changing geometrical framework and increased permeabilities of the fault zones during the Late Cretaceous inversion phase, was the complete disappearance of overpressured conditions in the central inverted part of the basin (Figure 78). One of the repercussions of the changed geometry of the basin fill was an increase in the drainage area, of the P6 permeable fault zones. During the subsequent period of non-deposition in the Early Paleocene the overpressures also dissipated in the northern platform area due to continued absence of pressure-generating mechanisms in the modelling.

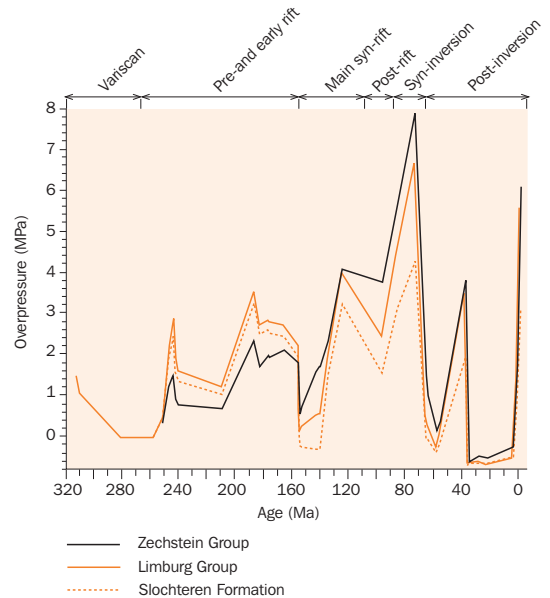


Figure 80 The calculated history of overpressures in the Ruurlo Formation, Slochteren Formation and Zechstein Group in the central part of the basin (at 50 km)



### Post-inversion phase

Post-inversion deposition of the Lower North Sea Group, in combination with some gas generation in selected parts of the basin, induced the return of overpressured conditions in the basin. The overpressures predicted in the southern part of the basin were: Baarlo Formation  $P_{ex} = 8$  MPa, Slochteren Formation  $P_{ex} \leq 1.5$  MPa, Triassic Formations  $P_{ex} \leq 2$  MPa; and in the central part of the basin: Baarlo Formation  $P_{ex} = 2 - 4.7$  MPa, Slochteren Formation  $P_{ex} = 2$  MPa.

Eocene–Oligocene uplift and erosion and the subsequent period of non-deposition or only minor sedimentation resulted in approximately near-hydrostatic conditions in the modelled cross-section in the period between between Oligocene and Miocene.

Increasing sedimentation rates in Pliocene and, especially, in Quaternary times, resulted in present-day mild overpressures in the poorly permeable deeper parts of the basin (Figure 79). The maximum overpressures predicted in the central part of the basin were: Zechstein Group  $P_{ex} = 6.5$  MPa, Slochteren Formation  $P_{ex} = 3$  MPa; Baarlo Formation  $P_{ex} = 6$  MPa.

The history of pore pressure outlined above is based on a modelling scenario including a no-flow boundary condition on the northern side of the cross-section. However, deep erosion northeast of the cross-section during the Early Cretaceous could have created a lateral escape route for groundwater in the permeable Slochteren Formation and Triassic units. To study this effect the history of overpressure and groundwater flow was also simulated with an open northern boundary. Figures 81 (pre-inversion) and 82 (present-day) show modelling results assuming such a boundary. The overpressures predicted in the Limburg, Upper Rotliegend and Zechstein Groups are significantly lower in the area north of Q1 in comparison with those predicted in the closed boundary simulations.

## 23.2 History of groundwater flow

The model predictions of the history of groundwater flow patterns and flow rates will be discussed below in relation to the previously identified periods of active paleo groundwater flow (Figure 83 and Table 16).

### Pre- and Early-rift phase

Continuous regional sedimentation during the pre- and early rift phase of basin evolution was the primary mechanism influencing the rates and patterns of groundwater flow accounted for in the modelling. In general, the predicted groundwater flow induced by the continuous regional sedimentary loading during the pre- and early rift phase, was directed vertically upwards in the poorly permeable units and was bedding-parallel in the relatively permeable units. The calculated mean vertical flow rates at shallow depths in newly deposited sediments were in the order of 10 - 50 m/My (mean Darcy flow rates). The bedding-parallel flow rates were higher than the vertical rates: > 100 m/My. The basin was subaerial during deposition of the terrestrial Slochteren Formation of the Upper Rotliegend Group, and rates – and as a consequence directions of groundwater flow – were also influenced by topography-driven flow: in the newly deposited sediments of the Slochteren Formation the flow directions varied and mean flow rates were 100 - 500 m/My. Figure 84 shows the

model-predicted directions of groundwater flow for parts of the flow system with the highest groundwater flow rates at the end of the early-rift subsidence phase. At a depth of approximately 1000 m, the mean rates of vertically upward groundwater flow in the poorly permeable Aalburg Formation were less than 5 m/My. At depths of more than 3000 m the vertical flow rates reduced to <1 m/My (in Limburg Group). Predicted-bedding parallel flow occurred in the following relatively permeable units: Middle Werkendam Member, sandstone units of the Lower Germanic Trias Group, Solling Formation and the Slochteren Formation.

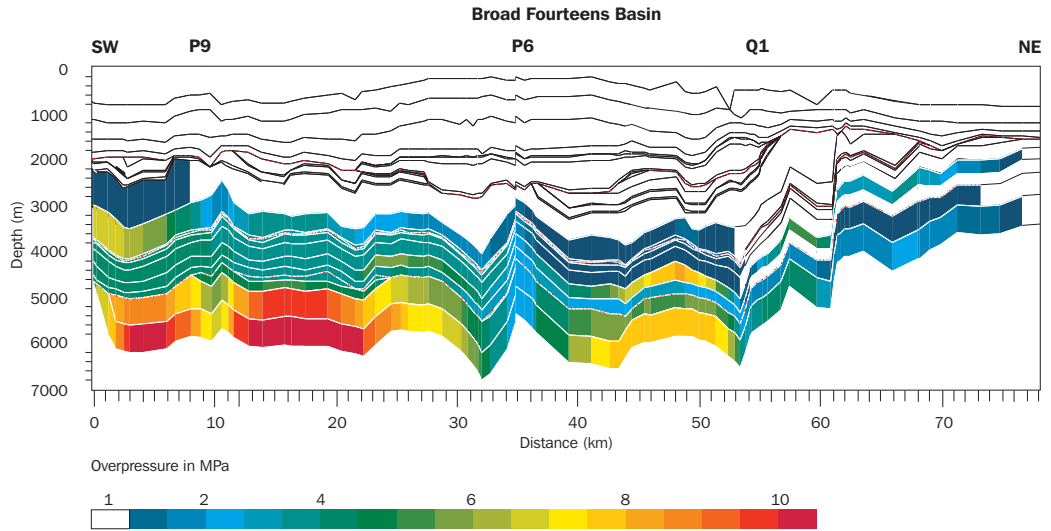


Figure 81 Predicted distribution of overpressures at the end of the post-rift phase of basin evolution (at 74 Ma; modelling assumption: open hydraulic boundary at northeastern side of cross-section)

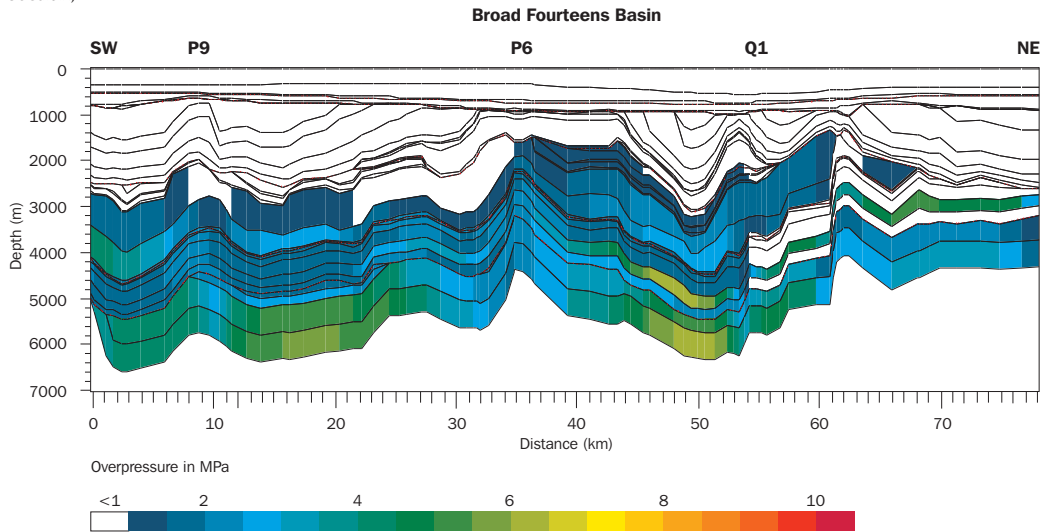
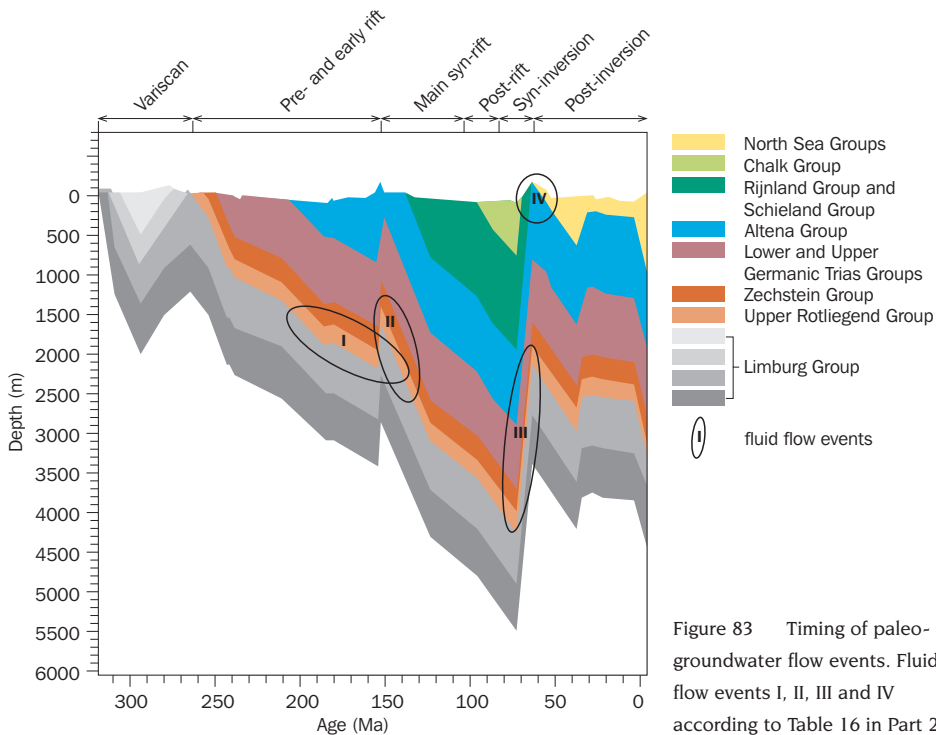


Figure 82 Predicted distribution of present-day overpressures at present-day (modelling assumption: open hydraulic boundary at northeastern side of cross-section)



Before the start of major gas generation in the syn-rift phase, the Carboniferous source rocks in the basin generated other volatile non-hydrocarbon compounds, such as  $\text{CO}_2$  (Section 21.1). The continuous expulsion of  $\text{CO}_2$ -rich groundwater from the Limburg Group into the Upper Rotliegend Group and overlying Zechstein Group is in accordance with the flow conditions required to explain kaolin cement and leached K-feldspar in the Slochteren Formation and calcite cements in Z3 Carbonate Member (Figure 83 and Table 16). This is also illustrated by the modelled history of overpressures in the Limburg Group, Slochteren Formation and Zechstein Group in the central part of the basin (Figure 80). During the Early-rift phase, overpressure gradients are consistent with vertical upward expulsion of groundwater from Limburg Group into Slochteren Formation and Zechstein Group.

Topography-driven flow developed again at shallow depths in the basin and flanking regions during the Mid Kimmerian phase of uplift at the end of the early-rift phase. Mean lateral groundwater flow in the Werkendam Formation attained mean Darcy flow rates of approximately 100 m/My at shallow depths of 500 m.

### Main syn-rift phase

Groundwater flow in the early part of the main syn-rift phase was modelled to be affected by the presence of fault zones with increased permeabilities, increased rates of sedimentation during deposition of the Delfland Subgroup, gas generation and the elevation of the basin above sea level. The resulting groundwater flow was dominated by bedding-parallel flow in the relatively permeable units, including the recently deposited Delfland Subgroup. The permeable fault zones dewatered the relatively

permeable units (Slochteren Formation, Triassic sandstones and Middle Werkendam Member) and bedding-parallel flow was towards the P6, P9 and Q1 fault zones. In comparison with the foregoing period, the predicted groundwater flow rates were higher both in the upper part of the basin (vertical flow regime) and in the permeable units in the deeper parts of the basin (e.g. a Darcy flow rate of 900 m/My in the Solling Formation at 26 km along the cross-section, and 400 m/My in the Slochteren Formation at 13 km). Average Darcy flow rates for the entire basin were approximately 500 m/My in Triassic sandstones and 100 m/My in Slochteren Formation.

During the main syn-rift phase the overpressure gradients of the groundwater were directed from the Limburg Group and the Zechstein Group towards the dewatering and lower overpressured Slochteren Formation (Figure 80). These modelled expulsion directions of water from both the Limburg and the Zechstein Group are consistent with one of the flow conditions required to explain illite cements in the Slochteren Formation (Table 16).

The fault zones were inactive and poorly permeable during the subsequent deposition of Rijnland Group sediments. The sedimentary loading and gas generation affected the groundwater system. Sedimentary loading induced the following vertical Darcy flow rates in the syn-rift deposits:  $<10$  m/My in the Holland Formation and  $<5$  m/My in the Vlieland Claystone Formation. Differential sedimentary loading induced lateral flow in the Vlieland Sandstone Formation ( $\leq 2000$  m/My). Deeper in the basin the calculated vertical flow rates fell to  $\leq 1$  m/My in the Aalburg Formation and  $\leq 0.1$  m/My in the Limburg Group.

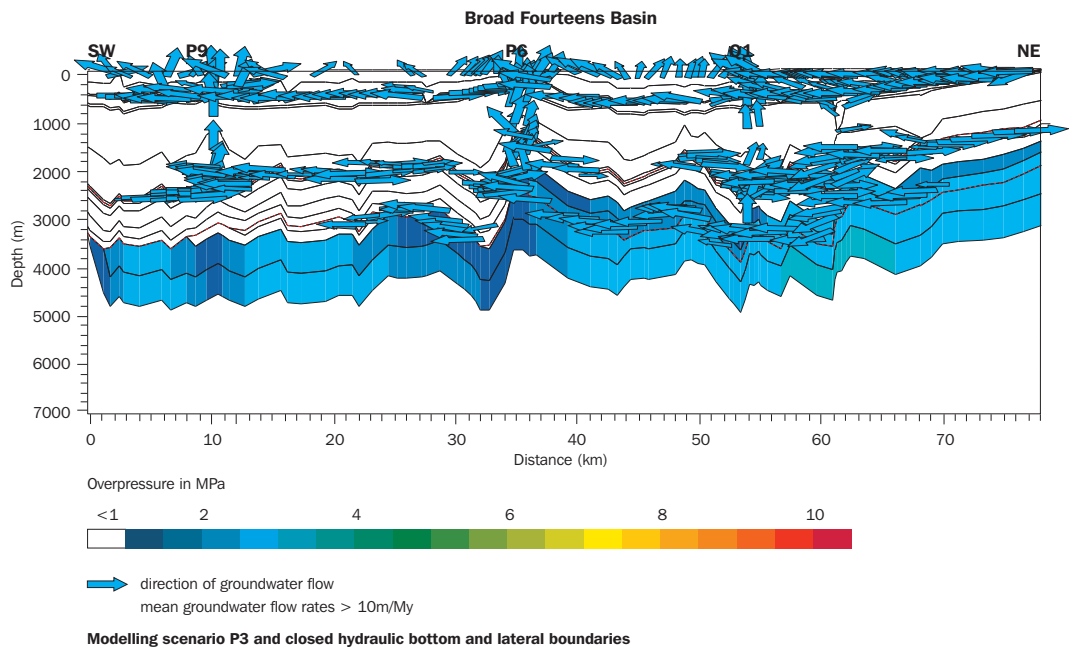


Figure 84 Predicted distribution of overpressures, pattern of groundwater flow and mean rates of groundwater flow at the end of the early-rift phase of basin evolution (modelling scenario P3)

### Post-rift phase

Post-rift regional subsidence and sedimentation and gas generation were the principal mechanisms influencing the groundwater and were calculated to result e.g. in continuation of the vertical upward flow of groundwater in the shallow part of the basin (25 m/My in Chalk; <10 m/My in Holland Formation; <5 m/My in Vlieland Claystone Formation). Figure 85 shows the modelling results at the end of the post-rift phase. Main flow was concentrated in the upper part of the basin (vertical flow) and in the relatively permeable units (bedding-parallel flow). The highest flow rates of bedding-parallel flow occurred in the sandstones of the Delfland Subgroup and in the Vlieland Sandstone Formation. Flow was restricted in the deeper poorly permeable parts of the basin as illustrated by the previously described extended zone of overpressuring (Figure 77).

### Syn-inversion phase

Figure 86 illustrates the syn-inversion groundwater flow system at the end of the Cretaceous. Continued sedimentary loading in the northern platform area maintained the vertically upward flow system until depths of approximately 2000 m. The mean vertical rate of groundwater flow in the Chalk Group and Holland Formation was 50 m/My.

The pre-inversion overpressured conditions did dissipate in the inverted part of the basin. The topographic relief of the water table (in the modelling represented by the topographic relief of the ground surface) of the inverted basin was the main mechanism inducing groundwater flow. The inversion-related tilting of the geological units exposed different permeable units (e.g. Vlieland Sandstone Formation) to inflow of surface-derived water. In addition, fault zones have assigned increased permeabilities during the Late Cretaceous part of the syn-inversion period. The predicted topography-induced flow was from the central inverted part of the basin towards its edges. In the southwestern part of the cross-section the groundwater discharged by vertical upward flow in the area between 0 and 12 km. In the northeast two more local discharge areas occurred above structural highs at 53 and 62 km. Shallow topography-induced flow systems developed in the Chalk Group deposits in the southwestern part of the basin. Regional topography-induced groundwater flow from the central part of the basin towards its edges was focussed through the outcropping Vlieland Sandstone Formation. Southward bedding-parallel flow in the P9 area had predicted mean Darcy flow rates of 700 m/My at a depth of 1300 m (corresponding to true flow rates of approximately 4400 m/My). The regional topography-induced flow towards the north through the Vlieland Sandstone Formation had predicted Darcy flow rates of 8000 m/My at a depth of 455 m in the Q1 area (corresponding to a true flow rate of approximately 46 000 m/My).

In modelling scenario P3, the permeable fault zone in the P6 area was located in the basin-wide recharge area of the topography-induced groundwater flow system and allowed deep infiltration of water feeding the permeable units in the deeper part of the basin (such as the Triassic sandstones of the Lower Germanic Trias Group, the Solling Formation, and even the Slochteren Formation). The present-day NW-SE trending fault-related fractures in the Upper Rotliegend Group and inversion-related fractures in Z3 Carbonates indicate that vertical permeability in the basin increased

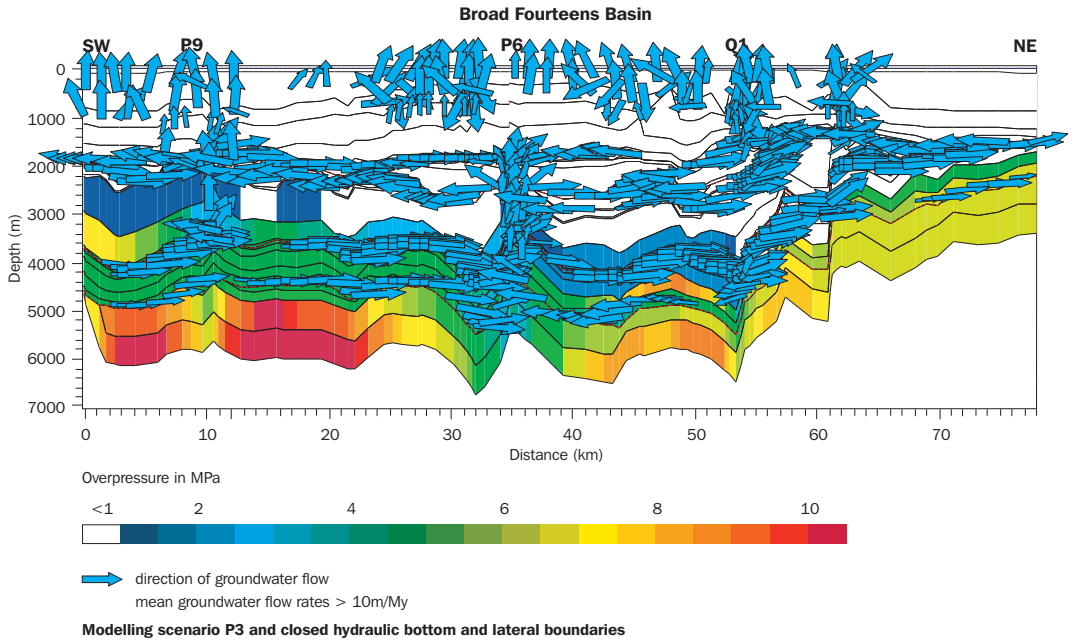


Figure 85 Predicted distribution of overpressures, pattern of groundwater flow and mean rates of groundwater flow at the end of the post-rift phase of basin evolution (at 74 Ma, modelling scenario P3)

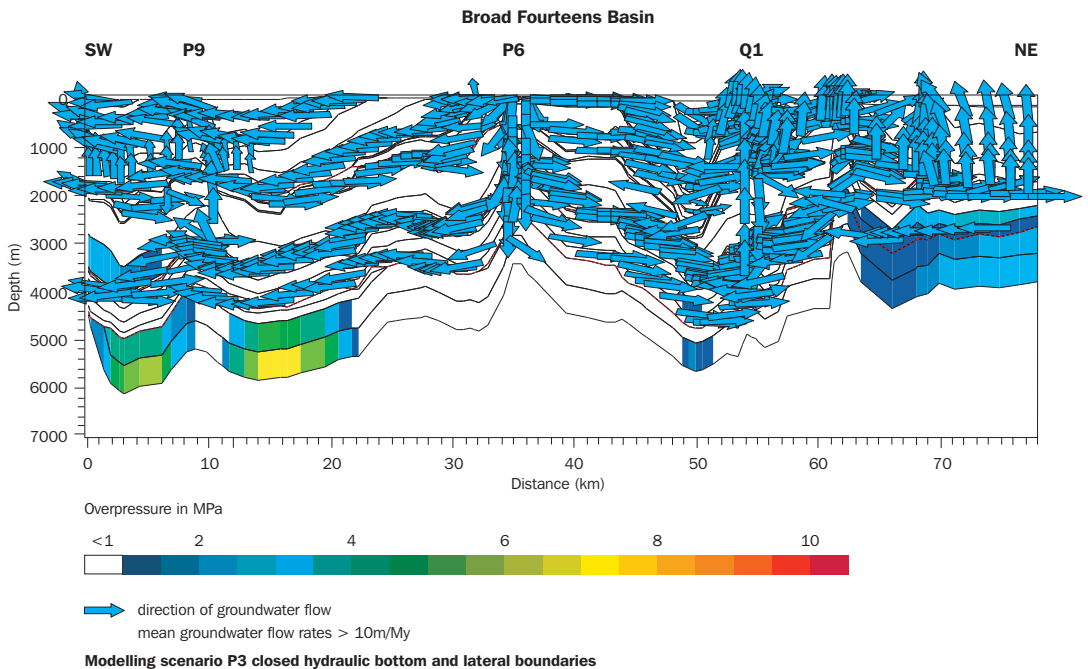


Figure 86 Predicted distribution of overpressures, pattern of groundwater flow and mean rates of groundwater flow during the syn-inversion phase of basin evolution (at 65 Ma, modelling scenario P3)

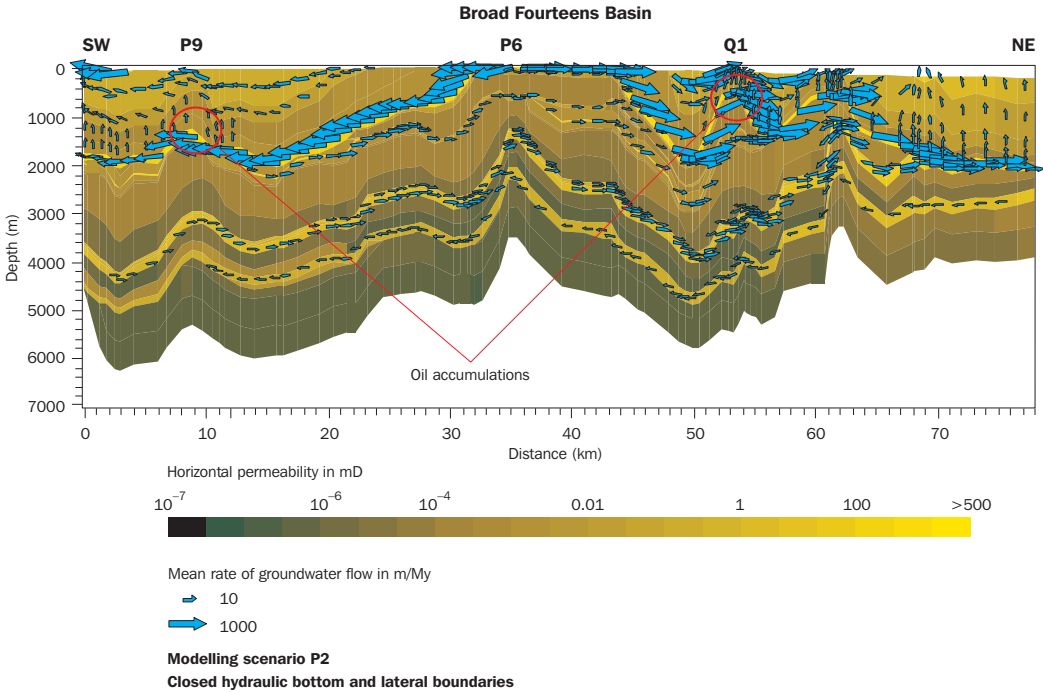


Figure 87 Predicted distribution of horizontal permeabilities, pattern of groundwater flow and mean rates of groundwater flow during the syn-inversion phase of basin evolution (at 65 Ma, modelling scenario P2)

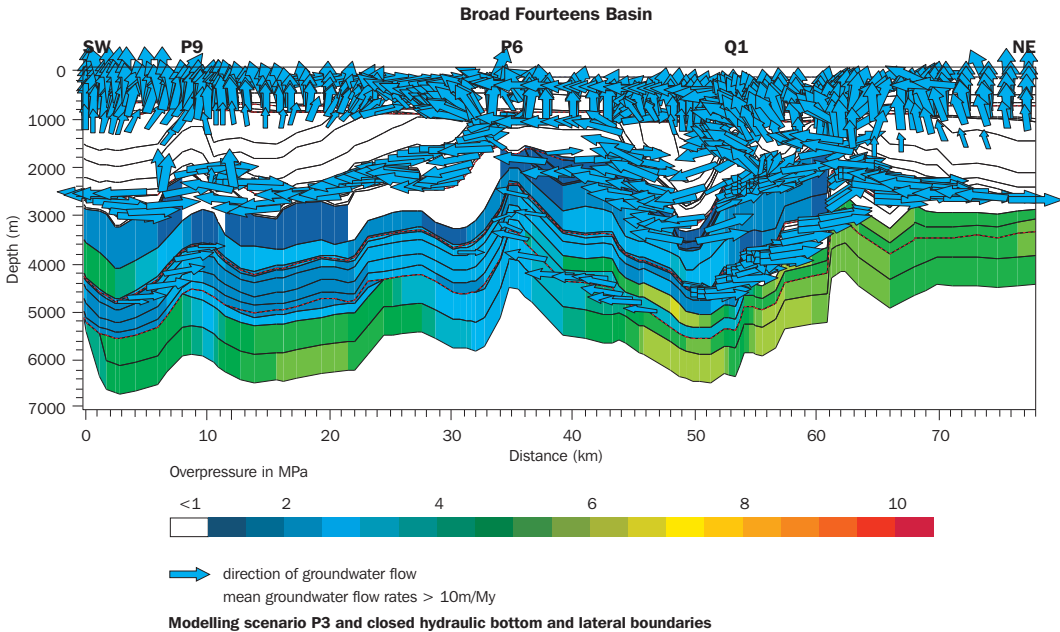


Figure 88 Predicted distribution of overpressures, pattern of groundwater flow and mean rates of groundwater flow at present-day (modelling scenario P3)



as a result of inversion (Gauthier et al. 2000, and Van der Poel 1989, respectively; Part 2). However, there are no published data known to the author, that support the actual syn-inversion flushing of these deep Triassic and Permian sandstone units in the southern part of the basin.

Model scenarios P2 and P3 of the present modelling study (Figure 87 and 86 respectively) both indicate the existence of active topography-induced groundwater flow through Chalk and Rijnland Group. The focussed topography-induced flow through the Vlieland Sandstone Formation occurred independently of the P6 fault system (Figure 87). Such focussed topography-driven flow is supported by flow conditions required to explain e.g. K-feldspar leaching in the Vlieland Sandstone Formation (Fluid flow event IV, Figure 83, Table 16).

The modelling package applied did not allow the introduction of variable densities of the groundwater during the modelling. A constant density of the groundwater of 1030 kg/m<sup>3</sup> was used (Appendix 4). Within the scope of this Broad Fourteens study Bouw (1999) studied the syn-inversion development of a freshwater lens in the more salt-dominated part of the basin north of the cross-section, by applying a density-dependent groundwater flow model. The results of her modelling scenarios (which do not include permeable faults, but do take into account different permeability assumptions for the hydrostratigraphic units) show that permeability distribution was the main factor of influence on the development of a freshwater lens. Predicted near steady-state conditions were established within 4 My. The maximum depth of the fresh-saltwater interface was 1200 m for a high permeability scenario. For a low permeability scenario, active topography-induced flow was mainly restricted to Rijnland and Chalk Group deposits.

### *Post-inversion phase*

The post-inversion deposition of the Lower North Sea Group deposits, the uplift and erosion of the basin during Eocene–Oligocene and the subsequent Oligocene–Miocene period of non-deposition or only minor deposition of Middle and Upper North Sea Group deposits resulted in prolonged periods of near-hydrostatic conditions in the basin (Section 23.1). The sedimentation rates increased during the Pliocene and, especially, Quaternary. Table 18 summarises the predicted evolution of overpressure build-up and changes in groundwater flow rates during the last 5 million years. The present-day result of the Pliocene–Quaternary sedimentary loading on the groundwater flow characteristics is illustrated in Figure 88, and includes the following characteristics:

- the main area of groundwater flow is located above the overpressured zone;
- in the upper part of the basin groundwater flow is cross-formational and mainly vertically upwards, flowing through Quaternary, Tertiary and Cretaceous units; flow is concentrated above structural highs at 31, 53 - 54 and 61 - 62 km along the cross-section;
- in the Quaternary deposits (with an assigned permeability anisotropy of 5) lateral flow is also observed; the flow is from the Quaternary depocentre (at 54 km) towards the edges of the Quaternary basin;
- bedding-parallel flow of groundwater through permeable sandstone units occurs at all depths.



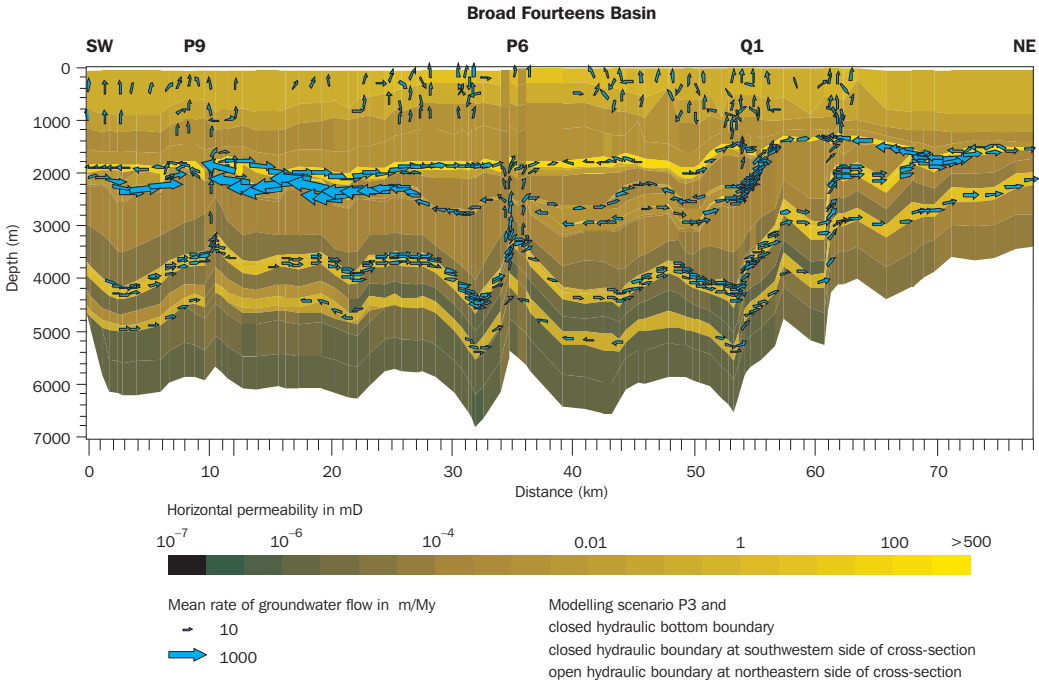


Figure 89 Predicted distribution of horizontal permeabilities, pattern of groundwater flow and mean rates of groundwater flow at the end of the post-rift phase of basin evolution (at 74 Ma; modelling assumption: open hydraulic boundary at northeastern side of cross-section)

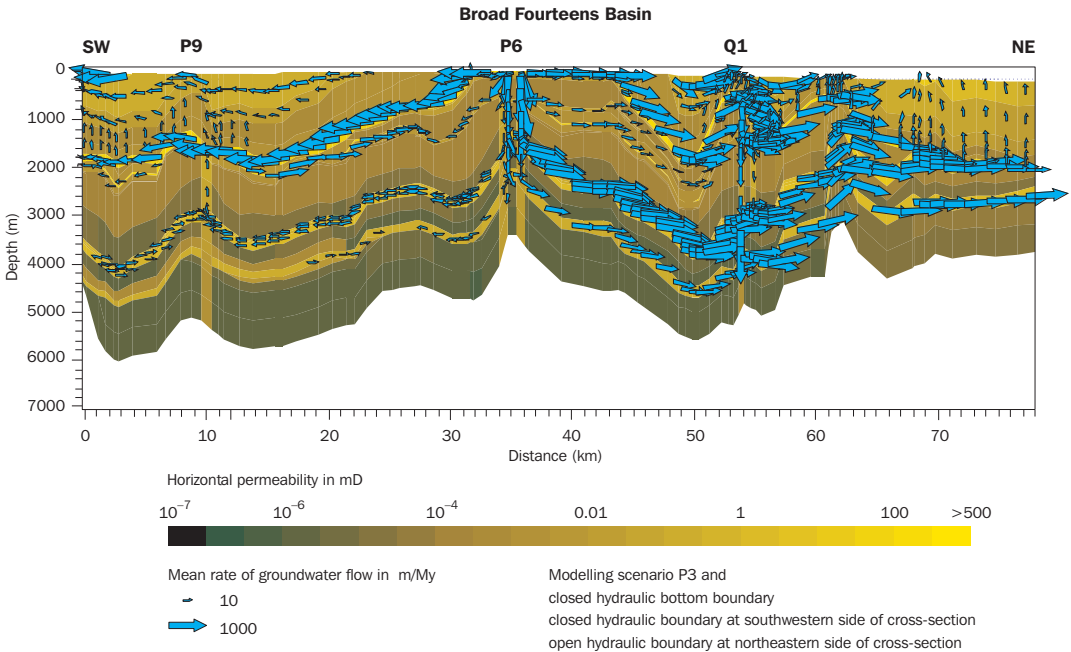


Figure 90 Predicted distribution of horizontal permeabilities, pattern of groundwater flow and mean rates of groundwater flow during the syn-inversion phase of basin evolution (modelling assumption: open hydraulic boundary at northeastern side of cross-section)

The increasing sedimentation rates induce increases in vertical rates of groundwater flow in the Lower Tertiary and the Cretaceous units, as well as the build-up of overpressures in relatively poorly permeable units and the extension of the overpressured zone towards younger units at shallower depths (Table 18).

Table 18 Predicted changes of overpressures and vertical rates of groundwater flow in relation to changes of sedimentation rates from the Miocene to present-day

|                                      | Time                     |                                |                          |                                |                                     |                                |
|--------------------------------------|--------------------------|--------------------------------|--------------------------|--------------------------------|-------------------------------------|--------------------------------|
|                                      | Miocene<br>23.3 - 5.2 Ma |                                | Pliocene<br>5.2 - 2.4 Ma |                                | Quaternary<br>2.4 - 0 Ma            |                                |
| Sedimentation rate (P9) (m/My)       | 0.7                      |                                | 30                       |                                | 190                                 |                                |
| Sedimentation rate (Q1) (m/My)       | 2                        |                                | 60                       |                                | 240                                 |                                |
|                                      | Flow rate<br>(m/My)      | Max Over-<br>pressure<br>(MPa) | Flow rate<br>(m/My)      | Max Over-<br>pressure<br>(MPa) | Flow rate<br>(m/My)                 | Max Over-<br>pressure<br>(MPa) |
| <b>Stratigraphic units:</b>          |                          |                                |                          |                                |                                     |                                |
| Quaternary                           |                          |                                |                          |                                | 40 - 130<br>(>2000<br>lateral flow) |                                |
| Tertiary – Pliocene<br>Oosterhout Fm |                          |                                | 15 - 30                  |                                | 30                                  |                                |
| Tertiary – Paleocene<br>Dongen Fm    | 0.1 - 1.5                |                                | <5                       |                                | 20                                  |                                |
| Cretaceous Chalk                     |                          | x                              | 1.4 - 3                  |                                | 10 - 15                             |                                |
| Jurassic shales                      |                          | x                              |                          | x                              |                                     | <1.5                           |
| Upper Triassic                       |                          | x                              |                          | x                              |                                     | <2.5                           |
| Permian (Zechstein)                  |                          | x                              |                          | <1                             |                                     | 6                              |
| Carboniferous Ruurlo Fm              | <<0.01                   | x                              | <0.01                    |                                | <0.05                               |                                |
| Carboniferous Baarlo Fm              |                          | x                              |                          | 2.5                            |                                     | 6                              |

The predicted history of groundwater flow assuming an open northern boundary since Early Cretaceous times, clearly shows an increase in northward bedding-parallel flow along the cross-section in the area north of 50 km. All flow through the permeable Triassic sandstone units and the Slochteren Formation in this area was northward at the end of the post-rift phase, at syn-inversion and at present-day (Figures 89, 90 and 91).

### 23.3 Discussion and conclusions

As described above, the overpressure scenario P2 (scenario without dynamic permeability of fault zones) does not adequately represent the conditions prevailing along the modelled cross-section. However, the simulation of overpressure generation and groundwater flow based on scenario P2 conditions does illustrate an important mechanism of overpressure evolution during inversion in reservoirs in creстал structures that remain sealed during inversion. The history of overpressures in the Slochteren Formation in the P6 area shows that overpressures increased during

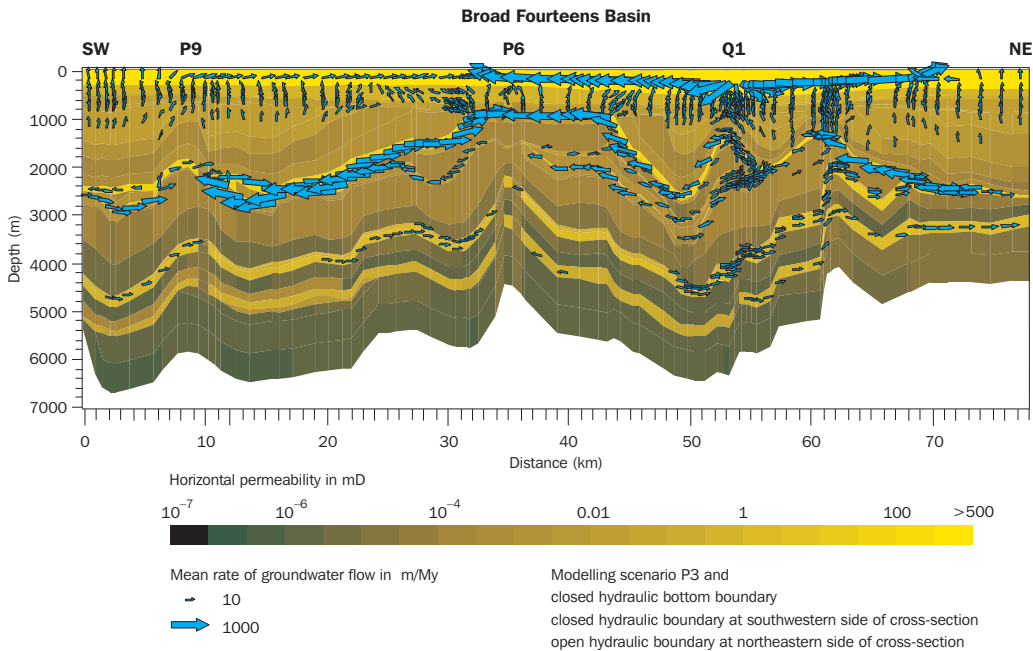


Figure 91 Predicted distribution of horizontal permeabilities, pattern of groundwater flow and mean rates of groundwater flow at present-day (modelling assumption: open hydraulic boundary at northeastern side of cross-section)

inversion (Figure 73). The most inverted area along the cross-section is P6. During inversion it developed into a crestal high and its drainage area for both gas and groundwater increased. Bedding-parallel migration of both gas and groundwater through the Slochteren Formation was from the deepest central part of the basin towards P6. Pre-inversion gas accumulations remigrated towards P6. As a consequence the gas saturations increased in the P6 crestal high area and the Slochteren Formation at P6 became fully saturated (predicted gas saturation >90%). The groundwater flow through the Slochteren Formation from the deepest and only mildly inverted part of the basin towards the P6 area transferred the relatively high overpressures from the deeply buried Slochteren Formation towards the P6 crestal high. This process may explain the increase in overpressures at P6 predicted by the modelling for P2 scenario. Figure 73 shows that after inversion the overpressure in the Slochteren Formation at P6 increased further as a result of Early Tertiary sedimentation ( $P_{ex} = 8$  MPa). At present-day the Slochteren reservoir unit has calculated constant overpressures of 8 - 8.5 MPa from the structural crest at P6 to its deepest position in the central part of the basin, indicating that the reservoir unit in this part of the basin permitted lateral flow of groundwater and associated redistribution of overpressures. Modelling results of the P2 scenario further showed that the Slochteren Formation south of the structural high at P6 was not overpressured. The absence of the Zechstein evaporite seal in this part of the basin allowed the Slochteren Formation to dewater vertically. However, the model results do not indicate any pressure equilibration between the overpressured Slochteren Formation in the central and northern parts of the section and the hydrostatically pressured southern extension of the formation. At the structural high of P6 there seems to have been a barrier

boundary obstructing fluid flow since syn-inversion times. It seems likely that the accumulated gases in the crestal parts of the P6 area acted as a barrier boundary for lateral groundwater flow. As a consequence, the Slochteren Formation between P6 and the northern closed boundary of the cross-section behaved as a closed pressure compartment in modelling scenario P2 since syn-inversion times. This predicted overpressure build-up and maintenance of overpressured conditions in the closed compartment of the Slochteren Formation requires that the overlying caprock maintains its sealing capacities during basin history (especially during inversion). As discussed earlier this is probably not the case along the modelled cross-section. However, in the northwestern part of the Broad Fourteens Basin there are thick Zechstein salt deposits that may have maintained their sealing capacities during inversion. This means that since syn-inversion times overpressured conditions may have been augmented by lateral pressure transfer and maintained in selected parts of the northwestern Broad Fourteens Basin. If so, present-day relatively high overpressures can be expected to occur in association with gas fields in reservoirs capped by a thick seal in crestal structures in the inverted parts of the Broad Fourteens Basin.

In addition to the possible influence of the gas system on the overpressure distribution discussed above, the generation of gas and the associated volume increase may have affected the pressure generation in the source rocks. Comparison of the modelling results based on overpressure scenario P1 (one-phase flow, no dynamic fault permeability) and scenario P2 conditions showed only a minor effect, however. For the P2 conditions the predicted overpressure values in the Limburg Group source rocks in the southern part of the cross-section are slightly higher than the values predicted for the P1 conditions.

The history of overpressures and groundwater flow predicted by the modelling is valid for the assumptions underlying the Temispack programme, the applied boundary conditions and input parameters (Chapter 18, Appendix 4). Below follows a discussion on the possible influence on the modelling results of a selection of assumptions, and of conditions and properties identified in the conceptual model (Part 2) but not included in the modelling.

**3D flow of groundwater.** The modelled cross-section is perpendicular to the strike of the basin and basin boundary fault directions and crosses the major depocentre of the combined Triassic to Lower Cretaceous deposits as well as the area of maximum uplift and erosion during syn-inversion times (see also Appendix 4). It thus captures the main directions of the driving forces for groundwater flow.

**Supra-regional topography-induced flow.** The conceptual model of evolution of the Broad Fourteens Basin (Part 2) includes six main periods of topography-induced flow (Table 9). These flow periods are taken into account in the modelling by introducing subaerial topography – and therefore a water table – along the cross-section (Tables 27 - 30 give the paleotopography at the wells P09-01A, P06-02, Q01-03 and L14-02). However, lateral inflow of groundwater from outside the modelled cross-section has not been included in the boundary conditions. Table 9 shows that during three periods the Broad Fourteens Basin was part of major supraregional flow systems with recharge areas outside the basin. Especially of interest for both the

groundwater and the petroleum systems is the possible influence of supraregional flow during syn-rift times. During the syn-rift period the Broad Fourteens Basin probably was the discharge area of different supraregional flow systems surrounding the basin. The southern part of the basin was in the realm of the supraregional flow system with the Texel IJsselmeer High as a recharge area. Deep syn-rift erosion of this High (Chapters 3 and 13) allowed infiltration of meteoric water into e.g. Triassic and Rotliegend reservoir units and subsequent flow towards the basin. Given the syn-rift geometry of the basin-fill along the cross-section the groundwater flow through these reservoir units was mainly discharged along the basin boundary fault zone (at 61 - 62 km along the cross-section, Figures 49e and 76) and probably did not exert a major influence on fluid flow in the basin itself. However, in order to evaluate the influence of this supraregional flow system on the fluid flow condition in the Broad Fourteens Basin, the modelled cross-section (Figure 48) should be extended to include the Texel IJsselmeer High. Modelling along this extended cross-section requires the quantitative reconstruction of the evolution of the Texel IJsselmeer High.

**Tectonic stresses.** In addition to sedimentary loading, erosional unloading and water table elevations, changes of regional stresses may also have influenced the evolution of overpressure and groundwater flow in the basin (Chapters 1 and 14). As outlined in Chapter 1 the effect of tectonic stresses on overpressure development is still poorly understood. It is subject of active research. For example, within the scope of the study of the Broad Fourteens basin, Simmelink and Orlic (2001) carried out a preliminary geomechanical modelling of basin inversion to investigate the effect of compressive stresses on overpressure buildup in the basin fill; lateral compression of a simple basin bounded by faults assuming undrained conditions led to very high overpressures prior to fault reactivation. More detailed geomechanical modelling is needed, however, to establish the influence of regional stress changes (e.g. prior to and during inversion of the basin) on the evolution of overpressure in combination with fluid flow in the complex sedimentary basin fill of the Broad Fourteens Basin.

**Permeability anisotropy.** In Temispack, the permeability of each layer consisting of different end-member lithologies is treated as the permeability of a homogeneous anisotropic unit that is the equivalent of a layered sequence of the lithologies. Although the default anisotropies calculated by Temispack were adjusted for each model layer (Appendix 4), the averaging method may still have influenced the modelling results. For example, a layer containing 20% salt is modelled as a layered sequence with a continuous – very poorly permeable – salt layer. The modelling will have overestimated the sealing capacity of the Zechstein Group if in reality the salt is not continuous. In a model layer with 20% sand, the modelling may have underestimated the vertical permeability, if in reality the sand is distributed and interconnected throughout the layer. In general, the interpreted seismic stratigraphy and the lithostratigraphic well data available to this study did not provide detailed information on occurrence, distribution and spatial continuity of different lithotypes within the distinguished model layers (Appendix 4). The greatest uncertainty with respect to distribution and spatial continuity of different lithotypes concerns the Schieland Group/Delfland Subgroup (characterised by significant facies changes) and the Limburg Group (no well data).

## Modelling results

The results of the integrated basin modelling provided the first quantitative understanding of the hydrogeological and pore pressure and groundwater flow response of the basin fill of the Broad Fourteens Basin to its sedimentation, uplift and erosion history. The steering influence of the conceptual model of integrated basin evolution (Part 2) proved to be indispensable.

The modelled history of overpressures and groundwater flow shows the following characteristics:

- The main period of overpressuring of the basin occurred at pre-inversion time in the poorly permeable Carboniferous units at depths >5000 m ( $P_{ex} = 11$  MPa) and was principally induced by sedimentary loading and to a minor extent by active gas generation.
- Present-day overpressures are mild in the poorly permeable deeper parts of the basin. The pressure-generating mechanism is the Pliocene and, especially, Quaternary sedimentary loading.
- During the evolution of the basin there were no overpressures of  $P_{ex} \geq 1$  MPa predicted in the shallow parts of the basin (depths to 2000 m).
- During the evolution of the basin, the area of maximum overpressures shifted along the cross-section in accordance with changing depocentres. At the end of the Early-rift phase it was located at 56 - 66 km in the central part of the basin; subsequently it shifted southwards and reached the area around 40 - 44 km in the central part of the basin in the Early Cretaceous. During Late Cretaceous pre-inversion times two main areas of overpressuring developed in the basin: one south of P6, and the other in the central part of the basin. In Early-Tertiary times the highest overpressured values occurred south of the P6 area. At present-day the area of maximum overpressuring has returned again to the central part of the basin in accordance with the location of the Quaternary depocentre.
- The distributions of overpressures in permeable and poorly permeable units and the history of the overpressures in the units show their difference in hydraulic behaviour. At a certain time during basin history, the overpressure distribution in poorly permeable units, such as Zechstein evaporites and Carboniferous shales, is characterised by lateral variation of overpressures, while the overpressures in the relatively permeable Slochteren Formation are approximately constant. The history of overpressures of the relatively permeable units, such as the Slochteren Formation, was strongly influenced by the availability of permeable escape routes (e.g. permeable fault zones) tapping the formation: such an escape route drained a large part of the permeable unit and as a consequence dissipated the overpressures. In contrast, a permeable fault zone tapping poorly permeable overpressured units, such as Zechstein evaporites and Carboniferous shales, only allowed the overpressures to dissipate in a relatively restricted area.
- During basin evolution mean Darcy rates of vertical upward flow of groundwater induced by sedimentary loading in the upper part of the basin varied between approximately 20 and 200 m/My.
- The vertical upward expulsion of groundwater from Carboniferous units into the Slochteren Formation and Z3 Carbonates during the early-rift period is in accordance with flow conditions required to explain observed kaolin cements

and leached K-feldspar in the Slochteren Formation, and calcite cements in the Zechstein Carbonate Member (Table 16).

- During basin evolution, sedimentary loading induced bedding-parallel flow of groundwater through permeable hydrostratigraphic units (principally sandstone units) at all depths; bedding-parallel flow rates were higher (by at least one order of magnitude) than vertical flow rates at the same depth; the bedding-parallel flow equilibrated the overpressures in the permeable hydrostratigraphic units.
- The reactivation of the groundwater flow system in Quaternary times was induced by the recent increase in sedimentation rates.
- Topography-induced groundwater flow systems developed during the syn-inversion period of basin evolution; the topography-induced flow of groundwater was focussed through the Vlieland Sandstone Formation, which is in accordance with observed K-feldspar leaching of this Formation (Table 16).

## 24 History of petroleum expulsion, migration and accumulation

The 2D forward modelling of the petroleum systems in the Broad Fourteens Basin aimed to increase the understanding of and provide a time framework for petroleum expulsion, migration, accumulation and preservation (Chapter 1). A specific objective of the modelling was to increase the process-based understanding of the geochemical compositions of the P9 and Q1 oils and the absence of commercially exploited gas accumulations along the cross-section (Chapters 1 and 17).

The migration module of the Temispack modelling tool simulates the history of petroleum expulsion from the source rocks and the subsequent secondary migration and accumulation of petroleum as a separate phase flow adopting a two-phase Darcy equation. This two-phase Darcy equation includes buoyancy, pressure gradients and capillary pressure gradients as forces of influence on separate phase flow. The migration module links the previously described modules. In the present study it simulated the gas system (with the Limburg Group coal measures as gas-prone source rocks) and the oil system separately. The oil system simulations included the Posidonia Shale Formation and the Aalburg Formation simultaneously as the oil-prone source rocks. The parameters in the Darcy equation influence both the timing of petroleum expulsion from the source rock and the pattern of petroleum migration. Important input parameters for the expulsion and migration module are the fluid properties, magnitude of capillary pressures and the effective permeabilities of the rocks to the fluids (Appendix 4). The fluid densities were kept constant during the modelling. The values used were  $1030 \text{ kg/m}^3$  for the density of the water,  $300 \text{ kg/m}^3$  for the density of gas and  $500 \text{ kg/m}^3$  for the density of the oil. Default Temispack values were used for the viscosities of water, oil and gas. For two-phase flow each fluid has its own effective permeability of the rock to the fluid. The higher the

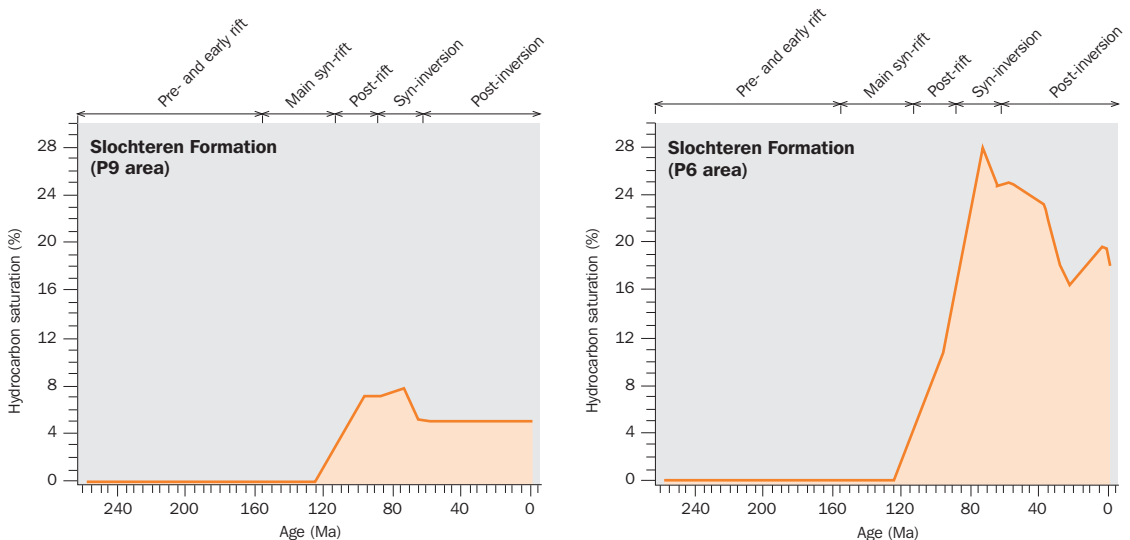


Figure 92 Carboniferous gas system: predicted history of hydrocarbon saturation in the Slochteren Formation in the P9 and the P6 areas



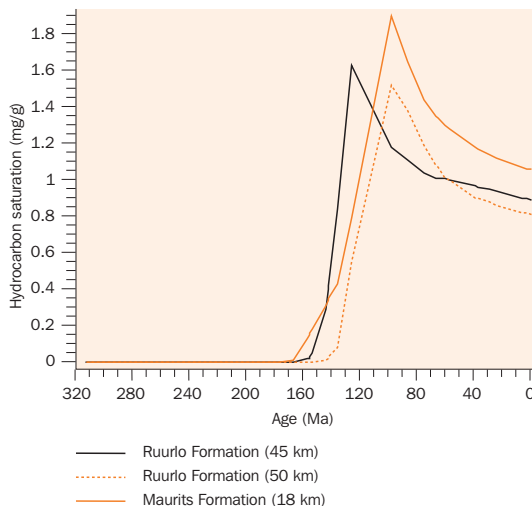
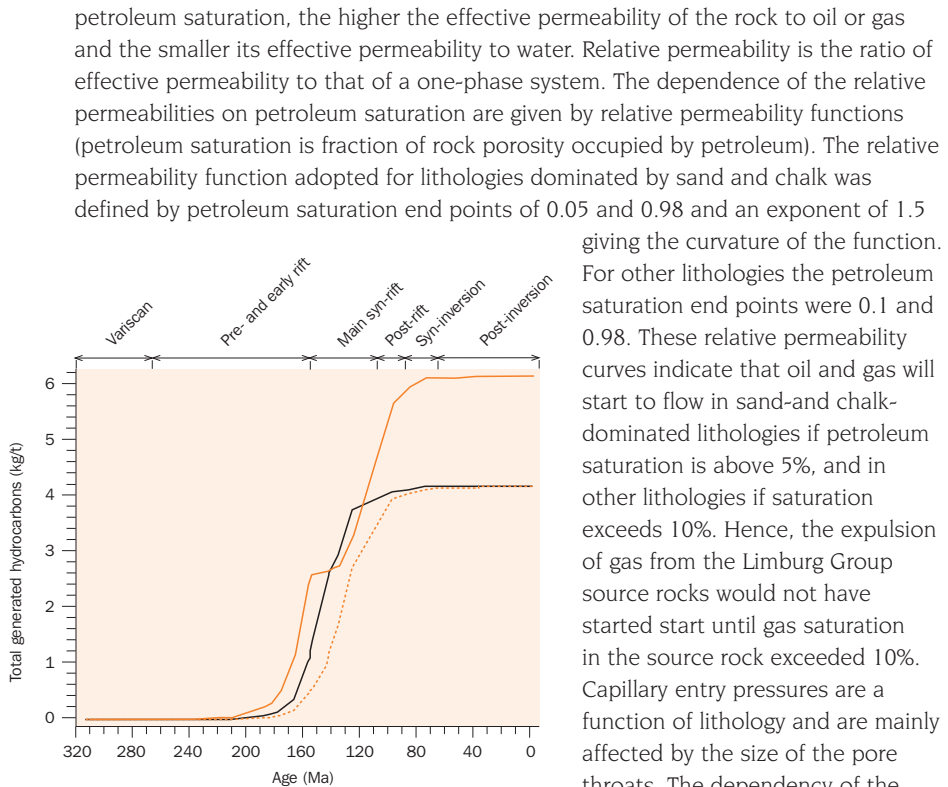


Figure 93 Carboniferous gas system: predicted history of hydrocarbon generation and saturation in the Ruurlo Formation in the central part of the Broad Fourteens Basin (at 45 - 50 km along the cross-section) and in the Maurits Formation in the southern part of the basin (at 18 km along the cross-section)

Group sandstones and the Vlieland Sandstone Formation), and for the evaporite containing layers of the Zechstein Group the capillary pressure was taken to be 5 MPa. The fault columns were defined with a constant capillary pressure of 0.1 MPa. For all lithologies the capillary entry pressures at the surface were 0.

## 24.1 Expulsion, migration and accumulation of gas

### *Main syn-rift phase*

The model results indicate that expulsion of gas from the Limburg Group source rocks in the central and southern part of the cross-section started during the main syn-rift period. At 125 Ma the gas migration system along the cross-section was dominated by this vertical upward expulsion from the Limburg Group source rocks. The overpressure gradients at this time were directed vertically upwards from the Limburg Group towards the Upper Rotliegend Group and provided an additional force driving upward migration of gas (Chapter 23). As a consequence, the gas invaded the Upper Rotliegend Group as early as main syn-rift times (Figure 92). Figure 93 shows that the expulsion rate of gas from the source rocks started to exceed the generation rates in the Ruurlo Formation (at 45 km) at approximately 125 Ma, in the Maurits Formation (at 18 km) and the Ruurlo Formation (at 50 km) at approximately 100 Ma. This timing coincides with the predicted decrease in gas generation rates.

### *Post-rift phase*

The expulsion of gas from the Limburg Group source rocks continued during post-rift times.

During these times the secondary migration system in the southern part of the cross-section is characterised by bedding-parallel updip migration through the Upper Rotliegend Group from 32 to 26 km, and subsequent vertically upwards cross-formational migration through Zechstein and Triassic Group units until the gas reached the reservoir-type Detfurth and Solling Formations, where it accumulated in structural traps (for example in a trap located at 25 km along the cross-section). Further south at P9 and 18 km, the secondary migration system was also dominated by vertical upward cross-formational migration through Zechstein and Triassic Group units, followed by the introduction of gas into the Detfurth and Solling reservoir units. At the end of the post-rift period predicted gas saturations were high in the Solling Formation at 16 km (Figure 94). Figure 94 shows that the Upper Triassic and Jurassic poorly permeable units did not halt the vertical upward migration of gas in the crestral structures in the southern part of the cross-section. Obviously, the gas that accumulated in the Solling Formation in the crestral areas provided enough buoyancy to overcome the capillary entry pressures in the overlying poorly permeable units. The buoyancy-related driving force was supported by the upward directed overpressure gradients in the groundwater. The fault zones in the P6 area breached the Zechstein seal and allowed gas to escape vertically upwards from the Upper Rotliegend Group. This modelling effect was caused by the difference in magnitude of the capillary pressures and vertical permeabilities assigned to the faults in comparison with those assigned to the Zechstein evaporites (e.g. at 10% porosity the fault zone  $k_v = 3 \times 10^{-5}$  mD, and evaporitic Zechstein  $k_v = 2.4 \times 10^{-6}$  mD).

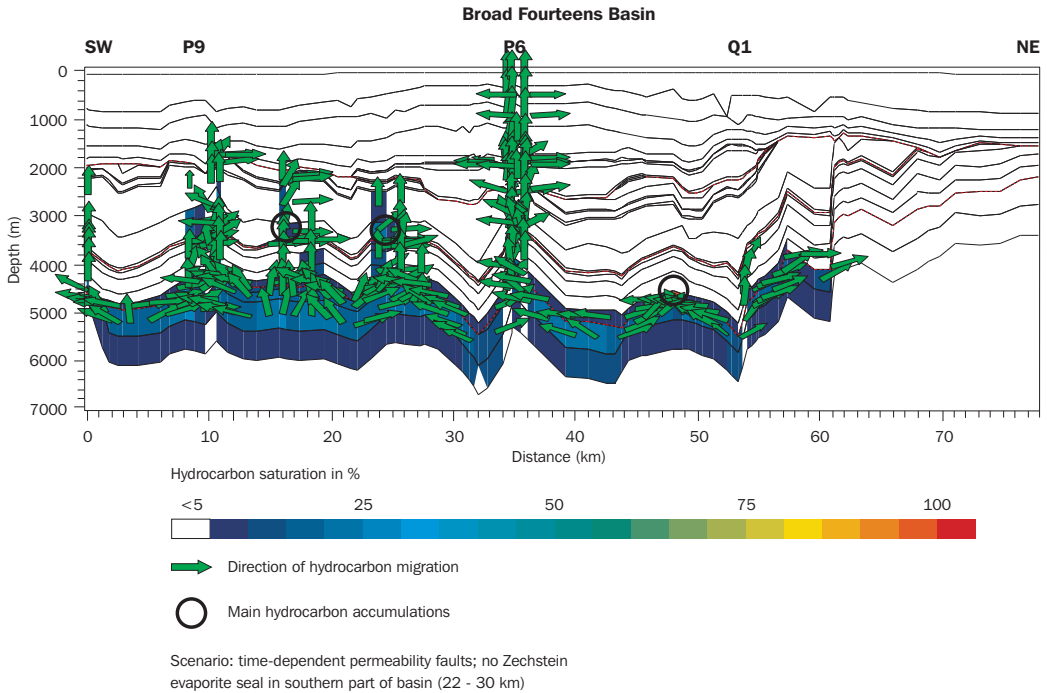


Figure 94 Predicted hydrocarbon saturation and migration in the Carboniferous gas system at the end of the post-rift period

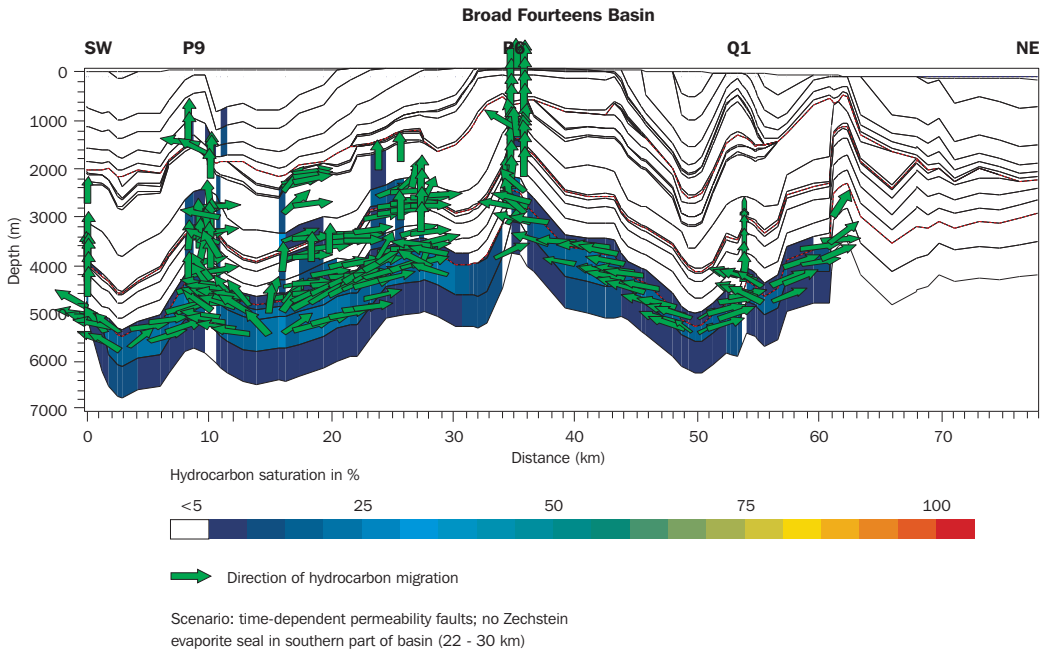


Figure 95 Predicted hydrocarbon saturation and migration in the Carboniferous gas system at syn-inversion time

The high capillary pressures of the Zechstein evaporites, in combination with their low permeabilities and the magnitude of the groundwater overpressures during post-rift times, effectively sealed the Upper Rotliegend Group in the central part of the basin north of P6. After gas had been expelled from the Limburg Group source rock it migrated updip through the Upper Rotliegend Group and accumulated in crestral structures, e.g at 50 km (Figure 94).

### *Syn-inversion phase*

Since the Late Cretaceous inversion period the expulsion of gas from the Limburg Group source rock levelled out (Figure 93).

The changing geometries of the hydrostratigraphic framework, in combination with the modelled increased permeabilities of the fault zones during the syn-inversion period were the major factors of influence on the secondary gas migration system. Figure 95 shows the gas migration system during syn-inversion times. In the central part of the basin the secondary migration through the Upper Rotliegend Group was mainly from the deepest part of the Upper Rotliegend Group towards the faulted crestral high area at P6. It included remigration of gas from the former gas accumulation at 50 km. After reaching the fault zone at P6 the gas moved vertically upwards along the faults. At shallower levels part of the gas left the fault zone and invaded reservoir-type horizons and part of the gas escaped into the atmosphere. In the northern half of the central part of the basin, the gas migrated updip through the Upper Rotliegend Group towards the Q1 fault system.

South of the P6 area – between 16 and 28 km along the cross-section – updip migration of gas through the Slochteren and Solling Formations was also towards the faulted crestral high P6 area. Gas that had previously accumulated remigrated (for example the gas previously accumulated in the Solling Formation at 16 km), and some accumulated again in an updip trapping structure (for example in the Solling Formation at 28 km).

The model results show that the syn-inversion topography-induced groundwater flow system did not prevent the vertical upward migration of gas through the P6 fault zone, nor the updip migration of gas in the Slochteren Formation and the Triassic sandstones (Figure 95).

### *Present-day*

In the southern part of the basin, where most of the gas was generated during basin history, the gas was distributed throughout the post-Carboniferous section by bedding-parallel and cross-formational migration. As a consequence, only a restricted number of gas fields were predicted to be present in the southern part of the basin at present-day (Figure 96). Increased gas saturations of >90% were predicted in the Solling Formation in structural traps at approximately 20 and 28 km along the cross-section.

The preserved saturation of gas in the Slochteren Formation in the P6 crestral area was calculated to be 18% (Figure 92). At shallower levels in the P6 area, some of the gas that escaped along the P6 fault zone during periods of tectonic activity,

accumulated in Triassic reservoirs (Detfurth/Volpriehausen/Solling Formations) and in Delfland Subgroup sandstones. The model predicted increased gas saturations in these reservoir units at present-day. North of the P6 structural high, the vertical escape of the gas from the Slochteren Formation was effectively stopped during basin history by the continuous Zechstein seal rock. Much of the pre-inversion gas accumulations remigrated towards the P6 area during the syn-inversion period. Since no favourable trapping structure was available in which the remigrating gas could accumulate, no significant present-day gas fields were predicted in the Slochteren Formation north of P6. In the Q1 fault zone the Zechstein seal was breached during the syn-inversion and Eocene–Oligocene periods of tectonic activity and associated modelled increase in fault permeability. This enabled some of the Slochteren gas to escape vertically upward along the Q1 fault zone and infiltrate into the Vlieland Sandstone Formation at shallower depths. The modelling predicted a minor amount of gas trapped in this reservoir in the anticlinal structure at Q1 at present-day.

As the Zechstein Group in the central and northern part of the cross-section includes evaporite deposits it was modelled with lithology-based poor permeabilities and a high capillary entry pressure (5 MPa). The modelling results clearly show that these characteristics of the Zechstein evaporites prohibited gas migration, an effect augmented by overpressure gradients counteracting cross-formational migration through the Zechstein. In contrast, the results show that fine-grained clastic lithologies of poor permeabilities with a capillary pressure of  $\leq 1$  MPa may still allow cross-formational migration of gas. The uninterrupted presence of a Zechstein evaporite caprock effectively sealed the Slochteren Formation in the central part of the basin. Only if this Zechstein evaporite seal is breached e.g. by active fault zones (P6 and Q1 fault zones), did the model predict escape of gas through the caprock. An early modelling scenario, assuming a basin hydrogeological framework without dynamically permeable fault zones, predicted present-day gas saturations of more than 90% in the Slochteren Formation in the P6 crestal structure, instead of the 18% reported above. In that scenario the continuous evaporite seal prevented the escape of gas. In the southern part of the cross-section the Zechstein Group does not include evaporite deposits and is principally composed of clastic lithologies (53% shale, 17% sandstone, 30% carbonates) with an assigned capillary pressure of 0.1 MPa. The model results indicate that in the southern part of the basin the Zechstein Group allowed the vertical escape of gas. The comparison of two distinct modelling scenarios gives another clear illustration of this dominant influence of the lithology-based fluid migration parameters controlling gas migration and accumulation. The modelling scenario including a more southward extension the Zechstein evaporites resulted in the prediction of a major gas accumulation in the Slochteren Formation at the structural trap at 26 km along the cross-section (Figure 97). As indicated in Appendix 4, the Zechstein Group evaporites probably do not extend so far south.

The histories of gas migration and accumulation discussed so far are based on modelling scenarios that include a no-flow hydraulic boundary at the northern side of the cross-section. Simulations based on the assumption of an open hydraulic boundary on the northern side, show the influence of the increase in northward flow of groundwater on migration and accumulation in the Slochteren Formation.

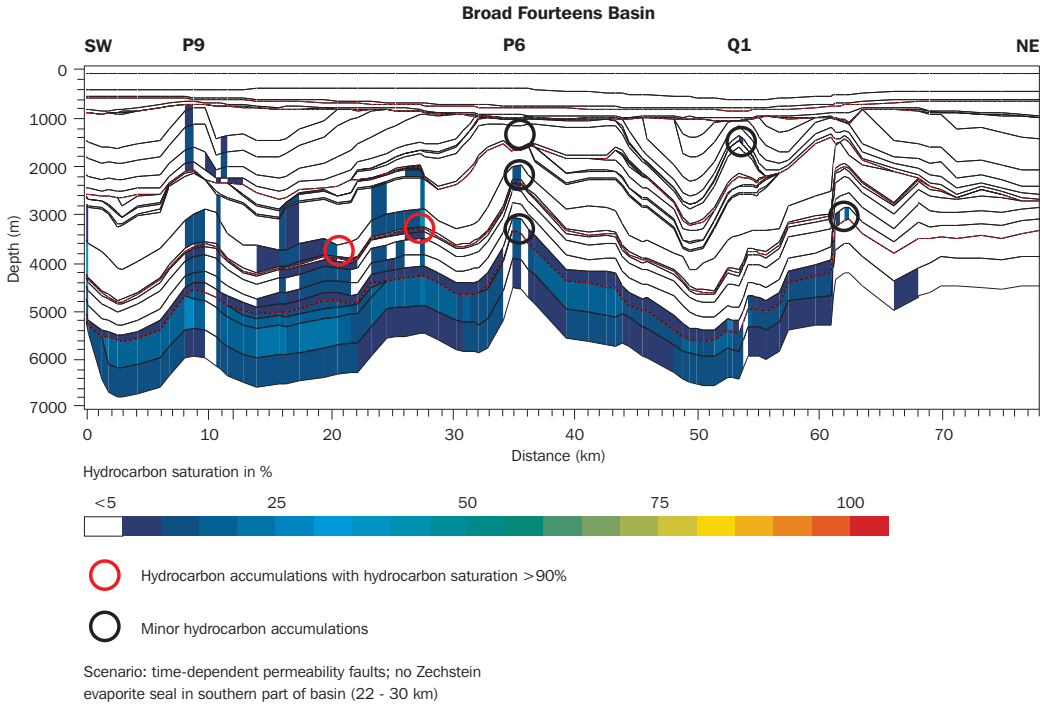


Figure 96 Predicted present-day hydrocarbon saturation in the Carboniferous gas system

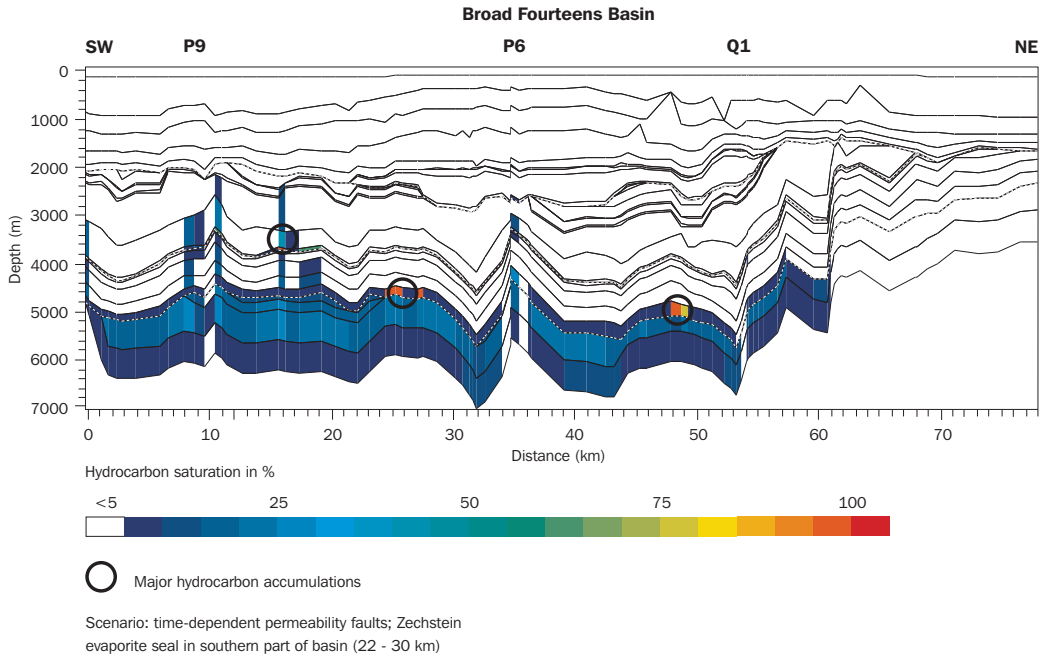


Figure 97 Predicted hydrocarbon saturation in the Carboniferous gas system at the end of the post-rift period (based on modelling scenario including southward extension of Zechstein evaporite seal to location 22 km along cross-section)

For example, the simulations with an open northern boundary predict a present-day saturation of gas of 26% in the Slochteren Formation at 62 km in the northern part of the cross-section. The predicted percentage of trapped gas at the same location, assuming a closed northern hydraulic boundary was 16%. It seems that the changed boundary condition not only enhanced the northward flow of groundwater (Chapter 23) but also the northward updip migration of gas through the Slochteren Formation.

## 24.2 Expulsion, migration and accumulation of oil

Expulsion of oil from the Jurassic source rocks starts if oil saturation exceeds 10% in the source rocks. The model results predict a negligible expulsion of oil from the Aalburg Formation during basin history. Figure 98 indicates that the present-day mass of oil in these Lower Jurassic shales is approximately equal to the total mass generated, that is  $\leq 5$  kg oil/ton source rock. The conditions in the Aalburg Formation are unfavourable for drainage: in the model the organic matter was assumed to be dispersed throughout the Aalburg Formation; in addition, the shale unit is thick (present-day thickness up to 896 m at P9) and of poor porosity and permeability, and as a consequence could not permit an efficient primary migration and expulsion.

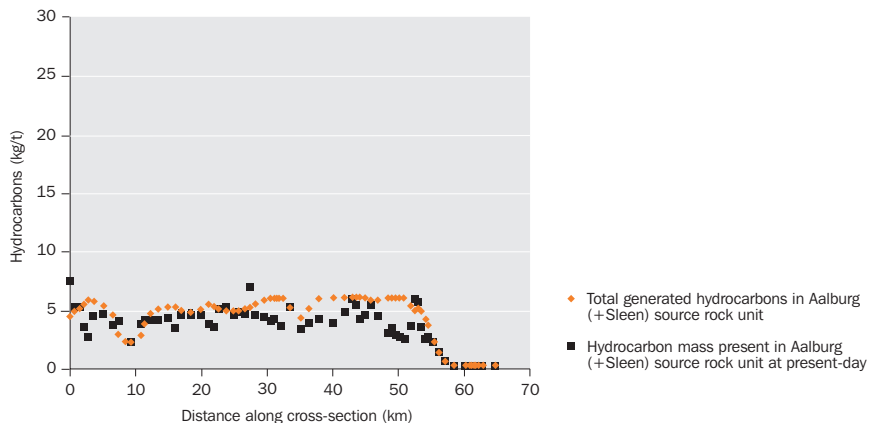


Figure 98 Calculated total amount of hydrocarbons generated in the oil-prone Aalburg/Sleen source rock unit and the hydrocarbon mass present in the Aalburg/Sleen unit at present-day

Figure 99 shows that during basin history oil saturation in the Posidonia Shale Formation remained below 10% at relatively shallow depths in the southern part of the cross-section, not allowing oil to migrate through the source rock. Only the parts of the Posidonia Shale Formation buried more deeply in the southern part of the cross-section reached oil saturations that allowed expulsion of oil (e.g. at 3 km and 13 km).

In the central – deepest – part of the pre-inversion basin (at 40 km), expulsion of oil from the Posidonia Shale Formation started at approximately 125 Ma (Figure 100), i.e. during the latest part of the main syn-rift period. The expulsion rates in this part of the basin started to exceed generation rates in post-rift times (Figure 101). In the central part of the basin, the expulsion of oil from part of the Posidonia Shale Formation, that was buried at relatively shallow depths during pre-inversion times, did not start until post-rift times (e.g. at approximately 90 Ma in the Q1 area; Figure 102).



### Post-rift phase

Due to the anisotropy assigned to the Posidonia Shale Formation, the generated oil first migrated updip through the source rock. After arriving at the crestal structures in the central part of the basin north of P6, migration continued vertically upwards through the Lower Werkendam Member until the oil reached the Middle Werkendam Member. At the end of the post-rift period oil had accumulated in the Werkendam Member in structural traps at several locations (37.9, 46.9 and 53 km). In the crestal high area of P6, the expelled oil migrated into the sandstones of the Delfland Subgroup during pre-inversion times (predicted oil saturation of 60% at 74 Ma). In the southern part of the cross-section the cross-formational migration of oil was also concentrated in crestal structures (Figure 103). Cross-formational migration introduced oil into the Middle Werkendam Member and the sand-dominated units of the Delfland Subgroup. In pre-inversion times oil accumulated in the sandstones in structural traps (e.g. predicted oil saturation was >90% at 26 km).

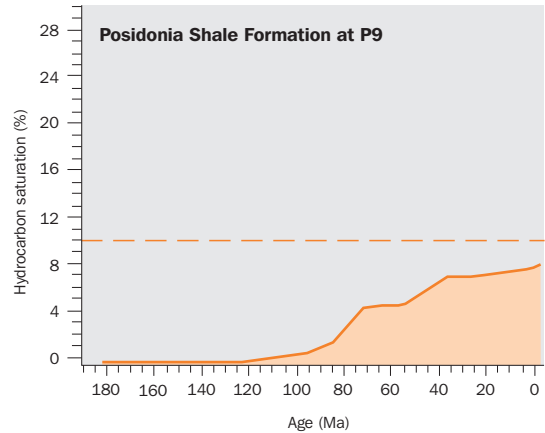


Figure 99 Predicted history of hydrocarbon saturation in the Posidonia Shale source rock at P9 in the southern part of the cross-section

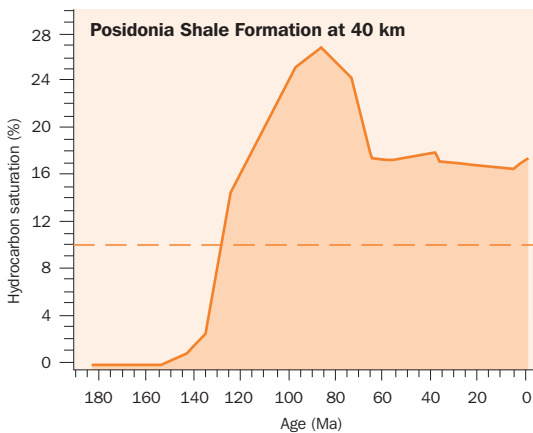


Figure 100 Predicted history of hydrocarbon saturation in the Posidonia Shale source rock in the central part of the Broad Fourteens Basin at 40 km along the cross-section

### Syn-inversion phase

The migration and remigration of oil during the syn-inversion period were strongly influenced by the changing geometry of the basin fill and the increased permeability of the active fault zones. Remigration was mainly towards the P6 and Q1 fault zone areas. The post-rift oil accumulations in the Middle Werkendam Member at 46.9 and 53 km were emptied and the southward and updip remigrating oils filled the Middle Werkendam Member in the crestal structure at 42 km (Figure 104). During inversion, oil reached the Delfland Subgroup sandstones by cross-formational flow at 45 km and subsequently migrated updip towards the P6 area.

The previously accumulated oils in the Middle Werkendam Member at 37.9 km and in the Delfland Subgroup at approximately 26 km were preserved during inversion.

North of 50 km along the cross-section oil remigrated updip through the Middle Werkendam Member towards the Q1 fault zone. Remigrated oil included the oil previously accumulated at 53 km. The model results indicated that the permeable



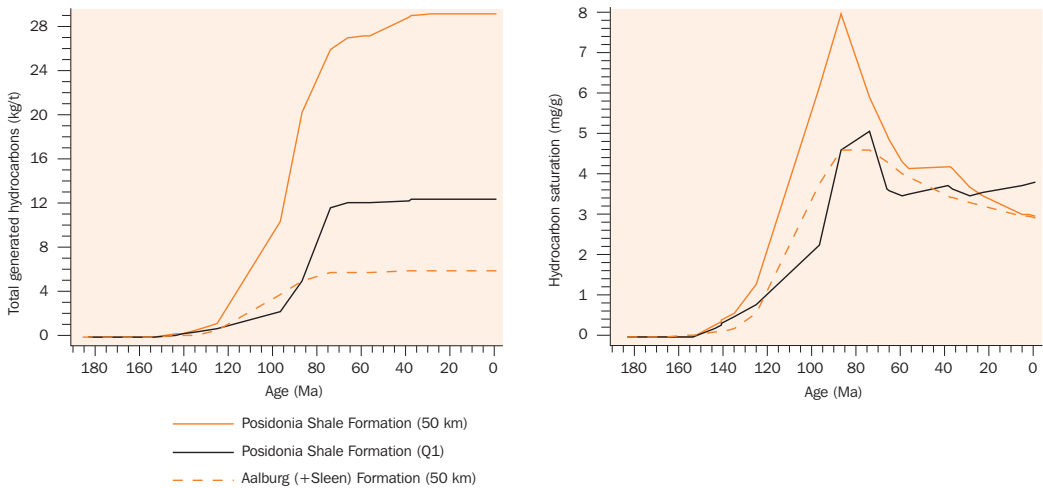


Figure 101 Predicted history of hydrocarbon generation and saturation in the Posidonia Shale and the Aalburg/Sleen source rocks in the central part of the Broad Fourteens Basin

Q1 fault zone drained additional oil directly from the tapped Jurassic source rocks (Figure 104). After migrating vertically upward through the fault zone, oil penetrated the Vlieland Sandstone Formation, where it accumulated (Figure 105). During syn-inversion times the accumulating oils in the Vlieland Sandstone Formation in the Q1 area were in the realm of the active regional topography-induced groundwater flow system (Section 23.2).

In the area south of the P6 fault zone, remigration of oil through the Middle Werkendam Member and the Delfland Subgroup sandstones was principally updip. Oil accumulated in the slightly changed crestal structure at approximately 26 km. At pre-inversion times, an oil-filled crestal structure was already present at approximately the same location. The oil migrating northward from 29 km towards the P6 fault zone escaped through the faults.

In the southernmost part of the cross-section (0 - 20 km) no oil reached the Vlieland Sandstone Formation during the inversion period.

#### Post-inversion phase

In the southernmost part of the cross-section the expulsion rate of oil from the Posidonia Shale Formation began to exceed the generation rate of oil in the source rock since Eocene-Oligocene (Figure 106; it seems that expulsion continued to

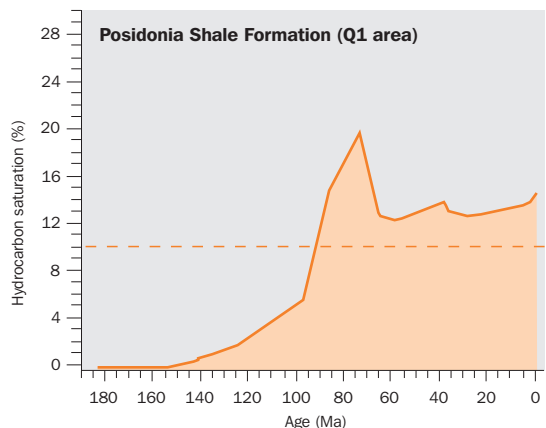


Figure 102 Predicted history of hydrocarbon saturation in the Posidonia Shale source rock in the Q1 area

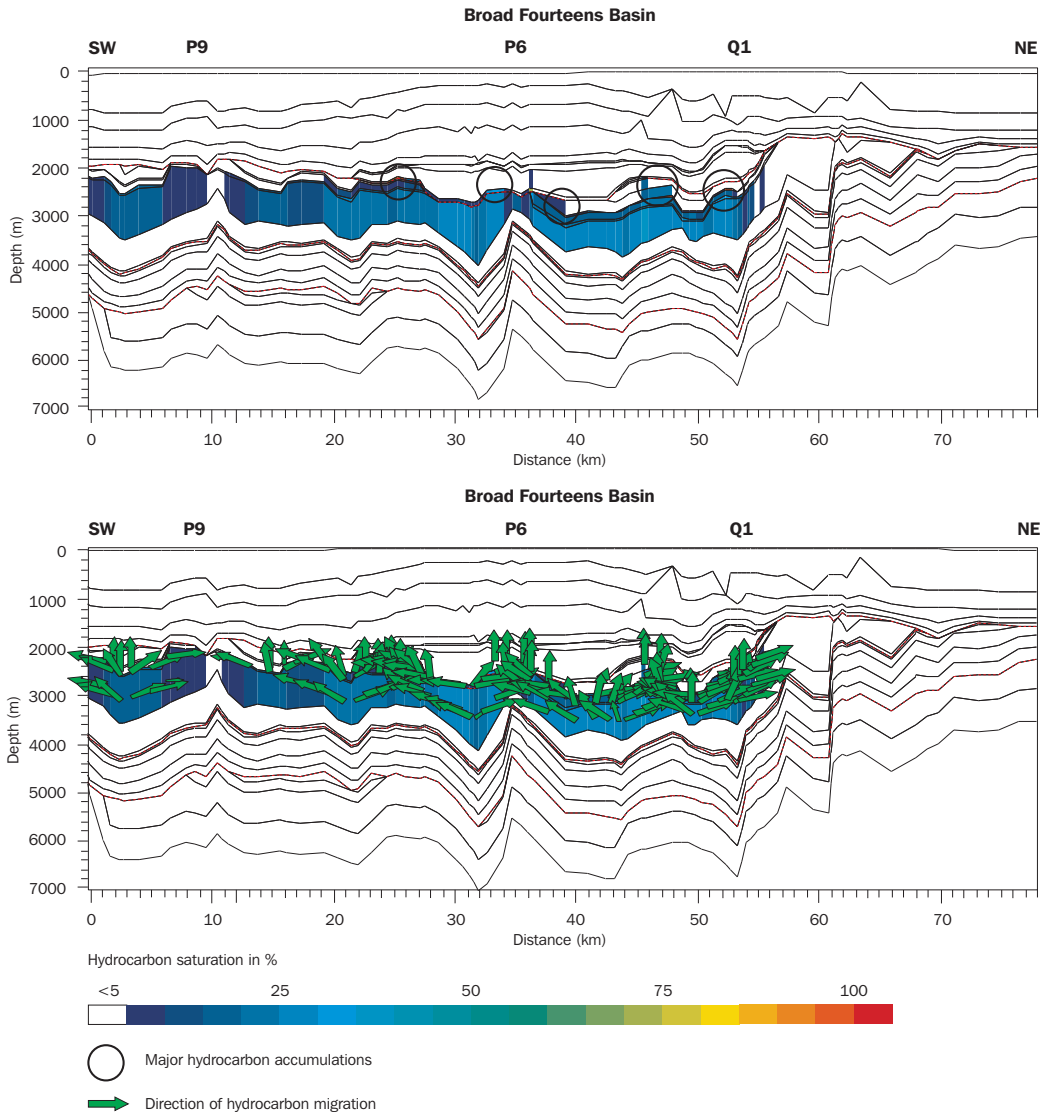


Figure 103 Predicted hydrocarbon saturation and migration in the Lower Jurassic oil system at the end of the post-rift period

present-day, while generation of oil levelled out). The oil expelled from the Posidonia Shale Formation south of P9 migrated vertically upwards until it reached the Middle Werkendam Member and subsequently moved updip towards the P9 crestal area. In the basin north of the P9 structure, the expelled oil also reached the Middle Werkendam Member. However, the oil saturations in the Middle Werkendam Member north of P9 were too low to permit updip secondary migration of oil towards P9. The predicted oil saturation history of the Lower Cretaceous Vlieland Formation in the crestal structure at P9 shows that the trap started to fill during the Eocene-Oligocene phase of tectonic activity (Figure 105). In the model, the increased fault zone permeability allowed the faults to drain the oil from the Middle Werkendam Member.

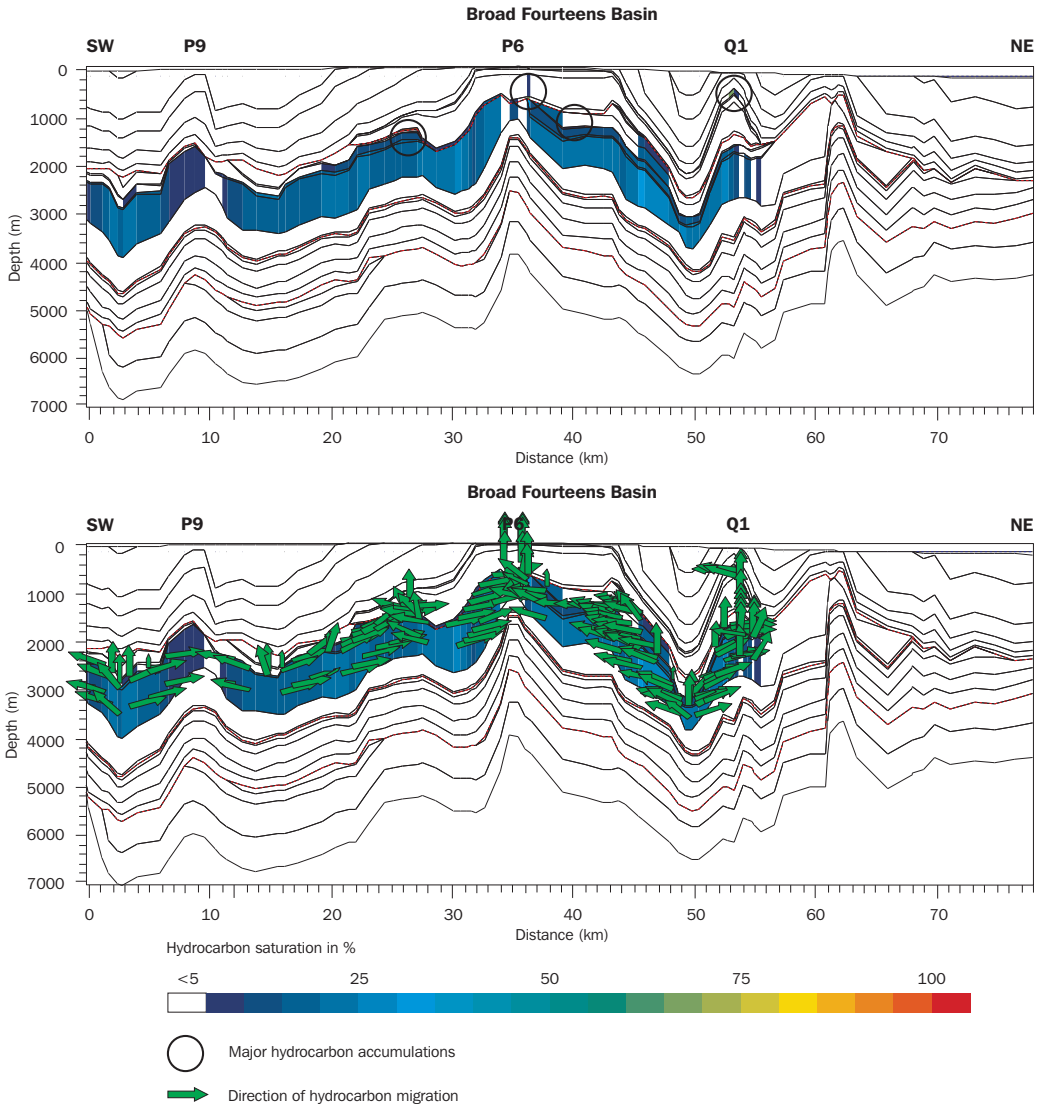


Figure 104 Predicted hydrocarbon saturation and migration in the Lower Jurassic oil system at syn-inversion time

### Present-day

The model reproduced the two known oil accumulations in the Vlieland Sandstone Formation, that is the oil accumulations in the crestal structures at Q1 and P9 (Figure 107). The results of the modelling show that the Lower Cretaceous reservoir at Q1 was filled during the syn-inversion phase by oil expelled prior to inversion from possibly both early and late mature Posidonia Shale Formation (Figure 68). The known oil field in the Vlieland Sandstone Formation in the Q1 area contains waterwashed and biodegraded oils (Roelofsens and De Boer 1991). The syn-inversion filling of the oil reservoir exposed the oils to syn-inversion topography-driven groundwater flow that may have induced the waterwashing and biodegradation of the oils. The P9 reservoir

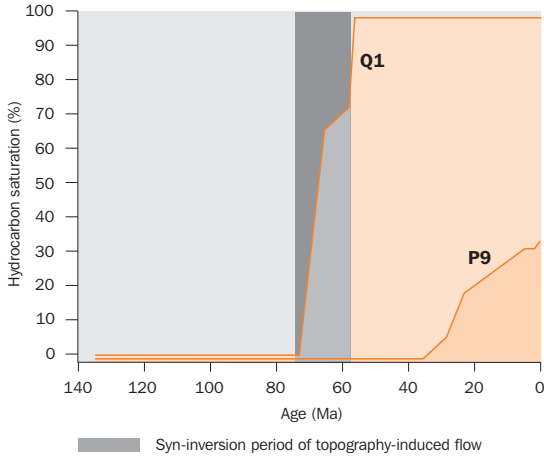
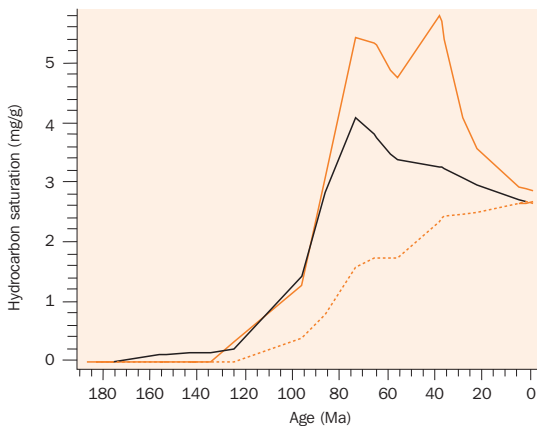
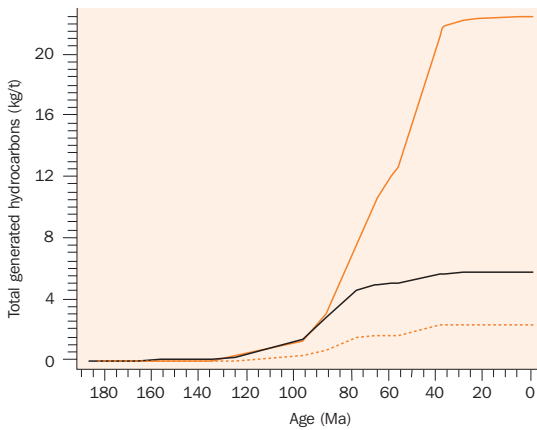


Figure 105 Predicted history of oil saturation in the Vlieland Sandstone Formation at Q1 and P9



was filled after the main inversion period (Figure 105) and the associated topography-induced flow event. In contrast to the Q1 oils, the accumulated oils in the P9 area are principally sourced from early mature Posidonia source rock south of P9 (Figure 68), and probably do not show signs of waterwashing and biodegradation. The differences in oil compositions are confirmed by in-house geochemical analyses of the oils.

The model predicted that oil saturations exceeding 80% would occur in the southern part of the cross-section in the Middle Werkendam Member at 18 km and 26.5 km and in the Delfland Subgroup sandstones at 26.5 km, and in the central part of the cross-section in the Middle Werkendam Member at 42 km. In addition increased saturations were predicted in the sandstones of the Delfland Subgroup at the P6 crestal high (at 33 - 34 km and 36 km) and in the Middle Werkendam Member just north of P6 (38 km). The P6 area was the basin-wide recharge area of the topography-induced groundwater flow system during syn-inversion times. Oils remigrating and reservoirized in the P6 area at that time were in the realm of active meteoric flow, and as a consequence will have been affected by waterwashing and biodegradation.

Figure 106 Predicted history of oil generation and saturation/oil masses in the Posidonia Shale source rock and the Aalburg source rock in the southern part of the Broad Fourteens Basin

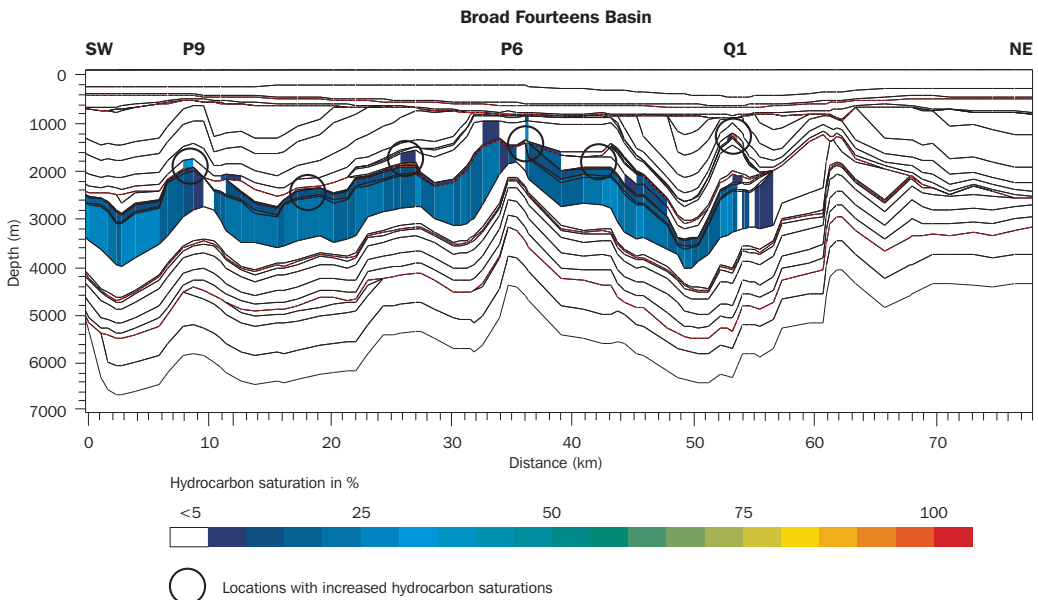


Figure 107 Predicted hydrocarbon saturation in the Lower Jurassic oil system at present-day

## 24.3 Discussion and conclusions

### *Migration of petroleum*

The migration of petroleum through a basin fill is a multiphase fluid flow process (e.g. Schowalter, 1979, England et al. 1987, 1991, Verweij 1993) driven by fluid potential gradients. These gradients are induced by differences in excess groundwater pressures, buoyancy forces (related to density differences between petroleum and water), and differences in capillary pressures. In turn, capillary pressures are a function of pore throat radii, interfacial tension and pore throat wettability. The actual migration rates of petroleum, as described by the multiphase Darcy equation, are controlled by the effective permeability of the basin fill to petroleum. Hence, the distributions of pore sizes and permeability in a basin highly control the migration process. The migration pathways of petroleum are largely controlled by units of relatively high porosity and permeability, such as permeable fault and fracture zones and sand-dominated lithostratigraphic units, and their structural dip or geometry. This is illustrated by the results of the 2D modelling of the petroleum system in the Broad Fourteens Basin. The geometry of these carrier-bed units and fault zones controlling the evolution of the migration pathways, remigration and accumulation changed dramatically during the evolution of the basin. In the modelling the basin is laterally constrained and, in addition, the modelling does not allow actual fault deformation. As a consequence, it should be realised that the modelled reconstructions of paleogeometries are not structurally correct. The modelled cross-section was chosen perpendicular to the strike of the basin and basin boundary fault directions and it crosses the major depocentre of the combined Triassic to Lower Cretaceous deposits as well as the area of maximum uplift and erosion during syn-inversion times. In this way it captures the principal dip directions of the stratigraphic units and the major variations in dip directions of direct influence on petroleum migration pathways.

The 2D basin modelling thus allows capturing the essence of the petroleum migration system. Although most buoyancy-driven updip migration is in the direction of largest dip (that is along the cross-section), additional out-of-plane migration of oil and gas is likely to have occurred during basin history. Today, the maximum depths of the basin extend from block Q1, towards blocks P3 and F18 (see depth map of top Carboniferous, e.g. Heybroek and Van Wijhe 1987). This suggests that updip migration may be possible from block F18 towards block L16, and from block P3 towards block Q1; i.e. migration towards the cross-section. In general, it is recognised that actual charging of a structure as well as the integrity of a petroleum-filled structure at any time during basin history should ideally be evaluated in 3D.

In order to fill the known oil fields in the Vlieland Sandstone Formation in the Q1 and P9 areas with oil generated from the Posidonia Shale Formation, the oil somehow had to pass through the shale-dominated Werkendam Formation and Delfland Subgroup. The interpreted seismic data and lithostratigraphic well data available to this study did not provide detailed information on the occurrence, distribution and horizontal and vertical continuity of sand-dominated permeable facies within the Werkendam Formation and the Delfland Subgroup. Therefore, regional information was used instead to reconstruct the lithostratigraphy and hydrostratigraphy between wells. In the model lateral continuity of permeable sandy facies was assumed, but no vertical connectivity between these facies. As a consequence the lithostratigraphic build-up adopted in the oil migration module, does not provide a potential cross-formational pathway for oil through the Delfland Subgroup. This is illustrated by the modelling results. The predicted Posidonia Shale–Vlieland Sandstone oil system (Q1) is dominated by focussed updip flow through the Middle Werkendam Member and subsequent vertical upward flow through the fault zone. The shales of the Upper Werkendam Member and the Delfland Subgroup do not allow widespread cross-formational flow. It is clear that more detailed information is required on the lithostratigraphic build-up especially of the Delfland Subgroup, in order to evaluate more confidently its actual role in oil history.

### *Dynamic permeability of fault zones*

Given the tectonic activity during basin history and the indicators of permeability alterations and paleofluid flow through fracture and fault zones (Part 2), there is no doubt that dynamic fault and fracture permeability played a role in fluid migration during the evolution of the Broad Fourteens Basin. The introduction of the dynamic permeability of the three fault zones in the modelled cross-section should be considered as an initial modelling effort to take such dynamic permeabilities into account in fluid migration in the basin. The real magnitude of changes in permeability, storativity, capillary pressures, the duration of the changed properties and the volumes of fluids involved are unknown.

The model results revealed the influence of the dynamic permeability of the three fault zones on the secondary migration and remigration of oil and gas. The interpreted seismic section (Figure 48) shows more widespread faults in the Broad Fourteens Basin. These additional fault zones may also have played a role in the history of petroleum systems in the basin, for example, in the filling and preservation history of the predicted oil accumulations in the Middle Werkendam Member in the

fault-bounded crestal structures at 26.5 and 42 km. These structures were filled prior to and during inversion. To be able to reliably evaluate the fault activity and related variations in permeability on the petroleum system, requires the dating and timing of fault movement and the reconstruction of phases of paleo groundwater flow.

### *Comparison Broad Fourteens Basin and West Netherlands Basin*

In a general sense, the Broad Fourteens Basin and the West Netherlands Basin (Figure 12) have similar geological histories. There are clear differences in lithostratigraphic characteristics, however. The more southern location of the West Netherlands Basin close to the London Brabant Massif partly explains these differences: for example, in the West Netherlands Basin, Zechstein evaporites are absent and only a thin layer of clastics of the Zechstein Group and a thin layer of Upper Rotliegend sands are present in part of the basin (Bodenhausen and Ott 1981); the Keuper Formation is free of salt and the lithological composition of the Schieland Group is more sand-rich than in the Broad Fourteens Basin (Bodenhausen and Ott 1981, TNO-NITG 2002, Van Adrichem Boogaert and Kouwe 1993-1997). In addition, Late Cretaceous inversion and erosion of the West Netherlands Basin was less intense: the Rijnland Group (including its sandy reservoir units) is largely preserved in this basin (TNO-NITG 2002). The petroleum systems of the West Netherlands Basin were also studied by 2D basin modelling (Van Balen et al. 2000). The strong dependence of maturation on burial history (Chapter 21) can probably explain the relatively minor differences between the modelled histories of the Westphalian gas system and the Jurassic oil system in both basins. Differences in the migration characteristics of the gas and oil systems might be related to the above described differences in lithology and associated differences in porosity and permeability.

### *Petroleum saturation*

Petroleum saturation has a major influence on the initiation of petroleum migration. Suggested magnitudes of bulk threshold saturations of the total available pore space for carrier rocks range between 1% (Hirsch and Thompson 1995), 3 - 5% for thick units (Mann et al. 1997) to 20% for thin units only several tens of metres thick (Mann et al. 1997). These breakthrough saturations also indicate the residual petroleum saturation, that is the percentage of petroleum that will be left behind in the carrier rock after migration. Residual saturations of the total available pore space have been estimated at 1 - 3% (Mackenzie and Quickley 1988) and 5% (England et al. 1987). The threshold petroleum saturation assumed in the modelling (5%) is well within these published ranges of values.

The saturation values that control initial expulsion from source rocks in separate phase are generally assumed to be higher than those used for initial migration through carrier rocks (Mann et al. 1997). However, when modelling the petroleum systems in different basins Burrus (1997) used threshold saturations of only 2%. In addition, Mann et al. (1997) consider threshold saturations of 2 - 5% typical for modelling purposes if the source rock cells are in the order of several tens of metres to 500 m in size. A single 10% threshold saturation for both the thin oil-prone Posidonia Shale Formation and the thick gas-prone Limburg Group source rocks was used in the modelling of the Broad Fourteens Basin. Source rocks with lower assigned threshold saturations would have started to expell their hydrocarbons earlier during

basin history. In the modelling of the Broad Fourteens basin kerogen was assumed to be distributed throughout the source rock. In the actual Limburg Group source rock, however, the kerogen is concentrated in distinct organic-rich coal layers. A value of 10% for petroleum threshold saturations – as assumed in the model – can probably be considered as a maximum saturation at which petroleum starts to migrate in the source rocks. Given these considerations, it is unlikely that the petroleum expulsion from the source rocks in the Broad Fourteens Basin started later than the times the model predicted.

### Modelling results

The modelling identified the following main characteristics of the gas and oil migration systems in the Broad Fourteens Basin:

#### Gas system

- Expulsion of gas from the Limburg Group source rocks in the central and southern part of the cross-section started during the main syn-rift period. Peak expulsion of gas occurred in Cretaceous pre-inversion times. Gas expulsion levelled out after the Late Cretaceous inversion period.
- The spatial variation in lithology and associated sealingness of the Zechstein Group results in different gas migration patterns along the cross-section. In the area south of the P6 structural high, where the clastic Zechstein Group is non-sealing, gas was distributed throughout the post-Carboniferous section by bedding-parallel migration through sand-dominated units and by cross-formational migration. North of the P6 area gas was prevented from escaping vertically from the Slochteren Formation by the sealing evaporite deposits of the Zechstein Group. The migration system was dominated by updip flow through the Slochteren Formation. Breaching of the Zechstein seal by the P6 and Q1 fault zones allowed gas to escape vertically upward, especially during the syn-inversion and Pyrenean periods of tectonic activity.
- Major pre-inversion gas accumulations were predicted in the Slochteren Formation at 50 km along the cross-section and in the Triassic sand-dominated units at 16 and 25 km. The accumulation at 50 km was emptied during inversion and the remigrating gas escaped through the P6 fault zone. Inversion-induced remigrated gas in the Triassic reservoirs in the southern part of the basin was trapped again updip in the Triassic reservoirs, e.g. at 28 km.
- For present-day the model predicted gas saturations exceeding 90% in the Triassic sand-dominated units at 20 and 28 km. No major gas accumulations were predicted in the Slochteren Formation. Gas migrating through the fault zones in the P6 and Q1 area during periods of tectonic activity were in part introduced into post-Permian reservoirs and trapped there.

#### Oil system

- Total expulsion of oil from the Aalburg Formations is negligible. Oil was expelled first from the Posidonia Shale Formation in the central part of the basin, namely during the most recent stage of the main syn-rift period. The post-rift period was the main period of oil expulsion in the central part of the basin, while in the southern part of the basin significant expulsion did not start until post-inversion times.



- The oil migration system in the central part of the basin during post-rift times was characterised by initial updip migration of oil through anisotropic source rock, expulsion of oil from the source rock and subsequent cross-formational migration of oil in crestal structures, followed by the introduction of oil into the Middle Werkendam Member and – south of P6 – also in the sand-dominated units in the Delfland Subgroup, and finally the updip migration of oils and their entrapment in these reservoir units.
- Just prior to inversion, the main oil accumulations predicted by the model occurred in crestal structures in the Middle Werkendam Member at 26, 38, 47 and 53 km and in the sandy units of the Delfland Subgroup at 26 km. Secondary accumulations were predicted in the Delfland Subgroup at P6.
- The oil accumulations at 38 and 47 km were preserved during inversion, while remigration of oils resulted in a new accumulation in the Middle Werkendam Member at 42 km and in the Vlieland Sandstone Formation in the Q1 area. An inversion-related increase in fault permeability permitted oil to remigrate from the Middle Werkendam Member into the Vlieland Sandstone Formation at Q1.
- The Vlieland Sandstone Formation in the crestal structure at P9 started to be charged at the end of the Eocene.
- At present oil accumulations occur in the Vlieland Sandstone Formation in the Q1 and the P9 crestal structures that are sealed by the Vlieland Shale Formation. The model predicted that oil saturations exceeding 80% occur in the southern part of the cross-section in the Middle Werkendam Member at 18 km and 26.5 km and in the sandstones of the Delfland Subgroup at 26.5 km, and in the central part of the cross-section in the Middle Werkendam Member at 42 km. In addition increased saturations were predicted in the sandstones of the Delfland Subgroup at the P6 crestal high (at 33 - 34 km and 36 km) and in the Middle Werkendam Member just north of P6 (38 km).
- Although the Q1 and P9 oil fields were charged with oil from the same Posidonia Shale source rock, their chemical characteristics were predicted to be different. The oils accumulated in the Q1 oil field were sourced by remigrated oils expelled for a prolonged period from – probably – early to mature Posidonia shales. In addition, the oils were exposed to syn-inversion topography-induced flow of groundwater that may have induced their waterwashing and biodegradation. The accumulated oils in the P9 area were sourced from an early mature part of the Posidonia Shale Formation and were probably not affected by waterwashing and biodegradation because of post-inversion charging of the structure.

The modelling study provided the time framework for expulsion, migration, accumulation and preservation of petroleum along a 2D cross section in the Broad Fourteens Basin and offered an explanation for the differences in geochemical composition of oil accumulations in the basin and for the absence of major gas accumulations in the centre of the basin. Thus attaining this part of the objective of the thesis (Chapter 1).

## 25 Relations between the groundwater flow system and the petroleum system

The results of the integrated modelling of the Broad Fourteens Basin clearly illustrate the overall effect of the geodynamic and sedimentation history on the evolution of the groundwater and petroleum migration systems and provide a number of illustrations of the interrelations between the two systems.

The gas and oil system events charts (Figure 108 and Figure 109, respectively) summarise the time framework for petroleum generation, migration, accumulation and preservation in the basin as derived from the modelling study and previous data analysis. In comparison with the classical petroleum system events charts, as introduced by Magoon and Dow (1994), Figures 108 and 109 also incorporate the aspects of the hydrodynamic and hydrogeologic history of importance for evaluating the history of petroleum systems in the Basin.

Migration of groundwater and petroleum are both influenced by groundwater potential gradients (including the overpressure gradients) in a sedimentary basin and the hydrogeological framework of the sedimentary fill. The groundwater potential gradients and the characteristics of the hydrogeological framework evolve continuously during

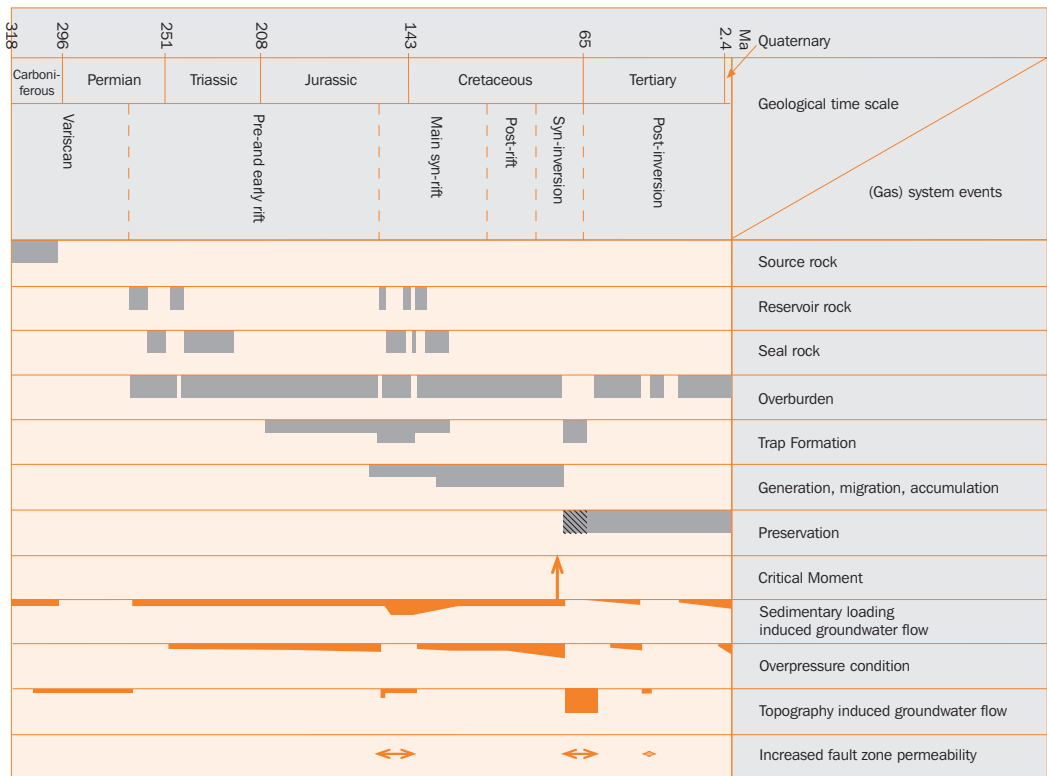


Figure 108 Events chart showing model-predicted timing of essential elements and processes of the Carboniferous gas system in the central part of the southern Broad Fourteens Basin

basin evolution. The groundwater has most impact on the petroleum system in zones of focussed active groundwater flow and in parts of the basin with large groundwater potential gradients (Verweij 1993, 1999). Focussed active groundwater flow and large groundwater potential gradients are associated with, for example, a pronounced topographic relief of the water table and high sedimentary and tectonic loading rates (Chapter 1). These in turn are related to distinct periods of basin evolution (Figures 108 and 109).

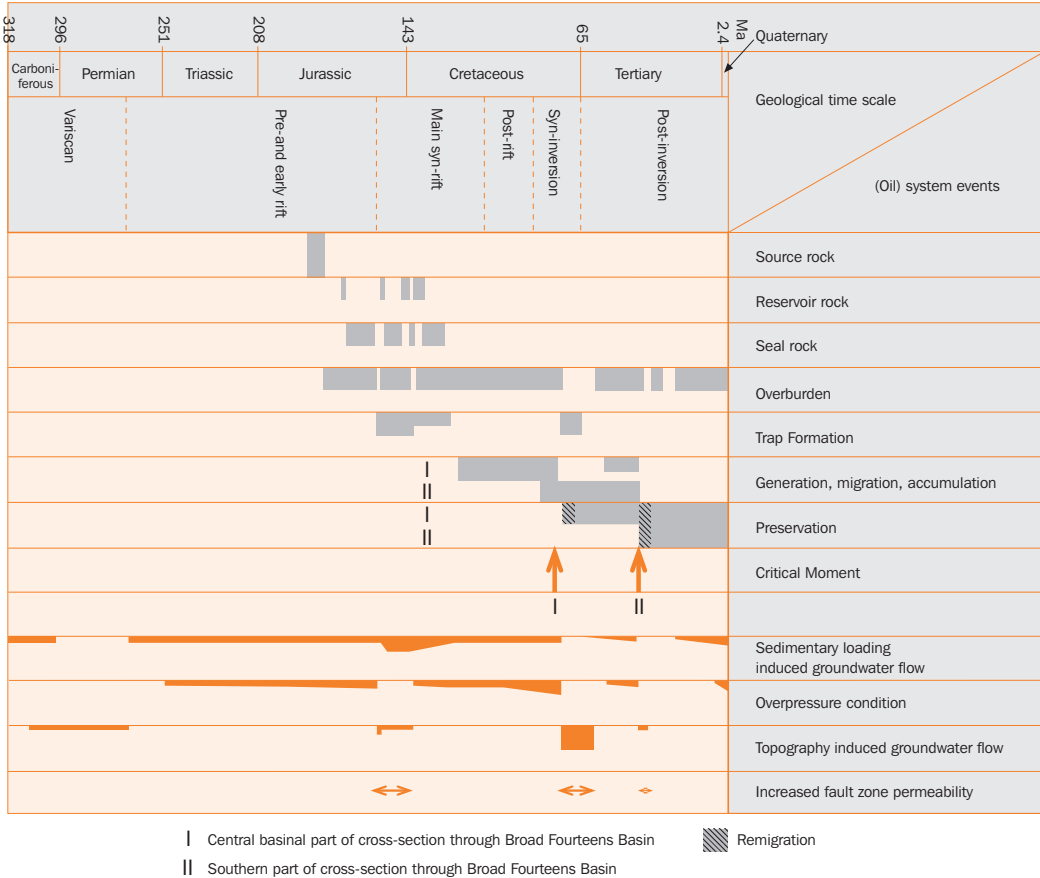


Figure 109 Events chart showing model-predicted timing of essential elements and processes of the Posidonia Shale oil system in the central part of the southern Broad Fourteens Basin

The following aspects of the geodynamic and sedimentary evolution of the Broad Fourteens Basin have been identified from the modelling results to have greatly influenced the evolution of groundwater potential gradients and the permeability distribution and thus also the evolution of groundwater and petroleum systems:

- Significant tectonic activities that caused faulting and fracturing during the main syn-rift and syn-inversion periods, changing the permeability of the basin fill and disrupting the lateral continuity of pre-inversion lithostratigraphic units. During periods of tectonic activity, fluid flow focussed into the fault zones of increased permeability.

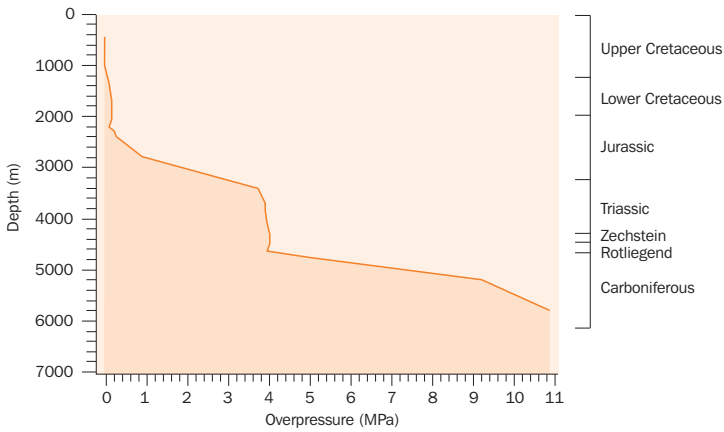
- Dramatically changing geometries of the lithostratigraphic units and as a consequence dramatically changing hydrostratigraphy, especially during the main syn-rift period and the syn-inversion period;
- Generally moderate sedimentation rates that induced overpressures with maximum values well below the values of minimum horizontal stress;
- Continued sedimentation during the main syn-rift and the post-rift times, leading to maximum overpressures in the basin at the end of the post-rift period (Figure 108);
- Relatively high sedimentation rates during the main syn-rift period and during the Quaternary, inducing active flow of groundwater in the basin (Figure 108);
- Syn-inversion erosion;
- Broad Fourteens Basin standing out as a regional high during the syn-inversion period, inducing active regional topography-induced flow of groundwater (Figure 108).

### 25.1 Influence of the groundwater flow system on the petroleum system

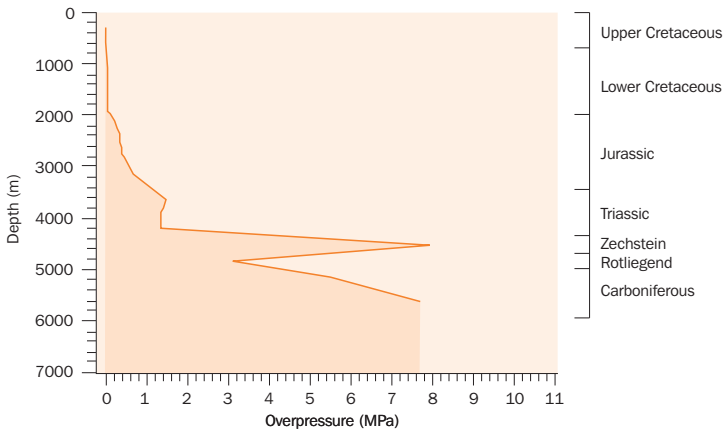
Overpressure gradients affect the sealing capacity of poorly permeable layers, and affect the petroleum migration through the poorly permeable layers (Verweij 1993). Examples of modelling results indicating these effects in the Broad Fourteens Basin, are:

- The predicted gradients of groundwater overpressure in the Limburg Group source rocks were vertically upwards from the Limburg Group towards the Slochteren Formation and thus provided an additional force driving the upward expulsion of gas from the source rock during main syn-rift and post-rift times (Chapter 24);
- The predicted downward gradients of groundwater overpressure during post-rift times (Figure 110) increased the effectiveness of the Zechstein seal in the central part of the basin north of P6. The modelling showed that in the central part of the basin the Zechstein acted as a perfect seal. In contrast, the contemporaneous gradients of groundwater overpressure in much of the southern section of the basin were vertically upward from the Slochteren Formation and in the overlying poorly permeable units (Figure 110). These upward directed overpressure gradients enhanced the cross-formational migration of gas, which was predicted to be widespread during post-rift times (Chapter 24).

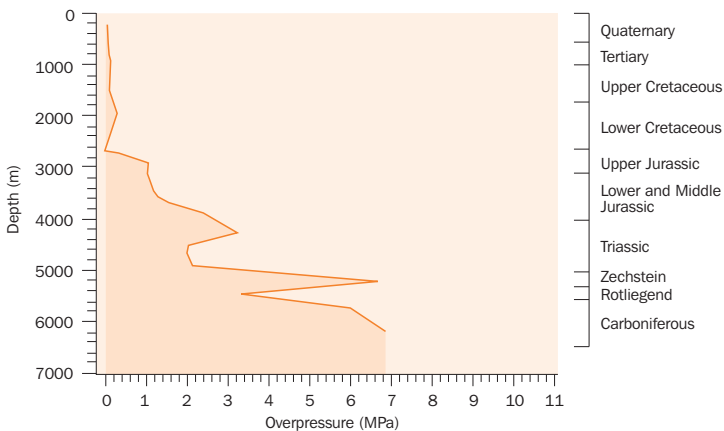
In theory, groundwater flow parallel to the buoyancy-induced direction of oil and gas migration will enhance the petroleum migration (increase the rates of petroleum migration, lengthen the migration paths; Verweij 1993). Modelling results indicate that transport of oil, gas and groundwater was focussed through permeable hydrostratigraphic units during different phases of basin evolution. The predicted principal direction of bedding-parallel migration of oil and gas is updip. The direction of lateral groundwater flow through the permeable hydrostratigraphic units varied during basin evolution. A major period of focussed downdip flow of groundwater was predicted for syn-inversion times: downdip flow occurred in the regional topography-induced groundwater flow system. Tectonically active periods were important periods of updip flow of groundwater towards the crestal high areas with permeable fault zones. From the Early Cretaceous onward the model results (based on the scenario with an open hydraulic northern boundary) indicated focussed updip flow of groundwater through Triassic and Upper Rotliegend permeable units northwards. An example of enhancement of petroleum migration in the direction of groundwater



a. Southern part basin: end post-rift times



b. Central part basin: end post-rift times



c. Central part basin: present-day

Figure 110 Predicted variation of overpressure with depth in the southern and central parts of the Broad Fourteens Basin during post-rift times, and in the central part of the basin at present-day

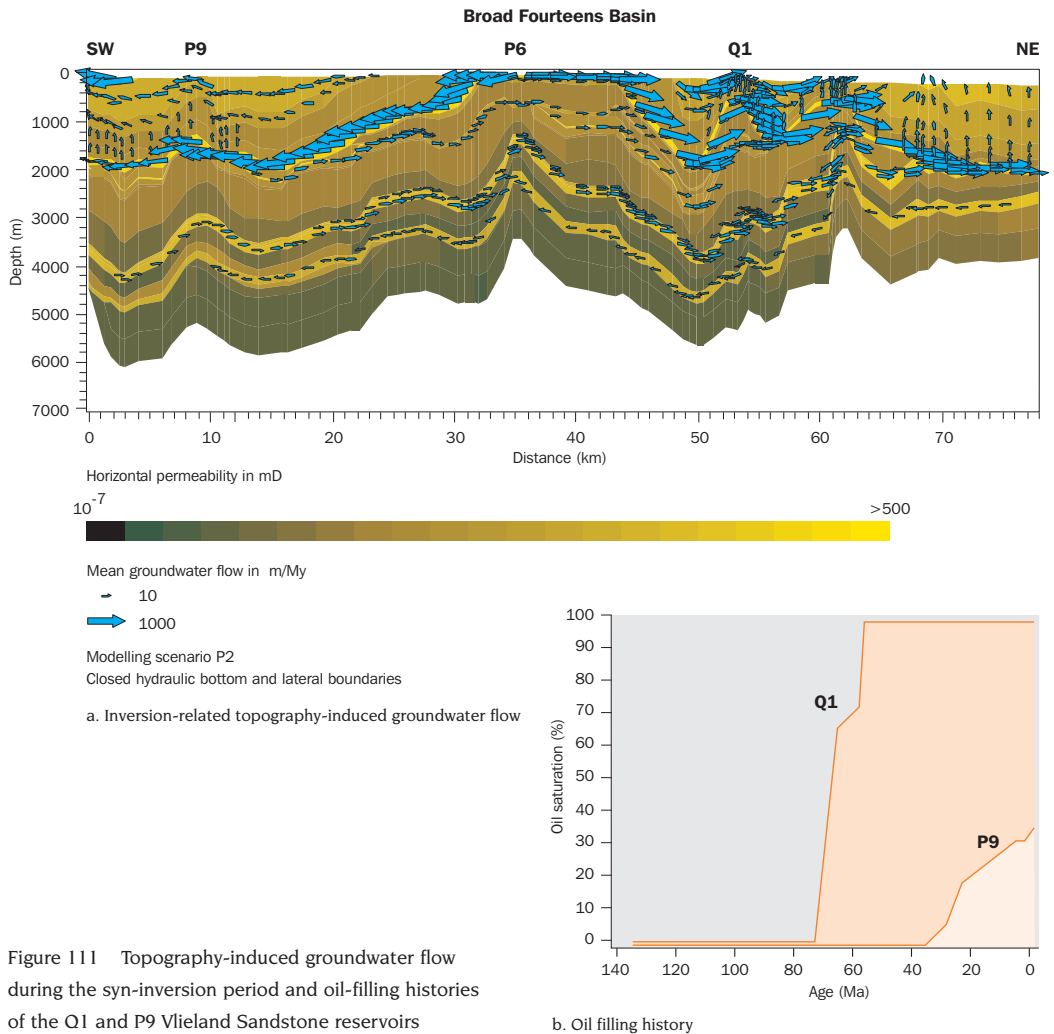


Figure 111 Topography-induced groundwater flow during the syn-inversion period and oil-filling histories of the Q1 and P9 Vlieland Sandstone reservoirs

flow is the modelled increase of the present-day saturation of gas (from 16 to 26%) in the Slochteren Formation at 62 km along the cross-section (Section 24.1). The predicted updip migration of oil and gas during the syn-inversion period showed that the updip-directed component of the buoyancy force for petroleum migration dominated the downdip-directed groundwater potential gradient of the topography-driven groundwater flow system.

An example of the influence of the groundwater flow system on the chemical characteristics of the petroleum system is the predicted concentrated topography-induced groundwater flow through the Vlieland Sandstone Formation during syn-inversion times. This phenomenon provided an explanation for the waterwashed and biodegraded nature of the Q1 oil reservoir charged in the Late Cretaceous (Figure 111).

## 25.2 Influence of the petroleum system on the groundwater flow system

The modelling results also revealed the influence of the petroleum system on the groundwater system; for example, the – minor – influence of gas generation on the development of overpressures in the Limburg Group source rocks (Section 23.1). In addition, as discussed in Section 23.3, the presence of a gas accumulation may affect the groundwater flow system: gas accumulation in a reservoir in a crestal high area will decrease the effective permeability for groundwater flow, and at high gas saturations may even form a barrier for groundwater flow through the reservoir, thus enhancing the formation of a pressure compartment.

## 25.3 Influence of the groundwater and petroleum systems on permeability evolution

Groundwater flow exerts direct and indirect influences on the evolution of the porosity and permeability in a basin. Its influence on the compaction process is direct. Examples of the indirect role of groundwater flow derived from the modelling results and data analysis, include:

- The observed secondary porosity and K-feldspar leaching in the Vlieland Sandstone Formation. This is consistent with the model-predicted concentration of topography-induced groundwater flow through this formation during syn-inversion times.
- The overpressure gradients of the groundwater calculated for the main syn-rift phase were directed from the Limburg Group and Zechstein Group towards the lower-pressured Slochteren Formation. These modelled directions of groundwater expulsion from both the Limburg Group and the Zechstein Group are consistent with one of the flow conditions required to explain the permeability-influencing illite cements in the Slochteren Formation.

The modelling results also provide further evidence for the combined role of the groundwater and the gas systems in modifying the porosity and permeability conditions in the basin. An example is the inferred generation of CO<sub>2</sub> in the Limburg Group source rocks, and the contemporaneous vertical upward expulsion of groundwater from the source rocks into the Slochteren Formation and overlying Zechstein Group that was induced by sedimentary loading. These processes and their timing are in accordance with the conditions required to explain the observed formation of kaolin cement and leaching of K-feldspar in the Slochteren Formation and calcite cements in the Z3 Carbonate Member of the Zechstein Group.

The modelling results in combination with the previous data analysis showed that the geodynamic and the sedimentary evolution of the Broad Fourteens Basin exerted an important influence on the development of both the groundwater flow and the petroleum migration systems. Furthermore, the groundwater and the petroleum systems influenced each other, and, the groundwater and petroleum systems, separately and in combination, affected the evolution of porosity and permeability in the basin.

## 26 Conclusions Part 3 and continued analysis of fluid flow systems on geological timescales

### 26.1 Conclusions

The integrated basin modelling provided quantitative insight into a number of key aspects of the histories of temperature and heat flow, the maturation and petroleum generation from the oil-prone Posidonia Shale Formation and Aalburg Formation and gas-prone Limburg Group source rocks, the pore pressures and groundwater flow, and the petroleum expulsion, migration and accumulation in the southern part of the Broad Fourteens Basin. It was recognised that the basin modelling did not incorporate all the processes and forces influencing the pore pressure, fluid geology and fluid dynamics in the Broad Fourteens Basin identified in Part 2; for example it did not include tectonic compression and chemical compaction. The results of the basin modelling presented in Part 3 do not provide evidence that these processes have no influence on e.g. pore pressures or fluid flow.

Important findings of the modelling are:

- The occurrence of lateral and vertical variations in heat flow along the cross-section at different times during basin history. These variations could be related to differential vertical displacements of the basin and the evolution of the temperature at the surface and bottom boundary; e.g. the contrasting uplift and subsidence histories of the central part of the basin and the northern platform during the main syn-rift and the syn-inversion period, resulted in lateral variations in heat flow along the cross-section of approximately 8 mW/m<sup>2</sup>.
- The modelling demonstrated that large differences in the burial histories of the Carboniferous and Jurassic source rocks along the cross-section resulted in very different temperature and maturation histories for the source rocks depending on their structural evolution. As a result, the Limburg Group source rocks in the central and southern part of the cross-section first entered the gas window at the end of early-rift times, while in the northern platform area a first phase of gas generation was reached in the Early Tertiary.
- It provided the time framework for expulsion, migration, and accumulation of oil and gas. Expulsion of gas from the Limburg Group source rocks in the central and southern part of the cross-section started during the main syn-rift period. First expulsion of oil from the Posidonia Shale Formation started at approximately 125 Ma in the central part of the pre-inversion basin. Given – amongst other things – the threshold saturation values controlling initial expulsion from source rocks used in the modelling, it is unlikely that the petroleum expulsion from the source rocks in the Broad Fourteens Basin started later than the modelling predicted. The modelling revealed that present-day oil and gas accumulations were largely charged by migrating and remigrating oil and gas during Late Cretaceous inversion and Eocene-Oligocene uplift; large part of the previously accumulated hydrocarbons escaped to the atmosphere during inversion especially in the central part of the basin (P6 area): only minor amounts of gas are preserved in e.g. Slochteren Formation and Triassic sandstones in the central part of the basin.
- The results provided a time framework for overpressure generation and dissipation and for groundwater flow, and a characterisation of the permeability framework, pressure system and groundwater system at different times during basin history.



The main period of overpressuring induced by sedimentary loading occurred at the end of post-rift times:  $P_{\text{excess}}$  reached 11 MPa in the Limburg Group at burial depths exceeding 5000 m. Sedimentary loading induced bedding-parallel flow of groundwater through permeable hydrostratigraphic units (principally sandstones) at all depths; the bedding parallel flow equilibrated the overpressures in these permeable units. In the inverted part of the basin these overpressures dissipated during Late Cretaceous inversion, because of the combined effect of the absence of sedimentation as a pressure-generating mechanism, decreased rates of gas generation, erosional unloading, a changing geometrical framework and increased permeabilities of the fault zones. Major topography-induced flow systems developed during the syn-inversion period; flow of groundwater was focussed through the Vlieland Sandstone Formation, which is in accordance with observed K-feldspar leaching of this formation; the focussed flow of groundwater is contemporaneous with oil migration, remigration and accumulation in the Vlieland Sandstone Formation.

- The results of the integrated modelling of the Broad Fourteens Basin clearly illustrated the overall effect of the geodynamic and sedimentary history on the evolution of groundwater and petroleum migration systems along the cross section and provided a number of illustrations of the interrelations between the two systems (Chapter 25); e.g. during basin evolution, the area of maximum overpressure shifted along the cross-section in accordance with changing depocentres.
- It demonstrated that the presence of an – assumed continuous – layer of evaporites in the Zechstein in the northeastern part of the cross-section exerted a major influence on pore pressure build-up, groundwater flow and petroleum migration.
- It showed that the assigned dynamic permeability of fault zones did affect the migration and accumulation history of oil and gas.

Forward modelling results of the heat flow system, and the groundwater and petroleum systems in the basin show the following present-day features:

- A relatively low heat flow in the shallow part of the basin; resulting from Pleistocene surface temperature fluctuations and the relatively high porosities of the Pliocene and Quaternary sediments.
- Temperatures in the Carboniferous and Jurassic source rocks along the cross-section that are lower than the maximum temperatures experienced during previous burial.
- There is no to only minor generation of gas from the Limburg Group source rocks and no to only minor generation of oil from the Posidonia Shale Formation along the cross-section.
- The occurrence of – mild – overpressures is restricted to the poorly permeable deeper parts of the basin, with maximum overpressures in the evaporites of the Zechstein Group and in the shales of the Limburg Group. The modelling identified Pliocene and Quaternary sedimentary loading as the mechanisms responsible for these present-day overpressures. Today, and during the entire evolution of the basin, no overpressures of  $P_{\text{excess}} > 1$  MPa occur in the shallow parts of the basin (depths to 2000 m).
- Increased fluid flow in the shallow part of the basin related to Pliocene and Quaternary sedimentary loading.
- The model reproduced the two known oil accumulations in the Vlieland Sandstone Formation sealed by Vlieland Claystone Formation in the P9 and Q1 crestal structures. Additional oil accumulations were predicted in the southern part of

the cross-section in the Middle Werkendam Member at 18 km and 26.5 km, and in the sandstones of the Delfland Subgroup at 26.5 km, and in the central part of the cross-section in the Middle Werkendam Member. The model revealed increased saturations in the sandstones of the Delfland Subgroup at the P6 creстал high, and in the Middle Werkendam Member just north of P6.

- Different geochemical compositions of the oils in the Q1 and P9. Oils in Q1 were sourced from the early mature to mature Posidonia Shale Formation and were exposed to syn-inversion topography-induced flow of groundwater that may have induced waterwashing and biodegradation. The P9 oil accumulation was sourced from an early mature part of the Posidonia Shale Formation and was probably not affected by waterwashing and biodegradation because of post-inversion charging of the P9 structure.
- No major gas accumulations in the Slochteren Formation; pre-inversion gas accumulations were not preserved during inversion. Two gas accumulations occur in Triassic sandstone-dominated units in structural traps in the southern part of the basin.

In general Part 3 showed the significance of the combination of a powerful conceptual model with predictive abilities in geofluid evolution and the use of a wide variety of actual data with basin modelling for a process-based understanding of present-day characteristics of the hydrogeological framework and the fluids.

## 26.2 Continued analysis of fluid flow systems on geological timescales in sedimentary basins in onshore and offshore Netherlands

The analysis of fluid flow systems is part of different ongoing studies in onshore and offshore Netherlands (e.g. Schroot and Schüttenhelm 2003, Simmelink et al. 2003, Winthagen and Verweij 2003). Some of these studies include the application of basin modelling. The modelling results and discussions in Part 3 in combination with the findings of the Parts 1 and 2 enable to identify factors that will increase the confidence of basin modelling of sedimentary basins in onshore and offshore Netherlands. These factors include: a. parameters and processes which need to be specified more accurately; b. additional information on present-day and paleo characteristics of the subsurface of the Netherlands; c. tool improvement; d. improvement basin analysis approach.

- a. Tectonic processes played an important role during different phases of basin development in onshore and offshore Netherlands (Chapters 3, 12 and 13). It was found that changes in tectonic stress included gradual long-term changes in tectonic stress regime from an active extensional stress regime (Triassic to Early Cretaceous) towards a compressional stress regime (Late Cretaceous to present-day), short term stress fluctuations related to distinct rifting pulses (e.g. Late Jurassic rifting of the Mesozoic basins, Late Oligocene to recent rifting of the Roer Valley Graben) and pulse-like changes in compressive stress during the Late Cretaceous and Cenozoic. It is likely that these changes in stress influenced the magnitude and distribution of fluid pressures and groundwater and petroleum migration to a greater or lesser extent (Chapters 4 and 14). There is a need for a quantitative understanding of the effect of both the long-term and pulse-like tectonic loading on overpressure development and fluid flow in sedimentary basins.

- b. In general it is important to calibrate the modelling using different types of – reliable – data and information. The confidence of the integrated basin modelling of the Dutch basins will increase from, e.g.
- A database of present-day temperatures and indicators of paleotemperatures, such as vitrinite reflectance values.
  - Database of porosity and permeability of poorly permeable lithotypes (clays, shales).
  - A database of present-day pressures. At present, well data are used to set up a quality-controlled data base of pressures, temperatures and salinities in offshore Netherlands (Chapter 10).
  - Information on sand connectivity. For the Broad Fourteens Basin: the distribution and spatial continuity of different lithotypes (presence/absence sand connectivity) especially in the Schieland Group and the Limburg Group; the distribution and spatial continuity of evaporites in the Zechstein Group.
  - Present-day fault zone properties (permeability, storativity, capillary pressures);
  - Quantitative information on the erosional history. Quantitative information on the uninterrupted time-stratigraphic sequence of events during the evolution of a basin is the basic input for the basin modelling; quantitative information on erosional history is largely lacking.
  - Quantitative reconstructions of paleotopography.
- In addition, (3D) structural reconstructions of the geological framework (including salt deformation) will enable to assess geometrically accurate paleo groundwater flow and paleo petroleum migration patterns.
- c. The need for continuous improvement of basin modelling tools is widely recognised and much discussed (e.g. EAGE Workshop 2002 on multidimensional geological modelling). Improvements relevant for basin modelling of the sedimentary basins in onshore and offshore Netherlands include:
- Incorporation of dynamic fault properties (permeabilities, storativities, capillary pressures) in fluid flow modules;
  - Incorporation of salt deformation (dynamic salt doming, salt depletion);
  - Incorporation of link of structural restoration tool with fluid flow module;
- d. Incorporation of the identification and quantification of uncertainties in the basin analysis process will enable the assessment of the probability of e.g. overpressure or of trapped oil or gas.

The approach to study the evolution of groundwater and petroleum systems on geological timescales outlined in Part 2 and 3 for the southern Broad Fourteens Basin can readily be applied to the other basins in onshore and offshore Netherlands, such as the West Netherlands Basin, Roer Valley Graben, Central Netherlands Basin, Vlieland Basin, Central North Sea Graben and Terschelling Basin. The general evolution of the Broad Fourteens Basin and these basins show important similarities; e.g. all basins are inverted Mesozoic basins that contain gas-prone Limburg Group source rocks and oil-prone Jurassic source rocks. However, the timing and intensity of the geological events, such as subsidence and sedimentation and uplift and erosion, were different for each basin (Chapter 3). The present-day characteristics of rocks and fluids in the basins reflect these differences (Part 1; Chapters 5, 7 and 8). Part 1 provides the general fluid dynamics context for the analysis of fluid flow systems in the sedimentary basins of the Netherlands.

The onshore and offshore Netherlands is a mature exploration area for gas and oil. Over the past few decades seismic surveys, measurements in exploration and production wells and measurements on core samples have resulted in a large amount of data and information on the rock matrix and the subsurface fluids. An increasing number of quality-controlled geoscientific data and information on the Netherlands subsurface is becoming publicly available. This thesis shows that the analysis of fluid flow systems on geological time scales – including the application of basin modelling – allows the integrated interpretation of such a wide variety of data and information. Hence, the analysing procedure is very well suited for application in mature areas. Here it may be used for detailed studies to identify and evaluate e.g. new exploration concepts as well as for obtaining a better theoretical understanding of fluid flow systems on geological time scales to be applied subsequently in less explored areas.

## Summary

### General objectives and research questions

The strategic objective of the research that is described in this thesis was improvement of safety and economics of oil and gas field exploration and exploitation and of subsurface storage of energy and energy residues in onshore and offshore Netherlands. The thesis aims to contribute to this strategic objective by increasing the knowledge of the evolution of fluid flow systems on geological timescales.

For this purpose it intends to provide:

1. A general description of the present-day hydrogeological framework of the sedimentary fill in onshore and offshore Netherlands and an overview of present-day characteristics of the fluids it contains (pressures, salinities, hydrochemical characteristics, temperatures);
2. The fluid dynamics context for an improved process-based understanding of the present-day characteristics of the hydrogeological framework and the fluids in onshore and offshore Netherlands;
3. A quantitative understanding of the hydrogeological and pore pressure and groundwater flow response of the basin fill of a selected basin—the Broad Fourteens Basin—to important aspects of its geological, geothermal and climatic evolution and an understanding of this response for the evolution of the oil and gas systems in the basin;
4. A time framework for petroleum generation, migration, accumulation and preservation along a 2D cross-section in the Broad Fourteens Basin.

Specific research questions that are addressed in the thesis include:

1. What are the main forces and processes that influenced, directly or indirectly, the hydrogeological, pore pressure and fluid flow conditions during the evolution of onshore and offshore Netherlands since the Late Carboniferous?
2. What was the temporal and spatial distribution of these forces and processes?
3. Could any of these processes have induced significant overpressuring of the subsurface in past or present?
4. Are there any indications of distinct phases of increased fluid flow?
5. What is the pattern of paleo fluid flow in the Broad Fourteens Basin (paleo flow of groundwater and petroleum)?
6. What causes the differences in observed geochemical compositions of oil accumulations in Broad Fourteens Basin?
7. Where did all the gas go in the Broad Fourteens Basin?

The unifying approach of the thesis is the analysis of the evolution of fluid flow systems on geological timescales. The analysing procedure is based on the premise that geodynamics and climate are the major external mechanisms influencing the hydrogeological and hydrodynamic evolution of a sedimentary basin and with the concept of fluid flow system as mechanism linking intrabasinal processes. In the analysis, the evolution of fluid flow systems was reconstructed in relation to the major external and internal processes operating on the basin fill of onshore and offshore Netherlands. The various present-day manifestations of paleo and present-day fluid flow in the Netherlands subsurface were used to verify this evolution of fluid flow systems and to identify distinct periods of permeability alterations and distinct

periods of fluid flow. The resulting conceptual model of the evolution of the geology, hydrogeology and fluid dynamics provided the basic understanding of the complexity of fluid flow evolution in onshore and offshore Netherlands. The conceptual model and the compiled database of present-day fluid and rock characteristics allowed the selection of a subbasin (the Broad Fourteens Basin) for subsequent more detailed analysis. In the second research phase the same analysing procedure was applied to the Broad Fourteens Basin and resulted in a powerful conceptual model that steered subsequent quantitative analysis of fluid flow evolution by 2D basin modelling. This 2D basin modelling was used to acquire more quantitative understanding of the evolution of the coupled processes of sedimentation/uplift/erosion, heat transport, groundwater flow, maturation of source rocks, and generation, migration and accumulation of petroleum.

The three parts of the thesis treat the analysis of fluid flow evolution in increasing detail. The analysis is applied to onshore and offshore Netherlands (Part 1) and the Broad Fourteens Basin (Parts 2 and 3). Each Part follows approximately the same systematic approach to assess the history of the fluid geology and the fluid dynamics. Because geology is the basis for the analysis, each Part starts with an outline of the geodynamic and geological history. Parts 1 and 2 present the approach for reconstructing the evolution of fluid flow systems based on the analysis and interpretation of a wide variety of data and information (geological, geophysical, thermal, geochemical, hydrochemical) both from published sources and public wells. The data analysis in Part 2 provided both the understanding as well as the input data, boundary conditions and different scenarios required for the 2D basin modelling of the Broad Fourteens Basin treated in Part 3.

## Part 1. Overview of the post-Carboniferous hydrogeohistory of onshore and offshore Netherlands

Part 1 addresses the general objectives 1 and 2 and the specific research questions 1 - 4. It gives an overview of the characteristic features of the external and internal processes acting on the sedimentary fill of onshore and offshore Netherlands and their role in shaping the hydrogeological and hydrodynamic setting of the Netherlands from Late Carboniferous to the present day. The main mechanical and thermal forces and processes controlling the fluid dynamic and permeability conditions of the sedimentary fill of the Netherlands during six main phases of evolution (Variscan, pre- and early rift, main syn-rift, post-rift, main syn-inversion, and post-inversion) identified, are: topography of the water table, sedimentary loading, erosional unloading, tectonic compression and extension, and, to a minor extent, heating and cooling, and ice loading and unloading:

- **Topography of the water table.** It was found that the only time period without any subaerial exposure and hence without any topography-induced flow was the post-rift period. The reconstructed history of subaerial exposure indicates that supra-regional topography-induced flow systems with recharge areas in the highs located south of the Netherlands border could have been active repeatedly and for prolonged periods of time: e.g. during the Permian, the main syn-rift period and from Miocene to present day. Geological history suggests that regional flow systems with recharge areas in onshore and offshore Netherlands could develop in distinct intrabasinal highs, such as the main syn-rift highs, the Late Cretaceous

inverted basins, and the Southern Early Tertiary High. In Quaternary times, local and regional groundwater flow systems developed in onshore and offshore Netherlands in addition to the supraregional Ardenno-Rhenish groundwater flow system.

- **Sedimentary loading.** Calculated average long-time sedimentation rates did not exceed 100 m/My during most of geological history, and the associated groundwater flow was probably in equilibrium with sedimentary loading in much of the sedimentary fill. Periods of high average long time sedimentation rates that may have induced significant overpressures of the pore water occurred in the depocentres of the Southern Permian Basin during Zechstein (140 m/My) and Early Triassic (160 m/My), in Mesozoic basins during the main syn-rift period (220 m/My), and in northern offshore Netherlands during Pliocene-Quaternary times (400 m/My).
- **Erosional unloading.** Three important phases of erosional unloading could be identified: uplift and erosion of Mesozoic highs during the main syn-rift period, uplift and erosion of Mesozoic basins during the syn-inversion period, and Eocene-Oligocene uplift and erosion of the Southern Early Tertiary High.
- **Changes in tectonic stress.** Identified changes in tectonic stress include both long-term gradual changes in tectonic stress regime from an active extensional stress regime (Triassic to Early Cretaceous) towards a compressional stress regime (Late Cretaceous to present-day), short-term stress fluctuations related to distinct rifting pulses (such as Late Jurassic rifting of Mesozoic basins, Late Oligocene to recent rifting of the Roer Valley Graben) and pulse-like changes in compressive stress during e.g. the Late Cretaceous and Eocene-Oligocene. Each of these stress changes might have had a distinct influence on permeability, storativity and fluid dynamics. For example, the long change from an extensional towards a compressional regime had the potential to increase the pressures of the pore water in the sedimentary fill, while active deformation associated with Late Jurassic rifting, Late Cretaceous inversion and Eocene-Oligocene uplift and Late Oligocene to Recent rifting affected fault and fracture permeability, creating permeable pathways for fluids.

The analysis in Part 1 shows that the type, magnitude and areal distribution of the driving forces and processes influencing fluid flow systems changed continuously during the geological evolution of the Netherlands. It also demonstrates that during each phase of basin evolution different forces and processes have acted simultaneously on the fluids, largely because of the differential subsidence and uplift history of the various structural units. During the main syn-rift period, for example, the following mechanisms were active: sedimentary loading, tectonic forces and heating in the Mesozoic basins, topography of the water table and erosional unloading in platform areas and highs, while topography of the water table and, to a minor extent, cooling, operated in the area south and southeast of the Netherlands. Hence, different fluid flow systems have probably coexisted and interacted laterally and vertically in onshore and offshore Netherlands.

Direct and indirect indicators of fluid flow (pressure, sediment-diagenetic minerals, salinity, hydrochemistry, and to a minor extent temperature) were a valuable tool in delineating and characterising present-day and paleo hydrodynamic conditions.

The indicators allowed distinct periods of fluid flow to be identified in each of the main phases of evolution of the Netherlands, with the exception of expected fluid flow induced by sedimentary loading during the post-rift period. The fluid flow events identified showed a qualitative relation with the previously established driving mechanisms for fluid flow derived from geological history.

Measured groundwater overpressures are direct indicators of flow conditions. Analysis of pressure data showed the existence of severely overpressured conditions in pre-Tertiary aquifer-type hydrostratigraphic units (Chalk Group, Central Graben Group, Lower Germanic Trias Group; Upper Rotliegend Group) in the Central North Sea Graben, Step Graben, Terschelling Basin and southwest of the Elbow Spit High. Normal to slightly overpressured conditions were observed in the main aquifer-type hydrostratigraphic units in the Broad Fourteens Basin (Upper Rotliegend Group, Main Buntsandstein Subgroup, Delfland Subgroup, Vlieland Sandstone Formation) and in the Vlieland Sandstone Formation in the West Netherlands Basin. These overpressured conditions in each unit are described in relation to fluid flow through these units. The combined effect of differences in magnitude and duration of Tertiary and Quaternary sedimentary loading and the distribution and sealing capacity of the Zechstein Group might explain the present-day difference between the northern overpressured area and the southern normal to slightly overpressured area.

Finally Part 1 outlines the present-day hydrodynamic setting of onshore and offshore Netherlands, including natural topography-induced flow systems, artificial fluid flow systems, density-induced flow, and fluid flow systems induced by sedimentary loading and associated burial-related processes.

## **Part 2. Fluid flow systems analysis of the Broad Fourteens Basin: conceptual model of its geodynamic and fluiddynamic evolution**

Part 2 focusses on the Broad Fourteens Basin and addresses the general objectives 1 and 2 and the research questions 1 - 4.

The first phase of the Broad Fourteens Basin study involved the analysis and interpretation of a wide variety of publicly available data on rocks and fluids in the basin. It resulted in the identification of the major mechanical processes involved in overpressure and fluid flow evolution in the Broad Fourteens Basin (sedimentary loading and unloading, tectonic compression and extension, topography of the water table) and provided a time framework for the important permeability alterations in the basin and the distinct phases of fluid flow. A number of present-day diagenetic features in the basin point to important permeability alterations during Late Jurassic rifting and Late Cretaceous inversion, and others clearly indicate distinct periods of paleo fluid flow, namely: 1. Early to syn-rift period: expulsion of CO<sub>2</sub>-rich water from the Limburg Group; 2. Syn-rift period: hydrothermal flow along faults, expulsion of potassium-rich water from the Zechstein and/or Limburg Group; 3. Syn-inversion period: expulsion of sulfate-rich water from the Zechstein Group evaporites and Limburg Group; 4. After 90 Ma: flushing and flow of oxygen-rich water of meteoric origin through the Vlieland Sandstone Formation. Data analysis provided different scenarios to explain observed features in the basin. Part 2 includes an outline of the conceptual model of the geodynamic and fluiddynamic evolution of the Broad Fourteens Basin for four important phases of basin evolution.



Data analysis allowed the characterisation of the Broad Fourteens Basin, including the present-day geological and hydrogeological framework, temperature and heat flow distribution, distribution of groundwater pressures, distribution of hydrochemical properties, and distribution and characteristics of petroleum accumulations:

- **Hydrogeological framework.** Identified important characteristics of the sedimentary fill controlling fluid flow conditions are the dominance of shaly deposits of poor matrix permeability in the basin and the occurrence of Zechstein Salt Members of very poor permeability in the central and northern parts of the basin. The lateral continuity of pre-Tertiary hydrostratigraphic units is restricted by the numerous faults in the basin. Lateral continuity in the northern part of the basin is also affected by the presence of salt diapirs. In much of the basin the pre-rift, early-rift and syn-rift sequences are not at their maximum depth of burial due to the previous inversion of the basin and show signs of overcompaction. Fracture permeability affects the overall permeability of the hydrostratigraphic units in the basin. Based on the distribution of Zechstein Salt Members, the basin can be subdivided hydrogeologically in a northern area where the Zechstein Group is laterally and vertically sealing the hydrostratigraphic units, and a southern area where the Zechstein Group is increasingly clastic and as a consequence less sealing.
- **Temperatures.** The present-day temperature gradient of the Broad Fourteens Basin, based on the published data and sediment-water interface temperature of 8 °C, was calculated at approximately 32 °C/km. Heat flow calculations indicated a relatively low heat flow in the shallow parts of the basin and heat flows increasing with depth.
- **Groundwater pressures and chemical compositions.** The published pressure data indicated near-hydrostatic to slightly overpressured conditions in reservoir units at depths exceeding 1200 m. No pressure data were available for poorly permeable units. The composition of water samples revealed that groundwaters of Upper Permian to Lower Cretaceous hydrostratigraphic units are chloride-dominated type brines. The salinity of the water showed large variations in all units.
- **Oil and gas.** It was observed that most oil and gas accumulations are located along the margins of the basin. Four oil fields in block Q1 contain waterwashed and biodegraded oils.

The nature and distribution of the presented characteristics of the basin also revealed the need for additional information on specific rock and fluid properties and in addition gave rise to various questions concerning the origins of the identified characteristics. These questions were addressed in Part 3.

### Part 3. Fluid flow systems analysis of the Broad Fourteens Basin: results of integrated 2D basin modelling

This final part of the thesis discusses the quantitative analysis of fluid flow systems on geological timescales and addresses the general objectives 3 and 4 and the research questions 3 - 7.

The Temispack 2D basin modelling package was used to quantify, date and time the coupled processes of sedimentation/uplift/erosion, heat transport, groundwater flow,

maturation of source rocks, and generation, migration and accumulation of petroleum during the development of the basin, along a SW-NE cross-section through the southern part of the Broad Fourteens Basin.

The favoured modelling scenario for simulating the evolution of the groundwater and petroleum systems includes sedimentary loading, erosional unloading, topography of the water table and generation of gas as the pressure-influencing mechanisms. Among the factors it takes into account are time-dependent changes in basal heat flow for the basal thermal boundary condition and the evolution of the sediment-water interface temperature (incorporating a detailed evolution sediment-water interface temperature from Pliocene to recent) as the top thermal boundary condition. It also incorporates the dynamic permeability of fault zones. The integrated basin modelling provided quantitative insight into a number of key aspects of the histories of temperature and heat flow, the maturation and petroleum generation from the oil-prone Posidonia Shale Formation and Aalburg Formation and gas-prone Limburg Group source rocks, the pore pressures and groundwater flow, and the petroleum expulsion, migration and accumulation in the southern part of the Broad Fourteens Basin. It was recognised that the basin modelling did not incorporate all the processes and forces influencing the pore pressure, fluid geology and fluid dynamics in the Broad Fourteens Basin identified in Part 2; for example it did not include tectonic compression and chemical compaction. The results of the basin modelling presented in Part 3 do not provide evidence that these processes have no influence on e.g. pore pressures or fluid flow.

Important findings of the modelling are:

- The occurrence of lateral and vertical variations in heat flow along the cross-section at different times during basin history. These variations could be related to differential vertical displacements of the basin and the evolution of the temperature at the surface and bottom boundary; e.g. the contrasting uplift and subsidence histories of the central part of the basin and the northern platform during the main syn-rift and the syn-inversion period, resulted in lateral variations in heat flow along the cross-section of approximately 8 mW/m<sup>2</sup>.
- The modelling demonstrated that large differences in the burial histories of the Carboniferous and Jurassic source rocks along the cross-section resulted in very different temperature and maturation histories for the source rocks depending on their structural evolution. As a result, the Limburg Group source rocks in the central and southern part of the cross-section first entered the gas window at the end of early-rift times, while in the northern platform area a first phase of gas generation was reached in the Early Tertiary.
- It provided the time framework for expulsion, migration, and accumulation of oil and gas. Expulsion of gas from the Limburg Group source rocks in the central and southern part of the cross-section started during the main syn-rift period. First expulsion of oil from the Posidonia Shale Formation started at approximately 125 Ma in the central part of the pre-inversion basin. Given – amongst other things – the threshold saturation values controlling initial expulsion from source rocks used in the modelling, it is unlikely that the petroleum expulsion from the source rocks in the Broad Fourteens Basin started later than the modelling predicted. The modelling revealed that present-day oil and gas accumulations were largely charged by migrating and remigrating oil and gas during Late Cretaceous

inversion and Eocene-Oligocene uplift; large part of the previously accumulated hydrocarbons escaped to the atmosphere during inversion especially in the central part of the basin (P6 area); only minor amounts of gas are preserved in e.g. Slochteren Formation and Triassic sandstones in the central part of the basin.

- The results provided a time framework for overpressure generation and dissipation and for groundwater flow, and a characterisation of the permeability framework, pressure system and groundwater system at different times during basin history. The main period of overpressuring induced by sedimentary loading occurred at the end of post-rift times:  $P_{\text{excess}}$  reached 11 MPa in the Limburg Group at burial depths exceeding 5000 m. Sedimentary loading induced bedding-parallel flow of groundwater through permeable hydrostratigraphic units (principally sandstones) at all depths; the bedding parallel flow equilibrated the overpressures in these permeable units. In the inverted part of the basin these overpressures dissipated during Late Cretaceous inversion, because of the combined effect of the absence of sedimentation as a pressure-generating mechanism, decreased rates of gas generation, erosional unloading, a changing geometrical framework and increased permeabilities of the fault zones. Major topography-induced flow systems developed during the syn-inversion period; flow of groundwater was focussed through the Vlieland Sandstone Formation, which is in accordance with observed K-feldspar leaching of this Formation; the focussed flow of groundwater is contemporaneous with oil migration, remigration and accumulation in the Vlieland Sandstone Formation.
- The results of the integrated modelling of the Broad Fourteens Basin clearly illustrated the overall effect of the geodynamic and sedimentary history on the evolution of groundwater and petroleum migration systems along the cross-section and provided a number of illustrations of the interrelations between the two systems; e.g. during basin evolution, the area of maximum overpressure shifted along the cross-section in accordance with changing depocentres.
- It demonstrated that the presence of an – assumed continuous – layer of evaporites in the Zechstein in the northeastern part of the cross-section exerted a major influence on pore pressure build-up, groundwater flow and petroleum migration.
- It showed that – the assigned – dynamic permeability of fault zones did significantly affect the migration and accumulation history of oil and gas.

Forward modelling results of the heat flow system, and the groundwater and petroleum systems in the basin predict the following present-day features:

- A relatively low heat flow in the shallow part of the basin; resulting from Pleistocene surface temperature fluctuations and the relatively high porosities of the Pliocene and Quaternary sediments.
- Temperatures in the Carboniferous and Jurassic source rocks along the cross-section that are lower than the maximum temperatures experienced during previous burial.
- There is no to only minor generation of gas from the Limburg Group source rocks and no to only minor generation of oil from the Posidonia Shale Formation along the cross-section.
- The occurrence of – mild – overpressures is restricted to the poorly permeable deeper parts of the basin, with maximum overpressures in the evaporites of

the Zechstein Group and in the shales of the Limburg Group. The modelling identified Pliocene and Quaternary sedimentary loading as the mechanisms responsible for these present-day overpressures. Today, and during the entire evolution of the basin, no overpressures of  $P_{\text{excess}} > 1 \text{ MPa}$  occur in the shallow parts of the basin (depths to 2000 m).

- Increased fluid flow in the shallow part of the basin related to Pliocene and Quaternary sedimentary loading.
- The model reproduced the two known oil accumulations in the Vlieland Sandstone Formation sealed by the Vlieland Claystone Formation in the P9 and Q1 crestal structures. Additional oil accumulations were predicted in the southern part of the cross-section in the Middle Werkendam Member and in the sandstones of the Delfland Subgroup, and in the central part of the cross-section in the Middle Werkendam Member. The model revealed increased saturations in the sandstones of the Delfland Subgroup at the P6 crestal high, and in the Middle Werkendam Member just north of P6.
- Different geochemical compositions of the oils in the Q1 and P9 blocks. Oils in block Q1 were sourced from the early mature to mature Posidonia Shale Formation and were exposed to syn-inversion topography-induced flow of groundwater that may have induced waterwashing and biodegradation. The P9 oil accumulation was sourced from an early mature part of the Posidonia Shale Formation and was probably not affected by waterwashing and biodegradation because of post-inversion charging of the P9 structure.
- No major gas accumulations in the Slochteren Formation; pre-inversion gas accumulations were not preserved during inversion. Two gas accumulations occur in Triassic sandstone-dominated units in structural traps in the southern part of the basin.

It should be realised that the above findings are the outcome of 2D basin modelling and as a consequence their validity depends on the assumptions underlying the modelling programme and on the input parameters and boundary conditions used. Part 3 includes discussions on the main factors that affect the confidence of the basin modelling.

In general Part 3 shows the significance of the combination of a powerful conceptual model with predictive abilities in fluid flow evolution and the integrated use of a wide variety of actual data with basin modelling for a process-based understanding of present-day characteristics of the hydrogeological framework and the fluids.

The approach to study the evolution of groundwater and petroleum systems on geological timescales outlined in Part 2 and 3 for the southern Broad Fourteens Basin can readily be applied to the other basins in onshore and offshore Netherlands, such as the West Netherlands Basin, Roer Valley Graben, Central Netherlands Basin, Vlieland Basin, Central North Sea Graben and Terschelling Basin. The general evolution of the Broad Fourteens Basin and these basins show important similarities; e.g. all basins are inverted Mesozoic basins that contain gas-prone Limburg Group source rocks and oil-prone Jurassic source rocks. However, the timing and intensity of the geological events, such as subsidence and sedimentation and uplift and erosion, were different for each basin. The present-day characteristics of rocks

and fluids in the basins reflect these differences (Part 1). Part 1 provides the general fluid dynamics context for the analysis of fluid systems in the sedimentary basins of the Netherlands.

The onshore and offshore Netherlands are mature exploration areas for gas and oil. Over the past few decades seismic surveys, measurements in exploration and production wells and measurements on core samples have resulted in a large amount of data and information on the rock matrix and the subsurface fluids. An increasing number of quality-controlled geoscientific data and information on the Netherlands subsurface is becoming available for geoscientific research. This thesis shows that the analysis of fluid flow systems on geological time scales – including the application of basin modelling – allows the integrated interpretation of such a wide variety of data and information. Hence, the analysing procedure is very well suited for application in mature areas. Here it may be used for detailed studies to identify and evaluate e.g. new exploration concepts as well as for obtaining a better theoretical understanding of fluid flow systems on geological time scales to be applied subsequently in less explored areas.

# Analyse van vloeistofstromingsystemen op geologische tijdschaal in Nederland en het Nederlandse deel van het Continentale Plat; met speciale aandacht voor het Breeveertien Bekken

## Samenvatting

Dit proefschrift betreft de resultaten van onderzoek naar de ontwikkeling van vloeistofstromingsystemen op geologische tijdschaal in de ondergrond van het vasteland van Nederland en van het Nederlandse gedeelte van de Noordzee. Het onderzoek is primair gericht op grondwaterstromingssystemen en in tweede instantie op petroleumsystemen.

Het inleidend hoofdstuk 1 besteedt uitgebreid aandacht aan de doelstellingen en de aanpak van het onderzoek en beschrijft beknopt de concepten betreffende grondwaterstroming op geologische tijdschaal die zijn toegepast in het onderzoek.

De fysisch-chemische eigenschappen van gesteenten en vloeistoffen in een sedimentair bekken veranderen voortdurend in de loop van de geologische geschiedenis. Grondwater vormt een belangrijke schakel tussen de verschillende geodynamische, geothermische en geochemische processen die plaatsvinden in een sedimentair bekken. Kennis van grondwatersystemen op bekken-schaal biedt een raamwerk om deze processen te bestuderen en maakt een geïntegreerde interpretatie mogelijk van de fysisch-chemische eigenschappen van gesteente en grondwater. De evolutie van grondwaterstromingsystemen op geologische tijdschaal in een sedimentair bekken bepaalt mede de ontwikkeling van petroleumsystemen in zo'n bekken. Grondwaterstroming beïnvloedt, bijvoorbeeld via zijn invloed op de drukverdeling in de ondergrond, de processen van petroleummigratie en -accumulatie, en heeft, via zijn effect op compactie en sedimentdiagenese, ook invloed op de reservoirkwaliteit.

Kennis met betrekking tot de evolutie op geologische tijdschaal van grondwaterstromingsystemen in Nederland en het Nederlandse deel van het Continentale Plat was tot dusverre beperkt. De nieuwe kennis betreffende de evolutie op geologische tijdschaal van grondwaterstromingsystemen is met name van belang voor de opsporing en winning van aardolie en aardgas, en tevens voor een evenwichtige evaluatie van duurzame opslagmogelijkheden van energie-residuen en chemisch afval in de ondergrond.

De drie prioritaire doelstellingen van het onderzoek zijn:

1. Verschaffen van een algemene karakterisatie van de huidige hydrogeologische opbouw, de hydrodynamische toestand en de relevante fysisch-chemische eigenschappen van grondwater op bekken-schaal in het onderzoeksgebied;

2. Verschaffen van inzicht in de invloed van belangrijke aspecten van, met name, de geologische ontwikkeling van Nederland op de hydrogeologische en hydrodynamische ontwikkeling; dit mede in relatie tot de ontwikkeling van petroleumsystemen;
3. Verschaffen van een kwantitatief inzicht in de ontwikkeling in de tijd van petroleumsystemen in een geselecteerd sedimentair bekken.

Daar vloeistofstroming op geologische tijdschaal – ten tijde van de start van het onderzoek – een voor Nederland nieuw type onderzoek betrof, waren er een reeks van onderzoeksvragen die voor het bereiken van deze doelstellingen beantwoord dienden te worden. Onderzoeksvragen, waarop in het proefschrift specifiek antwoord gegeven wordt, betreffen:

1. Wat zijn de belangrijkste krachten en invloeden die – direct of indirect – de hydrogeologische eigenschappen, de verdeling van de druk van het grondwater en de grondwaterstroming beïnvloed hebben tijdens de evolutie van de Nederlandse ondergrond vanaf het Carboon;
2. Wat is de verdeling in ruimte en tijd van deze krachten en processen;
3. Is het mogelijk dat een van deze krachten of processen een hoge overdruk van het grondwater veroorzaakt heeft in heden of verleden;
4. Zijn er aanwijzingen voor het voorkomen van actieve grondwaterstroming dan wel petroleummigratie in heden en verleden;
5. Wat zijn de kenmerken van het grondwaterstromingspatroon en van het patroon van petroleummigratie in het Breeveertien Bekken in heden en verleden;
6. Wat is de oorzaak van de waargenomen verschillen in geochemische samenstelling van aardolieaccumulaties in het Breeveertien Bekken;
7. Waar is al het aardgas gebleven dat in het Breeveertien Bekken gegenereerd is in de loop van de geologische geschiedenis.

Voor het beantwoorden van de onderzoeksvragen en het bereiken van de doelstellingen is in eerste instantie een grote verscheidenheid aan geowetenschappelijke data en informatie bewerkt en geanalyseerd. Deze betreffen gepubliceerde geologische, geofysische, geothermische, geochemische, hydrogeologische en petroleumgeologische data en informatie van de Nederlandse ondergrond en vrij beschikbare data en informatie van aardolie- en aardgasboringen. Het 2D bekkenmodelleringsprogramma Temispac is gebruikt om een kwantitatief inzicht te verkrijgen in de ontwikkeling van vloeistofsystemen in relatie tot de geologische evolutie in een geselecteerd deel van het onderzoeksgebied: het Breeveertien Bekken.

Het proefschrift behandelt de resultaten van het onderzoek in drie delen.

### **Deel 1. Overzicht van de hydrogeologische en hydrodynamische geschiedenis van Nederland en het Nederlandse deel van het Continentale Plat vanaf het Carboon tot heden**

Dit deel beschrijft de resultaten van de analyse van de beschikbare geowetenschappelijke data en informatie. Deel 1 draagt bij aan het bereiken van de bovengenoemde doelstellingen 1 en 2, en het beantwoorden van de onderzoeksvragen 1 - 4.

Eerst wordt een overzicht van de geodynamische en geologische geschiedenis van het gebied gepresenteerd voor zes opeenvolgende ontwikkelingsfasen. De onderverdeling in ontwikkelingsfasen is in belangrijke mate gebaseerd op de invloed van de laatste fase van de Varistische orogenese en van twee perioden van tektonische activiteit tijdens het Mesozoïcum: a. De Kimmerische fase (Trias – Vroeg-Krijt) gekenmerkt door rekbewegingen waardoor sneldalende riftbekkens gevormd werden; b. Subhercynische fase gekenmerkt door drukk Bewegingen, die inversie en erosie van de eerder gevormde bekkens tot gevolg hadden. De belangrijkste factoren en mechanismen van invloed op de hydrogeologische en hydrodynamische ontwikkeling konden direct uit de geologische geschiedenis afgeleid worden voor elk van de zes ontwikkelingsfasen. Deze mechanismen zijn sedimentatie, opheffing en erosie, tektonische druk- en rekbewegingen, en het ontstaan van een grondwaterspiegel. Uit de berekende sedimentatiesnelheden blijkt dat relatief hoge sedimentatiesnelheden ( $> 100$  m/My) optraden in het Zuidelijk Perm Bekken tijdens het Zechstein en Vroeg-Trias, in de Mesozoïsche riftbekkens tijdens snelle daling van de bekkens in het Laat-Jura – Vroeg-Krijt, en in de noordelijke helft van het Nederlandse Noordzee Bekken tijdens het Plioceen en Kwartair. Hoge sedimentatiesnelheden kunnen leiden tot het ontstaan van overdruk. Erosie daarentegen zal afname van de druk van het grondwater tot gevolg kunnen hebben. Belangrijke erosiefasen betreffen: opheffing en erosie van de Mesozoïsche hogen tijdens het Laat-Jura en vooral het Vroeg-Krijt, inversie en erosie van Mesozoïsche riftbekkens tijdens het Laat-Krijt – Vroeg-Tertiair, opheffing en erosie van Midden- en West-Nederland tijdens de Tertiaire Pyreneïsche drukfase. Tektonische activiteit van belang voor de hydrodynamische toestand betreffen met name de Laat-Kimmerische fase van riftvorming, de Subhercynische fase van inversie, alsmede de veranderingen in het regionale spanningsregime. Gedurende 5 van de 6 ontwikkelingsfasen heeft het onderzoeksgebied en/of de direct aangrenzende gebieden ten zuiden en zuidoosten van Nederland geheel of gedeeltelijk boven zeeniveau gelegen, zodat neerslag in deze gebieden grondwatersystemen kon voeden. Het gecompileerde overzicht van de geïdentificeerde mechanismen laat zien dat het type, de intensiteit en de ruimtelijke verdeling van de mechanismen voortdurend veranderden in de loop van de geologische geschiedenis. Tevens blijken verschillende mechanismen tegelijkertijd actief geweest te zijn.

De geïnventariseerde huidige eigenschappen van de ondergrond (zoals de verdeling van druk van het grondwater, het voorkomen van sediment-digenetische mineralen, de saliniteit en hydrochemische samenstelling van het grondwater) bleken een belangrijk hulpmiddel bij het identificeren en karakteriseren van de huidige en paleo-hydrodynamische omstandigheden. Zo was het mogelijk om verschillende perioden met actieve grondwaterstroming te identificeren, die gecorreleerd konden worden met de eerder vastgestelde geologische mechanismen. De huidige drukgegevens van het grondwater leverden inzicht in de regionale verdeling van overdruk in de belangrijkste watervoerende hydrostratigrafische eenheden, c.q. reservoir-eenheden. Significante overdruk komt voor in de reservoir-eenheden van pre-Tertiaire ouderdom in de Centrale Noordzee Slenk, de Step Graben, het Terschelling Bekken en ten zuidwesten van het Elbow Spit Hoog (het betreft reservoir-eenheden uit Krijtkalk Groep, Central Graben Subgroep, Onder-Germaanse Trias Groep, Boven-Rotliegend Groep). De verdeling van de overdruk in de afzonderlijke eenheden wordt beschreven in relatie tot grondwaterstroming door deze eenheden. Het verschil in snelheid en



duur van Tertiaire en Kwartaire sedimentatie in combinatie met het verschil in afsluitend vermogen van de Zechstein Groep verschaft een mogelijke verklaring voor het waargenomen verschil tussen significante overdruk in pre-Tertiaire eenheden in het noordoosten van Nederland en noordelijke helft van het Noordzeegebied en weinig of geen overdruk in het gebied ten zuiden van het Texel-IJsselmeer Hoog.

In het laatste hoofdstuk van deel 1 worden de nieuw geïdentificeerde kenmerken van de huidige hydrodynamische toestand van de diepere ondergrond van Nederland en het Nederlands deel van het Continentaal Plat gecombineerd met de reeds eerder bekende natuurlijke en kunstmatige grondwaterstromingssystemen van het vasteland van Nederland.

Op basis van de resultaten van het onderzoek beschreven in deel 1 en de beschikbaarheid van data en informatie is het Breeveertien Bekken geselecteerd voor het uitvoeren van een meer gedetailleerde analyse van vloeistofstromingssystemen op geologische tijdschaal.

## **Deel 2. Analyse van vloeistofstromingssystemen in het Breeveertien Bekken: conceptueel model van zijn geodynamische en vloeistofdynamische ontwikkeling**

Dit deel beschrijft de analyse van vloeistofstromingssystemen met behulp van geowetenschappelijke data en informatie in één van de belangrijkste bekken in het Noordzeegebied. Het eerste hoofdstuk betreft de geodynamische en geologische geschiedenis. De analyse is uitgevoerd ter voorbereiding op de bekkenmodellering beschreven in deel 3. Deel 2 betreft de eerder genoemde doelstellingen 1 en 2 en de onderzoeksvragen 1 - 4.

De mechanismen van belang voor de ontwikkeling van overdruk en vloeistofstroming in het Breeveertien Bekken zijn geïdentificeerd. Daarnaast bleek het ook mogelijk om belangrijke veranderingen in de permeabiliteit van het bekken alsmede perioden van actieve vloeistofstroming vast te stellen. Hierbij waren met name geochemische indicatoren van belang. Belangrijke veranderingen in breukpermeabiliteiten treden op tijdens de tektonische rekfase in het Laat-Jura en tijdens de Laat-Krijt inversie. Geïdentificeerde perioden met actieve vloeistofstroming betreffen: fase van riftvorming (Trias – Laat-Jura): expulsie CO<sub>2</sub>-rijk grondwater uit Limburg Groep; Laat-Jura – Vroeg-Krijtperiode van riftvorming: hydrothermale stroming langs breuken, alsmede expulsie van Kalium-rijk water uit de Zechstein Groep en/of Limburg Groep; Laat-Krijt inversie periode: expulsie van sulfaatrijk grondwater uit evaporieten van de Zechstein Groep en uit Limburg Groep; en in een periode na 90 Ma: stroming van zuurstofrijk water door de Vlieland Zandsteen Formatie.

De analyse van de geowetenschappelijke data en informatie heeft geresulteerd in een karakterisatie van het Breeveertien Bekken met betrekking tot de huidige geologische en hydrogeologische opbouw, de verdeling van temperatuur en warmtedoorvoer, de verdeling van druk, saliniteit en hydrochemie van het grondwater, en eigenschappen van de petroleumvoorkomens.

- **Hydrogeologische opbouw.** Een belangrijk kenmerk van de hydrostratigrafische opbouw betreft het grote percentage slechtdoorlatende lagen in het bekken: in het gehele bekken komen kleistenen en schalies voor van Carboon tot Kwartaire ouderdom; de zeer slechtdoorlatende steenzoutafzettingen van de Zechstein Groep worden in het centrale en noordelijke deel van het bekken aangetroffen. Watervoerende pakketten komen goeddeels overeen met de bekende reservoir-eenheden uit de Boven-Rotliegend Groep (Slochteren Formatie), Zechstein Groep (kalksteen laagpakketten), Onder-Germaanse Trias Groep (zandsteen laagpakketten), Boven-Germaanse Trias Groep (Solling Formatie), Altena Groep (Midden Werkendam Laagpakket), Schieland Groep (zandsteen laagpakketten), Rijnland Groep (Mieland Zandsteen Formatie) en Kwartaire zandpakketten. De permeabiliteiten van deze watervoerende pakketten worden gekenmerkt door zowel matrixpermeabiliteit als ook breukpermeabiliteit. De hydrogeologische opbouw wordt mede bepaald door de vele breuken die het bekken doorsnijden. De hydrostratigrafische eenheden van pre-Tertiaire ouderdom hebben daarom een geringe laterale continuïteit in het bekken. In het noordelijk deel worden de eenheden ook lateraal begrensd door de aanwezige zoutstructuren.
- **Temperatuur.** De berekende huidige temperatuurgradiënt in het bekken bedraagt 32 °C/km. De warmtedoorvoer in het ondiepe deel van het bekken blijkt relatief laag te zijn.
- **Druk.** Informatie betreffende de druk van het grondwater was alleen beschikbaar voor reservoir-eenheden op diepte van meer dan 1200 m. Deze informatie wijst op het bestaan van een overwegend normale (hydrostatische tot een in beperkte mate superhydrostatische) drukverdeling in de reservoir-eenheden.
- **Saliniteit.** Het grondwater in de reservoir-eenheden van Boven-Rotliend tot Onder-Krijt is een brijn met chloride als belangrijkste anion. Het zoutgehalte vertoont zeer grote variatie in alle reservoir-eenheden.
- **Aardolie en aardgas.** De bekende aardolie- en aardgasvoorkomens – behorende tot respectievelijk het Jura aardoliesysteem en het Carboon aardgassysteem – liggen langs de randen van het bekken. Vier aardolievoorkomens in het blok Q1 bevatten olie die sporen vertonen van biodegradatie en uitspoeling.

De analyse van de geowetenschappelijke data en informatie heeft geresulteerd in een conceptueel model van de geologische en vloeistofdynamische ontwikkeling van het Breeveertien Bekken en in verschillende scenario's om de huidige eigenschappen van gesteenten en vloeistoffen in het bekken (met name drukverdeling, temperatuurverdeling, locatie en eigenschappen van petroleumvoorkomens) te kunnen verklaren.

### Deel 3. Analyse van vloeistofstromingssystemen in het Breeveertien Bekken: resultaten van een geïntegreerde 2D bekkenmodellering

Het Temispack 2D bekkenmodelleringprogramma (versie 2.5 en 2.6) is gebruikt om de in deel 2 geïdentificeerde mechanismen die de vloeistofgeologische en vloeistofdynamische ontwikkeling van het Breeveertien Bekken beïnvloeden, geïntegreerd te kunnen bestuderen. Deel 3 draagt bij aan het bereiken van de bovengenoemde doelstellingen 3 en 4, en het beantwoorden van onderzoeksvragen 3 - 7.

De bekkenmodellering is toegepast op een zuidwest-noordoost profiel door het zuidelijke deel van het Breeveertien Bekken. Het was mogelijk de invloed te bestuderen van daling en sedimentatie, compactie, opheffing en erosie, en de ontwikkeling van een grondwaterspiegel op de ontwikkeling van de druk van het grondwater en de grondwaterstroming, alsmede – in combinatie met warmte-transport – op de ontwikkeling van maturatie van petroleummoedergesteenten, en de generatie, migratie en accumulatie van petroleum. Na evaluatie van verschillende modelleringsscenario's, waarbij het conceptuele model van het Breeveertien Bekken (deel 2) een sturende invloed had, is gekozen voor toepassing van een modelleringsscenario, waarin o.m. dynamische permeabiliteit van breuken een rol speelt. Deel 2 verschaft een gedetailleerd inzicht in de gebruikte parameters en randvoorwaarden.

### Grondwatersysteem

Resultaten van de bekkenmodellering illustreren duidelijk het effect van de geodynamische en sedimentatiegeschiedenis op de ontwikkeling van overdruk in het bekken. Gedurende de loop van de geologische geschiedenis verplaatsen de gebieden met maximale overdruk zich langs het profiel overeenkomstig de verplaatsing van de depocentra. De maximale overdruk gerelateerd aan de invloed van sedimentatie treedt op in het diepste deel van het bekken na een langdurige periode van sedimentatie vlak voor de Laat-Krijt inversie. De modellering laat zien dat het proces van sedimentatie laterale stroming van grondwater door watervoerende eenheden tot gevolg heeft op alle dieptes in het bekken. Deze laterale stroming minimaliseert de overdrukverschillen in deze eenheden. Tijdens de Laat-Krijt inversie blijkt de overdruk in het bekken te verdwijnen; dit zowel onder invloed van erosie, alsook door de veranderende geometrische opbouw van het bekken en de verhoogde permeabiliteit van de breukzones. Het verloop van de grondwaterspiegel in het – tijdens de inversie – boven zeeniveau gelegen Breeveertien Bekken induceert een actieve laterale grondwaterstroming door de Vlieland Zandsteen Formatie; deze gesimuleerde grondwaterstroming is in overeenstemming met de waargenomen uitloging van Kalium-veldspaat in deze formatie. De resultaten van de modellering tonen de gevolgen van de toegenomen sedimentatiesnelheden in het Pliocen en Kwartiair op het grondwaterstromingssysteem: een toename van grondwaterstroming in het ondiepe deel van het bekken, alsmede de ontwikkeling van – een geringe – overdruk in de diepgelegen slechtdoorlatende eenheden (schalies van de Limburg Groep, evaporieten van de Zechstein Groep).

### Petroleumsysteem

2D bekkenmodellering is gebruikt om de ontwikkeling van het Carboon aardgassysteem en Jura aardoliesysteem te onderzoeken. Resultaten van de modellering laten grote verschillen zien in het verloop van de temperatuur, de maturatie en petroleumgeneratie en de migratie van petroleum. Deze verschillen konden gerelateerd worden aan de grote verschillen in begravingsgeschiedenis langs het gemodelleerde profiel. In het centrale en zuidelijke deel van het profiel heeft het Carboon het meeste gas al gegenereerd voor de Laat-Krijt inversie. Echter op het platform, ten noordoosten van het bekken, vindt een eerste fase van gasgeneratie plaats in het Vroeg-Tertiair. Modelberekeningen wijzen er op dat er geen belangrijke gasvoorkomens bewaard gebleven zijn in de Slochteren Formatie langs het profiel. Remigratie en vervolgens

migratie naar het oppervlak tijdens de inversie verklaart in belangrijke mate deze afwezigheid van gasvoorkomens. Mogelijk zijn nog wel gasaccumulaties bewaard gebleven in Trias zandstenen in het zuidwestelijk deel van profiel. De belangrijkste fase van oliegeneratie vond plaats in het centrum van het bekken vóór de Laat-Krijt inversie. In het zuidelijk deel van het bekken is het Vroeg-Tertiair een belangrijke periode van oliegeneratie. Modelresultaten voorspellen de aanwezigheid van aardolievoorkomens in de Vlieland Zandsteen Formatie in de P9 en Q1 blokken; dit is in overeenstemming met de locatie van reeds bekende olievelden. Tevens worden additionele olievoorkomens voorspeld in de zandstenen van het Midden Werkendam Laagpakket en zandstenen van de Delfland Subgroep.

De uitkomsten van de modellering bieden een verklaring voor de verschillen in geochemische samenstelling van de aardolie in de blokken P9 en Q1. De in blok Q1 geaccumuleerde aardolie bestaat uit, tijdens inversie geremigreerde, olievoorkomens die voorheen gedurende langere tijd aangevuld werden met olie uit het vroegrijpe tot rijpe aardoliemoedergesteente (Posidonia Schalie). Tijdens de inversie stroomde grondwater van meteorische origine door de Vlieland Zandsteen Formatie en zal daar in contact gekomen zijn met de olievoorkomens; grondwaterstroming bevordert biologische afbraak en uitspoeling van aardolie. De aardolievoorkomens in P9 zijn afkomstig uit een vroegrijp deel van de Posidonia Schalie. Deze olievoorkomens zijn waarschijnlijk niet aangetast door biodegradatie en uitspoeling, omdat die zijn gevormd ná de belangrijke inversiefase.

De belangrijkste mechanismen die het aardolie- en aardgassysteem in het Breeveertien Bekken beïnvloeden in de loop van de geologische geschiedenis, zijn samengevat in 'gas and oil system events charts'. Deze schema's zijn een combinatie van de resultaten van de gegevensanalyse en de resultaten van de bekkenmodellering. In vergelijking met standaard 'events charts' bevatten deze ook de hydrogeologische en hydrodynamische aspecten die van belang zijn om de geschiedenis van petroleumssystemen te kunnen evalueren.

Niet alle geïdentificeerde geologische mechanismen van invloed op vloeistofstromingssystemen konden m.b.v. het bekkenmodelleringprogramma bestudeerd worden (zoals tektonische drukbewegingen en chemische compactie). Deel 3 bevat een discussie met betrekking tot belangrijke factoren die de betrouwbaarheid van de modelresultaten beïnvloeden.

Deel 3 demonstreert het belang van het gebruik van een ver ontwikkeld conceptueel model met betrekking tot de evolutie van vloeistofstromingssystemen – gebaseerd op een analyse van zowel zoveel mogelijk alsook een grote verscheidenheid aan data en informatie – in combinatie met een geïntegreerde bekkenmodellering, teneinde de huidige eigenschappen van de gesteenten en van de vloeistoffen te kunnen verklaren. De methodiek die ontwikkeld is voor de analyse van de evolutie van grondwater- en petroleumssystemen op geologische tijdschaal in het Breeveertien Bekken (Deel 2 en Deel 3), kan worden toegepast op de andere sedimentaire bekkens in Nederland. Deel 1 verschaft de algemene hydrodynamische context voor dergelijk onderzoek.

De afgelopen tientallen jaren zijn – in verband met de opsporing en winning van aardolie en aardgas – vele seismische onderzoeken, metingen in exploratie- en productieputten, en metingen aan kernen uitgevoerd in Nederland. Deze hebben een grote hoeveelheid geowetenschappelijke data en informatie opgeleverd met betrekking tot de eigenschappen van gesteenten en vloeistoffen. In toenemende mate komen hiervan op kwaliteit gecontroleerde data en informatie voor onderzoek beschikbaar. In dit onderzoek is aangetoond dat de systeembenadering voor analyse van grondwaterstroming op geologische tijdschaal, met inbegrip van toepassing van bekkenmodellering, de geïntegreerde interpretatie van zo'n grote verscheidenheid aan data en informatie mogelijk maakt. Deze benadering is met name geschikt om onderzoek uit te voeren teneinde bijvoorbeeld nieuwe concepten voor opsporing van olie en gas te identificeren en te evalueren. Tevens kan het hierbij verkregen theoretische inzicht in het gedrag van grondwater en petroleum op geologische tijdschaal vervolgens gebruikt worden in nieuwe exploratiegebieden waar nog weinig geowetenschappelijke data en informatie beschikbaar zijn.

---

## Acknowledgements

The research presented in this thesis started in 1995 and was largely carried out at the Netherlands Institute of Applied Geoscience TNO – *National Geological Survey* and – during 1997 - 2001 – also at the Centre of Hydrology of Utrecht University (ICHU).

Before the start of the research my promotor Prof. dr Sierd Cloetingh (Vrije Universiteit Amsterdam) introduced me into the fascinating world of formation and evolution of sedimentary basins. My research on fluid flow systems on geological timescales benefited from the acquired knowledge on these large-scale processes. I gratefully acknowledge his continuous confidence and support from the early phases of the research onward. I also thank my promotor Prof. dr Jacobus de Vries for his support during the final phase of thesis preparation.

For the pleasant atmosphere and co-operation I am grateful to my colleagues at TNO-NITG – especially the section Geo-Energy Mapping and Systems under the friendly guidance of Drs Henk Pagnier – and to my former colleagues at Utrecht University, in particular my roommate Dr Hans Peter Broers.

My special thanks go to my colleague and roommate at TNO-NITG for many years, Ir. Erik Simmelink for his great help and enthusiastic co-operation during the basin-modelling phase of the Broad Fourteens Basin research. Former colleague Drs Mark Geluk and Nora Parker are thanked for the fruitful discussions on the geology of the Netherlands. Carla Elmers is kindly acknowledged for providing the seismic section of the Broad Fourteens Basin. Dr Petra David and Kathrin Reimer are thanked for their analysis and interpretation of source rock and oil samples. I thank former colleague Dr Ronald van Balen for contributing the reconstruction by tectonic forward modelling of the heat flow history along the cross-section of the Broad Fourteens Basin.

I gratefully acknowledge the members of the reading committee of the thesis, Dr Claus Otto (CSIRO Petroleum, Australia), Dr Frédéric Schneider (Institut Français du Pétrole, France), Dr József Tóth (Professor Emeritus, University of Alberta, Canada), Dr Ronald van Balen (Vrije Universiteit Amsterdam) and Dr Ide van der Molen (Nederlandse Aardoliemaatschappij B.V.) for their thoughtful and constructive comments and suggestions. Dr Henk Kooi (Vrije Universiteit Amsterdam) is thanked for his constructive criticism.

I am grateful to Dr Joy Burrough for her detailed advice to improve the English text.

Furthermore I would like to thank André Koers and Roel van der Kraan for preparing the figures and Jos Rietstap Vormgeving for the final versions of the figures and the beautiful lay-out of the thesis.

Working at home – hidden behind the computer and between piles of papers on my desk and on the floor – Hessel, Eveline and Laurens approached me with continuous indulgence for many years: the completion of this thesis would not have been possible without their understanding, moral support and love.

## References

- Adams, J.J. and Bachu, S. 2002. Equations of state for basin geofluids: algorithm review and intercomparison for brines. *Geofluids* 2, 257 - 271.
- Ahisan, A., Karlsen, D.A. and Patience, R.L. 1997. Petroleum biodegradation in the Tertiary reservoirs of the North Sea. *Marine and Petroleum Geology* 14, 55 - 64.
- Al-Aasm, I.S., Scotchman, I.C. and Verweij, J.M. (eds) 2002. *Marine and Petroleum Geology* 19 (no. 3). Thematic set on origins, characterization and significance of fluids in sedimentary basins, 207 - 388.
- Ames, R. and Farfan, P.F. 1996. The environments of deposition of the Triassic Main Buntsandstein Formation in the P and Q quadrants, offshore the Netherlands. In: Rondeel, H.E., Batjes, D.A.J. & Nieuwenhuijs, W.H. (eds) 1996. *Geology of gas and oil under the Netherlands*. Kluwer Academic Publishers, Dordrecht, the Netherlands, 167 - 178.
- Anthor, J.E. and Okkerman, J. 1998. Influence of early-diagenesis on reservoir quality of Rotliegende sandstones, Northern Netherlands. *AAPG Bulletin* 82, 2246 - 2265.
- Andrews-Speed, C.P., Oxburgh, E.R. and Cooper, B.A. 1984. Temperatures and depth-dependent heat flow in western North Sea. *AAPG Bulletin* 68, 1764 - 1781.
- Bachu, S. 1995. Flow of variable-density formation water in deep sloping aquifers: review of methods of representation with case studies. *Journal of Hydrology* 164, 19 - 39.
- Baldwin, B. and Butler, C.O. 1985. Compaction curves. *AAPG Bulletin* 69, 622 - 626.
- Barker, C. 1972. Aquathermal pressuring: role of temperature in the development of abnormal pressure zones. *AAPG Bulletin* 56, 2068 - 2071.
- Barson, D., Rakhit, K., Groves-Gidney, M., Bathurst, P. and Standley, B. 1997. Present and paleo hydrodynamic petroleum migration patterns in the Chalk, Central Graben, North Sea. Paper presented at The AAPG Hedberg Conference 'Applied hydrogeology in petroleum exploration', Banff, Alberta, Canada, July 27 - 30, 1997.
- Bayer, U., Lünenschloß, B., Negendank, J.F.W. and Springer, J. 1995. Modellierung der geologischen Entwicklung und der Temperaturgeschichte in Variszidenvorland und an der variszischen Front. Scientific Technical Report STR 95/27, Geoforschungszentrum Potsdam, Germany, 104 p.
- Bayer, U., Lünenschloß, B., Springer, J. and Von Winterfeld, C. 1996. Thermal modeling at an ancient orogenic front with special regard to the uncertainty of heat-flow predictions. In: Förster, A. and Merriam, D.F. (eds). *Geologic modeling and mapping*. Plenum Press, New York and London, 79 - 93.
- Beck, A.E. 1988. Methods for determining thermal conductivity and thermal diffusivity. In: Haenel, R., Rybach, L. and L. Stegena (eds). *Handbook of terrestrial heat-flow density determination*. Kluwer Academic Publishers. Dordrecht, 87 - 124.
- Bethke, C.M. 1985. A numerical model of compaction-driven groundwater flow and heat transfer and its application to the paleohydrology of intracratonic sedimentary basins. *Journal of Geophysical Research* 90, B8, 6817 - 6828.
- Bethke, C.M. 1986. Hydrologic constraints on the genesis of the Upper Mississippi Valley mineral district from Illinois basin brines. *Economic Geology* 81, 233 - 249.
- Bethke, C.M. 1986b. Inverse hydrologic analysis of the distribution and origin of Gulf Coast-type geopressed zones. *Journal of Geophysical Research* 91, B6, 6535 - 6545.
- Bethke, C.M. 1989. Modeling subsurface flow in sedimentary basins. *Geologische Rundschau* 78/1, 129 - 154.
- Bethke, C.M. and Marshak, S. 1990. Brine migrations across North America - The plate tectonics of groundwater. *Annual Review of Earth and Planetary Sciences* 18, 287 - 315.
- Bjørlykke, K. and Hoeg, K. 1997. Effects of burial diagenesis on stresses, compaction and fluid flow in sedimentary basins. *Marine and Petroleum Geology* 14 (no.3), 267 - 276.
- Bjørlykke, K.O. 1989. *Sedimentology and petroleum geology*. Springer Verlag, Berlin, 363 p.
- Bloch, G., Doyle, M., Kukla, P. 1993. Subsurface pressures and leak-off tests in the Netherlands and their implications for prospectivity, safety and well design. Paper presented at the American Association of Petroleum Geologists International Conference and Exhibition, The Hague, the Netherlands, October 17 - 20, 1993.
- Bless, M.J.M., Felder, P.J. and Meessen, J.P.M.T. 1987. Late Cretaceous sea level rise and inversion: their influence on the depositional environment between Aachen and Antwerp. *Ann Soc. Géol. Belgique* 109, 333 - 355.
- Bodenhausen, J.W.A. and Ott, W.F. 1981. Habitat of the Rijswijk oil province, onshore, The Netherlands. In: Illing, L.V. and Hobson, G.D. (eds). *Petroleum geology of the continental shelf of North-West Europe*. Institute of Petroleum, London, 301 - 309.
- Boulton, G.S., Slot, T., Blessing, K., Glasbergen, P., Leijnse, T. and Van Gijsel, K. 1993. Deep circulation of groundwater in overpressured subglacial aquifers and its geological consequences. *Quaternary Science Reviews* 12, 739 - 745.
- Bouw, L. 1999. *Geology, hydrogeology and hydrodynamics of the northern Broad Fourteens, southern North Sea: a conceptual model*. Centre of Hydrology Utrecht (ICHU), Utrecht University, and The Netherlands Institute of Applied Geoscience TNO - National Geological Survey, MSc Thesis, 159 p.
- Bredehoeft, J.D. and Norton, D.L. (eds) 1990. *The role of fluids in crustal processes*. Studies in Geophysics. National Academy Press, Washington D.C., 165 p.
- Bredehoeft, J.D., Back, W. and Hanshaw, B.B. 1982. Regional groundwater flow concepts in the United States: historical perspective. In: Narasimhan, T.M. (ed.). *Recent trends in hydrogeology*. Geological Society of America Special Paper 189, 297 - 316.
- Bredehoeft, J.D., Blyth, C.R., White, W.A. and Maxey, G.B. 1963. A possible mechanism for concentration of brines in subsurface formations. *AAPG Bulletin* 47 no. 2, 257 - 269.
- Bredehoeft, J.D., Djevanshir, R.D. and Belitz, K.R. 1988. Lateral fluid flow in a compacting sand-shale sequence: South Caspian Basin. *AAPG Bulletin* 72, 416 - 424.
- Brun, J.-P. and Nalpas, T. 1996. Graben inversion in nature and experiments. *Tectonics* 15 ( 2), 677 - 687.
- Burgers, W.F.J. and Mulder, G.G. 1991. Aspects of the Late Jurassic and Cretaceous history of the Netherlands. *Geologie en Mijnbouw* 70, no. 4, 347 - 354.
- Burley, S.D. 1993. Models of burial diagenesis for deep exploration in Jurassic fault traps of the Central and Northern North Sea. In: Parker, J.R. (ed.). *Petroleum Geology of Northwest Europe: Proceedings of the 4<sup>th</sup> Conference*. The Geological Society, London, 1353 - 1375.

- Burrus, J. 1997. Contribution à l'étude du fonctionnement des systèmes pétroliers: apport d'une modélisation bi-dimensionnelle. Thèse. École des Mines de Paris. Centre d'Informatique Géologique, Paris, France.
- Burrus, J. 1998. Overpressure models for clastic rocks, their relation to hydrocarbon expulsion: a critical reevaluation. In: Law, B.E., Ulmishek, G.F. and Slavin, V.I. (eds). Abnormal pressures in hydrocarbon environments. AAPG Memoir 70, 35 - 63.
- Burrus, J., Kuhfuss, A., Doligez, B. and Ungerer, P. 1991. Are numerical models useful in reconstructing the migration of hydrocarbons? A discussion based on the Northern Viking Graben. In: England, W.A. and Fleet, A.J. (eds) Petroleum migration. Geological Society Special Publication 59, 89 - 109.
- Caillet, G., Judge, N.C., Bramwell, N.P., L. Meciani, L., Green, M. and Adam, P. 1997. Overpressure and hydrocarbon trapping in the Chalk of the Norwegian Central Graben. *Petroleum Geoscience* 3, 33 - 42.
- Cartwright, J.A. and Lonergan, L. 1996. Volumetric contraction during the compaction of mudrocks: a mechanism for the development of regional scale polygonal fault systems. *Basin Research* 8, 183 - 193.
- Caston, V.N.D. 1977. A new isopachyte map of the Quaternary of the North Sea. *Rep. Inst. Geol. Sci.* 77/11, 3 - 8.
- Cayley, G.T. 1987. Hydrocarbon migration in the Central North Sea. In: Brooks, J. and Glennie, K. (eds). *Petroleum Geology of North West Europe*. Graham and Trotman Ltd., London. 549 - 555.
- Chapman, D.S. and Rybach, L. 1985. Heat flow anomalies and their interpretation. *Journal of Geodynamics* 4, 3 - 37.
- Clauer, N., Zwingman, H. and Chaudhuri, S. 1996. Isotopic (K-Ar and oxygen) constraints on the extent and importance of the Liassic hydrothermal activity in Western Europe. *Clay Minerals* 31, 301 - 318.
- Cloetingh, S., Gradstein, F.M., Kooi, H., Grant, A.C. and Kaminski, M. 1990. Plate reorganization: a cause of rapid late Neogene subsidence and sedimentation around the North Atlantic? *Journal of the Geological Society of London* 147, 495 - 506.
- Collins, A.G. 1975. *Geochemistry of oilfield waters*. Elsevier, Amsterdam, 495 p.
- Connan, J. 1984. Biodegradation of crude oils in reservoirs. In: Brooks, J. and Welte, D.H. (eds). *Advances in petroleum geochemistry*, Vol.1. Academic Press, London, 299 - 335.
- Cornford, C. 1998. Source rocks and hydrocarbons of the North Sea. In Glennie, K.W. (ed.) 1998. *Petroleum geology of the North Sea area*. Basic concepts and recent advances. Fourth edition. Blackwell Science Ltd., Oxford. 376 - 462.
- Cottençon, A., Parant, B. and Flacelière, G. 1975. Lower Cretaceous gas fields in Holland. In: Woodland, A.W. (ed.) *Petroleum and the continental shelf of NW Europe Vol 1 Geology*. Applied Science Publishers Ltd, Barking, England. 403 - 412.
- Crépieux, N., Sacleux, M. and Mathis, B. 1998. Influence of the pressure on the petroleum system. Example from Triassic in the Netherlands Central Graben. In: Mitchell, A. and Grauls, D. (eds). *Overpressures in Petroleum Exploration*. Proceedings of the workshop 7<sup>th</sup> - 8<sup>th</sup> April 1998, Pau, France. Elf Exploration Production Memoir 22, 123 - 131.
- Crouch, S.V., Baumgartner, W.E.L., Houllberg, E.J.M.J. and Walzebuck, J.P. 1996. Developments of a tight gas reservoir by a multiple fracted horizontal well: Ameland-204, the Netherlands. In: Rondeel, H.E., Batjes, D.A.J. and Nieuwenhuis, W.H. (eds) 1996. *Geology of gas and oil under the Netherlands*. Kluwer Academic Publishers, Dordrecht, the Netherlands, 93 - 102.
- Dahlberg, E.C. 1994. *Applied hydrodynamics in petroleum exploration*. 2nd edition. Springer-Verlag, New York, 295 p.
- Daines, S.R. 1982. Aquathermal pressuring and geopressure evaluation. *AAPG Bulletin* 66, 931 - 939.
- Darby, D., Haszeldine, R.S. and Couples, G.D. 1996. Pressure cells and pressure seals in the UK Central Graben. *Marine and Petroleum Geology* 13, 865 - 878.
- Davis, R.W. 1987. Analysis of hydrodynamic factors in petroleum migration and entrapment. *AAPG Bulletin* 71, 643 - 649.
- De Jager, J., Doyle, M.A., Grantham, P.J. and Mabillard, J.E. 1996. Hydrocarbon habitat of the West Netherlands Basin. In: Rondeel, H.E., Batjes, D.A.J. and Nieuwenhuis, W.H. (eds) 1996. *Geology of gas and oil under the Netherlands*. Kluwer Academic Publishers, Dordrecht, the Netherlands, 191 - 209.
- De Jong, M.G.G. and Laker, N. 1992. Reservoir modelling of the Vlieland Sandstone of the Koter Field (Block K18b), offshore. *The Netherlands. Geologie en Mijnbouw* 71, 173 - 188.
- De Marsily, G. 1986. *Quantitative hydrogeology. Groundwater hydrology for engineers*. Academic Press Inc., London, 440 p.
- De Sitter, L.U. 1947. Diagenesis of oil-field brines. *Bulletin of the AAPG*. 31 no 11, 2030 - 2040.
- Deming, D. 1989. Application of bottom-hole temperature corrections in geothermal studies. *Geothermics* 18 (no. 5/6), 775 - 786.
- Deming, D. 1992. Catastrophic release of heat and fluid flow in the continental crust. *Geology* 20, 83 - 86.
- Deming, D. 1994a. Overburden rock, temperature, and heat flow. In: Magoon, L.B. and Dow, W.G. (eds). *The Petroleum system - From source to trap*. AAPG Memoir 60, 165 - 186.
- Deming, D. 1994b. Fluid flow and heat transport in the upper continental crust. In: Parnell, J. (ed.). *Geofluids Origin, migration and evolution of fluids in sedimentary basins*. Geological Society Special Publication 78. The Geological Society, London, 27 - 42.
- Dickey, P.A. 1988. Regional variations in formation water chemistry, Frio Formation (Oligocene), Texas Gulf Coast: discussion. *AAPG Bulletin* 72, 856 - 857.
- Dirkzwager, J.B., Van Wees, J.D., Cloetingh, S.A.P.L., Geluk, M.C., Dost, B., Beekman, F. 2000. Geo-mechanical and rheological modelling of upper crustal faults and their near-surface expression in the Netherlands. *Global and Planetary Change* 27, 67 - 88.
- Dixon, J.E., Fitton, J.G. and Frost, R.T.C. 1981. The tectonic significance of post-Carboniferous igneous activity in the North Sea Basin. In: Illing, L.V. and Hobson, G.D. (eds) 1981. *Petroleum geology of the continental shelf of North-West Europe*. Heyden and Son Ltd/Institute of Petroleum, London, 121 - 137.
- Doligez, B. (ed.) 1987. *Migration of hydrocarbons in sedimentary basins*. 3<sup>rd</sup> IFP Exploration and Production Research Conference. Éditions Technip, Paris, 681 p.
- Domenico, P.A. and Palciauskas, V.V. 1973. Theoretical analysis of forced convective heat transfer in regional groundwater flow. *Geological Society of America Bulletin* 84, 3803 - 3814.
- Domenico, P.A. and Schwartz, F.W. 1990. *Physical and Chemical Hydrogeology*. John Wiley & Sons Inc. New York, 824 p.
- Domenico, P.A. and Schwartz, F.W. 1998. *Physical and Chemical Hydrogeology*. 2<sup>nd</sup> Edition. John Wiley & Sons Inc. New York, 506 p.
- Doornhof, D. 1992. Surface subsidence in the Netherlands: the Groningen gas field. *Geologie en Mijnbouw* 71, 119 - 130.
- Dronkers, A.J. and Mrozek, F.J. 1991. Inverted basins of The Netherlands. *First Break* 9, 409 - 425.



- Dronkert, H. and Remmelts, G. 1993. Influence of salt structures on reservoir rocks in block L-2, Dutch Continental Shelf. Paper presented at the American Association of Petroleum Geologists International Conference and Exhibition, The Hague, the Netherlands, October 17 - 20, 1993.
- Dronkert, H., Nio, S.D., Kouwe, W., Van der Poel, N. and Baumfalk, Y. 1989. Buntsandstein of the Netherlands offshore. International Geoservices, the Netherlands, Reportno EP 890020.
- Du Rouchet, J. 1981. Stress fields, a key to oil migration. AAPG Bulletin 65, 74 - 85.
- Dufour, F.C. 1998. Grondwater in Nederland. Onzichtbaar water waarop wij lopen. Netherlands Institute of Applied Geoscience TNO – National Geological Survey. Utrecht/Delft, the Netherlands, 265 p. (in Dutch).
- Dufour, F.C. 2000. Groundwater in the Netherlands – Facts and figures. Netherlands Institute of Applied Geoscience TNO – National Geological Survey. Utrecht/Delft, the Netherlands, 96 p.
- ECL Exploration Consultants Ltd. 1983. Offshore Netherlands. Petroleum Exploration Appraisal. Volume I. Regional Exploration review.
- Ehrenberg, S.N. 1990. Relationship between diagenesis and reservoir quality in sandstones of the Garn Formation, Haltenbanken, Mid Norwegian Continental Shelf. AAPG Bulletin 74, 1538 - 1558.
- Einsele, G. 1992. Sedimentary basins. Evolution, facies and sediment budget. Springer-Verlag, Berlin, 628 p.
- Elderhorst, W.I.M. and Zijl, W. 1992. Large-scale palaeo-hydrological modelling. TNO Institute of Applied Geoscience, the Netherlands, Report no. OS 92-44C.
- Emery, D. and Robinson, A. 1993. Inorganic Geochemistry: Applications to petroleum geology. Blackwell Scientific Publications, Oxford, 254 p.
- Engelen, G.B. and Kloosterman, F.H. 1996. Hydrological systems analysis: methods and applications. Water Science and Technology Library 20. Kluwer Academic Publishers, Dordrecht, the Netherlands, 152 p.
- England, W.A., Mackenzie, A.S., Mann, D.M. and Quigley, T.M. 1987. The movement and entrapment of petroleum fluids in the surface. Journal of the Geological Society, London 144, 327 - 347.
- England, W.A., Mann, A.L. and Mann, D.M. 1991. Migration from source to trap. In: Merrill, R.K. (ed.) 1991. Source and migration processes and evaluation techniques. Handbook of petroleum geology. The American Association of Petroleum Geologists, Tulsa, USA, 23 - 46.
- Evans, T.R. and Coleman, N.C. 1974. North sea geothermal gradients. Nature 247, 28 - 30.
- Fertl, W.H. 1976. Abnormal formation pressures. Implications to exploration, drilling and production of oil and gas resources. Developments in Petroleum Science 2. Elsevier, Amsterdam, 382 p.
- Fisher, M.J. and Mudge, D.C. 1998. Triassic. In: Glennie, K.W. (ed.) 1998. Petroleum geology of the North Sea area. Basic concepts and recent advances. Fourth edition. Blackwell Science Ltd., Oxford, 212 - 244.
- Fisher, O.J. and Knipe, R.J. 1998. Fault sealing processes in siliciclastic sediments. In: Jones, G., Fisher, O.J. and Knipe, R.J. (eds) 1998. Faulting, fault sealing and fluid flow in hydrocarbon reservoirs. Geological Society, London, Special Publications, 147, 117 - 134.
- Fleming, C.G., Couples, G.D. and Haszeldine, R.S. 1998. Thermal effects of fluid flow in steep fault zones. In: Jones, G., Fisher, O.J. and Knipe, R.J. (eds.) 1998. Faulting, fault sealing and fluid flow in hydrocarbon reservoirs. Geological Society, London, Special Publications 147, 217 - 229.
- Flemings, P.B., Stump, B.B., Finkbeiner, Th. and Zoback, M. 2002. Flow focusing in overpressured sandstones: theory, and applications. American Journal of Science 302, 827 - 855.
- Fontaine, J.M., Guastella, G., Jouault, P. and De la Vega, P. 1993. F15-A: a Triassic gas field on the eastern limit of the Dutch Central Graben. In: Parker, J.R. (ed) 1993. Petroleum Geology of Northwest Europe: Proceedings of the 4th Conference. The Geological Society, London, 583 - 593.
- Frakes, L.A. 1979. Climates throughout geologic time. Elsevier, Amsterdam, 310 p.
- Frikken, H.W. 1996. CBIL logs: vital for evaluating disappointing well and reservoir performance, K15-FG field, central offshore Netherlands. In: Rondeel, H.E, Batjes, D.A.J. and Nieuwenhuis, W.H. (eds.). Geology of oil and gas under the Netherlands. Kluwer Academic Publishers. Dordrecht, the Netherlands, 103 - 114.
- Frikken, H.W. 1999. Reservoir-geological aspects of productivity and connectivity of gasfields in the Netherlands. Technical University Delft, PhD thesis, 91 p.
- Gaarenstroom, L., Tromp, R.A.J., De Jong, M.C. and Brandenburg, A.M. 1993. Overpressures in the Central North Sea: implications for trap integrity and drilling safety. In: Parker, J.R. (ed.) Petroleum Geology of Northwest Europe: Proceedings of the 4th Conference. The Geological Society, London, 1305 - 1313.
- GAPS Geological Consultants 1991. Lithostratigraphy, sedimentology and reservoir quality of the Rotliegend in the Dutch sector of the Southern North Sea. Volume 1.
- Garven, G. 1985. The role of regional fluid flow in the genesis of the Pine Point deposit. Economic Geology 80, 307 - 324.
- Garven, G. 1995. Continental-scale groundwater flow and geologic processes. Annual Review of Earth Planetary Sciences 23, 89 - 117.
- Garven, G. and Freeze, 1984a. Theoretical analysis of the role of groundwater flow in the genesis of stratabound ore deposits. 1. Mathematical and numerical model. American Journal of Science 284, 1085 - 1124.
- Garven, G. and Freeze, 1984b. Theoretical analysis of the role of groundwater flow in the genesis of stratabound ore deposits. 2. Quantitative results. American Journal of Science 284, 1125 - 1174.
- Gas Atlas 1998: Northwest European Gas Atlas – Composition and isotope ratios of natural gases. CD ROM Netherlands Institute of Applied Geoscience TNO – National Geological Survey.
- Gaupp, R., Matter, A., Platt, J., Ramseyer, K. and Walzebeck, J. 1993. Diagenesis and fluid evolution of deeply buried Permian (Rotliegend) gas reservoirs, Northwest Germany. AAPG Bulletin 77, 1111 - 1128.
- Gauthier, B.D.M., Franssen, R.C.W.M. and Drei, S. 2000. Fracture networks in Rotliegend gas reservoirs of the reservoirs of the Dutch offshore: implications for reservoir behaviour. Geologie en Mijnbouw/Netherlands Journal of Geosciences 79 (1), 45 - 57.
- Ge, S. and Garven, G. 1989. Tectonically induced transient groundwater flow in foreland basin. In: Price, R.A. (ed.). Origin and evolution of sedimentary basins and their energy and mineral resources. Geophysical Monograph 48. IUGG Volume 3, 145 - 157.
- Geluk, M. 1999. Late Permian (Zechstein) rifting in the Netherlands: models and implications for petroleum geology. Petroleum Geoscience 5, 189 - 199.

- Geluk, M.C. and Röhring, H.G. 1997. High-resolution sequence stratigraphy of the Lower Triassic 'Buntsandstein' in the Netherlands and northwestern Germany. *Geologie en Mijnbouw* 76, 227 - 246.
- Geluk, M.C., Duin, E.J.Th., Dusar, M., Rijkers, R.H.B., Van den Berg, M.W. and Van Rooijen, P. 1994. Stratigraphy and tectonics of the Roer Valley Graben. *Geologie en Mijnbouw* 73, 95 - 98.
- Geluk, M.C., Plomp, A. and Van Doorn, Th.H.M. 1996. Development of the Permo-Triassic succession in the basin fringe area, southern Netherlands. In: Rondeel, H.E., Batjes, D.A.J. and Nieuwenhuis, W.H. (eds) 1996. *Geology of gas and oil under the Netherlands*. Kluwer Academic Publishers, Dordrecht, the Netherlands, 57 - 78.
- Geological Survey of the Netherlands and IMNES Investering Maatschappij Nederland Energy Services 1984. Geological sections through the onshore and adjacent part of the continental shelf.
- Geological Survey of the Netherlands RGD 1991 - 1995. Atlas of the Deep Subsurface of the Netherlands. Sheets I-V
- Giesen, M.H. 1995. Een onderzoek naar de akoestische snelheden in de Nederlandse ondergrond on- and offshore. Geological Survey of the Netherlands. Internal Report (in Dutch).
- Giles, M.R., Cocksorth, G.R., Sanchez-Rodriguez, L., Bettembourg, S., Dufour, E., McNutt, J.F., Kukla, P., Indrelid, S.L. and De Jong, M.C. 2000. 4D overpressure modelling and prospectivity. Paper presented at Overpressure 2000 Workshop. Drilling and exploiting overpressured reservoirs: a research workshop for the millennium, London, UK, April 4<sup>th</sup> - 6<sup>th</sup> 2000.
- Giles, M.R., Indrelid, S.L., Kuszniir, N.J., Loopik, A., Meijerink, J.A., McNutt, J., Dijkstra, P., Heidug, W., Totfi, J., Willis, M., Rutten, K., Elsinga, B., Huyse, P., Riviere, P., Bürgisser, H. and Rowley, E. 1999. Charge and overpressure modelling in the North Sea: multi-dimensional modelling and uncertainty analysis. In: Fleet, A.J. and Boldy, S.A.R. (eds). *Petroleum Geology of Northwest Europe: Proceedings of the 5<sup>th</sup> Conference*. The Geological Society, London, 1313 - 1324.
- Glasbergen, P. 1984. Enkele voorbeelden van de grondwaterkwaliteit in paleogene watervoerende lagen. Rijksinstituut voor Volksgezondheid en Milieuhygiëne. Mededelingen 84-1, 31 p. (in Dutch).
- Glennie, K.W. (ed.) 1990. Introduction to the petroleum geology of the North Sea. Third edition. Blackwell Scientific Publications, Oxford, 402 p.
- Glennie, K.W. (ed.) 1998. Petroleum geology of the North Sea area. Basic concepts and recent advances. Fourth edition. Blackwell Science Ltd., Oxford, 636 p.
- Glennie, K.W. and Underhill, J.R. 1998. Origin, development and evolution of structural styles. In: Glennie, K.W. (ed.) 1998. *Petroleum geology of the North Sea area. Basic concepts and recent advances*. Fourth edition. Blackwell Science Ltd., Oxford, 42 - 103.
- Goes, S., Govers, R. and Vacher, P. 2000b. Shallow upper mantle temperatures under Europe from P and S wave tomography. *Journal of Geophysical Resources* 105, 11153 - 11169.
- Goes, S., Loohuis, J.J.P., Wortel, M.J.R. and Govers, R. 2000a. The effect of plate stresses and shallow mantle temperatures on tectonics of Northwestern Europe. *Global and Planetary Change* 27, 23 - 38.
- Gof, L.S. 1996. The Logger oil field (Netherlands offshore): reservoir architecture and heterogeneity. In: Rondeel, H.E., Batjes, D.A.J. & Nieuwenhuis, W.H. (eds) 1996. *Geology of gas and oil under the Netherlands*. Kluwer Academic Publishers, Dordrecht, the Netherlands, 255 - 263.
- Gölke, M. and Coblenz, D. 1996. Origins of the European regional stress field. *Tectonophysics* 266, 11 - 24.
- Goultly, N.R. 1998. Relationships between porosity and effective stress in shales. *First Break* 16, 413 - 1998.
- Graf, D.L. 1982. Chemical osmosis, reverse chemical osmosis, and the origin of subsurface brines. *Geochimica et Cosmochimica Acta* 46, 1431 - 1448.
- Gras, R. 1995. Late Cretaceous sedimentation and tectonic inversion, southern Netherlands. *Geologie en Mijnbouw* 74, 117 - 127.
- Gras, R. and Geluk, M.C. 1999. Late Cretaceous – Early Tertiary sedimentation and tectonic inversion in the southern Netherlands. *Geologie en Mijnbouw* 78, 1 - 19.
- Grauls, D. 1997. Minimum principal stress as a control of overpressures in sedimentary basins. Extended Abstracts. *Geofluids II '97*. Contributions to the Second International Conference on fluid evolution, migration and interaction in sedimentary basins and orogenic belts, Belfast, Northern Ireland, March 10 - 14, 1997, 219 - 222.
- Gvirtzman, H. and Stanislavski, E. 2000a. Large-scale flow of geofluids at the Dead Sea Rift. *Journal of Geochemical Exploration* 69 - 70, 207 - 211.
- Gvirtzman, H. and Stanislavski, E. 2000b. Palaeohydrology of hydrocarbon maturation, migration and accumulation in the Dead Sea Rift. *Basin Research* 12, 79 - 93.
- Hallam, A. 1985. A review of Mesozoic climates. *J. Geol. Soc. London* 142, 433 - 445.
- Hancock, J.M. 1990. Cretaceous. In: Glennie, K.W. (ed.) 1990. *Introduction to the Petroleum Geology of the North Sea*. 3<sup>rd</sup> Edition. Blackwell Scientific Publications, London, 255 - 272.
- Hanor, J.S. 1994. Origin of saline fluids in sedimentary basins. In: Parnell, J. (ed.) *Geofluids: Origin, migration and evolution of fluids in sedimentary basins*. Geological Society Special Publication 78, 151 - 174.
- Hanor, J.S. and Sassen, R. 1990. Evidence for large-scale vertical and lateral migration of formation waters, dissolved salt, and crude oil in the Louisiana Gulf Coast. In: Schumacher, D. and Perkins, B.F. (eds). *Gulf Coast oil and gases: their characteristics, origin, distribution, and exploration and production significance*. Proceedings 9<sup>th</sup> Annual research conference, Gulf Coast section Society of Economic Paleontologists and Mineralogists Foundation, 293 - 296.
- Harland, W.B., Armstrong, R.L., Cox, A.V., Craig, L.E., Smith, A.G. and Smith, D.G. 1990. *A geologic time scale 1989*. Cambridge University Press, 263 p.
- Harrison, W.J. 1990. Modelling fluid/rock interactions in sedimentary basins. In: Cross, T.A. (ed.). *Quantitative dynamic stratigraphy*. Prentice-Hall, Englewood Cliffs, N.J., 195 - 231.
- Harrison, W.J. and Summa, L.L. 1991. Paleohydrology of the Gulf of Mexico Basin. *American Journal of Science* 291, 109 - 176.
- Harrison, W.J. and Tempel, R.N. 1993. Diagenetic pathways in sedimentary basins. In: Horbury, A.D. and Robinson, A.G. (eds). *AAPG Studies in Geology* 36, 69 - 86.
- Harrold, T.W.D., Swarbrick, R.E. and Goultly, N.R. 2000. Overpressure estimation from mudrock porosity and mean effective stress relationships. Paper presented at Overpressure 2000 Workshop. Drilling and exploiting overpressured reservoirs: a research workshop for the millennium, London, UK, April 4<sup>th</sup> - 6<sup>th</sup> 2000.
- Hastings, A., Murphy, P. and Stewart, L. 1991. A multi-disciplinary approach to reservoir characterization: Helm field, Dutch North Sea. In: Spencer, A.M. (ed). *Generation, accumulation and production of Europe's hydrocarbons*. Special Publication of the European Association of Petroleum Geoscientists No. 1, Oxford University Press, Oxford, 193 - 202.

- Hayward, A.B. and Graham, R.H. 1989. Some geometrical characteristics of inversion. In: Cooper, M.A. and Williams, G.D. (eds.). Inversion tectonics. Geological Society Special Publication 44, 17 - 39.
- Heederik, J.P. and Haurdeman, A.J.M. 1988. Geothermal study of the Central Graben (North Brabant); Evaluation of the results of an exploratory geothermal well in Asten. In: Hooghart, J.C. (ed.). Geothermal energy and heat storage in aquifers. TNO Committee on Hydrological Research, The Hague. Proceedings and information No. 40, 77 - 97.
- Hendry, J.P. 1993. Geological controls on regional subsurface carbonate cementation: An isotopic-paleohydrologic investigation of Middle Jurassic Limestones in Central England. In: Horbury, A.D. and Robinson, A.G. (eds). Diagenesis and basin development. AAPG Studies in Geology 36, 231 - 260.
- Herczeg, A.L., Torgersen, T., Chivas, A.R., and Habermehl, M.A. 1991. Geochemistry of ground waters from the Great Artesian Basin, Australia. Journal of Hydrology 126, 225 - 245.
- Hermanrud, C., Cao, S. and Lerche, I. 1990. Estimates of virgin rock temperature derived from BHT measurements: bias and error. Geophysics 55 (no. 7), 924 - 931.
- Herrgreen, G.F.W., Eillebrecht, A.T.J.M., Gortemaker, R.E., Remmelts, G., Schuurman, H.A.H.M. and Verbeek, J.W. 1996. Upper Cretaceous Chalk Group stratigraphy near the isle of Texel, the Netherlands (a multidisciplinary approach). Mededelingen Rijks Geologische Dienst 56, 63 p.
- Heybroek, P. and Van Wijfe, D.H. 1987. Structural interpretation of the subsurface since 1956. In: Visser, W.A., Zonneveld, J.I.S. and Van Loon, A.J. Seventy-five years of geology and mining in The Netherlands. Royal Geological and Mining Society of The Netherlands (KNGMG), The Hague, 259 - 268.
- Hinch, H.H. 1980. The nature of shales and the dynamics of hydrocarbon expulsion in the Gulf Coast Tertiary section. In: Roberts III, W.H. and Cordell, R.J. (eds). Problems of petroleum migration. The AAPG Studies in Geology 10, 1 - 18.
- Hirsch, L.M. and Thompson, A.H. 1995. Minimum saturations and buoyancy in secondary migration. AAPG Bulletin 79, 696 - 710.
- Holm, G.M. 1996. The Central Graben: a dynamic overpressure system. In: Glennie, K. and Hurst, A. (eds). NW Europe's hydrocarbon Industr.Geological Society, London, 107 - 122.
- Hooper, R.J., Goh, L.S. and Dewey, F. 1995. The inversion history of the northeastern margin of the Broad Fourteens Basin. In: Buchanan, J.G. and Buchanan, P.G. (eds). Basin Inversion.Geological Society Special Publication 88, 307 - 317.
- Horst, P. 2000. Geological development during the Tertiary in the Broad Fourteens area. Faculty of Earth Sciences Utrecht University and Netherlands Institute of Applied Geoscience TNO – National Geological Survey, MSc Thesis.
- Houtgast, R.F. and Van Balen, R.T. 2000. Neotectonics of the Roer Valley Rift System, the Netherlands. Global and Planetary Change 27, 131 - 146.
- Hovland, M., Gardner, J.V. and Judd, A.G. 2002. The significance of pockmarks to understanding fluid flow processes and geohazards. Geofluids 2, 127 - 136.
- Hubbert, M.K. 1953. Entrapment of petroleum under hydrodynamic conditions. The AAPG Bulletin 37, 1954 - 2026.
- Hubbert, M.K. and Rubey, W.W. 1959. Role of fluid pressure in mechanics of overthrust faulting. Bulletin of the Geological Society of America 70, 115 - 166.
- Huisman, P., Cramer, W., Van Ee, G., Hooghart, J.C., Salz, H. and Zuidema, F.C. (eds) 1998. Water in the Netherlands. Netherlands Hydrological Society, Delft, the Netherlands, 186 p.
- Hunt, J.M. 1979. Petroleum geochemistry and geology. W.H. Freeman and Company, San Francisco, 617 p.
- Huyghe, P. and Mugnier, J.-L. 1994. Intra-plate stresses and basin inversion: A case from the Southern North Sea. In: Roure, F. (ed.) Peri-Tethyan Platforms. Édition Technip, Paris, 211 - 226.
- Huyghe, P. and Mugnier, J.-L. 1995. A comparison of inverted basins of the Southern North Sea and inverted structures of the external Alps. In: Buchanan, J.G. and Buchanan, P.G. Basin inversion. Geological Society Special Publication 88, 339 - 353.
- Ingebritsen, S.E. and Sandford, W.E. 1998. Groundwater in geologic processes. Cambridge University Press, 341 p.
- Intergeos – International Geoservices BV 1991. Tertiary sequence stratigraphy of the Netherlands.
- Jamtveit, B. and Yardley, B.W.D. (eds) 1997. Fluid flow and transport in rocks. Mechanisms and effects. Chapman and Hall, London, 319 p.
- Japsen, P. 1997. Regional Neogene exhumation of Britain and the western North Sea. Journal of the Geological Society London 154, 239 - 247.
- Japsen, P. 1998. Regional velocity-depth anomalies, North Sea Chalk: a record of overpressure and Neogene uplift and erosion. AAPG Bulletin 82, 2031 - 2074.
- Japsen, P. 1999. Overpressured Cenozoic shale mapped from velocity anomalies relative to a base line for marine shale, North Sea. Petroleum Geoscience 5, 321 - 336.
- Jensenius, J. and Munkgaard, N.C. 1989. Large-scale hot water migration systems around salt diapirs in the Danish Central Trough and their impact on diagenesis of Chalk reservoirs. Geochimica et Cosmochimica Acta 53, 79 - 88.
- Jessop, A.M. and Majorowicz, J.A. 1994. Fluid flow and heat transfer in sedimentary basins. In: Parnell, J. (ed.). Geofluids Origin, migration and evolution of fluids in sedimentary basins. Geological Society Special Publication 78. The Geological Society, London, 43 - 54.
- Jones, G., Fisher, Q.J. and Knipe, R.J. (eds) 1998. Faulting, fault sealing and fluid flow in hydrocarbon reservoirs. Geological Society, London, Special Publications 147, 319 p.
- Joon, B., Laban, C. and Van der Meer, J.J.M. 1990. The Saalian glaciation in the Dutch part of the North Sea. Geologie en Mijnbouw 69, 151 - 158.
- Keary, P. (ed.) 1993. The encyclopedia of the solid earth sciences. Blackwell Scientific Publications, Oxford, 713 p.
- Knaap, W.A. and M.J. Coenen. 1987. Exploration for oil and natural gas. In: Visser, W.A., Zonneveld, J.I.S. and A.J. van Loon (eds) 1987. Seventy-five years of geology and mining in The Netherlands. Royal Geological and Mining Society of the Netherlands, 207 - 230.
- Kooi, H. and De Vries, J. 1998. Land subsidence and hydrodynamic compaction of sedimentary basins. Hydrology and Earth System Sciences 2, 159 - 171.
- Kooi, H., Cloetingh, S. and Remmelts, G. 1989. Intraplate stresses and the stratigraphic evolution of the North Sea Central Graben. Geologie en Mijnbouw 68, 49 - 72.
- Kooi, H., Hettema, M. and Cloetingh, S. 1991. Lithospheric dynamics and the rapid Pliocene-Quaternary subsidence phase in the southern North Sea basin. Tectonophysics 192, 245 - 259.

- Kooi, H., Johnstone, P., Lambeck, K., Smither, C. and Molendijk, R. 1998. Geological causes of recent (~100 yr) vertical land movement in the Netherlands. *Tectonophysics* 299, 297 - 316.
- Laban, C. 1995. The Pleistocene glaciations in the Dutch sector of the North Sea. A synthesis of sedimentary and seismic data. University of Amsterdam. PhD Thesis.
- Laban, C. 1999. Gaskraters in de Noordzee. *Mens en Wetenschap* 2, 96 - 99 (in Dutch).
- Lachenbruch, A.H. and Sass, J.H. 1977. Heat flow in the United States and the thermal regime of the crust. In: Heacock, J.G. (ed). *The earth's crust, its nature and physical properties*. American Geophysical Union, Geophysical Monographs 20, 626 - 675.
- Lafargue, E. and Barker, C. 1988. Effect of waterwashing on crude oil compositions. *AAPG Bulletin* 72, 263 - 276.
- Lampe, C. and Person, M. 2000. Episodic hydrothermal fluid flow in the Upper Rhinegraben (Germany). *Journal of Geochemical Exploration* 69 - 70, 37 - 40.
- Lanson, B., Beaufort, D., Berger, G., Baradat, J. and Lacharpagne, J.-C. 1996. Illitization of diagenetic kaolinite-to-dickite conversion series: Late stage diagenesis of the Lower Permian Rotliegend sandstone reservoir, offshore of the Netherlands. *Journal of Sedimentary Research* 66, 501 - 518.
- Lanson, B., Beaufort, D., Berger, G., Petit, S. and Lacharpagne, J.-C. 1995. Evolution of clay minerals crystallographic structure in the Dutch Rotliegende sandstone reservoir. *Centres de Recherches Exploration-Production Elf Aquitaine Bulletin* 19, 243 - 265.
- Latin, D.M., Dixon, J.E. and Fitton, J.G. 1990a. Rift-related magmatism in the North Sea Basin. In: Blundell, D.J. and Gibbs, A.D. 1990. *Tectonic evolution of the North Sea Rifts*. Clarendon Press, Oxford, 101-144.
- Latin, D.M., Dixon, J.E., Fitton, J.G. and White, N. 1990b. Mesozoic magmatic activity in the North Sea Basin: implications for stretching history. In: Hardman, R.F.P. and Brooks, J. 1990. *Tectonic events responsible for Britain's oil and gas reserves*. Geological Society Special Publication 55, 207 - 227.
- Law, B.E., Ulmishek, G.F. and Slavin, V.I. (eds) 1998. *Abnormal pressures in hydrocarbon environments*. AAPG Memoir 70, 264 p.
- Lee, M., Aronson, J.L. and Savin, S.M. 1985. K/Ar dating of time of gas emplacement in Rotliegendes sandstone, Netherlands. *AAPG Bulletin* 69, 1381 - 1385.
- Lee, M., Aronson, J.L. and Savin, S.M. 1989. Timing and conditions of Permian Rotliegende sandstone diagenesis, Southern North Sea: K/Ar and oxygen isotopic data. *AAPG Bulletin* 73, 195 - 215.
- Leeder, M.R. and Hardman, M. 1990. Carboniferous of the Southern North Sea Basin and controls on hydrocarbon prospectivity. In: Hardman, R.F.P. and Brooks, J. (eds). *Tectonic events responsible for Britain's oil and gas reserves*. Geological Society Special Publication 55, 87 - 105.
- Lepoutre, M., Mathis, B., Perez, Ph. and Gossart, M. 1996. F15-A Triassic gas field - facies related diagenesis implication on production. Extended Abstract Volume EAGE 58th Conference and Technical Exhibition, Amsterdam, the Netherlands, 3 - 7 June 1996.
- Lerche, I. and Thomsen, R.O. 1994. *Hydrodynamics of oil and gas*. Plenum Press, New York and London, 308 p.
- Letsch, W.J. and Sissing, W. 1983. Tertiary stratigraphy of The Netherlands. *Geologie en Mijnbouw* 62, 305 - 318.
- Leveille, G.P., Primmer, T.J., Dudley, G., Ellis, D. and Allison, G.J. 1997. Diagenetic controls on reservoir quality in Permian Rotliegende sandstones, Jupiter Fields area, southern North Sea. In: Ziegler, K., Turner, P. and Daines, S.R. (eds). *Petroleum Geology of the Southern North Sea: Future Potential*. Geological Society Special Publication 123, 105 - 122.
- Liewig, N., Clauer, N. and Sommer, F. 1987. Rb-Sr and K-Ar dating of clay diagenesis in Jurassic sandstone oil reservoirs, North Sea. *AAPG Bulletin* 71, 1467 - 1474.
- Loneragan, L. and Cartwright, J.A. 1999. Polygonal faults and their influence on deep-water sandstone reservoir geometries, Alba Field, United Kingdom Central North Sea. *AAPG Bulletin* 83, 410 - 432.
- Losh, S., Eglinton, L., Schoell, M. and Wood, J. 1999. Vertical and lateral fluid flow related to a large growth fault, south Eugene Island Block 330 Field, Offshore Louisiana. *AAPG Bulletin* 83, 244 - 276.
- Lünensloss, B., Bayer, U. and Muecher, Ph. 1997. Coalification anomalies induced by fluid flow at the Variscan thrust front: A numerical model of the palaeotemperature field. *Geologie en Mijnbouw* 76, 271 - 275.
- Luo, X. and Vasseur, G. 1992. Contributions of compaction and aquathermal pressuring to geopressure and the influence of environmental conditions. *AAPG Bulletin* 76, 1550-1559.
- Macaulay, C.I., Boyce, A.J., Fallick, A.E. and Haszeldine, R.S. 1997. Quartz veins record vertical flow at a graben edge: Fulmar Oil Field, Central North Sea. *AAPG Bulletin* 81, 2024 - 2035.
- Mackenzie, A.S. and Quigley, T.M. 1988. Principles of geochemical prospect appraisal. *AAPG Bulletin* 72, 399 - 415.
- Magara, K. 1986. *Geological models of petroleum entrapment*. Elsevier, Barking, England, 319 p.
- Magoon, L.B. and Dow, W.G. 1994. *The Petroleum system from source to trap*. AAPG Memoir 60, 655 p.
- Mann, D.M. and Mackenzie, A.S. 1990. Prediction of pore fluid pressures in sedimentary basins. *Marine and Petroleum Geology* 7, 55 - 65.
- Mann, U., Hantschel, T., Schaefer, R.G., Krooss, B., Leythaeuser, D., Litke, R. and Sachsenhofer, R.F. 1997. Petroleum migration: mechanisms, pathways, efficiencies and numerical simulations. In: Welte, D.H., Horsfield, B. and Baker, D.R. (eds) 1997. *Petroleum and Basin evolution. Insights from petroleum geochemistry, geology and basin modeling*. Springer-Verlag, Berlin Heidelberg New York, 403 - 520.
- Mathis, B. and Nieuwland, F. 1999. F15A Triassic gas field - offshore Netherlands: an example of a mixed structural and stratigraphic trap. Paper presented at Petroleum Geologische Kring January meeting, The Hague, the Netherlands, January 27, 1999.
- McCaffrey, K.J.W., Loneragan, L. and Wilinson, J.J. (eds) 1999. *Fractures, fluid flow and mineralization*. Geological Society, London, Special Publication 155, 328 p.
- McKenzie, D.P. 1978. Some remarks on the development of sedimentary basins. *Earth and Planetary Science Letters* 40, 25 - 32.
- McNeil, B., Shaw, H.F. and Rankin, A.H. 1998. The timing of cementation in the Rotliegende sandstones of the Southern North Sea: a petrological and fluid inclusion study of cements. *Journal of Petroleum Geology* 21 (3), 311 - 328.
- McPherson, B.J.O.L. and Garven, G. 1999. Hydrodynamics and overpressure mechanisms in the Sacramento Basin, California. *American Journal of Science* 299, 429 - 466.
- Megson, J. 1998. Discussion: Overpressure and hydrocarbon trapping in the Chalk of the Norwegian Central Graben by Caillet et al. *Petroleum Geoscience* 4, 181 - 185.

- Megson, J.B. 1992. The North Sea chalk play; examples from the Danish Central Graben. In: Hardman, R.F.P. (ed.). Exploration Britain: geological insights for the next decade. Geological Society Special Publication 67, London, 247 - 282.
- Menning, M. 1995. A numerical time scale for the Permian and Triassic periods: an integrated time analysis. In: Scholle, P.A., Peryt, T.M., Ulmer-Scholler, D.S. (eds). The Permian of northern Pangea. Volume 1: Paleogeography, paleoclimates, stratigraphy. Springer-Verlag, Berlin, 77 - 97.
- Michon, L., Van Balen, R. and Simmelink, E. 2002. Cenozoic geodynamics of the Roer Valley Graben. Netherlands Institute of Applied Geoscience TNO - National Geological Survey. Information 9, 22 - 23.
- Mitchell, A. and Grauls, D. (eds) 1998. Overpressures in petroleum exploration. Bulletin du Centre de Recherches Elf Exploration Production Memoir 22.
- Moretti, I. 1998. The role of faults in hydrocarbon migration. Petroleum Geoscience 4, 81 - 94.
- Morton, R.A. and Land, L.S. 1987. Regional variations in formation water chemistry, Frio Formation (Oligocene), Texas Gulf Coast. AAPG Bulletin 71, 191 - 206.
- Muchez, Ph., Slobodnik, M., Viaene, W. and Keppens, E. 1994. Mississippi Valley-type Pb-Zn mineralization in eastern Belgium: Indications for gravity-driven flow. Geology 22, 1011 - 1014.
- Muchez, Ph., Slobodnik, M., Viaene, W.A. and Keppens, E. 1995. Geochemical constraints on the origin and migration of paleofluids at the northern margin of the Variscan foreland, southern Belgium. Sedimentary Geology 96, 191 - 200.
- Muir-Wood, R. 1994. Earthquakes, strain-cycling and the mobilization of fluids. In: Parnell, J. (ed). Geofluids: Origin, migration and evolution of fluids in sedimentary basins. Geological Society, London, Special Publications 78, 85 - 98.
- Muir-Wood, R. and King, G.C.P. 1993. Hydrological signatures of earthquake strain. Journal of Geophysical Research 98 (B12), 22035 - 22068.
- Müller, B., Zoback, M.L., Fuchs, K., Mastin, L., Gregersen, S., Pavoni, N., Stephansson, O. and Ljunggren, C. 1992. Regional patterns of tectonic stress in Europe. Journal of Geophysical Research 97 (B8), 11783 - 11803.
- Nalpas, T., Le Douaran, S., Brun, J.-P., Unternehr, P. and Richert, J.-P. 1995. Inversion of the Broad Fourteens Basin (offshore Netherlands), a small-scale model investigation. Sedimentary Geology 95, 237 - 250.
- Nalpas, T., Richert, J.-P., Mulder, T. et Unternehr, P. 1996. Inversion du Broad Fourteens Basin ou Graben de La Haye (sud de la Mer du Nord) - apports de la sismique 3D. Centres de Recherches Exploration-Production Elf Aquitaine Bulletin 20 (2), 309 - 321.
- Neuzil, C.E. 1995. Abnormal pressures as hydrodynamic phenomena. American Journal of Science 295, 742 - 786.
- Nieuwenhuis, J.D. 1994. Liquefaction and the 1992 Roermond earthquake, the Netherlands. Geologie en Mijnbouw 73, 357 - 364.
- Nolte, A. 1996. Hydrochemie van de Centrale en Roerdal Senk en het optreden van diepe kwel. TNO Grondwater en Geo-Energie, Delft, the Netherlands. Report no. 96 - 90 B (in Dutch).
- Nur, A. and Walder, J. 1990. Time-dependent hydraulics of the earth's crust. Studies in Geophysics: The role of fluids in crustal processes. National Academy Press, Washington, USA, 113 - 127.
- Oakman, C.D. and Partington, M.A. 1998. Cretaceous. In: Glennie, K.W. (ed.) 1998. Petroleum geology of the North Sea area. Basic concepts and recent advances. Fourth edition. Blackwell Science Ltd., Oxford, 294 - 349.
- Oele, J.A., Hol, A.C.P.J. and Tiemens, J. 1981. Some Rotliegend gas fields of the K and L Blocks, Netherlands Offshore (1968 - 1978) - A case history. In: Illing, L.V. and Hobson, G.D. (eds). Petroleum geology of the continental shelf of north-west Europe. Heyden and Son Ltd/The Institute of Petroleum, London, 289 - 300.
- Oliver, J. 1986. Fluids expelled tectonically from orogenic belts: Their role in hydrocarbon migration and other geologic phenomena. Geology 14, 99 - 102.
- Oliver, J. 1992. The spots and stains of plate tectonics. Earth-Science Reviews 32, 77 - 106.
- Ostrom, M., Van Gijssel, K. and Zijl, W. 1993. Modelling subsrosion and groundwater flow in the vicinity of the Zuidwending diapir on the basis of geometrical and (paleo)hydrological boundary conditions for the northeastern Netherlands. National Institute of Public Health and Environmental Protection. RIVM report 715205004.
- Osborne, M.J. and Swarbrick, R.E. 1997. Mechanisms for generating overpressure in sedimentary basins: a reevaluation. AAPG Bulletin 81, 1023 - 1041.
- Overeem, I., Weltje, G.J., Bishop-Kay, C. and Kroonenberg, S.B. 2001. The Late Cenozoic Eridanos delta system in the Southern North Sea Basin: a climate signal in sediment supply? Basin Research 13, 293 - 312.
- Palciauskas, V.V. and Domenico, P.A. 1989. Fluid pressures in deforming porous rocks. Water Resources Research 25, no.2, 203 - 213.
- Palmer, S.E. 1993. Effects of biodegradation and water washing on crude oil composition. In: Engel, M.H. and Macko, S.A. (eds). Organic geochemistry. Plenum Press, New York, 511 - 533.
- Parnell, J. (ed.) 1994. Geofluids: Origin, migration and evolution of fluids in sedimentary basins. Geological Society, London, Special Publication 78, 372 p.
- Parnell, J. (ed.) 1998. Dating and duration of fluid flow and fluid-rock interaction. Geological Society, London, Special Publication 144, 284 p.
- Perrot, J. and Van der Poel, 1987. Zuidwal - a Neocomian gas field. In: Brooks, J. and Glennie, K. (eds). Petroleum geology of North West Europe. Graham & Trotman, London, 325 - 335.
- Person, M. and Garven, G. 1992. Hydrologic constraints on petroleum generation within continental rift basins: Theory and application to the Rhine Graben. AAPG Bulletin 76, 468 - 488.
- Person, M., Raffensperger, J.P., Ge, S., and Garven, G. 1996. Basin-scale hydrogeologic modeling. Reviews of Geophysics 34, 61 - 87.
- Platt, J.D. 1993. Controls on clay mineral distribution and chemistry in the Early Permian Rotliegend of Germany. Clay Minerals 28, 393 - 416.
- Platt, J.D. 1994. Geochemical evolution of pore waters in the Rotliegend (Early Permian) of northern Germany. Marine and Petroleum Geology 11, 66 - 78.
- Price, L.C. 1980. Utilization and documentation of vertical oil migration in deep basins. Journal of Petroleum Geology, 2, 353 - 387.
- Pueyo, J.J., Cardellach, E., Bitzer, K. and Taberner, C. (eds) 2000. Proceedings of GeofluidsIII: Third international Conference on fluid evolution, migration and interaction in sedimentary basins and orogenic belts, Barcelona, July 12 - 14. Journal of Geochemical Exploration 69 - 70, 714 p.



- Purvis, K. and Okkerman, J.A. 1996. Inversion of reservoir quality by early diagenesis, an example from the Triassic Buntsandstein, offshore the Netherlands. In: Rondeel, H.E., Batjes, D.A.J. and Nieuwenhuis, W.H. (eds) 1996. *Geology of gas and oil under the Netherlands*. Kluwer Academic Publishers, Dordrecht, the Netherlands, 179 - 189.
- Quirk, D.G. 1993. Interpreting the Upper Carboniferous of the Dutch Cleaver Bank High. In: Parker, J.R. (ed.), 1993. *Petroleum geology of northwest Europe: Proceedings of the 4<sup>th</sup> Conference*. The Geological Society London, 697 - 706.
- Quirk, D.G. and J.F. Aitken 1997. The structure of the Westphalian in the northern part of the southern North Sea. In: Ziegler, K., Turner, P. and Daines, S.R. (eds) 1997. *Petroleum geology of the Southern North Sea. Future potential*. Geological Society Special Publication 123, 143 - 152.
- Ramaekers, J.J.F. 1992. The Netherlands. In: Hurtig, E., Cermak, V., Haenel, R. and Zui, V. 1992. *Geothermal atlas of Europe*, 81 - 83.
- Ranganathan, V. and Hanor, J.S. 1987. A numerical model for the formation of saline fluids due to diffusion of dissolved NaCl in subsiding sedimentary basins with evaporites. *Journal of Hydrology*, 92, 97 - 120.
- Remmelts, G. 1996. Salt tectonics in the southern North Sea, the Netherlands. In: Rondeel, H.E., Batjes, D.A.J. and Nieuwenhuis, W.H. (eds) 1996. *Geology of gas and oil under the Netherlands*. Kluwer Academic Publishers, Dordrecht, the Netherlands, 143 - 158.
- RGD 1991-1996. *Atlas of the Deep Subsurface of the Netherlands*. Geological Survey of the Netherlands.
- Rieke III, H.H. and Chilingarian, G.V. 1974. *Compaction of argillaceous sediments*. Developments in Sedimentology 16. Elsevier, Amsterdam, 424 p.
- Rijkers, R. and Van Doorn, Th.H.M. 1997. *Atlas of Geothermal resources in the European Community, the Netherlands*. Netherlands Institute of Applied Geoscience TNO – *National Geological Survey*, Report 97-24-A.
- Rijkers, R.H.B. and Duin, E.J.Th. 1994. Crustal observations beneath the southern North Sea and their tectonic and geological implications. *Tectonophysics* 240, 215 - 224.
- Rijkers, R.H.B. and Geluk, M.C. 1996. Sedimentary and structural history of the Texel-IJsselmeer High, the Netherlands. In: Rondeel, H.E., Batjes, D.A.J. and Nieuwenhuis, W.H. (eds) 1996. *Geology of gas and oil under the Netherlands*. Kluwer Academic Publishers, Dordrecht, the Netherlands, 265 - 284.
- Roelofsen, J.W. and De Boer, W.D. 1991. Geology of the Lower Cretaceous Q/1 oil-fields, Broad Fourteens Basin, The Netherlands. In: Spencer, A.M. (ed). *Generation, accumulation and production of Europe's hydrocarbons*. Special Publication of the European Association of Petroleum Geoscientists 1. Oxford University Press, Oxford, 203 - 216.
- Rondeel, H.E., Batjes, D.A.J. & Nieuwenhuis, W.H. (eds) 1996. *Geology of gas and oil under the Netherlands*. Kluwer Academic Publishers, Dordrecht, the Netherlands, 284 p.
- Roos, B.M. and Smits, B.J. 1983. Rotliegend and Main Buntsandstein gas fields in block K/13 - a case history. *Geologie en Mijnbouw* 62, 75 - 82.
- Rossel, N.C. 1982. Clay mineral diagenesis in Rotliegend aeolian sandstones of the Southern North Sea. *Clay Minerals* 17, 69 - 77.
- Royden, L. and Keen, C.E. 1980. Rifting process and thermal evolution of the continental margin of eastern Canada determined from subsidence curves. *Earth and Planetary Science Letters* 51, 343 - 361.
- RRI – *Robertson Research International* 1984. The Dutch North Sea area: the stratigraphy and petroleum geochemistry of the Jurassic to Tertiary sediments.
- RRI – *Robertson Research International* 1985. The Permian, Triassic and Carboniferous reservoirs of the Dutch North Sea. A petroleum geology and engineering evaluation Volume 3.
- RRI – *Robertson Research International* 1988. Netherlands North Sea Study: an integrated analytical and evaluation study incorporating petroleum geology, geophysics and reservoir engineering.
- RRI – *Robertson Research International* 1990. The Netherlands North Sea Well updates.
- Rubey, W.W. and Hubbert, M.K. 1959. Role of fluid pressure in mechanics of overthrust faulting. II Overthrust belt in synclinal area of Western Wyoming in light of fluid pressure hypothesis. *Bulletin of the Geological Society of America* 70, 167 - 206.
- Schneider, F., Potdevin, J.L., Wolf, S. and Faille, I. 1996. Mechanical and chemical compaction model for sedimentary basin simulators. *Tectonophysics* 263, 307 - 317.
- Schokking, F. 1990. On estimating the thickness of the Saalian ice sheet from a vertical profile of preconsolidation loads of a lacustro-glacial clay. *Geologie en Mijnbouw* 69, 305 - .
- Schowalter, T.T. 1979. Mechanics of secondary hydrocarbon migration and entrapment. *AAPG Bulletin* 63, 723-760.
- Schroot, B. 2001. TNO shallow gas seepage study for NASCENT. Netherlands Institute of Applied Geoscience TNO – *National Geological Survey*. Information 8, 20 - 21.
- Schroot, B.M. and Schüttenhelm, R.T.E. 2003. Expressions of shallow gas in the Netherlands North Sea. *Netherlands Journal of Geosciences/Geologie en Mijnbouw* 82-1, 91 - 105.
- Sclater, J.G. and Christie, P.A.F. 1980. Continental stretching: an explanation of the post-Mid Cretaceous subsidence of the Central North Sea Basin. *Journal of Geophysical Research* 85, 3711 - 3739.
- Seemann, U. 1979. Diagenetically formed interstitial clay minerals as a factor in Rotliegend sandstone reservoir quality in the Dutch sector of the North Sea. *Journal of Petroleum Geology* 1 (3), 55 - 62.
- Shi, Y. and Wang, Ch.-Y. 1986. Pore pressure generation in sedimentary basins: overloading versus aquathermal. *Journal of Geophysical Research* 91, B2, 2153 - 2162.
- Sibson, R.H. 1994. Crustal stress, faulting and fluid flow. In: Parnell, J. (ed). *Geofluids: Origin, migration and evolution of fluids in sedimentary basins*. Geological Society, London, Special Publications 78, 69 - 84.
- Sibson, R.H. 1995. Selective fault reactivation during basin inversion: potential for fluid redistribution through fault-valve action. In: Buchanan, J.G. and Buchanan, P.G. (eds). *Basin Inversion*. Geological Society, London, Special Publications 88, 3 - 19.
- Sibson, R.H. 2000. Tectonic controls on maximum sustainable overpressure: fluid redistribution from stress transitions. *Journal of Geochemical Exploration* 69 - 70, 471 - 475.
- Simmelink, H.J. and Orlic, B. 2001. A geomechanical model. Compressive stress and overpressures in inverted basins. Netherlands Institute of Applied Geoscience TNO – *National Geological Survey*, Information 7, 18 - 19.
- Simmelink, H.J. and Verweij, J.M. 2000. Basin modelling of the Broad Fourteens Basin. Explanation of modelling steps, sensitivity analysis and results. Netherlands Institute of Applied Geoscience TNO – *National Geological Survey*, Report 00-36-A.

- Simmelink, H.J., Orlic, B. and Van Wees, J.D. 2001. Geomechanical modelling of compressive stress and overpressures in inverted basins. Paper O-30 in Extended Abstracts Volume 1 of the EAGE 63<sup>rd</sup> Conference and Technical Exhibition, Amsterdam, the Netherlands, 11 - 15 June 2001.
- Simmelink, H.J., Underschultz, J.R., Verweij, J.M., Henning, A., Pagnier, H.J.M., Otto, C.J. 2003. A pressure and fluid dynamic study of the Southern North Sea Basin. *Geofluids* special issue of the *Journal of Geochemical Exploration* 78 - 79.
- Somerton, W.H. 1992. Thermal properties and temperature-related behavior of rock/fluid systems. *Developments in Petroleum Science* 37, Elsevier, Amsterdam.
- Sørensen, J.C., Gregersen, U., Breiner, M. and Michelsen, O. 1997. High frequency sequence stratigraphy of Upper Cenozoic deposits in the central and southeastern North Sea areas. *Marine and Petroleum Geology* 14 (2), 99 - 123.
- Speelman, H. and Breunese, J.N. 1985. Permeabiliteit, porositeit en kleigehalte van Tertiaire en Onder-Kwartaire afzettingen in Nederland. Rijks Geologische Dienst Rapportnummer 10371. Haarlem (in Dutch).
- Steeghs, P., Overeem, I and Tigrek, S. 2000. Seismic volume attribute analysis of the Cenozoic succession in the L08 block (Southern North Sea). *Global and Planetary Change* 27, 245 - 262.
- Stheeman, H.A. 1963. Petroleum development in the Netherlands, with special reference to the origin, subsurface migration and geological history of the country's oil and gas resources. *Verhandelingen van het Nederlands Geologisch Mijnbouwkundig Genootschap Geologische Serie* 21-1, 57 - 95.
- Stuurman, R. and Vermeulen, P. 2000. Cross-border groundwater flow in the Roer Valley Graben. Netherlands Institute of Applied Geoscience TNO – *National Geological Survey*. Information, edition geohydrology, geochemistry and geomechanics, 1 - 4.
- Stuurman, R., Van Beusekom, G. en Reckman, J. 2000. Watersystemen in beeld. Een beschrijving en kaarten van de grond- en oppervlaktewatersystemen van Noord-Brabant. Nederlands Instituut voor Toegepaste Geowetenschappen TNO. Report 00-10-A (in Dutch).
- Stuyfzand, P.J. 1993. Hydrochemistry and hydrology of the coastal dune area of the Western Netherlands. PhD thesis, Vrije Universiteit, Amsterdam, the Netherlands.
- Sullivan, M.D., Haszeldine, R.S., Boyce, A.J., Rogers, G. and Fallick, A.E. 1994. Late anhydrite cements mark basin inversion: isotopic and formation water evidence, Rotliegend Sandstone, North Sea. *Marine and Petroleum Geology* 11 (1), 46 - 54.
- Swarbrick, R.E. and Osborne, M.J. 1998. Mechanisms that generate abnormal pressures: an overview. In: Law, B.E., Ulmishek, G.F. and Slavin, V.I. (eds). *Abnormal pressures in hydrocarbon environments*. AAPG Memoir 70, 13 - 34.
- TNO-GG 1991-1996. National analysis of regional groundwater flow systems. TNO Institute of Applied Geoscience, Delft, the Netherlands, Reports.
- TNO-NITG 1997 - 2002. Geological Atlas of the deep subsurface of the Netherlands. Netherlands Institute of Applied Geoscience TNO – *National Geological Survey*.
- TNO-NITG 1998. Geological Atlas of the deep subsurface of the Netherlands. Sheet X: Almelo-Winterswijk. Netherlands Institute of Applied Geoscience TNO – *National Geological Survey*.
- TNO-NITG 1999. Geological Atlas of the deep subsurface of the Netherlands. Sheet XV: Sittard-Maastricht. Netherlands Institute of Applied Geoscience TNO – *National Geological Survey*.
- TNO-NITG 2001. Geological Atlas of the deep subsurface of the Netherlands. Sheet XIII-XIV. Netherlands Institute of Applied Geoscience TNO – *National Geological Survey*.
- TNO-NITG 2002. Geological Atlas of the deep subsurface of the Netherlands. Sheets VII and VIII: Noordwijk-Rotterdam and Amsterdam-Gorinchem. Netherlands Institute of Applied Geoscience TNO – *National Geological Survey*.
- Tóth, J. 1963. A theoretical analysis of groundwater flow in small drainage basins. *Journal of Geophysical Research* 68, 4795 - 4812.
- Tóth, J. 1966. Mapping and interpretation of field phenomena for groundwater reconnaissance in a prairie environment, Alberta, Canada. *International Association of Scientific Hydrology Bulletin* 9 (2), 20-68.
- Tóth, J. 1971. Groundwater discharge: A common generator of diverse geologic and morphologic phenomena. *International Association of Scientific Hydrology Bulletin* 16 (1), 7 - 24.
- Tóth, J. 1980. Cross-formational gravity-flow of groundwater: A mechanism of the transport and accumulation of petroleum (The generalized hydraulic theory of petroleum migration). In: Roberts III, W.H. and Cordell, R.J. (eds). *Problems of petroleum migration*. The AAPG Studies in Geology 10, 121 - 167.
- Tóth, J. 1984. The role of regional gravity flow in the chemical and thermal evolution of ground water. In: Hitchon, B. and Wallick, E. (eds). *Proceedings First Canadian/American Conference on Hydrogeology*, Worthington. National Water Well Association and Alberta Research Council, 3 - 39.
- Tóth, J. 1987. Petroleum hydrogeology: a new basic in exploration. *World oil*, September 1987, 48 - 50.
- Tóth, J. 1995. Hydraulic continuity in large sedimentary basins. *Hydrogeology Journal* 44, 4 - 16.
- Tóth, J. 1999. Groundwater as a geologic agent: An overview of the causes, processes, and manifestations. *Hydrogeology Journal* 7, 1 - 14.
- Tseng, H.-Y., Person, M. and Onstott, T.C. 1998. Hydrogeologic constraint on the origin of deep subsurface microorganisms within a Triassic basin. *Water Resources Research* 34, 937 - 948.
- Tuncay, K., Park, A. and Ortoleva, P. 2000. Sedimentary basin deformation: and incremental stress approach. *Tectonophysics* 323, 77 - 104.
- Tuncay, K. and Ortoleva, P. 2001. Salt tectonics as a self-organizing process: A reaction, transport, and mechanics model. *Journal of Geophysical Research* 106 (B1), 803 - 817.
- Underhill, J.R. and Partington, M.A. 1993. Jurassic thermal doming and deflation in the North Sea: implications of the sequence stratigraphic evidence. In: Parker, J.R. (ed.) 1993. *Petroleum Geology of Northwest Europe*. Proceedings of the 4<sup>th</sup> Conference. The Geological Society London, 337 - 345.
- Ungerer, P., Burrus, J., Doligez, B., Chénet, and Bessis, F. 1990. Basin evaluation by integrated two-dimensional modeling of heat transfer, fluid flow, hydrocarbon generation and migration. *AAPG Bulletin* 74, 309 - 335.
- Van Adrichem Boogaert, H.A. and Burgers, W.F.J. 1983. The development of the Zechstein in the Netherlands. *Geologie en Mijnbouw* 62, 83 - 92.
- Van Adrichem Boogaert, H.A. and Kouwe, W.F.P. 1993 - 1997. Stratigraphic nomenclature of the Netherlands, revision and update by RGD and NOGPA. Mededelingen Rijks Geologische Dienst nr 50.
- Van Balen, R.T. 1995. Tectonic control on the hydrodynamics and sedimentary record of extensional basins; inferences from numerical modelling and analyses of the Pannonian Basin. PhD thesis Vrije Universiteit Amsterdam, 201 p.

- Van Balen, R.T. and Cloetingh, S. 1994. Tectonic control of the sedimentary record and stress-induced fluid flow: constraints from basin modelling. In: Parnell, J. (ed.). *Geofluids: Origin, migration and evolution of fluids in sedimentary basins*. Geological Society, London, Special Publication 78, 9 - 26.
- Van Balen, R.T., Houtgast, R.F., Van der Wateren, F.M., Vandenbergh, J. and Bogaart, R.W. 2000a. Sediment budget and tectonic evolution of the Meuse catchment in the Ardennes and the Roer Valley Rift System. *Global and Planetary Change* 27, 113 - 130.
- Van Balen, R.T., Podlachikov, Yu. Yu., Cloetingh, S. 1998. A new multilayered model for intraplate stress-induced differential subsidence of faulted lithosphere, applied to rifted basins. *Tectonics* 17, 938 - 954.
- Van Balen, R.T., Van Bergen, F., De Leeuw, C., Pagnier, H., Simmelink, H., Van Wees, J.D. and Verweij, J.M. 2000b. Modelling the hydrocarbon generation and migration in the West Netherlands Basin, the Netherlands. *Geologie en Mijnbouw/Netherlands Journal of Geosciences* 79, 29 - 44.
- Van Balen, R.T., Verweij, J.M., Van Wees, J.D., Simmelink, H., Van Bergen, F. and Pagnier, H. 2002. Deep subsurface temperatures in the Roer Valley Graben and the Peelblock, the Netherlands – new results. *Netherlands Journal of Geosciences/Geologie en Mijnbouw* 81, 19 - 26.
- Van Bergen, F. 1998. Basin modelling and hydrocarbon generation in the WNB – an organic petrological and organic geochemical approach. Netherlands Institute of Applied Geoscience TNO – National Geological Survey, Report 98-148B.
- Van Dalfsen, W. 1983. Het ondiepe ondergrondse temperatuurveld in Nederland. Dienst Grondwaterverkenning TNO, Delft, the Netherlands, Report OS 83-31 (in Dutch).
- Van den Bosch, W.J. 1983. The Harlingen field, the only gas field in the Upper Cretaceous Chalk of The Netherlands. *Geologie en Mijnbouw* 62, 145 - 156.
- Van der Poel, A.B. 1989. A case study on the hydrocarbon geology of Upper Permian (Zechstein-3) carbonates in licence P6, the Netherlands' offshore. *Geologie en Mijnbouw*, 68, 285 - 296.
- Van der Weiden, M.J.J. 1983. Een hydrogeochemisch onderzoek in verband met de winning van aardwarmte uit het West-Nederland bekken, toegespitst op het demonstrieringsproject Delfland. Vening Meinesz Laboratorium, Afdeling Geochemie. Rijksuniversiteit Utrecht. Rapport, 34 p. (in Dutch).
- Van Engen, H. 1975. An interpretation of Groningen subsurface temperature data. *Geologie en Mijnbouw* 54, 177 - 183.
- Van Gijssel, K. 1995. A hydrogeological and palaeoenvironmental data set for large-scale groundwater flow model simulations in the northeastern Netherlands. *Mededelingen Rijks Geologische Dienst* 52, 105 - 134.
- Van Wees, J.D. and Beekman, F. 2000. Lithosphere rheology during intraplate extension and inversion: inferences from automated forward modelling of four basins in Western Europe. *Tectonophysics* 320, 219-242.
- Van Wees, J.D. and Cloetingh, S. 1996. 3D flexure and intraplate compression in the North Sea Basin. *Tectonophysics* 266, 343 - 359.
- Van Wees, J.D., Arche, A., Beijdorff, C.G., López-Gómez, J. and Cloetingh, S.A.-PL. 1998. Temporal and spatial variations in tectonic subsidence in the Iberian Basin (eastern Spain): inferences from automated forward modelling of high-resolution stratigraphy (Permian-Mesozoic). *Tectonophysics* 300, 285 - 310.
- Van Wees, J.D., Stephenson, R.A., Ziegler, P.A., Bayer, U., McCann, T., Dadlez, R., Gaupp, R., Narkiewicz, M., Bitzer, F. and Scheck, M. 2000. On the origin of the Southern Permian Basin, Central Europe. *Marine and Petroleum Geology* 17, 43 - 59.
- Van Wijfe, D.H. 1987a. The structural evolution of the Broad Fourteens Basin. In: Brooks, J. and Glennie, K. (eds). *Petroleum Geology of North West Europe*. Graham and Trotman, 315 - 323.
- Van Wijfe, D.H. 1987b. Structural evolution of inverted basins in the Dutch offshore. *Tectonophysics* 137, 171 - 219.
- Van Wijfe, D.H., Lutz, M. and Kaasschieter, J.P.H. 1980. The Rotliegend in the Netherlands and its gas accumulations. *Geologie en Mijnbouw* 59, 3 - 24.
- Vasseur, G. and Demongodin, L. 1995. Convective and conductive heat transfer in sedimentary basins. *Basin Research* 7, 67 - 79.
- Veld, H., Fermont, W.J.J., Kerp, H. and Visscher, H. 1996. Geothermal history of the Carboniferous in South Limburg, the Netherlands. In: Rondeel, H.E., Batjes, D.A.J. and Nieuwenhuis, W.H. (eds) 1996. *Geology of gas and oil under the Netherlands*. Kluwer Academic Publishers, Dordrecht, the Netherlands, 31 - 43.
- Vercoutere, C. and Van den Haute, P. 1993. Post-Palaeozoic cooling and uplift of the Brabant Massif as revealed by apatite fission track analysis. *Geol. Mag.* 130 (5), 639 - 646.
- Verweij, J.M. 1989. Hydrocarbon migration; With special reference to regional secondary hydrocarbon migration and its significance for basin evaluation. TNO Institute of Applied Geoscience, Delft, the Netherlands. Reportno. OS 89-67.
- Verweij, J.M. 1990a. Outline of the Cenozoic hydrogeohistory of the Dutch Section of the North Sea Basin. TNO Institute of Applied Geoscience, Delft, the Netherlands. Reportno. OS 90-41B.
- Verweij, J.M. 1990b. Preliminary assessment of the secondary hydrocarbon migration patterns in the Dutch section of the North Sea Basin. TNO Institute of Applied Geoscience, Delft, the Netherlands, Reportno. OS 90-56.
- Verweij, J.M. 1993. Hydrocarbon migration systems analysis. *Developments in Petroleum Science* 35, Elsevier, Amsterdam, the Netherlands, 276 p.
- Verweij, J.M. 1994a. Overview evolution Western Canada Sedimentary Basin in relation to the evolution of secondary oil migration conditions in Pembina and Crossfield case study areas. Report. Secondary Oil Migration Project. Projectno. Jou2 CT 93-0368.
- Verweij, J.M. 1994b. Aqueous and petroleum fluid systems in sedimentary basins. Paper presented at 2<sup>nd</sup> Aardwetenschappelijk Congres Veldhoven, the Netherlands, 21 April 1994.
- Verweij, J.M. 1997. Post-Carboniferous hydrogeohistory of the onshore and offshore Netherlands and its control on the evolution of petroleum systems. Oral presentation. Abstract. AAPG Hedberg Research Conference 'Applied hydrogeology in Petroleum exploration'. July 27 - 30, 1997, Banff, Canada.
- Verweij, J.M. 1999. Application of fluid flow systems analysis to reconstruct the post-Carboniferous hydrogeohistory of the onshore and offshore Netherlands. *Marine and Petroleum Geology* 16, 561 - 579.
- Verweij, J.M. (ed.) 2003. *Geofluids in the Netherlands*. Special issue of The Netherlands Journal of Geosciences/Geologie en Mijnbouw 82-1, 1 - 105.
- Verweij, J.M., Simmelink, H.J., David, P., Van Balen, R.T., Van Bergen, F., Van Wees, J.D.A.M. 2000. Geodynamic and hydrodynamic evolution of the Broad Fourteens Basin and the development of its petroleum systems: an integrated 2D modelling approach. *Journal of Geochemical Exploration* 69 - 70, 635 - 639.



- Verweij, J.M., Simmelink, H.J., Van Balen, R.T., David, P., Van Bergen, F. 2001. History of petroleum generation and migration in the Broad Fourteens Basin. Oral presentation. Extended Abstract Volume 1, O-16 of the EAGE 63<sup>rd</sup> Conference and Exhibition, 11 - 15 June, Amsterdam.
- Verweij, J.M. and Simmelink, H.J. 2002. Geodynamic and hydrodynamic evolution of the Broad Fourteens Basin (The Netherlands) in relation to its petroleum systems. *Marine and Petroleum Geology* 19, 339 - 359.
- Verweij, J.M., Simmelink, H.J., Van Balen, R.T. and David, P. 2003. History of petroleum systems in the Broad Fourteens Basin. *Netherlands Journal of Geosciences/Geologie en Mijnbouw* 82-1 Special issue 'on Geofluids in the Netherlands', 71 - 90.
- Vinken, R. (compiler) 1988. The northwest European Tertiary Basin. Results of the International Geological Correlation Programme Project no. 124. *Geol. Jb. A100*, 7-508.
- Von Winterfeld, C., Bayer, U., Oncken, O., Lünenschloß, B. and Springer, J. 1994. Das westlichen Rheinische Schiefergebirge Krustenstruktur und heutiges Temperaturfeld. *Geowissenschaften* 12, Heft 10-11, 320 - 324.
- Warren, E.A. and Smalley, P.C. (eds.) 1994. North Sea Formation Waters Atlas. Geological Society Memoir 15. The Geological Society, London, 208 p.
- Wassing, F. 1968. Data for investigation of the North Sea. Coastal Engineering Survey Consultants CESCO NV the Netherlands. Cescso Information no. 10.00.13/1.
- Webatlas of North Sea fields 1999. <http://www.nitg.tno.nl/webatlas>.
- Welle, D.H., Horsfield, B. and Baker, D.R. (eds) 1997. Petroleum and Basin evolution. Insights from petroleum geochemistry, geology and basin modeling. Springer-Verlag, Berlin Heidelberg New York, 535 p.
- Wiers, J. 2001. A hydrogeological characterization and groundwater model of the Roer Valley Graben. Centre of Hydrology Utrecht (ICHU), Utrecht University, and the Netherlands Institute of Applied Geoscience TNO – *National Geological Survey*, MSc Thesis.
- Wildenborg, A.F.B., Orlic, B., De Lange, G., De Leeuw, C.S., Zijl, W., Van Weert, F., Veling, E.J.M., De Cock, S., Thimus, J.F., Lehnen-De Rooij, C. and Den Haan, E.J. 2000. Transport of radionuclides disposed of in clay of Tertiary origin (TRACTOR). Netherlands Institute of Applied Geoscience TNO – *National Geological Survey*. Report 00-223-B.
- Willett, S.D. and Chapman, D.S. 1987. Temperatures, fluid flow, and the thermal history of the Uinta Basin. In: Doligez, B. (ed.). Migration of hydrocarbons in sedimentary basins. *Éditions Technip*, Paris, 533 - 551.
- Winstanley, A.M. 1993. A review of the Triassic play in the Roer Valley Graben, SE onshore Netherlands. In: Parker, J.R. (ed) 1993. *Petroleum Geology of Northwest Europe: Proceedings of the 4<sup>th</sup> Conference*. The Geological Society, London, 595 - 607.
- Winthagen, P.L.A. and Verweij, J.M. 2003. Estimating regional pore pressure distribution using 3D seismic velocities in the Dutch Central North Sea Graben. *GeofluidsIV special issue of the Journal of Geochemical Exploration* 78 - 79.
- Wong, Tfr.E., Parker, N. and Horst, P. 2001. Tertiary sedimentary development of the Broad Fourteens area, the Netherlands. *Netherlands Journal of Geosciences/Geologie en Mijnbouw* 80, 85 - 94.
- Wride, W.C. 1995. Structural features and structural styles from the Five Countries Area of the North Sea Central Graben. *First Break Vol. 13*, no. 10, 395 - 407.
- Yang, C.S. and Nio, S.D. 1993. Application of high-resolution sequence stratigraphy to the Upper Rotliegend in the Netherlands offshore. In: Weimer, P. and Rosamentier, H. 1993. *Siliciclastic sequence stratigraphy. Recent developments and applications*. AAPG Memoir 58, American Association of Petroleum Geologists, Tulsa, USA, 285 - 316.
- Yardley, G.S. and Swarbrick, R.E. 2000. Lateral transfer: a source of additional overpressure?. *Marine and Petroleum Geology* 17, 523 - 537.
- Yassir, N.A. and Bell, J.S. 1996. Abnormally high fluid pressures and associated porosities and stress regimes in sedimentary basins. *SPE Formation evaluation*, March 1996, 5 - 10.
- Zagwijn, W.H. 1975. De palaeogeografische ontwikkeling van Nederland in de laatste drie miljoen jaar. *Koninklijk Nederlands Aardrijkskundig Genootschap Geografisch Tijdschrift* IX, no. 3, 181 - 201 (in Dutch).
- Zagwijn, W.H. 1989. The Netherlands during the Tertiary and the Quaternary: A case history of Coastal Lowland Evolution. *Geologie en Mijnbouw* 68 (1), 107 - 120.
- Zagwijn, W.H. 1992. The beginning of the ice age in Europe and its major subdivisions. *Quaternary Science Reviews* 11, 583-591.
- Ziegler, K., Sellwood, B.W. and Fallick, A.E. 1994. Radiogenic and stable isotope evidence for age and origin of authigenic illites in the Rotliegend, Southern North Sea. *Clay Minerals* 29, 555 - 565.
- Ziegler, P.A. 1987. Late Cretaceous and Cenozoic intra-plate compressional deformations in the Alpine foreland – a geodynamic model. *Tectonophysics* 137, 389 - 420.
- Ziegler, P.A. 1990a. Geological Atlas of Western and Central Europe. Second and completely revised edition. Shell Internationale Petroleum Maatschappij, the Netherlands, 239 p, 56 annexes.
- Ziegler, P.A. 1990b. Tectonic and palaeogeographic development of the North Sea rift system. In: Blundell, D.J. and A.D. Gibbs. 1990. *Tectonic evolution of the North Sea rifts*. Clarendon Press, Oxford, 1 - 36.
- Ziegler, P.A. 1992. North Sea rift system. *Tectonophysics* 208, 55 - 75.
- Ziegler, P.A. 1994. Cenozoic rift system of western and central Europe: an overview. *Geologie en Mijnbouw* 73, 99 - 127.
- Zoback, M.L. 1992. First- and second-order patterns of stress in the lithosphere: The World Stress Map Project. *Journal of Geophysical Research* 97 (B), 11703 - 11728.
- Zoth, G. and Haenel, R. 1988. Chapter 10. Appendix . In: Haenel, R., Rybach, L. and L. Stegena (eds). *Handbook of terrestrial heat-flow density determination*. Kluwer Academic Publishers. Dordrecht. 449 - 466.
- Zuurdeeg, B.W. and Coenegracht, Y.M.A. 1986. Genesis of the mineral water of Nieuweschans. University of Utrecht, Institute of Earth Sciences, Department of Geochemistry Internal Report.
- Zuurdeeg, B.W., Coenegracht, Y.M.A. en Van Gaans, P.F.M. 1989. Geothermische reserves Centrale Slenk, Nederland. Geochemische aspecten formatiewater. Rijksuniversiteit Utrecht, Faculteit Geologie en Geofysica, en Dienst Grondwaterverkenning TNO, Delft, the Netherlands. Report OS 89-20 (in Dutch).

## Appendix 1 Calculated bulk thermal conductivities for offshore Netherlands

Bulk thermal conductivities were calculated for 52 wells in the following chronostratigraphic units: Quaternary, Tertiary, Upper Cretaceous (Chalk Group), Lower Cretaceous, Jurassic, Upper Triassic, Lower Triassic, Upper Permian (Zechstein Group), Upper Permian (Upper Rotliegend Group) and Carboniferous. The bulk thermal conductivities of the chronostratigraphic units are based on matrix thermal conductivities given by Andrews-Speed et al. (1984) and groundwater temperature-dependent thermal conductivities given in Somerton (1992) and take the influence of porosity into account. The temperature dependence of the thermal conductivity of halite and carbonates has also been included in the calculations.

The following paragraphs present the lithology, and values for the porosity, matrix thermal conductivity and groundwater thermal conductivity used in calculating the bulk thermal conductivities for each chronostratigraphic unit.

### 1 Quaternary

#### *Lithology*

1. Predominantly fine to medium grained sand
2. Clay

#### *Porosity*

Both sands and clay: 40%

#### *Bulk density*

Both sands and clay: 1900 kg/m<sup>3</sup>

#### *Matrix thermal conductivity*

$$\lambda_r = 2.8 \text{ Wm}^{-1}\text{K}^{-1}$$

#### *Groundwater thermal conductivity*

$$\lambda_w = 0.6 \text{ Wm}^{-1}\text{K}^{-1}$$

#### *Bulk thermal conductivity Quaternary*

$$\lambda = \lambda_w^\phi \cdot \lambda_r^{1-\phi} = 0.6^{0.4} \cdot 2.8^{0.6} = 1.5 \text{ Wm}^{-1}\text{K}^{-1}$$

This value of the bulk thermal conductivity of Quaternary sediments is in accordance with the value for unconsolidated sands of 40% porosity presented by Somerton (1992).

#### *Data sources*

- Lithology, porosity, bulk density: BGS & RGD Maps Flemish Bight & Indefatigable, 1984.
- Matrix thermal conductivity: Andrews-Speed et al. (1984).
- Groundwater thermal conductivity: Table C-1 in Somerton (1992; see also De Marsily 1986).

## 2 Tertiary

### Lithology

1. Predominantly clay;
2. Sandy intercalations in wells P02-01, Q01-01, F03-03, and in northern Dutch Central Graben blocks B14, B17, B18, F2, F3, F5, F6, F8, F9. (The total thermal resistivity  $R$  of the Tertiary will decrease only a few % because of the sandy intercalations: influence of sandy intercalations is very small especially in relation to the uncertainties in estimated porosity values of the Tertiary).

### Porosity

Porosity values were calculated with porosity–depth relations given in Sclater and Christie (1980):

porosity shale  $\phi = \phi_0 e^{-cz} = 0.63 e^{-0.51z}$  ( $z$  = depth below sea bottom in km);

porosity sand  $\phi = \phi_0 e^{-cz} = 0.49 e^{-0.27z}$  ( $z$  = depth below sea bottom in km).

The calculated sand porosities are slightly higher than values for Tertiary sands in the onshore Netherlands given in Speelman and Breunese (1985).

The shale porosities have also been calculated with the help of the porosity–depth relations given by Baldwin and Butler (1985).

### Matrix thermal conductivity

Shale:  $\lambda_r = 2.0 \text{ Wm}^{-1}\text{K}^{-1}$

Sandy intercalations:  $\lambda_r = 2.3 \text{ Wm}^{-1}\text{K}^{-1}$

Data source : Andrews-Speed et al. (1984).

### Groundwater thermal conductivity

$\lambda_w = 0.62 \text{ Wm}^{-1}\text{K}^{-1}$  Data source: Table C-1 in Somerton (1992).

### Bulk thermal conductivity of the Tertiary (for shale porosities calculated with the Sclater and Christie 1980 porosity–depth relations)

Bulk thermal conductivity was calculated for each well using  $\lambda = \lambda_w^\phi \cdot \lambda_r^{1-\phi}$ .

The bulk thermal conductivity  $\lambda = 1.3 \text{ Wm}^{-1}\text{K}^{-1}$  except for well A12-01, P02-01, Q01-01 where  $\lambda = 1.4 \text{ Wm}^{-1}\text{K}^{-1}$  (sandy intercalations).

### Bulk thermal conductivity of the Tertiary (for shale porosities calculated with the Baldwin and Butler 1985 porosity–depth relations)

Bulk thermal conductivities are  $\lambda = 1.3 - 1.6 \text{ Wm}^{-1}\text{K}^{-1}$  ( $\lambda_{\text{mean}} = 1.4 \text{ Wm}^{-1}\text{K}^{-1}$ ).

## 3 Upper Cretaceous (Chalk)

### Lithology

Limestone

### Porosity

No measured porosity values are available for the Chalk Group.

Porosity values were calculated with porosity–depth relations for normally pressured Chalk given in Sclater and Christy (1980):

$\phi = \phi_0 e^{-cz} = 0.63 e^{-0.71z}$  ( $z$  = depth below sea bottom in km).

### Matrix thermal conductivity

Mean matrix conductivity Chalk  $\lambda_r = 3.2 \text{ Wm}^{-1}\text{K}^{-1}$

Data source: Andrews-Speed et al. (1984).

### Groundwater thermal conductivity

$\lambda_w = 0.63 \text{ Wm}^{-1}\text{K}^{-1}$  Data source: Table C-1 in Somerton (1992).

### Bulk thermal conductivity for the Upper Cretaceous (Chalk)

Bulk thermal conductivity was calculated for each well using  $\lambda = \lambda_w^\phi \cdot \lambda_r^{1-\phi}$ .

$\lambda = 1.8 - 2.5 \text{ Wm}^{-1}\text{K}^{-1}$

$\lambda_{\text{mean}} = 2.1 \text{ Wm}^{-1}\text{K}^{-1}$

## 4 Lower Cretaceous

### Lithology

Claystone/shale; sandstone

### Porosity

Measured porosities for Lower Cretaceous sandstone are available for most of the wells.

There are no measured porosity values of Lower Cretaceous shales.

Porosity values for Lower Cretaceous shales and remaining sandstones were calculated with porosity–depth relations given in Sclater and Christie (1980), including inversion corrections.

Shales  $\phi = \phi_0 e^{-cz} = 0.63 e^{-0.51z}$  ( $z$  = depth below sea bottom in km);

Sandstones  $\phi = \phi_0 e^{-cz} = 0.49 e^{-0.27z}$  ( $z$  = depth below sea bottom in km).

The shale porosities were also calculated with the porosity–depth relations given by Baldwin and Butler (1985), including inversion corrections.

### Matrix thermal conductivity

Shale:  $\lambda_r = 2.5 \text{ Wm}^{-1}\text{K}^{-1}$

Sandstone :  $\lambda_r = 3.6 \text{ Wm}^{-1}\text{K}^{-1}$

Data source: Andrews-Speed et al. (1984).

### Groundwater thermal conductivity

$\lambda_w = 0.63 \text{ Wm}^{-1}\text{K}^{-1}$

Data source Table C-1 in Somerton (1992) (for a depth range 1.5 - 2.5 km, the temperature is 50 - 70 °C and salinity is 65,000 - 110,000 mg/l).

### Bulk thermal conductivity of the Lower Cretaceous (for shale porosities calculated with the Sclater and Christie 1980 porosity–depth relations, including inversion correction)

Bulk thermal conductivity was calculated for each well using  $\lambda = \lambda_w^\phi \cdot \lambda_r^{1-\phi}$ .

$\lambda = 1.6 - 2.1 \text{ Wm}^{-1}\text{K}^{-1}$

$\lambda_{\text{mean}} = 2.8 \text{ Wm}^{-1}\text{K}^{-1}$

*Bulk thermal conductivity of the Lower Cretaceous (for shale porosities calculated with the Baldwin and Butler 1985 porosity-depth relations, including inversion correction)*

Bulk thermal conductivity was calculated for each well using  $\lambda = \lambda_w^\phi \cdot \lambda_r^{1-\phi}$ .

$$\lambda = 1.8 - 2.2 \text{ Wm}^{-1}\text{K}^{-1}$$

$$\lambda_{\text{mean}} = 2.0 \text{ Wm}^{-1}\text{K}^{-1}$$

## 5 Jurassic

### *Lithology*

Claystone/shale; sandstone; carbonate

### *Porosity*

There are no measured porosity values available for shales and carbonates.

Missing porosity values for shales, sandstones and carbonates were calculated with porosity-depth relations given in Sclater and Christie (1980), including depth correction for inversion.

More reliable shale porosities were calculated with the porosity-depth relations given by Baldwin and Butler (1985), including depth corrections for inversion.

### *Matrix thermal conductivity*

Shale:  $\lambda_r = 2.4 \text{ Wm}^{-1}\text{K}^{-1}$

Sandstone :  $\lambda_r = 3.6 \text{ Wm}^{-1}\text{K}^{-1}$

Limestone:  $\lambda_r = 2.8 \text{ Wm}^{-1}\text{K}^{-1}$

Sandstone + shale:  $\lambda_r = 3.4 \text{ Wm}^{-1}\text{K}^{-1}$  ('Graben sand')

$2/3$  Shale +  $1/3$  sandstone:  $\lambda_r = 2.8 \text{ Wm}^{-1}\text{K}^{-1}$  (Delfland Subgroup and Puzzle Hole Formation)

Data source: Andrews-Speed et al. (1984).

### *Groundwater thermal conductivity*

$\lambda_w = 0.63 \text{ Wm}^{-1}\text{K}^{-1}$

In well A12-01:  $\lambda_w = 0.66 \text{ Wm}^{-1}\text{K}^{-1}$

Data source Table C-1 in Somerton (1992).

Bulk thermal conductivity of the Jurassic (for shale porosities calculated with the Sclater and Christie 1980 porosity–depth relations, including inversion correction)

Bulk thermal conductivity was calculated for each well using  $\lambda = \lambda_w^\phi \cdot \lambda_r^{1-\phi}$ .

$$\lambda = 1.7 - 2.5 \text{ Wm}^{-1}\text{K}^{-1}$$

$$\lambda_{\text{mean}} = 2.0 \text{ Wm}^{-1}\text{K}^{-1}$$

Bulk thermal conductivity of the Jurassic (for shale porosities calculated with the Baldwin and Butler 1985 porosity–depth relations, including inversion correction)

Bulk thermal conductivity was calculated for each well using  $\lambda = \lambda_w^\phi \cdot \lambda_r^{1-\phi}$ .

$$\lambda = 1.9 - 2.5 \text{ Wm}^{-1}\text{K}^{-1}$$

$$\lambda_{\text{mean}} = 2.1 \text{ Wm}^{-1}\text{K}^{-1}$$

## 6 Upper Triassic

### Lithology

Shale, halite, limestone, dolomite, anhydrite

### Porosity

There are no measured porosity values available for the Upper Triassic lithologies. Missing porosity values for shales, sandstones and carbonates were calculated with porosity-depth relations given in Sclater and Christie (1980), including depth correction for inversion.

More reliable shale porosities were calculated with the porosity-depth relations given by Baldwin and Butler (1985), including depth corrections for inversion. The halite porosity was assumed.

Shale:  $\phi = 11 - 16\%$

Limestone:  $\phi = 11 - 15\%$

Halite:  $\phi = 1\%$

### Matrix thermal conductivity

Shale:  $\lambda_r = 2.6 \text{ Wm}^{-1}\text{K}^{-1}$

Limestone:  $\lambda_r = 2.8 \text{ Wm}^{-1}\text{K}^{-1}$

Halite:  $\lambda_r = 5.5 \text{ Wm}^{-1}\text{K}^{-1}$  (at room temperature; corrected for subsurface temperature in each wells)

Data source: Andrews-Speed et al. (1984).

### Groundwater thermal conductivity

$\lambda_w = 0.65 \text{ Wm}^{-1}\text{K}^{-1}$  Data source Table C-1, Somerton (1992).

### Generalised bulk thermal conductivity

Shale:  $\lambda = \lambda_w^\phi \cdot \lambda_r^{1-\phi}$ ; for  $\phi = 11\%$ ,  $\lambda = 0.65^{0.11} \cdot 2.6^{0.89} = 2.2 \text{ Wm}^{-1}\text{K}^{-1}$ ;

for  $\phi = 16\%$ ,  $\lambda = 0.65^{0.16} \cdot 2.6^{0.84} = 2.1 \text{ Wm}^{-1}\text{K}^{-1}$

Limestone: for  $\phi = 11\%$ ,  $\lambda = 0.65^{0.11} \cdot 2.8^{0.89} = 2.4 \text{ Wm}^{-1}\text{K}^{-1}$ ;

for  $\phi = 15\%$ ,  $\lambda = 0.65^{0.15} \cdot 2.8^{0.85} = 2.2 \text{ Wm}^{-1}\text{K}^{-1}$

Halite:  $\lambda = \lambda_w^\phi \cdot \lambda_r^{1-\phi} = 0.65^{0.01} \cdot 5.5^{0.99} = 5.4 \text{ Wm}^{-1}\text{K}^{-1}$

Halite thermal conductivity is temperature dependent. For the Upper Triassic

$\lambda_{\text{salt}} = \lambda_w^\phi \cdot \lambda_r^{1-\phi} = 3.8 - 4.6 \text{ Wm}^{-1}\text{K}^{-1}$

### Bulk thermal conductivity of the Upper Triassic (for shale porosities calculated with the Sclater and Christie 1980 porosity-depth relations, including inversion correction)

Bulk thermal conductivity was calculated for each well using  $\lambda = \lambda_w^\phi \cdot \lambda_r^{1-\phi}$ .

$\lambda = 2.1 - 3.2 \text{ Wm}^{-1}\text{K}^{-1}$

$\lambda_{\text{mean}} = 2.4 \text{ Wm}^{-1}\text{K}^{-1}$

### *Bulk thermal conductivity of the Upper Triassic (for shale porosities calculated with the Baldwin and Butler 1985 porosity-depth relations, including inversion correction)*

Bulk thermal conductivity was calculated for each well using  $\lambda = \lambda_w^\phi \cdot \lambda_r^{1-\phi}$ .

$$\lambda = 2.2 - 3.2 \text{ Wm}^{-1}\text{K}^{-1}$$

$$\lambda_{\text{mean}} = 2.4 \text{ Wm}^{-1}\text{K}^{-1}$$

## 7 Lower Triassic ('Bunter')

### *Lithology*

Shale:

Lower Buntsandstein Formation (Rogenstein Member, Main Claystone Member);  
Volpriehausen Clay-Siltstone Member and Detfurth Claystone Member (of the Main Buntsandstein Subgroup);

Sandstone:

Lower Volpriehausen Sandstone Member and Lower Detfurth Sandstone Member (of the Main Buntsandstein Subgroup);

Sandstone + shale:

Hardeggen Formation (of the Main Buntsandstein Subgroup).

### *Porosity*

There are no measured porosity values available for the shales. Measured porosities of sandstone units were used in the calculations for the respective wells. Sandstone porosities of 15% were assumed to occur on the Mesozoic Highs (e.g. Cleaverbank High, RRI 1988).

General:

Shale:  $\phi = 10\%$

Sandstone:  $\phi = 10 - 15\%$

### *Matrix thermal conductivity*

Shale:  $\lambda_r = 2.8 \text{ Wm}^{-1}\text{K}^{-1}$

Sandstone:  $\lambda_r = 4.0 \text{ Wm}^{-1}\text{K}^{-1}$

'Hardeggen':  $\lambda_r = 3.2 \text{ Wm}^{-1}\text{K}^{-1}$

Data source: Andrews-Speed et al. (1984).

### *Groundwater thermal conductivity*

$\lambda_w = 0.66 \text{ Wm}^{-1}\text{K}^{-1}$       Data source Table C-1, Somerton (1992).

### *Generalised bulk thermal conductivity*

Shale:  $\lambda = \lambda_w^\phi \cdot \lambda_r^{1-\phi}$ ; for  $\phi = 10\%$ ,  $\lambda = 0.66^{0.10} \cdot 2.8^{0.9} = 2.4 \text{ Wm}^{-1}\text{K}^{-1}$ ;

Sandstone: for  $\phi = 10\%$ ,  $\lambda = 0.66^{0.10} \cdot 4.0^{0.9} = 3.3 \text{ Wm}^{-1}\text{K}^{-1}$ ; for  $\phi = 15\%$ ,

$$\lambda = 0.66^{0.15} \cdot 4.0^{0.85} = 3.1 \text{ Wm}^{-1}\text{K}^{-1}$$

Hardeggen:  $\lambda = \lambda_w^\phi \cdot \lambda_r^{1-\phi} = 0.66^{0.10} \cdot 3.2^{0.9} = 2.7 \text{ Wm}^{-1}\text{K}^{-1}$

### *Bulk thermal conductivity for the Lower Triassic*

Bulk thermal conductivity was calculated for each well using  $\lambda = \lambda_w^\phi \cdot \lambda_r^{1-\phi}$ .

$$\lambda = 2.4 - 2.8 \text{ Wm}^{-1}\text{K}^{-1}$$

$$\lambda_{\text{mean}} = 2.6 \text{ Wm}^{-1}\text{K}^{-1}$$

## 8 Upper Permian (Zechstein Group)

### Lithology

Halite; anhydrite; dolomite; limestone; shale; sandstone (very fine grained to medium grained).

### Porosity

|                         |  |
|-------------------------|--|
| Halite:                 | $\phi = \text{max. } 1\%$ (Domenico and Schwartz 1990) |
| Anhydrite:              | $\phi = 3\%$ (assumed; see Domenico and Schwartz 1990) |
| Dolomite and limestone: | $\phi = 5\%$ (Van Adrichem Boogaert 1983; ECL 1983)    |
| Shale:                  | $\phi = 10\%$ (assumed)                                |
| Sandstone:              | $\phi = 10\%$  |

### Matrix thermal conductivity

|            |  |
|------------|--|
| Halite:    | $\lambda_r = 5.5 \text{ Wm}^{-1}\text{K}^{-1}$ |
| Anhydrite: | $\lambda_r = 5.5 \text{ Wm}^{-1}\text{K}^{-1}$ |
| Dolomite:  | $\lambda_r = 5.0 \text{ Wm}^{-1}\text{K}^{-1}$ |
| Limestone: | $\lambda_r = 2.8 \text{ Wm}^{-1}\text{K}^{-1}$ |
| Shale:     | $\lambda_r = 2.9 \text{ Wm}^{-1}\text{K}^{-1}$ |
| Sandstone: | $\lambda_r = 4.0 \text{ Wm}^{-1}\text{K}^{-1}$ |

Data source: Andrews-Speed et al. (1984) (for sandstone the thermal conductivities were derived from values given for Triassic and Carboniferous sandstones).

### Groundwater thermal conductivity

$$\lambda_w = 0.65 \text{ Wm}^{-1}\text{K}^{-1}$$

Data source Table C-1, Somerton (1992).

### Bulk thermal conductivity Halite

$$\lambda = \lambda_w^\phi \cdot \lambda_r^{1-\phi}; \text{ for } f = 1\%, \lambda = 0.65^{0.10} \cdot 5.5^{0.9} = 5.4 \text{ Wm}^{-1}\text{K}^{-1}.$$

### Temperature dependence of thermal conductivity of halite

Zoth and Haenel 1988 present the following expression for the temperature dependence of salt:

$$\lambda_T = \{(2960)/(350 + T) - 2.11\} \text{ (T in } ^\circ\text{C, } \lambda \text{ in } \text{Wm}^{-1}\text{K}^{-1}\text{)}.$$

For  $T = 20 \text{ } ^\circ\text{C}$  and  $\lambda_{\text{salt}} = 5.4 \text{ Wm}^{-1}\text{K}^{-1}$ , the equation becomes

$$\lambda_T = \{(2960)/(350 + T) - 2.6\}$$

| Temperature ( $^\circ\text{C}$ ) | $\lambda_{\text{salt}}$ ( $\text{Wm}^{-1}\text{K}^{-1}$ ) | Temperature ( $^\circ\text{C}$ ) | $\lambda_{\text{salt}}$ ( $\text{Wm}^{-1}\text{K}^{-1}$ ) |
|----------------------------------|---|----------------------------------|---|
| 20                               | 5.4   | 100                              | 4.0   |
| 30                               | 5.2   | 110                              | 3.8   |
| 40                               | 5.0   | 120                              | 3.7   |
| 50                               | 4.8   | 130                              | 3.6   |
| 60                               | 4.6   | 140                              | 3.4   |
| 70                               | 4.4   | 150                              | 3.3   |
| 80                               | 4.3   | 160                              | 3.2   |
| 90                               | 4.1   |                                  |   |



### Bulk thermal conductivity Limestone

Zoth and Haenel's (1988) expression for the temperature dependence of limestones is:

$$\lambda_T = \{(1073)/(350 + T) + 0.13\}$$

| Temperature (°C) | $\lambda_{\text{limestone}}$ ( $\text{Wm}^{-1}\text{K}^{-1}$ ) |
|------------------|--|
| 20               | 2.8  |
| 100              | 2.5  |
| 150              | 2.3  |

### Generalised bulk thermal conductivity

|            |  |
|------------|--|
| Halite:    | $\lambda = 3.6 - 4.5 \text{ Wm}^{-1}\text{K}^{-1}$   |
| Anhydrite: | $\lambda = \lambda_w^\phi \cdot \lambda_r^{1-\phi}$ ; for $\phi = 3\%$ , $\lambda = 0.65^{0.03} \cdot 5.5^{0.97} = 5.2 \text{ Wm}^{-1}\text{K}^{-1}$ ; |
| Dolomite:  | $\lambda = \lambda_w^\phi \cdot \lambda_r^{1-\phi}$ ; for $\phi = 5\%$ , $\lambda = 0.65^{0.05} \cdot 5.0^{0.95} = 4.5 \text{ Wm}^{-1}\text{K}^{-1}$ ; |
| Limestone: | $\lambda = \lambda_w^\phi \cdot \lambda_r^{1-\phi}$ ; for $\phi = 5\%$ , $\lambda = 0.65^{0.05} \cdot 2.8^{0.95} = 2.6 \text{ Wm}^{-1}\text{K}^{-1}$ ; |
| Shale:     | $\lambda = \lambda_w^\phi \cdot \lambda_r^{1-\phi}$ ; for $\phi = 10\%$ , $\lambda = 0.65^{0.10} \cdot 2.9^{0.9} = 2.5 \text{ Wm}^{-1}\text{K}^{-1}$ ; |
| Sandstone: | for $\phi = 10\%$ , $\lambda = 0.65^{0.10} \cdot 4.0^{0.9} = 3.3 \text{ Wm}^{-1}\text{K}^{-1}$ ;   |

### Bulk thermal conductivity of the Upper Permian (Zechstein Group)

Bulk thermal conductivity for the Zechstein:

$$\lambda = 2.8 - 5.0 \text{ Wm}^{-1}\text{K}^{-1}$$

## 9 Upper Permian (Upper Rotliegend Group)

### Lithology

Slochteren Formation:

predominantly sandstones;

Silverpit Formation:

Ameland and Ten Boer Members: claystones and siltstones

Silverpit Evaporite Member: claystones and halite

### Porosity

Slochteren Formation: measured porosities available:  $\phi = 6 - 19\%$ ;  $\phi_{\text{mean}} = 12\%$ .

Porosities of the claystones were calculated from porosity–depth relations given by Sclater and Christie (1980).

Ten Boer and Ameland claystones:  $\phi = 9 - 14\%$ ;  $\phi_{\text{mean}} = 10\%$ .

Silverpit claystones:  $\phi = 10 - 11\%$ ;  $\phi_{\text{mean}} = 10\%$ .

Halite:  $\phi = 3\%$

### Matrix thermal conductivity

Shale:  $\lambda_r = 2.9 \text{ Wm}^{-1}\text{K}^{-1}$

Sandstone:  $\lambda_r = 4.7 \text{ Wm}^{-1}\text{K}^{-1}$

Halite:  $\lambda_r = 5.5 \text{ Wm}^{-1}\text{K}^{-1}$  (at room temperature)

Data source: Andrews-Speed et al. (1984).

### Groundwater thermal conductivity

$\lambda_w = 0.67 \text{ Wm}^{-1}\text{K}^{-1}$  Data source Table C-1, Somerton (1992).

### Generalised bulk thermal conductivity

Shale:  $\lambda = \lambda_w^\phi \cdot \lambda_r^{1-\phi}$ ; for  $\phi = 10\%$ ,  $\lambda = 0.67^{0.10} \cdot 2.9^{0.9} = 2.5 \text{ Wm}^{-1}\text{K}^{-1}$ ;

Sandstone: for  $\phi = 12\%$ ,  $\lambda = 0.67^{0.12} \cdot 4.7^{0.88} = 3.7 \text{ Wm}^{-1}\text{K}^{-1}$ ;

Halite:  $\lambda = \lambda_w^\phi \cdot \lambda_r^{1-\phi} = 0.67^{0.03} \cdot 5.5^{0.97} = 5.2 \text{ Wm}^{-1}\text{K}^{-1}$   
(at room temperature)

### Bulk thermal conductivity for the Upper Permian (Upper Rotliegend Group)

Bulk thermal conductivity was calculated for each well using  $\lambda = \lambda_w^\phi \cdot \lambda_r^{1-\phi}$ .

$\lambda = 2.5 - 3.7 \text{ Wm}^{-1}\text{K}^{-1}$

$\lambda_{\text{mean}} = 3.4 \text{ Wm}^{-1}\text{K}^{-1}$

## 10 Carboniferous

### Lithology

1. Mudstones + coal intercalations
2. Mudstones + sandstone intercalations
3.  $\frac{2}{3}$  Mudstones +  $\frac{1}{3}$  sandstones

### Porosity

Measured porosities were available for sandstone intercalations in 5 wells.

No measured porosities were available for the mudstones.

Mudstones + coal intercalations:  $\phi = 8\%$  (assumed porosities)

Mudstones + sandstone intercalations:  $\phi = 10\%$  (assumed porosities).

### Matrix thermal conductivity

Shale:  $\lambda_r = 2.0 \text{ Wm}^{-1}\text{K}^{-1}$

Sandstone:  $\lambda_r = 4.0 \text{ Wm}^{-1}\text{K}^{-1}$

Data source: Andrews-Speed et al. 1984.

### Groundwater thermal conductivity

$\lambda_w = 0.67 \text{ Wm}^{-1}\text{K}^{-1}$  Data source Table C-1, Somerton 1992.

### Generalised bulk thermal conductivity

Mudstones + coal intercalations:

$\lambda = \lambda_w^\phi \cdot \lambda_r^{1-\phi}$ ; for  $\phi = 8\%$ ,  $\lambda = 0.67^{0.08} \cdot 2.0^{0.92} = 1.8 \text{ Wm}^{-1}\text{K}^{-1}$ ;

Mudstones + sandstone intercalations:

for  $\phi = 10\%$ ,  $\lambda = 0.67^{0.10} \cdot 2.5^{0.90} = 2.2 \text{ Wm}^{-1}\text{K}^{-1}$ .

### Bulk thermal conductivity for the Carboniferous

Bulk thermal conductivity has been calculated for each well using  $\lambda = \lambda_w^\phi \cdot \lambda_r^{1-\phi}$ .

$\lambda = 1.8 - 2.2 \text{ Wm}^{-1}\text{K}^{-1}$

## Appendix 2 Temperature differences, temperature gradients and steady-state heat flows between successive temperature measurements in wells in the Broad Fourteens area

| Well no.  | Depth below sea-bottom m | Temperature measured °C | Sediment-water temperature °C | Chronostratigraphic unit           |
|-----------|--------------------------|-------------------------|-------------------------------|------------------------------------|
| K14-01    | 1009                     | 43                      | 9                             | Quaternary                         |
|           | 1950.1                   | 75                      | 9                             | Tertiary                           |
|           | 3196                     | 100                     | 9                             | Upper Cretaceous & Lower Paleocene |
|           |                          |                         |                               | Lower Cretaceous                   |
|           |                          |                         |                               | Jurassic                           |
|           |                          |                         |                               | Middle & Upper Triassic            |
|           |                          |                         |                               | Lower Triassic                     |
|           |                          |                         |                               | Permian (Zechstein)                |
|           |                          |                         |                               | Permian (Upper Rotliegend)         |
|           |                          |                         |                               | Carboniferous                      |
| K14-07    | 1979.7                   | 60                      | 8.5                           | Quaternary                         |
|           | 2449.7                   | 81                      | 8.5                           | Tertiary                           |
|           | 3474.5                   | 112                     | 8.5                           | Lower Cretaceous                   |
|           | 3779.5                   | 117                     | 8.5                           | Jurassic                           |
|           |                          |                         |                               | Middle & Upper Triassic            |
|           |                          |                         |                               | Lower Triassic                     |
|           |                          |                         | Permian (Zechstein)           |                                    |
|           |                          |                         | Permian (Upper Rotliegend)    |                                    |
|           |                          |                         | Carboniferous                 |                                    |
| K15-01    | 1234.7                   | 56                      | 9                             | Quaternary                         |
|           | 2141.7                   | 71                      | 9                             | Tertiary                           |
|           | 2698.7                   | 91                      | 9                             | Upper Cretaceous & Lower Paleocene |
|           |                          |                         |                               | Lower Cretaceous                   |
|           |                          |                         | Jurassic                      |                                    |
|           |                          |                         | Middle & Upper Triassic       |                                    |
| K15-03-S1 | 1588                     | 67                      | 9                             | Quaternary                         |
|           | 3145                     | 109                     | 9                             | Tertiary                           |
|           | 3727                     | 126                     | 9                             | Upper Cretaceous & Lower Paleocene |
|           | 3962                     | 132                     | 9                             | Lower Cretaceous                   |
|           |                          |                         |                               | Jurassic                           |
|           |                          |                         | Middle & Upper Triassic       |                                    |
|           |                          |                         | Lower Triassic                |                                    |
|           |                          |                         | Permian (Zechstein)           |                                    |
|           |                          |                         | Permian (Upper Rotliegend)    |                                    |
| K15-06    | 1715.1                   | 64                      | 8.5                           | Quaternary                         |
|           | 3130.1                   | 112                     | 8.5                           | Tertiary                           |
|           | 3961.1                   | 127                     | 8.5                           | Upper Cretaceous & Lower Paleocene |
|           |                          |                         |                               | Lower Cretaceous                   |
|           |                          |                         | Jurassic                      |                                    |
|           |                          |                         | Middle & Upper Triassic       |                                    |
|           |                          |                         | Lower Triassic                |                                    |
|           |                          |                         | Permian (Zechstein)           |                                    |
|           |                          |                         | Permian (Upper Rotliegend)    |                                    |
|           |                          |                         | Carboniferous                 |                                    |

| Thickness<br>m | Bulk thermal<br>resistivity<br>$\text{m}^2\text{KW}^{-1}$ | Bulk thermal<br>conductivity<br>$\text{Wm}^{-1}\text{K}^{-1}$ | Temperature<br>difference<br>$^{\circ}\text{C}$ | Temperature<br>gradient<br>$^{\circ}\text{C}10^{-3}\text{m}^{-1}$ | Steady-state<br>heat flow<br>$\text{mW m}^{-2}$ | Data source |
|----------------|---|---|---|---|---|-------------|
| 399            | 266   | 1.5   | 34  | 34  | 49  | RRI, 1984   |
| 646            | 461   | 1.4   | 32  | 34  | 70  | RRI, 1984   |
| 3              | 1.6   | 1.9   | 25  | 20  | 60  | RRI, 1984   |
| 176            | 88  | 2   |   |   |   |             |
| 343            | 172   | 2   |   |   |   |             |
| 488            | 202   | 2.4   |   |   |   |             |
| 503            | 196   | 2.6   |   |   |   |             |
| 326            | 79  | 4.1   |   |   |   |             |
| 249            | 67  | 3.7   |   |   |   |             |
| 65             | 36  | 1.8   |   |   |   |             |
| 3198           | 1569  |   |   |   |   |             |
| 396            | 264   | 1.5   | 52  | 26  | 43  | RRI, 1990   |
| 660            | 471   | 1.4   | 21  | 45  | 126   | RRI, 1990   |
| 104            | 52  | 2   | 31  | 30  | 103   | RRI, 1990   |
| 786            | 387   | 2   | 5   | 16  | 53  | RRI, 1990   |
| 235            | 74  | 3.2   |   |   |   |             |
| 623            | 237   | 2.6   |   |   |   |             |
| 675            | 169   | 4   |   |   |   |             |
| 271            | 77  | 3.5   |   |   |   |             |
| 29             | 16  | 1.8   |   |   |   |             |
| 3779           | 1748  |   |   |   |   |             |
| 398            | 265   | 1.5   | 47  | 38  | 56  | RRI, 1984   |
| 687            | 491   | 1.4   | 15  | 17  | 32  | RRI, 1984   |
| 24             | 13  | 1.9   | 20  | 36  | 75  | RRI, 1984   |
| 393            | 218   | 1.8   |   |   |   |             |
| 1157           | 568   | 2   |   |   |   |             |
| 66             | 30  | 2.2   |   |   |   |             |
| 2725           | 1585  |   |   |   |   |             |
| 398            | 265   | 1.5   | 58  | 37  | 56  | RRI, 1988   |
| 814            | 581   | 1.4   | 42  | 27  | 62  | RRI, 1988   |
| 293            | 140   | 2.1   | 17  | 29  | 114   | RRI, 1988   |
| 264            | 139   | 1.9   | 6   | 26  | 88  | RRI, 1988   |
| 468            | 227   | 2.1   |   |   |   |             |
| 302            | 128   | 2.4   |   |   |   |             |
| 541            | 211   | 2.6   |   |   |   |             |
| 647            | 166   | 3.9   |   |   |   |             |
| 235            | 68  | 3.5   |   |   |   |             |
| 3962           | 1926  |   |   |   |   |             |
| 397            | 265   | 1.5   | 56  | 32  | 51  | RRI, 1990   |
| 673            | 481   | 1.4   | 48  | 34  | 74  | RRI, 1990   |
| 192            | 101   | 1.9   | 15  | 18  | 56  | RRI, 1990   |
| 223            | 117   | 1.9   |   |   |   |             |
| 944            | 488   | 1.9   |   |   |   |             |
| 491            | 194   | 2.5   |   |   |   |             |
| 547            | 213   | 2.6   |   |   |   |             |
| 197            | 53  | 3.7   |   |   |   |             |
| 298            | 88  | 3.4   |   |   |   |             |
| 42             | 19  | 2.2   |   |   |   |             |
| 4004           | 2019  |   |   |   |   |             |

| Well no. | Depth below sea-bottom m | Temperature measured °C | Sediment-water temperature °C | Chronostratigraphic unit           |
|----------|--------------------------|-------------------------|-------------------------------|------------------------------------|
| K15-07   | 2331.2                   | 74                      | 9                             | Quaternary                         |
|          | 2794.3                   | 85                      | 9                             | Tertiary                           |
|          | 2896.3                   | 97                      | 9                             | Upper Cretaceous & Lower Paleocene |
|          | 3668.8                   | 129                     | 9                             | Lower Cretaceous                   |
|          | 4015.1                   | 135                     | 9                             | Jurassic                           |
|          |                          |                         |                               | Middle & Upper Triassic            |
|          |                          |                         |                               | Lower Triassic                     |
|          |                          |                         |                               | Permian (Zechstein)                |
|          |                          |                         |                               | Permian (Upper Rotliegend)         |
|          |                          |                         |                               | Carboniferous                      |
| K17-02   | 1236.1                   | 68                      | 8.5                           | Quaternary                         |
|          | 2008.6                   | 79                      | 8.5                           | Tertiary                           |
|          | 2379.6                   | 84                      | 8.5                           | Upper Cretaceous & Lower Paleocene |
|          | 2810.6                   | 106                     | 8.5                           | Jurassic                           |
|          |                          |                         |                               | Middle & Upper Triassic            |
|          |                          |                         |                               | Permian (Zechstein)                |
|          |                          |                         |                               | Permian (Upper Rotliegend)         |
|          |                          |                         |                               | Carboniferous                      |
| L16-03   | 1838.8                   | 61                      | 8                             | Quaternary                         |
|          | 3508.1                   | 116                     | 8                             | Tertiary                           |
|          | 4126.8                   | 135                     | 8                             | Upper Cretaceous & Lower Paleocene |
|          | 4188.3                   | 143                     | 8                             | Lower Cretaceous                   |
|          |                          |                         |                               | Jurassic                           |
|          |                          |                         |                               | Middle & Upper Triassic            |
|          |                          |                         |                               | Lower Triassic                     |
|          |                          |                         |                               | Permian (Zechstein)                |
|          |                          |                         |                               | Permian (Upper Rotliegend)         |
| P02-01   | 1045.6                   | 45                      | 8                             | Quaternary                         |
|          | 2396.4                   | 87                      | 8                             | Tertiary                           |
|          | 3728.4                   | 123                     | 8                             | Upper Cretaceous & Lower Paleocene |
|          |                          |                         |                               | Jurassic                           |
|          |                          |                         |                               | Middle & Upper Triassic            |
|          |                          |                         |                               | Lower Triassic                     |
|          |                          |                         |                               | Permian (Zechstein)                |
|          |                          |                         |                               | Permian (Upper Rotliegend)         |
|          |                          |                         |                               | Carboniferous                      |
| P03-01   | 1144                     | 54                      | 8                             | Quaternary                         |
|          | 2580                     | 96                      | 8                             | Tertiary                           |
|          | 3626                     | 152?                    | 8                             | Upper Cretaceous & Lower Paleocene |
|          |                          |                         |                               | Jurassic                           |
|          |                          |                         |                               | Middle & Upper Triassic            |
|          |                          |                         |                               | Lower Triassic                     |
|          |                          |                         |                               | Permian (Zechstein)                |
|          |                          |                         |                               | Permian (Upper Rotliegend)         |
| P06-01   | 1086.8                   | 13                      | 8.5                           | Quaternary                         |
|          | 2163.8                   | 76                      | 8.5                           | Tertiary                           |
|          | 3624.8                   | 120                     | 8.5                           | Lower Cretaceous                   |
|          |                          |                         |                               | Jurassic                           |
|          |                          |                         |                               | Middle & Upper Triassic            |
|          |                          |                         |                               | Lower Triassic                     |
|          |                          |                         |                               | Permian (Zechstein)                |
|          |                          |                         |                               | Permian (Upper Rotliegend)         |

| Thickness<br>m | Bulk thermal<br>resistivity<br>$m^2KW^{-1}$ | Bulk thermal<br>conductivity<br>$Wm^{-1}K^{-1}$ | Temperature<br>difference<br>$^{\circ}C$ | Temperature<br>gradient<br>$^{\circ}C10^{-3}m^{-1}$ | Steady-state<br>heat flow<br>$mW m^{-2}$ | Data source |
|----------------|---|---|--|---|--|-------------|
| 399            | 266   | 1.5   | 65                                       | 28  | 46                                       | RRI, 1990   |
| 829            | 592   | 1.4   | 11                                       | 24  | 58                                       | RRI, 1990   |
| 258            | 123   | 2.1   | 12                                       | 118   | 447                                      | RRI, 1990   |
| 458            | 239   | 1.9   | 32                                       | 41  | 157                                      | RRI, 1990   |
| 342            | 174   | 2   | 6  | 17  | 57                                       | RRI, 1990   |
| 365            | 157   | 2.3   |  |   |  |             |
| 120            | 45  | 2.7   |  |   |  |             |
| 904            | 238   | 3.8   |  |   |  |             |
| 297            | 84  | 3.5   |  |   |  |             |
| 41             | 19  | 2.2   |  |   |  |             |
| 4013           | 1937  |   |  |   |  |             |
| 395            | 263   | 1.5   | 60                                       | 48  | 73                                       | RRI, 1984   |
| 616            | 440   | 1.4   | 11                                       | 14  | 41                                       | RRI, 1984   |
| 6              | 3   | 1.8   | 5  | 13  | 55                                       | RRI, 1984   |
| 235            | 118   | 2   | 22                                       | 51  | 178                                      | RRI, 1984   |
| 507            | 196   | 2.6   |  |   |  |             |
| 1010           | 264   | 4.1   |  |   |  |             |
| 234            | 63  | 3.7   |  |   |  |             |
| 40.5           | 18  | 2.2   |  |   |  |             |
| 3043.5         | 1366  |   |  |   |  |             |
| 400            | 267   | 1.5   | 53                                       | 29  | 47                                       | RRI, 1990   |
| 582            | 416   | 1.4   | 55                                       | 33  | 75                                       | RRI, 1990   |
| 446            | 223   | 2   | 19                                       | 31  | 105                                      | RRI, 1990   |
| 467            | 242   | 1.9   | 8  | 130   | 481                                      | RRI, 1990   |
| 563            | 282   | 2   |  |   |  |             |
| 533            | 220   | 2.4   |  |   |  |             |
| 538            | 213   | 2.5   |  |   |  |             |
| 554            | 163   | 3.4   |  |   |  |             |
| 152            | 41  | 3.7   |  |   |  |             |
| 4235           | 2066  |   |  |   |  |             |
| 468            | 312   | 1.5   | 37                                       | 35  | 53                                       | RRI, 1984   |
| 549            | 366   | 1.5   | 42                                       | 31  | 68                                       | RRI, 1984   |
| 15             | 8   | 1.8   | 36                                       | 27  | 86                                       | RRI, 1984   |
| 795            | 391   | 2   |  |   |  |             |
| 557            | 226   | 2.5   |  |   |  |             |
| 622            | 233   | 2.7   |  |   |  |             |
| 427            | 111   | 3.9   |  |   |  |             |
| 302            | 82  | 3.7   |  |   |  |             |
| 1.7            | 1   | 1.8   |  |   |  |             |
| 3736.7         | 1730  |   |  |   |  |             |
| 417            | 278   | 1.5   | 46                                       | 40  | 59                                       | RRI, 1988   |
| 661            | 472   | 1.4   | 42                                       | 29  | 67                                       | RRI, 1988   |
| 20             | 11  | 1.9   | 56                                       | 54  | 183                                      | RRI, 1988   |
| 874            | 434   | 2   |  |   |  |             |
| 537            | 187   | 2.9   |  |   |  |             |
| 570            | 221   | 2.6   |  |   |  |             |
| 514            | 104   | 5   |  |   |  |             |
| 137            | 37  | 3.7   |  |   |  |             |
| 3730           | 1744  |   |  |   |  |             |
| 345            | 230   | 1.5   | 4  | 4   | 6  | RRI, 1984   |
| 515            | 368   | 1.4   | 63                                       | 59  | 126                                      | RRI, 1984   |
| 1026           | 489   | 2.1   | 44                                       | 30  | 81                                       | RRI, 1984   |
| 392            | 171   | 2.3   |  |   |  |             |
| 300            | 131   | 2.3   |  |   |  |             |
| 540            | 208   | 2.6   |  |   |  |             |
| 282            | 89  | 3.2   |  |   |  |             |
| 225            | 61  | 3.7   |  |   |  |             |
| 3625           | 1746  |   |  |   |  |             |

| Well no. | Depth below sea-bottom m | Temperature measured °C | Sediment-water temperature °C | Chronostratigraphic unit           |
|----------|--------------------------|-------------------------|-------------------------------|------------------------------------|
| P06-02   | 256.5                    | 29                      | 8.5                           | Quaternary                         |
|          | 1096.5                   | 41                      | 8.5                           | Tertiary                           |
|          | 3082.5                   | 109                     | 8.5                           | Jurassic                           |
|          |                          |                         |                               | Middle & Upper Triassic            |
|          |                          |                         |                               | Lower Triassic                     |
|          |                          |                         | Permian (Zechstein)           |                                    |
|          |                          |                         | Permian (Upper Rotliegend)    |                                    |
| P09-01-A | 1249.1                   | 50                      | 8.5                           | Quaternary                         |
|          | 2562.3                   | 78                      | 8.5                           | Tertiary                           |
|          | 3924.8                   | 128                     | 8.5                           | Upper Cretaceous & Lower Paleocene |
|          | 4664.3                   | 149                     | 8.5                           | Lower Cretaceous                   |
|          |                          |                         |                               | Jurassic                           |
|          |                          |                         | Middle & Upper Triassic       |                                    |
|          |                          |                         | Lower Triassic                |                                    |
|          |                          |                         | Permian (Zechstein)           |                                    |
|          |                          |                         | Permian (Upper Rotliegend)    |                                    |
| Q01-01   | 1007.1                   | 37                      | 8                             | Quaternary                         |
|          | 2559.1                   | 79                      | 8                             | Tertiary                           |
|          | 3286.1                   | 99                      | 8                             | Upper Cretaceous & Lower Paleocene |
|          |                          |                         |                               | Lower Cretaceous                   |
|          |                          |                         |                               | Jurassic                           |
|          |                          |                         | Middle & Upper Triassic       |                                    |
|          |                          |                         | Lower Triassic                |                                    |
|          |                          |                         | Permian (Zechstein)           |                                    |
|          |                          |                         | Permian (Upper Rotliegend)    |                                    |
| Q01-03   | 1385.7                   | 52                      | 9                             | Quaternary                         |
|          | 2375.7                   | 87                      | 9                             | Tertiary                           |
|          | 3194.7                   | 121                     | 9                             | Lower Cretaceous                   |
|          |                          |                         | Jurassic                      |                                    |
| Q01-04   | 1364.7                   | 55                      | 9                             | Quaternary                         |
|          | 1833.7                   | 68                      | 9                             | Tertiary                           |
|          |                          |                         |                               | Lower Cretaceous                   |
|          |                          |                         | Jurassic                      |                                    |
| Q01-05   | 1220.4                   | 54                      | 9                             | Quaternary                         |
|          | 1334.1                   | 60                      | 9                             | Tertiary                           |
|          |                          |                         |                               | Lower Cretaceous                   |
|          |                          |                         | Jurassic                      |                                    |
| Q04-01   | 1004.6                   | 57                      | 9                             | Quaternary                         |
|          | 1981.6                   | 89                      | 9                             | Tertiary                           |
|          | 3071.6                   | 110                     | 9                             | Jurassic                           |
|          |                          |                         |                               | Middle & Upper Triassic            |
|          |                          |                         | Lower Triassic                |                                    |
|          |                          |                         | Permian (Zechstein)           |                                    |
|          |                          |                         | Permian (Upper Rotliegend)    |                                    |

| Thickness<br>m | Bulk thermal<br>resistivity<br>$\text{m}^2\text{KW}^{-1}$ | Bulk thermal<br>conductivity<br>$\text{Wm}^{-1}\text{K}^{-1}$ | Temperature<br>difference<br>$^{\circ}\text{C}$ | Temperature<br>gradient<br>$^{\circ}\text{C}10^{-3}\text{m}^{-1}$ | Steady-state<br>heat flow<br>$\text{mW m}^{-2}$ | Data source |
|----------------|---|---|---|---|---|-------------|
| 365            | 243   | 1.5   | 21  | 82  | 122   | RRI, 1984   |
| 531            | 379   | 1.4   | 12  | 14  | 21  | RRI, 1984   |
| 908            | 443   | 2.1   | 68  | 34  | 82  | RRI, 1984   |
| 390            | 162   | 2.4   |   |   |   |             |
| 517            | 200   | 2.6   |   |   |   |             |
| 290            | 91  | 3.2   |   |   |   |             |
| 90             | 24  | 3.7   |   |   |   |             |
| 3091           | 1543  |   |   |   |   |             |
| 345            | 230   | 1.5   | 42  | 33  | 53  | RRI, 1984   |
| 327            | 234   | 1.4   | 28  | 21  | 43  | RRI, 1984   |
| 556            | 309   | 1.8   | 50  | 37  | 81  | RRI, 1984   |
| 939            | 464   | 2   | 21  | 29  | 80  | RRI, 1984   |
| 978            | 489   | 2   |   |   |   |             |
| 681            | 291   | 2.3   |   |   |   |             |
| 500            | 190   | 2.6   |   |   |   |             |
| 233            | 84  | 2.8   |   |   |   |             |
| 107            | 29  | 3.7   |   |   |   |             |
| 4666           | 2319  |   |   |   |   |             |
| 417            | 278   | 1.5   | 29  | 29  | 44  | RRI, 1984   |
| 531            | 354   | 1.5   | 42  | 27  | 58  | RRI, 1984   |
| 338            | 178   | 1.9   | 20  | 28  | 101   | RRI, 1984   |
| 473            | 237   | 2   |   |   |   |             |
| 35             | 16  | 2.2   |   |   |   |             |
| 229            | 106   | 2.2   |   |   |   |             |
| 540            | 213   | 2.5   |   |   |   |             |
| 535            | 149   | 3.6   |   |   |   |             |
| 194            | 52  | 3.7   |   |   |   |             |
| 3292           | 1582  |   |   |   |   |             |
| 425            | 283   | 1.5   | 43  | 31  | 49  | RRI, 1988   |
| 525            | 375   | 1.4   | 35  | 35  | 74  | RRI, 1988   |
| 342            | 171   | 2   | 34  | 42  | 85  | RRI, 1988   |
| 1904           | 915   | 2.1   |   |   |   |             |
| 3196           | 1744  |   |   |   |   |             |
| 425            | 283   | 1.5   | 46  | 34  | 54  | RRI, 1990   |
| 467            | 334   | 1.4   | 13  | 28  | 60  | RRI, 1990   |
| 654            | 323   | 2   |   |   |   |             |
| 299            | 137   | 2.2   |   |   |   |             |
| 1845           | 1077  |   |   |   |   |             |
| 425            | 283   | 1.5   | 45  | 37  | 57  | RRI, 1990   |
| 490            | 350   | 1.4   | 6   | 53  | 105   | RRI, 1990   |
| 382            | 193   | 2   |   |   |   |             |
| 37             | 17  | 2.2   |   |   |   |             |
| 1334           | 843   |   |   |   |   |             |
| 425            | 283   | 1.5   | 48  | 48  | 72  | RRI, 1984   |
| 471            | 336   | 1.4   | 32  | 32  | 69  | RRI, 1984   |
| 854            | 420   | 2   | 21  | 19  | 54  | RRI, 1984   |
| 470            | 196   | 2.4   |   |   |   |             |
| 399            | 158   | 2.5   |   |   |   |             |
| 251            | 80  | 3.1   |   |   |   |             |
| 212            | 57  | 3.7   |   |   |   |             |
| 3082           | 1531  |   |   |   |   |             |



### Appendix 3 Water analyses data from nine wells in the Broad Fourteens Basin

| Well no.                            | Depth (m)  | pH  | TDS mg/l | Na mg/l | K mg/l | Mg mg/l | Ca mg/l | Sr mg/l |
|-------------------------------------|------------|-----|----------|---------|--------|---------|---------|---------|
| <b>Vlieland Sandstone Formation</b> |            |     |          |         |        |         |         |         |
| Q01-03                              | 1300       | 7.2 | 95360    | 27940   | 380    | 770     | 7360    |         |
|                                     | 1300       | 6.9 | 97600    | 29620   | 480    | 760     | 6600    |         |
| Q04-04                              | 1023-1087  | 7.8 | 74200    | 24830   | 215    | 920     | 2400    | 155     |
| P08-03                              | 2830-2839  | 5.1 | 142930   | 40710   | 270    | 4300    | 7400    | 655     |
| <b>Detfurth Formation</b>           |            |     |          |         |        |         |         |         |
| P06-05                              | 1335       | 4.9 | 312340   | 99660   | 2040   | 2550    | 15800   | 470     |
|                                     | 1335       | 5.3 | 320640   | 100470  | 3200   | 4070    | 15200   | 440     |
| P06-06                              |            | 8   | 331920   | 128260  | 1010   | 4.8     | 310     | 6.9     |
| <b>Z2 Formation</b>                 |            |     |          |         |        |         |         |         |
| P02-05                              | 3011       | 5.8 | 311080   | 101080  | 7100   | 1760    | 11750   | 300     |
|                                     | 3011       | 5.6 | 306910   | 100110  | 6100   | 1840    | 11700   | 370     |
|                                     | 3011       | 6.5 | 303730   | 100700  | 7000   | 1530    | 9850    | 300     |
|                                     | 3011       | 6.4 | 309920   | 102450  | 6500   | 1650    | 10650   | 325     |
|                                     | 3011       | 6.2 | 312000   | 102260  | 6150   | 1720    | 11700   | 395     |
| <b>Slochteren Formation</b>         |            |     |          |         |        |         |         |         |
| K12-03                              | 3600       | 4.2 | 257445   | 76906   |        | 3246    | 17495   |         |
| P05-01                              | 3053-3088  | 7   | 103152   | 35600   | 1160   | 61      | 3210    |         |
|                                     |            | 8.2 | 50513    | 16500   | 700    | 61      | 2000    |         |
|                                     | 3053-3088  | 6.5 | 152311   | 49700   | 1580   | 300     | 7310    |         |
|                                     | 3053-3088  | 6.4 | 149978   | 49000   | 1590   | 426     | 7010    |         |
| Q07-01                              | 2375-2378; | 5.6 | 256084   | 83841   |        | 1290    | 13555   |         |
|                                     | 2380-2385; |     |          |         |        |         |         | (Na&K)  |
|                                     | 2405-2408  |     |          |         |        |         |         |         |
| <b>Lower Germanic Trias Group</b>   |            |     |          |         |        |         |         |         |
| P06-06                              |            | 4.6 | 306290   | 104370  | 5200   | 1770    | 4860    | 12      |
|                                     |            | 4.6 | 224955   | 27390   | 9450   | 19200   | 18500   | 130     |

| Ba<br>mg/l | Cl<br>mg/l | HCO <sub>3</sub><br>mg/l | CO <sub>3</sub><br>mg/l | SO <sub>4</sub><br>mg/l | Fe total<br>mg/l | Fe<br>mg/l | Sample | Date<br>sampled | Date<br>analysed |
|------------|------------|--------------------------|-------------------------|-------------------------|------------------|------------|--------|-----------------|------------------|
| 27         | 58380      | 270                      |                         | 230                     | 13               | 0.1        | DST    |                 | 12-01-1975       |
| 25         | 59880      | 230                      |                         | 10                      | 33               | 0.2        | DST    | 24-01-1975      | 12-02-1975       |
| 20         | 45360      | 260                      |                         | 43                      | 15               | 0.5        |        | 23-10-1979      | 12/13-11-83      |
| 7.4        | 89050      | 68                       |                         | 345                     | 250              | 125        | DST    | 21-07-1983      | 21-07-1983       |
| 0.1        | 191090     | 50                       |                         | 510                     | 810              | 170        | DST    | 29-07-1979      | 06-08-1979       |
| 0.1        | 196410     | 130                      |                         | 670                     | 220              | 45         | DST    | 29-07-1979      | 06-08-1979       |
| <0.1       | 190740     | 235                      |                         | 11350                   | 4.0              | <0.1       | RFT    |                 | 21-05-1980       |
| 39         | 187140     | 355                      |                         | 1520                    | 185              | 3.3        | DST    | 07-02-1983      | 23-26/05/83      |
| 48         | 185310     | 255                      |                         | 1130                    | 825              | 14         | DST    | 08-02-1983      | 23-26/05/83      |
| 30         | 182550     | 315                      |                         | 1390                    | 2000             | 14         | DST    | 08-02-1983      | 23-26/05/83      |
| 38         | 186680     | 255                      |                         | 1310                    | 3160             | 13         | DST    | 08-02-1983      | 23-26/05/83      |
| 40         | 188320     | 250                      |                         | 1130                    | 1850             | 5          | DST    | 08-02-1983      | 23-26/05/83      |
| 0          | 159007     | 12                       | 0                       | 483                     |                  | 297        | DST    |                 | 30-09-1976       |
|            | 58800      | 854                      | 0                       | 3340                    |                  | 111        | DST    | 07-09-1968      | 17-12-1968       |
|            | 27200      | 480                      | 360                     | 3210                    |                  | tr         | DST    | 07-09-1968      | 17-12-1968       |
|            | 90400      | 732                      | 0                       | 2150                    |                  | 111        | DST    | 07-09-1968      | 17-12-1968       |
|            | 88460      | 732                      | 0                       | 2620                    |                  | 111        | DST    | 07-09-1968      | 17-12-1968       |
|            | 156555     | 232                      | 0                       | 450                     | 161              |            |        | 29-05-1973      | 15-06-1973       |
| 0.8        | 170530     | 14520                    |                         | 3400                    | 1640             | 1630       | DST    |                 | 01-06-1980       |
| 4.6        | 143760     | 580                      |                         | 1530                    | 4480             | 4410       | DST    |                 | 10-06-1980       |

## Appendix 4 Conceptual model of basin history along the regional cross-section: input parameters and boundary conditions

This Appendix provides an overview of the input data and boundary conditions used in the integrated 2D basin modelling study along a SW-NE cross-section through the southern part of the Broad Fourteens Basin.

### Present-day geological framework

Figure 48 shows the present-day geological framework along the cross-section. It is based on in-house interpreted seismic sections SNST-83-02 and NNS-6, in combination with geological cross-sections published by Burgers and Mulder (1991). Necessary additional information on the geometry of the Upper Rotliegend Group, Limburg Group, and – in the southern part of the cross-section also – the Zechstein and Germanic Trias Groups was derived from declassified well data and regional information (Van Adrichem Boogaert and Kouwe 1993-1997, RRI 1988, Quirk 1993, Quirk and Aitken 1997 and Van Wijhe et al. 1980). The lower boundary of the cross-section is the Epen Formation of the Geul Subgroup of the Limburg Group. The section includes gas- and oil-prone source rocks and intersects or runs in the vicinity of two oil accumulations (in the Q1 and the P9 blocks). The interpreted seismic stratigraphy and the lithostratigraphic well data available to this study did not provide detailed information on occurrence, distribution and spatial continuity of different lithotypes within the distinguished stratigraphic units.

### Time framework for conceptual model: geochronological units

The uninterrupted time-stratigraphic sequence of events during the evolution of the basin was quantified for three key wells along the cross-section (P09-01A, P06-02, Q01-03) and for two wells along the northern extension of the cross-section (L17-02, L14-02) (Tables 19-23).

Major hiatuses related to periods of syn-inversion uplift and erosion are present along the base of the Lower Tertiary North Sea Group. The main hiatus along the section – at well P06-02 – corresponds to a sedimentary thickness of 2.5km (Table 20). The missing stratigraphic units include the Chalk Group, the post-rift Rijnland Group and large part of the syn-rift Schieland Group. In large part of the Broad Fourteens Basin the Chalk Group deposits are absent.

Data and information available for the present study allow different scenarios for the depositional and erosional history during the Late Cretaceous and Danian times. Two scenarios were selected for the modelling studies. The 'Map showing reconstructed Triassic to Lower Cretaceous sedimentary thickness' and the 'Map showing amount of pre-Tertiary erosion due to Late Cretaceous inversion' (from Nalpas et al. 1995, see Figures 37 and 39 in Part 2) were used as boundary conditions for the reconstruction of Cretaceous depositional thicknesses and erosional thicknesses for both scenarios. These maps are based on sonic velocities of Lower Triassic shales and on maturation modelling calibrated by vitrinite reflectance measurements. In addition to burial, the compaction of the Lower Triassic shales may also have been influenced by

pre-inversion increase in lateral compression. If so, the reconstruction of the eroded thickness from sonic velocity data as given by Nalpas et al. (1995) should be considered as maximum values.

Pulsed inversion movements of the Broad Fourteens Basin are responsible for the uplift and erosion during the Late Cretaceous (see Part 2). At least two major inversion-related phases of erosion are recognised in the basin: a pre-Campanian and a Maastrichtian phase. The subsequent regional phase of erosion during the Mid-Palaeocene contributed to the total eroded thickness corresponding to the present hiatuses in the basin.

Scenario 1 represents the simplest scenario for the Late Cretaceous and Danian history and is based on the following assumptions:

- Pre-Campanian erosion started around 85 Ma;
- There was no net deposition of Chalk in the period 85 - 59.4 Ma (that is, deposition of Chalk in the basin may have occurred after 85 Ma, but it was eroded away before 59.4 Ma; no separate depositional and erosional events were included in the modelling in the period 85 - 59.4 Ma);
- Syn-inversion erosion and subsequent Mid-Paleocene erosion stripped off the currently missing stratigraphic units corresponding to the hiatus at the base of the North Sea Group;
- The entire net eroded thickness of Chalk was deposited before 85 Ma;
- The pre-erosional thickness of the Chalk Group (CKTX plus CKGR) is constant along the cross-section and is approximately 1000 m (this value is in accordance with information presented in Ziegler 1990a, Figure 51).

Scenario 2 allows for Chalk to be deposited in the basin after the first major inversion pulse, and concentrates erosion in the Maastrichtian to Mid Paleocene. The subaerial topography of the Broad Fourteens Basin is restricted to the Maastrichtian (74.0 - 65 Ma) and Danian (65 - 59.4 Ma). Scenario 2 is based, among other things, on the lithological characteristics of the Chalk Group encountered in well L17-02: these seem to indicate the possible renewed or continued deposition of Chalk in the basin during the Late Cretaceous syn-inversion period. The Ommelanden Formation has a present-day thickness of 1430 m in well L17-02. The upper 50 m of the formation consists of occasionally argillaceous chalks and includes a 4 m thick shale interval. The 4 m thick shale interval may be related to a major erosion phase of the nearby Broad Fourteens Basin. The middle part (approx. 600 m) of the formation consists of predominantly chalks, while the lower part ( $\pm 800$  m) is again occasionally argillaceous with shale intercalations. The presence of 600 m of relatively pure chalks with few such intercalations may indicate the absence of a nearby subaerial source of such terrestrial input during deposition of these chalks. Continued syn-inversion sedimentation in inverted basins has been recognised in the nearby Vlieland Basin. Herngreen et al. (1996) studied the Cretaceous Chalk Group stratigraphy in and around the inverted Vlieland Basin and found that this Chalk sequence thins dramatically from the Texel IJsselmeer High towards the Vlieland Basin. But even along the inversion axis of this basin, a condensed sequence of sediments representing almost all Cretaceous stages has been encountered in the wells.

Scenario 2 includes the following assumptions:

- Mean average sedimentation rates for the Ommelanden Formation, as based on data from well L17-02 are approx. 56 m/My;
- Before the first major inversion phase (85 Ma) the sedimentation rates are equal for all wells along the cross-section: the net thickness of Ommelanden Chalk is approx. 300 m ( $56 \times (90.4 - 85)$ );
- Between 85 and 74 Ma, deposition is affected by inversion movements and sedimentary sequences are condensed in the central part of the basin (due to less sedimentation and/or syn-sedimentary erosion); the effective sedimentation rate is assumed to be  $1/2 \times 56$  m/My; this results in a net thickness of Ommelanden Chalk of  $28 \times (85 - 74) \sim 308$  m;
- For the edges of the basin, deposition of the Ommelanden Formation continues between 90.4 and 74 Ma and proceeds at sedimentation rates of 56 m/My. This results in a total pre-erosional thickness of approximately 920 m;
- Erosion of the centre and the edges of the basin starts at 74 Ma and ends at 59.4 Ma; that is only the Maastrichtian and Danian erosional phases are taken into account; the result of the first major syn-inversion erosional period is assumed to be included in the pre-Campanian thickness of the Ommelanden Formation;
- Deposition of the Ommelanden Formation is continuous outside the basin between 90.4 and 65 Ma: the total depositional thickness equals the residual thickness of the Ommelanden Formation encountered in the wells (e.g. L17-02).

Not all events given in Tables 19 - 23 were taken into account as separate events in the basin modelling (this applies, for example, to the deposition of the Rupel Formation and the subsequent Savian erosion, and to the intrabasinal erosion during Kimmerian II event).

From the viewpoint of fluid dynamics the quantified uninterrupted time-stratigraphic sequence of events during the evolution of the basin requires the Triassic, Jurassic and Lower Cretaceous units to be subdivided further on the basis of the lithology-dependent hydraulic characteristics of the rocks. Table 24 shows the additional events taken into account in both scenarios.

## Properties of rocks and fluids

The lithology and corresponding hydraulic and thermal parameters are given in Table 25.

### *Porosity and permeability*

The model requires the input of porosity-effective stress relationships for each lithotype or each model layer. Default porosity-effective stress relationships were used for each lithotype, except for shale. The shale relationship applied is based on the porosity-depth relations presented by Baldwin and Butler (1985). Verification of modelling results with published porosity–depth relations for Permian and Triassic reservoir units (e.g. Verweij 1999) and log-derived reservoir porosities (Webatlas 1999; RRI 1985, 1988) led to some additional modifications (Simmelink and Verweij 2000). The intrinsic permeabilities were derived from the lithology-related porosities by applying the Kozeny-Carman equation, and were verified against the permeability data available for the main reservoir units (Simmelink and Verweij 2000).

The Temispack programme calculated for each layer consisting of different end-member lithologies, harmonic means for vertical permeability and arithmetic means for horizontal permeabilities. These averaging rules provide the horizontal and vertical permeabilities of a single homogeneous anisotropic layer that is the equivalent of a layered sequence of lithologies. The calculated default anisotropies were adjusted for each layer using published anisotropy and permeability data in combination with the lithostratigraphic data given in the stratigraphic nomenclature of the Netherlands (Van Adrichem Boogaert and Kouwe 1993 - 1997).

### *Thermal properties*

The matrix thermal conductivities in Table 25 are based on the results of heat flow studies in the southern North Sea area (Andrews-Speed et al. 1984; Verweij 1999). The heat capacities were calculated from Temispack default values for end member lithologies. The radiogenic heat production data were based on values derived from gamma log readings from wells O01-03 and P06-02 by using the Rybach equation (Simmelinck and Verweij 2000).

### *Relative permeability*

The relative permeability curves applied are characterised by saturation end points (0.05 - 0.10 and 0.98) and an exponent of 1.5. The curves indicate that hydrocarbons will start to flow in lithologies dominated by sand and chalk, if the hydrocarbon saturation is above 5%, and in other lithologies if the saturation exceeds 10%.

### *Capillary pressures*

The capillary entry pressures are a function of lithology and are mainly affected by the size of the pore throats. The dependency of the capillary pressures on saturation was not taken into account in the modelling. Three classes of capillary entry pressures, as related to lithology, can be distinguished (Burrus 1997; Welte et al. 1997):  $C_p = 1 - 5$  MPa for tight lithologies (shales and evaporites);  $C_p = 0.1$  MPa for intermediate lithologies;  $C_p = 0.01$  MPa for porous and permeable lithologies. The values in Table 25 are based on this classification. For all lithologies the capillary entry pressures at the surface are 0.

### *Fluid properties*

The densities of the fluids were kept constant during the modelling, at 300 kg/m<sup>3</sup> for the in-situ density of gas, 500 kg/m<sup>3</sup> for that of oil and 1030 kg/m<sup>3</sup> for the water density. Default Temispack values were used for the fluid viscosities.

### *Source rock properties*

The Westphalian coal measures of the Limburg Group (model layers 1, 2, 3 and 4) are considered to be the main source rock for gas in the basin. The source rock is of kerogen type III. The TOC contents of model layers 1, 2, 3 and 4 are 0.7%, 2.8%, 4.2% and 0.7%, respectively.

The Posidonia Shale Formation (model layer 16), is the most important source rock for oil. It is a kerogen type II source rock with a TOC of 5%. The oil-prone Lower Jurassic shales (model layer 15) were taken into account as an additional kerogen type II source rock for oil (estimated TOC = 1%).

Table 26 shows the in-house measured maturity parameters (vitrinite reflectance Rr% and pyrolyses – RockEval –  $T_{\max}$  values) of source rock horizons at wells P09-01A, P06-02 and Q01-03. The number of reliable vitrinite reflectance measurements on source rocks is unfortunately very limited. In addition, the measurements of the Posidonia Shale Formation at well Q01-03 probably had limited value as calibration data for the basin modelling. The northward thrusting of the basin fill in the Q1 area during Late Cretaceous inversion (e.g. Roelofsen and De Boer, 1991) induced a considerable increase in the thickness of the Altena Formation due to fault movement, as observed at well Q01-03. Because of the lateral displacement of – at least the Altena and younger – pre-inversion units from the deeper part of the basin towards the north, it can be expected that the Posidonia shales are actually more mature than than predicted by the 2D basin modelling, because in the basin modelling only vertical displacements were taken into account. The  $T_{\max}$  values measured at well Q01-03 at different depths show a relatively low  $T_{\max}$  value for the deepest sample that indicates at least that  $T_{\max}$  does not increase steadily with depth.

In conclusion, the only reliable vitrinite reflectance measurement that can be used with confidence for calibration of the reconstruction of temperature history is that of well P09-01A.

## Boundary conditions

### *Paleogeography; topography and bathymetry*

The paleobathymetry (Tables 27 - 30) was principally derived from Van Adrichem Boogaert and Kouwe (1993-1997) and – for the Chalk Group – also from Herngreen et al. (1996).

In the basin modelling package, the topographic relief of the ground surface is assumed to be equal to the topographic relief of the water table. The reconstructed history of the ground surface along the cross-section incorporates this assumption. In reality, the topographic relief of the water table is determined by the topographic relief of the ground surface in combination with the climatological conditions and the hydrogeological characteristics of the subsurface. The highest elevations above sea level of the ground surface (and of the water table) occurred during the Saalian, Kimmerian I and II and Late Cretaceous inversion events. The assumed water tables were approximately 100 m above sea level during Saalian and Kimmerian events and 175 m in the intrabasinal part of the cross-section during the Late Cretaceous event.

The paleotopography and the associated topographic relief of the water table at the end of the Late Cretaceous inversion period were estimated, based on the following assumptions:

- The total regional thickness of the sediments eroded along the cross-section during the Late Cretaceous inversion period is 1200 m (reconstructed from sedimentary history and residual thicknesses of the sedimentary sequences);
- The maximum thickness of the sediments eroded in the central part of the basin (P6 area) is approximately 2400 m;

- The subaerial topography of Broad Fourteens Basin is restricted to the Maastrichtian (74.0 - 65 Ma);
- The major phase of erosion coincided with eustatic lowering of sea level between 69.0 - 65.0 Ma (lowest level at approximately 66 Ma, Hancock 1990); this major erosion phase is possibly related to shale intercalation of 4 m in Chalk Group encountered in well L17-02;
- Denudation rates were high, because of probably relatively small drainage basins in the Broad Fourteens area, easily erodable sedimentary rocks especially at the start of erosion (chalk, marl, claystones), and a warm and humid climate.
- Uplift during inversion was discontinuous: 4 pulses of uplift between 74 and 69 Ma (duration and rate of each pulse is 0.5 My and 1 mm/year, respectively); erosion started after first uplift with a time lag of 2 My's; the regional rate of erosion was 200 m/My.

For the above assumptions, the calculated maximum elevation of the basin along the cross-section was 350 m above sea level at 67 Ma. At this time the Chalk Group, and the marls and claystones of the Rijnland Group had been eroded and the Vlieland Sandstones were outcropping at the surface. The water table in the P6 area was estimated at 175 m above sea level, taking into account the warm and humid climate and the lithostratigraphy/hydrostratigraphy at P6 (Vlieland Sandstone Formation on top of sandstones and claystones of the Schieland Group). This elevation of 175 m above sea level was taken as the paleotopography (= paleowater table) during the Late Cretaceous event.

### *Thermal boundary conditions*

#### *Paleo surface temperatures/sediment-water interface temperatures*

The evolution of the sediment-water interface temperature along the section (Table 31) was reconstructed from the general evolution of ocean surface temperatures for paleolatitudes of London, the paleobathymetries along the section and the relation between the mean annual North Sea bottom temperature and water depth given in Evans and Coleman (1974). The evolution of the temperatures in the near past (Pliocene and Quaternary) is given in more detail because of its possible influence on the present-day temperature distribution (Table 32).

#### *Paleo basal heat flow*

The lower boundary condition for simulating the paleo heat transport and paleo temperature distribution in the Broad Fourteens Basin is determined by the evolution of the heat flow input into the sedimentary basin per unit time and unit area. This heat flow input is controlled by radiogenic heat flow induced by the decay of radioactive isotopes in the crust, and subcrustal heat flow. For the parameters given in Table 33, the present-day heat flow input into the upper crust (a boundary condition required by the basin modelling package) is approximately 36.5 mW/m<sup>2</sup> in the Broad Fourteens Basin.

The history of heat flow along the cross-section was estimated in-house by tectonic forward modelling, using the reconstructed history of sedimentation, uplift and erosion of well P09-01A, L16-02 and a pseudo-well representing the central part



of the Broad Fourteens Basin. The applied tectonic forward model (Van Wees et al. 1998, Van Balen et al. 2000) is based on a depth-dependent stretching mechanism (McKenzie, 1978; Royden and Keen, 1980). In this model, the crustal and subcrustal parts of the lithosphere are thinned during rifting. The synrift subsidence is caused by the local isostatic response to the decreased lithospheric load and the postrift subsidence is caused by the lithospheric density increase due to thermal contraction. As a consequence the results of tectonic subsidence modelling incorporate a model for the temperature evolution of the basin. Figure 60 shows the history of tectonic subsidence and surface heat flow reconstructed for well P09-01A. The two periods of increasing surface heat flow follow the Triassic and Late Jurassic rifting phases with a time delay.

#### *Hydraulic boundary conditions*

The following boundary conditions were used: no flow conditions at the lateral boundaries and the lower sediment–basement interface; the upper boundary condition is given by the hydraulic head, which is related to the ground surface topography. In addition, several simulations were run testing the influence of open boundary conditions at the northern side boundary.

The conceptual model of geodynamic and hydrodynamic evolution of the Broad Fourteens Basin (Part 2) included a distinct period of basement-derived groundwater flow. Hydrothermal flow of groundwater may have entered the basin along deep-reaching faults during periods of tectonic activity in the early part of the main syn-rift period. Because no data were available on possible fluxes involved, the effect of this flow was not included in the hydraulic boundary conditions of the modelling study.

**Tables 19-23 History of sedimentation, uplift, erosion and nondeposition for well P09-01A (Table 19), P06-02 (Table 20), Q01-03 (Table 21), L17-02 (Table 22) and L14-02 (Table 23).**

Bottom ages of the stratigraphic units of the North Sea Groups to Altena Group, and of the Baarlo Formation are derived from Van Adrichem Boogaert and Kouwe (1993-1997). Bottom ages of the Lower Germanic Trias Group, Zechstein Group and Upper Rotliegend Group are after Menning (1995).

Thicknesses of stratigraphic units are indicated as present-day (compacted) thicknesses.

Reconstructed thicknesses of missing and eroded units for all the wells are based on declassified well data from wells in and surrounding the Broad Fourteens Basin, the interpreted seismic section through the basin and on information presented in Van Adrichem Boogaert and Kouwe 1993 - 1997.

In addition the following information was used to reconstruct missing and eroded units:

**Limburg Group:** Present-day residual thicknesses were also derived from the 'restored isopachyte map of the Westphalian – early Stephanian' given in Quirk and Aitken (1997). Amount of erosion estimated from 'Pre-Perm subcrop map of the Netherlands' (Figure C4 in Van Adrichem Boogaert and Kouwe (1993-1997) and 'Pre-Perm subcrop of chronostratigraphic units' (Gas Atlas 1998);

**Upper Rotliegend Group:** Regional information presented in Van Wijhe et al. (1980) and RRI (1988);

**Zechstein Group:** Present-day thicknesses are based on declassified well data only;

**Germanic Trias Group:** Present-day thicknesses at well Q01-03, L14-02 and L17-02 reconstructed from regional distributions published in Ames and Farfan (1996), Rijkers and Geluk (1996) and Geluk and Röhling (1997). Hardegsen phase of erosion/nondeposition is also based on information given in Ames and Farfan (1996), Geluk and Röhling (1997) and the 'Subcrop map Base Solling unconformity' in Van Adrichem Boogaert and Kouwe (1993-1997; Figure E2);

**Altena Group:** Thicknesses of Sleen and Aalburg Formations are based on additional regional information from Van Wijhe (1987a,b) and Rijkers and Geluk (1996). Thicknesses of Posidonia Shale Formation are based on well data only. Thicknesses of Werkendam and Brabant Formation are based on additional information derived from paleogeographic maps given in Ziegler (1990a); Mid Kimmerian and Late Kimmerian I erosion: Reconstructed thicknesses based on additional information from Burgers and Mulder (1991), Roelofsen and De Boer (1991) and Van Wijhe (1987a,b);

**Schieland Group:** Regional information presented in Hooper et al. (1995);

**Rijnland Group:** Reconstructed thicknesses from 'Map restored isopach Early Cretaceous' (Ziegler 1990a; enclosure 40, Figure 51) and 'Map reconstructed Triassic and Lower Cretaceous thicknesses (Nalpas et al. 1995; Figure 39 in Part 2);

**Chalk Group (scenario 1):** Reconstruction of thicknesses is based on additional information given in 'Structural cross-section through West Netherlands Basin and Late Cretaceous palinspastic reconstruction' (Ziegler 1990a, Figure 51), 'Cross section across the Broad Fourteens Basin schematically restored to Upper Cretaceous' (Hayward and Graham 1989, Figure 8b), 'Map showing amount of pre-Tertiary erosion due to Late Cretaceous inversion' (Nalpas et al. 1995; Figure 39) and 'Map showing reconstructed Triassic to Lower Cretaceous sedimentary thickness' (Nalpas et al. 1995; Figure 37).

**Subhercynian and Laramide erosion (scenario 1):** reconstructed eroded thicknesses verified with information given by Nalpas et al. (1995);

**Pyrenean erosion:** Eroded thicknesses reconstructed using regional information from Nalpas et al. (1995, 1996) and Zagwijn (1989).

**Savian erosion:** De Lugt (2000, pers. com).

Table 19 History of sedimentation, uplift, erosion and nondeposition for well P09-01A

| Stratigraphic Unit   | Unit Code | Bottom age<br>Ma | Thickness<br>m | Missing<br>m | Data source<br>'Thickness' | Data Source<br>'Missing' |
|--|-----------|------------------|----------------|--------------|----------------------------|--------------------------|
| North Sea Groups   |           | 59.4             | 661.8          |              | NITG database              |                          |
| Upper North Sea Group  | NU        | 23.3             | 567.8          |              | Horst 2000                 |                          |
| — Maassluis Formation  | NUMS      | 2.4              | 463.8          |              | Horst 2000                 |                          |
| — Oosterhout Formation   | NUOT      | 5.2              | 90.5           |              | Horst 2000                 |                          |
| — Breda Formation  | NUBA      | 23.3             | 13.5           |              | Horst 2000                 |                          |
| <i>Nondeposition/erosion (Savian)</i>                            |           | 29.3             | >30            |              | Reconstructed              |                          |
| Middle North Sea Group   | NM        | 35               | —              | >30          | Horst 2000                 | Reconstructed            |
| — Rupel Formation  | NMRF      | 35               | —              | >30          | Horst 2000                 | Reconstructed            |
| <i>Uplift/erosion (Pyrenean)</i>                                 |           | 38.6             | <500           |              | Reconstructed              |                          |
| Lower North Sea Group  | NL        | 59.4             | 8              | <500         |                            | Reconstructed            |
| — Dongen Formation   | NLFF      | 56.6             | 46.5           | <500         | Horst 2000                 | Reconstructed            |
| — Asse Member  | NLFFB     |                  | —              |              | Horst 2000                 |                          |
| — Brussels Marl Member   | NLFFM     |                  | —              |              | Horst 2000                 |                          |
| — Brussels Sand Member   | NLFFS     |                  | —              |              | Horst 2000                 |                          |
| — Ieper Member   | NLFFY     |                  | 38.5           |              | Horst 2000                 |                          |
| — Basal Dongen Tuffite Member                                    | NLFFT     |                  | —              |              | Horst 2000                 |                          |
| — Basal Dongen Sand Member                                       | NLFFD     | 56.6             | 8              |              | Horst 2000                 |                          |
| — Landen Formation   | NLLF      | 59.4             | 47.5           |              | Horst 2000                 |                          |
| <i>Uplift &amp; erosion (Subhercynean &amp; Laramide)</i>        |           | 85               | 433.5          |              | Reconstructed              |                          |
| Chalk Group  | CK        | 97               | 566.5          | 433.5**      | NITG database              | Reconstructed            |
| — Ekofisk Formation  | CKEK      | 65               | —              |              | NITG database              |                          |
| — Ommelanden Formation   | CKGR      | 90.4             | 493.5          |              | NITG database              |                          |
| — Texel Formation  | CKTX      | 97               | 73             |              | NITG database              |                          |
| Rijnland Group   | KN        | 138.7            | 938.5          |              | NITG database              |                          |
| Schieland Group  | SLD       |                  |                |              |                            |                          |
| <i>Erosion/nondeposition (Mid and Late Kimmerian I &amp; II)</i> |           | 156              | <b>567.5</b>   |              | Reconstructed              |                          |
| Altena Group   | AT        | 209.5            | 989            | 567.5        | NITG database              | Reconstructed            |
| — Brabant Formation  | ATBR      | 166              | —              | 200          | NITG database              | Reconstructed            |
| — Werkendam Formation  | ATWD      | 180              | 32.5           | 367.5        | NITG database              | Reconstructed            |
| — Posidonia Shale Formation                                      | ATPO      | 187              | 60             |              | NITG database              |                          |
| — Sleen and Aalburg Formations                                   | ATRT+ATAL | 209.5            | 896.5          |              | NITG database              |                          |
| Upper Germanic Trias Group                                       | RN        | 243              | 703.5          |              | NITG database              |                          |
| <i>Erosion/nondeposition (Hardegse)</i>                          |           | 244.5            | 0-50           |              | Reconstructed              |                          |
| Lower Germanic Trias Group                                       | RB        | 251              | 468            | 0-50         | NITG database              | Reconstructed            |
| Zechstein Group  | ZE        | 258              | 232            |              | NITG database              |                          |
| Upper Rotliegend Group   | RO        | 266              | 135            |              | Reconstructed              |                          |
| <i>Uplift &amp; erosion (Saalian)</i>                            |           | 296              | 700            |              | Reconstructed              |                          |
| Limburg Group  | DC        | 318.3            | 1300           | 700          | Reconstructed              | Reconstructed            |
| — Dinkel/Hunze Subgroups   | DCD/DCH   |                  |                | 600          |                            | Reconstructed            |
| — Maurits Formation  | DCCU      |                  | 100            | 100          | Reconstructed              | Reconstructed            |
| — Ruurlo Formation   | DCCR      |                  | 600            |              | Reconstructed              |                          |
| — Baarlo Formation   | DCCB      | 318.3            | 600            |              | Reconstructed              |                          |

Table 20 History of sedimentation, uplift, erosion and nondeposition for well P06-02

| Stratigraphic Unit  | Unit Code | Bottom age<br>Ma | Thickness<br>m | Missing<br>m | Data source<br>'Thickness' | Data Source<br>'Missing' |
|---|-----------|------------------|----------------|--------------|----------------------------|--------------------------|
| North Sea Groups  | N         | 59.4             | 894.5          |              | NITG database              |                          |
| Upper North Sea Group                                     | NU        | 23.3             | 722.5          |              | Horst 2000                 |                          |
| — Maassluis Formation                                     | NUMS      | 2.4              | 593.5          |              | Horst 2000                 |                          |
| — Oosterhout Formation                                    | NUOT      | 5.2              | 100            |              | Horst 2000                 |                          |
| — Breda Formation   | NUBA      | 23.3             | 29             |              | Horst 2000                 |                          |
| <i>Nondeposition/erosion (Savian)</i>                     |           | 29.3             | >15            |              | Reconstructed              |                          |
| Middle North Sea Group                                    | NM        | 15               | >15            |              | Horst 2000                 | Reconstructed            |
| — Rupel Formation   | NMRF      | 35               | 15             | >15          | Horst 2000                 | Reconstructed            |
| <i>Uplift/erosion (Pyrenean)</i>                          |           | 38.6             | <435           |              | Reconstructed              |                          |
| Lower North Sea Group                                     | NL        | 59.4             | 157            | <435         | Horst 2000                 | Reconstructed            |
| — Dongen Formation  | NLFF      | 56.6             | 126            | <435         | Horst 2000                 | Reconstructed            |
| — Asse Member   | NLFFB     |                  | —              |              | Horst 2000                 |                          |
| — Brussels Marl Member                                    | NLFFM     |                  | —              |              | Horst 2000                 |                          |
| — Brussels Sand Member                                    | NLFFS     |                  | —              |              | Horst 2000                 |                          |
| — Ieper Member  | NLFFY     |                  | 105            |              | Horst 2000                 |                          |
| — Basal Dongen Tuffite Member                             | NLFFT     |                  | 12.5           |              | Horst 2000                 |                          |
| — Basal Dongen Sand Member                                | NLFFD     | 56.6             | 8.5            |              | Horst 2000                 |                          |
| — Landen Formation  | NLLF      | 59.4             | 31             |              | Horst 2000                 |                          |
| <i>Uplift &amp; erosion (Subhercynian &amp; Laramide)</i> |           | 85               | 2528           |              | Reconstructed              |                          |
| Chalk Group   | CK        | 97               | 1000*          |              |                            | Reconstructed            |
| — Ekofisk Formation                                       | CKEK      | 65               |                |              |                            |                          |
| — Ommelanden Formation                                    | CKGR      | 90.4             | 850            |              |                            | Reconstructed            |
| — Texel Formation   | CKTX      | 97               | 150            |              |                            | Reconstructed            |
| Rijnland Group  | KN        | 138.7            | 1200           |              |                            | Reconstructed            |
| <i>Erosion/nondeposition (Late Kimmerian II)</i>          |           | 140.7            | 100            |              | Reconstructed              |                          |
| Schieland Group   | SLD       | 154.7            | 672            | 428          | NITG database              | Reconstructed            |
| <i>Erosion/nondeposition (Mid and Late Kimmerian I)</i>   |           | 156              | 564            |              | Reconstructed              |                          |
| Altena Group  | AT        | 209.5            | 236            | 564          | NITG database              | Reconstructed            |
| — Brabant Formation                                       | ATBR      | 166              | 130            |              |                            | Reconstructed            |
| — Werkendam Formation                                     | ATWD      | 180              | 270            |              |                            | Reconstructed            |
| — Posidonia Shale Formation                               | ATPO      | 187              | 30             |              |                            | Reconstructed            |
| — Sleen and Aalburg Formations                            | ATRT+ATAL | 209.5            | 236            | 134          | NITG database              | Reconstructed            |
| Upper Germanic Trias Group                                | RN        | 243              | 404            |              | NITG database              |                          |
| <i>Erosion/nondeposition (Hardegsen)</i>                  |           | 244.5            | 0-50           |              | Reconstructed              |                          |
| Lower Germanic Trias Group                                | RB        | 251              | 488            | 0-50         | NITG database              | Reconstructed            |
| Zechstein Group   | ZE        | 258              | 305            |              | NITG database              |                          |
| Upper Rotliegend Group                                    | RO        | 266              | 235            |              | Reconstructed              |                          |
| <i>Uplift &amp; erosion (Saalian)</i>                     |           | 296              | 800            |              | Reconstructed              |                          |
| Limburg Group   | DC        | 318.3            | 1200           | 800          | Reconstructed              | Reconstructed            |
| — Dinkel/Hunze Subgroups                                  | DCD/DCH   |                  | 600            |              |                            | Reconstructed            |
| — Maurits Formation                                       | DCCU      |                  | 200            |              |                            | Reconstructed            |
| — Ruurlo Formation  | DCCR      | 600              |                |              | Reconstructed              |                          |
| — Baarlo Formation  | DCCB      | 318.3            | 600            |              | Reconstructed              |                          |

\* Scenario 1

Table 21 History of sedimentation, uplift, erosion and nondeposition for well Q01-03

| Stratigraphic Unit  | Unit Code | Bottom age<br>Ma | Thickness<br>m | Missing<br>m | Data source<br>'Thickness' | Data Source<br>'Missing' |
|---|-----------|------------------|----------------|--------------|----------------------------|--------------------------|
| North Sea Groups  |           | 59.4             | 949.7          |              | NITG database              |                          |
| Upper North Sea Group                                     | NU        | 23.3             | 772.7          |              | Horst 2000                 |                          |
| — Maassluis Formation                                     | NUMS      | 2.4              | 569.7          |              | Horst 2000                 |                          |
| — Oosterhout Formation                                    | NUOT      | 5.2              | 168            |              | Horst 2000                 |                          |
| — Breda Formation   | NUBA      | 23.3             | 35             |              | Horst 2000                 |                          |
| <i>Nondeposition/erosion (Savian)</i>                     |           | 29.3             | >23            |              | Reconstructed              |                          |
| Middle North Sea Group                                    | NM        | 35               | 7              | >23          | Horst 2000                 | Reconstructed            |
| — Rupel Formation   | NMRF      | 35               | 7              | >23          | Horst 2000                 | Reconstructed            |
| <i>Uplift/erosion (Pyrenean)</i>                          |           | 38.6             | <400           |              | Reconstructed              |                          |
| Lower North Sea Group                                     | NL        | 59.4             | 170            | <400         | Horst 2000                 | Reconstructed            |
| — Dongen Formation  | NLFF      | 56.6             | 135            | <400         | Horst 2000                 | Reconstructed            |
| — Asse Member   | NLFFB     |                  | —              |              | Horst 2000                 |                          |
| — Brussels Marl Member                                    | NLFFM     |                  | —              |              | Horst 2000                 |                          |
| — Brussels Sand Member                                    | NLFFS     |                  | —              |              | Horst 2000                 |                          |
| — Ieper Member  | NLFFY     |                  | 119.5          |              | Horst 2000                 |                          |
| — Basal Dongen Tuffite Member                             | NLFFT     |                  | 9.5            |              | Horst 2000                 |                          |
| — Basal Dongen Sand Member                                | NLFFD     | 56.6             | 6              |              | Horst 2000                 |                          |
| — Landen Formation  | NLLF      | 59.4             | 35             |              | Horst 2000                 |                          |
| <i>Uplift &amp; erosion (Subhercynean &amp; Laramide)</i> |           | 85               | 1550           |              | Reconstructed              |                          |
| Chalk Group   | CK        | 97               |                | 1000*        |                            | Reconstructed            |
| — Ekofisk Formation                                       | CKEK      | 65               |                |              |                            |                          |
| — Ommelanden Formation                                    | CKGR      | 90.4             |                | 850          |                            | Reconstructed            |
| — Texel Formation   | CKTX      | 97               |                | 150          |                            | Reconstructed            |
| Rijnland Group  | KN        | 138.7            | 348.5          | 550          |                            | Reconstructed            |
| <i>Erosion/nondeposition (Late Kimmerian II)</i>          |           | 140.7            | 100            |              | Reconstructed              |                          |
| Schieland Group   | SLD       | 154.7            | 842.5          | 100          | NITG database              | Reconstructed            |
| <i>Erosion/nondeposition (Mid and Late Kimmerian I)</i>   |           | 156              | <474           |              | Reconstructed              |                          |
| Altena Group  | AT        | 209.5            | 1054           | <474         |                            | Reconstructed            |
| — Brabant Formation                                       | ATBR      | 166              |                | <200         |                            | Reconstructed            |
| — Werkendam Formation                                     | ATWD      | 180              | 126            | <274         | NITG database              | Reconstructed            |
| — Posidonia Shale Formation                               | ATPO      | 187              | 40             |              | NITG database              |                          |
| — Sleen and Aalburg Formations                            | ATRT+ATAL | 209.5            | 888**          |              | NITG database              |                          |
| Upper Germanic Trias Group                                | RN        | 243              | 400            |              | Reconstructed              |                          |
| <i>Erosion/nondeposition (Hardegse)</i>                   |           | 244.5            | 0-50           |              | Reconstructed              |                          |
| Lower Germanic Trias Group                                | RB        | 251              | 500            | 0-50         | Reconstructed              | Reconstructed            |
| Zechstein Group   | ZE        | 258              | 280            |              | Reconstructed              |                          |
| Upper Rotliegend Group                                    | RO        | 266              | 235            |              | Reconstructed              |                          |
| <i>Uplift &amp; erosion (Saalian)</i>                     |           | 296              | 1060           |              | Reconstructed              |                          |
| Limburg Group   | DC        | 318.3            | 940            | 1060         | Reconstructed              | Reconstructed            |
| — Dinkel/Hunze Subgroups                                  | DCD/DCH   |                  | —              | 600          |                            | Reconstructed            |
| — Maurits Formation                                       | DCCU      |                  | —              | 200          |                            | Reconstructed            |
| — Ruurlo Formation  | DCCR      |                  | 340            | 260          | Reconstructed              | Reconstructed            |
| — Baarlo Formation  | DCCB      | 318.3            | 600            |              | Reconstructed              |                          |

\* Scenario 1

\*\* ATAL: thickness doubled due to fault movement

Table 22 History of sedimentation, uplift, erosion and nondeposition for well L17-02

| Stratigraphic Unit   | Unit Code | Bottom age<br>Ma | Thickness<br>m | Missing<br>m | Data source<br>'Thickness' | Data Source<br>'Missing' |
|--|-----------|------------------|----------------|--------------|----------------------------|--------------------------|
| North Sea Groups   | N         | 59.4             | 1096           |              | NITG database              |                          |
|  | N         | 59.4             | 1160           |              | Seismic                    |                          |
| Upper North Sea Group  | NU        | 23.3             | 540            |              | Seismic                    |                          |
| <i>Nondeposition/erosion (Savian)</i>                            |           | 29.3             |                |              |                            |                          |
| Middle North Sea Group   | NM        | 35               | –              |              | Seismic                    |                          |
| <i>Uplift/erosion (Pyrenean)</i>                                 |           | 38.6             |                |              |                            |                          |
| Lower North Sea Group  | NL        | 59.4             | 620            |              |                            |                          |
| — Dongen Formation   | NLFF      | 56.6             | 540            |              | Seismic                    |                          |
| — Landen Formation   | NLLF      | 59.4             | 80             |              | Seismic                    |                          |
| <i>Uplift &amp; erosion (Subhercynian &amp; Laramide)</i>        |           |                  |                |              |                            |                          |
| Chalk Group  | CK        | 97               | 1551           |              | NITG database              |                          |
| — Ekofisk Formation  | CKEK      | 65               | 35             |              | NITG database              |                          |
| — Ommelanden Formation   | CKGR      | 90.4             | 1430           |              | NITG database              |                          |
| — Texel Formation  | CKTX      | 97               | 86             |              | NITG database              |                          |
| Rijnland Group   | KN        | 138.7            | 271            |              | NITG database              |                          |
| Schieland Group  | SLD       | 154.7            | –              |              |                            |                          |
| <i>Erosion/nondeposition (Mid and Late Kimmerian I &amp; II)</i> |           |                  | 156            | <1637        |                            | Reconstructed            |
| Altena Group   | AT        | 209.5            |                | 600          |                            | Reconstructed            |
| — Brabant Formation  | ATBR      | 166              |                | –            |                            | Reconstructed            |
| — Werkendam Formation  | ATWD      | 180              |                | –            |                            | Reconstructed            |
| — Posidonia Shale Formation                                      | ATPO      | 187              |                | –            |                            | Reconstructed            |
| — Sleen and Aalburg Formations                                   | ATRT+ATAL | 209.5            |                | 600          |                            | Reconstructed            |
| Upper Germanic Trias Group                                       | RN        | 243              |                | 400          |                            | Reconstructed            |
| <i>Erosion/nondeposition (Hardegse)</i>                          |           | 244.5            | 100            |              |                            | Reconstructed            |
| Lower Germanic Trias Group                                       | RB        | 251              |                | 500          |                            | Reconstructed            |
| Zechstein Group  | ZE        | 258              | 43             | <237         | NITG database              | Reconstructed            |
| Upper Rotliegend Group   | RO        | 266              | 234            |              | NITG database              |                          |
| <i>Uplift &amp; erosion (Saalian)</i>                            |           | 296              | 880            |              |                            | Reconstructed            |
| Limburg Group  | DC        | 318.3            | 1120           | 880          | Reconstructed              | Reconstructed            |
| — Dinkel/Hunze Subgroups   | DCD/DCH   |                  | 600            |              | Reconstructed              |                          |
| — Maurits Formation  | DCCU      |                  | 200            |              | Reconstructed              |                          |
| — Ruurlo Formation   | DCCR      |                  | 520            | 80           | Reconstructed              | Reconstructed            |
| — Baarlo Formation   | DCCB      | 318.3            | 600            |              | Reconstructed              |                          |

Table 23 History of sedimentation, uplift, erosion and nondeposition for well L14-02

| Stratigraphic Unit   | Unit Code | Bottom age<br>Ma | Thickness<br>m | Missing<br>m | Data source<br>'Thickness' | Data Source<br>'Missing' |
|--|-----------|------------------|----------------|--------------|----------------------------|--------------------------|
| North Sea Groups   | N         | 59.4             | 1281.7         |              | NITG database              |                          |
|  | N         | 59.4             | 1300           |              | Seismic                    |                          |
| Upper North Sea Group  | NU        | 23.3             | 560            |              | Seismic                    |                          |
| <i>Nondeposition/erosion (Savian)</i>                            |           | 29.3             |                |              |                            |                          |
| Middle North Sea Group   | NM        | 35               | –              |              | Seismic                    |                          |
| <i>Uplift/erosion (Pyrenean)</i>                                 |           | 38.6             |                |              |                            |                          |
| Lower North Sea Group  | NL        | 59.4             | 740            |              |                            |                          |
| — Dongen Formation   | NLFF      | 56.6             | 640            |              | Seismic                    |                          |
| — Landen Formation   | NLLF      | 59.4             | 100            |              | Seismic                    |                          |
| <i>Uplift &amp; erosion (Subhercynean &amp; Laramide)</i>        |           |                  |                |              |                            |                          |
| Chalk Group  | CK        | 97               | 1360           |              | NITG database              |                          |
| — Ekofisk Formation  | CKEK      | 65               | –              |              |                            |                          |
| — Ommelanden Formation   | CKGR      | 90.4             | 1270           |              | NITG database              |                          |
| — Texel Formation  | CKTX      | 97               | 90             |              | NITG database              |                          |
| Rijnland Group   | KN        | 138.7            | 356            |              | NITG database              |                          |
| Schieland Group  | SLD       | 154.7            | –              |              |                            |                          |
| <i>Erosion/nondeposition (Mid and Late Kimmerian I &amp; II)</i> |           | 156              | <1620          |              | Reconstructed              |                          |
| Altena Group   | AT        | 209.5            |                | 600          |                            | Reconstructed            |
| — Brabant Formation  | ATBR      | 166              |                | –            |                            | Reconstructed            |
| — Werkendam Formation  | ATWD      | 180              |                | –            |                            | Reconstructed            |
| — Posidonia Shale Formation                                      | ATPO      | 187              |                | –            |                            | Reconstructed            |
| — Sleen and Aalburg Formations                                   | ATRT+ATAL | 209.5            |                | 600          |                            | Reconstructed            |
| Upper Germanic Trias Group                                       | RN        | 243              |                | 400          |                            | Reconstructed            |
| <i>Erosion/nondeposition (Hardegsen)</i>                         |           | 244.5            | 100            |              | Reconstructed              |                          |
| Lower Germanic Trias Group                                       | RB        | 251              |                | 500          |                            | Reconstructed            |
| Zechstein Group  | ZE        | 258              | 60             | <220         | NITG database              | Reconstructed            |
| Upper Rotliegend Group   | RO        | 266              | 233.5          |              | NITG database              |                          |
| <i>Uplift &amp; erosion (Saalian)</i>                            |           | 296              | 840            |              | Reconstructed              |                          |
| Limburg Group  | DC        | 318.3            | 1160           | 840          | Reconstructed              | Reconstructed            |
| — Dinkel/Hunze Subgroups   | DCD/DCH   |                  |                | 600          |                            | Reconstructed            |
| — Maurits Formation  | DCCU      |                  |                | 200          |                            | Reconstructed            |
| — Ruurlo Formation   | DCCR      |                  | 560            | 40           | Reconstructed              | Reconstructed            |
| — Baarlo Formation   | DCCB      | 318.3            | 600            |              | Reconstructed              |                          |

Table 24 Additional geochronological units

| Geochronological unit                 | Code | Additional units  | Code                     |
|---------------------------------------|------|---|--------------------------|
| Rijnland Group                        | KN   | Holland Formation   | KNGL                     |
|                                       |      | Vlieland Claystone Formation  | KNNC                     |
|                                       |      | Vlieland Sandstone Formation  | KNNS                     |
| Schieland Group                       | SLD  | Helm Member   | SLDBH                    |
|                                       |      | Bloemendaal Member  | SLDBB                    |
|                                       |      | Fourteens Claystone Member  | SLDBC                    |
|                                       |      | Aerdenhout Member   | SLDBA                    |
| Werkendam Formation<br>(Altena Group) | ATW  | Upper Werkendam Member  | ATWDU                    |
|                                       |      | Middle Werkendam Member   | ATWDM                    |
|                                       |      | Lower Werkendam Member  | ATWDL                    |
| Upper Germanic<br>Trias Group         | RN   | Röt + Muschelkalk +<br>Keuper Formations                                      | RNRO +<br>RNMU +<br>RNKP |
|                                       |      | Solling Formation   | RNSO                     |
|                                       |      |   |                          |
| Lower Germanic<br>Trias Group         | RB   | Dethfurth Claystone Member +<br>Hardegse Formation                            | RBMDL +<br>RBMH          |
|                                       |      | Lower Volpriehausen Sandstone Member<br>+ Volpriehausen Clay-Siltstone Member | RBMVL +<br>RBMVC +       |
|                                       |      | + Lower Dethfurth Sandstone Member  | RBMDL                    |
|                                       |      | Main Claystone Member   | RBSHM +                  |
|                                       |      | + Rogenstein Member   |                          |



Table 25 Lithology and corresponding hydraulic and thermal parameters

| Stratigraphy            | Model stages | Lithology |       |        |         |        |              |              |        |        |
|-------------------------|--------------|-----------|-------|--------|---------|--------|--------------|--------------|--------|--------|
|                         |              | Shale %   | Sst % | Silt % | Chalk % | Marl % | Carbon-ate % | Anhy-drite % | Salt % | Coal % |
| Limburg                 | 1            | 90        | 9     |        |         |        |              |              |        | 1      |
| Limburg                 | 2            | 85        | 11    |        |         |        |              |              |        | 4      |
| Limburg                 | 3            | 80        | 14    |        |         |        |              |              |        | 6      |
| Limburg                 | 4            | 59        | 40    |        |         |        |              |              |        | 1      |
| Upper Rotliegend        | 7            | 0         | 100   |        |         |        |              |              |        |        |
| Zechstein               | 8            | 6         |       |        |         |        | 34           | 38           | 22     |        |
| Zechstein               | 8            | 8         |       |        |         |        | 43           | 37           | 12     |        |
| Zechstein               | 8            | 53        | 17    |        |         |        | 30           |              |        |        |
| Lower Germanic Trias    | 9            | 100       |       |        |         |        |              |              |        |        |
| Lower Germanic Trias    | 10           | 37        | 63    |        |         |        |              |              |        |        |
| Lower Germanic Trias    | 11           | 67        | 33    |        |         |        |              |              |        |        |
| Lower Germanic Trias    | 11           | 50        | 50    |        |         |        |              |              |        |        |
| Upper Germanic Trias    | 13           | 67        | 33    |        |         |        |              |              |        |        |
| Upper Germanic Trias    | 13           | 50        | 50    |        |         |        |              |              |        |        |
| Upper Germanic Trias    | 13           | 40        | 60    |        |         |        |              |              |        |        |
| Upper Germanic Trias    | 14           | 50        |       |        |         |        | 25           | 7            | 18     |        |
| Upper Germanic Trias    | 14           | 68        |       |        |         |        | 14           | 16           | 2      |        |
| Altena                  | 15           | 99        |       |        |         | 1      |              |              |        |        |
| Altena (Posidonia)      | 16           | 100       |       |        |         |        |              |              |        |        |
| Altena                  | 17           | 97        | 3     |        |         |        |              |              |        |        |
| Altena                  | 18           | 0         | 100   |        |         |        |              |              |        |        |
| Altena                  | 19           | 97        | 3     |        |         |        |              |              |        |        |
| Altena                  | 20           | 15        | 3     |        |         | 64     | 18           |              |        |        |
| Schieland               | 23           | 43        | 57    |        |         |        |              |              |        |        |
| Schieland               | 24           | 98        | 1     |        |         |        | 1            |              |        |        |
| Schieland               | 25           | 76        | 17    |        |         |        | 7            |              |        |        |
| Schieland               | 26           | 0         | 8     | 92     |         |        |              |              |        |        |
| Rijnland (Vlieland Sst) | 27           | 0         | 100   |        |         |        |              |              |        |        |
| Rijnland                | 28           | 100       |       |        |         |        |              |              |        |        |
| Rijnland                | 29           | 10        |       |        |         | 90     |              |              |        |        |
| Chalk                   | 30           | 0         |       |        | 100     |        |              |              |        |        |
| Lower North Sea         | 34           | 100       |       |        |         |        |              |              |        |        |
| Lower North Sea         | 35           | 100       |       |        |         |        |              |              |        |        |
| Upper North Sea         | 40           | 100       |       |        |         |        |              |              |        |        |
| Upper North Sea         | 41           | 80        | 20    |        |         |        |              |              |        |        |
| Upper North Sea         | 42           |           | 100   |        |         |        |              |              |        |        |

| Matrix density<br>(g/cm <sup>3</sup> ) | Permeability (mD) |            |          |            | Matrix thermal properties            |                          |  |
|--|-------------------|------------|----------|------------|--------------------------------------|--------------------------|--|
|  | Intrinsic         | Horizontal | Vertical | Anisotropy | T conductivity<br>(W/mK)<br>at 20° C | Heat capacity<br>(J/KgK) | Radiogenic<br>heat production<br>(W/m <sup>3</sup> ) |
| 2.785                                  | 3.00E-05          | 1.0E-04    | 1.0E-05  | 1.00E+01   | 2                                    | 856                      | 1.2E-06  |
| 2.784                                  | 3.00E-05          | 9.0E-05    | 3.0E-06  | 3.00E +01  | 1.9                                  | 858                      | 1.2E-06  |
| 2.779                                  | 4.00E-05          | 1.2E-04    | 4.0E-06  | 3.00E+01   | 1.8                                  | 862                      | 1.2E-06  |
| 2.74                                   | 6.00E-04          | 6.0E-02    | 6.0E-04  | 1.00E+02   | 2.5                                  | 904                      | 1.2E-06  |
| 2.65                                   | 1.00E+00          | 1.0E+00    | 4.0E-01  | 2.50E+00   | 4                                    | 1000                     | 8.0E-07  |
| 2.673                                  | 2.00E-05          | 7.0E-04    | 2.0E-06  | 3.50E+02   | 4                                    | 957                      | 1.0E-06  |
| 2.728                                  | 4.00E-05          | 1.0E-03    | 2.4E-06  | 4.20E+02   | 3.7                                  | 969                      | 1.0E-06  |
| 2.746                                  | 3.00E-04          | 1.5E-02    | 3.0E-04  | 5.00E+01   | 2.9                                  | 915                      | 1.0E-06  |
| 2.800                                  | 1.00E-05          | 1.0E-04    | 1.0E-04  | 1.00E+00   | 2.8                                  | 840                      | 1.2E-06  |
| 2.707                                  | 1.00E-01          | 1.0E+01    | 2.0E-04  | 5.00E+04   | 3.6                                  | 878                      | 1.0E-06  |
| 2.751                                  | 1.50E-03          | 3.3E+00    | 7.5E-05  | 4.40E+04   | 3                                    | 860                      | 1.0E-06  |
| 2.726                                  | 1.50E-02          | 6.8E+00    | 2.3E-04  | 3.00E+04   | 3.2                                  | 870                      | 1.0E-06  |
| 2.751                                  | 1.50E-03          | 3.3E+00    | 7.5E-05  | 4.40E+04   | 3                                    | 860                      | 1.0E-06  |
| 2.726                                  | 1.50E-02          | 6.8E+00    | 2.3E-04  | 3.00E+04   | 3.2                                  | 870                      | 1.0E-06  |
| 2.711                                  | 6.00E-02          | 7.8E+00    | 4.2E-04  | 1.86E+04   | 2.9                                  | 876                      | 1.0E-06  |
| 2.670                                  | 2.50E-05          | 6.5E-04    | 6.3E-06  | 1.04E+02   | 2.9                                  | 893                      | 1.2E-06  |
| 2.794                                  | 2.00E-05          | 6.0E-04    | 6.0E-06  | 1.00E+02   | 2.9                                  | 888                      | 1.2E-06  |
| 2.799                                  | 1.00E-05          | 6.0E-05    | 6.2E-06  | 1.00E+01   | 2.4                                  | 841                      | 1.2E-06  |
| 2.800                                  | 1.00E-05          | 5.0E-05    | 1.0E-05  | 5.00E+00   | 2.1                                  | 840                      | 1.2E-06  |
| 2.795                                  | 2.00E-05          | 3.0E-04    | 1.5E-05  | 2.00E+01   | 2.1                                  | 845                      | 1.2E-06  |
| 2.650                                  | 1.00E+00          | 1.0E+00    | 4.0E-01  | 2.50E+00   | 4                                    | 1000                     | 8.0E-07  |
| 2.795                                  | 2.00E-05          | 3.0E-04    | 1.5E-05  | 2.00E+01   | 2.1                                  | 845                      | 1.2E-06  |
| 2.708                                  | 1.50E-04          | 1.0E-03    | 1.0E-04  | 1.00E+01   | 2.1                                  | 912                      | 1.0E-06  |
| 2.716                                  | 3.00E-02          | 3.0E-02    | 3.0E-05  | 1.00E+03   | 2.6                                  | 874                      | 1.0E-06  |
| 2.797                                  | 1.00E-05          | 5.0E-05    | 1.0E-05  | 5.00E+00   | 2.1                                  | 843                      | 1.2E-06  |
| 2.768                                  | 1.50E-04          | 7.5E-03    | 7.5E-06  | 1.00E+03   | 2.6                                  | 861                      | 1.0E-06  |
| 2.650                                  | 1.50E-02          | 1.5E-02    | 7.5E-04  | 2.00E+01   | 2.2                                  | 1073                     | 1.2E-06  |
| 2.653                                  | 2.50E+01          | 2.5E+01    | 5.0E+00  | 5.00E+00   | 3.2                                  | 900                      | 8.0E-07  |
| 2.800                                  | 1.00E-05          | 5.0E-04    | 5.0E-05  | 1.00E+01   | 2.1                                  | 840                      | 1.2E-06  |
| 2.701                                  | 1.00E-04          | 2.0E-04    | 5.0E-05  | 4.00E+00   | 2.1                                  | 894                      | 1.0E-06  |
| 2.700                                  | 1.00E-02          | 1.0E-02    | 1.0E-02  | 1.00E+00   | 2.7                                  | 950                      | 8.0E-07  |
| 2.800                                  | 1.00E-05          | 1.0E-03    | 1.0E-04  | 1.00E+01   | 2                                    | 840                      | 1.2E-06  |
| 2.800                                  | 1.00E-05          | 1.0E-03    | 1.0E-04  | 1.00E+01   | 2                                    | 840                      | 1.2E-06  |
| 2.800                                  | 1.00E-05          | 4.0E-03    | 2.0E-04  | 2.00E+01   | 2                                    | 840                      | 1.2E-06  |
| 2.771                                  | 2.00E-04          | 2.0E-02    | 2.0E-04  | 1.00E+02   | 2.1                                  | 852                      | 1.0E-06  |
| 2.653                                  | 2.50E+01          | 2.5E+01    | 5.0E+00  | 5.00E+00   | 2.8                                  | 900                      | 8.0E-07  |

Table 26 Maturity parameters

| Well           | Log depth<br>m | Stratigraphic<br>unit | T <sub>max</sub><br>°C | R <sub>p</sub> % | Number of<br>measurements | Standard<br>deviation |
|----------------|----------------|-----------------------|------------------------|------------------|---------------------------|-----------------------|
| <b>P09-01A</b> | 2285           | ATPO                  | 431                    | 0.84             | 8                         | 0.04                  |
|                | 2545           | ATAL                  | 431                    | 0.81             | 6                         | 0.12                  |
|                | 2780           | ATAL                  | 436                    |                  |                           |                       |
| <b>P06-02</b>  | 1428           | SLD                   | 435                    |                  |                           |                       |
| <b>Q01-03</b>  | 1658           | SLD                   | 442                    |                  |                           |                       |
|                | 1812           | SLD                   | 447                    |                  |                           |                       |
|                | 2340           | ATPO                  | 444                    | 0.93             | 6                         | 0.01                  |
|                | 2352           | ATPO                  | 446                    | 0.92             | 6                         | 0.01                  |
|                | 2362           | ATPO                  | 443                    |                  |                           |                       |
|                | 2458           | ATAL                  | 445                    |                  |                           |                       |
|                | 2556           | ATAL                  | 436                    |                  |                           |                       |

Table 27 Paleobathymetry and paleotopography for Well P09-01A

| Stratigraphic Unit   | Bottom age<br>Ma | Thickness<br>m | Missing<br>m | Water depth<br>m | Topography<br>m asl |
|--|------------------|----------------|--------------|------------------|---------------------|
| North Sea Groups   | 59.4             | 661.8          |              |                  |                     |
| Upper North Sea Group  | 23.3             | 567.8          |              |                  |                     |
| — Maassluis Formation  | 2.4              | 463.8          |              | 0-30             |                     |
| — Oosterhout Formation   | 5.2              | 90.5           |              | 50               |                     |
| — Breda Formation  | 23.3             | 13.5           |              | 50               |                     |
| <i>Nondeposition/erosion (Savian)</i>                            | 29.3             | >30            |              |                  | 10                  |
| Middle North Sea Group   | 35               | -              | >30          |                  |                     |
| — Rupel Formation  | 35               | -              | >30          | 25               |                     |
| <i>Uplift/erosion (Pyrenean)</i>                                 | 38.6             | <500           |              |                  | 10-50               |
| Lower North Sea Group  | 59.4             | 8              | <500         | 50-100           |                     |
| — Dongen Formation   | 56.6             | 46.5           | <500         |                  |                     |
| — Asse Member  |                  | -              |              |                  |                     |
| — Brussels Marl Member   |                  | -              |              |                  |                     |
| — Brussels Sand Member   |                  | -              |              |                  |                     |
| — Ieper Member   | 38.5             | 50-100         |              |                  |                     |
| — Basal Dongen Tuffite Member                                    |                  | -              |              |                  |                     |
| — Basal Dongen Sand Member                                       | 56.6             | 8              |              | 25-50            |                     |
| — Landen Formation   | 59.4             | 47.5           |              | 50               |                     |
| <i>Uplift &amp; erosion (Subhercynian &amp; Laramide)</i>        | 85               | 433.5          |              |                  | 100                 |
| Chalk Group  | 97               | 566.5          | 433.5*       |                  |                     |
| — Ekofisk Formation  | 65               | -              |              |                  |                     |
| — Ommelanden Formation   | 90.4             | 493.5          |              | 50-200           |                     |
| — Texel Formation  | 97               | 73             |              | 50-150           |                     |
| Rijnland Group   | 138.7            | 938.5          |              | 25-100           |                     |
| Schieland Group  |                  |                |              |                  |                     |
| <i>Erosion/nondeposition (Mid and Late Kimmerian I &amp; II)</i> | 156              | 567.5          |              |                  | 100                 |
| Altena Group   | 209.5            | 989            | 567.5        |                  |                     |
| — Brabant Formation  | 166              | -              | 200          | 25-50            |                     |
| — Werkendam Formation  | 180              | 32.5           | 367.5        | 75               |                     |
| — Posidonia Shale Formation                                      | 187              | 60             |              | >100             |                     |
| — Sleen and Aalburg Formations                                   | 209.5            | 896.5          |              | 50-100           |                     |
| Upper Germanic Trias Group                                       | 243              | 703.5          |              | 30-50            |                     |
| <i>Erosion/nondeposition (Hardeggen)</i>                         | 244.5            | 0-50           |              | 0                |                     |
| Lower Germanic Trias Group                                       | 251              | 468            | 0-50         | 0                |                     |
| Zechstein Group  | 258              | 232            |              | 0-10             |                     |
| Upper Rotliegend Group   | 266              | 135            |              |                  | 10                  |
| <i>Uplift &amp; erosion (Saalian)</i>                            | 296              | 700            |              |                  | 100                 |
| Limburg Group  | 318.3            | 1300           | 700          |                  |                     |
| Dinkel/Hunze Subgroups   |                  |                | 600          |                  | 10                  |
| — Maurits Formation  |                  | 100            | 100          |                  | 10                  |
| — Ruurlo Formation   |                  | 600            | 0            |                  |                     |
| — Baarlo Formation   | 318.3            | 600            | 0            |                  |                     |

\* Scenario 1

Table 28 Paleobathymetry and paleotopography for Well P06-02

| Stratigraphic Unit  | Bottom age<br>Ma | Thickness<br>m | Missing<br>m | Water depth<br>m | Topography<br>m asl |
|---|------------------|----------------|--------------|------------------|---------------------|
| North Sea Groups  | 59.4             | 894.5          |              |                  |                     |
| Upper North Sea Group                                     | 23.3             | 722.5          |              |                  |                     |
| — Maassluis Formation                                     | 2.4              | 593.5          |              | 0-30             |                     |
| — Oosterhout Formation                                    | 5.2              | 100            |              | 50               |                     |
| — Breda Formation   | 23.3             | 29             |              | 50               |                     |
| <i>Nondeposition/erosion (Savian)</i>                     | 29.3             | >15            |              | 0                |                     |
| Middle North Sea Group                                    |                  | 15             | >15          |                  |                     |
| — Rupel Formation   | 35               | 15             | >15          | 25               |                     |
| <i>Uplift/erosion (Pyrenean)</i>                          | 38.6             | <435           |              |                  | 10-50               |
| Lower North Sea Group                                     | 59.4             | 157            | <435         | 50-100           |                     |
| — Dongen Formation  | 56.6             | 126            | <435         | 50-100           |                     |
| — Asse Member   |                  | -              |              |                  |                     |
| — Brussels Marl Member                                    |                  | -              |              |                  |                     |
| — Brussels Sand Member                                    |                  | -              |              |                  |                     |
| — Ieper Member  |                  | 105            |              | 50-100           |                     |
| — Basal Dongen Tuffite Member                             |                  | 12.5           |              |                  |                     |
| — Basal Dongen Sand Member                                | 56.6             | 8.5            |              | 25-50            |                     |
| — Landen Formation  | 59.4             | 31             |              | 50-100           |                     |
| <i>Uplift &amp; erosion (Subhercynian &amp; Laramide)</i> | 85               | 2528           |              |                  | 175                 |
| Chalk Group   | 97               |                | 1000*        |                  |                     |
| — Ekofisk Formation                                       | 65               |                |              |                  |                     |
| — Ommelanden Formation                                    | 90.4             | 850            |              | 50-200           |                     |
| — Texel Formation   | 97               | 150            |              | 50-150           |                     |
| Rijnland Group  | 138.7            | 1200           |              | 25-100           |                     |
| <i>Erosion/nondeposition (Late Kimmerian II)</i>          | 140.7            | 100            |              | 0                |                     |
| Schieland Group   | 154.7            | 672            | 428          |                  | 10                  |
| <i>Erosion/nondeposition (Mid and Late Kimmerian I)</i>   | 156              | 564            |              |                  | 100                 |
| Altena Group  | 209.5            | 236            | 564          |                  |                     |
| — Brabant Formation                                       | 166              | 130            |              | 25-50            |                     |
| — Werkendam Formation                                     | 180              | 270            | 75           |                  |                     |
| — Posidonia Shale Formation                               | 187              | 30             | >100         |                  |                     |
| — Sleen and Aalburg Formations                            | 209.5            | 236            | 134          | 50-100           |                     |
| Upper Germanic Trias Group                                | 243              | 404            |              | 30-50            |                     |
| <i>Erosion/nondeposition (Hardeggen)</i>                  | 244.5            | 0-50           |              | 0                |                     |
| Lower Germanic Trias Group                                | 251              | 488            | 0-50         | 0                |                     |
| Zechstein Group   | 258              | 305            |              | 0-20             |                     |
| Upper Rotliegend Group                                    | 266              | 235            |              | 0                |                     |
| <i>Uplift &amp; erosion (Saalian)</i>                     | 296              | 800            |              |                  | 100                 |
| Limburg Group   | 318.3            | 1200           | 800          |                  |                     |
| — Dinkel/Hunze Subgroups                                  |                  |                | 600          |                  | 10                  |
| — Maurits Formation                                       |                  |                | 200          |                  | 10                  |
| — Ruurlo Formation  |                  | 600            |              | 0                |                     |
| — Baarlo Formation  | 318.3            | 600            |              | 0                |                     |

\* Scenario 1

Table 29 Paleobathymetry and paleotopography for Well Q01-03

| Stratigraphic Unit  | Bottom age<br>Ma | Thickness<br>m | Missing<br>m | Water depth<br>m | Topography<br>m asl |
|---|------------------|----------------|--------------|------------------|---------------------|
| North Sea Groups  | 59.4             | 949.7          |              |                  |                     |
| Upper North Sea Group                                     | 23.3             | 772.7          |              |                  |                     |
| — Maassluis Formation                                     | 2.4              | 569.7          |              | 0-30             |                     |
| — Oosterhout Formation                                    | 5.2              | 168            |              | 50               |                     |
| — Breda Formation   | 23.3             | 35             |              | 50               |                     |
| <i>Nondeposition/erosion (Savian)</i>                     | 29.3             | >23            |              | 0                |                     |
| Middle North Sea Group                                    | 35               | 7              | >23          |                  |                     |
| — Rupel Formation   | 35               | 7              | >23          | 25               |                     |
| <i>Uplift/erosion (Pyrenean)</i>                          | 38.6             | <400           |              |                  | 10-50               |
| Lower North Sea Group                                     | 59.4             | 170            | <400         | 50-100           |                     |
| — Dongen Formation  | 56.6             | 135            | <400         |                  |                     |
| — Asse Member   |                  | -              |              |                  |                     |
| — Brussels Marl Member                                    |                  | -              |              |                  |                     |
| — Brussels Sand Member                                    |                  | -              |              |                  |                     |
| — Ieper Member  |                  | 119.5          |              | 50-100           |                     |
| — Basal Dongen Tuffite Member                             |                  | 9.5            |              |                  |                     |
| — Basal Dongen Sand Member                                | 56.6             | 6              |              |                  |                     |
| — Landen Formation  | 59.4             | 35             |              | 50-100           |                     |
| <i>Uplift &amp; erosion (Subhercynian &amp; Laramide)</i> | 85               | 1550           |              |                  | 175                 |
| Chalk Group   | 97               |                | 1000*        |                  |                     |
| — Ekofisk Formation                                       | 65               |                |              |                  |                     |
| — Ommelanden Formation                                    | 90.4             |                | 850          | 50-200           |                     |
| — Texel Formation   | 97               |                | 150          | 50-150           |                     |
| Rijnland Group  | 138.7            | 348.5          | 550          | 25-100           |                     |
| <i>Erosion/nondeposition (Late Kimmerian II)</i>          | 140.7            | 100            |              | 0                |                     |
| Schieland Group   | 154.7            | 842.5          | 100          |                  | 10                  |
| <i>Erosion/nondeposition (Mid and Late Kimmerian I)</i>   | 156              | <474           |              |                  | 10                  |
| Altena Group  | 209.5            | 1054           | <474         |                  |                     |
| — Brabant Formation                                       | 166              |                | <200         | 25-50            |                     |
| — Werkendam Formation                                     | 180              | 126            | <274         | 75               |                     |
| — Posidonia Shale Formation                               | 187              | 40             |              | >100             |                     |
| — Sleen and Aalburg Formations                            | 209.5            | 888            |              | 50-100           |                     |
| Upper Germanic Trias Group                                | 243              | 400            |              | 30-50            |                     |
| <i>Erosion/nondeposition (Hardeggen)</i>                  | 244.5            | 0-50           |              | 0                |                     |
| Lower Germanic Trias Group                                | 251              | 500            | 0-500        |                  |                     |
| Zechstein Group   | 258              | 280            |              | 0-20             |                     |
| Upper Rotliegend Group                                    | 266              | 235            |              |                  | 10                  |
| <i>Uplift &amp; erosion (Saalian)</i>                     | 296              | 1060           |              |                  | 100                 |
| Limburg Group   | 318.3            | 940            | 1060         |                  |                     |
| — Dinkel/Hunze Subgroups                                  |                  | -              | 600          |                  | 10                  |
| — Maurits Formation                                       |                  | -              | 200          |                  | 10                  |
| — Ruurlo Formation  |                  | 340            | 260          | 0                |                     |
| — Baarlo Formation  | 318.3            | 600            |              | 0                |                     |

\* Scenario 1

Table 30 Paleobathymetry and paleotopography for Well L14-02

| Stratigraphic Unit   | Bottom age<br>Ma | Thickness<br>m | Missing<br>m | Water depth<br>m | Topography<br>m asl |
|--|------------------|----------------|--------------|------------------|---------------------|
| North Sea Groups   | 59.4             | 1300           |              |                  |                     |
| Upper North Sea Group  | 23.3             | 560            |              | 0-50             |                     |
| <i>Nondeposition/erosion (Savian)</i>                            | 29.3             |                |              | 0                |                     |
| Middle North Sea Group   | 35               | -              |              | 0                |                     |
| Uplift/erosion (Pyrenean)  | 38.6             |                |              | 0                |                     |
| Lower North Sea Group  | 59.4             | 740            |              |                  |                     |
| — Dongen Formation   | 56.6             | 640            |              | 50-100           |                     |
| — Landen Formation   | 59.4             | 100            |              | 100              |                     |
| <i>Uplift &amp; erosion (Subhercynean &amp; Laramide)</i>        |                  |                |              |                  |                     |
| Chalk Group  | 97               | 1360           |              |                  |                     |
| — Ekofisk Formation  | 65               | -              |              | 0                |                     |
| — Ommelanden Formation   | 90.4             | 1270           |              | 50-200           |                     |
| — Texel Formation  | 97               | 90             |              | 50-150           |                     |
| Rijnland Group   | 138.7            | 356            |              | 25-100           |                     |
| Schieland Group  | 154.7            | -              |              |                  | 10                  |
| <i>Erosion/nondeposition (Mid and Late Kimmerian I &amp; II)</i> | 156              | <1620          |              |                  | 100                 |
| Altena Group   | 209.5            |                | 600          |                  |                     |
| — Brabant Formation  | 166              |                | -            |                  | 10                  |
| — Werkendam Formation  | 180              |                | -            |                  | 10                  |
| — Posidonia Shale Formation                                      | 187              |                | -            |                  | 10                  |
| — Sleen and Aalburg Formations                                   | 209.5            |                | 600          | 50-100           |                     |
| Upper Germanic Trias Group                                       | 243              |                | 400          | 30-50            |                     |
| <i>Erosion/nondeposition (Hardeggen)</i>                         | 244.5            | 100            |              |                  | 10                  |
| Lower Germanic Trias Group                                       | 251              |                | 500          | 0                |                     |
| Zechstein Group  | 258              | 60             | <220         | 0-20             |                     |
| Upper Rotliegend Group   | 266              | 233.5          |              |                  | 10                  |
| <i>Uplift &amp; erosion (Saalian)</i>                            | 296              | 840            |              |                  | 100                 |
| Limburg Group  | 318.3            | 1160           | 840          |                  |                     |
| — Dinkel/Hunze Subgroups   |                  |                | 600          |                  | 10                  |
| — Maurits Formation  |                  |                | 200          |                  | 10                  |
| — Ruurlo Formation   |                  | 560            | 40           | 0                |                     |
| — Baarlo Formation   | 318.3            | 600            |              | 0                |                     |

Table 31 Evolution of sediment–water interface temperatures along the SW–NE section through the Broad Fourteens Basin. Ocean surface temperatures are estimated from the paleolatitudes derived from Glennie (1990, Figure 2.7) in combination with the relation between ocean surface temperature and paleolatitudes given in Welte et al. (1997, Figure 1.5). Subsequently, the sediment–water interface temperatures were estimated using paleobathymetries along the section and the relation between water depth and bottom temperatures of the North Sea given in Evans and Coleman (1974)

| Time (Ma) | Ocean surface temperature (latitude London) (°C) | Sediment-water interface temperature (°C) (well P09-01A, P06-02, Q01-03, Q01-19) | Sediment-water interface temperature (°C) (well L14-02) |
|-----------|--|--|---|
| 0         | 10   | 8  | 8   |
| 10        | 14.5   | 12.5   | 12.5  |
| 20        | 19.5   | 17.5   | 17.5  |
| 40        | 22.5   | 22.5   | 22.5  |
| 60        | 23   | 21   | 19  |
| 80        | 25   | 25   | 21  |
| 100       | 26.5   | 22.5 (-18.5)   | 22.5 (-18.5)  |
| 120       | 26.5   | 23.5   | 22  |
| 140       | 25.5   | 25.5   | 25.5  |
| 160       | 24   | 23   | 24  |
| 180       | 22.5   | 19.5   | 22.5  |
| 200       | 22   | 19   | 21  |
| 220       | 25.5   | 23.5   | 23.5  |
| 240       | 28   | 27   | 27  |
| 280       | 25   | 25   | 25  |
| 293       | 25   | 25   | 25  |
| 320       | >25  | >25  | >25   |
| 360       | >25  | >25  | >25   |



Table 32 Paleotemperatures from Pliocene to Holocene. Temperatures for Holocene to Saalian (135 000 years B.P.) estimated from Van Gijssel (1995). Remaining temperatures estimated from Zagwijn (1992)

|                         | Time period<br>(years B.P.) | Mean annual temperature<br>(°C) |
|-------------------------|-----------------------------|---------------------------------|
| Holocene                | 0 - 5000                    | 8                               |
| Holocene                | 5000 - 10 000               | 4                               |
| Weichselian             | 10 000 - 13 000             | -2                              |
|                         | 13 000 - 25 000             | -10                             |
|                         | 25 000 - 60 000             | -2                              |
|                         | 60 000 - 70 000             | -10                             |
|                         | 70 000 - 75 000             | -5                              |
|                         | 75 000 - 82 000             | 0                               |
|                         | 82 000 - 94 000             | -2                              |
|                         | 94 000 - 105 000            | 0                               |
|                         | 105 000 - 116 000           | -2                              |
| Eemian                  | 116 000 - 126 000           | 8                               |
| Saalian                 | 126 000 - 135 000           | -2                              |
|                         | 135 000 - 150 000           | -8                              |
|                         | 150 000 - 280 000           | 0                               |
| Holsteinian             | 280 000 - 325 000           | 8                               |
| Elsterian               | 325 000 - 350 000           | -2                              |
| Cromerian – Praetiglian | 350 000 - 2.3 Ma            | 2                               |
| Pliocene                | 2.3 - 5.2 Ma                | 8                               |

Table 33 Present-day basal heat flow

|  |  |
|--|--|
| Present-day heat flow in sedimentary fill of Broad Fourteens Basin (depths 0 - 3000 m) | 62 mW/m <sup>2</sup><br>(55 - 65 mW/m <sup>2</sup> )       |
| Present-day thickness crust Broad Fourteens Basin                                      | 29 - 30 km*  |
| Present-day thickness upper crust Broad Fourteens Basin                                | 15 km*<br>(+ 5 km sediments)                               |
| Present-day thickness lower crust Broad Fourteens basin                                | 10 km*   |
| Radiogenic heat production rate upper crust  | 1.5 × 10 <sup>-6</sup> W/m <sup>3</sup>                    |
| Radiogenic heat production rate lower crust  | 0.4 × 10 <sup>-6</sup> W/m <sup>3</sup>                    |
| Thermal conductivity upper crust   | 2.5 W/mK   |
| Thermal conductivity lower crust   | 2.5 W/mK   |
| ⇒ Basal heat flow  | 32.5 mW/m <sup>2</sup><br>(25.5 - 35.5 mW/m <sup>2</sup> ) |
| ⇒ Heat flow input into upper crust   | 36.5 mW/m <sup>2</sup><br>(29.5 - 39.5 mW/m <sup>2</sup> ) |
| ⇒ Heat flow input into base sedimentary fill   | 59 mW/m <sup>2</sup><br>(52 - 62 mW/m <sup>2</sup> )       |

\* Rijkers and Duin (1994)

